Metabolic Regulation of Antiviral Immune Responses in Macrophages

By

Duale Ahmed, M.Sc.

A thesis submitted to the Faculty of Graduate and Postdoctoral Affairs

in partial fulfillment of the requirements for the degree of

Doctor of Philosophy

in

Biology

Carleton University

Ottawa, Ontario

ABSTRACT

It is increasingly clear that there is an intimate link between cellular metabolism and macrophage function. Several studies in the last decade have established that alterations in cellular metabolism both drive and regulate macrophage function, allowing them to mount a functional immune response against viruses by promoting viral resistance, antigen presentation and the production of inflammatory and antiviral cytokines. As a result, metabolic reprogramming of macrophages allows them to adapt the spectrum and magnitude of their response depending on the microenvironment, stimuli, and stage of infection. Yet, it is unclear how different viral ligands alter metabolism to induce specific immune responses and if specific metabolic components can act as rheostats to amplify these responses based on the microenvironment.

The central hypothesis of my thesis is that cellular metabolism is crucial to regulating antiviral immune responses. Specifically, I hypothesized that differential mitochondrial reprogramming allows macrophages to modulate ligand-specific effector response. Moreover, mitochondria further function as rheostats, fine-tuning immune responses based on the microenvironment.

First, I used publicly available microarray datasets to develop a metabolic signature associated with early IFN-α responses in mouse BMMs and human MDMs. >500 metabolic genes related to cellular bioenergetics, cellular redox status, amino acid, and lipid metabolism were identified. Next, I show that TLR3 and TLR4 engagement in mouse BMMs drive differential ETC remodeling, linked to differential mitochondrial activity and subsequent ROS generation, to support ligand-specific inflammatory and antiviral profiles. Furthermore, when exploring different types of TLR3 engagement, based on ligand length, they trigger distinct inflammatory and antiviral

programs, due to unique regulatory mechanisms surrounding HIF-1α function as well as altered ETC architecture and function, respectively.

The aim of this thesis is to gain a more thorough understanding of the critical role of cellular metabolism in regulating macrophage antiviral responses. A systematic understanding of these critical processes to regulating effector function under non-diseased conditions can provide critical insights into the dysregulation of metabolic processes during chronic viral infections. The data presented may be the foundation towards the development of new antiviral therapeutics by targeting selective mitochondrial components.

DEDICATION

To **HODAN NALAYEH**

Your legacy lives on through us!

To all the dream chasers in the world, keep chasing!

This is an important discussion and I'm glad we're having it!

PREFACE

This thesis "Metabolic Regulation of Antiviral Immune Responses in Macrophages" is comprised of four chapters adapted from research manuscripts. Chapters 2 (*Mediators of Inflammation*, 2018) and 3 (*Scientific Reports*, 2019) have been published. Chapter 4 (*Journal of Immunology*, 2020) has been submitted for publication and Chapter 5 is in preparation for submission at *Frontiers of Immunology*. D.A. is the primary co-author on each of these chapters. The authors contributions for each chapter are as follows:

Chapter 2

This chapter is a finished manuscript published at *Mediators of Inflammation* in 2018 and is a collaborative work of D.A., Jaworski, A., Roy, D., Willmore, W., Golshani, A., and Cassol, E. entitled "Transcriptional profiling suggests extensive metabolic rewiring of human and mouse macrophages during early interferon alpha responses." D.A. is the main contributor, having curated the dataset and conducted the analysis, aided by A.J, D.R., W.W., and E.C. A.G. and E.C. supervising the research. All contributors contributed to the writing and editing of the manuscript.

Chapter 3

This chapter is a completed manuscript published at *Scientific Reports* in 2019 and is a collaborative work of D.A., Roy, D., Jaworski, A., Edwards, A., Abizaid, A., Kumar, A., Golshani, A., and Cassol, E. entitled "Differential remodeling of the electron transport chain is required to support TLR3 and TLR4 signaling and cytokine production in macrophages." A.G. and E.C supervised the work in this chapter. D.A. performed all of the experiments, with D.R. assisting and D.A. and E.C. designing the experiments. A.J., A.E. and A.A. helped procured the mouse bone marrow progenitors used in this chapter. D.A., D.R., A.K., and E.C. assisted in the analysis and interpretation. All co-authors contributed to the writing and critiquing of the manuscript.

Chapter 4

This chapter is a completed manuscript submitted at *Journal of Immunology* in 2020 and is a collaborative work of D.A., Humphrey, A., Roy, D., Sheridan, M-E, Jaworski, A., Edwards, A., Donner, J., Abizaid, A., Willmore, W., Kumar, A., Golshani, A., and Cassol, E. entitled "HIF-1α regulation of pro-inflammatory cytokine production following TLR3 engagement is dependent on viral nucleic acid length and glucose availability." D.A. is the main contributor of this experiment, conducting all of the experiments with the help of A.H., D.R., M.E.S, and J.D, supervised by A.G. and E.C. The experiments were designed by D.A. and E.C. A.J., A.E. and A.A. helped harvested the mouse bone marrow progenitor cells used in this study. D.A., A.H., D.R., M.E.S., J.D., W.W., A.K. and E.C. participated in the analysis and interpreting of the data. All contributors on this chapter assisted in the careful writing of this manuscript.

Chapter 5

This chapter is a manuscript in preparation to be submitted at *Frontiers of Immunology* and is a collaborative work of D.A., Humphrey, A., Roy, D., Sheridan, M-E, Versey, Z., Jaworski, A., Edwards, A., Abizaid, A., Kumar, A., Golshani, A., and Cassol, E. entitled "dsRNA strand length dictates the manner of mitochondrial reprogramming and ROS-activated antiviral response during TLR3 engagement." D.A. is the primary co-author, conducting all of the experiments of this chapter with support from A.H., D.R., M.E.S, and Z.V, with supervision from A.G. and E.C. The experiments of this chapter were designed by D.A. and E.C., and mouse bone marrow progenitors were collected A.J., A.E., and A.A. D.A., A.H., D.R., M.E.S., Z.V., A.K. and E.C. contributed to the analysis and interpreting of the data. All co-authors on this chapter assisted in the creation of this manuscript.

ACKNOWLEDGEMENTS

There is an old African proverb that says, "It takes a village to raise a child." One person's success is not only due to their skills and expertise, but the infrastructure that surrounds them. The completion of this Ph.D. would not have been possible with the numerous pillars that held me up. Firstly, I would like to thank Dr. Edana Cassol for giving me the opportunity to work under her supervision. There is no doubt that this Ph.D. experience can be considered one of the more "unique" experiences that one could go through. There has been lots of ups, lots of downs, lots of relocations and readjustments. But through it all, we were able to find a way to make it work. I've worked harder during this Ph.D. than I ever have for anything in my life and even though some of that can be attributed to circumstances out of our control, you pushed me to be the best that I could be. There is absolutely no way I would be in the position that I am in today without your guidance. I am a better person because I was a part of your lab. I am a better person because of what we went through. And like Super Saiyans, what doesn't kill you can only make you stronger!

Next, I would like to extend my appreciation to my advisory committee for their guidance through this Ph.D.: Dr. Ashok Kumar, Dr. Bruce McKay, and especially Dr. Ashkan Golshani. When I had to switch labs in the middle of this process, you did not hesitate to help and lend a hand. You all had a hand in pushing me to be better, and this would not be possible without you!

To my fellow and former lab mates, Mary-Elizabeth Sheridan, Adam Kemp, Allan Humphrey, David Roy, Zoya Versey: Thank you for your help and support throughout our time together. You all also played a part in this, and for that I am forever grateful. To the undergraduate students that I worked alongside during my time in the lab: Garrett, Aleksandra, Morgan, Melinda, Olivia, Claudia, Marwa, Kamaara, Mara, Catherine, James, Dan, Millie, Kylen, Emma, Romanah, and Emily: Thank you all for helping me with my research and know that you all have taught me

something even though it was my job to teach you. To all the people I have worked alongside within the Biology and Health Sciences departments over the years: Mohsen, Bahram, Katayoun, Kristina, Dan, Dominique, Eddy, Emily, Tom, Taylor, Nathalie, Houman, Anna, Thet, Krishna, Ziggy, Hailey, Lilian, Waleska, and Carole: Thank you for providing a welcoming and friendly environment. And to the thousands of undergraduate students, I had the pleasure of TAing: Thank you! You have made me a better person and a better teacher!

Lastly, but certainly not least, I would not be the person that I am today without the support of my closest family and friends. Hooyo and Aabo, you brought me into this world, nurtured me and raised me to become someone who can accomplished anything that they set their mind to. While life was not always easy for us, you still gave everything you had to make sure that my three brothers and I never felt those hardships. Hopefully, I have and will continue to live up to the name you have bestowed onto me. To the rest of my support system: My brothers Mohamed, Mubarak, and Mukhtar; my cousins Kombe and Samia; my aunt Muna and my friends Hussein, Brandon, Vernon, Frank, and Allison: Thank you for being there for me whenever I needed you. To the members of my family that I have not mentioned (and there is a lot of you!), I am grateful for you as I would not be here without you. You are the foundation from which I prosper! Without you, I would fail!

The completion of this Ph.D. is a monumental achievement in my life. This is a cumulation of the buckets of blood, sweat and tears that I have put into this project. But I still have a lot to give and a long way to go before I have reached my full potential. What I do know is that without all of you, I would not have gotten this far. And whatever I end up doing next, I do with all of you propelling me forward. And because of each and every one of you: I'm Ph.Ding it! How 'bout that! Now, heeeeerrrre's what I want to talk to you about…

TABLE OF CONTENTS

LIST OF FIGURES

LIST OF SUPPLEMENTAL FIGURES

LIST OF TABLES

LIST OF ABBREVIATIONS

25-HC   25-hydroxycholesterol

2-DG   2-deoxyglucose

ACLY   ATP citrate lyase

ACR   Acriflavine

ADP   Adenosine diphosphate

AMP   Adenosine monophosphate

AMPK   AMP-activated protein kinase

APC   Antigen-presenting cells

ATG   Autophagy related protein

ATP   Adenosine triphosphate

BCAA   Branched-chain amino acid

BCAT   BCAA aminotransferase

BCKDH   Branched-chain alpha-keto acid dehydrogenase

BCL2   B cell lymphoma 2

BMM   Mouse bone marrow-derived macrophage

BSA   Bovine serum albumin

CARD   Caspase active recruitment domain

CCR5   C-C chemokine receptor type 5

CD   Cluster of differentiation

CH25H	Cholesterol 25-hydroxylase
CoA	Coenzyme A
CpG	Cytosine-Guanine regions in DNA
CPT	Carnitine palmitoyltransferase
CXCL10	C-X-C motif chemokine ligand 10
DAMP	Danger-associated molecular pattern
DAVID	Database for Annotation, Visualization, and Integrated Discovery
DC	Dendritic cell
DMEM	Dulbecco's Modified Eagle Medium
DMSO	Dimethylsulfoxide
DNA	Deoxyribonucleic acid
Drp1	Dynamin-related protein 1
dsRNA	Double-stranded ribonucleic acid
ECAR	Extracellular acidification rate
EHMN	Edinburgh Human Metabolic Network
ERK	Extracellular signal-regulated kinase
ETC	Electron transport chain
FA	Fatty acid
FAD/FADH$_2$	Flavin adenine dinucleotide

FAO	Fatty acid oxidation
FBS	Fetal bovine serum
FC	Fold change
FCCP	Carbonyl cyanide 4-(trifluoromethoxy)phenylhydrazone
FDR	False discovery rate
FIH-I	Factor inhibiting HIF-I
G3P	Glycerol 3-phosphate
G6PD	Glucose 6-phosphate dehydrogenase
GAPDH	Glyceraldehyde 3-phosphate dehydrogenase
GAS	Interferon-γ-associated site
GEO	Gene expression omnibus
GLUT	Glucose transporter
GPD	Glycerol 3-phosphate dehydrogenase
GPS	Glycerol phosphate shuttle
GPX4	Glutathione peroxidase 4
GSEA	Gene set enrichment analysis
H_2O_2	Hydrogen peroxide
HCMV	Human cytomegalovirus
HCV	Hepatitis C virus

HG	High glucose
HIF-1α	Hypoxic-inducible factor-1α
HIV	Human immunodeficiency virus
HSV	Herpes simplex virus
IAV	Influenza A virus
IDH	Isocitrate dehydrogenase
IFN	Interferon
IFNAR	Interferon-α receptor
IKK	IκB kinase
IL	Interleukin
iNOS	inducible NO synthase
IRAK	Interleukin-1 receptor associated kinase
IRF	Interferon regulatory factor
IRG1	Immunoresponsive gene 1
ISG	Interferon stimulating gene
ISGF3	Interferon-stimulated gene factor 3 complex
ISRE	Interferon-stimulated responsive element
IκB	Nuclear factor of kappa light polypeptide gene enhancer in B-cells inhibitor
JAK	Janus activated kinase

KEGG	Kyoto Encyclopedia of Genes and Genomes
LDH	Lactate dehydrogenase
LG	Low glucose
LPS	Lipopolysaccharide
LXR	Liver X receptor
MAPK	Mitogen-activated protein kinase
MAVS	Mitochondrial antiviral signaling protein
M-CSF	Macrophage-colony stimulating factor
MDA5	Melanoma differentiation-associated protein 5
MDM	Human monocyte derived macrophage
MEF	Mouse embryonic fibroblasts
MFI	Mean fluorescence intensity
MFN	Mitofusin
MMP	Mitochondrial membrane potential
MPC	Mitochondrial pyruvate carrier
mRNA	Messenger ribonucleic acid
MSigDB	Molecular Signatures Database
MT	MitoTEMPO
mtDNA	Mitochondrial DNA

mTOR	Mechanistic target of rapamycin
mtROS	Mitochondrial reactive oxygen species
MyD88	Myeloid differentiation primary response-88
NAC	N-acetylcysteine
NAD⁺/NADH	Nicotinamide adenine dinucleotide
NADP⁺/NADPH	Nicotinamide adenine dinucleotide phosphate
NCBI	National center for biotechnology information
NEMO	NF-kappa-B essential modulator
NFAT	Nuclear factor of activated T cells
NF-κB	Nuclear factor of kappa light polypeptide gene enhancer in B-cells
NK	Natural Killer cell
NLRP3	NOD-like receptor family pyrin domain containing 3
NO	Nitric Oxide
NOX	NADPH oxidase
NRF2	NF-E2–related factor 2
OCR	Oxygen consumption rate
O-GlcNAc	O-linked β-N-acetylglucosamine
OM	Oligomycin
OPA1	Optic atrophy 1

OXPHOS   Oxidative phosphorylation

PAMP   Pathogen-associated molecular pattern

PBS   Phosphate buffered saline

PCA   Principal component analysis

PDH   Pyruvate dehydrogenase

PDK   PDH kinase

PenStrep   Penicillin/Streptomycin

PER   Proton efflux rate

PFKFB   6-phosphofructo-2-kinase/fructose-2,6-biphosphatase

PHD   Prolyl hydroxylase

PI3K   Phosphoinositide 3-kinase

PKM2   Pyruvate kinase muscle isozyme 2

Poly(I:C)/PIC   Polyinosinic:polycytidylic acid

PPP   Pentose phosphate pathway

PRR   Pathogen Recognition Receptor

R837   Imiquimod

R848   Resiquimod

RET   Reverse electron transport

RF   Random forest

RIG-I	Retinoic acid-inducible gene-I
RISP	Rieske iron-sulfur protein
RLR	RIG-I-like receptors
RNA	Ribonucleic acid
ROS	Reactive oxygen species
ROT/AA	Rotenone + Antimycin A
RSV	Respiratory syncytial virus
S1QEL	Suppressors of site I_Q Electron Leak
S3QEL	Suppressors of site III_{Qo} Electron Leak
SDH	Succinate dehydrogenase
shRNA	short hairpin RNA
siRNA	Small interfering RNA
SOD	Superoxide dismutase
SPHK2	Sphingosine kinase 2
SRC	Spare respiratory capacity
SREBP	Sterol regulatory element-binding protein
ssRNA	Single-stranded ribonucleic acid
STAT	Signal transducer and activator of transcription
STING	Stimulator of type I interferon genes

TBK1   TANK-binding kinase 1

TBS   Tris buffered saline

TCA   Tricarboxylic acid cycle

TGF-β   Transforming growth factor-β

TIR   Toll/Interleukin-1 receptor

TLR   Toll-like receptor

TMRM   Tetramethylrhodamine

TNF   Tumour necrosis factor

TRAF   TNF receptor-associated factor

TRAM   Translocating chain-associated membrane protein

TRIF   Toll/Interleukin-1 receptor-domain-containing adapter-inducing IFN-β

TYK2   Tyrosine kinase 2

UCP   Uncoupling protein

UQ/UQH$_2$ Ubiquinone/Ubiquinol

VIP   Variable Importance in Projection

Chapter 1. INTRODUCTION

The immune system consists of a variety of cells and complex biological processes that protect the host organism against foreign agents (1). It is made up of two interconnected subsystems: the innate and adaptive immune systems. The innate immune system provides the first line of defense against pathogens by undertaking nonspecific defense mechanisms against foreign microorganisms (1-3). This first line acts quickly to prevent the spread of the infection *via* the sensing of conserved components and the initiation of inflammation (1-3). They also phagocytose and destroy local invaders, secrete antibacterial and antiviral molecules, and recruit other cells to the site of infection through the release of chemokines (1-3). The innate immune system is comprised of a diverse set of cells capable of exerting tissue-protective mechanisms in their fight against pathogens, such as neutrophils, dendritic cells (DCs), natural killer (NK) cells, monocytes and macrophages (1, 3). DCs, monocytes, macrophages, known as antigen-presenting cells (APCs), can engulf the pathogen and present an antigen to activate adaptive immune cells (2).

Once activated, the adaptive immune response provides an antigen-specific response against pathogens (1, 4). Adaptive immune cells include B cells and T cells, named based on the initial tissue of discovery: the bursa of Fabricius of birds and the human thymus respectively (1, 4). B cells are responsible for producing antigen-specific antibodies that can bind to the pathogen and facilitate their recognition by APCs, triggering phagocytosis *via* Fc receptor recognition (1). T cells can trigger the death of infected cells, activate B cells, and secrete cytokines to attract other immune cells to the site of infection (1, 4). After the initial infection, adaptive immunity maintains immunological memory against the defeated pathogen, leading to a quicker and heightened response upon secondary exposure (1, 4). Together, the innate and adaptive systems provide host defense against a vast number of organisms of bacterial, viral, or fungal origin.

1.1. Macrophages and the Mononuclear Phagocyte System

Macrophages were first discovered by Ilya Metchnikoff in 1882, who was later awarded the Nobel Prize in Physiology or Medicine in 1908 for this discovery (5, 6). Van Furth et al. (7, 8) proposed that macrophages are derived from bone marrow progenitors, which differentiate into circulating monocytes. However, recent work has found that macrophages can originate from at least three different progenitors that give rise to macrophages at different stages of fetal development and adulthood: Yolk sac-derived macrophages, fetal liver-derived macrophages, and bone marrow-derived macrophages (9-11). Macrophages originating from yolk sac progenitors are initially developed during the embryonic phase prior to fetal monocyte development, circumventing the monocytic intermediary stage (12). These cells are maintained locally and persist throughout the life (5, 6). Yolk sac-derived macrophages make up the majority of tissue-resident macrophages found in the body. Examples include heart macrophages, alveolar macrophages of the lung, microglia of the brain, Kupffer cells of the liver and Langerhans cells of the skin (10-12). Later in development, hematopoietic stem cells seed the fetal liver and their progenitors also lead to the development of tissue-resident macrophages excluding microglia, which only originate from the yolk sac (6). The third known macrophage lineage is the well-discussed bone marrow progenitors (6). Cellular descendants of this lineage give rise to circulating monocytes in adults, which are newly recruited into inflamed tissue microenvironments during infection and stress. A small number also maintain tissue-resident populations under conditions of homeostasis (5, 6). As a result, macrophages populations can arise through different origins which may be a contributing factor to the plasticity of this cell type.

Circulating monocytes can be classified based on specific surface marker expression in mice and humans. In mice, circulating monocytes are categorized based on Ly6C expression (13).

Ly6C$^+$ monocytes are inflammatory cells, infiltrating tissues in response to damage or infection and differentiate into macrophages (14). Conversely, Ly6C$^-$ monocytes do not enter tissues and survey the vascular system to clear damaged endothelial cells (14, 15). Human circulating monocytes are separated into three distinct classes based on the expression of Cluster of differentiation (CD)-14 and CD16 (14, 16-19). Similar to Ly6C$^+$ monocytes in mice, CD14^{++}CD16$^-$ monocytes are recruited to inflamed tissues and they differentiate into inflammatory macrophages (14, 19). CD14$^+$CD16^{++} monocytes shared functions similar to mice LyC6$^-$ cells, in that they patrol the vascular system and contribute to wound healing (16-18). CD14^{++}CD16$^+$ monocytes are intermediary monocytes, performing the functions of the other two classes (17, 18).

Once in the tissue, resident tissue macrophages maintain their ability to detect microorganisms and cellular debris while adapting suppressive strategies to prevent hyper-activation and associated cellular damage due to the constant exposure to microbes and cellular debris (20). When these immunomodulatory mechanisms are absent, macrophage hyper-activation can lead to severe inflammation and tissue damage (21-23). As a result, macrophages display regional heterogeneity depending on the specific tissue microenvironment (24). For example, alveolar macrophages in the lung express higher levels of pathogen recognition receptors (PRRs) and scavenger receptors to clear pathogens and inhaled environmental particles (25). Yet, these cells are relatively anergic due to high levels of Transforming growth factor-β (TGF-β) expression, critical for the development and differentiation of alveolar macrophages (26). Another regional tissue macrophage, Kupffer cells of the liver, possess heightened scavenger and bactericidal activities (27), yet are highly sensitive to entering a state of hypo-responsiveness due to stimuli overexposure (28). Intestinal macrophages are also inflammatory anergic due to TGF-β-driven inhibition of NF-κB-associated inflammation (29, 30), yet retain their scavenger and bactericidal

activities (29, 31). This highlights the immense pressure that a macrophage's microenvironment places on its function and the versatility of the macrophage to adapt its function to its environment.

Macrophages perform a diverse set of roles that are central to a proper immune response. During early infection, this includes the ability to phagocytose microorganisms or pathogenic components, to produce pro-inflammatory cytokines that can help recruit and activate other innate and adaptive immune cells, and the processing and presenting of pathogen-specific antigens to further activate adaptive immune cells. To promote the resolution of the inflammatory process, macrophages expressed anti-inflammatory cytokines to quell inflammation and take up apoptotic debris to help facilitate tissue remodeling and repair (24, 32-34). This establishes the macrophages as an invaluable link between the innate and adaptive immune systems. This adaptability of macrophages to facilitate a wide range of response is governed by the metabolic re-programming that occurs due to specific pathogen recognition and the resulting cellular microenvironment (35).

1.2.   Host Pathogen Recognition by Macrophages

Macrophages survey their tissue microenvironment for pathogens, microbial components/proteins or host biomolecules by recognizing conserved molecular motifs known as pathogen-associated molecular patterns (PAMPs) or host components released from damaged or dying cells, that otherwise would not be present in the extracellular space, known as danger-associated molecular patterns (DAMPs) (1, 36). PAMPs and DAMPs are detected by specific extracellular and intracellular PRRs (1, 36). Several classes of PRRs have been identified that sense viruses, among the most important are Toll-like receptors (TLRs) and Retinoic acid-inducible gene I (RIG-I)-like receptors (RLRs) (37, 38).

1.2.1. *Toll Like Receptors (TLRs)*

The best characterized class of PRRs are TLRs. Each member is a single-pass type I membrane protein with a N-terminal ectodomain of leucine-rich repeats and a cytosolic C-terminal Toll/Interleukin-1 receptor (TIR) domain (37). Mammals possess up to 12 distinct TLRs that can be categorized by their ligand specificity and by their location (Figure 1.1). Bacterial PAMPs are detected by surface TLRs such as TLR1/2/6 (lipoproteins from Gram-positive bacteria), TLR4 (lipopolysaccharide [LPS] of Gram-negative bacteria), and TLR5 (Flagellin) (39-44) (Figure 1.1). Viral PAMPs are detected by TLRs that mainly reside in endosomes including TLR3 (dsRNA), and TLR7/8 (ssRNA) (45-47) (Figure 1.1). TLR9 can detect both bacterial and viral unmethylated CpG DNA motifs (48, 49) (Figure 1.1).

PAMP engagement results in TLR dimerization and the initiation of downstream signalling either through Myeloid differentiation primary response 88 (MyD88) or TIR-domain-containing adapter-inducing interferon-β (TRIF) (50). All TLRs except TLR3 utilized MyD88-dependent signalling, which recruit Interleukin (IL)-1 receptor associated kinase (IRAK) proteins to activate Tumour necrosis factor (TNF) receptor-associated factor 6 (TRAF6) (2) (Figure 1.2). TRAF6 then drives the activation of the Nuclear factor of kappa light polypeptide gene enhancer in B-cells (NF-κB) inhibitor (IκB) kinase (IKK) complex, which subsequently phosphorylates IκBα. This results in the detachment of IκBα from NF-κB, allowing free NF-κB to translocate into the nucleus and induce the expression of inflammatory cytokines (51). To maintain this activation state, NF-κB also directly suppresses the expression of other gene targets, such as Fos and the early growth response protein (EGR), as well as up-regulate NF-kB-induced transcription factors, including Myc and Interferon regulatory factor 1 (IRF1) (52). Both TLR3 and TLR4 employ the TRIF-dependent pathway (2) (Figure 1.2). For TLR3, TRIF triggers both the activation of TRAF6-

mediated NF-κB signalling and TANK-binding kinase 1 (TBK1)/IKKε-mediated IRF3/7 signalling (50). Conversely, TRIF activation during TLR4 engagement only results in the activation of TBK1/IKKε-mediated IRF3/7 signalling (53) (Figure 1.2). The phosphorylation and dimerization of IRF3 and IRF7 triggers the expression of type I interferons (IFNs), a family of antiviral cytokines (50, 54).
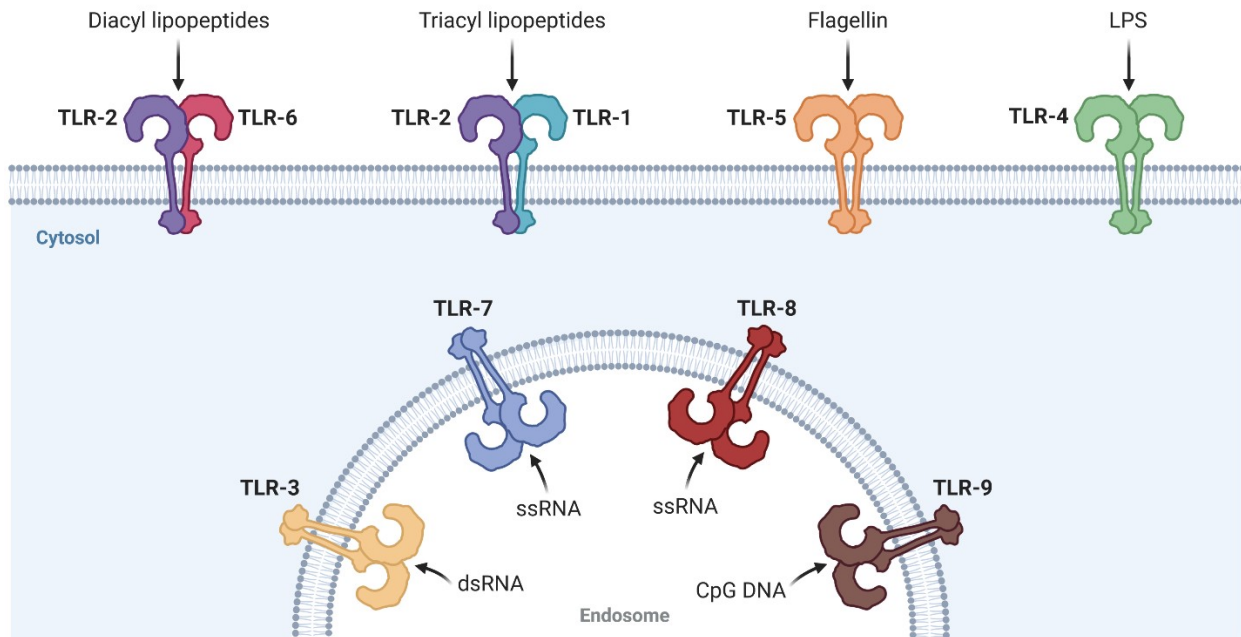
Figure 1.1: A summary of the bacterial and viral PAMPs that are detected by Toll-like receptors (TLRs). Bacterial-sensing TLRs are located along the surface of plasma membrane whereas, RNA/DNA-sensing TLRs are primarily located in the endosomes. Image created with BioRender.com.
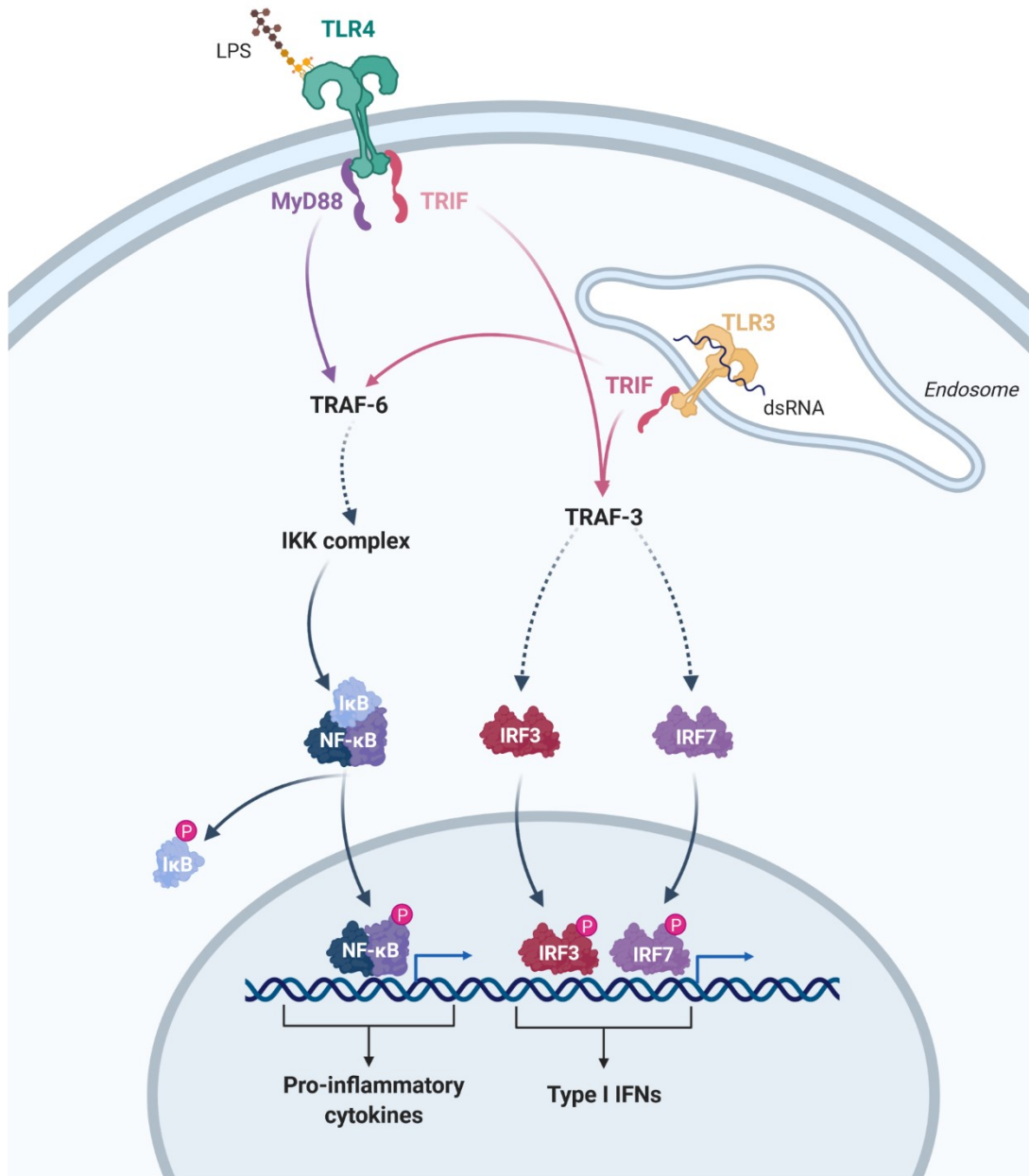
Figure 1.2: TLR3 (viral dsRNA) vs TLR4 (bacterial LPS) signaling dynamics. TLR4 induces MyD88 and TRIF activation to support the production of pro-inflammatory cytokine and Type I IFNs, respectively. Conversely, TLR3-mediated TRIF activation results in the activation of the same pro-inflammatory and IFN cascades. Image created with BioRender.com.

1.2.2. RIG-I-like Receptors (RLRs)

RLRs are a family of DExD/H box RNA helicases found in the cytosol and are responsible for the detection of cytosolic viral dsRNA (55). These receptors possess a C-terminal domain and catalytic helicase core responsible for binding viral RNA, accompanied by N-terminal caspase active recruitment domains (CARD) which are essential for downstream signalling (55-57). There are two major receptors responsible for triggering effector responses: RIG-I and Melanoma differentiation-associated protein 5 (MDA5). These receptors detect dsRNA of specific lengths. RIG-I recognize short RNA strands preferentially (<1kb) whereas MDA5 prefers longer RNA strands (>2kb) (58, 59) (Figure 1.3). This differs from the TLR family, where one receptor (TLR3) is responsible for dsRNA engagement irrespective of length (46).

Upon engagement, both RIG-I and MDA5 form filaments along their preferred dsRNA strands, leading to the polymerization of their respective CARD domains (60-63). These oligomeric formations facilitate the recruitment of the mitochondrial antiviral signaling protein (MAVS), forming the MAVS signalosome along the outer membrane of mitochondria (61, 64-67) (Figure 1.3). Additional MAVS proteins are then recruited to the signalosome site, leading to signal amplification (67). The MAVS signalosome drives the activation of NF-κB-mediated inflammation and the IRF3/7-driven antiviral response, *via* the recruitment of the IKK complex and TBK1/IKKε respectively (56) (Figure 1.3).
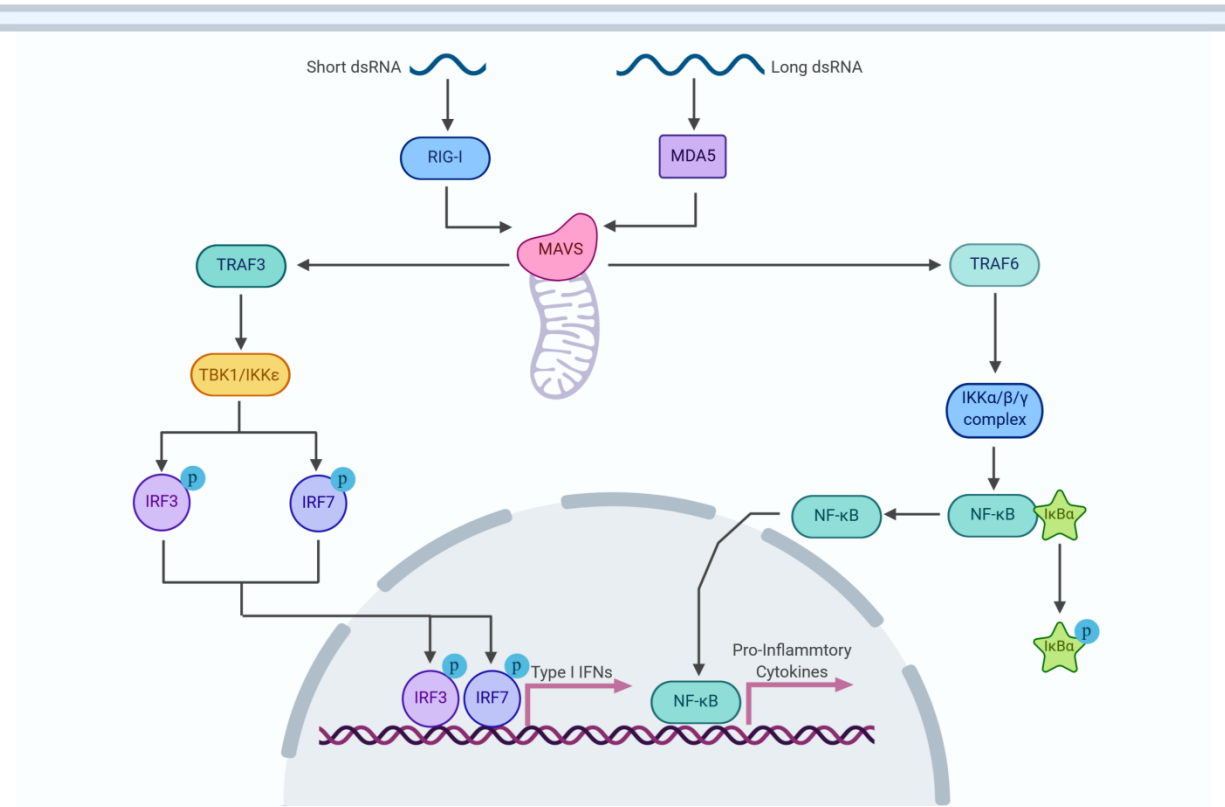
Figure 1.3: Overview of RLR signaling. RIG-I and MDA5 detect dsRNA of different lengths before engaging MAVS, initiating NF-κB and IRF signaling. The activation of NF-κB results in pro-inflammatory cytokine production while IRF3/7 activation leads to type I IFNs production. Image created with BioRender.com.

1.2.3. Type I IFN signalling

The one commonality between TLR and RLR signalling is the induction of type I IFNs, triggered by IRF3/7 signalling. Type I IFNs are the largest class of IFNs, consisting of IFN-δ, IFN-ε, IFN-κ, IFN-τ, IFN-ω, IFN-β, and 13 different subtypes of IFN-α (68, 69). They act in an autocrine and paracrine manner to induce antiviral states in infected and bystander cells in the local microenvironment (Figure 1.4). This state is associated with the upregulation of IFN-stimulating genes (ISGs) and expression of antiviral proteins, which prevent further viral propagation and replication. Type I IFNs also regulate antigen presentation and phagocytic activity to support adaptive immune system activation, which is critical to the locating and killing of infected cells (70-72).

Type I IFNs interact with either IFN-α receptor 1 or 2 (IFNAR1/2) leading to IFNAR dimerization (73) (Figure 1.4). This results in the autophosphorylation and activation of the Janus activated kinase (JAK) proteins, JAK1 and Tyrosine kinase 2 (TYK2), which are constitutively associated with IFNAR1 and IFNAR2 respectively (73). Both proteins activate the signal transducer and activator of transcription (STAT) proteins STAT1 and STAT2, leading to their subsequent nuclear translocation (74). Two different mechanisms exist resulting in ISG expression. First, STAT1 and STAT2 can bind to IRF9 to form the IFN-stimulated gene factor 3 complex (ISGF3) which recognizes the IFN-stimulated responsive elements (ISREs) resulting in ISG expression (73) (Figure 1.4). Second, phosphorylated STAT proteins can form homo- or heterodimers that are capable of binding to IFN-γ-associated sites (GAS) elements leading to ISG expression (75). ISGs can have an ISRE site and/or a GAS site, thus a combination of different STAT complex formations may be required for the expression of >1000 known ISGs and therefore facilitating specific immune responses (76) (Figure 1.4). In addition to the traditional JAK-STAT

11

pathway, IFNAR engagement can also activate the phosphoinositide 3-kinase (PI3K)-Akt-Mechanistic target of rapamycin (mTOR) pathway, critical for the transcription and translation of ISGs as well as the phosphorylation of STAT proteins (77-79). In addition, this pathway is responsible for the expression of genes related to energy metabolism in activated immune cells such as Hypoxic-inducible factor-1α (HIF-1α) and pyruvate kinase muscle isozyme 2 (PKM2) (80-82).
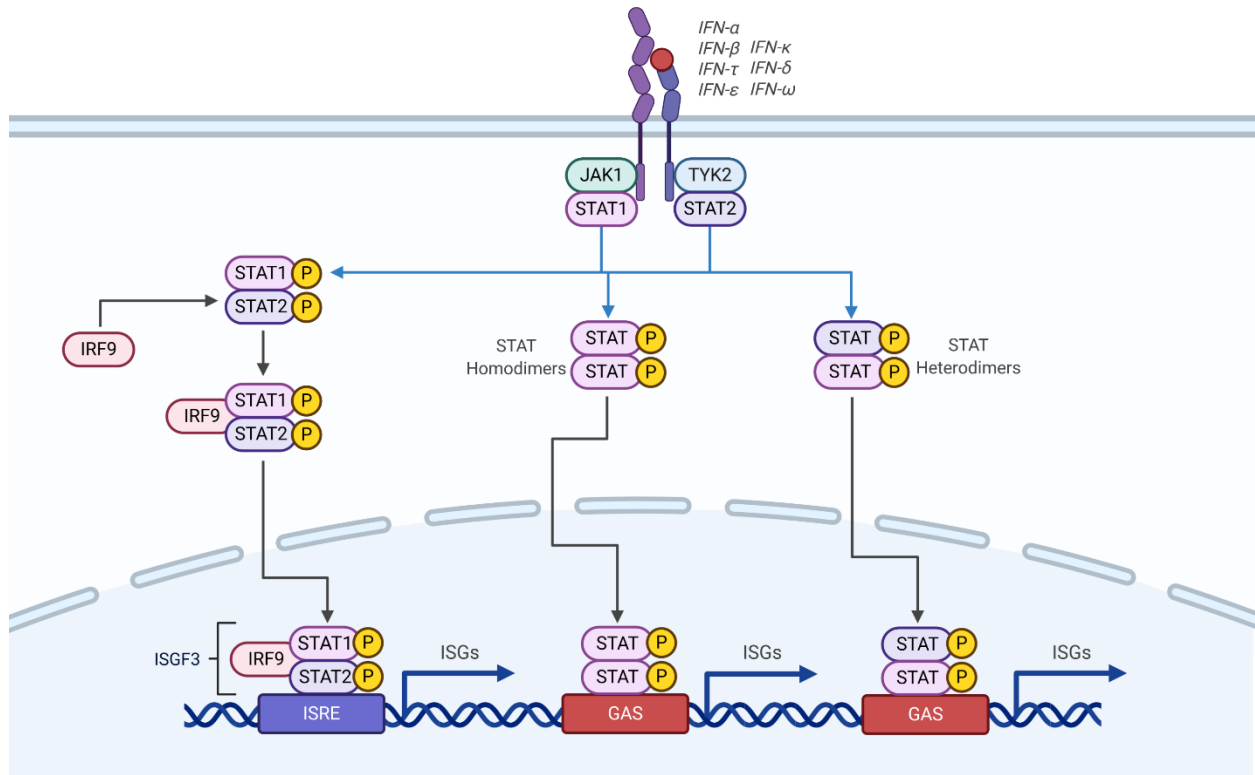
Figure 1.4: Traditional type I IFN signaling cascade. Type I IFNs act through IFNAR1 and IFNAR2, leading to the activation of JAK proteins JAK1 and TYK2. They, in turn, phosphorylate STAT family of transcription factors. STAT proteins can either form homo- or heterodimers and activate GAS-mediated ISG expression. In addition, STAT1 and STAT2 interact with IRF9 to form the ISGF3 complex and drive ISRE-mediated ISG expression. Image created with BioRender.com.

1.3. Mitochondria: Master Regulator of Cell Function

Mitochondria are the central hub for several metabolic processes and play a critical role in modulating diverse cellular functions. These functions include catabolizing nutrients for energy, producing biosynthetic precursors for macromolecules (e.g., nucleotides, proteins, lipids), maintaining redox balance, and regulating apoptosis (83-85) (Figure 1.5). Here, I will outline these mitochondrial-associated processes and highlight their importance in regulating immune function.

1.3.1. *Mitochondrial Bioenergetic Pathways*

Glucose is the primary source of energy to the mitochondrion (86, 87). Its breakdown *via* glycolysis involves a ten-enzyme pathway and nets 2 pyruvate, 2 nicotinamide adenine dinucleotide (NAD^+ or NADH) and 2 ATP molecules per glucose molecule (86, 87). Other sugars, such as fructose and galactose, can feed into this pathway at various points, providing a focal point for the breakdown of sugars in cells (88) (Figure 1.6). The intermediates produced by this pathway also serves as metabolites for several different pathways critical to immune function. For example, naïve DCs build up their glycogen stores by taking up extracellular glucose and initially use these stores to support DC function in the early activation phase (89) (Figure 1.6). The pentose phosphate pathway (PPP) (responsible for nucleotide and NAD phosphate (NADPH) synthesis) has been linked to T cell activation and its need for NADPH (90, 91) (Figure 1.6). Glucose-derived amino acids, such as serine, are also used during T cell activation to drive their proliferation due to its link to *de novo* purine biosynthesis (92) (Figure 1.6). This highlights the fundamental role of glycolysis in cell function.
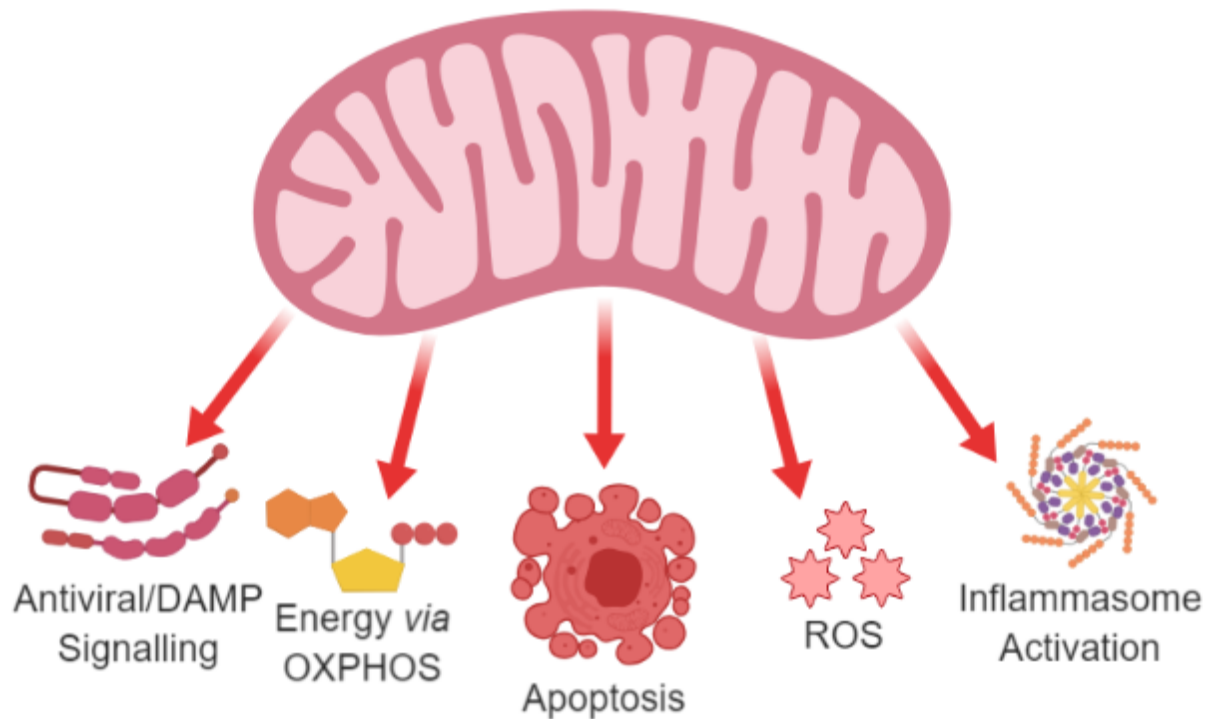
Figure 1.5: Mitochondria are the central hubs for innate immune responses. Mitochondria play a central role in several metabolic and immune processes such as functioning as scaffold for antiviral signaling, energy production *via* oxidative phosphorylation (OXPHOS), as well as mediate apoptosis and facilitates inflammation through regulation mitochondrial reactive oxygen species (ROS) production and inflammasome activation. Image created with BioRender.com.
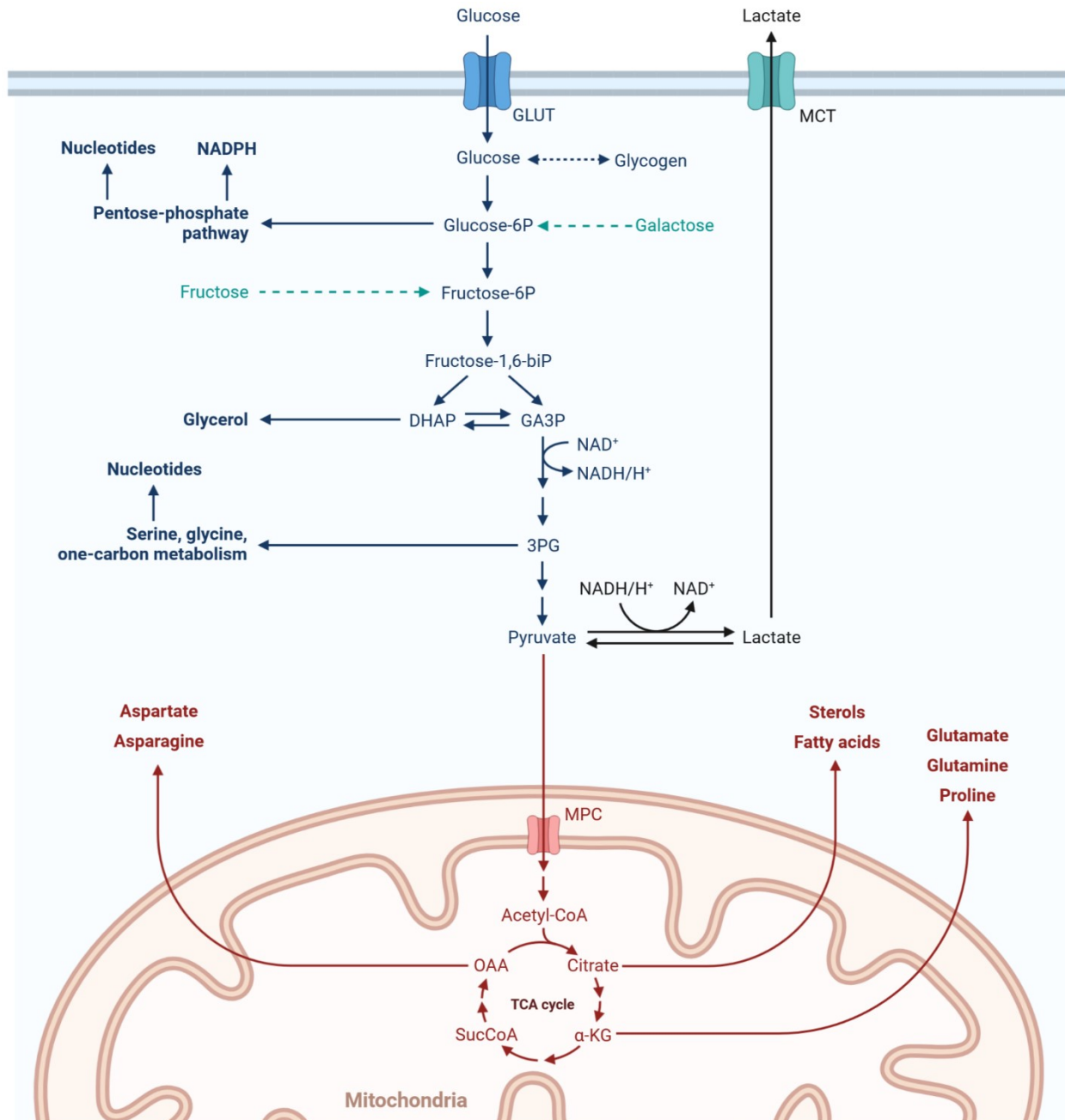
Figure 1.6: The importance of Glycolysis and the TCA cycle intermediates as building blocks for various biosynthetic pathways. Glucose and the other sugars that feed into its catalytic pathway (fructose and galactose) are processed and can be used in the generation of nucleotides, NADPH, glycerol, serine, and glycine. TCA cycle metabolites can be used to produce sterols, fatty acids, and a variety of amino acids. Image created with BioRender.com.

Glycolytic-derived pyruvate can be further metabolized by anaerobic or aerobic means. While initially discovered in bacteria, mammalian cells can process pyruvate in the absence of oxygen in a process known as lactic acid fermentation (88). In this process, pyruvate is converted into lactate by lactate dehydrogenase (LDH), providing a rapid and anaerobic means of NAD^+ recycling to maintain this cycle of rapid glycolytic-derived ATP production (86, 88) (Figure 1.6). Inflammatory immune cells produce large amounts of lactate as a consequence of their need for rapid energy production (93-96). Interestingly, emerging evidence suggests that lactate possesses immunosuppressive properties to control inflammation and may serve as a feedback loop to regulate these responses (97, 98).

Pyruvate is differentially consumed under aerobic conditions leading to slower, yet more efficient ATP production. First, it is transported across the mitochondrial membranes by the mitochondrial pyruvate carrier (MPC) before it is consumed by the pyruvate dehydrogenase (PDH) protein complex, producing acetyl-CoA and NADH (86, 99) (Figure 1.6). Acetyl-CoA enters the tricarboxylic acid (TCA) cycle, and through a 10-step cycle, generates three NADH molecules and one flavin adenine dinucleotide ($FADH_2$) molecule (86, 88). TCA intermediates are also used to synthesize several macromolecules. Citrate can be transported out of mitochondria where it is used for lipid synthesis, *via* ATP citrate lyase (ACLY), which under inflammatory conditions assists in the production in prostaglandins, nitric oxide (NO), and reactive oxygen species (ROS) (100-102) (Figure 1.6). Both oxaloacetate and α-ketoglutarate serve as the backbone for the generation of amino acids such as aspartate, asparagine, glutamine, and arginine (86, 88) (Figure 1.6). Other TCA metabolites are critical to regulating other cellular functions. Succinate accumulation can protect key inflammatory and metabolic transcription factor, HIF-1α, from degradation (103). Conversely, α-ketoglutarate can boost prolyl hydroxylase (PHD) activity, responsible for targeting

HIF-1α for degradation (104). In addition, α-ketoglutarate is a key substrate to regulating epigenetic modifications (105). This demonstrates the TCA cycle's position as a central metabolic network regulating immune function.

In addition to providing pyruvate to mitochondria, glycolysis also generates NADH that are transferred into mitochondria *via* two different "electron shuttles" which transport electrons from cytosolic NADH across the membranes to accepting mitochondrial NAD^+ (86, 88) (Figure 1.7). As a vital energy source, maintaining adequate levels of NADH is vital to mounting a functional inflammatory response (106, 107). The first shuttle, the malate-aspartate shuttle, transfers electrons from glycolytic NADH to cytosolic oxaloacetate to generate malate (86, 88) (Figure 1.7). Once in mitochondria, malate is re-oxidized by mitochondrial NAD^+ to form oxaloacetate and NADH. Oxaloacetate is recycled, *via* its conversion to aspartate, and transported to the cytosol (86, 88) (Figure 1.7). Inflammatory macrophages utilized this shuttle to replenish cytosolic NAD^+ to maintain the rapid glycolytic ATP production (108). The second shuttle, the glycerol phosphate shuttle (GPS), cytosolic glycerol 3-phosphate (G3P) dehydrogenase 1 (GPD1) reduces dihydroxyacetone using cytosolic NADH, to form G3P (Figure 1.7). G3P readily transverse the outer mitochondrial membrane where it is re-oxidized by mitochondrial GPD2, which reduces FAD within the inner mitochondrial membrane (86, 88) (Figure 1.7). GPD2$^{-/-}$ macrophages produce less inflammatory mediators (IL-6 and IL-1β) due to reduced glycolytic activity (109).
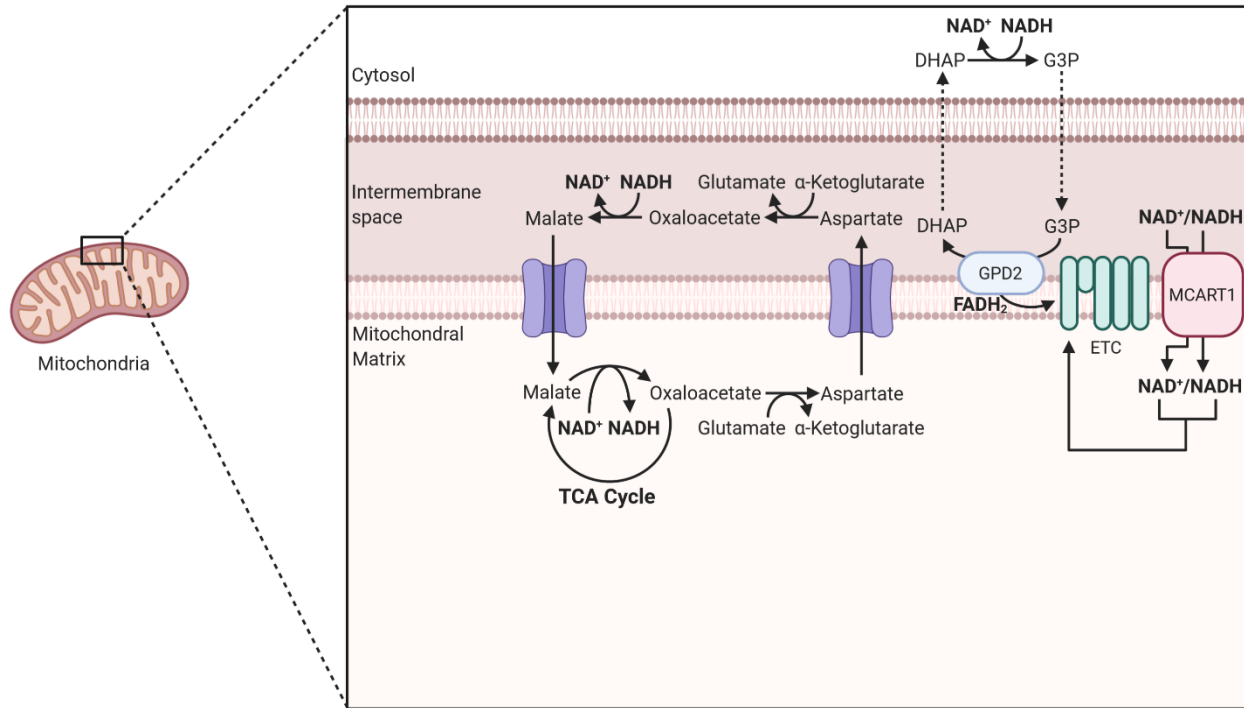
Figure 1.7: Methods of NAD$^+$/NADH transport into the mitochondria. NAD$^+$/NADH can be transported into mitochondria *via* three methods: The malate-aspartate shuttle, the glycerol phosphate shuttle and the newly discovered SLC25A51/MCART1 transporter. Image created with BioRender.com.

It has long been believed that the inner mitochondrial membrane was impermeable to NAD$^+$/NADH and thus cytosolic NAD$^+$/NADH could only enter mitochondria *via* these "shuttles" (86, 88). Recently, two independent groups have identified a mitochondrial NAD$^+$/NADH transporter (SLC25A51/MCART1), providing a direct mechanism of glycolytic NADH to enter mitochondria (110, 111). More work is required to determine which mechanism is the primary means of NAD$^+$/NADH transfer or if specific pathways are important under certain conditions.

The generated NADH molecules from these pathways then enter the mitochondrial process called oxidative phosphorylation (OXPHOS) (99). NADH molecules are shuttled into the electron transport chain (ETC), a series of protein complexes that transfer electrons through a series of electron donors embedded within the inner mitochondrial membrane (86, 99) (Figure 1.8). NADH is oxidized by Complex I (NADH ubiquinone oxidoreductase) and the electrons are passed to the electron carrier ubiquinone (UQ) forming ubiquinol (UQH$_2$) (86, 99). The energy generated by the electron transfer is used by Complex I to transport four protons into the mitochondrial intermembrane space (Figure 1.8). Complex II (Succinate dehydrogenase [SDH]) is a parallel electron transfer pathway, linked to the TCA cycle. Succinate oxidation leads to the reduction of FAD which transfers its electrons to UQ forming UQH$_2$ (86, 99) (Figure 1.8). However, Complex II does not participate in the shuttling of protons out of mitochondria and thus generates less energy compared to Complex I. The reduced UQH$_2$ then passes the electrons onto Complex III (Coenzyme Q: cytochrome c–oxidoreductase), where it is shuttled to cytochrome c and results in the translocation of four protons out of the mitochondrial matrix (Figure 1.8). Cytochrome c interacts with Complex IV (Cytochrome c oxidase), transferring electrons to molecular oxygen, producing water (86, 99). Another four protons are shuttled into the intermembrane space by Complex IV (Figure 1.8). The shuttling of these protons across the mitochondrial inner membrane creates a

proton gradient, which is used by Complex V (ATP synthase) to generate ATP (Figure 1.8). In short, Complex V transports three protons back into the mitochondrial matrix and uses the energy of that transfer to create a single ATP molecule (Figure 1.8). In total, under aerobic conditions, one glucose molecule can generate 36 ATP molecules compared to 2 ATP molecules from anaerobic glycolysis, making OXPHOS the more efficient means of producing cellular energy (86, 99).

To further increase the efficiency of electron flow and limit electron leakage, Complexes I, III, and IV can also form a series of ETC supercomplexes (112). These complexes work with the mitochondrial uncoupling protein family (UCP) to reduce mitochondrial membrane potential (MMP) by funneling protons back into the mitochondria, reduce the electron leakage and prevent ROS production (112, 113). These higher-level structures are critical to maximize energy efficiency of the organelle. Interestingly, under inflammatory conditions (e.g., LPS activation), macrophages undergo ETC supercomplex disassembly, which increases mitochondrial ROS (mtROS) production/release and activates NOD-like receptor family pyrin domain containing 3 (NLRP3) inflammasome (114).
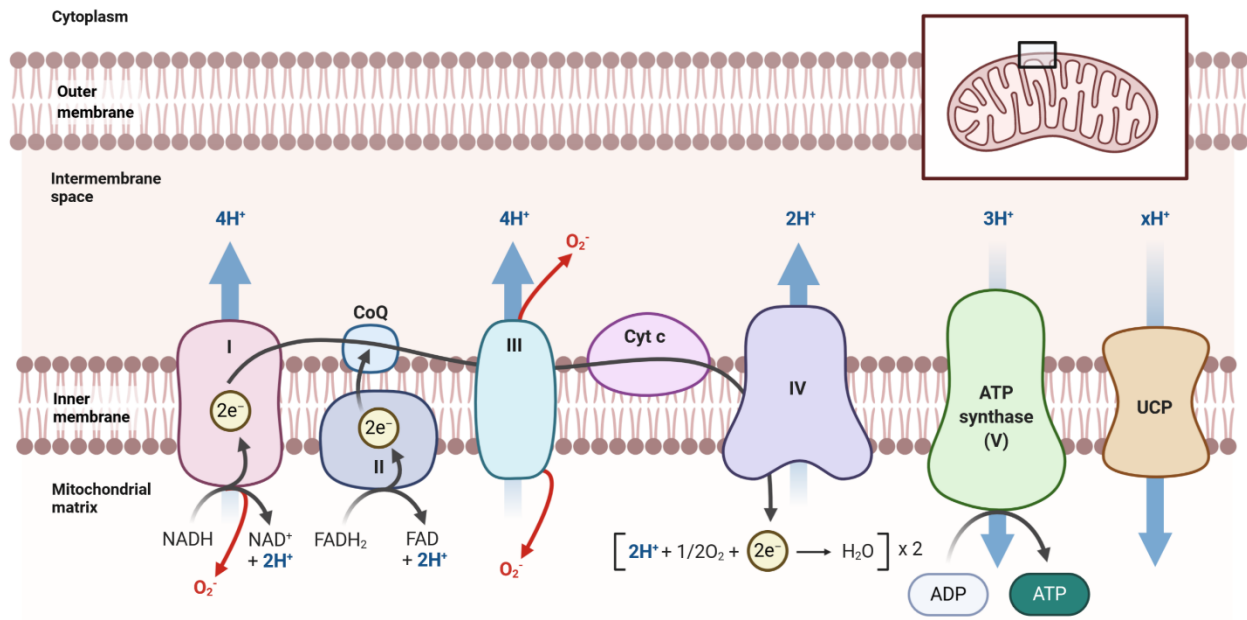
Figure 1.8: Oxidative phosphorylation is coupled with the electron transport chain to generate ATP in the mitochondria. Located in the inner mitochondrial membrane, electrons from NADH are transferred across the four complexes of the ETC. The electron movement is coupled with the pumping of protons out of the mitochondrial matrix into the intermembrane space, where ATP synthase (Complex V) transports the protons back into the matrix, using the energy created to produce ATP. Uncoupling proteins are capable of transporting protons back into the matrix absent of ATP production. Image created with BioRender.com.

There are alternative energy pathways that make use of OXPHOS without any input from glycolysis (Figure 1.9). Fatty acid (FA) oxidation (FAO) breaks down FAs to produce acetyl-CoA (99) (Figure 1.9). However, before they can be broken down, they are transported into mitochondria using the carnitine shuttle. Long chain fatty acid-CoA ligase attaches coenzyme A (CoA) to free FAs to facilitate transport (99). The resulting Acyl-CoA is transferred onto carnitine by the outer mitochondrial membrane-embedded carnitine palmitoyltransferase (CPT) 1 (99). Carnitine-acylcarnitine translocase relocates acyl-carnitine into mitochondria where CPT2, located on the inner mitochondrial membrane, separates carnitine and the attached FA (99). The released carnitine is then transported back to the cytosol to continue the cycle. Once in the mitochondrial matrix, acyl-CoA undergoes β-oxidation by cleaving two carbons from the acyl group to form acetyl-CoA and the shorter acyl-CoA (99). This cycle is continued until the final cycle yields two acetyl-CoA molecules. Each cycle of β-oxidation yields 1 NADH and acetyl-CoA molecule which feeds into OXPHOS and TCA cycle, respectively (Figure 1.9). This results in 14 ATP molecules per cycle (86, 99). This alternative energy pathway is mainly utilized during anti-inflammatory and antiviral responses (115-117). In addition, the overexpression of a constitutively active CPT1 mutant led to reduced inflammation and improved insulin sensitivity in RAW 264.7 macrophages. (118).

Another mitochondrial bioenergetic pathway is glutaminolysis, or the breakdown of glutamine (Figure 1.9). Glutamine is transported into mitochondria where it converted into glutamate (86, 88, 99). The subsequent glutamate is directed into the TCA cycle, *via* its transformation into α-ketoglutarate (86, 88, 99) (Figure 1.9). This pathway generates one NADH molecule, in addition to the 2 NADH produced due to α-ketoglutarate's insertion into the TCA

cycle (86, 88, 99) (Figure 1.9). In addition, this pathway is used under inflammatory conditions to replenish citrate and itaconate levels in the cell (108).

Lastly, the catabolism of branched-chain amino acids (BCAAs), such as leucine, isoleucine, and valine, is another source of energy into mitochondria (86, 88, 99) (Figure 1.9). Broken down by the branched-chain alpha-keto acid dehydrogenase (BCKDH) complex, BCAAs are converted into various acyl-CoA derivatives which eventually result in acetyl-CoA and/or succinyl-CoA generation that enter the TCA cycle (86, 88, 99) (Figure 1.9). This process directly nets 1 NADH plus either 1 or 3 NADH due to succinyl-CoA or acetyl-CoA entry into the TCA cycle (86, 88, 99). This pathway is critical to macrophage effector function. Intestinal macrophages with a selective knockout of BCAA transporter CD98hc were found to be more prone to apoptosis (119). Further, the cytosolic BCAA aminotransferase (BCAT1) is upregulated during antibacterial responses to provide additional fuel to mount an immune response (120, 121). Interestingly, this is independent of its role in BCAA catabolism as leucine levels were unchanged, suggesting a possible moonlighting role for BCAT1 (120). This assortment of energetic pathways to support cellular activation and function provides the cell with some level of flexibility in tissue microenvironments with varied levels of nutrients available and/or under conditions of stress such as infections where nutrients are rapidly consumed.
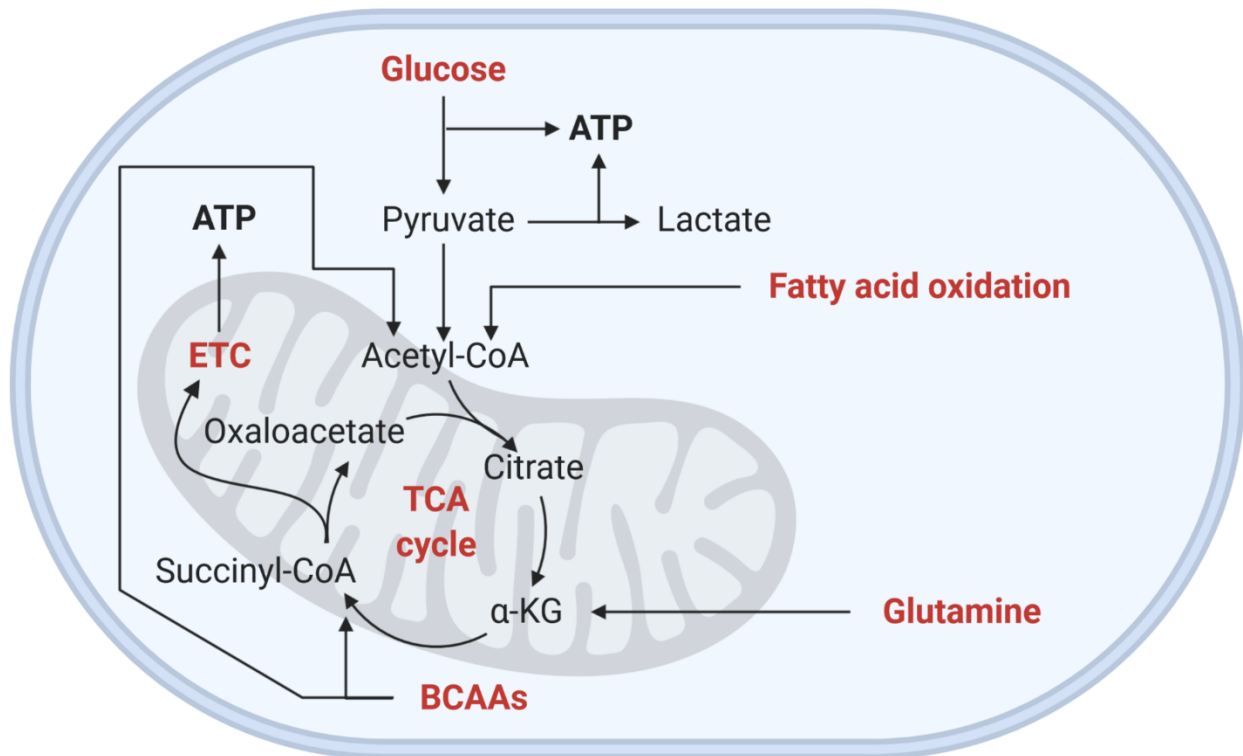
Figure 1.9: The Mitochondrial Bioenergetic Pathways. Several different bioenergetic pathways feed into mitochondria to produce ATP. While glycolysis can rapidly generate ATP, pyruvate directed into mitochondria produces more ATP per glucose molecule. Fatty acid oxidation, glutamine, and branched-chain amino acids (BCAAs) can feed into the TCA cycle, leading to the generation of ATP *via* oxidative phosphorylation. Image created with BioRender.com.

1.3.2. Other important mitochondrial functions

In addition to being the powerhouse of the cell, mitochondria produce several other bioactive molecules, which regulate cell function. Among the most potent of these are mtROS, which are generated as a by-product of electron flux through the ETC (Voet et al., 2016; Berg et al., 2008; Spinelli & Haigis, 2018) (Figure 1.8). ROS are generated because of electron leakage from Complexes I and III (86, 99) (Voet et al., 2016; Spinelli & Haigis, 2018). Initially thought to be detrimental to cells, it is now recognized that low levels of ROS regulate several cellular processes including cell proliferation, differentiation, and migration (122, 123). In plasmacytoid DCs, mitochondrial superoxide is a key driver of antiviral responses *via* increased MAVS protein expression (124). Mitochondrial-derived hydrogen peroxide (H_2O_2) has been also shown to support antiviral and inflammatory responses through the activation of redox-sensitive NF-κB and IRF signalling (125-128). Further, mtROS contributes to NLRP3 inflammasome activation (114) and drive the transcription of inflammatory genes (129) (Figure 1.5). For the most part, the damaging effects of ROS on mitochondria is limited by the presence of antioxidant proteins (86, 88, 99). However, if the redox balance is lost, accumulating ROS trigger the intrinsic apoptosis pathway *via* activation of the B cell lymphoma 2 (BCL2) protein family (130). Damaged mitochondria released mitochondrial DNA (mtDNA) as a danger signal and recent evidence has pointed to this being a key promoter of inflammation, *via* PRR and NLRP3 activation (131-133).

1.4. Metabolic Regulation of Macrophages

The last decade of research has placed a spotlight on the central role that cellular metabolism plays in controlling the magnitude and specificity of the innate immune response (35, 83). It is well recognized that cellular metabolism provides the necessary biosynthetic and bioenergetic requirements to support effector function and survival. Consistent with these findings,

initial work done by Warburg and colleagues, demonstrated that activated leukocytes and cancer cells were metabolically similar, in that they favoured glycolysis as a primary energy producer over the more efficient OXPHOS (134-136). This was done to provide essential metabolic precursors quickly for rapid cell division and function (Figure 1.6). However, an increasing number of studies from researchers in the field have shown it is so much more complicated and interesting than that. Metabolic enzymes, metabolites and bioactive molecules also play a central role in regulating gene transcription, epigenetics and signalling cascades, which contribute to immune cell differentiation, maturation, and activation (103, 137-139).

Macrophages are highly plastic and heterogeneous cells that are responsible for a wide range of responses along the inflammatory spectrum (140). Macrophages initiate and suppress inflammation and as a result it has been customary to bifurcate activated cells based on those primary functions (140). The M1 state, induced by inflammatory ligands LPS and IFN-γ, drives a pro-inflammatory state by producing inflammatory cytokines (TNF-α, IL-1β, IL-6) to attract other immune cells to the infection site to target and kill microorganisms (93, 94) (Figure 1.10). Conversely, M2 macrophages, due to IL-4 and IL-10 activation, generate anti-inflammatory cytokines (IL-10, TGF-β), clearing cellular debris to quell inflammation and drive tissue remodeling and repair (5) (Figure 1.10). M2 macrophages can be further divided into three separate sub-phenotypes based on function: M2a, M2b, M2c (141, 142). M2a macrophages arises in response to IL-4 and are involved in the T helper 2 cell-type immune response; M2b macrophages are induced in response to immune complexes and TLR and IL-1 receptor agonists and regulate the magnitude of immune responses; M2c macrophages arises in response to IL-10 or TGF-β and are involved in tissue remodeling (141, 142).

Interestingly, these activation states are associated with distinct metabolic profiles driven in part by differential mitochondrial function (140). Supported by the Warburg effect, M1 macrophages are heavily reliant on glycolysis as its primary energy source (134-136) (Figure 1.9). Mitochondria are reprogrammed from an ATP-producing to a ROS-generating organelle *via* reduced SDH activity, driving reverse electron transport (RET), a buildup of electrons at Complex I of the ETC and subsequent ROS generation (143). The altered SDH activity leads to succinate accumulation, which inhibits PHDs and results in the stabilization of HIF-1α, responsible for the upregulation of glycolytic and inflammatory genes (103, 144). Alternatively, M2 macrophages are dependent on OXPHOS and FAO as their primary energy sources, mediated by nutrient-sensing AMP-activated protein kinase (AMPK) activation (145, 146) (Figure 1.9). The plasticity of macrophages allows them to adapt their phenotype based on their microenvironment, but this ability is dependent on the degree of mitochondrial impairment in the cell (147, 148), highlighting the importance of mitochondria as the dynamic regulator of proper innate immune function.
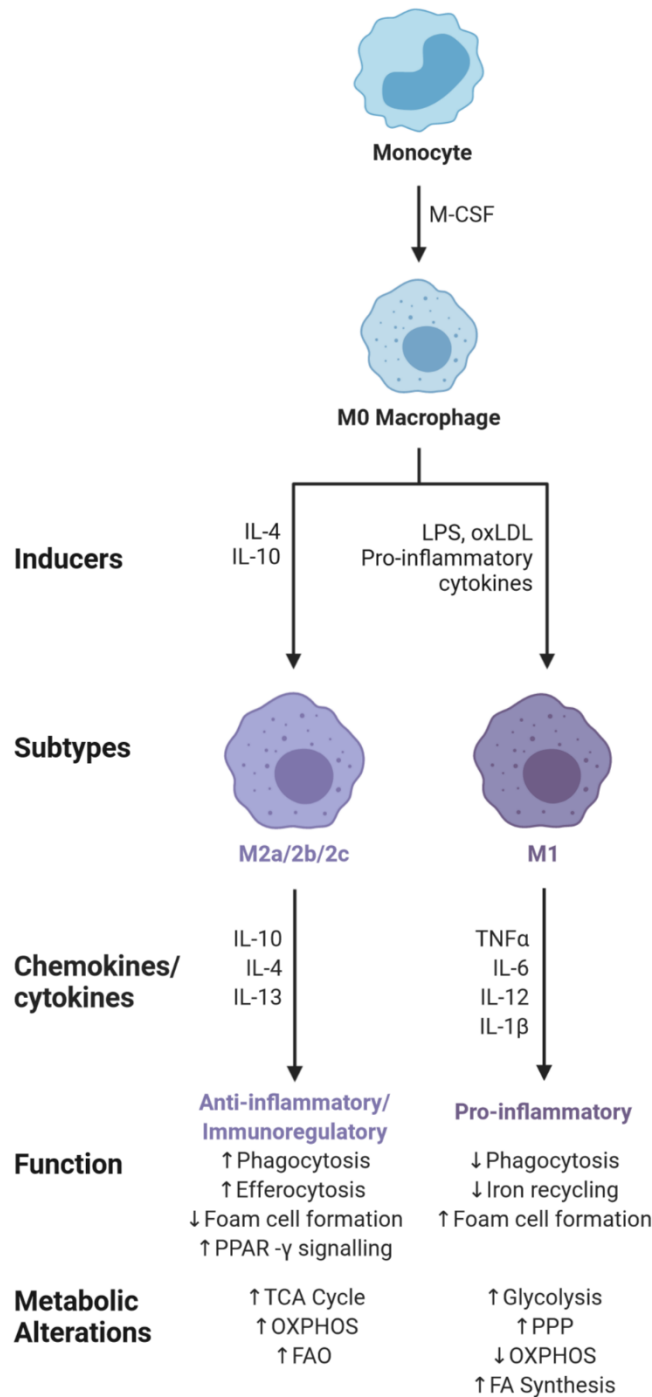
Figure 1.10: The differences between M1 and M2 macrophages. M1 and M2 are functionally distant macrophage phenotypes. While M1 macrophages are pro-inflammatory in nature, M2 macrophages are considered anti-inflammatory. These divergent functions are associated with differential metabolic re-programming which supports their respective functions. M1 macrophages rely on glycolysis for ATP production, whereas M2 macrophages are fueled by OXPHOS and FAO. Image created with BioRender.com.

1.4.1. *Metabolic Reprogramming of LPS engagement of TLR4*

LPS stimulation is thought to induce an M1 profile and has been widely used to model changes in cellular metabolism across inflammatory cells. However, it is increasingly recognized that the metabolic alterations associated with LPS stimulation are not observed in all inflammatory conditions. A plethora of studies have outlined that diverse pro-inflammatory and anti-inflammatory stimuli possess their own distinct metabolic profiles and suggest that the M1/M2 dichotomy is more of a spectrum of macrophages activation states with varying degrees of metabolic reprogramming (32).

1.4.1.1 Reprogramming of Glycolysis

A key feature of LPS-associated metabolic reprogramming is an increased reliance on glycolysis, mediated by HIF-1α and NF-κB (93, 149, 150). This reprogramming starts within minutes of receiving the stimuli by increasing glucose influx through Glucose transporter (GLUT)-1 and GLUT6 (150, 151). This influx is required to initiate inflammatory responses (152). To handle the increased influx of glucose, glycolytic genes (e.g. LDHA, PDK1, PFKFB3) are upregulated to quickly metabolize glucose to pyruvate and funnel pyruvate towards the production of lactate, and not acetyl-CoA (93, 153, 154). Interestingly, these glycolytic enzymes also participate in secondary "moon-lighting" roles to facilitate inflammation. For instance, Glyceraldehyde 3-phosphate dehydrogenase (GAPDH) is recruited to the mRNAs of inflammatory genes such as IFN-γ and TNF-α and suppresses their translation under resting conditions (155-157). Following LPS activation, GAPDH malonylation results in its dissociation from these mRNAs, leading to inflammatory cytokine expression (157). Similarly, PKM2 traditionally functions as a tetramer in glycolysis (158). However, under inflammatory conditions, PKM2 is converted into its dimer form and translocates to the nucleus to co-activate HIF-1α and STAT3,

boosting IL-1β and IL-6 levels respectively (Palsson-McDermott et al., 2015; Shirai et al., 2016). This increased dependence on glycolysis for energy leads to rapid ATP and NADH production from the pathway (93, 106).

The intermediary molecules of glycolysis are also used as precursors to biomolecules that serve critical roles in regulating LPS-mediated inflammation. For example, PPP gene expression (e.g. G6PD) and activity is elevated in LPS-stimulated mouse bone marrow-derived macrophages (BMM) (108, 159). The PPP is a major producer of the cofactor NADPH, a critical substrate for ROS-producing NADPH oxidase (NOX) and various enzymes involved in energy metabolism, cholesterol, and FA synthesis (108). Further, in its dephosphorylated form, NADH serves as the main source of energy transport throughout the macrophage. High levels of NAD^+ are also consumed during inflammatory responses to protect against excess ROS-associated DNA damage (107). To maintain a sufficient supply of NAD^+, two separate NAD-related pathways are activated during LPS activation: Tryptophan-driven *de novo* NAD^+ synthesis (160) and NAD^+ salvaging pathway (106, 107). Both pathways allow for the sustaining of Warburg metabolism during LPS activation. Finally, glycolytic-derived NADH is funnelled into mitochondria using the GPS, to fuel various vital mitochondrial reactions supporting IL-6 and IL-1β production (109).

1.4.1.2 Reprogramming of Mitochondrial Function

Another central feature of LPS engagement is the multi-faceted impairment of OXPHOS activity. During LPS stimulation, two breaks occur along the TCA cycle: at isocitrate dehydrogenase (IDH) and SDH (108). LPS-induced IFN-β downregulates the expression of IDH *via* IL-10 production (161). Itaconate is capable of inducing IFN-β production, creating a feed-forward mechanism to quell inflammation (162). The resulting break at IDH forces citrate into two directions. First, citrate is transported out of mitochondria to facilitate FA and prostaglandin

biosynthesis *via* increased activity of mitochondrial citrate carrier and ACLY (101, 163). Second, citrate is directed towards immunoresponsive gene 1 (IRG1), responsible for producing antibacterial and immunosuppressive itaconate (161, 164, 165). Itaconate targets several different proteins including NF-E2–related factor 2 (NRF2) (responsible for blocking IL-6 and IL-1β production), and SDH (162, 164, 166-169). This decrease in SDH activity leads to succinate accumulation and the inhibition of PHDs, stabilizing HIF-1α (103, 164, 168). However, some SDH activity is required to drive the RET phenomenon, funnelling electrons to Complex I and ROS generation and further stabilizing HIF-1α by inactivating the iron cofactor of PHDs (114, 143, 170-172). This can be blocked with the use diabetic drug Metformin, which inhibits Complex I activity and boosts IL-10 expression (173). It also blocks glucose uptake and glycolytic activity to further quell the inflammatory response (174). Other TCA metabolites, such as fumarate and α-ketoglutarate, also play a role in driving epigenetic reprograming to augment TNF-α and IL-6 production (175).

In addition to the repurposing of the TCA cycle, the ETC undergoes a considerable rearrangement during LPS activation. Activated macrophages force ETC supercomplex disassembly *via* Optic atrophy 1 (OPA1) downregulation, facilitating the increased reliance on glycolytic energy and amplified inflammatory response observed in LPS-activated macrophages (114, 176). This disassembly leads to increased mtROS-mediated NLRP3 activation (114, 177). The conversion of mitochondria from an energy-producing organelle to a ROS-generating organelle augments the bactericidal activity of macrophages as they are recruited to bacteria-containing phagosomes to facilitate bacteria killing (170). Furthermore, Complex III-derived H_2O_2 drives disulfide bond formation within the IKK complex, activating it and driving NF-κB translation (128, 178). To prevent hyper-inflammation, UCP2 reduces MMP to lessen mtROS

levels (179-181). Although the mitochondrion is not used in its traditional role as a central energy hub, ETC activity still is vital to LPS-driven effector functions.

1.4.1.3 Reprogramming of Amino Acid Metabolism

Amino acids metabolism serves diverse roles during LPS activation. This includes the catabolism of glutamine, arginine, serine, and leucine. In LPS-stimulated macrophages, glutamine is broken down, *via* glutaminolysis, and funnelled into the TCA cycle as α-ketoglutarate (103, 108). This is done to replenish the carbons lost due to the various diversions of citrate and further drive succinate accumulation (103, 108). Arginine transport is upregulated during LPS activation, facilitating NO production by the inducible NO synthase (iNOS) (182-184). The molecule NO is a powerful bactericide and inhibitor of OXPHOS activity, both of which further enable the pro-inflammatory state (183, 184). Additionally, NO inhibits TCA enzyme aconitase and PDH, blocking glucose-derived carbon flow through the TCA cycle (185). The other product of the iNOS reaction, citrulline, is then directed towards the feedforward aspartate-arginosuccinate shunt, to continuously generate arginine for iNOS-derived NO production (108). Glucose-derived serine and serine uptake is critical for IL-1β expression (186, 187). Serine is used to generate glycine, which is required for glutathione synthesis as well as to fuel the epigenetic modification of pro-inflammatory genes such as IL-1β (186, 187). BCAAs (e.g. leucine, valine, isoleucine) are also used to maintain the inflammatory state, with increased uptake and expression of BCAT1 (121, 188). The loss of BCAT1 resulted in reduced itaconate and IRG1 levels due to decreased glycolytic activity (120, 121). Interestingly, this occurs independent to its native function by driving NRF2-mediated antioxidant response and glucose-derived TCA metabolite production (120). This further demonstrates the complicated networks of pathways integral to driving effector function.

1.4.1.4 Reprogramming of Lipid Metabolism

Lipid metabolism plays a critical role in regulating LPS-driven responses in macrophages. LPS-stimulated macrophages diminish cholesterol biosynthesis and promotes cholesterol ester formation in a type I IFN-dependent manner (189-191). Autocrine IFN-β signalling also diverts excess cholesterol towards Cholesterol 25-hydroxylase (CH25H)-mediated 25-hydroxycholesterol (25-HC) production (189). This removal of cholesterol and the reprogramming of its lipid membrane composition, mediated by MyD88-dependent NRF2 and Sterol regulatory element-binding protein (SREBP) signalling, increases membrane fluidity and improves phagocytotic capabilities (190, 192). 25-HC provides resistance against the binding of cholesterol-dependent cytolysins to cellular membranes (193). Moreover, the production of 25-HC also reduces SREBP2-driven translation, responsible for the expression of cholesterol biosynthetic genes (189). Its counterpart, SREBP1, is upregulated in the later stages of activation phase to drive anti-inflammatory FA production in a Liver X receptor (LXR)-dependent manner (194). Another late expressing protein, Sphingosine kinase 2 (SPHK2) is degraded within 6hrs of activation to promote inflammation before its induction 24hrs post-stimulation to quell inflammation in a Stimulator of type I interferon genes (STING)- and NF-κB-dependent manner (195, 196).

1.5.   Role of cellular metabolism in viral infections

The role of cellular metabolism in regulating macrophage effector function is not limited to antibacterial responses. Recent evidence has indicated that antiviral responses are supported by a rewiring of metabolic networks (197). In addition, viruses attempt to manipulate these cellular networks to favour viral replication and expansion and subvert the host immune response (197, 198). A better understanding of this complex interplay is required to elucidate their individual contributions as well as their cumulative effect on macrophage metabolism during viral infections.

1.5.1. *Virus-mediated hijacking of cellular metabolism*

Viruses are obligate intracellular microorganisms that use the host cell machinery to support their life cycle. To do this, they hijack the host cell's metabolism to build the macromolecules required to promote viral replication and assembly as well as to support the survival of infected cells (197). Rapid viral replication depends on an immense amount of energy and requires rapid and robust energy production (198). One key metabolic pathway that provides rapid energy and the production of macromolecule precursors is glycolysis. Human cytomegaloviruses (HCMV) increase glucose uptake and consumption in infected cells by promoting the expression of GLUT4, which has three times higher glucose affinity than GLUT1 (199). This increases glucose-derived TCA metabolite flux, providing the building blocks to facilitate inflammation (200). Metabolomic analysis of Influenza A (IAV)-infected macrophages revealed that the virus upregulates glycolytic-derived citrate and succinate to drive FA synthesis, for viral envelope assembly, and HIF-1α accumulation respectively (201). IAV is not the only virus that upregulates HIF-1α. Both the Human immunodeficiency virus (HIV) and Hepatitis C (HCV) increased HIF-1α levels to boost glycolysis (202-206). During HIV infection, HIF-1α expression is elevated in both infected and bystander cells to promote a pro-inflammatory state and viral replication (207). Alternatively, Adenovirus and the Herpes simplex virus (HSV) upregulate glycolysis to drive intermediates to PPP and boost nucleotide synthesis to support viral genome replication (208-210).

In addition to altered glucose metabolism, viruses employ strategies to altered mitochondrial function to support viral replication. For instance, Dengue virus infection is associated with increased mtROS and blocked mitochondrial fusion, which drives mitochondrial damage and DNA release leading to a dependency on glycolysis and the production of

biomolecular precursors required for viral replication (211-213). Conversely, Hepatitis B infection increases Dynamin-related protein 1 (DRP1) activation while promoting mitofusin 2 (MFN2) degradation, favouring mitochondrial fission (214). HCV expresses several proteins that alter mitochondrial function by either reducing the levels of Complex IV subunits (215, 216), inhibiting Complex I activity to induce mtROS (217, 218), or by altering mitochondrial fusion/fission (219). These processes force the cell to rely on glycolysis for rapid energy production. Interestingly, HIV-1 selectively infects high energy CD4+ T cells irrespective of their activation phenotype (220). Yet, HIV-infected macrophages that survive the initial infection have reduced ATP production, suggesting differential cell type machinery adaptation to ensure viral survival (221).

Viral replication is an energy intensive process and as a result requires access to multiple bioenergetic pathways for viral propagation. Adenovirus and HCV infections cause increased glutaminolysis and glutamine dependence to support robust viral replication and cell growth (208, 222). In addition, HIV-infected macrophages have an increased reliance of glutamine as an energy source (221). Vaccinia viral infection preferentially increase intracellular glutamine levels as it is the primary energy source during viral replication (223). This dependency on glutamine for energy has the added benefit of maintaining TCA cycle metabolites to generate amino acids for Vaccinia viral protein synthesis (223). Dengue-infected cells increase FAO *via* AMPK activation (224). Other viruses preferentially use lipids to support viral replication and assembly. For example, HIV infection promotes FA and cholesterol biosynthesis to support viral propagation (225). HCMV also induces lipogenesis *via* SREBP1 and SREBP2 upregulation (226). Interestingly, a Dengue component protein recruits fatty acid synthase to sites of viral particle replication and stimulates its activity (227). Targeting *de novo* fatty acid biosynthesis during vaccinia infection reduced viral load (228). HCV infection boost lipid metabolism by activating SREBP protein translation and

increasing its proteolytic cleavage into its mature form (229-232). As a result, host immune cells must enact defense strategies to counteract the re-programming driven by viruses and central to these strategies is the ability of cellular metabolism to manipulate the degree and magnitude of the host response.

1.5.2. *The regulation of antiviral immune responses by cellular metabolism*

In response to viral infection, macrophage employ countermeasures against the co-opting of cell machinery by the virus (197). Central to these responses is the revamping of metabolic networks, such as glycolysis, OXPHOS, amino acid metabolism and lipid metabolism. These alterations play critical roles in supporting viral resistance, antigen presentation and the production of inflammatory and antiviral mediators (76, 233-236).

1.5.2.1 Relationship between metabolism and RLR-mediated responses

The best characterized viral PPR pathway shown to reprogram cellular metabolism in macrophages are the cytosolic RLRs. This is likely given their intimate link between the signalling of these receptors and the mitochondria. The MAVS protein participates in several interactions which propel RLR-mediated responses. MAVS undergoes O-linked β-N-acetylglucosamine (O-GlcNAc) modifications *via* O-GlcNAc transferase, leading to MAVS ubiquitination and MAVS aggregation (237). A component of Complex IV (COX5B) directly interacts with MAVS, preventing MAVS aggregation, ROS production and ultimately suppressing antiviral responses (238). This provides a direct link between the homeostatic functions of the ETC and MAVS-mediated signalling. MAVS also interacts with glycolytic protein hexokinase 2 (HK2) natively (97). Upon RLR activation, this interaction is lost resulting in reduced glycolytic activity (97). This is because lactate naturally binds to MAVS and prevents its aggregation and subsequent RLR-mediated activation (97) (Zhang et al., 2019). While glycolysis suppresses RLR activation,

increased PFKFB3 is required for type I IFN induction (236), suggesting some glycolytic activity is required for RLR-mediated antiviral responses.

There are other mechanisms by which mitochondria have been shown to regulate RLR-mediated responses independent of its signalling dynamics. Examples include the mitochondrial fusion proteins MFN1 and MFN2, which are critical to eliciting type I IFN and pro-inflammatory cytokine expression following RLR engagement. Whereas MFN1 facilitates RLR signalling, MFN2 maintains MMP (212, 239). The latter is crucial to maintaining OXPHOS activity, which is required for ROS-mediated potentiation of RLR signalling (240, 241). To prevent hyper-activation, Autophagy related 5 (ATG5)-mediated autophagy of dysfunctional mitochondria, a large source of mtROS during RLR activation, limits the degree of RLR activation (240).

1.5.2.2 TLR3-mediated responses depend on altered metabolic flux

In response to dsRNA, TLR3 engagement propels an antiviral immune response. However, little is known regarding the role of cellular metabolism in regulating these responses in macrophages. One key regulator that has been identified is ROS. To et al. (242) have shown that NOX2-generated ROS facilitates the expression of IFN-β, IL-1β, TNF-α, and IL-6 at supraphysiological concentrations of the artificial dsRNA ligand Polyinosinic:polycytidylic acid (Poly(I:C) or PIC). This is essential for the activation of NF-κB, IRF3 and STAT1 signalling (243). This is accompanied by reduced Complex I-associated ATP production, partly linked to a loss ETC supercomplex assembly which forces a reliance on glycolysis (114, 176). This dependency on glycolysis is reliant on PFKFB3 activity, which supports phagocytotic activity (236). The immunosuppressive itaconate can block type I IFN induction during Poly(I:C) activation as a feedback mechanism to limit overactivation (169). In addition, proteomic analysis has directly connected the expression of 18 different proteins to the proper activation of TYK2, a member of

the JAK-STAT signalling pathway (244). These proteins are linked to glucose metabolism (e.g. TIM) as well as FA synthesis (e.g. ACLY, ACSL4) and degradation (e.g. ACSL4) (163, 244). This suggests that TLR-driven metabolic re-programming is partly due to autocrine type I IFN signalling.

As shown in Grunert et al. (244), lipid metabolism is important to TLR3-mediated responses. Activated macrophages have significantly lower levels of saturated and unsaturated long-chain FAs as well as cholesterol and thus rely on lipid import rather than *de novo* synthesis regulated by SREBP (235). This is partly to a funneling of cholesterol towards the generation of 25-HC, which replaces cholesterol in the plasma membrane, reducing viral entry (245). To further assist in preventing viral entry, TRIF-induced type I IFN signalling promote a reprogramming of lipid membrane composition (192).

1.5.2.3 The metabolic reprogramming induced by other viral TLRs

Other viral-sensing TLRs are considerably less studied in the context of immunometabolism, with most of the work done on these TLR ligands conducted as an accessory to either global TLR studies or used as a comparison to TLR4-focused studies. The ssRNA-sensing TLR7/8 possess a few artificial ligands capable of initiating their activation, including Imidazoquinolinones (Imiquimod/R837, Resiquimod/R848, CL097) (246-248). While NOX2-derived ROS is produced during TLR7 activation, unlike TLR3, ROS represses cytokine production and the use of apocynin (NOX2 inhibitor) enhances cytokine secretion in a MyD88-dependent manner (242). In accordance with this, proteomic analysis of R848 treated macrophages found 27 differentially expressed protein, including several antioxidant proteins (SOD2, GPX, PRDX1/6) (178). Yet, imidazoquinolinone engagement also inhibits Complex I activity, leading

to increased ROS and ROS-mediated NLRP3 activation, suggesting that mtROS, but not cytosolic ROS, may be key in modulating TLR7/8 responses (249, 250).

Similar to other viral ligand receptors, activation of TLR7/8 alters macrophage lipid metabolism to protect the cell against infection. This occurs *via* MyD88-dependent lipid membrane re-composition by NRF2 and SREBP, which facilitates inflammatory cytokine production (192, 251). Yet, uncontrolled TLR7/8-mediated inflammation can result in foam cell formation due to excess cellular lipid accumulation (252). A key modulator of this homeostatic balance is SPHK2, which is degraded in the early phase of activation but induced in the late phase to quell inflammation (195). Another immunosuppressive molecule produced during TLR7/8 activation is itaconate, which assists in preventing hyper-inflammation (167).

Very little is known regarding the role of cellular metabolism in regulating the activation of the DNA-sensing TLR9. Like TLR3 and TLR4, TLR9 activation with CpG oligonucleotides has been shown to induce ETC supercomplex disassembly and increase dependency on glycolysis for energy (176, 253). Yet, TLR9-activated macrophages also require other energy sources for proper activation. CpG activation reduce glucose input into the TCA cycle to favour carbons from glutaminolysis (115). Furthermore, TCA metabolites are shunted towards *de novo* lipid biosynthesis *via* increased CPT1A and ACLY activity (115, 251). In addition to their incorporation into the plasma membrane akin to other MyD88-dependent TLRs (TLR3/7/8) (192), newly generated lipids are used to increase FAO's energy contribution (115).

1.6.   Study Objectives

The literature presented above demonstrates that like other inflammatory responses, the ability of macrophages to mount an effective antiviral response depends on metabolic re-

programming of critical pathways. Yet, there are several gaps in the literature that yet have not been addressed. Initial assumptions in the literature were that TLR4-mediated responses in macrophages were representative for all TLR-mediated responses. However, based on limited data available, the metabolic reprogramming associated with TLR3-medaited responses differ from LPS activation. In addition, there has yet to be a systematic characterization of which metabolic pathways are associated with type I IFN responses and which metabolic pathways contribute to specific aspects of the response. Moreover, it is currently unknown if specific metabolic proteins or pathways are capable of functioning as rheostats, capable of fine-tuning individual components of the response and regulate its magnitude. For example, increased glycolysis in macrophages is associated with increase inflammation yet it has not been elucidated if the altered expression of specific proteins controls the magnitude of the inflammation and can it be done without altering other aspects of the response. In this vein, this thesis endeavours to build a better understanding of the role of cellular metabolism in regulating antiviral responses.

Despite activating the same family of transcription factors, TLR-associated antibacterial and antiviral responses produce distinct inflammatory and antiviral responses. While the role of cellular metabolism in driving antibacterial responses, such as LPS, has been well-established (93, 96, 98, 103, 143, 144, 173, 254-256), there has yet to be a comprehensive characterization of the metabolic processes that are altered during TLR-associated antiviral responses and their specific role in regulating effector function during these responses. In addition, there is limited knowledge as to the direct contribution of type I IFNs in the metabolic reprogramming of macrophages, which are induced by antibacterial and antiviral responses. Therefore, my thesis aims to show that changes to cellular metabolism are key drivers of the antiviral function of macrophages. To

accomplish this, this project has mainly focus on IFN-α as well as two vital, yet divergent producers of type I IFNs: LPS and Poly(I:C). The aims of this thesis are as follows:

1. The systematic characterization of metabolic processes associated with type I IFN-mediated responses in macrophages

2. Examine the differences in mitochondrial re-programming in TLR3- and TLR4-mediated responses

3. Investigate the differential responses of Poly(I:C) of different strand lengths in macrophages

    A. Assess the inflammatory profiles of Poly(I:C)-mediated responses based on strand length

    B. Probe the differential mitochondrial re-programming of Poly(I:C)-mediated responses based on strand length

1.7.   References

1.   Murphy, K. M. 2011. *Janeway's Immunobiology*. Taylor & Francis Group.
2.   Akira, S., S. Uematsu, and O. Takeuchi. 2006. Pathogen Recognition and Innate Immunity. *Cell* 124: 783-801.
3.   Gasteiger, G., A. D'Osualdo, D. A. Schubert, A. Weber, E. M. Bruscia, and D. Hartl. 2017. Cellular innate immunity: An old game with new players. *J Innate Immun* 9: 111-125.
4.   Bonilla, F. A., and H. C. Oettgen. 2010. Adaptive immunity. *J Allergy Clin Immunol* 125: S33-S40.
5.   Wynn, T. A., A. Chawla, and J. W. Pollard. 2013. Origins and Hallmarks of Macrophages: Development, Homeostasis, and Disease. *Nature* 496: 445-455.
6.   Theret, M., R. Mounier, and F. Rossi. 2019. The origins and non-canonical functions of macrophages in development and regeneration. *Development* 146: dev156000.
7.   van Furth, R., and Z. A. Cohn. 1968. The origin and kinetics of mononuclear phagocytes. *J Exp Med* 128: 415-435.
8.   van Furth, R., Z. A. Cohn, J. G. Hirsch, J. H. Humphrey, W. G. Spector, and H. L. Langevoort. 1972. The mononuclear phagocyte system: a new classification of macrophages, monocytes, and their precursor cells. *Bull World Health Organ* 46: 845-852.
9.   Schulz, C., E. Gomez Perdiguero, L. Chorro, H. Szabo-Rogers, N. Cagnard, K. Kierdorf, M. Prinz, B. Wu, S. E. Jacobsen, J. W. Pollard, J. Frampton, K. J. Liu, and F. Geissmann. 2012. A lineage of myeloid cells independent of Myb and hematopoietic stem cells. *Science* 336: 86-90.
10. Ginhoux, F., M. Greter, M. Leboeuf, S. Nandi, P. See, S. Gokhan, M. F. Mehler, S. J. Conway, L. G. Ng, E. R. Stanley, I. M. Samokhvalov, and M. Merad. 2010. Fate mapping analysis reveals that adult microglia derive from primitive macrophages. *Science* 330: 841-845.
11. Hoeffel, G., Y. Wang, M. Greter, P. See, P. Teo, B. Malleret, M. Leboeuf, D. Low, G. Oller, F. Almeida, S. H. Y. Choy, M. Grisotto, L. Renia, S. J. Conway, E. R. Stanley, J. K. Y. Chan, L.-G. Ng, I. M. Samokhvalov, M. Merad, and F. Ginhoux. 2012. Adult Langerhans cells derive predominantly from embryonic fetal liver monocytes with a minor contribution of yolk sac-derived macrophages. *J Exp Med* 209: 1167-1181.
12. Hoeffel, G., and F. Ginhoux. 2015. Ontogeny of tissue-resident macrophages. *Front Immunol* 6: 486.
13. Yona, S., K.-W. Kim, Y. Wolf, A. Mildner, D. Varol, M. Breker, D. Strauss-Ayali, S. Viukov, M. Guilliams, and A. Misharin. 2013. Fate mapping reveals origins and dynamics of monocytes and tissue macrophages under homeostasis. *Immunity* 38: 79-91.
14. Geissmann, F., S. Jung, and D. R. Littman. 2003. Blood Monocytes Consist of Two Principal Subsets with Distinct Migratory Properties. *Immunity* 19: 71-82.
15. Carlin, L. M., E. G. Stamatiades, C. Auffray, R. N. Hanna, L. Glover, G. Vizcay-Barrena, C. C. Hedrick, H. T. Cook, S. Diebold, and F. Geissmann. 2013. Nr4a1-dependent Ly6Clow monocytes monitor endothelial cells and orchestrate their disposal. *Cell* 153: 362-375.
16. Cros, J., N. Cagnard, K. Woollard, N. Patey, S.-Y. Zhang, B. Senechal, A. Puel, S. K. Biswas, D. Moshous, C. Picard, J.-P. Jais, D. D'Cruz, J.-L. Casanova, C. Trouillet, and F. Geissmann. 2010. Human CD14dim Monocytes Patrol and Sense Nucleic Acids and Viruses via TLR7 and TLR8 Receptors. *Immunity* 33: 375-386.

17. Belge, K.-U., F. Dayyani, A. Horelt, M. Siedlar, M. Frankenberger, B. Frankenberger, T. Espevik, and L. Ziegler-Heitbrock. 2002. The Proinflammatory CD14+CD16+DR++ Monocytes Are a Major Source of TNF. *The Journal of Immunology* 168: 3536-3542.

18. Ziegler-Heitbrock, L. 2007. The CD14+ CD16+ blood monocytes: their role in infection and inflammation. *Journal of Leukocyte Biology* 81: 584-592.

19. Ziegler-Heitbrock, L., P. Ancuta, S. Crowe, M. Dalod, V. Grau, D. N. Hart, P. J. M. Leenen, Y.-J. Liu, G. MacPherson, G. J. Randolph, J. Scherberich, J. Schmitz, K. Shortman, S. Sozzani, H. Strobl, M. Zembala, J. M. Austyn, and M. B. Lutz. 2010. Nomenclature of monocytes and dendritic cells in blood. *Blood* 116: e74.

20. Varol, C., A. Mildner, and S. Jung. 2015. Macrophages: Development and Tissue Specialization. *Annual Review of Immunology* 33: 643-675.

21. Toth, C. A., and D. P. Thomas. 1992. Liver endocytosis and Kupffer cells. *Hepatology* 16: 255-266.

22. Tate, M. D., D. L. Pickett, N. van Rooijen, A. G. Brooks, and P. C. Reading. 2010. Critical Role of Airway Macrophages in Modulating Disease Severity during Influenza Virus Infection of Mice. *Journal of Virology* 84: 7569-7580.

23. Kühl, A. A., U. Erben, L. I. Kredel, and B. Siegmund. 2015. Diversity of Intestinal Macrophages in Inflammatory Bowel Diseases. *Frontiers in Immunology* 6: 613.

24. Ross, J. A., and M. J. Auger. 2002. The biology of the macrophage. In *The macrophage*, 2nd ed. B. Burke, and C. E. Lewis, eds. Oxford University Press, New York, New York. 1-57.

25. Gordon, S., and P. R. Taylor. 2005. Monocyte and macrophage heterogeneity. *Nat Rev Immunol* 5: 953-964.

26. Yu, X., A. Buttgereit, I. Lelios, S. G. Utz, D. Cansever, B. Becher, and M. Greter. 2017. The cytokine TGF-β promotes the development and homeostasis of alveolar macrophages. *Immunity* 47: 903-912 e904.

27. Naito, M., G. Hasegawa, Y. Ebe, and T. Yamamoto. 2004. Differentiation and function of Kupffer cells. *Medical Electron Microscopy* 37: 16-28.

28. Biswas, S. K., and E. Lopez-Collazo. 2009. Endotoxin tolerance: new mechanisms, molecules and clinical significance. *Trends in Immunology* 30: 475-487.

29. Smythies, L. E., R. Shen, D. Bimczok, L. Novak, R. H. Clements, D. E. Eckhoff, P. Bouchard, M. D. George, W. K. Hu, S. Dandekar, and P. D. Smith. 2010. Inflammation Anergy in Human Intestinal Macrophages Is Due to Smad-induced IκBα Expression and NF-κB Inactivation. *Journal of Biological Chemistry* 285: 19593-19604.

30. Zigmond, E., C. Varol, J. Farache, E. Elmaliah, Ansuman T. Satpathy, G. Friedlander, M. Mack, N. Shpigel, Ivo G. Boneca, Kenneth M. Murphy, G. Shakhar, Z. Halpern, and S. Jung. 2012. Ly6Chi Monocytes in the Inflamed Colon Give Rise to Proinflammatory Effector Cells and Migratory Antigen-Presenting Cells. *Immunity* 37: 1076-1090.

31. Schenk, M., and C. Mueller. 2007. Adaptations of intestinal macrophages to an antigen-rich environment. *Semin Immunol* 19: 84-93.

32. Mosser, D. M., and J. P. Edwards. 2008. Exploring the full spectrum of macrophage activation. *Nat Rev Immunol* 8: 958-969.

33. Fadok, V. A., D. L. Bratton, A. Konowal, P. W. Freed, J. Y. Westcott, and P. M. Henson. 1998. Macrophages that have ingested apoptotic cells in vitro inhibit proinflammatory cytokine production through autocrine/paracrine mechanisms involving TGF-beta, PGE2, and PAF. *Journal of Clinical Investigation* 101: 890-898.

34. Fadok, V. A., P. P. McDonald, D. L. Bratton, and P. M. Henson. 1998. Regulation of macrophage cytokine production by phagocytosis of apoptotic and post-apoptotic cells. *Biochem Soc Trans* 26: 653-656.

35. Murray, P. J., J. Rathmell, and E. Pearce. 2015. SnapShot: Immunometabolism. *Cell Metabolism* 22: 190-190.e191.

36. Bianchi, M. E. 2007. DAMPs, PAMPs and alarmins: all we need to know about danger. *J. Leukoc. Biol.* 81: 1-5.

37. Fitzgerald, K. A., and J. C. Kagan. 2020. Toll-like receptors and the control of immunity. *Cell* 180: 1044-1066.

38. Reikine, S., J. B. Nguyen, and Y. Modis. 2014. Pattern recognition and signaling mechanisms of RIG-I and MDA5. *Front Immunol* 5: 342-342.

39. Takeuchi, O., K. Hoshino, T. Kawai, H. Sanjo, H. Takada, T. Ogawa, K. Takeda, and S. Akira. 1999. Differential roles of TLR2 and TLR4 in recognition of gram-negative and gram-positive bacterial cell wall components. *Immunity* 11: 443-451.

40. Takeuchi, O., S. Sato, T. Horiuchi, K. Hoshino, K. Takeda, Z. Dong, R. L. Modlin, and S. Akira. 2002. Cutting edge: Role of Toll-like receptor 1 in mediating immune response to microbial lipoproteins. *J Immunol* 169: 10-14.

41. Kang, J. Y., X. Nan, M. S. Jin, S.-J. Youn, Y. H. Ryu, S. Mah, S. H. Han, H. Lee, S.-G. Paik, and J.-O. Lee. 2009. Recognition of lipopeptide patterns by Toll-like receptor 2-Toll-like receptor 6 heterodimer. *Immunity* 31: 873-884.

42. Poltorak, A., X. He, I. Smirnova, M.-Y. Liu, C. Van Huffel, X. Du, D. Birdwell, E. Alejos, M. Silva, and C. Galanos. 1998. Defective LPS signaling in C3H/HeJ and C57BL/10ScCr mice: mutations in Tlr4 gene. *Science* 282: 2085-2088.

43. Shimazu, R., S. Akashi, H. Ogata, Y. Nagai, K. Fukudome, K. Miyake, and M. Kimoto. 1999. MD-2, a molecule that confers lipopolysaccharide responsiveness on Toll-like receptor 4. *J Exp Med* 189: 1777-1782.

44. Hayashi, F., K. D. Smith, A. Ozinsky, T. R. Hawn, C. Y. Eugene, D. R. Goodlett, J. K. Eng, S. Akira, D. M. Underhill, and A. Aderem. 2001. The innate immune response to bacterial flagellin is mediated by Toll-like receptor 5. *Nature* 410: 1099-1103.

45. Heil, F., H. Hemmi, H. Hochrein, F. Ampenberger, C. Kirschning, S. Akira, G. Lipford, H. Wagner, and S. Bauer. 2004. Species-specific recognition of single-stranded RNA via Toll-like receptor 7 and 8. *Science* 303: 1526-1529.

46. Alexopoulou, L., A. C. Holt, R. Medzhitov, and R. A. Flavell. 2001. Recognition of double-stranded RNA and activation of NF-[kappa]B by Toll-like receptor 3. *Nature* 413: 732-738.

47. Lund, J. M., L. Alexopoulou, A. Sato, M. Karow, N. C. Adams, N. W. Gale, A. Iwasaki, and R. A. Flavell. 2004. Recognition of single-stranded RNA viruses by Toll-like receptor 7. *Proc Natl Acad Sci U S A* 101: 5598-5603.

48. Lund, J., A. Sato, S. Akira, R. Medzhitov, and A. Iwasaki. 2003. Toll-like receptor 9–mediated recognition of herpes simplex virus-2 by plasmacytoid dendritic cells. *J Exp Med* 198: 513-520.

49. Hemmi, H., O. Takeuchi, T. Kawai, T. Kaisho, S. Sato, H. Sanjo, M. Matsumoto, K. Hoshino, H. Wagner, K. Takeda, and S. Akira. 2000. A Toll-like receptor recognizes bacterial DNA. *Nature* 408: 740-745.

50. Kawai, T., and S. Akira. 2010. The role of pattern-recognition receptors in innate immunity: update on Toll-like receptors. *Nat Immunol* 11: 373-384.

51. Bhoj, V. G., and Z. J. Chen. 2009. Ubiquitylation in innate and adaptive immunity. *Nature* 458: 430-437.

52. Zhao, M., J. Joy, W. Zhou, S. De, W. H. I. Wood, K. G. Becker, H. Ji, and R. Sen. 2018. Transcriptional outcomes and kinetic patterning of gene expression in response to NF-κB activation. *PLoS Biol* 16.

53. Hacker, H., and M. Karin. 2006. Regulation and function of IKK and IKK-related kinases. *Sci STKE* 2006: re13.

54. Taniguchi, T., K. Ogasawara, A. Takaoka, and N. Tanaka. 2001. IRF family of transcription factors as regulators of host defense. *Annu Rev Immunol* 19: 623-655.

55. Yoneyama, M., M. Kikuchi, K. Matsumoto, T. Imaizumi, M. Miyagishi, K. Taira, E. Foy, Y.-M. Loo, M. Gale, and S. Akira. 2005. Shared and unique functions of the DExD/H-box helicases RIG-I, MDA5, and LGP2 in antiviral innate immunity. *J Immunol* 175: 2851-2858.

56. Yoneyama, M., M. Kikuchi, T. Natsukawa, N. Shinobu, T. Imaizumi, M. Miyagishi, K. Taira, S. Akira, and T. Fujita. 2004. The RNA helicase RIG-I has an essential function in double-stranded RNA-induced innate antiviral responses. *Nat Immunol* 5: 730-737.

57. Saito, T., R. Hirai, Y.-M. Loo, D. Owen, C. L. Johnson, S. C. Sinha, S. Akira, T. Fujita, and M. Gale. 2007. Regulation of innate antiviral defenses through a shared repressor domain in RIG-I and LGP2. *Proc Natl Acad Sci U S A* 104: 582-587.

58. Kato, H., O. Takeuchi, S. Sato, M. Yoneyama, M. Yamamoto, K. Matsui, S. Uematsu, A. Jung, T. Kawai, K. J. Ishii, O. Yamaguchi, K. Otsu, T. Tsujimura, C.-S. Koh, C. Reis e Sousa, Y. Matsuura, T. Fujita, and S. Akira. 2006. Differential roles of MDA5 and RIG-I helicases in the recognition of RNA viruses. *Nature* 441: 101-105.

59. Kato, H., O. Takeuchi, E. Mikamo-Satoh, R. Hirai, T. Kawai, K. Matsushita, A. Hiiragi, T. S. Dermody, T. Fujita, and S. Akira. 2008. Length-dependent recognition of double-stranded ribonucleic acids by Retinoic acid-inducible gene-I and Melanoma differentiation-associated gene 5. *J Exp Med* 205: 1601-1610.

60. Peisley, A., C. Lin, B. Wu, M. Orme-Johnson, M. Liu, T. Walz, and S. Hur. 2011. Cooperative assembly and dynamic disassembly of MDA5 filaments for viral dsRNA recognition. *Proc Natl Acad Sci U S A* 108: 21010-21015.

61. Berke, I. C., and Y. Modis. 2012. MDA5 cooperatively forms dimers and ATP-sensitive filaments upon binding double-stranded RNA. *EMBO J* 31: 1714-1726.

62. Kowalinski, E., T. Lunardi, A. A. McCarthy, J. Louber, J. Brunel, B. Grigorov, D. Gerlier, and S. Cusack. 2011. Structural basis for the activation of innate immune pattern-recognition receptor RIG-I by viral RNA. *Cell* 147: 423-435.

63. Jiang, F., A. Ramanathan, M. T. Miller, G.-Q. Tang, M. Gale, S. S. Patel, and J. Marcotrigiano. 2011. Structural basis of RNA recognition and activation by innate immune receptor RIG-I. *Nature* 479: 423-427.

64. Peisley, A., B. Wu, H. Xu, Z. J. Chen, and S. Hur. 2014. Structural basis for ubiquitin-mediated antiviral signal activation by RIG-I. *Nature* 509: 110-114.

65. Seth, R. B., L. Sun, C.-K. Ea, and Z. J. Chen. 2005. Identification and characterization of MAVS, a mitochondrial antiviral signaling protein that a ctivates NF-κB and IRF3. *Cell* 122: 669-682.

66. Kawai, T., K. Takahashi, S. Sato, C. Coban, H. Kumar, H. Kato, K. J. Ishii, O. Takeuchi, and S. Akira. 2005. IPS-1, an adaptor triggering RIG-I- and MDA5-mediated type I interferon induction. *Nat Immunol* 6: 981-988.

67. Hou, F., L. Sun, H. Zheng, B. Skaug, Q.-X. Jiang, and Z. J. Chen. 2011. MAVS forms functional prion-like aggregates to activate and propagate antiviral innate immune response. *Cell* 146: 448-461.

68. Pestka, S., C. D. Krause, and M. R. Walter. 1987. Interferons, interferon-like cytokines, and their receptors. *Immunol. Rev.* 202 8-32.

69. Pestka, S. 1997. The human interferon-alpha species and hybrid proteins. *Semin Oncol* 24: S9-4-S9-17.

70. Ivashkiv, L. B., and L. T. Donlin. 2014. Regulation of type I interferon responses. *Nat Rev Immunol* 14: 36-49.

71. Trinchieri, G. 2010. Type I interferon: friend or foe? *J. Exp. Med.* 207: 2053-2063.

72. Stark, G. R., I. M. Kerr, B. R. G. Williams, R. H. Silverman, and R. D. Schreiber. 1998. How cells respond to interferons. *Annu. Rev. Biochem.* 67: 227-264.

73. Ihle, J. N. 1995. Cytokine receptor signalling. *Nature* 377: 591-594.

74. Darnell, J., I. Kerr, and G. Stark. 1994. Jak-STAT pathways and transcriptional activation in response to IFNs and other extracellular signaling proteins. *Science* 264: 1415-1421.

75. Nakaya, T., M. Sato, N. Hata, M. Asagiri, H. Suemori, S. Noguchi, N. Tanaka, and T. Taniguchi. 2001. Gene Induction Pathways Mediated by Distinct IRFs during Viral Infection. *Biochem Biophys Res Commun* 283: 1150-1156.

76. Schoggins, J. W., and C. M. Rice. 2011. Interferon-stimulated genes and their antiviral effector functions. *Curr. Opin. Virol.* 1: 519-525.

77. Lekmine, F., S. Uddin, A. Sassano, S. Parmar, S. M. Brachmann, B. Majchrzak, N. Sonenberg, N. Hay, E. N. Fish, and L. C. Platanias. 2003. Activation of the p70 S6 Kinase and Phosphorylation of the 4E-BP1 Repressor of mRNA Translation by Type I Interferons. *J. Biol. Chem.* 278: 27772-27780.

78. Uddin, S., B. Majchrzak, P.-C. Wang, S. Modi, M. K. Khan, E. N. Fish, and L. C. Platanias. 2000. Interferon-Dependent Activation of the Serine Kinase PI 3′-Kinase Requires Engagement of the IRS Pathway but Not the Stat Pathway. *Biochem. Biophys. Res. Commun.* 270: 158-162.

79. Huang, J., and Brendan D. Manning. 2009. A complex interplay between Akt, TSC2 and the two mTOR complexes. *Biochemical Society Transactions* 37: 217-222.

80. Sun, Q., X. Chen, J. Ma, H. Peng, F. Wang, X. Zha, Y. Wang, Y. Jing, H. Yang, R. Chen, L. Chang, Y. Zhang, J. Goto, H. Onda, T. Chen, M.-R. Wang, Y. Lu, H. You, D. Kwiatkowski, and H. Zhang. 2011. Mammalian target of rapamycin up-regulation of pyruvate kinase isoenzyme type M2 is critical for aerobic glycolysis and tumor growth. *Proceedings of the National Academy of Sciences* 108: 4129-4134.

81. Dang, Eric V., J. Barbi, H.-Y. Yang, D. Jinasena, H. Yu, Y. Zheng, Z. Bordman, J. Fu, Y. Kim, H.-R. Yen, W. Luo, K. Zeller, L. Shimoda, Suzanne L. Topalian, Gregg L. Semenza, Chi V. Dang, Drew M. Pardoll, and F. Pan. 2011. Control of TH17/Treg Balance by Hypoxia-Inducible Factor 1. *Cell* 146: 772-784.

82. Shi, L. Z., R. Wang, G. Huang, P. Vogel, G. Neale, D. R. Green, and H. Chi. 2011. HIF1α–dependent glycolytic pathway orchestrates a metabolic checkpoint for the differentiation of TH17 and Treg cells. *J Exp Med* 208: 1367-1376.

83. O'Neill, L. A. J., R. J. Kishton, and J. Rathmell. 2016. A guide to immunometabolism for immunologists. *Nature Reviews Immunology* 16: 553-565.

84. Angajala, A., S. Lim, J. B. Phillips, J.-H. Kim, C. Yates, Z. You, and M. Tan. 2018. Diverse roles of mitochondria in immune responses: Novel insights into immuno-metabolism. *Front Immunol* 9: 1605.

85. Arnoult, D., F. Soares, I. Tattoli, and S. E. Girardin. 2011. Mitochondria in innate immunity. *EMBO Rep* 12: 901-910.

86. Voet, D., J. G. Voet, and C. W. Pratt. 2016. *Fundamentals of biochemistry: life at the molecular level*. John Wiley & Sons.

87. Tanner, L. B., A. G. Goglia, M. H. Wei, T. Sehgal, L. R. Parsons, J. O. Park, E. White, J. E. Toettcher, and J. D. Rabinowitz. 2018. Four key steps control glycolytic flux in Mammalian cells. *Cell Syst* 7: 49-62.e48.

88. Berg, J. M., J. L. Tymoczko, and L. Stryer. 2008. *Biochemistry*. Macmillan.

89. Thwe, P. M., L. R. Pelgrom, R. Cooper, S. Beauchamp, J. A. Reisz, A. D'Alessandro, B. Everts, and E. Amiel. 2017. Cell-intrinsic glycogen metabolism supports early glycolytic reprogramming required for Dendritic cell immune responses. *Cell Metab* 26: 558-567.e555.

90. Ghergurovich, J. M., J. C. García-Cañaveras, J. Wang, E. Schmidt, Z. Zhang, T. TeSlaa, H. Patel, L. Chen, E. C. Britt, M. Piqueras-Nebot, M. C. Gomez-Cabrera, A. Lahoz, J. Fan, U. H. Beier, H. Kim, and J. D. Rabinowitz. 2020. A small molecule G6PD inhibitor reveals immune dependence on pentose phosphate pathway. *Nat Chem Biol* 16: 731-739.

91. Wang, R., C. P. Dillon, L. Z. Shi, S. Milasta, R. Carter, D. Finkelstein, L. L. McCormick, P. Fitzgerald, H. Chi, and J. Munger. 2011. The transcription factor Myc controls metabolic reprogramming upon T lymphocyte activation. *Immunity* 35: 871-882.

92. Ma, E. H., G. Bantug, T. Griss, S. Condotta, R. M. Johnson, B. Samborska, N. Mainolfi, V. Suri, H. Guak, M. L. Balmer, M. J. Verway, T. C. Raissi, H. Tsui, G. Boukhaled, S. Henriques da Costa, C. Frezza, C. M. Krawczyk, A. Friedman, M. Manfredi, M. J. Richer, C. Hess, and R. G. Jones. 2017. Serine is an essential metabolite for effector T cell expansion. *Cell Metabolism* 25: 345-357.

93. Rodríguez-Prados, J., P. G. Través, J. Cuenca, D. Rico, J. Aragonés, P. Martín-Sanz, M. Cascante, and L. Boscá. 2010. Substrate fate in activated macrophages: A comparison between innate, classic, and alternative activation. *J Immunol* 185: 605-614.

94. Vazquez, A., J. Liu, Y. Zhou, and Z. N. Oltvai. 2010. Catabolic efficiency of aerobic glycolysis: The Warburg effect revisited. *BMC Syst. Biol.* 4: 1-9.

95. Wang, T., H. Liu, G. Lian, S.-Y. Zhang, X. Wang, and C. Jiang. 2017. HIF1α-induced glycolysis metabolism is essential to the activation of inflammatory macrophages. *Mediators Inflamm* 2017: 10.

96. Aki, T., T. Funakoshi, K. Noritake, K. Unuma, and K. Uemura. 2020. Extracellular glucose is crucially involved in the fate decision of LPS-stimulated RAW264.7 murine macrophage cells. *Scientific Reports* 10: 10581.

97. Zhang, W., G. Wang, Z. G. Xu, H. Tu, F. Hu, J. Dai, Y. Chang, Y. Chen, Y. Lu, H. Zeng, Z. Cai, F. Han, C. Xu, G. Jin, L. Sun, B. S. Pan, S. W. Lai, C. C. Hsu, J. Xu, Z. Z. Chen, H. Y. Li, P. Seth, J. Hu, X. Zhang, H. Li, and H. K. Lin. 2019. Lactate is a natural suppressor of RLR signaling by targeting MAVS. *Cell* 178: 176-189.e115.

98. Errea, A., D. Cayet, P. Marchetti, C. Tang, J. Kluza, S. Offermanns, J.-C. Sirard, and M. Rumbo. 2016. Lactate Inhibits the Pro-Inflammatory Response and Metabolic Reprogramming in Murine Macrophages in a GPR81-Independent Manner. *PLoS ONE* 11: e0163694.

99.   Spinelli, J. B., and M. C. Haigis. 2018. The multifaceted contributions of mitochondria to cellular metabolism. *Nat Cell Biol* 20: 745-754.

100.   Williams, N. C., and L. A. J. O'Neill. 2018. A role for the Krebs cycle intermediate Citrate in metabolic reprogramming in innate immunity and inflammation. *Front Immunol* 9: 141.

101.   Infantino, V., P. Convertini, L. Cucci, Maria A. Panaro, Maria A. Di Noia, R. Calvello, F. Palmieri, and V. Iacobazzi. 2011. The mitochondrial citrate carrier: a new player in inflammation. *Biochem. J.* 438: 433-436.

102.   Ratter, J. M., H. M. M. Rooijackers, G. J. Hooiveld, A. G. M. Hijmans, B. E. de Galan, C. J. Tack, and R. Stienstra. 2018. In vitro and in vivo effects of Lactate on metabolism and cytokine production of Human primary PBMCs and onocytes. *Front Immunol* 9: 2564.

103.   Tannahill, G. M., A. M. Curtis, J. Adamik, E. M. Palsson-McDermott, A. F. McGettrick, G. Goel, C. Frezza, N. J. Bernard, B. Kelly, N. H. Foley, L. Zheng, A. Gardet, Z. Tong, S. S. Jany, S. C. Corr, M. Haneklaus, B. E. Caffrey, K. Pierce, S. Walmsley, F. C. Beasley, E. Cummins, V. Nizet, M. Whyte, C. T. Taylor, H. Lin, S. L. Masters, E. Gottlieb, V. P. Kelly, C. Clish, P. E. Auron, R. J. Xavier, and L. A. J. O/'Neill. 2013. Succinate is an inflammatory signal that induces IL-1β through HIF-1α. *Nature* 496: 238-242.

104.   Tennant, D. A., C. Frezza, E. D. MacKenzie, Q. D. Nguyen, L. Zheng, M. A. Selak, D. L. Roberts, C. Dive, D. G. Watson, and E. O. Aboagye. 2009. Reactivating HIF prolyl hydroxylases under hypoxia results in metabolic catastrophe and cell death. *Oncogene* 28: 4009-4021.

105.   Liu, P.-S., H. Wang, X. Li, T. Chao, T. Teav, S. Christen, G. Di Conza, W.-C. Cheng, C.-H. Chou, and M. Vavakova. 2017. α-ketoglutarate orchestrates macrophage activation through metabolic and epigenetic reprogramming. *Nature Immunol* 18: 985-994.

106.   Liu, T. F., C. M. Brown, M. El Gazzar, L. McPhail, P. Millet, A. Rao, V. T. Vachharajani, B. K. Yoza, and C. E. McCall. 2012. Fueling the flame: bioenergy couples metabolism and inflammation. *J Leukoc Biol* 92: 499-507.

107.   Cameron, A. M., A. Castoldi, D. E. Sanin, L. J. Flachsmann, C. S. Field, D. J. Puleston, R. L. Kyle, A. E. Patterson, F. Hässler, J. M. Buescher, B. Kelly, E. L. Pearce, and E. J. Pearce. 2019. Inflammatory macrophage dependence on NAD+ salvage is a consequence of reactive oxygen species–mediated DNA damage. *Nature Immunology* 20: 420-432.

108.   Jha, A. K., S. C.-C. Huang, A. Sergushichev, V. Lampropoulou, Y. Ivanova, E. Loginicheva, K. Chmielewski, K. M. Stewart, J. Ashall, B. Everts, E. J. Pearce, E. M. Driggers, and M. N. Artyomov. 2015. Network Integration of Parallel Metabolic and Transcriptional Data Reveals Metabolic Modules that Regulate Macrophage Polarization. *Immunity* 42: 419-430.

109.   Langston, P. K., A. Nambu, J. Jung, M. Shibata, H. I. Aksoylar, J. Lei, P. Xu, M. T. Doan, H. Jiang, M. R. MacArthur, X. Gao, Y. Kong, E. T. Chouchani, J. W. Locasale, N. W. Snyder, and T. Horng. 2019. Glycerol phosphate shuttle enzyme GPD2 regulates macrophage inflammatory responses. *Nat Immunol* 20: 1186-1195.

110.   Kory, N., J. Uit de Bos, S. van der Rijt, N. Jankovic, M. Güra, N. Arp, I. A. Pena, G. Prakash, S. H. Chan, T. Kunchok, C. A. Lewis, and D. M. Sabatini. 2020. MCART1/SLC25A51 is required for mitochondrial NAD transport. *Sci Adv* 6.

111.   Luongo, T. S., J. M. Eller, M. J. Lu, M. Niere, F. Raith, C. Perry, M. R. Bornstein, P. Oliphint, L. Wang, M. R. McReynolds, M. E. Migaud, J. D. Rabinowitz, F. B. Johnson, K. Johnsson, M. Ziegler, X. A. Cambronne, and J. A. Baur. 2020. SLC25A51 is a mammalian mitochondrial NAD(+) transporter. *Nature* 2020: 1-10.

112. Acín-Pérez, R., P. Fernández-Silva, M. L. Peleato, A. Pérez-Martos, and J. A. Enriquez. 2008. Respiratory active mitochondrial supercomplexes. *Mol Cell* 32: 529-539.

113. Garlid, K. D., M. Jabůrek, P. Ježek, and M. Vařecha. 2000. How do uncoupling proteins uncouple? *Biochim Biophys Acta* 1459: 383-389.

114. Garaude, J., R. Acín-Pérez, S. Martínez-Cano, M. Enamorado, M. Ugolini, E. Nistal-Villán, S. Hervás-Stubbs, P. Pelegrín, L. E. Sander, J. A. Enríquez, and D. Sancho. 2016. Mitochondrial respiratory-chain adaptations in macrophages contribute to antibacterial host defense. *Nat Immunol* 17: 1037-1045.

115. Liu, M., R. S. O'Connor, S. Trefely, K. Graham, N. W. Snyder, and G. L. Beatty. 2019. Metabolic rewiring of macrophages by CpG potentiates clearance of cancer cells and overcomes tumor-expressed CD47−mediated 'don't-eat-me' signal. *Nature Immunology* 20: 265-275.

116. Vats, D., L. Mukundan, J. I. Odegaard, L. Zhang, K. L. Smith, C. R. Morel, R. A. Wagner, D. R. Greaves, P. J. Murray, and A. Chawla. 2006. Oxidative metabolism and PGC-1beta attenuate macrophage-mediated inflammation. *Cell Metab* 4: 13-24.

117. Wang, T., J. F. Fahrmann, H. Lee, Y.-J. Li, S. C. Tripathi, C. Yue, C. Zhang, V. Lifshitz, J. Song, and Y. Yuan. 2018. JAK/STAT3-regulated fatty acid β-oxidation is critical for breast cancer stem cell self-renewal and chemoresistance. *Cell Metab* 27: 136-150.

118. Malandrino, M. I., R. Fucho, M. Weber, M. Calderon-Dominguez, J. F. Mir, L. Valcarcel, X. Escoté, M. Gómez-Serrano, B. Peral, L. Salvadó, S. Fernández-Veledo, N. Casals, M. Vázquez-Carrera, F. Villarroya, J. J. Vendrell, D. Serra, and L. Herrero. 2015. Enhanced fatty acid oxidation in adipocytes and macrophages reduces lipid-induced triglyceride accumulation and inflammation. *Am J Physiol Endocrinol Metab* 308: E756-769.

119. Wuggenig, P., B. Kaya, H. Melhem, C. K. Ayata, I. B. D. C. I. Swiss, P. Hruz, A. E. Sayan, H. Tsumura, M. Ito, J. Roux, and J. H. Niess. 2020. Loss of the branched-chain amino acid transporter CD98hc alters the development of colonic macrophages in mice. *Commun Biol* 3: 130.

120. Ko, J. H., A. Olona, A. E. Papathanassiu, N. Buang, K. S. Park, A. S. H. Costa, C. Mauro, C. Frezza, and J. Behmoaras. 2020. BCAT1 affects mitochondrial metabolism independently of leucine transamination in activated human macrophages. *J Cell Sci* 2020: jcs.247957.

121. Papathanassiu, A. E., J.-H. Ko, M. Imprialou, M. Bagnati, P. K. Srivastava, H. A. Vu, D. Cucchi, S. P. McAdoo, E. A. Ananieva, C. Mauro, and J. Behmoaras. 2017. BCAT1 controls metabolic reprogramming in activated human macrophages and is associated with inflammatory diseases. *Nat Commun* 8: 16040.

122. Nathan, C., and A. Cunningham-Bussel. 2013. Beyond oxidative stress: an immunologist's guide to reactive oxygen species. *Nature Reviews Immunology* 13: 349.

123. Holmström, K. M., and T. Finkel. 2014. Cellular mechanisms and physiological consequences of redox-dependent signalling. *Nature Reviews Molecular Cell Biology* 15: 411.

124. Agod, Z., T. Fekete, M. M. Budai, A. Varga, A. Szabo, H. Moon, I. Boldogh, T. Biro, A. Lanyi, A. Bacsi, and K. Pazmandi. 2017. Regulation of type I interferon responses by mitochondria-derived reactive oxygen species in plasmacytoid dendritic cells. *Redox Biol* 13: 633-645.

125. Takada, Y., A. Mukhopadhyay, G. C. Kundu, G. H. Mahabeleshwar, S. Singh, and B. B. Aggarwal. 2003. Hydrogen Peroxide Activates NF-κB through Tyrosine Phosphorylation

of IκBα and Serine Phosphorylation of p65: Evidence for the Involvement of IκBα Kinase and Syk Protein-Tyrosine Kinase. *J Biol Chem* 278: 24233-24241.

126. Indukuri, H., S. M. Castro, S.-M. Liao, L. A. Feeney, M. Dorsch, A. J. Coyle, R. P. Garofalo, A. R. Brasier, and A. Casola. 2006. Ikkε regulates viral-induced interferon regulatory factor-3 activation via a redox-sensitive pathway. *Virology* 353: 155-165.

127. Gonzalez-Dosal, R., K. A. Horan, S. H. Rahbek, H. Ichijo, Z. J. Chen, J. J. Mieyal, R. Hartmann, and S. R. Paludan. 2011. HSV infection induces production of ROS, which potentiate signaling from pattern recognition receptors: Role for S-glutathionylation of TRAF3 and 6. *PLOS Pathog* 7: e1002250.

128. Herb, M., A. Gluschko, K. Wiegmann, A. Farid, A. Wolf, O. Utermöhlen, O. Krut, M. Krönke, and M. Schramm. 2019. Mitochondrial reactive oxygen species enable proinflammatory signaling through disulfide linkage of NEMO. *Sci Signal* 12: eaar5926.

129. Bell, E. L., T. A. Klimova, J. Eisenbart, C. T. Moraes, M. P. Murphy, G. R. S. Budinger, and N. S. Chandel. 2007. The Qo site of the mitochondrial complex III is required for the transduction of hypoxic signaling via reactive oxygen species production. *J Cell Biol* 177: 1029-1036.

130. Kale, J., E. J. Osterlund, and D. W. Andrews. 2018. BCL-2 family proteins: changing partners in the dance towards death. *Cell Death Differ* 25: 65-80.

131. Zhang, Q., M. Raoof, Y. Chen, Y. Sumi, T. Sursal, W. Junger, K. Brohi, K. Itagaki, and C. J. Hauser. 2010. Circulating mitochondrial DAMPs cause inflammatory responses to injury. *Nature* 464: 104.

132. Zhang, Q., K. Itagaki, and C. J. Hauser. 2010. Mitochondrial DNA is released by shock and activates neutrophils via p38 map kinase. *Shock* 34: 55-59.

133. Nakahira, K., J. A. Haspel, V. A. K. Rathinam, S.-J. Lee, T. Dolinay, H. C. Lam, J. A. Englert, M. Rabinovitch, M. Cernadas, and H. P. Kim. 2011. Autophagy proteins regulate innate immune responses by inhibiting the release of mitochondrial DNA mediated by the NALP3 inflammasome. *Nat Immunol* 12: 222-230.

134. Warburg, O. 1956. On the origin of cancer cells. *Science* 123: 309-314.

135. Warburg, O., K. Gawehn, and A. W. Geissler. 1958. Metabolism of leukocytes. *Z Naturforsch B* 13b: 515-516.

136. Deberardinis, R. J., N. Sayed, D. Ditsworth, and C. B. Thompson. 2008. Brick by brick: metabolism and tumor cell growth. *Curr Opin Genet Dev* 18: 54-61.

137. Kesarwani, P., A. K. Murali, A. A. Al-Khami, and S. Mehrotra. 2013. Redox regulation of T-cell function: from molecular mechanisms to significance in human health and disease. *Antioxid. Redox Signal.* 18: 1497-1534.

138. Wang, H., Y. Hsieh, W. Cheng, C. Lin, Y. Lin, S. Yang, C. Chen, Y. Izumiya, J. Yu, H. Kung, and W. Wang. 2014. JMJD5 regulates PKM2 nuclear translocation and reprograms HIF-1α–mediated glucose metabolism. *Proc. Natl. Acad. Sci. U. S. A* 111: 279-284.

139. Wang, H., H. Flach, M. Onizawa, L. Wei, M. T. McManus, and A. Weiss. 2014. Negative regulation of Hif1a expression and TH17 differentiation by the hypoxia-regulated microRNA miR-210. *Nat. Immunol.* 15: 393-401.

140. Murray, Peter J., Judith E. Allen, Subhra K. Biswas, Edward A. Fisher, Derek W. Gilroy, S. Goerdt, S. Gordon, John A. Hamilton, Lionel B. Ivashkiv, T. Lawrence, M. Locati, A. Mantovani, Fernando O. Martinez, J.-L. Mege, David M. Mosser, G. Natoli, Jeroen P. Saeij, Joachim L. Schultze, Kari A. Shirey, A. Sica, J. Suttles, I. Udalova, Jo A.

van Ginderachter, Stefanie N. Vogel, and Thomas A. Wynn. 2014. Macrophage Activation and Polarization: Nomenclature and Experimental Guidelines. *Immunity* 41: 14-20.

141. Mantovani, A., A. Sica, S. Sozzani, P. Allavena, A. Vecchi, and M. Locati. 2004. The chemokine system in diverse forms of macrophage activation and polarization. *Trends in Immunology* 25: 677-686.

142. Gordon, S. 2003. Alternative activation of macrophages. *Nat Rev Immunol* 3: 23-35.

143. Mills, E. L., B. Kelly, A. Logan, A. S. H. Costa, M. Varma, C. E. Bryant, P. Tourlomousis, J. H. M. Däbritz, E. Gottlieb, I. Latorre, S. C. Corr, G. McManus, D. Ryan, H. T. Jacobs, M. Szibor, R. J. Xavier, T. Braun, C. Frezza, M. P. Murphy, and L. A. O'Neill. 2016. Succinate dehydrogenase supports metabolic repurposing of mitochondria to drive inflammatory macrophages. *Cell* 167: 457-470.e413.

144. Palsson-McDermott, E. M., A. M. Curtis, G. Goel, M. A. R. Lauterbach, F. J. Sheedy, L. E. Gleeson, M. W. M. van den Bosch, S. R. Quinn, R. Domingo-Fernandez, D. G. W. Johnston, J.-k. Jiang, W. J. Israelsen, J. Keane, C. Thomas, C. Clish, M. Vander Heiden, R. J. Xavier, and L. A. J. O'Neill. 2015. Pyruvate kinase M2 regulates Hif-1α activity and IL-1β induction and is a critical determinant of the warburg effect in LPS-activated macrophages. *Cell Metab.* 21: 65-80.

145. Sag, D., D. Carling, R. D. Stout, and J. Suttles. 2008. Adenosine 5'-monophosphate-activated protein kinase promotes macrophage polarization to an anti-inflammatory functional phenotype. *Journal of immunology (Baltimore, Md. : 1950)* 181: 8633-8641.

146. Steinberg, G. R., and J. D. Schertzer. 2014. AMPK promotes macrophage fatty acid oxidative metabolism to mitigate inflammation: implications for diabetes and cardiovascular disease. *Immunology & Cell Biology* 92: 340-345.

147. Stout, R. D., C. Jiang, B. Matta, I. Tietzel, S. K. Watkins, and J. Suttles. 2005. Macrophages Sequentially Change Their Functional Phenotype in Response to Changes in Microenvironmental Influences. *The Journal of Immunology* 175: 342-349.

148. Van den Bossche, J., J. Baardman, Natasja A. Otto, S. van der Velden, Annette E. Neele, Susan M. van den Berg, R. Luque-Martin, H.-J. Chen, Marieke C. S. Boshuizen, M. Ahmed, Marten A. Hoeksema, Alex F. de Vos, and Menno P. J. de Winther. 2016. Mitochondrial Dysfunction Prevents Repolarization of Inflammatory Macrophages. *Cell Rep* 17: 684-696.

149. Cramer, T., Y. Yamanishi, B. E. Clausen, I. Förster, R. Pawlinski, N. Mackman, V. H. Haase, R. Jaenisch, M. Corr, V. Nizet, G. S. Firestein, H.-P. Gerber, N. Ferrara, and R. S. Johnson. 2003. HIF-1α is essential for myeloid cell-mediated inflammation. *Cell* 112: 645-657.

150. Maedera, S., T. Mizuno, H. Ishiguro, T. Ito, T. Soga, and H. Kusuhara. 2019. GLUT6 is a lysosomal transporter that is regulated by inflammatory stimuli and modulates glycolysis in macrophages. *FEBS Lett* 593: 195-208.

151. Fukuzumi, M., H. Shinomiya, Y. Shimizu, K. Ohishi, and S. Utsumi. 1996. Endotoxin-induced enhancement of glucose influx into murine peritoneal macrophages via GLUT1. *Infection and Immunity* 64: 108-112.

152. Varanasi, S. K., D. Donohoe, U. Jaggi, and B. T. Rouse. 2017. Manipulating Glucose Metabolism during Different Stages of Viral Pathogenesis Can Have either Detrimental or Beneficial Effects. *J Immunol*.

153. Liu, L., Y. Lu, J. Martinez, Y. Bi, G. Lian, T. Wang, S. Milasta, J. Wang, M. Yang, G. Liu, D. R. Green, and R. Wang. 2016. Proinflammatory signal suppresses proliferation and

shifts macrophage metabolism from Myc-dependent to HIF1α-dependent. *Proc Natl Acad Sci U S A* 113: 1564.

154.   Tan, Z., N. Xie, H. Cui, D. R. Moellering, E. Abraham, V. J. Thannickal, and G. Liu. 2015. Pyruvate Dehydrogenase Kinase 1 Participates in Macrophage Polarization via Regulating Glucose Metabolism. *J Immunol* 194: 6082.

155.   Chang, C. H., J. D. Curtis, L. B. Maggi, B. Faubert, A. V. Villarino, D. O'sullivan, S. C. Huang, G. L. van der Windt, J. Blagih, J. Qiu, J. D. Weber, E. J. Pearce, R. G. Jones, and E. L. Pearce. 2013. Posttranscriptional control of T cell effector function by aerobic glycolysis. *Cell* 153.

156.   Blagih, J., F. Coulombe, Emma E. Vincent, F. Dupuy, G. Galicia-Vázquez, E. Yurchenko, Thomas C. Raissi, Gerritje J. W. van der Windt, B. Viollet, Erika L. Pearce, J. Pelletier, Ciriaco A. Piccirillo, Connie M. Krawczyk, M. Divangahi, and Russell G. Jones. 2015. The Energy Sensor AMPK Regulates T Cell Metabolic Adaptation and Effector Responses In Vivo. *Immunity* 42: 41-54.

157.   Galván-Peña, S., R. G. Carroll, C. Newman, E. C. Hinchy, E. Palsson-McDermott, E. K. Robinson, S. Covarrubias, A. Nadin, A. M. James, M. Haneklaus, S. Carpenter, V. P. Kelly, M. P. Murphy, L. K. Modis, and L. A. O'Neill. 2019. Malonylation of GAPDH is an inflammatory signal in macrophages. *Nature Commun* 10: 338-338.

158.   Zhang, Z., X. Deng, Y. Liu, Y. Liu, L. Sun, and F. Chen. 2019. PKM2, function and expression and regulation. *Cell Biosci* 9: 52.

159.   Ham, M., J.-W. Lee, A. H. Choi, H. Jang, G. Choi, J. Park, C. Kozuka, D. D. Sears, H. Masuzaki, and J. B. Kim. 2013. Macrophage glucose-6-phosphate dehydrogenase stimulates proinflammatory responses with oxidative stress. *Mol Cell Biol* 33: 2425-2435.

160.   Minhas, P. S., L. Liu, P. K. Moon, A. U. Joshi, C. Dove, S. Mhatre, K. Contrepois, Q. Wang, B. A. Lee, M. Coronado, D. Bernstein, M. P. Snyder, M. Migaud, R. Majeti, D. Mochly-Rosen, J. D. Rabinowitz, and K. I. Andreasson. 2019. Macrophage de novo NAD(+) synthesis specifies immune function in aging and inflammation. *Nat Immunol* 20: 50-63.

161.   De Souza, D. P., A. Achuthan, M. K. Lee, K. J. Binger, M.-C. Lee, S. Davidson, D. L. Tull, M. J. McConville, A. D. Cook, A. J. Murphy, J. A. Hamilton, and A. J. Fleetwood. 2019. Autocrine IFN-I inhibits isocitrate dehydrogenase in the TCA cycle of LPS-stimulated macrophages. *The Journal of clinical investigation* 129: 4239-4244.

162.   Swain, A., M. Bambouskova, H. Kim, P. S. Andhey, D. Duncan, K. Auclair, V. Chubukov, D. M. Simons, T. P. Roddy, K. M. Stewart, and M. N. Artyomov. 2020. Comparative evaluation of itaconate and its derivatives reveals divergent inflammasome and type I interferon regulation in macrophages. *Nat Metab* 2: 594-602.

163.   Infantino, V., V. Iacobazzi, F. Palmieri, and A. Menga. 2013. ATP-citrate lyase is essential for macrophage inflammatory response. *Biochem. Biophys. Res. Commun.* 440: 105-111.

164.   Lampropoulou, V., A. Sergushichev, M. Bambouskova, S. Nair, E. E. Vincent, E. Loginicheva, L. Cervantes-Barragan, X. Ma, S. C.-C. Huang, T. Griss, C. J. Weinheimer, S. Khader, G. J. Randolph, E. J. Pearce, R. G. Jones, A. Diwan, M. S. Diamond, and M. N. Artyomov. 2016. Itaconate Links Inhibition of Succinate Dehydrogenase with Macrophage Metabolic Remodeling and Regulation of Inflammation. *Cell Metab.* 24: 158-166.

165.   Michelucci, A., T. Cordes, J. Ghelfi, A. Pailot, N. Reiling, O. Goldmann, T. Binz, A. Wegner, A. Tallam, A. Rausell, M. Buttini, C. L. Linster, E. Medina, R. Balling, and K. Hiller. 2013. Immune-responsive gene 1 protein links metabolism to immunity by

catalyzing itaconic acid production. *Proceedings of the National Academy of Sciences* 110: 7820.

166. Kobayashi, E. H., T. Suzuki, R. Funayama, T. Nagashima, M. Hayashi, H. Sekine, N. Tanaka, T. Moriguchi, H. Motohashi, K. Nakayama, and M. Yamamoto. 2016. Nrf2 suppresses macrophage inflammatory response by blocking proinflammatory cytokine transcription. *Nat Commun* 7: 11624.

167. Bambouskova, M., L. Gorvel, V. Lampropoulou, A. Sergushichev, E. Loginicheva, K. Johnson, D. Korenfeld, M. E. Mathyer, H. Kim, L.-H. Huang, D. Duncan, H. Bregman, A. Keskin, A. Santeford, R. S. Apte, R. Sehgal, B. Johnson, G. K. Amarasinghe, M. P. Soares, T. Satoh, S. Akira, T. Hai, C. de Guzman Strong, K. Auclair, T. P. Roddy, S. A. Biller, M. Jovanovic, E. Klechevsky, K. M. Stewart, G. J. Randolph, and M. N. Artyomov. 2018. Electrophilic properties of itaconate and derivatives regulate the IκBζ-ATF3 inflammatory axis. *Nature* 556: 501-504.

168. Cordes, T., M. Wallace, A. Michelucci, A. S. Divakaruni, S. C. Sapcariu, C. Sousa, H. Koseki, P. Cabrales, A. N. Murphy, K. Hiller, and C. M. Metallo. 2016. Immunoresponsive Gene 1 and Itaconate Inhibit Succinate Dehydrogenase to Modulate Intracellular Succinate Levels. *J Biol Chem* 291: 14274-14284.

169. Mills, E. L., D. G. Ryan, H. A. Prag, D. Dikovskaya, D. Menon, Z. Zaslona, M. P. Jedrychowski, A. S. H. Costa, M. Higgins, E. Hams, J. Szpyt, M. C. Runtsch, M. S. King, J. F. McGouran, R. Fischer, B. M. Kessler, A. F. McGettrick, M. M. Hughes, R. G. Carroll, L. M. Booty, E. V. Knatko, P. J. Meakin, M. L. J. Ashford, L. K. Modis, G. Brunori, D. C. Sévin, P. G. Fallon, S. T. Caldwell, E. R. S. Kunji, E. T. Chouchani, C. Frezza, A. T. Dinkova-Kostova, R. C. Hartley, M. P. Murphy, and L. A. O'Neill. 2018. Itaconate is an anti-inflammatory metabolite that activates Nrf2 via alkylation of KEAP1. *Nature* 556: 113-117.

170. West, A. P., I. E. Brodsky, C. Rahner, D. K. Woo, H. Erdjument-Bromage, P. Tempst, M. C. Walsh, Y. Choi, G. S. Shadel, and S. Ghosh. 2011. TLR signalling augments macrophage bactericidal activity through mitochondrial ROS. *Nature* 472: 476-480.

171. Chua, Y. L., E. Dufour, E. P. Dassa, P. Rustin, H. T. Jacobs, C. T. Taylor, and T. Hagen. 2010. Stabilization of Hypoxia-inducible factor-1α protein in hypoxia occurs independently of mitochondrial reactive oxygen species production. *J Biol Chem* 285: 31277-31284.

172. Brüne, B., and J. Zhou. 2007. Hypoxia-inducible factor-1α under the control of Nitric oxide. *Methods Enzymol* 435: 463-478.

173. Kelly, B., G. M. Tannahill, M. P. Murphy, and L. A. J. O'Neill. 2015. Metformin Inhibits the Production of Reactive Oxygen Species from NADH:Ubiquinone Oxidoreductase to Limit Induction of Interleukin-1β (IL-1β) and Boosts Interleukin-10 (IL-10) in Lipopolysaccharide (LPS)-activated Macrophages. *J Biol Chem* 290: 20348-20359.

174. Ip, W. K. E., N. Hoshi, D. S. Shouval, S. Snapper, and R. Medzhitov. 2017. Anti-inflammatory effect of IL-10 mediated by metabolic reprogramming of macrophages. *Science* 356: 513-519.

175. Arts, R. J. W., B. Novakovic, R. Ter Horst, A. Carvalho, S. Bekkering, E. Lachmandas, F. Rodrigues, R. Silvestre, S.-C. Cheng, S.-Y. Wang, E. Habibi, L. G. Gonçalves, I. Mesquita, C. Cunha, A. van Laarhoven, F. L. van de Veerdonk, D. L. Williams, J. W. M. van der Meer, C. Logie, L. A. O'Neill, C. A. Dinarello, N. P. Riksen, R. van Crevel, C. Clish, R. A. Notebaart, L. A. B. Joosten, H. G. Stunnenberg, R. J. Xavier, and M. G. Netea. 2016.

Glutaminolysis and fumarate accumulation integrate immunometabolic and epigenetic programs in trained immunity. *Cell Metab* 24: 807-819.

176. Su, Y., T. P. Miettinen, L. Mu, E. Mirek, S. R. Manalis, T. G. Anthony, H. Sesaki, and J. Chen. 2020. Disassembly of ETC Complexes Drives Macrophage Inflammatory Responses by Reprogramming Cellular Metabolism and Translation [Manuscirpt submitted for publication]. *Cell Rep* Available at SSRN: https://ssrn.com/abstract=3611881: 1-54.

177. Zhou, R., A. S. Yazdi, P. Menu, and J. Tschopp. 2011. A role for mitochondria in NLRP3 inflammasome activation. *Nature* 469: 221-225.

178. Rakkola, R., S. Matikainen, and T. A. Nyman. 2007. Proteome analysis of human macrophages reveals the upregulation of manganese-containing superoxide dismutase after toll-like receptor activation. *Proteomics* 7: 378-384.

179. Emre, Y., C. Hurtaud, T. Nübel, F. Criscuolo, D. Ricquier, and A.-M. Cassard-Doulcier. 2007. Mitochondria contribute to LPS-induced MAPK activation via uncoupling protein UCP2 in macrophages. *Biochemical Journal* 402: 271-278.

180. Kizaki, T., K. Suzuki, Y. Hitomi, N. Taniguchi, D. Saitoh, K. Watanabe, K. Onoé, N. K. Day, R. A. Good, and H. Ohno. 2002. Uncoupling protein 2 plays an important role in nitric oxide production of lipopolysaccharide-stimulated macrophages. *Proceedings of the National Academy of Sciences* 99: 9392-9397.

181. Arsenijevic, D., H. Onuma, C. Pecqueur, S. Raimbault, B. S. Manning, B. Miroux, E. Couplan, M.-C. Alves-Guerra, M. Goubern, R. Surwit, F. Bouillaud, D. Richard, S. Collins, and D. Ricquier. 2000. Disruption of the uncoupling protein-2 gene in mice reveals a role in immunity and reactive oxygen species production. *Nat Genet* 26: 435-439.

182. Dreißig, M. D. M., R. Hammermann, J. Mössner, M. Göthert, and K. Racké. 2000. In rat alveolar macrophages lipopolysaccharides exert divergent effects on the transport of the cationic amino acids L-arginine and L-ornithine. *Naunyn Schmiedebergs Arch Pharmacol* 361: 621-628.

183. Sun, C., L. Sun, H. Ma, J. Peng, Y. Zhen, K. Duan, G. Liu, W. Ding, and Y. Zhao. 2012. The phenotype and functional alterations of macrophages in mice with hyperglycemia for long term. *J Cell Physiol.* 227: 1670-1679.

184. Everts, B., E. Amiel, G. J. W. van der Windt, T. C. Freitas, R. Chott, K. E. Yarasheski, E. L. Pearce, and E. J. Pearce. 2012. Commitment to glycolysis sustains survival of NO-producing inflammatory dendritic cells. *Blood* 120: 1422-1431.

185. Palmieri, E. M., C. McGinity, D. A. Wink, and D. W. McVicar. 2020. Nitric oxide in macrophage immunometabolism: Hiding in plain sight. *Metabolites* 10: 429.

186. Rodriguez, A. E., G. S. Ducker, L. K. Billingham, C. A. Martinez, N. Mainolfi, V. Suri, A. Friedman, M. G. Manfredi, S. E. Weinberg, J. D. Rabinowitz, and N. S. Chandel. 2019. Serine metabolism supports macrophage IL-1β production. *Cell Metab* 29: 1003-1011.e1004.

187. Yu, W., Z. Wang, K. Zhang, Z. Chi, T. Xu, D. Jiang, S. Chen, W. Li, X. Yang, X. Zhang, Y. Wu, and D. Wang. 2019. One-Carbon metabolism supports S-Adenosylmethionine and histone methylation to drive inflammatory macrophages. *Mol Cell* 75: 1147-1160.e1145.

188. Yoon, B. R., Y.-J. Oh, S. W. Kang, E. B. Lee, and W.-W. Lee. 2018. Role of SLC7A5 in metabolic reprogramming of Human monocyte/macrophage immune responses. *Front Immunol* 9: 53.

189. Dang, E. V., J. G. McDonald, D. W. Russell, and J. G. Cyster. 2017. Oxysterol Restraint of Cholesterol Synthesis Prevents AIM2 Inflammasome Activation. *Cell* 171: 1057-1071.e1011.

190. Araldi, E., M. Fernández-Fuertes, A. Canfrán-Duque, W. Tang, G. W. Cline, J. Madrigal-Matute, J. S. Pober, M. A. Lasunción, D. Wu, C. Fernández-Hernando, and Y. Suárez. 2017. Lanosterol Modulates TLR4-Mediated Innate Immune Responses in Macrophages. *Cell Reports* 19: 2743-2755.

191. Lopes-Virella, M. F., R. L. Klein, and H. C. Stevenson. 1987. Low density lipoprotein metabolism in human macrophages stimulated with microbial or microbial-related products. *Arteriosclerosis* 7: 176-184.

192. Hsieh, W.-Y., Q. D. Zhou, A. G. York, K. J. Williams, P. O. Scumpia, E. B. Kronenberger, X. P. Hoi, B. Su, X. Chi, V. L. Bui, E. Khialeeva, A. Kaplan, Y. M. Son, A. S. Divakaruni, J. Sun, S. T. Smale, R. A. Flavell, and S. J. Bensinger. 2020. Toll-Like Receptors Induce Signal-Specific Reprogramming of the Macrophage Lipidome. *Cell Metabolism* 32: 128-143.e125.

193. Zhou, Q. D., X. Chi, M. S. Lee, W. Y. Hsieh, J. J. Mkrtchyan, A.-C. Feng, C. He, A. G. York, V. L. Bui, and E. B. Kronenberger. 2020. Interferon-mediated reprogramming of membrane cholesterol to evade bacterial toxins. *Nat Immunol*: 1-10.

194. Oishi, Y., N. J. Spann, V. M. Link, E. D. Muse, T. Strid, C. Edillor, M. J. Kolar, T. Matsuzaka, S. Hayakawa, J. Tao, M. U. Kaikkonen, A. F. Carlin, M. T. Lam, I. Manabe, H. Shimano, A. Saghatelian, and C. K. Glass. 2017. SREBP1 contributes to resolution of pro-inflammatory TLR4 signaling by reprogramming fatty acid metabolism. *Cell Metab* 25: 412-427.

195. Weigert, A., A. von Knethen, D. Thomas, I. Faria, D. Namgaladze, E. Zezina, D. Fuhrmann, A. Petcherski, D. M. z. Heringdorf, H. H. Radeke, and B. Brüne. 2019. Sphingosine kinase 2 is a negative regulator of inflammatory macrophage activation. *Biochimica et Biophysica Acta (BBA) - Molecular and Cell Biology of Lipids* 1864: 1235-1246.

196. Joshi, J. C., B. Joshi, I. Rochford, S. Rayees, M. Z. Akhter, S. Baweja, K. R. Chava, M. Tauseef, H. Abdelkarim, V. Natarajan, V. Gaponenko, and D. Mehta. 2020. SPHK2-generated S1P in CD11b(+) macrophages blocks STING to suppress the inflammatory function of alveolar macrophages. *Cell Rep* 30: 4096-4109.e4095.

197. Fritsch, S. D., and T. Weichhart. 2016. Effects of Interferons and Viruses on Metabolism. *Front. Immunol.* 7: 630.

198. Zhang, S., J. Carriere, X. Lin, N. Xie, and P. Feng. 2018. Interplay between cellular metabolism and cytokine responses during viral infection. *Viruses* 10: 521.

199. Yu, Y., T. G. Maguire, and J. C. Alwine. 2011. Human cytomegalovirus activates glucose transporter 4 expression to increase glucose uptake during infection. *J Virol* 85: 1573-1580.

200. Munger, J., B. D. Bennett, A. Parikh, X. J. Feng, J. McArdle, H. A. Rabitz, T. Shenk, and J. D. Rabinowitz. 2008. Systems-level metabolic flux profiling identifies fatty acid synthesis as a target for antiviral therapy. *Nat Biotechnol* 26.

201. Ritter, J. B., A. S. Wahl, S. Freund, Y. Genzel, and U. Reichl. 2010. Metabolic effects of influenza virus infection in cultured animal cells: intra- and extracellular metabolite profiling. *BMC Syst Biol* 4.

202. Deshmane, S. L., S. Amini, S. Sen, K. Khalili, and B. E. Sawaya. 2011. Regulation of the HIV-1 promoter by HIF-1α and Vpr proteins. *Virol J* 8: 477.

203. Ripoli, M., A. D'Aprile, G. Quarato, M. Sarasin-Filipowicz, J. Gouttenoire, R. Scrima, O. Cela, D. Boffoli, M. H. Heim, D. Moradpour, N. Capitanio, and C. Piccoli. 2010. Hepatitis C virus-linked mitochondrial dysfunction promotes Hypoxia-inducible factor 1α-mediated glycolytic adaptation. *J Virol* 84: 647-660.

204. Palmer, C. S., T. Hussain, G. Duette, T. J. Weller, M. Ostrowski, I. Sada-Ovalle, and S. M. Crowe. 2016. Regulators of Glucose Metabolism in CD4+ and CD8+ T Cells. *International Reviews of Immunology* 35: 477-488.

205. Palmer, C. S., G. A. Duette, M. C. E. Wagner, D. C. Henstridge, S. Saleh, C. Pereira, J. Zhou, D. Simar, S. R. Lewin, M. Ostrowski, J. M. McCune, and S. M. Crowe. 2017. Metabolically active CD4+ T cells expressing Glut1 and OX40 preferentially harbor HIV during in vitro infection. *Febs Letters* 591: 3319-3332.

206. Anzinger, J. J., T. R. Butterfield, M. Gouillou, J. M. McCune, S. M. Crowe, and C. S. Palmer. 2018. Glut1 Expression Level on Inflammatory Monocytes is Associated With Markers of Cardiovascular Disease Risk in HIV-Infected Individuals. *J Acquir Immune Defic Syndr* 77.

207. Duette, G., P. Pereyra Gerber, J. Rubione, P. S. Perez, A. L. Landay, S. M. Crowe, Z. Liao, K. W. Witwer, M. P. Holgado, J. Salido, J. Geffner, O. Sued, C. S. Palmer, and M. Ostrowski. 2018. Induction of HIF-1α by HIV-1 infection in CD4(+) T cells promotes viral replication and drives extracellular vesicle-mediated inflammation. *mBio* 9: e00757-00718.

208. Thai, M., S. K. Thaker, J. Feng, Y. Du, H. Hu, T. T. Wu, T. G. Graeber, D. Braas, and H. R. Christofk. 2015. MYC-induced reprogramming of glutamine catabolism supports optimal virus replication. *Nature communications* 6: 1-9.

209. Vastag, L., E. Koyuncy, S. L. Grady, T. E. Shenk, and J. D. Rabinowitz. 2011. Divergent effects of human cytomegalovirus and herpes simplex virus-1 on cellular metabolism. *PLoS Pathog.* 7: e1002124.

210. Grady, S. L., J. G. Purdy, J. D. Rabinowitz, and T. Shenk. 2013. Argininosuccinate synthetase 1 depletion produces a metabolic state conducive to herpes simplex virus 1 infection. *Proc Natl Acad Sci U S A* 110.

211. Sun, B., K. B. Sundström, J. J. Chew, P. Bist, E. S. Gan, H. C. Tan, K. C. Goh, T. Chawla, C. K. Tang, and E. E. Ooi. 2017. Dengue virus activates cGAS through the release of mitochondrial DNA. *Sci Rep* 7: 1-8.

212. Yu, C.-Y., J.-J. Liang, J.-K. Li, Y.-L. Lee, B.-L. Chang, C.-I. Su, W.-J. Huang, M. M. C. Lai, and Y.-L. Lin. 2015. Dengue virus impairs mitochondrial fusion by cleaving mitofusins. *PLoS pathog* 11: e1005350.

213. Chatel-Chaix, L., M. Cortese, I. Romero-Brey, S. Bender, C. J. Neufeldt, W. Fischl, P. Scaturro, N. Schieber, Y. Schwab, and B. Fischer. 2016. Dengue virus perturbs mitochondrial morphodynamics to dampen innate immune responses. *Cell Host Microbe* 20: 342-356.

214. Kim, S.-J., M. Khan, J. Quan, A. Till, S. Subramani, and A. Siddiqui. 2013. Hepatitis B virus disrupts mitochondrial dynamics: induces fission and mitophagy to attenuate apoptosis. *PLoS Pathog* 9: e1003722.

215. Peng, Y.-T., P. Chen, R.-Y. Ouyang, and L. Song. 2015. Multifaceted role of prohibitin in cell survival and apoptosis. *Apoptosis* 20: 1135-1149.

216. Tsutsumi, T., M. Matsuda, H. Aizaki, K. Moriya, H. Miyoshi, H. Fujie, Y. Shintani, H. Yotsuyanagi, T. Miyamura, T. Suzuki, and K. Koike. 2009. Proteomics analysis of

mitochondrial proteins reveals overexpression of a mitochondrial protein chaperon, prohibitin, in cells expressing hepatitis C virus core protein. *Hepatology* 50: 378-386.

217. Deng, L., T. Adachi, K. Kitayama, Y. Bungyoku, S. Kitazawa, S. Ishido, I. Shoji, and H. Hotta. 2008. Hepatitis C virus infection induces apoptosis through a Bax-triggered, mitochondrion-mediated, Caspase 3-dependent pathway. *J Virol* 82: 10375.

218. Korenaga, M., T. Wang, Y. Li, L. A. Showalter, T. Chan, J. Sun, and S. A. Weinman. 2005. Hepatitis C virus core protein inhibits mitochondrial electron transport and increases reactive oxygen species (ROS) production. *J Biol Chem* 280: 37481-37488.

219. Nomura-Takigawa, Y., M. Nagano-Fujii, L. Deng, S. Kitazawa, S. Ishido, K. Sada, and H. Hotta. 2006. Non-structural protein 4A of Hepatitis C virus accumulates on mitochondria and renders the cells prone to undergoing mitochondria-mediated apoptosis. *J Gen Virol* 87: 1935-1945.

220. Valle-Casuso, J. C., M. Angin, S. Volant, C. Passaes, V. Monceaux, A. Mikhailova, K. Bourdic, V. Avettand-Fenoel, F. Boufassa, M. Sitbon, O. Lambotte, M. I. Thoulouze, M. Müller-Trutwin, N. Chomont, and A. Sáez-Cirión. 2019. Cellular metabolism is a major determinant of HIV-1 reservoir seeding in CD4(+) T cells and offers an opportunity to tackle infection. *Cell Metab* 29: 611-626 e615.

221. Castellano, P., L. Prevedel, S. Valdebenito, and E. A. Eugenin. 2019. HIV infection and latency induce a unique metabolic signature in human macrophages. *Sci Rep* 9: 3941.

222. Lévy, P. L., S. Duponchel, H. Eischeid, J. Molle, M. Michelet, G. Diserens, M. Vermathen, P. Vermathen, J. F. Dufour, and H. P. Dienes. 2017. Hepatitis C virus infection triggers a tumor-like glutamine metabolism. *Hepatology* 65: 789-803.

223. Fontaine, K. A., R. Camarda, and M. Lagunoff. 2014. Vaccinia virus requires glutamine but not glucose for efficient replication. *Journal of virology* 88: 4366-4374.

224. Jordan, T. X., and G. Randall. 2017. Dengue virus activates the AMP kinase-mTOR axis to stimulate a proviral lipophagy. *J Virol* 91.

225. Rasheed, S., J. S. Yan, A. Lau, and A. S. Chan. 2008. HIV Replication Enhances Production of Free Fatty Acids, Low Density Lipoproteins and Many Key Proteins Involved in Lipid Metabolism: A Proteomics Study. *PLOS ONE* 3: e3003.

226. Yu, Y., T. G. Maguire, and J. C. Alwine. 2012. Human cytomegalovirus infection induces adipocyte-like lipogenesis through activation of sterol regulatory element binding protein 1. *J Virol* 86: 2942-2949.

227. Heaton, N. S., R. Perera, K. L. Berger, S. Khadka, D. J. LaCount, R. J. Kuhn, and G. Randall. 2010. Dengue virus nonstructural protein 3 redistributes fatty acid synthase to sites of viral replication and increases cellular fatty acid synthesis. *Proceedings of the National Academy of Sciences* 107: 17345-17350.

228. Greseth, M. D., and P. Traktman. 2014. De novo Fatty Acid Biosynthesis Contributes Significantly to Establishment of a Bioenergetically Favorable Environment for Vaccinia Virus Infection. *PLOS Pathogens* 10: e1004021.

229. Perlemuter, G., A. Sabile, P. Letteron, G. Vona, A. Topilco, Y. Chrétien, K. Koike, D. Pessayre, J. Chapman, and G. Barba. 2002. Hepatitis C virus core protein inhibits microsomal triglyceride transfer protein activity and very low density lipoprotein secretion: a model of viral-related steatosis. *FASEB J* 16: 185-194.

230. Moriishi, K., R. Mochizuki, K. Moriya, H. Miyamoto, Y. Mori, T. Abe, S. Murata, K. Tanaka, T. Miyamura, and T. Suzuki. 2007. Critical role of PA28γ in hepatitis C virus-

associated steatogenesis and hepatocarcinogenesis. *Proc Natl Acad Sci U S A* 104: 1661-1666.

231. Oem, J.-K., C. Jackel-Cram, Y.-P. Li, Y. Zhou, J. Zhong, H. Shimano, L. A. Babiuk, and Q. Liu. 2008. Activation of sterol regulatory element-binding protein 1c and fatty acid synthase transcription by hepatitis C virus non-structural protein 2. *J Gen Virol* 89: 1225.

232. Waris, G., D. J. Felmlee, F. Negro, and A. Siddiqui. 2007. Hepatitis C virus induces proteolytic cleavage of Sterol Regulatory Element Binding Proteins and stimulates their phosphorylation via oxidative stress. *J Virol* 81: 8122.

233. de Veer, M. J., M. Holko, M. Frevel, E. Walker, S. Der, J. M. Paranjape, R. H. Silverman, and B. R. G. Williams. 2001. Functional classification of interferon-stimulated genes identified using microarrays. *J. Leukoc. Biol.* 69: 912-920.

234. Honda, K., A. Takaoka, and T. Taniguchi. 2006. Type I Inteferon Gene Induction by the Interferon Regulatory Factor Family of Transcription Factors. *Immunity* 25: 349-360.

235. York, Autumn G., Kevin J. Williams, Joseph P. Argus, Quan D. Zhou, G. Brar, L. Vergnes, Elizabeth E. Gray, A. Zhen, Nicholas C. Wu, Douglas H. Yamada, Cameron R. Cunningham, Elizabeth J. Tarling, Moses Q. Wilks, D. Casero, David H. Gray, Amy K. Yu, Eric S. Wang, David G. Brooks, R. Sun, Scott G. Kitchen, T.-T. Wu, K. Reue, Daniel B. Stetson, and Steven J. Bensinger. 2015. Limiting Cholesterol Biosynthetic Flux Spontaneously Engages Type I IFN Signaling. *Cell* 163: 1716-1729.

236. Jiang, H., H. Shi, M. Sun, Y. Wang, Q. Meng, P. Guo, Y. Cao, J. Chen, X. Gao, E. Li, and J. Liu. 2016. PFKFB3-Driven Macrophage Glycolytic Metabolism Is a Crucial Component of Innate Antiviral Defense. *J. Immunol.* 197: 2880-2890.

237. Li, T., X. Li, K. S. Attri, C. Liu, L. Li, L. E. Herring, J. M. Asara, Y. L. Lei, P. K. Singh, C. Gao, and H. Wen. 2018. O-GlcNAc Transferase Links Glucose Metabolism to MAVS-Mediated Antiviral Innate Immunity. *Cell Host & Microbe* 24: 791-803.e796.

238. Zhao, Y., X. Sun, X. Nie, L. Sun, T.-s. Tang, D. Chen, and Q. Sun. 2012. COX5B Regulates MAVS-mediated Antiviral Signaling through Interaction with ATG5 and Repressing ROS Production. *PLOS Pathogens* 8: e1003086.

239. Koshiba, T., K. Yasukawa, Y. Yanagi, and S.-i. Kawabata. 2011. Mitochondrial membrane potential is required for MAVS-mediated antiviral signaling. *Sci Signal* 4: ra7.

240. Tal, M. C., M. Sasai, H. K. Lee, B. Yordy, G. S. Shadel, and A. Iwasaki. 2009. Absence of autophagy results in reactive oxygen species-dependent amplification of RLR signaling. *Proc Natl Acad Sci U S A* 106: 2770.

241. Yoshizumi, T., H. Imamura, T. Taku, T. Kuroki, A. Kawaguchi, K. Ishikawa, K. Nakada, and T. Koshiba. 2017. RLR-mediated antiviral innate immunity requires oxidative phosphorylation activity. *Sci Rep* 7: 5379.

242. To, E. E., R. Vlahos, R. Luong, M. L. Halls, P. C. Reading, P. T. King, C. Chan, G. R. Drummond, C. G. Sobey, B. R. S. Broughton, M. R. Starkey, R. van der Sluis, S. R. Lewin, S. Bozinovski, L. A. J. O'Neill, T. Quach, C. J. H. Porter, D. A. Brooks, J. J. O'Leary, and S. Selemidis. 2017. Endosomal NOX2 oxidase exacerbates virus pathogenicity and is a target for antiviral therapy. *Nature Communications* 8: 69.

243. Yang, C.-S., J.-J. Kim, S. J. Lee, J. H. Hwang, C.-H. Lee, M.-S. Lee, and E.-K. Jo. 2013. TLR3-triggered reactive oxygen species contribute to inflammatory responses by activating Signal transducer and activator of transcription-1. *J Immunol* 190: 6368.

244. Grunert, T., N. R. Leitner, M. Marchetti-Deschmann, I. Miller, B. Wallner, M. Radwan, C. Vogl, T. Kolbe, D. Kratky, M. Gemeiner, G. Allmaier, M. Müller, and B. Strobl. 2011. A

comparative proteome analysis links tyrosine kinase 2 (Tyk2) to the regulation of cellular glucose and lipid metabolism in response to poly(I:C). *J. Proteomics* 74: 2866-2880.

245. Blanc, M., Wei Y. Hsieh, Kevin A. Robertson, Kai A. Kropp, T. Forster, G. Shui, P. Lacaze, S. Watterson, Samantha J. Griffiths, Nathanael J. Spann, A. Meljon, S. Talbot, K. Krishnan, Douglas F. Covey, Markus R. Wenk, M. Craigon, Z. Ruzsics, J. Haas, A. Angulo, William J. Griffiths, Christopher K. Glass, Y. Wang, and P. Ghazal. 2013. The Transcription Factor STAT-1 Couples Macrophage Synthesis of 25-Hydroxycholesterol to the Interferon Antiviral Response. *Immunity* 38: 106-118.

246. Jurk, M., F. Heil, J. Vollmer, C. Schetter, A. M. Krieg, H. Wagner, G. Lipford, and S. Bauer. 2002. Human TLR7 or TLR8 independently confer responsiveness to the antiviral compound R-848. *Nat Immunol* 3: 499-499.

247. Lee, J., T.-H. Chuang, V. Redecke, L. She, P. M. Pitha, D. A. Carson, E. Raz, and H. B. Cottam. 2003. Molecular basis for the immunostimulatory activity of guanine nucleoside analogs: Activation of Toll-like receptor 7. *Proc Natl Acad Sci U S A* 100: 6646.

248. Gorden, K. B., K. S. Gorski, S. J. Gibson, R. M. Kedl, W. C. Kieper, X. Qiu, M. A. Tomai, S. S. Alkan, and J. P. Vasilakos. 2005. Synthetic TLR agonists reveal functional differences between human TLR7 and TLR8. *J Immunol* 174: 1259-1268.

249. Patoli, D., F. Mignotte, V. Deckert, A. Dusuel, A. Dumont, A. Rieu, A. Jalil, K. Van Dongen, T. Bourgeois, T. Gautier, C. Magnani, N. Le Guern, S. Mandard, J. Bastin, F. Djouadi, C. Schaeffer, N. Guillaumot, M. Narce, M. Nguyen, J. Guy, A. Dargent, J.-P. Quenot, M. Rialland, D. Masson, J. Auwerx, L. Lagrost, and C. Thomas. 2020. Inhibition of mitophagy drives macrophage activation and antibacterial defense during sepsis. *The Journal of Clinical Investigation* 130.

250. Groß, Christina J., R. Mishra, Katharina S. Schneider, G. Médard, J. Wettmarshausen, Daniela C. Dittlein, H. Shi, O. Gorka, P.-A. Koenig, S. Fromm, G. Magnani, T. Ćiković, L. Hartjes, J. Smollich, Avril A. B. Robertson, Matthew A. Cooper, M. Schmidt-Supprian, M. Schuster, K. Schroder, P. Broz, C. Traidl-Hoffmann, B. Beutler, B. Kuster, J. Ruland, S. Schneider, F. Perocchi, and O. Groß. 2016. K+ Efflux-Independent NLRP3 Inflammasome Activation by Small Molecules Targeting Mitochondria. *Immunity* 45: 761-773.

251. Carroll, R. G., Z. Zasłona, S. Galván-Peña, E. L. Koppe, D. C. Sévin, S. Angiari, M. Triantafilou, K. Triantafilou, L. K. Modis, and L. A. O'Neill. 2018. An unexpected link between fatty acid synthase and cholesterol synthesis in proinflammatory macrophage activation. *Journal of Biological Chemistry* 293: 5509-5521.

252. Bernard, M. A., X. Han, S. Inderbitzin, I. Agbim, H. Zhao, H. Koziel, and S. D. Tachado. 2014. HIV-Derived ssRNA Binds to TLR8 to Induce Inflammation-Driven Macrophage Foam Cell Formation. *PLOS ONE* 9: e104039.

253. Fensterheim, B., J. Bohannon, Y. Guo, and E. Sherwood. 2016. MyD88-associated Toll-like receptor ligands prime macrophage metabolism for infection. *The Journal of Immunology* 196: 203.224.

254. Frede, S., C. Stockmann, P. Freitag, and J. Fandrey. 2006. Bacterial lipopolysaccharide induces HIF-1 activation in human monocytes via p44/42 MAPK and NF-kappaB. *Biochem J* 396: 517-527.

255. Meiser, J., L. Krämer, S. C. Sapcariu, N. Battello, J. Ghelfi, A. F. D'Herouel, A. Skupin, and K. Hiller. 2016. Pro-inflammatory Macrophages Sustain Pyruvate Oxidation through

Pyruvate Dehydrogenase for the Synthesis of Itaconate and to Enable Cytokine Expression. *J. Biol. Chem.* 291: 3932-3946.

256. Al-Shabany, A., A. Moody, A. Foey, and R. Billington. 2016. Intracellular NAD(+) levels are associated with LPS-induced TNF-α release in pro-inflammatory macrophages. *Biosci. Rep.* 36: e00301.

Chapter 2. Transcriptional profiling suggests extensive metabolic rewiring of human and mouse macrophages during early interferon alpha responses (Ahmed *et al.,* 2018; Published in *Mediators of Inflammation*)

2.1. Introduction

Type I interferons (IFN) (IFN-α and IFN-β) play a seminal role in anti-viral, anti-bacterial, and anti-tumour responses and act as critical regulators of innate and adaptive immune responses (1-5). These pleiotropic cytokines are produced following engagement of pattern recognition receptors and signal through the ubiquitously expressed transmembrane IFN-α receptor (IFNAR), composed of IFNAR1 and IFNAR2 subunits (5-7). Cellular responses to type I IFN are cell- and context-dependent and vary during the course of an immune responses (8-11). The variability in these responses is due, in part, to the cumulative effects of JAK-STAT, the p38 MAP kinase, the MAP kinase kinase/ERK/MAPK signal-interacting kinase and the phosphatidylinositol 3-kinase (PI3K)/AKT/mammalian target of rapamycin (mTOR) signaling pathways (11-13).

Emerging evidence suggests cellular metabolism plays a critical role in regulating and fine-tuning immune function (14-16). Alterations in cellular bioenergetics, amino acid and lipid metabolism have been shown to affect cytokine production, signaling protein activity and cell differentiation (17-19). In macrophages, stimulation with type I IFNs, has been shown to increase glycolytic flux, inhibit sterol biosynthesis, shift lipid metabolism from *de novo* synthesis to lipid import, and increase tryptophan catabolism (20-25). This metabolic reprogramming is required to mount functional antiviral responses and has been shown to regulate antigen presentation, inflammatory mediator production, phagocytosis efficiency and intracellular killing (26, 27).

Recent studies suggest metabolic adaptions in macrophages occur at the molecular level (i.e., gene expression) very early during the process activation and functional polarization (28-30). In lipopolysaccharide (LPS) stimulated macrophages, cellular activation undergoes stages of time-

resolved metabolic reprogramming into initiation-, early- and amplification-phases (28). To date, there has been no systematic characterization of metabolic reprogramming associated with type I IFN responses, particularly when examined as a function of time. In the study, I used transcriptional profiling to evaluate global changes in metabolic gene expression following short term IFN-α stimulation (<4 hours) in two well-characterized primary macrophage model systems: mouse bone marrow-derived macrophages (BMM) and human monocyte derived macrophages (MDM). Our findings provide a systematic understanding of altered metabolic genes associated with early IFN-α responses in BMM and MDM and identify potential metabolic mechanisms that may contribute to initial establishment of antiviral immune responses.

2.2. Materials and Methods

2.2.1. Microarray normalization and processing

Microarray datasets were extracted from the Gene Expression Omnibus (GEO) repository from National Center for Biotechnology Information (NCBI). Datasets were identified using the search terms: "Macrophage Interferon" and "Type I Interferon" (31). A total of 10 datasets were identified using these search criteria. Two studies were identified that assessed short-term stimulation (<4 hours) in either mouse bone marrow-derived macrophages (BMM) or human monocyte-derived macrophages (MDM). The selected BMM dataset (32) differentiated bone marrow cells in DMEM media with 10ng/mL of Macrophage-Colony Stimulating Factor (M-CSF), 10% FBS, 1% penicillin/streptomycin for seven days before replacing the media on day six. BMM were stimulated with 62U/mL IFN-α (approximately 1 ng/ml) for 2.5 hours prior to cell lysis and RNA extraction (Supplemental Figure S2.1). The selected MDM dataset (33) isolated monocytes via adherence (4 hours) and differentiated cells in DMEM media with 2mM L-glutamine, 100U/mL penicillin, 100μg/mL streptomycin and 10% FCS for 7 days. After differentiation, MDM were treated with 10ng/mL IFN-α for 4 hours prior to cell lysis and RNA

extraction (Supplemental Figure S2.1). Raw gene expression data was normalized by median centering and preprocessing was performed in dChip (34). Probes were excluded from the analysis when present calls (P<0.05) were identified in less than 20% of samples.

2.2.2. *The identification of significant metabolic genes in IFN-stimulated macrophages (BMM & MDM)*

Metabolic genes were identified using the MetScape plugin in Cytoscape (35-37). These genes were identified by mapping Entrez Gene IDs to metabolic pathways found in the Kyoto Encyclopedia of Genes and Genomes (KEGG) and Edinburgh Human Metabolic Network (EHMN) databases. Manual curation was performed to identify metabolic genes that did not map to KEGG or EHMN pathways. Fold change (FC) analyses, p-values, and false discovery rates (FDR) were calculated in R. Differentially expressed genes were defined as a $-1.2 \leq FC \geq 1.2$, p-value ≤ 0.05 and FDR ≤ 0.1. This fold change cut-off was selected to be inclusive of small differences in gene expression. Biologically relevant alterations in metabolic gene expression were identified by combining FC with pathway and network analyses. Classification analyses including Principal Component Analysis (PCA), Partial Least Squares-Discriminant Analysis (PLS-DA), Random Forest (RF) and unsupervised hierarchical clustering were performed in MetaboAnalyst (38). Gene Set Enrichment Analysis (GSEA) (39) was performed using the hallmark gene sets (H; n=50), the curated gene sets (C2; n=4731) and the GO gene sets (C5; n=5917) from Molecular Signatures Database (MSigDB) version 6.0. Significant enrichment was defined as a p≤ 0.05 and FDR<0.25. Metabolic pathway enrichment and topology analysis was performed in MetaboAnalyst. Significant enrichment of metabolic data sets was defined with p≤ 0.05. Metabolic network annotation and analysis was performed in Cytoscape and the Database for Annotation, Visualization, and Integrated Discovery (DAVID) (40, 41). The workflow is shown in Figure 2.1A.
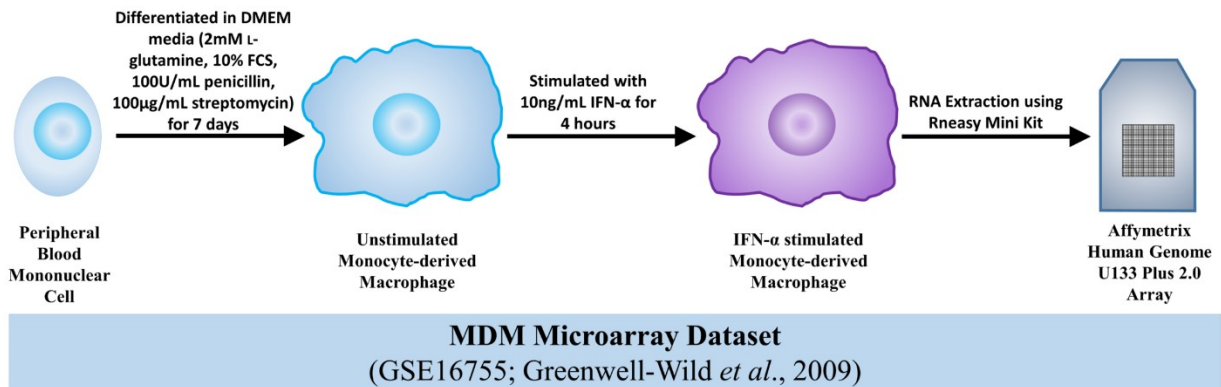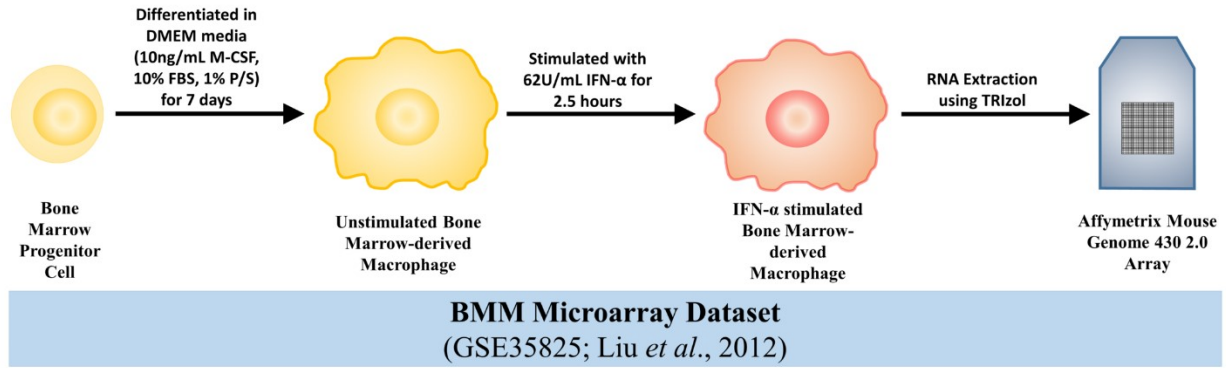
Supplemental Figure S2.1: Study workflow of BMM and MDM differentiation and IFN-α stimulation. Mouse bone marrow cells and human monocytes were differentiated for 7 days into BMM and MDM, respectively. Cells were then stimulated with IFN-α for less than 4 hours. RNA was extracted from total cells and prepared for microarray analysis.
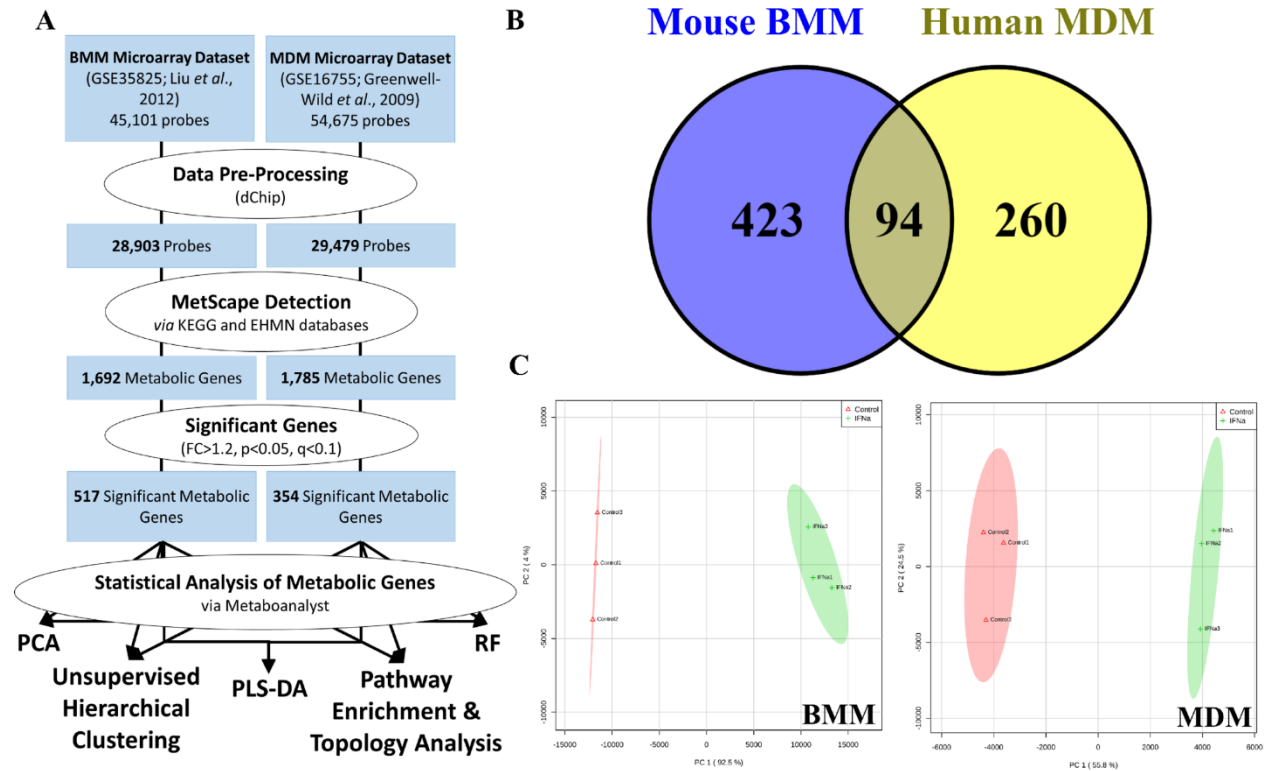
Figure 2.1: Short term IFN-α stimulation is associated with altered expression of metabolic genes in human monocyte-derived macrophages (MDM) and mouse bone marrow-derived macrophages (BMM). (**A**) Workflow used to identify differentially expressed metabolic genes in IFN-α-stimulated mouse BMM (2.5 hours) and human MDM (4 hours). Metabolic genes were identified in MetScape using the Kyoto Encyclopedia of Genes and Genomes (KEGG) and the Edinburgh Human Metabolic Network (EHMN) databases. (**B**) Venn diagram showing the number of metabolic genes common to the BMM (Yellow) and MDM (Blue) datasets (FC>1.2, p<0.05, FDR<0.10). (**C**) Principal component analysis (PCA) of metabolic gene sets from BMM (left) and MDM (right) following IFN-α stimulation (n = 517 and 354 metabolic genes in the BMM and MDM datasets, respectively).

2.3. Results

2.3.1. Type I IFN-stimulation of mouse BMM and human MDM is associated with enrichment of metabolic gene sets.

Of the >45,000 unique probe sets analyzed across the two datasets, 28,903 and 29,479 probes were identified as present in the BMM and MDM datasets, respectively. In total, 7,338 genes were differentially expressed in IFN-α stimulated BMM compared to unstimulated controls (Supplemental Table S2.1). Conversely, 3,804 genes were differentially expressed in IFN-α stimulated MDM compared to controls (Supplemental Table S2.2). GSEA identified significantly enriched gene sets within each dataset. Two hundred and eighty-five gene sets were enriched in BMM distributed across three main functional categories including immune signaling and function (n=151), cellular metabolism (n=40) and other biological states and processes (n=94). Enriched metabolic processes in BMM included glycolysis and gluconeogenesis, the regulation of NO biosynthetic process, and tryptophan, arginine, and proline metabolism (Supplemental Table S2.3). In MDM, GSEA identified 948 enriched gene sets (immune signaling and function: n=360, cellular metabolism: n=107, other biological states and processes: n=481). Enriched metabolic processes included reactive oxygen species (ROS) metabolism and biosynthesis, tryptophan metabolism, regulation of steroid biosynthetic process and regulation of oxidoreductase activity (Supplemental Table S2.4).

2.3.2. Metabolic genes represent important classifiers of early type I IFN responses in BMM and MDM

Given the significant enrichment of metabolic gene sets in GSEA analysis, I used MetScape to identify all metabolic genes detected across datasets. Of the >1600 metabolic genes identified, 517 and 354 were altered following short term IFN-α stimulation of BMM and MDM, respectively ($-1.2 \leq FC \geq 1.2$, p-value ≤ 0.05, FDR ≤ 0.1). Ninety-four genes were altered in both datasets with

the same directionality (either up or down regulated) (Figure 2.1B) including genes associated with cellular bioenergetics (*PFKFB3, PDP*), tryptophan metabolism (*KMO, WARS*), nucleotide metabolism (*NT5C3, CNP*) and lipid metabolism (*SPTLC2, AGPAT5, SQLE, SOAT1*). PCA showed a clear separation between the control and IFN-α treated samples in both BMM and MDM based on the metabolic gene subset (Figure 2.1C). Similarly, random forest analysis classified control and IFN-α-stimulated cells with 100% predictive accuracy using metabolic genes. Variable importance in projection (VIP) analysis identified genes involved in nucleotide degradation (*PNP, AMPD3*) and lipid metabolism (*ETNK1, HMGCS1*) as top classifiers in IFN-α stimulation in BMM. Top classifiers in MDM included genes associated with glycolysis (*PFKFB3*), tryptophan catabolism (*KYNU*) and reactive oxygen species production (*GCH1, SOD2*) (Figures 2.2C and 2.2D). Only *EIF2AK2, NAMPT, NT5C3* and the ubiquitin-related gene *USP18* overlapped as top classifiers across datasets. EIF2AK2 is involved in mRNA translation and inflammasome activation (42), NAMPT is a key NAD+ producing gene (43) and NT5C3 is an antiviral pyrimidine nucleotidase (44).

Pathway enrichment and topology analysis identified enrichment in purine, pyrimidine, inositol phosphate, and branched-chain amino acid metabolism in addition to lysine degradation in both BMM and MDM. Metabolic pathways uniquely enriched in BMM included arginine and proline metabolism, steroid biosynthesis, sphingolipid and glycerophospholipid metabolism. (Figure 2.2A, Supplemental Figure S2.2). Metabolic pathways uniquely enriched in MDM included amino sugar and nucleotide sugar metabolism, nicotinate and nicotinamide metabolism, galactose metabolism and fatty acid (FA) metabolism (Figure 2.2B, Supplemental Figure S2.2).
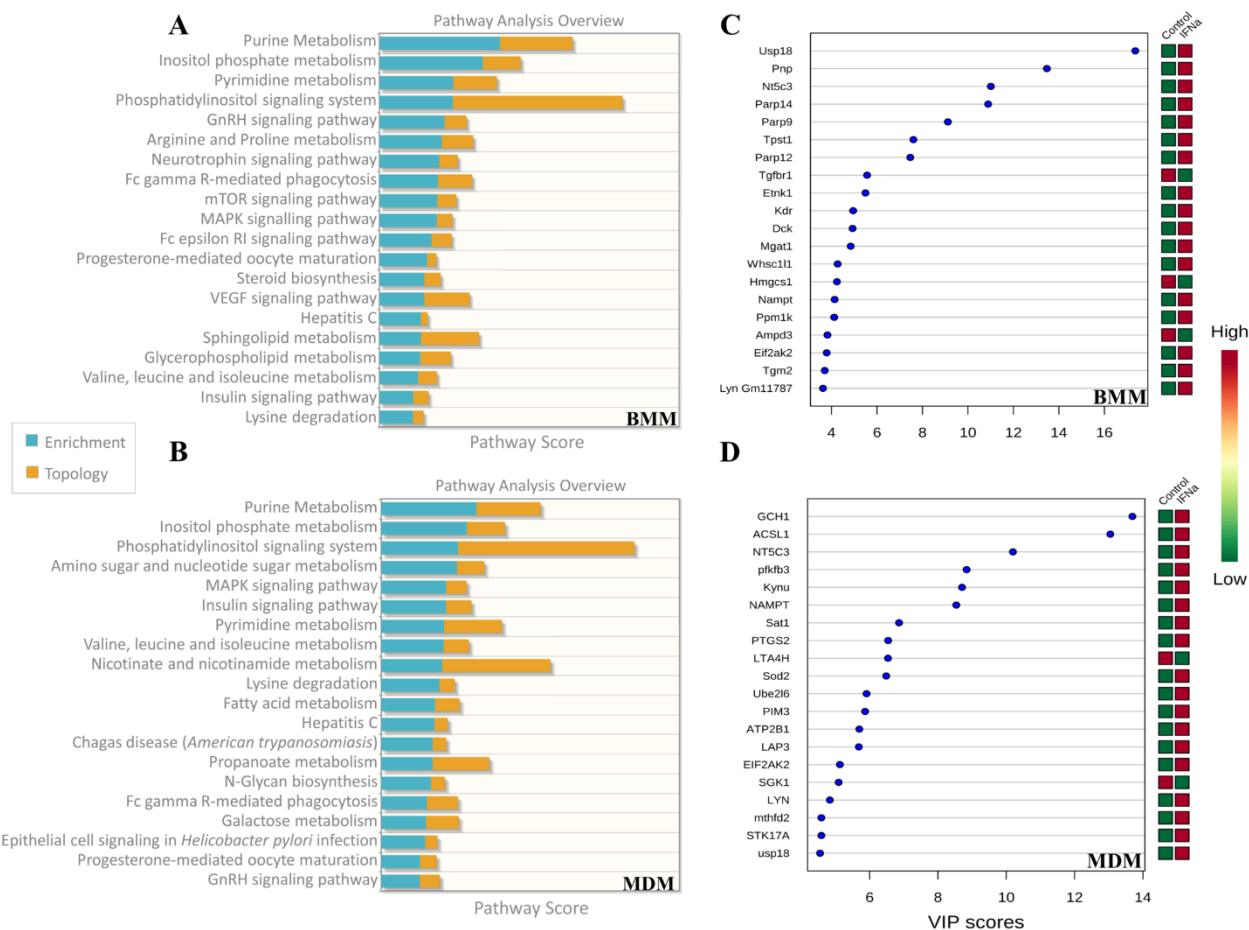
Figure 2.2: Metabolic genes are top classifiers of IFN-α stimulation in BMM and MDM. (**A**) Pathway enrichment and topology analysis of mouse BMM and human MDM following IFN-α stimulation (P<0.05). Analyses were performed using all metabolic genes. The blue bars represent enrichment analysis. The yellow bars represent topology scores. (**B**) Top metabolic classifiers of IFN-α stimulation were identified using Variable Importance in Projection (VIP) Scores based on PLS-DA models (P<0.05). Analyses were performed using all metabolic genes (P<0.05). Red and green in the heat map represent up and down regulation of gene expression, respectively.
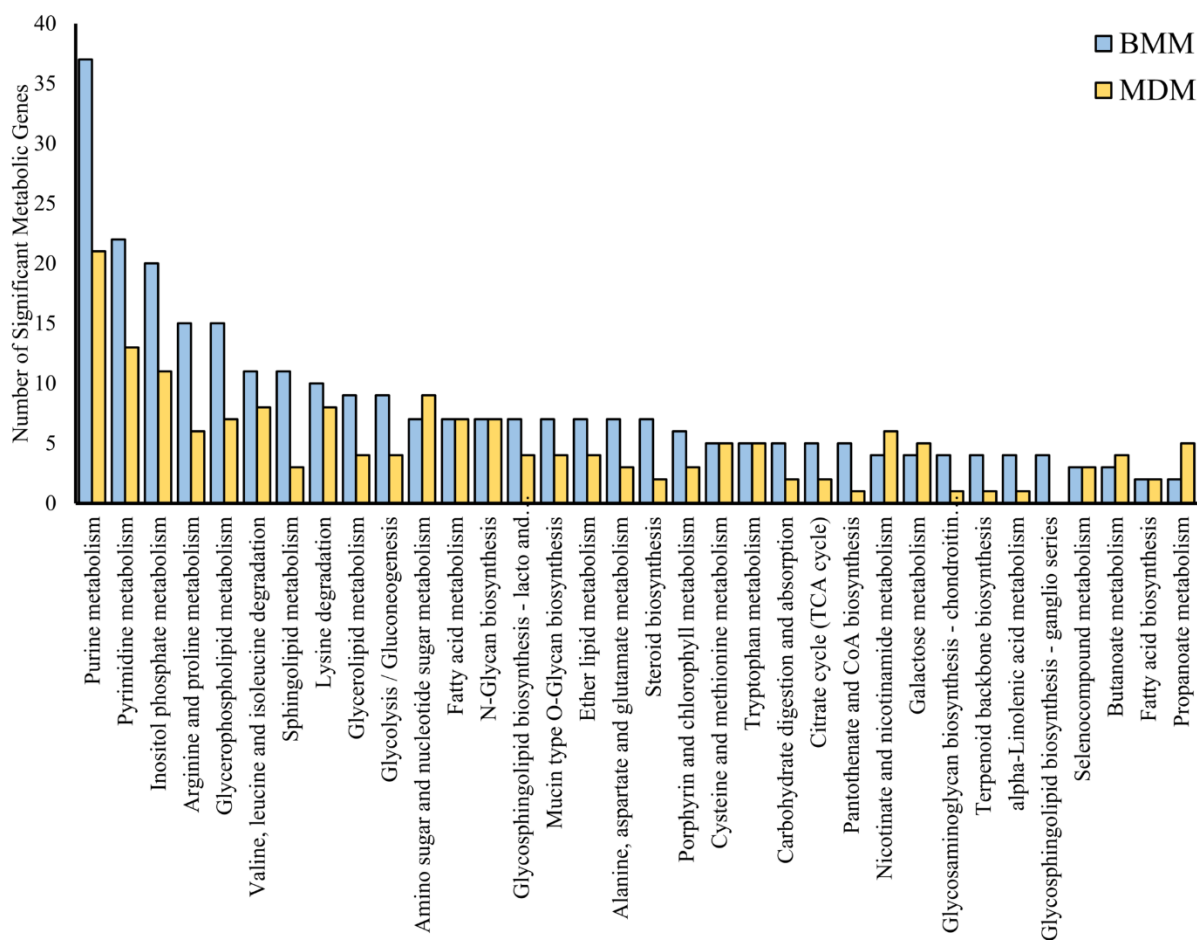
Supplemental Figure S2.2: IFN-α is associated with differential enrichment of metabolic pathways in mouse BMM compared to human MDM. Metabolite set enrichment analysis (MSEA) was performed in Metaboanalyst using metabolic gene datasets. Pathways shown were significantly enriched (P<0.05) in either IFN-stimulated BMM, MDM or both. Yellow and blue represent enrichment scores in BMM and MDM, respectively (Error bars = s.e.m.; n = 3).

2.3.3. *Short term IFN-α stimulation alters genes associated with energy metabolism in BMM and MDM.*

To better functionally characterize differential gene expression in IFN-α stimulated BMM and MDM, altered genes (-1.2 ≤ FC ≥1.2, p-value ≤0.05, FDR ≤0.1) were mapped to metabolic pathways and networks. Consistent with the literature (20), short-term IFN-α stimulation of BMM was associated with an upregulation of glycolytic genes (*HK2, HK3, PGM2, PFKP, PFKFB3, INSR*) compared to unstimulated controls (Figure 2.3, Supplemental Figure S2.3). Key genes involved in pyruvate metabolism were also altered in BMM following IFN-α stimulation. Whereas pyruvate dehydrogenase kinase 3 (*PDK3*) was upregulated, pyruvate dehydrogenase phosphatase 1 (*PDP1*) and dihydrolipoamide dehydrogenase (*DLD*) were downregulated. These alterations may affect the activity of the pyruvate dehydrogenase complex (*PDH*) and increase lactate production. Consistent with these findings, lactate dehydrogenase D (*LDHD*) was also upregulated in IFN-α stimulated BMM. Interestingly, IFN-α-stimulated BMMs also upregulated levels of isocitrate dehydrogenase (*IDH3A*) and the downregulation of *DLD* and dihydrolipoamide S-succinyltransferase (*DLST*) expression. DLD and DLST are key components of oxoglutarate dehydrogenase complex (OGDC) and play an important role in converting 2-oxoglutarate to succinyl-CoA. Along the succinate-fumarate-malate axis, succinate dehydrogenase complex subunit A (*SDHA*) was downregulated in stimulated compared to unstimulated BMM. SDHA is the major catalytic subunit of the succinate-ubiquinone oxidoreductase. Altered SDHA expression may also have significant effects on oxidative phosphorylation (OXPHOS).

Figure 2.3: Genes associated with bioenergetic processes are differentially expressed in mouse BMM and human MDM following IFN-α stimulation. Significantly altered (-1.2 ≤ FC ≥1.2, p-value ≤0.05, FDR ≤0.1) metabolic genes involved in energy production were mapped to their respective pathways using MetScape and DAVID. Green and red represent genes that have been significantly upregulated or downregulated, respectively. Blue represents genes that were not altered following IFN-α stimulation.

Mouse BMM

Human MDM

Supplemental Figure S2.3: IFN responses are associated with altered bioenergetic profiles in mouse and human macrophages. The bar plots show significantly altered genes associated with bioenergetics pathways (FC>1.2, p<0.05, FDR<0.10). Light blue and dark blue represent expression levels in unstimulated (control) and IFN-α treated macrophages, respectively (Error bars = s.e.m.; n = 3).

Short term IFN-α stimulation of MDM was not associated with significant alterations in glycolytic genes or genes linked to lactate production (Figure 2.3, Supplemental Figure S2.3). Alternatively, stimulation was associated with the downregulation of genes associated with the conversion of galactose to glucose (*GALK2, GALT, GALE*) and glycogen breakdown (*INSR, PHKA1, PHKA2, PHKG2, AGL*). Early responses in MDM were associated with increased levels of phosphofructokinase (PFK) activator *PFKFB3,* which assists in the production of pyruvate from glucose and pyruvate dehydrogenase complex component X (*PDHX*), which may facilitate acetyl-CoA production from pyruvate. IFN-α was also associated with the upregulation of genes associated with OXPHOS including genes from Complex I and V of the electron transport chain (*NDUFA9, NDUFS4, ATP5G3*) and the glycerol phosphate shuttle (glycerol 3-phosphate dehydrogenase 2 [*GPD2*]). Collectively, these results suggest early changes in energy metabolism may play an important role in the initiation of antiviral responses in both BMM and MDM.

2.3.4. *IFN-α stimulated BMM and MDM show signs of alterations in genes associated with redox regulation.*

Given the link between energy metabolism and ROS metabolism (45-47), I examined alterations between early IFN-α responses and genes linked to cellular redox status (oxidant and antioxidant genes). In BMM, IFN-α short term stimulation was associated with altered expression of genes associated with the nitric oxide cycle including the upregulation of argininosuccinate synthetase 1 (*ASS1*) and nitric oxide synthase 1 (*NOS1*), and down-regulation of arginase 2 (*ARG2*) expression, which may favour flux of arginine towards NO production (Figure 2.4, Supplemental Figure S2.4). Early IFN-α responses in BMM were also associated with the downregulation of genes associated with the antioxidant response (superoxide dismutase 2 (*SOD2*), glutamate-cysteine ligase, catalytic subunit (*GCLC*), NAD kinase (*NADK*), thioredoxin reductase 1 and 3

(*TXNRD1, TXNRD3*) and the upregulation of thioredoxin interacting protein (*TXNIP*), which inhibits the antioxidant activity of thioredoxin (48, 49).

Alternatively, IFN-α stimulation of MDM was associated with the upregulation of antioxidant genes including *SOD2* and myeloperoxidase (*MPO*) as well as genes associated with glutathione production (glutamate-cysteine ligase (*GLCM*) and *NADK*) (Figure 2.4, Supplemental Figure S2.4). Short term IFN-α was also associated with upregulation of *TXNIP,* glutaredoxin (*GLRX*), and thioredoxin 1 (*TXN1*). These alterations may help regulate electron linkage and subsequent ROS production associated with the upregulation of genes associated with OXPHOS in these cells (Figures 2.3 and 2.4).
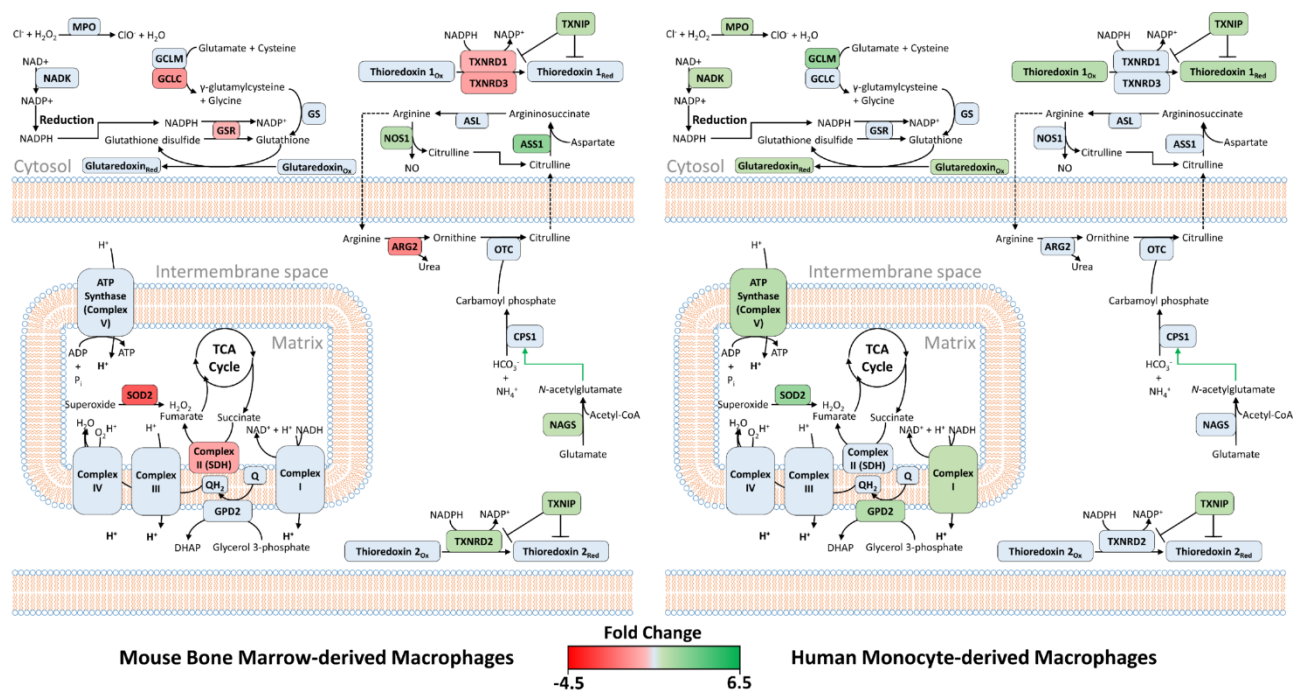
Figure 2.4: IFN-α stimulation of MDM is associated with increased expression of genes associated with ROS production and antioxidant responses. Differentially expressed metabolic genes ($-1.2 \leq$ FC ≥ 1.2, p-value ≤ 0.05, FDR ≤ 0.1) were mapped to pathways associated with cellular redox status using MetScape and DAVID. Green and red represent genes that have been significantly upregulated or downregulated, respectively. Blue represents genes that were not altered following IFN-α stimulation.
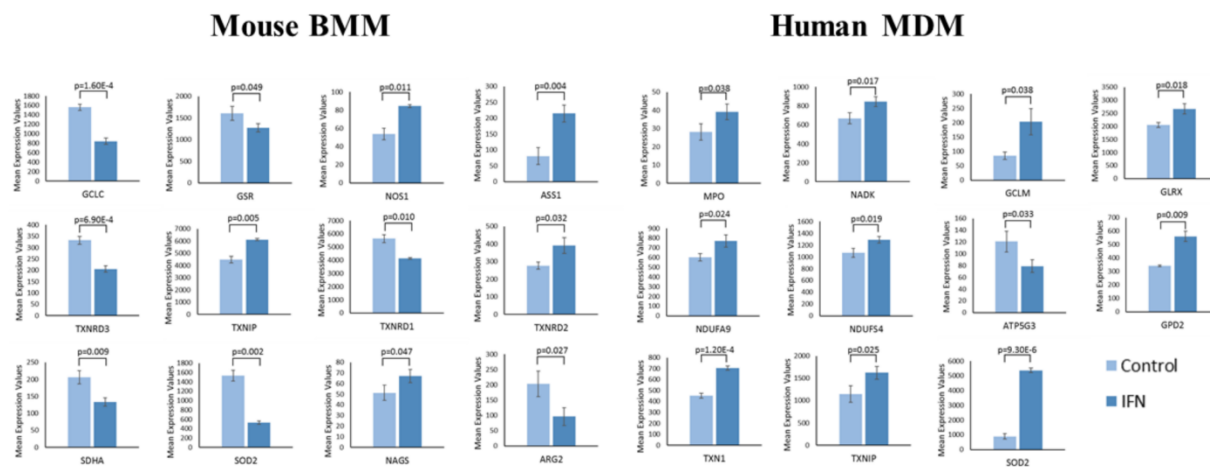
Supplemental Figure S2.4: BMM and MDM express redox-related genes following short term IFN-α stimulation. The bar plots show significantly altered genes associated with cellular redox pathways (FC>1.2, p<0.05, FDR<0.10). Light blue and dark blue represent expression levels in unstimulated (control) and IFN-α treated macrophages, respectively (Error bars = s.e.m.; n = 3).

2.3.5. Early type I IFN responses are associated with alterations in genes associated with cAMP and cGMP production.

Given the enrichment of gene sets associated with nucleotide metabolism in both data sets, I examined the specific effects on short term IFN-α stimulation on purine and pyrimidine metabolism. In BMM, short-term stimulation was associated with the downregulation of amidophosphoribosyltransferase (*PPAT*) and UMP synthetase (*UMPS*) (Figure 2.5, Supplemental Figure S2.5). These enzymes play a central role in ribose 5-phosphate incorporation during *de novo* purine and pyrimidine synthesis, which may represent an antiviral mechanism. At the level of purine degradation, IFN-α was associated with an upregulation of purine nucleoside phosphorylase (*PNP*), guanine deaminase (*GDA*), xanthine dehydrogenase (*XDH*), ectonucleoside triphosphate diphosphohydrolase 2 and 5 (*ENTPD2, ENTPD5*) suggesting increased degradation. Interestingly, IFN responses were also associated with alterations in genes that regulate cyclic guanine monophosphate (cGMP)/GMP and cyclic adenosine monophosphate (cAMP)/AMP ratios (Figure 2.5, Supplemental Figure S2.5). Four phosphodiesterases (*PDE4D, PDE7A, PDE7B, PDE8B*) and two adenylate cyclases (*ADCY2, ADCY4*) were upregulated and adenylate kinase (*ADK*) and AMP deaminase 3 (*AMPD3*) were downregulated in stimulated *vs.* unstimulated cells. These profiles suggest IFN-α-activated BMM may accumulate both AMP and cAMP. IFN-α stimulation of BMM was also associated with the upregulation of guanylate kinase (*GUK*) and down-regulation of phosphodiesterase 1B (*PDE1B*), suggesting these cells may favour cGMP production
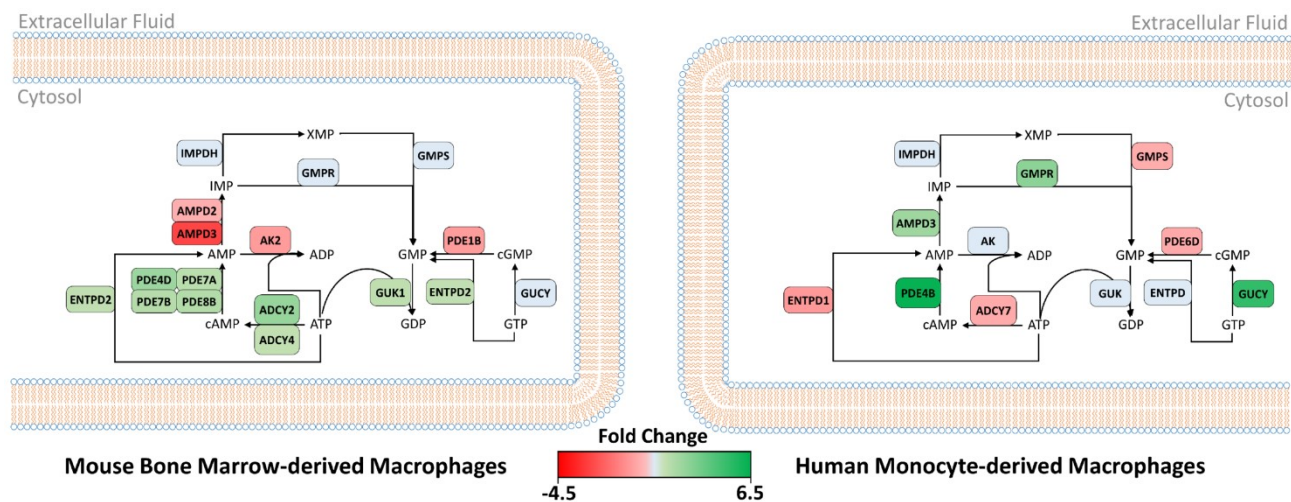
Figure 2.5: Type I IFN responses are associated with altered cAMP and cGMP production in BMM and MDM. Metabolic genes identified as significantly altered ($-1.2 \leq FC \geq 1.2$, p-value ≤ 0.05, FDR ≤ 0.1) were mapped to pathways associated with AMP and GMP production using MetScape and DAVID. Green and red represent genes that have been significantly upregulated or downregulated, respectively. Blue represents genes that were not altered following IFN-α stimulation.
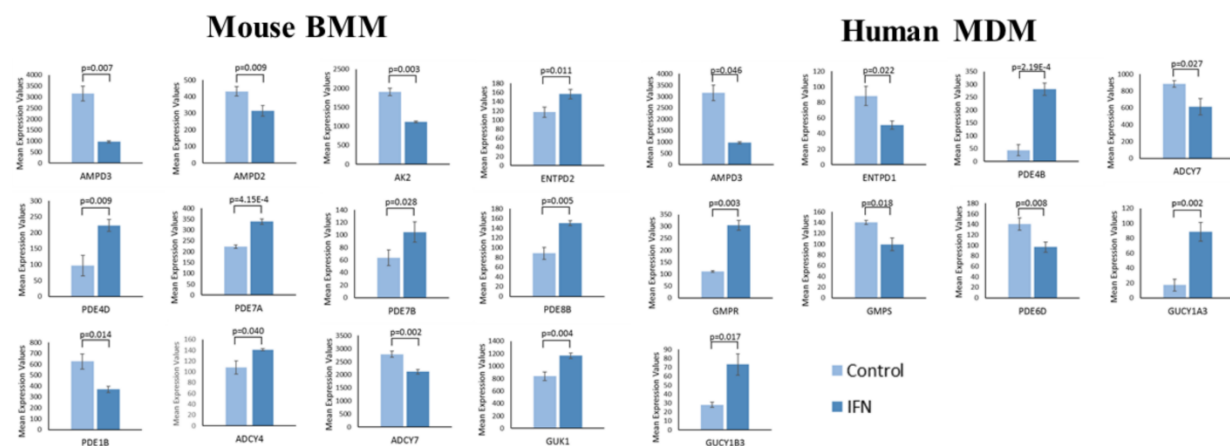
Supplemental Figure S2.5: IFN-α is associated with altered expression of genes that regulate nucleotide metabolism and cAMP/cGMP ratios. The bar plots show significantly altered genes associated with nucleotide metabolism (FC>1.2, p<0.05, FDR<0.10). Light blue and dark blue represent expression levels in unstimulated (control) and IFN-α treated macrophages, respectively (Error bars = s.e.m.; n = 3).

In MDM, IFN-α stimulation was not associated with significant changes in genes associated with *de novo* purine synthesis. However, IFN-α was associated with the downregulation of carbamoyl-phosphate synthetase 2, aspartate transcarbamylase and dihydroorotase (*CAD*), a protein responsible for the first three enzymatic steps of pyrimidine biosynthesis pathway (Figure 2.5, Supplemental Figure S2.5). Genes involved in nucleoside production within the purine and pyrimidine degradation pathways, such as GMP reductase (*GMPR*), AMPD3, 5`-nucleotidase, cytosolic II (*NT5C2*), adenosine deaminase (*ADA*), are found to be up-regulated in MDM which suggest an increase in nucleotide salvaging (Figure 2.5, Supplemental Figure S2.5). At the level of cGMP/GMP and cAMP/AMP regulation, the downregulation of *PDE6D* and adenylate cyclase 7 (*ADCY7*) as well as the upregulation of *PDE4B* and two soluble forms of guanylate cyclase (*GUCY1A3, GUCY1B3*) suggest a shift towards cGMP and AMP production. Varied expression of these bioactive nucleotides that function as intracellular secondary messengers may contribute to early type I IFN responses.

2.3.6. *Short term IFN-α stimulation is associated with alterations in tryptophan and branched-chain amino acid catabolism in BMM and MDM.*

Consistent with the literature (50, 51), alterations in genes associated with tryptophan and branched-chain amino acid catabolism were pronounced in early IFN-α responses. Both BMMs and MDMs exhibited a pronounced up-regulation of genes associated with tryptophan catabolism via the kynurenine pathway (Figure 2.6, Supplemental Figure S2.6). While IFN-α stimulated BMM upregulated tryptophan 2,3-dioxygenase (*TDO2*) and *KMO*, stimulation of MDM was associated with the upregulation of *KMO* and kynureninase (*KYNU*). This shift in tryptophan catabolism was accompanied by the upregulation of nicotinamide phosphoribosyltransferase (*NAMPT*), suggesting an increased flux of tryptophan towards NAD$^+$ production.

Figure 2.6: Tryptophan and branched-chain amino acid catabolism is altered in BMM and MDM following short-term IFN-α treatment. Metabolic genes altered in IFN-α stimulated cells compared to controls (-1.2 ≤ FC ≥1.2, p-value ≤0.05, FDR ≤0.1) were mapped to amino acid metabolism pathways using MetScape and DAVID. Green and red represent genes that have been significantly upregulated or downregulated, respectively. Blue represents genes that were not altered following IFN-α stimulation.

Supplemental Figure S2.6: Short term IFN-α stimulation is associated with alterations in tryptophan and branched chain amino acid catabolism. The bar plots show significantly altered genes associated with tryptophan and branched chain amino acid metabolism (FC>1.2, p<0.05, FDR<0.10). Light blue and dark blue represent expression levels in unstimulated (control) and IFN-α treated macrophages, respectively (Error bars = s.e.m.; n = 3).

Both IFN-α-activated BMM and MDM showed altered expression of genes associated with branched-chain amino acid (Figure 2.6, Supplemental Figure S2.6). In BMMs, IFN-α stimulation leads to the upregulation of genes associated with isoleucine (propionyl-CoA carboxylase; *PPCA*, 3-ketoacyl-CoA thiolase 1A and 2; *ACAA1A/2*) and valine (3-hydroxyisobutyrate dehydrogenase; *HIBADH*) catabolism. Upregulation of AU-RNA binding/methylglutaconyl-CoA hydratase (*AUH*) and the downregulation of methylcrotonoyl-CoA carboxylase 1 (*MCCC1*) and 3-hydroxymethyl-3-methylglutaryl-CoA lyase (*HMGCL*) suggest decreased leucine catabolism in BMM. However, AUH may be functioning in its secondary role in promoting mRNA degradation (52). In MDM, IFN-α stimulation was associated with a downregulation of multiple genes associated with branched chain amino acids catabolism including branched-chain aminotransferase 2 (*BCAT2*), isovaleryl-CoA dehydrogenase (*IVD*), hydroxyacyl-CoA dehydrogenase (*HADH*), and methylmalonyl-CoA epimerase (*MCEE*). Together, this indicates that alterations in branched-chain amino acid catabolism may be key to driver of early IFN-α responses in primary macrophage systems.

2.3.7. *IFN-α is associated with altered lipid metabolism in BMM and MDM.*

Lipid metabolism has been shown to play an important role in antiviral responses in BMM and MDM (53). Several studies have reported alterations in cholesterol metabolism during IFN and antiviral responses (22, 23, 54). Here, I also identified alterations in genes associated with phospholipid and sphingolipid metabolism and FA biosynthesis following short-term IFN responses. Consistent with previous studies, short term IFN-α stimulation of BMM and MDM was associated with the downregulation of genes associated with *de novo* cholesterol synthesis (Figure 2.7, Supplemental Figure S2.7). In BMM, IFN-α was associated with the downregulation of genes involved in mevalonate synthesis (*HMGCS1, HMGCR*), lanosterol synthesis (*FDFT1, SQLE, LSS*)

and cholesterol synthesis (*CYP51, MSMO1, HSD17B7, SC5D*). It was also associated with the downregulation of genes associated with cholesterol ester formation and the upregulation of carboxyl ester lipase (*CEL*), cholesterol 25-hydroxylase (*CH25H*) and sterol 27-hydroxylase (*CYP27A1*). In MDM, IFN-α stimulation was associated with decreased levels of *SQLE* and sterol O-acyltransferase 1 (*SOAT1*) and increased levels of *CH25H* (Figure 2.7, Supplemental Figure S2.7). SQLE catalyzes the first oxygenation step in sterol biosynthesis and is thought to be a rate-limiting enzyme of this process (55).

At the level of phospholipid and sphingolipid metabolism, IFN-α treated BMM upregulated phospholipid phosphatase 2 (*PLPP2*) and neutral ceramidase (*ASAH2*) and downregulated sphingolipid kinases (*SPHK2, CERK*) suggesting a shift away from phosphorylated sphingolipids to sphingosine in acute IFN responses (Figure 2.7, Supplemental Figure S2.7). Stimulation of BMM was also associated with the upregulation of 1-acylglycerol-3-phosphate O-acyltransferase 1 (*AGPAT1*) and phosphatidate cytidylyltransferase 1 (*CDS1*), which may increase cytidine diphosphate (CDP)-diacylglycerol production, a precursor for phosphatidylinositol, phosphatidylglycerol, and cardiolipin synthesis. Phosphatidylinositol is a minor component on the cytosolic side of cell membranes and cardiolipin is an important component of the inner mitochondrial membrane (56). Consistent with these findings, IFN-α stimulation was associated with the upregulation of three different phospholipase A2 (*PLA2G2D, PLA2G4A, PLA2G16*) genes and the downregulation of two phospholipase D (*PLD1, PLD2*) genes. These genes cleave phosphatidylcholine and phosphatidylethanolamine, which represent the major phospholipids found in mammalian membranes. The relative ratio of these lipids to one another within the cell membrane has significant implications on membrane integrity (56). In MDM, *PLA2G4A* and sphingomyelin synthase 1 (*SGMS1*) were upregulated and lysophospholipid acyltransferase

(*LPCAT4*) and *PLA2G15* were downregulated following IFN-α stimulation (Figure 2.7, Supplemental Figure S2.7). IFN-α stimulation was also associated with the downregulation of *AGPAT5*, choline kinase alpha (*CHKA*) and ethanolamine kinase 1 (*ETNK1*), which play an important role in the synthesis of phosphatidylglycerol, phosphatidylcholine and phosphotidylethanolamine. Collectively, these alterations suggest IFN-α responses may alter the composition of the plasma and mitochondrial membranes of BMM and MDM as part of early type I IFN responses.

Finally, at the level of fatty acid synthesis, IFN-α stimulation of BMM was also associated with the downregulation of FA synthase (*FAS*) and FA desaturase 1 (*FADS1*) as well as the upregulation of carnitine palmitoyltransferase 1A (*CPT1A*). Alternatively, in MDM, IFN-α was associated with the upregulation of long-chain fatty acid (LCFA)-producing aldehyde dehydrogenase 3b1 (*ALDH3B1*) and three acyl-CoA synthetase long-chain genes (*ACSL1, ACSL5, ACSL6*) and the downregulation of carbonyl reductase 4 (*CBR4*), acetyl-CoA carboxylase-α (*ACACA*), mitochondrial 3-oxoacyl-ACP synthase (*OXSM*), trimethylysine hydrolase ε (*TMLHE*) and hydroxyacyl-CoA dehydrogenase (*HADH*). Differences in fatty acid metabolism may indicate differential dependencies of BMM and MDM on β-oxidation for energy production.
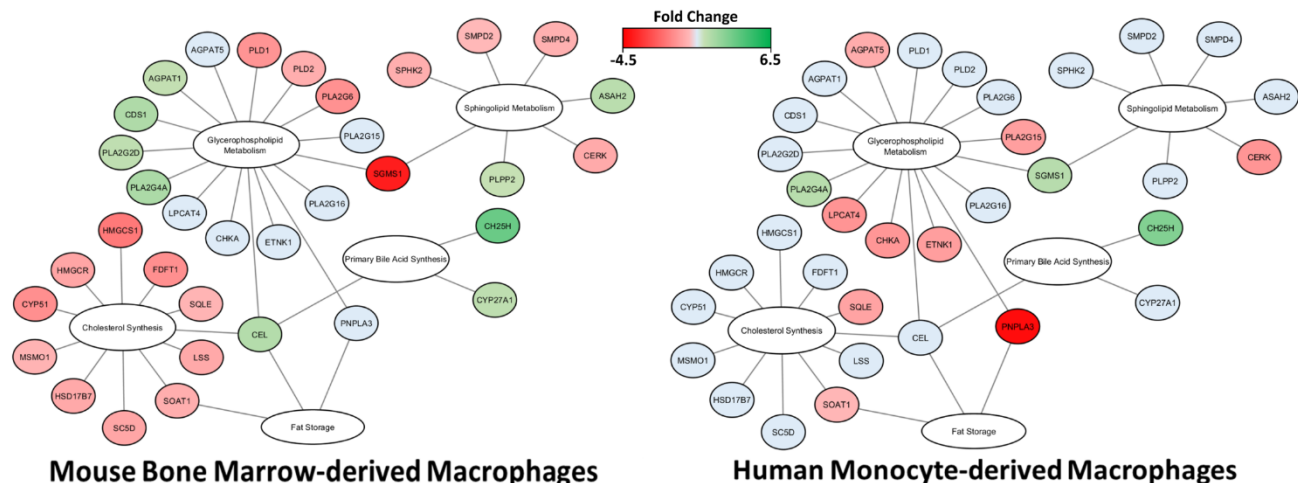
Figure 2.7: Expression of genes associated with lipid metabolism were differentially modulated in IFN-α stimulated BMM compared MDM. Differentially expressed metabolic genes (-1.2 ≤ FC ≥1.2, p-value ≤0.05, FDR ≤0.1) involved in cholesterol metabolism and phospholipid and sphingolipid synthesis were mapped using MetScape and DAVID. Green and red represent genes that have been significantly upregulated or downregulated, respectively. Blue represents genes that were not altered following IFN-α stimulation.
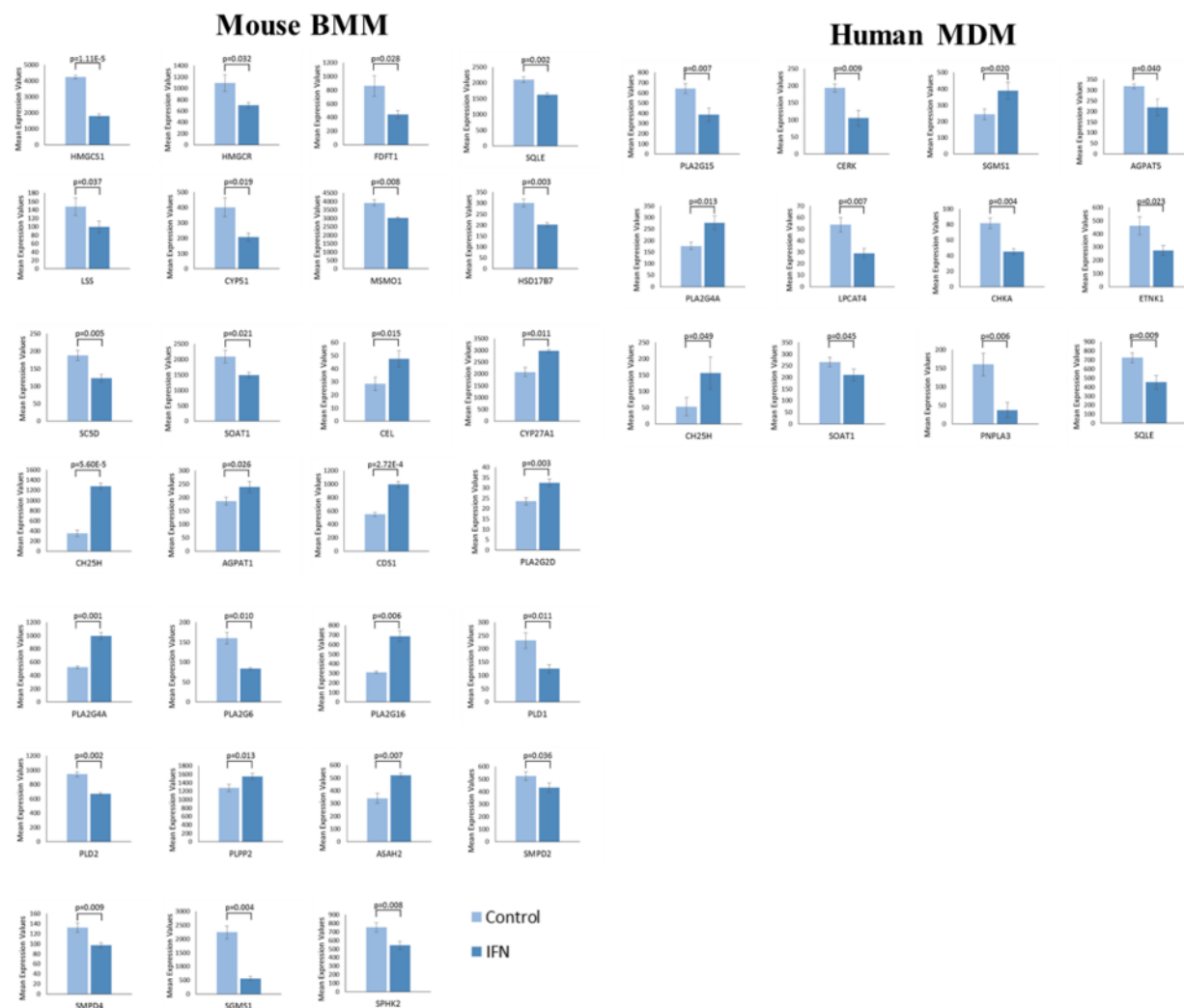
Supplemental Figure S2.7: Altered expression of genes associated with lipid metabolism is a key feature of Type I IFN responses. The bar plots show significantly altered genes associated with lipid metabolism (FC>1.2, p<0.05, FDR<0.10). Light blue and dark blue represent expression levels in unstimulated (control) and IFN-α treated macrophages, respectively (Error bars = s.e.m.; n = 3).

2.4. Discussion

In the current study, I used publicly available transcriptional profiling datasets to develop metabolic gene signatures associated with short term IFN-α stimulation in mouse and human macrophage models. Enrichment analysis, pathway mapping and network construction identified alterations in central metabolic pathways in early type I IFN responses including glycolysis, oxidative phosphorylation, redox regulation, nucleotide metabolism, amino acid catabolism, and lipid metabolism. BMM had increased expression of genes associated with aerobic glycolysis, nitric oxide production, branched-chain amino acid metabolism and fatty acid β-oxidation as well as decreased expression of genes associated with cholesterol biosynthesis. MDM had increased expression of genes associated with increased OXPHOS activity and antioxidant production and decreased expression of genes associated with branched-chain amino acid catabolism and fatty acid β-oxidation. While the current study only examines alterations in gene expression, these findings suggest that metabolic rewiring, at the level of transcription, is a key feature of early type I IFN responses. Future studies are required to validate the identified gene signatures and to validate the biological relevance of these alterations during early antiviral immune responses.

A number of studies have reported increased aerobic glycolysis and reduced oxidative phosphorylation in macrophages following activation with inflammatory stimuli (57-60). Consistent with the literature, short term IFN-α stimulation of BMM was associated with increased expression of genes associated with glycolysis (*HK2, HK3, PGM2, PFKP, PFKFB3, INSR*) and lactate production (*LDHD*) and decreased expression of genes associated with pyruvate production (*PDK3, PDP1, DLD*) and flux through the TCA cycle (*DLD, DLST, SDHA*). In addition to meeting bioenergetic requirements of the cells, these alterations may increase intracellular levels of bioactive metabolites such as D-lactate, α-ketoglutarate, and succinate. Lactate accumulation in

the microenvironment has been shown to suppress cytokine production and migration of human cytotoxic T cells (61, 62). Similarly, α-ketoglutarate has been shown to quell inflammatory processes by suppressing NF-κB-mediated inflammatory pathways (63). Succinate can also modulate inflammatory cytokine production. A recent study found that succinate stabilizes HIF-1α expression in LPS-activated macrophages (14), which facilitates HIF-1α transport into the nucleus where it induces the expression of glycolytic targets such as *LDHA, HK2, and PKM2*, as well as inflammatory genes such as *IL1B* (64, 65). Inhibition or decreased expression of succinate dehydrogenase (SDH) has been shown to promote IL-10 expression and to repurpose the mitochondria for ROS production (19). While functional studies are required to validate these profiles, our findings suggest bioenergetic reprogramming of BMM may represent a feedforward mechanism that may contribute to the immunomodulatory properties of type I IFNs during early antiviral immune responses.

Unlike BMM, short term IFN-α stimulation of MDM was associated with the upregulation of a range of genes associated with the electron transport chain, which may favour OXPHOS for energy production. While OXPHOS provides more ATP per glucose molecule compared to aerobic glycolysis, energy and metabolic precursor production occurs more slowly. Further, IFN-α stimulation of MDM was associated with the downregulation of genes associated with the Leloir pathway (*GALK2, GALT, GALE*), which is responsible for the conversion of galactose to glucose. Recent studies have shown that T cells, but not B cells, can be activated and proliferate in presence of galactose when glucose is absent (66, 67). However, unlike activation in glucose rich environments, T cells in galactose are forced to rely on OXPHOS for energy production, which occurs at significantly slower rates (66). This reliance on galactose also results in suboptimal IFN-γ and IL-2 production suggesting galactose should only be used when no other energy substrate is

available (66). Thus, decreased expression of genes associated with the Leloir pathway in MDM may represent a means by which cells can improve the efficiency of energy production while maintaining functional immune responses.

Transcriptional profiling also identified redox regulation as a key feature of early IFN-α responses in mouse and human primary macrophage models. In BMM, IFN-α reprogramming was associated with increased expression of genes associated with nitric oxide (NO) production (*ASS1, NOS1, NAGS*) and decreased antioxidants (*SOD2, GCLC, TXNRD1, TXNRD3*). NO is a potent antimicrobial molecule that has been shown to modulate cellular metabolism (68-71) and immune function (72). ASS1 and ASL are part of the aspartate-argininosuccinate shunt, which recycles citrulline to resynthesize arginine for prolonged NO production (73, 74). In M1 macrophages, increased expression of ASS1 and the subsequent increased flux through this shunt has been shown to replenish TCA cycle intermediates following decreased *IDH* and *SDH* gene expression (73). Unlike BMM, IFN-α stimulated MDM had increased expression of genes associated with OXPHOS and reactive oxygen species (ROS) production. ROS are also potent antimicrobial molecules, capable of killing intracellular pathogens (75). The matched upregulation of antioxidant genes (e.g., glutathione, glutaredoxin, thioredoxin) in conjunction with ROS, likely reflects a protective mechanism to limit any associated cellular damage. Interestingly, a recent study found that the reducing nature of glutathione can prime T cell inflammatory responses by promoting mTOR-activated metabolic reprogramming (76). It is currently unclear if similar priming occurs in macrophages. Collectively, our data suggest mouse BMM and human MDM may adopt differential metabolic strategies to mount intracellular antimicrobial responses during acute IFN responses.

Pathway mapping and network reconstruction identified IFN-α-associated alterations in nucleotide metabolism. In both BMM and MDM, IFN-α stimulation was associated with a downregulation of genes associated with *de novo* pyrimidine biosynthesis. A number of viruses including human cytomegalovirus and herpes simplex viruses require *de novo* pyrimidine synthesis for propagation and survival (77, 78). Furthermore, inhibitors of *de novo* pyrimidine biosynthesis have broad antiviral effects against RNA, DNA, and retroviruses such as influenza A, hepatitis C, human adenovirus, and human immunodeficiency virus (HIV) (79, 80). In MDM, IFN-α stimulation was also associated with increased expression of genes associated with purine and pyrimidine degradation pathways and nucleotide salvaging. The induction of nucleotide degradation pathways may act as a counterstrategy against viral-driven nucleotide biosynthesis (81). Moreover, the activation of nucleotide salvaging pathways may allow the cell to recycle degraded bases and nucleosides and produce nucleotides to maintain cellular function. Interestingly, IFN-α responses were also associated with alterations in genes that regulate cyclic guanine monophosphate (cGMP)/GMP and cyclic adenosine monophosphate (cAMP)/AMP ratios. Cyclic nucleotide second messengers, including cAMP and cGMP, are potent secondary messengers that contribute to the regulation of a variety of cellular processes including metabolism (82). cAMP has been shown to suppress innate immune function including inflammatory cytokine production, cell adhesion, phagocytosis, and intracellular killing (83, 84). Additionally, the cAMP axis plays an important role in antimicrobial defense as many microbes have evolved virulence-enhancing strategies that exploit this pathway (85-87). In BMM, LPS responses are associated with low levels of cAMP and cGMP accumulation, which inhibit inflammatory cytokine production (88, 89). Thus, alterations in (cAMP)/AMP and (cGMP)/GMP ratio may play an

important role in regulating inflammatory, antimicrobial and metabolism responses in acute type I IFN responses.

Alterations in genes associated with tryptophan and branched-chain amino acid catabolism were pronounced in early IFN responses. Consistent with previous studies (50, 90, 91), IFN-α stimulation was associated with increased levels of genes associated with tryptophan catabolism. While I did not observe alterations in *IDO1* expression, *TDO2, KMO* and *KYNU* were increased in both BMM and MDM. Many studies have shown that tryptophan catabolism (via IDO activation) represents a potent antiviral immune response (91-93). Our study suggests downstream enzymes of the kynurenine pathway may also contribute to this phenotype. Interestingly, I also found that *NAMPT* was upregulated following acute IFN-α stimulation, suggesting tryptophan may be directed towards NAD$^+$ salvaging. NAMPT plays an important role in regulating glycolytic flux, phagocytic activity and TNF-α production in LPS-stimulated macrophages and may also contribute to IFN responses (94, 95). At the level of branched-chain amino acid metabolism, BMM had increased expression of genes associated with branched-chain amino acid catabolism. Conversely, MDM downregulated genes associated with this pathway. Catabolic products of branched chain amino acid metabolism feed into the TCA cycle contributing to the production of succinyl-CoA and acetyl-CoA (96). Previous studies have shown that branched-chain amino acid availability is critical for lymphocyte proliferation and M1 macrophage activation, but little is known regarding the role of these amino acids in regulating immune responses (97, 98). Thus, upregulation of branched chain amino acid catabolism in BMM may compensate for the loss of OXPHOS activity, which is not required in MDM.

Lipid metabolism has been shown to play an important role in antiviral responses in BMM and MDM (23, 24, 53). Consistent with the literature, altered gene expression in BMM and MDM

suggest these cells may downregulate *de novo* cholesterol synthesis and shunt available free cholesterol towards the production of oxysterols including 25-hydroxycholesterol and 27-hydroxycholesterol. The role of cholesterol flux in antiviral responses has been described previously (22, 23, 54). Increased cholesterol levels help facilitate the entry of the dengue virus during the early phases of infection, which is reduced by the presence of oxysterols such as 25-hydroxycholesterol (22, 99-101). Macrophages can also counteract this demand by switching away from *de novo* synthesis towards lipid import (23). Limiting flux through the cholesterol biosynthetic pathway induces a STING-mediated type I IFN response, which can be attenuated by exogenous free cholesterol (23, 54). I also observed significant alterations in genes associated with phospholipid, sphingolipid, and FA metabolism. Lipid membrane composition can play a critical role in the antiviral capabilities of immune cells. Sphingolipids and phosphatidylserine have been shown to function as receptors for polyomavirus, HIV, and vesicular stomatitis virus (VSV) (102-104). Altering the lipid composition of the plasma membrane is a vital protective strategy against viral entry by altering the potential interaction sites for viruses (105, 106). Thus, altering the membrane lipid composition may be a critical feature of metabolic reprogramming in early antiviral responses.

Collectively, our study provides critical new insights into the molecular underpinnings of metabolic reprogramming associated with short term IFN-α responses in mouse BMM and human MDM. This is the first study to systematically characterize changes in metabolic gene expression using transcriptional profiling in this context. However, I acknowledge certain limitations of this study. The current study only evaluates gene expression profiles via microarray. Validation and functional testing are required to understand the biological relevance of these findings. While both BMM and MDM were stimulated with short term IFN-α, I cannot exclude the possibility that some

of the reported differences may reflect the length of time in stimulant (2.5h vs. 4h). Preliminary studies from our laboratory suggest metabolic profiles in stimulated BMM are similar within a 2-6-hour window. However, future time-course studies are required to examine how metabolic signatures change in BMM and MDM over short and long term IFN-α stimulation. Culture conditions and differentiation protocols may also affect metabolic profiles in BMM vs. MDM. This limitation should be an important consideration across all studies examining relationships between immune and metabolic processes *in vitro*, whether in humans or in mice. Careful consideration of the model system may be required depending on downstream applications of the findings. Meta-analyses of transcriptional data sets may represent a powerful tool to identify metabolic signatures that are consistently altered across different studies using different models, time points, culture conditions etc. To minimize these effects, only studies performed in high glucose DMEM (plus glutamine and sodium pyruvate) with 10% FBS were selected for analyses. Finally, both BMM and MDM were analyzed using Affymetrix technologies' microarray chips. However, I cannot exclude the possibility that the reported differences may be affected by the microarray used. Despite these limitations, I strongly believe this comparative study provides important new insights into metabolic processes that contribute to IFN responses in mouse and human macrophages. I believe that the power of an untargeted approach such as transcriptional profiling is to systematically characterize these differences, which may have important implications on effector function depending on the local microenvironment. In the future, more targeted studies are required to evaluate the effects of these gene expression profiles on protein expression and functional metabolic and immune responses.

2.5. Conclusions

In summary, this study identified a variety of metabolic pathways altered following short term IFN-α stimulation in mouse and human macrophage systems. This may have important implications for the initiation of early antiviral immune responses, including the induction of the specific antimicrobial and immunomodulatory functions of IFN-α. While functional studies are required to clearly elucidate the relationships between this metabolic reprogramming and effector function, it is clear that transcriptional regulation of metabolic processes is a key feature of early type I IFN responses. An in-depth understanding of this early reprogramming may lead to the development of targeted therapeutics that regulate and fine tune specific type I IFN effector function.

2.6. Data Availability

Gene expression data used in this study have been previously published in the GEO database under the accession numbers GSE16755 (https://www.ncbi.nlm.nih.gov/geo/query/acc.cgi?acc=GSE16755) and GSE35825 (https://www.ncbi.nlm.nih.gov/geo/query/acc.cgi?acc=GSE35825)

2.7.   References

1.   Isaacs, A., and J. Lindenmann. 1957. Virus Interference. I. The Interferon. *Proc. R. Soc. Lond. B. Biol. Sci.* 147: 258-267.
2.   Isaacs, A., J. Lindenmann, and R. C. Valentine. 1957. Virus Interference. II. Some Properties of Interferon. *Proc. R. Soc. Lond. B. Biol. Sci.* 147: 268-273.
3.   Pestka, S., C. D. Krause, and M. R. Walter. 1987. Interferons, interferon-like cytokines, and their receptors. *Immunol. Rev.* 202 8-32.
4.   Trinchieri, G. 2010. Type I interferon: friend or foe? *J. Exp. Med.* 207: 2053-2063.
5.   Samuel, C. E. 2001. Antiviral Actions of Interferons. *Clin. Microbiol. Rev.* 14: 778-809.
6.   Stark, G. R., I. M. Kerr, B. R. G. Williams, R. H. Silverman, and R. D. Schreiber. 1998. How cells respond to interferons. *Annu. Rev. Biochem.* 67: 227-264.
7.   Platanias, L. C. 2005. Mechanisms of type-I- and type-II-interferon-mediated signalling. *Nat. Rev. Immunol.* 5: 375-386.
8.   Ivashkiv, L. B., and L. T. Donlin. 2014. Regulation of type I interferon responses. *Nat. Rev. Immunol.* 14: 36-49.
9.   Arimoto, K. I., S. Lochte, S. A. Stoner, C. Burkart, Y. Zhang, S. Miyauchi, S. Wilmes, J.-B. Fan, J. J. Heinisch, Z. Li, M. Yan, S. Pellegrini, F. Colland, J. Piehler, and D.-E. Zhang. 2017. STAT2 is an essential adaptor in USP18-mediated suppression of type I interferon signaling. *Nat. Struct. Mol. Biol.* 24: 279-289.
10.   Schneider, W. M., M. D. Chevillotte, and C. M. Rice. 2014. Interferon-Stimulated Genes: A Complex Web of Host Defenses. *Annu. Rev. Immunol.* 32: 513-545.
11.   Schoggins, J. W., and C. M. Rice. 2011. Interferon-stimulated genes and their antiviral effector functions. *Curr. Opin. Virol.* 1: 519-525.
12.   Bianchi, M. E. 2007. DAMPs, PAMPs and alarmins: all we need to know about danger. *J. Leukoc. Biol.* 81: 1-5.
13.   Iannello, A., O. Debbeche, E. Martin, L. H. Attalah, S. Samarani, and A. Ahmad. 2006. Viral strategies for evading antiviral cellular immune responses of the host. *J. Leukoc. Biol.* 79: 16-35.
14.   Tannahill, G. M., A. M. Curtis, J. Adamik, E. M. Palsson-McDermott, A. F. McGettrick, G. Goel, C. Frezza, N. J. Bernard, B. Kelly, N. H. Foley, L. Zheng, A. Gardet, Z. Tong, S. S. Jany, S. C. Corr, M. Haneklaus, B. E. Caffrey, K. Pierce, S. Walmsley, F. C. Beasley, E. Cummins, V. Nizet, M. Whyte, C. T. Taylor, H. Lin, S. L. Masters, E. Gottlieb, V. P. Kelly, C. Clish, P. E. Auron, R. J. Xavier, and L. A. J. O'Neill. 2013. Succinate is an inflammatory signal that induces IL-1β through HIF-1α. *Nature* 496: 238-242.
15.   Errea, A., D. Cayet, P. Marchetti, C. Tang, J. Kluza, S. Offermanns, J.-C. Sirard, and M. Rumbo. 2016. Lactate Inhibits the Pro-Inflammatory Response and Metabolic Reprogramming in Murine Macrophages in a GPR81-Independent Manner. *PLoS ONE* 11: e0163694.
16.   Infantino, V., V. Iacobazzi, F. Palmieri, and A. Menga. 2013. ATP-citrate lyase is essential for macrophage inflammatory response. *Biochem. Biophys. Res. Commun.* 440: 105-111.
17.   Kesarwani, P., A. K. Murali, A. A. Al-Khami, and S. Mehrotra. 2013. Redox regulation of T-cell function: from molecular mechanisms to significance in human health and disease. *Antioxid. Redox Signal.* 18: 1497-1534.

18. Wang, H., H. Flach, M. Onizawa, L. Wei, M. T. McManus, and A. Weiss. 2014. Negative regulation of Hif1a expression and TH17 differentiation by the hypoxia-regulated microRNA miR-210. *Nat. Immunol.* 15: 393-401.

19. Mills, E. L., B. Kelly, A. Logan, A. S. H. Costa, M. Varma, C. E. Bryant, P. Tourlomousis, J. H. M. Däbritz, E. Gottlieb, I. Latorre, S. C. Corr, G. McManus, D. Ryan, H. T. Jacobs, M. Szibor, R. J. Xavier, T. Braun, C. Frezza, M. P. Murphy, and L. A. O'Neill. 2016. Succinate Dehydrogenase Supports Metabolic Repurposing of Mitochondria to Drive Inflammatory Macrophages. *Cell* 167: 457-470.e413.

20. Jiang, H., H. Shi, M. Sun, Y. Wang, Q. Meng, P. Guo, Y. Cao, J. Chen, X. Gao, E. Li, and J. Liu. 2016. PFKFB3-Driven Macrophage Glycolytic Metabolism Is a Crucial Component of Innate Antiviral Defense. *J. Immunol.* 197: 2880-2890.

21. Blanc, M., W. Y. Hsieh, K. A. Robertson, S. Watterson, G. Shui, P. Lacaze, M. Khondoker, P. Dickinson, G. Sing, S. Rodríguez-Martín, P. Phelan, T. Forster, B. Strobl, M. Müller, R. Riemersma, T. Osborne, M. R. Wenk, A. Angulo, and P. Ghazal. 2011. Host Defense against Viral Infection Involves Interferon Mediated Down-Regulation of Sterol Biosynthesis. *PLoS Biol* 9: e1000598.

22. Blanc, M., Wei Y. Hsieh, Kevin A. Robertson, Kai A. Kropp, T. Forster, G. Shui, P. Lacaze, S. Watterson, Samantha J. Griffiths, Nathanael J. Spann, A. Meljon, S. Talbot, K. Krishnan, Douglas F. Covey, Markus R. Wenk, M. Craigon, Z. Ruzsics, J. Haas, A. Angulo, William J. Griffiths, Christopher K. Glass, Y. Wang, and P. Ghazal. 2013. The Transcription Factor STAT-1 Couples Macrophage Synthesis of 25-Hydroxycholesterol to the Interferon Antiviral Response. *Immunity* 38: 106-118.

23. York, Autumn G., Kevin J. Williams, Joseph P. Argus, Quan D. Zhou, G. Brar, L. Vergnes, Elizabeth E. Gray, A. Zhen, Nicholas C. Wu, Douglas H. Yamada, Cameron R. Cunningham, Elizabeth J. Tarling, Moses Q. Wilks, D. Casero, David H. Gray, Amy K. Yu, Eric S. Wang, David G. Brooks, R. Sun, Scott G. Kitchen, T.-T. Wu, K. Reue, Daniel B. Stetson, and Steven J. Bensinger. 2015. Limiting Cholesterol Biosynthetic Flux Spontaneously Engages Type I IFN Signaling. *Cell* 163: 1716-1729.

24. Boshuizen, M. C. S., M. A. Hoeksema, A. E. Neele, S. van der Velden, A. A. J. Hamers, J. Van den Bossche, E. Lutgens, and M. P. J. de Winther. 2016. Interferon-β promotes macrophage foam cell formation by altering both cholesterol influx and efflux mechanisms. *Cytokine* 77: 220-226.

25. Maneglier, B., C. Rogez-Kreuz, O. Spreux-Varoquaux, B. Malleret, P. Thérond, B. Samah, I. Drouet, D. Dormont, C. Advenier, and P. Clayette. 2007. Comparative effects of two type I interferons, human IFN-α and ovine IFN-τ on indoleamine-2,3-dioxygenase in primary cultures of human macrophages. *Fundam. Clin. Pharmacol.* 21: 29-34.

26. Acosta-Iborra, B., A. Elorza, I. M. Olazabal, N. B. Martín-Cofreces, S. Martin-Puig, M. Miró, M. J. Calzada, J. Aragonés, F. Sánchez-Madrid, and M. O. Landázuri. 2009. Macrophage Oxygen Sensing Modulates Antigen Presentation and Phagocytic Functions Involving IFN-γ Production through the HIF-1α Transcription Factor. *J. Immunol.* 182: 3155-3164.

27. Peyssonnaux, C., V. Datta, T. Cramer, A. Doedens, E. A. Theodorakis, R. L. Gallo, N. Hurtado-Ziola, V. Nizet, and R. S. Johnson. 2005. HIF-1α expression regulates the bactericidal capacity of phagocytes. *J. Clin. Invest.* 115: 1806-1815.

28.   Nagy, C., and A. Haschemi. 2015. Time and Demand are Two Critical Dimensions of Immunometabolism: The Process of Macrophage Activation and the Pentose Phosphate Pathway. *Frontiers in Immunology* 6: 164.

29.   Kelly, B., and L. A. J. O'Neill. 2015. Metabolic reprogramming in macrophages and dendritic cells in innate immunity. *Cell Res.* 25: 771-784.

30.   O'Neill, L. A. J., and E. J. Pearce. 2016. Immunometabolism governs dendritic cell and macrophage function. *J. Exp. Med.* 213: 15-23.

31.   Barrett, T., S. E. Wilhite, P. Ledoux, C. Evangelista, I. F. Kim, M. Tomashevsky, K. A. Marshall, K. H. Phillippy, P. M. Sherman, M. Holko, A. Yefanov, H. Lee, N. Zhang, C. L. Robertson, N. Serova, S. Davis, and A. Soboleva. 2013. NCBI GEO: archive for functional genomics data sets—update. *Nucleic Acids Res.* 41: D991-D995.

32.   Liu, S.-Y., D. J. Sanchez, R. Aliyari, S. Lu, and G. Cheng. 2012. Systematic identification of type I and type II interferon-induced antiviral factors. *Proc. Natl. Acad. Sci. U. S. A.* 109: 4239-4244.

33.   Greenwell-Wild, T., N. Vázquez, W. Jin, Z. Rangel, P. J. Munson, and S. M. Wahl. 2009. Interleukin-27 inhibition of HIV-1 involves an intermediate induction of type I interferon. *Blood* 114: 1864-1874.

34.   Li, C., and W. H. Wong. 2001. Model-based analysis of oligonucleotide arrays: Expression index computation and outlier detection. *Proc. Natl. Acad. Sci. U. S. A.* 98: 31-36.

35.   Gao, J., V. G. Tarcea, A. Karnovsky, B. R. Mirel, T. E. Weymouth, C. W. Beecher, J. D. Cavalcoli, B. D. Athey, G. S. Omenn, C. F. Burant, and H. V. Jagadish. 2010. Metscape: a Cytoscape plug-in for visualizing and interpreting metabolomic data in the context of human metabolic networks. *Bioinformatics* 26: 971-973.

36.   Karnovsky, A., T. Weymouth, T. Hull, V. G. Tarcea, G. Scardoni, C. Laudanna, M. A. Sartor, K. A. Stringer, H. V. Jagadish, C. Burant, B. Athey, and G. S. Omenn. 2012. Metscape 2 bioinformatics tool for the analysis and visualization of metabolomics and gene expression data. *Bioinformatics* 28: 373-380.

37.   Cline, M. S., M. Smoot, E. Cerami, A. Kuchinsky, N. Landys, C. Workman, R. Christmas, I. Avila-Campilo, M. Creech, B. Gross, K. Hanspers, R. Isserlin, R. Kelley, S. Killcoyne, S. Lotia, S. Maere, J. Morris, K. Ono, V. Pavlovic, A. R. Pico, A. Vailaya, P.-L. Wang, A. Adler, B. R. Conklin, L. Hood, M. Kuiper, C. Sander, I. Schmulevich, B. Schwikowski, G. J. Warner, T. Ideker, and G. D. Bader. 2007. Integration of biological networks and gene expression data using Cytoscape. *Nat. Protocols* 2: 2366-2382.

38.   Xia, J., I. V. Sinelnikov, B. Han, and D. S. Wishart. 2015. MetaboAnalyst 3.0—making metabolomics more meaningful. *Nucleic Acids Res.* 43: W251-257.

39.   Subramanian, A., P. Tamayo, V. K. Mootha, S. Mukherjee, B. L. Ebert, M. A. Gillette, A. Paulovich, S. L. Pomeroy, T. R. Golub, E. S. Lander, and J. P. Mesirov. 2005. Gene set enrichment analysis: A knowledge-based approach for interpreting genome-wide expression profiles. *Prod. Natl. Acad. Sci. U.S.A.* 102: 15545-15550.

40.   Huang, D. W., B. T. Sherman, X. Zheng, J. Yang, T. Imamichi, R. Stephens, and R. A. Lempicki. 2009. Extracting Biological Meaning from Large Gene Lists with DAVID. In *Curr. Protoc. Bioinformatics.* John Wiley and Sons, Inc. 1-13.

41.   Huang, D. W., B. T. Sherman, and R. A. Lempicki. 2009. Systematic and integrative analysis of large gene lists using DAVID bioinformatics resources. *Nat. Protocols* 4: 44-57.

42. Lu, B., T. Nakamura, K. Inouye, J. Li, Y. Tang, P. Lundbäck, S. I. Valdes-Ferrer, P. S. Olofsson, T. Kalb, J. Roth, Y. Zou, H. Erlandsson-Harris, H. Yang, J. P. Y. Ting, H. Wang, U. Andersson, D. J. Antoine, S. S. Chavan, G. S. Hotamisligil, and K. J. Tracey. 2012. Novel role of PKR in inflammasome activation and HMGB1 release. *Nature* 488: 670.

43. Garten, A., S. Petzold, A. Körner, S.-i. Imai, and W. Kiess. 2009. Nampt: linking NAD biology, metabolism and cancer. *Trends in Endocrinology & Metabolism* 20: 130-138.

44. Schoggins, J. W., S. J. Wilson, M. Panis, M. Y. Murphy, C. T. Jones, P. Bieniasz, and C. M. Rice. 2011. A diverse range of gene products are effectors of the type I interferon antiviral response. *Nature* 472: 481-485.

45. Liemburg-Apers, D. C., P. H. G. M. Willems, W. J. H. Koopman, and S. Grefte. 2015. Interactions between mitochondrial reactive oxygen species and cellular glucose metabolism. *Arch. Toxicol.* 89: 1209-1226.

46. Quijano, C., M. Trujillo, L. Castro, and A. Trostchansky. 2016. Interplay between oxidant species and energy metabolism. *Redox Biol.* 8: 28-42.

47. Kang, S. W., S. Lee, and E. K. Lee. 2015. ROS and energy metabolism in cancer cells: alliance for fast growth. *Arch. Pharm. Res.* 38: 338-345.

48. Hwang, J., H.-W. Suh, Y. H. Jeon, E. Hwang, L. T. Nguyen, J. Yeom, S.-G. Lee, C. Lee, K. J. Kim, B. S. Kang, J.-O. Jeong, T.-K. Oh, I. Choi, J.-O. Lee, and M. H. Kim. 2014. The structural basis for the negative regulation of thioredoxin by thioredoxin-interacting protein. *Nat. Commun.* 5: 2958.

49. Watanabe, R., H. Nakamura, H. Masutani, and J. Yodoi. 2010. Anti-oxidative, anti-cancer and anti-inflammatory actions by thioredoxin 1 and thioredoxin-binding protein-2. *Pharmacol. Ther.* 127: 261-270.

50. Mellor, A. L., and D. H. Munn. 1999. Tryptophan catabolism and T-cell tolerance: immunosuppression by starvation? *Immunol. Today* 20: 469-473.

51. Boasso, A., A. W. Hardy, S. A. Anderson, M. J. Dolan, and G. M. Shearer. 2008. HIV-Induced Type I Interferon and Tryptophan Catabolism Drive T Cell Dysfunction Despite Phenotypic Activation. *PLoS ONE* 3: e2961.

52. Nakagawa, J., H. Waldner, S. Meyer-Monard, J. Hofsteenge, P. Jenö, and C. Moroni. 1995. AUH, a gene encoding an AU-specific RNA binding protein with intrinsic enoyl-CoA hydratase activity. *Proc. Natl. Acad. Sci. U. S. A.* 92: 2051-2055.

53. Coulombe, F., J. Jaworska, M. Verway, F. Tzelepis, A. Massoud, J. Gillard, G. Wong, G. Kobinger, Z. Xing, C. Couture, P. Joubert, Jörg H. Fritz, William S. Powell, and M. Divangahi. 2014. Targeted Prostaglandin E2 Inhibition Enhances Antiviral Immunity through Induction of Type I Interferon and Apoptosis in Macrophages. *Immunity* 40: 554-568.

54. Blanc, M., W. Y. Hsieh, K. A. Robertson, S. Watterson, G. Shui, P. Lacaze, M. Khondoker, P. Dickinson, G. Sing, and S. Rodriguez-Martin. 2011. Host defense against viral infection involves interferon mediated down-regulation of sterol biosynthesis. *PLoS Biol* 9: e1000598.

55. Chugh, A., A. Ray, and J. B. Gupta. 2003. Squalene epoxidase as hypocholesterolemic drug target revisited. *Prog. Lipid Res.* 42: 37-50.

56. van Meer, G., D. R. Voelker, and G. W. Feigenson. 2008. Membrane lipids: where they are and how they behave. *Nat. Rev. Mol. Cell Biol.* 9: 112-124.

57.   Rodríguez-Prados, J., P. G. Través, J. Cuenca, D. Rico, J. Aragonés, P. Martín-Sanz, M. Cascante, and L. Boscá. 2010. Substrate Fate in Activated Macrophages: A Comparison between Innate, Classic, and Alternative Activation. *J. Immunol.* 185: 605-614.

58.   Vazquez, A., J. Liu, Y. Zhou, and Z. N. Oltvai. 2010. Catabolic efficiency of aerobic glycolysis: The Warburg effect revisited. *BMC Syst. Biol.* 4: 1-9.

59.   Imtiyaz, H. Z., and M. C. Simon. 2010. Hypoxia-inducible factors as essential regulators of inflammation. *Curr. Top. Microbiol. Immunol.* 345: 105-120.

60.   Infantino, V., P. Convertini, L. Cucci, Maria A. Panaro, Maria A. Di Noia, R. Calvello, F. Palmieri, and V. Iacobazzi. 2011. The mitochondrial citrate carrier: a new player in inflammation. *Biochem. J.* 438: 433-436.

61.   Fischer, K., P. Hoffmann, S. Voelkl, N. Meidenbauer, J. Ammer, M. Edinger, E. Gottfried, S. Schwarz, G. Rothe, S. Hoves, K. Renner, B. Timischl, A. Mackensen, L. Kunz-Schughart, R. Andreesen, S. W. Krause, and M. Kreutz. 2007. Inhibitory effect of tumor cell–derived lactic acid on human T cells. *Blood* 109: 3812.

62.   Haas, R., J. Smith, V. Rocher-Ros, S. Nadkarni, T. Montero-Melendez, F. D'Acquisto, E. J. Bland, M. Bombardieri, C. Pitzalis, M. Perretti, F. M. Marelli-Berg, and C. Mauro. 2015. Lactate Regulates Metabolic and Pro-inflammatory Circuits in Control of T Cell Migration and Effector Functions. *PLoS Biol.* 13: e1002202.

63.   He, L., H. Li, N. Huang, X. Zhou, J. Tian, T. Li, J. Wu, Y. Tian, Y. Yin, and K. Yao. 2017. Alpha-ketoglutarate suppresses the NF-kappaB-mediated inflammatory pathway and enhances the PXR-regulated detoxification pathway. *Oncotarget*: 1-15.

64.   Luo, W., H. Hu, R. Chang, J. Zhong, M. Knabel, R. O'Meally, Robert N. Cole, A. Pandey, and Gregg L. Semenza. 2011. Pyruvate Kinase M2 Is a PHD3-Stimulated Coactivator for Hypoxia-Inducible Factor 1. *Cell* 145: 732-744.

65.   Luo, W., and G. L. Semenza. 2011. Pyruvate kinase M2 regulates glucose metabolism by functioning as a coactivator for hypoxia-inducible factor 1 in cancer cells. *Oncotarget* 2: 551-556.

66.   Chang, C.-H., J. D. Curtis, L. B. Maggi, B. Faubert, A. V. Villarino, D. O'Sullivan, S. C.-C. Huang, G. J. W. van der Windt, J. Blagih, J. Qiu, J. D. Weber, E. J. Pearce, R. G. Jones, and E. L. Pearce. 2013. Posttranscriptional Control of T Cell Effector Function by Aerobic Glycolysis. *Cell* 153: 1239-1251.

67.   Milasta, S., Christopher P. Dillon, Oliver E. Sturm, Katherine C. Verbist, Taylor L. Brewer, G. Quarato, Scott A. Brown, S. Frase, Laura J. Janke, S. S. Perry, Paul G. Thomas, and Douglas R. Green. 2016. Apoptosis-Inducing-Factor-Dependent Mitochondrial Function Is Required for T Cell but Not B Cell Function. *Immunity* 44: 88-102.

68.   Drapier, J. C., and J. B. Hibbs. 1988. Differentiation of murine macrophages to express nonspecific cytotoxicity for tumor cells results in L-arginine-dependent inhibition of mitochondrial iron-sulfur enzymes in the macrophage effector cells. *J. Immunol.* 140: 2829-2838.

69.   Clementi, E., G. C. Brown, M. Feelisch, and S. Moncada. 1998. Persistent inhibition of cell respiration by nitric oxide: Crucial role of S-nitrosylation of mitochondrial complex I and protective action of glutathione. *Proc. Natl. Acad. Sci. U.S.A.* 95: 7631-7636.

70.   Cleeter, M. W. J., J. M. Cooper, V. M. Darley-Usmar, S. Moncada, and A. H. V. Schapira. 1994. Reversible inhibition of cytochrome c oxidase, the terminal enzyme of

the mitochondrial respiratory chain, by nitric oxide. Implications for neurodegenerative diseases. *FEBS Lett.* 345: 50-54.

71.   Doulias, P.-T., M. Tenopoulou, J. L. Greene, K. Raju, and H. Ischiropoulos. 2013. Nitric oxide regulates mitochondrial fatty acid metabolism through reversible protein S-nitrosylation. *Sci. Signal.* 6: rs1.

72.   Herbst, S., U. E. Schaible, and B. E. Schneider. 2011. Interferon Gamma Activated Macrophages Kill Mycobacteria by Nitric Oxide Induced Apoptosis. *PLoS ONE* 6: e19105.

73.   Jha, Abhishek K., Stanley C.-C. Huang, A. Sergushichev, V. Lampropoulou, Y. Ivanova, E. Loginicheva, K. Chmielewski, Kelly M. Stewart, J. Ashall, B. Everts, Edward J. Pearce, Edward M. Driggers, and Maxim N. Artyomov. 2015. Network Integration of Parallel Metabolic and Transcriptional Data Reveals Metabolic Modules that Regulate Macrophage Polarization. *Immunity* 42: 419-430.

74.   El Kasmi, K. C., and K. R. Stenmark. 2015. Contribution of metabolic reprogramming to macrophage plasticity and function. *Seminars in Immunology* 27: 267-275.

75.   West, A. P., I. E. Brodsky, C. Rahner, D. K. Woo, H. Erdjument-Bromage, P. Tempst, M. C. Walsh, Y. Choi, G. S. Shadel, and S. Ghosh. 2011. TLR signalling augments macrophage bactericidal activity through mitochondrial ROS. *Nature* 472: 476-480.

76.   Mak, T. W., M. Grusdat, G. S. Duncan, C. Dostert, Y. Nonnenmacher, M. Cox, C. Binsfeld, Z. Hao, A. Brüstle, M. Itsumi, C. Jäger, Y. Chen, O. Pinkenburg, B. Camara, M. Ollert, C. Bindslev-Jensen, V. Vasiliou, C. Gorrini, P. A. Lang, M. Lohoff, I. S. Harris, K. Hiller, and D. Brenner. 2017. Glutathione Primes T Cell Metabolism for Inflammation. *Immunity* 46: 675-689.

77.   DeVito, S. R., E. Ortiz-Riaño, L. Martínez-Sobrido, and J. Munger. 2014. Cytomegalovirus-mediated activation of pyrimidine biosynthesis drives UDP–sugar synthesis to support viral protein glycosylation. *Proc. Natl. Acad. Sci. U. S. A.* 111: 18019-18024.

78.   Vastag, L., E. Koyuncu, S. L. Grady, T. E. Shenk, and J. D. Rabinowitz. 2011. Divergent Effects of Human Cytomegalovirus and Herpes Simplex Virus-1 on Cellular Metabolism. *PLoS Pathog.* 7: e1002124.

79.   Hoffmann, H.-H., A. Kunz, V. A. Simon, P. Palese, and M. L. Shaw. 2011. Broad-spectrum antiviral that interferes with de novo pyrimidine biosynthesis. *Proc. Natl. Acad. Sci. U. S. A.* 108: 5777-5782.

80.   Lucas-Hourani, M., D. Dauzonne, P. Jorda, G. Cousin, A. Lupan, O. Helynck, G. Caignard, G. Janvier, G. André-Leroux, S. Khiar, N. Escriou, P. Desprès, Y. Jacob, H. Munier-Lehmann, F. Tangy, and P.-O. Vidalain. 2013. Inhibition of Pyrimidine Biosynthesis Pathway Suppresses Viral Growth through Innate Immunity. *PLOS Pathog.* 9: e1003678.

81.   Gavegnano, C., E. M. Kennedy, B. Kim, and R. F. Schinazi. 2012. The Impact of Macrophage Nucleotide Pools on HIV-1 Reverse Transcription, Viral Replication, and the Development of Novel Antiviral Agents. *Mol Biol Int.* 2012: 625983.

82.   Tasken, K., B. S. Skalhegg, K. A. Tasken, R. Solberg, H. K. Knutsen, F. O. Levy, M. Sandberg, S. Orstavik, T. Larsen, A. K. Johansen, T. Vang, H. P. Schrader, N. T. Reinton, K. M. Torgersen, V. Hansson, and T. Jahnsen. 1997. Structure, function, and regulation of human cAMP-dependent protein kinases. *Adv. Second Messenger Phosphoprotein Res.* 31: 191-204.

83. Serezani, C. H., M. N. Ballinger, D. M. Aronoff, and M. Peters-Golden. 2008. Cyclic AMP: master regulator of innate immune cell function. *Am. J. Respir. Cell Mol. Biol.* 39: 127-132.

84. Jin, S. L. C., L. Lan, M. Zoudilova, and M. Conti. 2005. Specific Role of Phosphodiesterase 4B in Lipopolysaccharide-Induced Signaling in Mouse Macrophages. *J. Immunol.* 175: 1523-1531.

85. Rickman, L., C. Scott, D. M. Hunt, T. Hutchinson, M. C. Menéndez, R. Whalan, J. Hinds, M. J. Colston, J. Green, and R. S. Buxton. 2005. A member of the cAMP receptor protein family of transcription regulators in Mycobacterium tuberculosis is required for virulence in mice and controls transcription of the rpfA gene coding for a resuscitation promoting factor. *Mol. Microbiol.* 56: 1274-1286.

86. Smith, R. S., M. C. Wolfgang, and S. Lory. 2004. An Adenylate Cyclase-Controlled Signaling Network Regulates Pseudomonas aeruginosa Virulence in a Mouse Model of Acute Pneumonia. *Infect. Immun.* 72: 1677-1684.

87. Zhan, L., Y. Han, L. Yang, J. Geng, Y. Li, H. Gao, Z. Guo, W. Fan, G. Li, L. Zhang, C. Qin, D. Zhou, and R. Yang. 2008. The Cyclic AMP Receptor Protein, CRP, Is Required for Both Virulence and Expression of the Minimal CRP Regulon in Yersinia pestis Biovar microtus. *Infect. Immun.* 76: 5028-5037.

88. Connelly, L., A. T. Jacobs, M. Palacios-Callender, S. Moncada, and A. J. Hobbs. 2003. Macrophage Endothelial Nitric-oxide Synthase Autoregulates Cellular Activation and Pro-inflammatory Protein Expression. *J. Biol. Chem.* 278: 26480-26487.

89. Endres, S., H. J. Fülle, B. Sinha, D. Stoll, C. A. Dinarello, R. Gerzer, and P. C. Weber. 1991. Cyclic nucleotides differentially regulate the synthesis of tumour necrosis factor-alpha and interleukin-1 beta by human mononuclear cells. *Immunology* 72: 56-60.

90. Adams, O., K. Besken, C. Oberdörfer, C. R. MacKenzie, O. Takikawa, and W. Däubener. 2004. Role of Indoleamine-2,3-Dioxygenase in Alpha/Beta and Gamma Interferon-Mediated Antiviral Effects against Herpes Simplex Virus Infections. *J. Virol.* 78: 2632-2636.

91. Taylor, M. W., and G. S. Feng. 1991. Relationship between interferon-gamma, indoleamine 2,3-dioxygenase, and tryptophan catabolism. *FASEB J.* 5: 2516-2522.

92. Mellor, A. L., and D. H. Munn. 2004. IDO expression by dendritic cells: tolerance and tryptophan catabolism. *Nat. Rev. Immunol.* 4: 762-774.

93. Obojes, K., O. Andres, K. S. Kim, W. Däubener, and J. Schneider-Schaulies. 2005. Indoleamine 2,3-Dioxygenase Mediates Cell Type-Specific Anti-Measles Virus Activity of Gamma Interferon. *J. Virol.* 79: 7768-7776.

94. Venter, G., F. T. J. J. Oerlemans, M. Willemse, M. Wijers, J. A. M. Fransen, and B. Wieringa. 2014. NAMPT-Mediated Salvage Synthesis of NAD+ Controls Morphofunctional Changes of Macrophages. *PLoS ONE* 9: e97378.

95. Al-Shabany, A., A. Moody, A. Foey, and R. Billington. 2016. Intracellular NAD(+) levels are associated with LPS-induced TNF-α release in pro-inflammatory macrophages. *Biosci. Rep.* 36: e00301.

96. Harper, A. E., R. H. Miller, and K. P. Block. 1984. Branched-Chain Amino Acid Metabolism. *Annu. Rev. Nutr.* 4: 409-454.

97. Skaper, S. D., D. P. Molden, and J. E. Seegmiller. 1976. Maple syrup urine disease: branched-chain amino acid concentrations and metabolism in cultured human lymphoblasts. *Biochem Genet* 14: 527-539.

98. Meiser, J., L. Krämer, S. C. Sapcariu, N. Battello, J. Ghelfi, A. F. D'Herouel, A. Skupin, and K. Hiller. 2016. Pro-inflammatory Macrophages Sustain Pyruvate Oxidation through Pyruvate Dehydrogenase for the Synthesis of Itaconate and to Enable Cytokine Expression. *J. Biol. Chem.* 291: 3932-3946.

99. Soto-Acosta, R., C. Mosso, M. Cervantes-Salazar, H. Puerta-Guardo, F. Medina, L. Favari, J. E. Ludert, and R. M. del Angel. 2013. The increase in cholesterol levels at early stages after dengue virus infection correlates with an augment in LDL particle uptake and HMG-CoA reductase activity. *Virology* 442: 132-147.

100. Park, K., and A. L. Scott. 2010. Cholesterol 25-hydroxylase production by dendritic cells and macrophages is regulated by type I interferons. *J. Leukoc. Biol.* 88: 1081-1087.

101. Liu, S.-Y., R. Aliyari, K. Chikere, G. Li, Matthew D. Marsden, Jennifer K. Smith, O. Pernet, H. Guo, R. Nusbaum, Jerome A. Zack, Alexander N. Freiberg, L. Su, B. Lee, and G. Cheng. 2013. Interferon-Inducible Cholesterol-25-Hydroxylase Broadly Inhibits Viral Entry by Production of 25-Hydroxycholesterol. *Immunity* 38: 92-105.

102. Rawat, S. S., M. Viard, S. A. Gallo, R. Blumenthal, and A. Puri. 2006. Sphingolipids, cholesterol, and HIV-1: A paradigm in viral fusion. *Glycoconj. J.* 23: 189-197.

103. Smith, A. E., H. Lilie, and A. Helenius. 2003. Ganglioside-dependent cell attachment and endocytosis of murine polyomavirus-like particles. *FEBS Lett.* 555: 199-203.

104. Ewers, H., W. Romer, A. E. Smith, K. Bacia, S. Dmitrieff, W. Chai, R. Mancini, J. Kartenbeck, V. Chambon, L. Berland, A. Oppenheim, G. Schwarzmann, T. Feizi, P. Schwille, P. Sens, A. Helenius, and L. Johannes. 2010. GM1 structure determines SV40-induced membrane invagination and infection. *Nat. Cell Biol.* 12: 11-18.

105. Merino-Ramos, T., Á. Vázquez-Calvo, J. Casas, F. Sobrino, J.-C. Saiz, and M. A. Martín-Acebes. 2016. Modification of the Host Cell Lipid Metabolism Induced by Hypolipidemic Drugs Targeting the Acetyl Coenzyme A Carboxylase Impairs West Nile Virus Replication. *Antimicrob. Agents Chemother.* 60: 307-315.

106. Pezacki, J. P., S. M. Sagan, A. M. Tonary, Y. Rouleau, S. Bélanger, L. Supekova, and A. I. Su. 2009. Transcriptional profiling of the effects of 25-hydroxycholesterol on human hepatocyte metabolism and the antiviral state it conveys against the hepatitis C virus. *BMC Chem. Biol.* 9: 2.

2.8. Chapter 2 Supplemental Tables

Supplemental Table S2.1: A list of all metabolic genes identified in the BMM dataset.

Entrez Gene ID	Gene Symbol	Gene Title	Fold Change	P-value	FDR
210106	Papd7	PAP associated domain containing 7	6.763807	4.38E-07	0.000139
17308	Mgat1	mannoside acetylglucosaminyltransferase 1	2.781795	6.01E-07	0.000139
70052	Prpf4	PRP4 pre-mRNA processing factor 4 homolog (yeast)	3.405339	1.72E-06	0.000266
20449	St8sia1	ST8 alpha-N-acetyl-neuraminide alpha-2,8-sialyltransferase 1	7.746754	4.42E-06	0.000433
22375	Wars	tryptophanyl-tRNA synthetase	2.38714	8.39E-06	0.000535
53625	B3gnt2	UDP-GlcNAc:betaGal beta-1,3-N-acetylglucosaminyltransferase 2///COMM domain containing 1	2.102979	9.27E-06	0.000548
16542	Kdr	kinase insert domain protein receptor	6.182894	9.46E-06	0.000551
208715	Hmgcs1	3-hydroxy-3-methylglutaryl-Coenzyme A synthase 1	-2.33769	1.11E-05	0.000571
20620	Plk2	polo-like kinase 2	2.603204	1.94E-05	0.00081
12799	Cnp	2',3'-cyclic nucleotide 3' phosphodiesterase	2.532145	2.70E-05	0.000958
17423	Ndst2	N-deacetylase/N-sulfotransferase (heparan glucosaminyl) 2	1.793242	2.93E-05	0.000996
18472	Pafah1b1	platelet-activating factor acetylhydrolase, isoform 1b, subunit 1	-1.26278	3.26E-05	0.001045
22021	Tpst1	protein-tyrosine sulfotransferase 1	7.198429	3.54E-05	0.001081
15369	Hmox2	heme oxygenase (decycling) 2	1.460464	3.74E-05	0.001105
14538	Gcnt2	glucosaminyl (N-acetyl) transferase 2, I-branching enzyme	2.982574	3.86E-05	0.001119
18950	Pnp	purine-nucleoside phosphorylase	2.239241	4.27E-05	0.001165
11992	Auh	AU RNA binding protein/enoyl-coenzyme A hydratase	1.789546	6.16E-05	0.001438
22247	Umps	uridine monophosphate synthetase	-1.69624	8.01E-05	0.001639
71978	Ppp2r2a	protein phosphatase 2, regulatory subunit B, alpha	1.525692	8.16E-05	0.001653
22217	Usp12	predicted gene, 19496///ubiquitin specific peptidase 12	3.421452	8.18E-05	0.001654
16922	Phyh	phytanoyl-CoA hydroxylase	1.557676	9.08E-05	0.001734
22224	Usp10	ubiquitin specific peptidase 10	-1.60565	9.73E-05	0.001786
26433	Plod3	procollagen-lysine, 2-oxoglutarate 5-dioxygenase 3	1.635048	0.000101	0.00181
76630	Stambpl1	STAM binding protein like 1	2.262333	0.000107	0.001853
98256	Kmo	kynurenine 3-monooxygenase (kynurenine 3-hydroxylase)	3.808386	0.000109	0.001868
99929	Tiparp	TCDD-inducible poly(ADP-ribose) polymerase	3.036925	0.00012	0.001969
104418	Dgkz	diacylglycerol kinase zeta	-1.31347	0.000126	0.002016
235584	Dusp7	dual specificity phosphatase 7	-2.27693	0.00015	0.002225
17096	Lyn; Gm11787	Yamaguchi sarcoma viral (v-yes-1) oncogene homolog	1.693171	0.000157	0.002285
14629	Gclc	Glutamate-cysteine ligase, catalytic subunit	-1.8552	0.00016	0.002305
243771	Parp12	poly (ADP-ribose) polymerase family, member 12	3.268517	0.00021	0.002647
11669	Aldh2	aldehyde dehydrogenase 2, mitochondrial	-2.70208	0.000215	0.002674
14231	Fkbp7	FK506 binding protein 7	2.225479	0.000217	0.002686

12988	Csk	c-src tyrosine kinase	1.650648	0.000222	0.002715
14534	Kat2a	K(lysine) acetyltransferase 2A	1.410931	0.000239	0.002809
74596	Cds1	CDP-diacylglycerol synthase 1	1.8141	0.000272	0.002963
14081	Acsl1	acyl-CoA synthetase long-chain family member 1	-1.40739	0.000279	0.002995
74167	Nudt9	nudix (nucleoside diphosphate linked moiety X)-type motif 9	1.507661	0.000304	0.003097
18715	Pim2	proviral integration site 2	-1.5358	0.000321	0.003161
17330	Minpp1	multiple inositol polyphosphate histidine phosphatase 1	1.670051	0.000342	0.003234
110157	Raf1	v-raf-leukemia viral oncogene 1	1.307271	0.000349	0.003258
26410	Map3k8	mitogen-activated protein kinase kinase kinase 8	3.134357	0.000351	0.003264
13548	Dyrk1a	dual-specificity tyrosine-(Y)-phosphorylation regulated kinase 1a	-1.51587	0.000384	0.003366
22234	Ugcg	UDP-glucose ceramide glucosyltransferase	2.437817	0.000413	0.003444
18583	Pde7a	phosphodiesterase 7A	1.515764	0.000416	0.003451
26408	Map3k5	mitogen-activated protein kinase kinase kinase 5	1.417154	0.000432	0.003491
268470	Ube2z	ubiquitin-conjugating enzyme E2Z (putative)	-1.50424	0.000451	0.003537
217127	Kat7	K(lysine) acetyltransferase 7	-1.34363	0.000459	0.003555
69922	Vrk2	vaccinia related kinase 2	1.675036	0.000462	0.00356
69241	Polr2d	polymerase (RNA) II (DNA directed) polypeptide D	-1.4936	0.000462	0.003562
236900	Pdk3	pyruvate dehydrogenase kinase, isoenzyme 3	2.262069	0.000494	0.003629
17769	Mthfr	5,10-methylenetetrahydrofolate reductase	3.793631	0.000494	0.003629
24110	Usp18	ubiquitin specific peptidase 18	46.3677	0.000504	0.003649
211347	Pank3	pantothenate kinase 3	-1.3012	0.000515	0.003671
83813	Tnk1	tyrosine kinase, non-receptor, 1	1.483272	0.000521	0.003682
72349	Dusp3	dual specificity phosphatase 3 (vaccinia virus phosphatase VH1-related)	-1.3074	0.000523	0.003685
18707	Pik3cd	phosphatidylinositol 3-kinase catalytic delta polypeptide	1.998752	0.000535	0.003707
213452	Dstyk	dual serine/threonine and tyrosine protein kinase	-1.43624	0.000537	0.00371
14645	Glul	glutamate-ammonia ligase (glutamine synthetase)	-1.20573	0.000543	0.003721
19108	Prkx	protein kinase, X-linked	2.008997	0.000544	0.003723
214424	Parp16	poly (ADP-ribose) polymerase family, member 16	-1.98746	0.000552	0.003737
67618	Aasdhppt	aminoadipate-semialdehyde dehydrogenase-phosphopantetheinyl transferase	-1.21136	0.000558	0.003748
22214	Ube2h	ubiquitin-conjugating enzyme E2H	-1.42323	0.00056	0.003751
170768	Pfkfb3	6-phosphofructo-2-kinase/fructose-2,6-biphosphatase 3	5.291241	0.000574	0.003773
103534	Mgat4b	mannoside acetylglucosaminyltransferase 4, isoenzyme B	-1.50731	0.000577	0.003779
20779	Src	Rous sarcoma oncogene	-1.54227	0.000579	0.003782
26420	Mapk9	mitogen-activated protein kinase 9	1.32252	0.000583	0.003788
66878	Riok3	RIO kinase 3	-1.27173	0.0006	0.003814
56375	B4galt4	UDP-Gal:betaGlcNAc beta 1,4-galactosyltransferase, polypeptide 4	4.302791	0.000621	0.003844
69737	Ttl	tubulin tyrosine ligase	-1.85121	0.000639	0.003871
73914	Irak3	interleukin-1 receptor-associated kinase 3	-2.11207	0.000648	0.003883
30955	Pik3cg	phosphoinositide-3-kinase, catalytic, gamma polypeptide	-1.50705	0.000666	0.003906

11982	Atp10a	ATPase, class V, type 10A	3.81068	0.000691	0.003964
77976	Nuak1	NUAK family, SNF1-like kinase, 1	-15.2322	0.000714	0.004014
104015	Synj1	synaptojanin 1	2.199326	0.000736	0.004059
104458	Rars	arginyl-tRNA synthetase	1.303931	0.000764	0.004138
217837	Itpk1	inositol 1,3,4-triphosphate 5/6 kinase	1.52582	0.000802	0.004239
73086	Rps6ka5	ribosomal protein S6 kinase, polypeptide 5	-1.66255	0.00081	0.00426
207839	Galnt6	UDP-N-acetyl-alpha-D-galactosamine:polypeptide N-acetylgalactosaminyltransferase 6	-1.72417	0.000888	0.004453
20112	Rps6ka2	ribosomal protein S6 kinase, polypeptide 2	-1.5991	0.000918	0.004523
330260	Pon2	paraoxonase 2	-1.20562	0.000926	0.00454
20448	St6galnac4	ST6 (alpha-N-acetyl-neuraminyl-2,3-beta-galactosyl-1,3)-N-acetylgalactosaminide alpha-2,6-sialyltransferase 4	2.002204	0.000926	0.004541
20768	Sephs2	selenophosphate synthetase 2	-1.83655	0.000927	0.004543
80285	Parp9	poly (ADP-ribose) polymerase family, member 9	5.357382	0.000951	0.004596
12894	Cpt1a	carnitine palmitoyltransferase 1a, liver	1.239826	0.000999	0.004699
50877	Neu3	neuraminidase 3	2.789321	0.001017	0.004736
17768	Mthfd2	methylenetetrahydrofolate dehydrogenase (NAD+ dependent), methenyltetrahydrofolate cyclohydrolase	2.173051	0.001023	0.004747
101187	Parp11	poly (ADP-ribose) polymerase family, member 11	2.375364	0.001096	0.004889
67956	Kmt5a	SET domain containing (lysine methyltransferase) 8	-1.98859	0.001102	0.004901
67045	Riok2	RIO kinase 2 (yeast)	-1.59731	0.001122	0.004936
24086	Tlk2	tousled-like kinase 2 (Arabidopsis)	2.46983	0.00117	0.005022
19267	Ptpre	protein tyrosine phosphatase, receptor type, E	-2.10887	0.001185	0.005047
234135	Whsc1l1	Wolf-Hirschhorn syndrome candidate 1-like 1 (human)	2.092489	0.001185	0.005048
68603	Pmvk	phosphomevalonate kinase	1.578973	0.001191	0.005057
27399	Ip6k1	inositol hexaphosphate kinase 1	-1.32241	0.001218	0.005103
547253	Parp14	poly (ADP-ribose) polymerase family, member 14	5.081282	0.001221	0.005107
12566	Cdk2	cyclin-dependent kinase 2	-1.33454	0.001225	0.005114
170755	Sgk3	serum/glucocorticoid regulated kinase 3	2.03164	0.001233	0.005127
18099	Nlk	nemo like kinase	-1.34664	0.001239	0.005137
327951	Cyb5d1	cytochrome b5 domain containing 1	-1.55873	0.001269	0.005184
15277	Hk2	hexokinase 2	1.893444	0.001304	0.005238
14537	Gcnt1	glucosaminyl (N-acetyl) transferase 1, core 2	1.721606	0.00131	0.005247
101540	Prkd2	protein kinase D2	-1.49341	0.001359	0.00532
59027	Nampt	nicotinamide phosphoribosyltransferase	2.861968	0.001374	0.00534
19042	Ppm1a	protein phosphatase 1A, magnesium dependent, alpha isoform	-1.36846	0.001379	0.005348
14528	Gch1	GTP cyclohydrolase 1	2.090721	0.001389	0.005362
18783	Pla2g4a	phospholipase A2, group IVA (cytosolic, calcium-dependent)	1.901651	0.001434	0.005423
16891	Lipg	lipase, endothelial	3.397824	0.001464	0.005462
11545	Parp1	poly (ADP-ribose) polymerase family, member 1	-1.87172	0.001465	0.005464
110119	Mpi	mannose phosphate isomerase	1.714154	0.001481	0.005485
107823	Whsc1	Wolf-Hirschhorn syndrome candidate 1 (human)	-2.17186	0.001539	0.005557

20773	Sptlc2	serine palmitoyltransferase, long chain base subunit 2	2.274875	0.001543	0.005562
70750	Kdsr	3-ketodihydrosphingosine reductase	-1.24223	0.001546	0.005565
74568	Mlkl	mixed lineage kinase domain-like	5.262045	0.001548	0.005568
269181	Mgat4a	mannoside acetylglucosaminyltransferase 4, isoenzyme A	1.762276	0.001558	0.00558
18970	Polb	polymerase (DNA directed), beta	1.597279	0.001559	0.005581
30940	Usp25	ubiquitin specific peptidase 25	1.731778	0.00159	0.005617
21871	Atp6v0a2	ATPase, H+ transporting, lysosomal V0 subunit A2	1.647803	0.001595	0.005623
18519	Kat2b	K(lysine) acetyltransferase 2B	1.582017	0.001605	0.005635
81601	Kat5	K(lysine) acetyltransferase 5	-1.34364	0.001632	0.005677
17772	Mtm1	X-linked myotubular myopathy gene 1	-1.8719	0.001746	0.005841
107569	Nt5c3	5'-nucleotidase, cytosolic III	7.718086	0.001753	0.005851
78920	Dlst	dihydrolipoamide S-succinyltransferase (E2 component of 2-oxo-glutarate complex)	-1.37118	0.001766	0.005868
73699	Ppp2r1b	protein phosphatase 2, regulatory subunit A, beta	-1.43771	0.00179	0.005901
19088	Prkar2b	protein kinase, cAMP dependent regulatory, type II beta	-1.48713	0.001817	0.005937
71340	Riok1	RIO kinase 1 (yeast)	-1.56169	0.001826	0.005949
11513	Adcy7	adenylate cyclase 7	-1.31653	0.00186	0.005994
18706	Pik3ca	phosphatidylinositol 3-kinase, catalytic, alpha polypeptide	-2.12379	0.001893	0.006035
13178	Dck	deoxycytidine kinase	11.01118	0.001899	0.006043
233011	Itpkc	inositol 1,4,5-trisphosphate 3-kinase C	-4.10654	0.001935	0.006087
20775	Sqle	squalene epoxidase	-1.29846	0.001957	0.006114
381406	Trp53rka	RIKEN cDNA 2810408M09 gene	-2.92393	0.001957	0.006115
14660	Gls	glutaminase	-1.45952	0.001986	0.006149
93765	Ube2n; Mcg1038069	ubiquitin-conjugating enzyme E2N	-1.22274	0.002048	0.006221
22390	Wee1	WEE 1 homolog 1 (S. pombe)	-1.96865	0.002095	0.006275
19277	Ptpro	protein tyrosine phosphatase, receptor type, O	1.285696	0.002115	0.006298
56421	Pfkp	phosphofructokinase, platelet	1.462618	0.002132	0.006316
20656	Sod2	superoxide dismutase 2, mitochondrial	-2.8823	0.00215	0.006335
58193	Extl2	exostoses (multiple)-like 2	-1.38527	0.002151	0.006336
232533	Stk38l	serine/threonine kinase 38 like	1.854298	0.002206	0.006395
11432	Acp2	acid phosphatase 2, lysosomal	-1.3285	0.002216	0.006405
20963	Syk	spleen tyrosine kinase	-1.42526	0.002216	0.006405
75320	Etnk1	ethanolamine kinase 1	3.421538	0.002237	0.006427
26406	Map3k3	mitogen-activated protein kinase kinase kinase 3	-1.37786	0.002266	0.006456
56361	Pus1	pseudouridine synthase 1	-1.37161	0.002278	0.006468
14048	Eya1	eyes absent 1 homolog (Drosophila)	-1.91034	0.002301	0.006491
104831	Ptpn23	protein tyrosine phosphatase, non-receptor type 23	-1.72145	0.002312	0.006502
14718	Got1	glutamate oxaloacetate transaminase 1, soluble	1.318871	0.002335	0.006525
29869	Ulk2	unc-51 like kinase 2	-1.51079	0.002343	0.006532
269941	Chsy1	chondroitin sulfate synthase 1	-1.64039	0.002352	0.006541
72157	Pgm2	phosphoglucomutase 2	1.383666	0.002362	0.00655

12572	Cdk7	cyclin-dependent kinase 7	-1.21154	0.0024	0.006586
18806	Pld2	phospholipase D2	-1.40494	0.002402	0.006588
252870	Usp7	ubiquitin specific peptidase 7	1.35695	0.002403	0.006589
11479	Acvr1b	activin A receptor, type 1B	-1.24857	0.002459	0.006683
243382	Ppm1k	protein phosphatase 1K (PP2C domain containing)	11.89657	0.002546	0.006822
432486	Gnptab	N-acetylglucosamine-1-phosphate transferase, alpha and beta subunits	1.337376	0.0026	0.006907
20975	Synj2	synaptojanin 2	1.564419	0.002607	0.006918
18712	Pim1	proviral integration site 1	1.447229	0.002717	0.007086
72535	Aldh1b1	aldehyde dehydrogenase 1 family, member B1	7.98456	0.002724	0.007098
245841	Polr2h	polymerase (RNA) II (DNA directed) polypeptide H	-1.50153	0.002733	0.00711
18975	Polg	polymerase (DNA directed), gamma	-1.21695	0.00277	0.007166
67092	Gatm	glycine amidinotransferase (L-arginine:glycine amidinotransferase)	1.556465	0.002804	0.007216
381113	Cdkl4	cyclin-dependent kinase-like 4	1.689056	0.002856	0.007291
18720	Pip5k1a	phosphatidylinositol-4-phosphate 5-kinase, type 1 alpha	-1.58835	0.002857	0.007293
16068	Il18bp	interleukin 18 binding protein	3.267926	0.002899	0.007352
18557	Cdk18	cyclin-dependent kinase 18	-1.63624	0.002907	0.007364
12651	Chkb	choline kinase beta	-1.32428	0.002939	0.007409
192195	Ash1l	ash1 (absent, small, or homeotic)-like (Drosophila)	-1.25729	0.002976	0.007461
19260	Ptpn22	protein tyrosine phosphatase, non-receptor type 22 (lymphoid)	-1.6213	0.003011	0.007509
235587	Parp3	poly (ADP-ribose) polymerase family, member 3	1.32592	0.003018	0.007519
16330	Inpp5b	inositol polyphosphate-5-phosphatase B	2.015754	0.003185	0.007751
70974	Pgm2l1	phosphoglucomutase 2-like 1	-1.76471	0.003221	0.007799
13728	Mark2	MAP/microtubule affinity-regulating kinase 2	-1.28083	0.003289	0.00789
11637	Ak2	adenylate kinase 2	-1.70646	0.003326	0.007938
15490	Hsd17b7	hydroxysteroid (17-beta) dehydrogenase 7	-1.48856	0.003339	0.007955
18451	P4ha1	Procollagen-proline, 2-oxoglutarate 4-dioxygenase (proline 4-hydroxylase), alpha 1 polypeptide	3.933435	0.003411	0.008047
18782	Pla2g2d	phospholipase A2, group IID	1.383774	0.003418	0.008056
69051	Pycr2	pyrroline-5-carboxylate reductase family, member 2	-1.28045	0.003447	0.008093
11898	Ass1; Gm5424	argininosuccinate synthetase 1	2.675768	0.003508	0.008169
208449	Sgms1	sphingomyelin synthase 1	-3.97643	0.003558	0.008231
54667	Atp8b2	ATPase, class I, type 8B, member 2	1.542026	0.003566	0.008241
18797	Plcb3	phospholipase C, beta 3	1.319991	0.003591	0.008271
74112	Usp16	ubiquitin specific peptidase 16	-1.75364	0.00361	0.008294
235441	Usp3	ubiquitin specific peptidase 3	-1.30355	0.003623	0.008309
19106	Eif2ak2	eukaryotic translation initiation factor 2-alpha kinase 2	7.0627	0.003644	0.008335
17961	Nat2	N-acetyltransferase 2 (arylamine N-acetyltransferase)	1.871224	0.003658	0.008352
100198	H6pd	Hexose-6-phosphate dehydrogenase (glucose 1-dehydrogenase)	-1.40004	0.0037	0.008405
56335	Mettl3	methyltransferase like 3	-1.5812	0.00377	0.008498
20873	Plk4	polo-like kinase 4	-2.12422	0.003814	0.008554
170789	Acot8	acyl-CoA thioesterase 8	1.219281	0.003969	0.008751

217057	Ptrh2	peptidyl-tRNA hydrolase 2	-1.65671	0.004074	0.00888
50772	Mapk6	mitogen-activated protein kinase 6	-1.46808	0.004085	0.008894
74205	Acsl3	acyl-CoA synthetase long-chain family member 3	-1.86005	0.004162	0.008987
60525	Acss2	acyl-CoA synthetase short-chain family member 2	1.563718	0.004216	0.009051
11352	Abl2	v-abl Abelson murine leukemia viral oncogene 2 (arg, Abelson-related gene)	2.210896	0.004326	0.009179
12892	Cpox	coproporphyrinogen oxidase	1.315867	0.004342	0.009197
16452	Jak2	Janus kinase 2	1.880227	0.004349	0.009206
14923	Guk1	guanylate kinase 1	1.392089	0.004354	0.009211
18105	Nqo2	NAD(P)H dehydrogenase, quinone 2	1.44201	0.004478	0.009352
16453	Jak3	Janus kinase 3	1.373527	0.004486	0.009361
19053	Ppp2cb	protein phosphatase 2 (formerly 2A), catalytic subunit, beta isoform	-1.27934	0.004539	0.00942
14431	Gamt	guanidinoacetate methyltransferase	1.289126	0.004568	0.009451
235293	Sc5d	sterol-C5-desaturase (fungal ERG3, delta-5-desaturase) homolog (S. cerevisae)	-1.52971	0.004788	0.009688
69870	Polr3gl	polymerase (RNA) III (DNA directed) polypeptide G like	1.259242	0.004789	0.00969
244349	Kat6a	K(lysine) acetyltransferase 6A	1.615962	0.004857	0.00976
17309	Mgat3	mannoside acetylglucosaminyltransferase 3	1.330662	0.004871	0.009774
264064	Cdk8	cyclin-dependent kinase 8	-1.50981	0.004879	0.009783
107435	Hat1	histone aminotransferase 1	1.288675	0.004927	0.009833
19052	Ppp2ca	protein phosphatase 2 (formerly 2A), catalytic subunit, alpha isoform	-1.2089	0.005039	0.009945
218461	Pde8b	phosphodiesterase 8B	1.707761	0.005151	0.010056
110279	Bcr	breakpoint cluster region	1.42383	0.005189	0.010093
52552	Parp8	poly (ADP-ribose) polymerase family, member 8	2.366188	0.00527	0.010171
58875	Hibadh	3-hydroxyisobutyrate dehydrogenase	1.200547	0.005296	0.010196
67418	Ppil4	peptidylprolyl isomerase (cyclophilin)-like 4	-1.79395	0.005399	0.010293
16798	Lats1	large tumor suppressor	-1.37085	0.005434	0.010325
13000	Csnk2a2	casein kinase 2, alpha prime polypeptide	-1.2341	0.005472	0.01036
67292	Pigc	phosphatidylinositol glycan anchor biosynthesis, class C	-1.36049	0.005475	0.010363
18107	Nmt1	N-myristoyltransferase 1	-1.31844	0.005477	0.010365
67800	Dgat2	diacylglycerol O-acyltransferase 2	1.733422	0.005488	0.010375
108148	Galnt2	UDP-N-acetyl-alpha-D-galactosamine:polypeptide N-acetylgalactosaminyltransferase 2	1.277501	0.005584	0.010462
14158	Fer	fer (fms/fps related) protein kinase, testis specific 2	1.304868	0.005591	0.010469
17691	Sik1	salt inducible kinase 1	3.079703	0.005631	0.010504
217119	Xylt2	xylosyltransferase II	-1.41727	0.005744	0.010604
74178	Stk40	serine/threonine kinase 40	-2.01727	0.005823	0.010673
56791	Ube2l6	ubiquitin-conjugating enzyme E2L 6	5.899447	0.005833	0.010681
14544	Gda	guanine deaminase	1.29685	0.005845	0.010692
216136	Ilvbl	ilvB (bacterial acetolactate synthase)-like	-2.48152	0.005957	0.010787
19248	Ptpn12	protein tyrosine phosphatase, non-receptor type 12	-1.87284	0.005972	0.0108
56626	Poll	polymerase (DNA directed), lambda	1.245762	0.005978	0.010804
74340	Ahcyl2	S-adenosylhomocysteine hydrolase-like 2	1.329344	0.005992	0.010816

14583	Gfpt1	glutamine fructose-6-phosphate transaminase 1	-1.25349	0.005994	0.010818
70425	Csnk1g3	casein kinase 1, gamma 3	-1.7595	0.006028	0.010846
17289	Mertk	c-mer proto-oncogene tyrosine kinase	1.773021	0.0061	0.010905
71472	Usp19	ubiquitin specific peptidase 19	-1.33552	0.0062	0.010987
69635	Dapk1	death associated protein kinase 1	-1.35424	0.006242	0.011021
223775	Pim3	proviral integration site 3	-1.29374	0.006338	0.011096
18004	Nek1	NIMA (never in mitosis gene a)-related expressed kinase 1	1.260282	0.006397	0.011143
20443	St3gal4	ST3 beta-galactoside alpha-2,3-sialyltransferase 4	1.534809	0.006399	0.011144
22436	Xdh	xanthine dehydrogenase	1.295806	0.006497	0.011219
21812	Tgfbr1	transforming growth factor, beta receptor I	-1.85882	0.006515	0.011234
12499	Entpd5	ectonucleoside triphosphate diphosphohydrolase 5	-1.23394	0.00654	0.011252
14360	Fyn	Fyn proto-oncogene	1.296731	0.006567	0.011273
98432	Phlpp1	PH domain and leucine rich repeat protein phosphatase 1	1.780875	0.006604	0.011301
14229	Fkbp5	FK506 binding protein 5	1.247204	0.006609	0.011305
21951	Tnks	tankyrase, TRF1-interacting ankyrin-related ADP-ribose polymerase	1.853836	0.006612	0.011307
71701	Pnpt1	polyribonucleotide nucleotidyltransferase 1	3.584633	0.006785	0.011437
224860	Plcl2	phospholipase C-like 2	1.538249	0.006856	0.011489
11350	Abl1	c-abl oncogene 1, non-receptor tyrosine kinase	-1.78831	0.006862	0.011493
50776	Polg2	polymerase (DNA directed), gamma 2, accessory subunit	1.445073	0.00688	0.011506
18700	Piga	phosphatidylinositol glycan anchor biosynthesis, class A	-1.53693	0.006906	0.011525
54447	Asah2	N-acylsphingosine amidohydrolase 2	1.530461	0.00703	0.011615
11717	Ampd3	adenosine monophosphate deaminase 3	-3.25208	0.007069	0.011642
56294	Ptpn9	protein tyrosine phosphatase, non-receptor type 9	-1.28777	0.007296	0.0118
15117	Has2	hyaluronan synthase 2	-2.73741	0.007395	0.011867
54613	St3gal6	ST3 beta-galactoside alpha-2,3-sialyltransferase 6	1.908463	0.007412	0.011879
208266	Dot1l	DOT1-like, histone H3 methyltransferase (S. cerevisiae)	-2.32878	0.007419	0.011883
17169	Mark3	MAP/microtubule affinity-regulating kinase 3	-1.31985	0.007497	0.011935
223753	Cerk	ceramide kinase	-1.46525	0.007526	0.011954
22210	Ube2b	ubiquitin-conjugating enzyme E2B	-1.30514	0.007542	0.011965
56632	Sphk2	sphingosine kinase 2	-1.39043	0.00755	0.01197
244418	D8Ertd82e	DNA segment, Chr 8, ERATO Doi 82, expressed	-4.86986	0.007601	0.012003
13436	Dnmt3b	DNA methyltransferase 3B	-1.79897	0.007714	0.012076
74841	Usp38	ubiquitin specific peptidase 38	-1.31434	0.007775	0.012114
15356	Hmgcl	3-hydroxy-3-methylglutaryl-Coenzyme A lyase	-1.26188	0.007782	0.012119
21817	Tgm2	transglutaminase 2, C polypeptide	1.547159	0.007805	0.012134
230661	Tesk2	testis-specific kinase 2	-3.44003	0.00784	0.012155
56336	B4galt5	UDP-Gal:betaGlcNAc beta 1,4-galactosyltransferase, polypeptide 5	1.967004	0.007846	0.012159
171210	Acot2	acyl-CoA thioesterase 2	-1.23567	0.007986	0.012246
16337	Insr	insulin receptor	2.760092	0.008067	0.012295
320119	Rps6kc1	ribosomal protein S6 kinase polypeptide 1	1.564504	0.00808	0.012303

228005	Ppig	peptidyl-prolyl isomerase G (cyclophilin G)	-2.20418	0.008082	0.012304
66234	Msmo1	methylsterol monooxygenase 1	-1.29911	0.008121	0.012328
12795	Plk3	polo-like kinase 3	-3.51263	0.008144	0.012341
20454	St3gal5	ST3 beta-galactoside alpha-2,3-sialyltransferase 5	-1.76047	0.008153	0.012347
17161	Maoa	monoamine oxidase A	1.283626	0.00819	0.012369
76367	Trp53rkb	transformation related protein 53 regulating kinase	-1.43414	0.008233	0.012395
105689	Mycbp2	MYC binding protein 2	1.577058	0.008307	0.012444
26384	Gnpda1	glucosamine-6-phosphate deaminase 1	-1.35069	0.008386	0.012497
14426	Galnt4	UDP-N-acetyl-alpha-D-galactosamine:polypeptide N-acetylgalactosaminyltransferase 4	-1.56396	0.008572	0.012635
237898	Usp32	ubiquitin specific peptidase 32	-1.47249	0.008607	0.012661
20019	Polr1a	polymerase (RNA) I polypeptide A	-1.3512	0.008645	0.012688
67834	Idh3a	isocitrate dehydrogenase 3 (NAD+) alpha	1.31945	0.00882	0.012815
19043	Ppm1b	protein phosphatase 1B, magnesium dependent, beta isoform	-1.76458	0.008938	0.012899
18984	Por	P450 (cytochrome) oxidoreductase	-1.32617	0.008943	0.012902
238871	Pde4d	0	2.305055	0.009013	0.012951
66945	Sdha	Succinate dehydrogenase complex, subunit A, flavoprotein (Fp)	-1.54835	0.00907	0.01299
319594	Hif1an	hypoxia-inducible factor 1, alpha subunit inhibitor	-1.45904	0.009076	0.012995
227292	Ctdsp1	CTD (carboxy-terminal domain, RNA polymerase II, polypeptide A) small phosphatase 1	-1.23869	0.009102	0.013013
19766	Ripk1	receptor (TNFRSF)-interacting serine-threonine kinase 1	1.261217	0.009232	0.013102
14479	Usp15	ubiquitin specific peptidase 15	1.577083	0.009239	0.013107
109674	Ampd2	adenosine monophosphate deaminase 2	-1.37284	0.009281	0.013136
15258	Hipk2	homeodomain interacting protein kinase 2	-1.72615	0.009461	0.013256
218271	B4galt7	xylosylprotein beta1,4-galactosyltransferase, polypeptide 7 (galactosyltransferase I)	-1.39371	0.009532	0.013303
15368	Hmox1	heme oxygenase (decycling) 1	-1.3231	0.009602	0.013349
74137	Nuak2	NUAK family, SNF1-like kinase, 2	1.3503	0.009725	0.013429
140780	Bmp2k	BMP2 inducible kinase	1.74302	0.009781	0.013464
77626	Smpd4	sphingomyelin phosphodiesterase 4	-1.35765	0.009781	0.013465
53892	Ppm1d	protein phosphatase 1D magnesium-dependent, delta isoform	-1.77334	0.009861	0.013516
75292	Prkd3	protein kinase D3	1.25541	0.009889	0.013534
14254	Flt1	FMS-like tyrosine kinase 1	1.624418	0.009931	0.01356
52815	Ldhd	lactate dehydrogenase D	1.913965	0.010086	0.013657
53357	Pla2g6	phospholipase A2, group VI	-1.9055	0.010119	0.013678
76800	Usp42	ubiquitin specific peptidase 42	2.144848	0.010122	0.013679
11980	Atp8a1	ATPase, aminophospholipid transporter (APLT), class I, type 8A, member 1	1.596596	0.010126	0.013682
140499	Ube2j2	ubiquitin-conjugating enzyme E2J 2	-1.55329	0.010189	0.01372
50493	Txnrd1	thioredoxin reductase 1	-1.36409	0.010229	0.013745
67440	Mtpap	mitochondrial poly(A) polymerase	-1.26068	0.010242	0.013753
19023	Ppef2	protein phosphatase, EF hand calcium-binding domain 2	1.639406	0.010482	0.013898
235574	Atp2c1	ATPase, Ca++-sequestering	-2.09949	0.010528	0.013925

76267	Fads1	fatty acid desaturase 1	-1.27061	0.010544	0.013934
26939	Polr3e	polymerase (RNA) III (DNA directed) polypeptide E	-1.51073	0.010694	0.014022
23797	Akt3	thymoma viral proto-oncogene 3	1.371375	0.010754	0.014057
382985	Rrm2b	ribonucleotide reductase M2 B (TP53 inducible)	1.374619	0.010819	0.014094
23972	Papss2	3'-phosphoadenosine 5'-phosphosulfate synthase 2	-1.25264	0.010852	0.014113
12496	Entpd2	ectonucleoside triphosphate diphosphohydrolase 2	1.341714	0.010914	0.014149
216965	Taok1	TAO kinase 1	-1.6692	0.010933	0.014159
18805	Pld1	phospholipase D1	-1.84578	0.010957	0.014173
223722	Mcat	malonyl CoA:ACP acyltransferase (mitochondrial)	1.414553	0.011164	0.014289
17347	Mknk2	MAP kinase-interacting serine/threonine kinase 2	-1.36049	0.011173	0.014294
244650	Phlpp2	PH domain and leucine rich repeat protein phosphatase 2	1.237588	0.011291	0.014359
104086	Cyp27a1	cytochrome P450, family 27, subfamily a, polypeptide 1	1.426482	0.011308	0.014368
18578	Pde4b	phosphodiesterase 4B, cAMP specific	-3.08994	0.011327	0.014379
18125	Nos1	nitric oxide synthase 1, neuronal	1.568898	0.011379	0.014406
26403	Map3k11	mitogen-activated protein kinase kinase kinase 11	-2.27656	0.011438	0.014438
22367	Vrk1	vaccinia related kinase 1	1.434406	0.011641	0.014547
330177	Taok3	TAO kinase 3	1.658102	0.011685	0.01457
94192	C1galt1	core 1 synthase, glycoprotein-N-acetylgalactosamine 3-beta-galactosyltransferase, 1	1.219714	0.011886	0.014675
19063	Ppt1	palmitoyl-protein thioesterase 1	1.216261	0.011903	0.014683
327942	Pigl	phosphatidylinositol glycan anchor biosynthesis, class L	-1.86476	0.011942	0.014703
59028	Rcl1	RNA terminal phosphate cyclase-like 1	-1.41172	0.012008	0.014737
110821	Pcca	propionyl-Coenzyme A carboxylase, alpha polypeptide	1.704841	0.012016	0.014741
12747	Clk1	CDC-like kinase 1	-2.09933	0.012207	0.014838
27369	Dguok	deoxyguanosine kinase	1.328536	0.01221	0.014839
218294	Cdc14b	CDC14 cell division cycle 14B	-1.50503	0.012272	0.01487
18601	Padi3	peptidyl arginine deiminase, type III	-1.45729	0.012301	0.014884
50523	Lats2	large tumor suppressor 2	-1.53141	0.012463	0.015003
11477	Acvr1	activin A receptor, type 1	1.254986	0.012613	0.015111
50784	Plpp2	phosphatidic acid phosphatase type 2C	1.21339	0.012616	0.015113
30941	Usp21	ubiquitin specific peptidase 21	1.313759	0.012679	0.015158
216150	Cdc34	cell division cycle 34	-1.2241	0.012899	0.015314
19057	Ppp3cc	protein phosphatase 3, catalytic subunit, gamma isoform	-1.47316	0.012922	0.015331
66136	Znrd1	zinc ribbon domain containing, 1	1.227041	0.013034	0.015409
108083	Pip4k2b	phosphatidylinositol-5-phosphate 4-kinase, type II, beta	-1.46747	0.013344	0.015626
67005	Polr3k	polymerase (RNA) III (DNA directed) polypeptide K	-1.21192	0.01338	0.015651
67897	Rnmt	RNA (guanine-7-) methyltransferase	-1.96504	0.013416	0.015676
22245	Uck1	uridine-cytidine kinase 1	-1.25283	0.01356	0.015775
63953	Dusp10	dual specificity phosphatase 10	1.687271	0.013629	0.015822
18574	Pde1b	phosphodiesterase 1B, Ca2+-calmodulin dependent	-1.69355	0.013755	0.015907
57295	Icmt	isoprenylcysteine carboxyl methyltransferase	-1.53956	0.01403	0.016092

26409	Map3k7	mitogen-activated protein kinase kinase kinase 7	-1.20091	0.014046	0.016102
105278	Cdk20	cyclin-dependent kinase 20	-1.6885	0.014187	0.016196
17346	Mknk1	MAP kinase-interacting serine/threonine kinase 1	-1.56621	0.014199	0.016204
75735	Pank1	pantothenate kinase 1	-1.29244	0.014302	0.016271
69181	Dyrk2	dual-specificity tyrosine-(Y)-phosphorylation regulated kinase 2	-1.40152	0.01435	0.016303
16329	Inpp1	inositol polyphosphate-1-phosphatase	2.871469	0.014416	0.016346
20111	Rps6ka1	ribosomal protein S6 kinase polypeptide 1	-1.29241	0.014715	0.016538
66812	Ppcdc	phosphopantothenoylcysteine decarboxylase	1.39982	0.014803	0.016594
59047	Pnkp	polynucleotide kinase 3'- phosphatase	-1.38291	0.014864	0.016633
20874	Slk	STE20-like kinase	-1.45548	0.014916	0.016666
20868	Stk10	serine/threonine kinase 10	-1.52357	0.014939	0.01668
12613	Cel	carboxyl ester lipase	1.673997	0.014952	0.016688
70661	Sik3	SIK family kinase 3	1.41369	0.015102	0.016783
23939	Mapk7	mitogen-activated protein kinase 7	-2.63017	0.015265	0.016884
51789	Tnk2	tyrosine kinase, non-receptor, 2	1.352419	0.015663	0.017167
22213	Ube2g2	ubiquitin-conjugating enzyme E2G 2	-1.32789	0.015878	0.017317
18607	Pdpk1	3-phosphoinositide dependent protein kinase 1	-1.6214	0.015882	0.01732
59031	Chst12	carbohydrate sulfotransferase 12	-1.4617	0.016088	0.017463
217734	Pomt2	protein-O-mannosyltransferase 2	1.436724	0.016463	0.017719
19229	Ptk2b	PTK2 protein tyrosine kinase 2 beta	1.300954	0.016476	0.017728
20425	Shmt1	serine hydroxymethyltransferase 1 (soluble)	1.533136	0.016707	0.017884
12660	Chka	choline kinase alpha	-1.6828	0.016945	0.018043
15531	Ndst1	N-deacetylase/N-sulfotransferase (heparan glucosaminyl) 1	-1.221	0.017104	0.018148
269180	Inpp4a	inositol polyphosphate-4-phosphatase, type I	-1.26696	0.017126	0.018163
74493	Tnks2	tankyrase, TRF1-interacting ankyrin-related ADP-ribose polymerase 2	-1.26016	0.017165	0.018188
60507	Qtrt1	queuine tRNA-ribosyltransferase 1	-1.3732	0.017348	0.018308
70008	Ace2	angiotensin I converting enzyme (peptidyl-dipeptidase A) 2	-2.90032	0.017391	0.018336
74414	Polr3c	polymerase (RNA) III (DNA directed) polypeptide C	1.266901	0.017584	0.018462
192185	Nadk	NAD kinase	-1.27237	0.017658	0.018509
399510	Map4k5	mitogen-activated protein kinase kinase kinase kinase 5	-1.68361	0.017727	0.018554
192656	Ripk2	receptor (TNFRSF)-interacting serine-threonine kinase 2	1.595815	0.018076	0.018776
18218	Dusp8	dual specificity phosphatase 8	-2.81691	0.018349	0.018947
26405	Map3k2	mitogen-activated protein kinase kinase kinase 2	-1.65601	0.018523	0.019055
13382	Dld	dihydrolipoamide dehydrogenase	-1.23751	0.018609	0.019109
15162	Hck	hemopoietic cell kinase	1.260567	0.018667	0.019144
68082	Dusp19	dual specificity phosphatase 19	1.218342	0.018736	0.019187
67655	Ctdp1	CTD (carboxy-terminal domain, RNA polymerase II, polypeptide A) phosphatase, subunit 1	1.394635	0.018741	0.01919
17156	Man1a2	mannosidase, alpha, class 1A, member 2	1.266249	0.018747	0.019194
231327	Ppat	phosphoribosyl pyrophosphate amidotransferase	-1.28172	0.019061	0.019385
72039	Mccc1	methylcrotonoyl-Coenzyme A carboxylase 1 (alpha)	-1.40604	0.019189	0.019462

13121	Cyp51	cytochrome P450, family 51	-1.93693	0.019259	0.019505
64580	Ndst4	N-deacetylase/N-sulfotransferase (heparin glucosaminyl) 4	-1.71606	0.019409	0.019594
108960	Irak2	interleukin-1 receptor-associated kinase 2	-1.47996	0.019806	0.01983
108079	Prkaa2	protein kinase, AMP-activated, alpha 2 catalytic subunit	1.859203	0.019835	0.019847
78783	Brpf1	bromodomain and PHD finger containing, 1	-1.4743	0.019837	0.019848
26363	Btd	biotinidase	-1.25829	0.020051	0.019972
109979	Art3	ADP-ribosyltransferase 3	2.756145	0.02009	0.019995
20810	Srm	spermidine synthase	-1.24836	0.020133	0.02002
66590	Farsa	phenylalanyl-tRNA synthetase, alpha subunit	1.243331	0.02014	0.020024
108682	Gpt2	glutamic pyruvate transaminase (alanine aminotransferase) 2	1.248706	0.020187	0.020051
67486	Polr3g	polymerase (RNA) III (DNA directed) polypeptide G	-1.83334	0.02033	0.020134
13807	Eno2	enolase 2, gamma neuronal	-3.29195	0.020462	0.02021
330010	Ttll10	tubulin tyrosine ligase-like family, member 10	1.309144	0.020568	0.02027
235344	Sik2	salt inducible kinase 2	-1.3557	0.020587	0.020281
56542	Ick	intestinal cell kinase	-1.27013	0.020674	0.02033
24018	Rngtt	RNA guanylyltransferase and 5'-phosphatase	-1.25735	0.02133	0.020697
13666	Eif2ak3	eukaryotic translation initiation factor 2 alpha kinase 3	-1.83592	0.021498	0.020789
70686	Dusp16	dual specificity phosphatase 16	-1.50198	0.021515	0.020799
20652	Soat1	0	-1.4004	0.021599	0.020845
19134	Prpf4b	PRP4 pre-mRNA processing factor 4 homolog B (yeast)	-1.38407	0.021736	0.020919
14859	Gsta3	glutathione S-transferase, alpha 3	-1.66324	0.021832	0.020971
109232	Sccpdh	saccharopine dehydrogenase (putative)	-1.31675	0.021886	0.021
11655	Alas1	aminolevulinic acid synthase 1	-1.28258	0.021964	0.021042
69740	Dph5	DPH5 homolog (S. cerevisiae)	-1.52944	0.022093	0.021111
64436	Inpp5e	inositol polyphosphate-5-phosphatase E	-1.41245	0.022351	0.021249
16818	Lck	lymphocyte protein tyrosine kinase	2.599679	0.023085	0.021631
13026	Pcyt1a	phosphate cytidylyltransferase 1, choline, alpha isoform	1.350674	0.023118	0.021649
56720	Tdo2	tryptophan 2,3-dioxygenase	1.629909	0.023142	0.021661
66848	Fuca2	fucosidase, alpha-L- 2, plasma	-1.46667	0.02319	0.021685
13435	Dnmt3a	DNA methyltransferase 3A	-1.35289	0.023242	0.021712
328572	Ep300	E1A binding protein p300	1.246388	0.02332	0.021752
67980	Gnpda2	glucosamine-6-phosphate deaminase 2	1.549614	0.02335	0.021767
22241	Ulk1	unc-51 like kinase 1	-2.146	0.023422	0.021804
218232	Ptpdc1	protein tyrosine phosphatase domain containing 1	1.681793	0.023442	0.021814
71742	Ulk3	unc-51-like kinase 3	-1.39685	0.023599	0.021893
110960	Tars	threonyl-tRNA synthetase	-1.21244	0.02374	0.021964
237459	Cdk17	cyclin-dependent kinase 17	-1.61204	0.023915	0.022052
170707	Usp48	ubiquitin specific peptidase 48	-1.28824	0.024102	0.022153
26921	Map4k4	mitogen-activated protein kinase kinase kinase kinase 4	-4.64958	0.024257	0.022239
11652	Akt2	thymoma viral proto-oncogene 2	-1.26628	0.024321	0.022275

19255	Ptpn2	protein tyrosine phosphatase, non-receptor type 2	1.279237	0.024441	0.022341
27103	Eif2ak4	eukaryotic translation initiation factor 2 alpha kinase 4	-1.40149	0.02466	0.022467
53418	B4galt2	coiled-coil domain containing 24///UDP-Gal:betaGlcNAc beta 1,4- galactosyltransferase, polypeptide 2	1.551705	0.025354	0.022861
53859	1700028N14Rik	RIKEN cDNA 1700028N14 gene	-1.58298	0.025508	0.022948
98267	Stk17b	serine/threonine kinase 17b (apoptosis-inducing)	-2.01955	0.025615	0.023007
212032	Hk3	hexokinase 3	1.311769	0.025732	0.023072
55979	Agpat1	1-acylglycerol-3-phosphate O-acyltransferase 1 (lysophosphatidic acid acyltransferase, alpha)	1.283884	0.025892	0.023161
20442	St3gal1	ST3 beta-galactoside alpha-2,3-sialyltransferase 1	-1.33836	0.026443	0.023463
15159	Hccs	holocytochrome c synthetase	-1.47077	0.026605	0.023551
269252	Gtf3c4	general transcription factor IIIC, polypeptide 4	-1.39156	0.026685	0.023594
214897	Csnk1g1	casein kinase 1, gamma 1	-1.5867	0.026797	0.023654
27052	Aoah	acyloxyacyl hydrolase	-4.60746	0.026899	0.023709
11847	Arg2	arginase type II	-2.1052	0.027218	0.02388
18181	Nrf1	nuclear respiratory factor 1	-1.21371	0.027414	0.023984
14137	Fdft1	farnesyl diphosphate farnesyl transferase 1	-1.95442	0.027698	0.024133
29863	Pde7b	phosphodiesterase 7B	1.646263	0.027714	0.024142
546071	Mast3	microtubule associated serine/threonine kinase 3	-1.98685	0.028145	0.024366
14104	Fasn	fatty acid synthase	-1.40158	0.028175	0.024382
18753	Prkcd	protein kinase C, delta	-2.88952	0.028658	0.02463
26362	Axl	AXL receptor tyrosine kinase	1.709075	0.028998	0.024802
78943	Ern1	endoplasmic reticulum (ER) to nucleus signalling 1	1.392665	0.029091	0.02485
216578	Papolg; LOC553090	predicted gene, 19887///uncharacterized LOC553090	-1.88766	0.029503	0.025056
26447	Poli	polymerase (DNA directed), iota	1.391949	0.029567	0.025088
59125	Nek7	NIMA (never in mitosis gene a)-related expressed kinase 7	1.359472	0.029634	0.025121
20016	Polr1c	polymerase (RNA) I polypeptide C	-1.26527	0.029718	0.025163
230809	Pdik1l	PDLIM1 interacting kinase 1 like	-1.40269	0.029792	0.0252
69718	Ipmk	inositol polyphosphate multikinase	-1.26203	0.029828	0.025217
17164	Mapkapk2	MAP kinase-activated protein kinase 2	-1.49365	0.030583	0.025586
76187	Adhfe1	alcohol dehydrogenase, iron containing, 1	-1.7943	0.03059	0.02559
67128	Ube2g1	ubiquitin-conjugating enzyme E2G 1	-1.3979	0.031169	0.0259
76055	Mgea5	meningioma expressed antigen 5 (hyaluronidase)	-1.45901	0.031508	0.026081
15357	Hmgcr	3-hydroxy-3-methylglutaryl-Coenzyme A reductase	-1.55728	0.031846	0.026259
26462	Txnrd2	thioredoxin reductase 2	1.414386	0.032448	0.026573
71773	Ugt2b1	UDP glucuronosyltransferase 2 family, polypeptide B1	1.322566	0.03304	0.026877
240505	Cdc42bpg	CDC42 binding protein kinase gamma (DMPK-like)	-1.41541	0.033329	0.027025
18717	Pip5k1c	phosphatidylinositol-4-phosphate 5-kinase, type 1 gamma	-1.42534	0.033331	0.027026
18803	Plcg1	phospholipase C, gamma 1	-1.48674	0.033525	0.027124
103135	Pan2	PAN2 polyA specific ribonuclease subunit homolog (S. cerevisiae)	-1.25014	0.033675	0.0272

19878	Rock2	Rho-associated coiled-coil containing protein kinase 2	-1.79832	0.033724	0.027224
76500	Ip6k2	inositol hexaphosphate kinase 2	-1.52614	0.034196	0.027461
117592	B3galt6	UDP-Gal:betaGal beta 1,3-galactosyltransferase, polypeptide 6	-1.44205	0.034373	0.027549
320951	Pisd	phosphatidylserine decarboxylase	-1.21276	0.034497	0.02761
216134	Pdxk	pyridoxal (pyridoxine, vitamin B6) kinase	-1.22717	0.034647	0.027684
14194	Fh1	fumarate hydratase 1	1.227958	0.034754	0.027737
20598	Smpd2	sphingomyelin phosphodiesterase 2, neutral	-1.20759	0.035528	0.028115
235626	Setd2	SET domain containing 2	-1.29035	0.035709	0.028202
56318	Acpp	acid phosphatase, prostate	1.27834	0.035804	0.028248
11790	Speg	SPEG complex locus	-1.29609	0.035875	0.028282
19211	Pten	phosphatase and tensin homolog	-1.56514	0.03604	0.028361
76179	Usp31	ubiquitin specific peptidase 31	-1.70549	0.036284	0.028478
16987	Lss	lanosterol synthase	-1.48188	0.036924	0.02878
77697	Mmab	methylmalonic aciduria (cobalamin deficiency) type B homolog (human)	-1.4977	0.037195	0.028907
52123	Agpat5	1-acylglycerol-3-phosphate O-acyltransferase 5 (lysophosphatidic acid acyltransferase, epsilon)	-1.21852	0.037262	0.028938
67333	Stk35	serine/threonine kinase 35	-1.98887	0.03764	0.029113
110350	2610019N06Rik	uncharacterized LOC100505161///RIKEN cDNA 2610019N06 gene	-3.08925	0.038307	0.029419
269614	Pank4	pantothenate kinase 4	-1.37862	0.038512	0.029513
18711	Pikfyve	phosphoinositide kinase, FYVE finger containing	1.483283	0.038925	0.029699
52538	Acaa2	acetyl-Coenzyme A acyltransferase 2 (mitochondrial 3-oxoacyl-Coenzyme A thiolase)	1.234894	0.0391	0.029778
57813	Tk2	thymidine kinase 2, mitochondrial	-1.24443	0.03962	0.030029
113868	Acaa1a	acetyl-Coenzyme A acyltransferase 1A	1.209673	0.039994	0.03021
104110	Adcy4	adenylate cyclase 4	1.302206	0.040024	0.030225
20817	Srpk2	serine/arginine-rich protein specific kinase 2	-1.39881	0.040589	0.030496
55936	Ctps2	cytidine 5'-triphosphate synthase 2	-1.54353	0.040658	0.030529
12571	Cdk6	cyclin-dependent kinase 6	1.473677	0.04112	0.030749
225997	Trpm6	transient receptor potential cation channel, subfamily M, member 6	1.28623	0.041195	0.030785
53376	Usp2	ubiquitin specific peptidase 2	1.327027	0.041224	0.030798
19271	Ptprj	protein tyrosine phosphatase, receptor type, J	-1.20434	0.041543	0.030949
78894	Aacs	acetoacetyl-CoA synthetase	-1.31949	0.042598	0.03144
100756	Usp30	ubiquitin specific peptidase 30	-1.20304	0.043095	0.031669
210044	Adcy2	adenylate cyclase 2	2.480524	0.04354	0.031872
26419	Mapk8	mitogen-activated protein kinase 8	-1.7321	0.043732	0.031959
69562	Cdk13	cyclin-dependent kinase 13	-1.45115	0.044658	0.032374
56737	Alg2	asparagine-linked glycosylation 2 (alpha-1,3-mannosyltransferase)	-1.99622	0.044719	0.032401
109880	Braf	Braf transforming gene	-1.49128	0.044809	0.032441
13885	Gm2904; Esd	esterase D/formylglutathione hydrolase	-2.15361	0.044847	0.032458
381511	Pdp1	pyruvate dehydrogenase phosphatase catalytic subunit 1	-1.6266	0.045118	0.032579
93683	Glce	glucuronyl C5-epimerase	-1.28658	0.045532	0.032761

15257	Hipk1	homeodomain interacting protein kinase 1	-1.23139	0.046056	0.03299
26401	Map3k1	mitogen-activated protein kinase kinase kinase 1	1.286126	0.046773	0.033301
22138	Ttn	titin	-1.49931	0.047029	0.033411
217214	Nags	N-acetylglutamate synthase	1.304931	0.047036	0.033414
76295	Atp11b	ATPase, class VI, type 11B	1.343552	0.047218	0.033492
243085	Ugt2b35	UDP glucuronosyltransferase 2 family, polypeptide B35	1.328672	0.047271	0.033515
28169	Agpat3	1-acylglycerol-3-phosphate O-acyltransferase 3	-1.34678	0.047552	0.033635
19714	Rev3l	REV3-like, catalytic subunit of DNA polymerase zeta RAD54 like (S. cerevisiae)	1.849724	0.049033	0.034272
14782	Gsr	glutathione reductase	-1.26175	0.049253	0.034365
19280	Ptprs	protein tyrosine phosphatase, receptor type, S	1.289708	0.049669	0.034541

Supplemental Table S2.2: A list of all metabolic genes identified in the MDM dataset.

Entrez Gene ID	Gene Symbol	Gene Title	Fold Change	P-value	FDR
3717	Jak2	Janus kinase 2	3.176442	1.89E-05	0.009626
5533	PPP3CC	protein phosphatase 3 (formerly 2B), catalytic subunit, gamma isoform	2.236797	3.69E-05	0.009626
11011	TLK2	tousled-like kinase 2	2.723902	5.34E-05	0.009626
64761	PARP12	poly (ADP-ribose) polymerase family, member 12	2.268545	5.51E-05	0.009626
23032	usp33	ubiquitin specific peptidase 33	1.424304	8.84E-05	0.012347
5775	PTPN4	protein tyrosine phosphatase, non-receptor type 4 (megakaryocyte)	-2.01923	0.000127	0.014743
5142	Pde4b	phosphodiesterase 4B, cAMP-specific (phosphodiesterase E4 dunce homolog, Drosophila)	6.353167	0.000219	0.019543
8972	LOC642103	similar to Maltase-glucoamylase, intestinal	4.678397	0.000227	0.019862
2180	ACSL1	acyl-CoA synthetase long-chain family member 1	2.276471	0.0003	0.022328
10135	NAMPT	nicotinamide phosphoribosyltransferase	3.449473	0.000333	0.023236
2710	GK3P	glycerol kinase 3 pseudogene; glycerol kinase	1.73406	0.0004	0.024744
10114	Hipk3	homeodomain interacting protein kinase 3	1.428001	0.000437	0.025458
3631	INPP4A	inositol polyphosphate-4-phosphatase, type I, 107kDa	-2.21237	0.000534	0.02713
1540	CYLD	cylindromatosis (turban tumor syndrome)	2.37934	0.000579	0.027773
1545	CYP1B1	cytochrome P450, family 1, subfamily B, polypeptide 1	1.536851	0.000617	0.028272
5168	ENPP2	ectonucleotide pyrophosphatase/phosphodiesterase 2	4.555246	0.000659	0.02876
5610	EIF2AK2	eukaryotic translation initiation factor 2-alpha kinase 2	3.172761	0.000766	0.029828
80146	UXS1	UDP-glucuronate decarboxylase 1	1.726443	0.000832	0.030379
6793	STK10	serine/threonine kinase 10	-1.50535	0.000952	0.031219
7326	ube2g1	ubiquitin-conjugating enzyme E2G 1 (UBC7 homolog, yeast)	-1.46646	0.001118	0.032139
8050	PDHX	Pyruvate dehydrogenase complex, component X	1.515724	0.001146	0.03227
1847	dusp5	dual specificity phosphatase 5	3.340293	0.001176	0.032408
57205	ATP10D	ATPase, class V, type 10D	-1.77633	0.001202	0.032521
84446	Brsk1	BR serine/threonine kinase 1	1.901541	0.001206	0.032539
3735	KARS	lysyl-tRNA synthetase	1.388079	0.001277	0.032828
9334	B4galt5	UDP-Gal:betaGlcNAc beta 1,4- galactosyltransferase, polypeptide 5	3.402661	0.001314	0.032966
51056	LAP3	leucine aminopeptidase 3	1.775856	0.001383	0.033211
57194	ATP10A	ATPase, class V, type 10A	4.50366	0.001433	0.033375
4329	Aldh6a1	aldehyde dehydrogenase 6 family, member A1	-1.38328	0.001481	0.033524
1845	DUSP3	dual specificity phosphatase 3	1.37165	0.00153	0.033666
1358	Cpa2	carboxypeptidase A2 (pancreatic)	2.552861	0.001559	0.033748
644	BLVRA	biliverdin reductase A	1.543476	0.001573	0.033786
5566	PRKACA	protein kinase, cAMP-dependent, catalytic, alpha	-1.28369	0.001634	0.033945
2643	GCH1	GTP cyclohydrolase 1	22.51212	0.001689	0.034081
4507	mtaP	methylthioadenosine phosphorylase	-1.44946	0.00171	0.034132
5170	PDPK1	3-phosphoinositide dependent protein kinase-1	-1.86312	0.001931	0.035481
8767	RIPK2	receptor-interacting serine-threonine kinase 2	2.66792	0.001976	0.035733

4067	LYN	v-yes-1 Yamaguchi sarcoma viral related oncogene homolog	2.093221	0.001989	0.035802
57134	MAN1C1	mannosidase, alpha, class 1C, member 1	-1.58222	0.00208	0.036278
2982	GUCY1A3	guanylate cyclase 1, soluble, alpha 3	5.151509	0.002185	0.036792
6732	srpk1	SFRS protein kinase 1	-1.27224	0.002248	0.037084
83666	PARP9	poly (ADP-ribose) polymerase family, member 9	2.333172	0.002315	0.037381
23522	MYST4	MYST histone acetyltransferase (monocytic leukemia) 4	-1.62314	0.002325	0.037426
9360	PPIG	peptidylprolyl isomerase G (cyclophilin G)	-1.58321	0.002369	0.037616
7324	UBE2E1	ubiquitin-conjugating enzyme E2E 1 (UBC4/5 homolog, yeast)	1.442897	0.002653	0.038894
23235	sik2	salt-inducible kinase 2	-1.78666	0.002712	0.039135
7453	wars	tryptophanyl-tRNA synthetase	1.658944	0.002906	0.039878
2766	gmpr	guanosine monophosphate reductase	2.749062	0.003	0.040213
5156	pdgfra	platelet-derived growth factor receptor, alpha polypeptide	1.588831	0.003062	0.040429
9517	Sptlc2	serine palmitoyltransferase, long chain base subunit 2	1.875558	0.003371	0.041397
1786	dnmt1	DNA (cytosine-5-)-methyltransferase 1	-1.60668	0.003465	0.041666
7803	ptp4a1	protein tyrosine phosphatase type IVA, member 1	1.242832	0.003508	0.041786
440275	EIF2AK4	eukaryotic translation initiation factor 2 alpha kinase 4	-1.49734	0.003768	0.042463
8396	PIP4K2B	phosphatidylinositol-5-phosphate 4-kinase, type II, beta	-2.13808	0.003948	0.042888
3712	ivd	isovaleryl Coenzyme A dehydrogenase	-1.43586	0.00395	0.042893
79567	fam65a	family with sequence similarity 65, member A	-1.35494	0.004017	0.043045
53944	CSNK1G1	casein kinase 1, gamma 1	1.408734	0.004065	0.04315
2713	GK3P	glycerol kinase 3 pseudogene; glycerol kinase	1.619607	0.004097	0.04322
1119	CHKA	choline kinase alpha	-1.81576	0.004109	0.043245
7321	UBE2D1	ubiquitin-conjugating enzyme E2D 1 (UBC4/5 homolog, yeast)	1.479857	0.004119	0.043268
7375	USP4	ubiquitin specific peptidase 4 (proto-oncogene)	-1.71882	0.004201	0.043439
2530	fut8	fucosyltransferase 8 (alpha (1,6) fucosyltransferase)	-1.6802	0.004283	0.043606
11274	usp18	ubiquitin specific peptidase 18	13.47735	0.004391	0.043818
9246	Ube2l6	ubiquitin-conjugating enzyme E2L 6	2.006129	0.004572	0.044157
7328	Ube2h	ubiquitin-conjugating enzyme E2H (UBC8 homolog, yeast)	1.954939	0.00463	0.04426
9958	USP15	ubiquitin specific peptidase 15	1.552271	0.004717	0.044412
57695	USP37	ubiquitin specific peptidase 37	-1.71885	0.004861	0.044653
415116	PIM3	pim-3 oncogene	2.069768	0.004865	0.04466
7329	UBE2I	ubiquitin-conjugating enzyme E2I (UBC9 homolog, yeast)	-1.83281	0.004876	0.044678
9262	STK17B	serine/threonine kinase 17b	2.270061	0.004916	0.044742
84196	usp48	ubiquitin specific peptidase 48	-1.58416	0.005055	0.044961
51805	COQ3	coenzyme Q3 homolog, methyltransferase (S. cerevisiae)	-1.44833	0.00514	0.045088
84930	MASTL	microtubule associated serine/threonine kinase-like	4.491827	0.005216	0.0452
1267	CNP	2',3'-cyclic nucleotide 3' phosphodiesterase	1.982498	0.005324	0.045355
64324	NSD1	nuclear receptor binding SET domain protein 1	-1.98816	0.005375	0.045427
91	ACVR1B	activin A receptor, type IB	2.03274	0.005493	0.045587
4145	matK	megakaryocyte-associated tyrosine kinase	-1.22476	0.005519	0.04562

7046	tgfbr1	transforming growth factor, beta receptor 1	-5.35032	0.005529	0.045635
10007	gnpda1	glucosamine-6-phosphate deaminase 1	-1.83086	0.005583	0.045705
2592	galT	galactose-1-phosphate uridylyltransferase	-1.2438	0.005607	0.045736
7320	ube2b	ubiquitin-conjugating enzyme E2B (RAD6 homolog)	1.272066	0.00581	0.04599
23463	icmt	isoprenylcysteine carboxyl methyltransferase	-1.30094	0.005846	0.046033
1387	CREBBP	CREB binding protein	1.704567	0.00591	0.046109
29943	PADI1	peptidyl arginine deiminase, type I	1.552521	0.00611	0.046339
80222	TARS2	threonyl-tRNA synthetase 2, mitochondrial (putative)	-1.7581	0.006229	0.046469
5058	Pak1	p21 protein (Cdc42/Rac)-activated kinase 1	-1.76388	0.006339	0.046586
6872	TAF1	TAF1 RNA polymerase II, TATA box binding protein (TBP)-associated factor, 250kDa	-1.63093	0.006344	0.046591
2648	KAT2A	K(lysine) acetyltransferase 2A	-1.57085	0.006436	0.046686
80339	pnpla3	patatin-like phospholipase domain containing 3	-4.29169	0.006518	0.046769
84132	Usp42	ubiquitin specific peptidase 42	1.307377	0.006593	0.046843
490	ATP2B1	ATPase, Ca++ transporting, plasma membrane 1	4.468336	0.00664	0.046888
80854	setd7	SET domain containing (lysine methyltransferase) 7	-1.51194	0.006834	0.047071
10038	PARP2	poly (ADP-ribose) polymerase 2	-1.50724	0.006898	0.047129
79834	SGK269	NKF3 kinase family member	4.019939	0.006993	0.047214
5520	Ppp2r2a	protein phosphatase 2 (formerly 2A), regulatory subunit B, alpha isoform	1.885083	0.007159	0.047358
9263	STK17A	serine/threonine kinase 17a	4.099909	0.007166	0.047364
254531	lpcat4	lysophosphatidylcholine acyltransferase 4	-1.86205	0.007173	0.04737
11044	papd7	polymerase (DNA directed) sigma	1.799687	0.007213	0.047403
1854	dut	deoxyuridine triphosphatase	-1.53256	0.007214	0.047404
224	aldh3a2	aldehyde dehydrogenase 3 family, member A2	-1.68795	0.00725	0.047434
5128	Cdk17	PCTAIRE protein kinase 2	1.88957	0.007422	0.047574
8459	TPST2	tyrosylprotein sulfotransferase 2	-1.49668	0.007562	0.047683
23659	PLA2G15	phospholipase A2, group XV	-1.66229	0.007635	0.047739
55781	RIOK2	RIO kinase 2 (yeast)	-2.06321	0.007713	0.047798
8737	RIPK1	receptor (TNFRSF)-interacting serine-threonine kinase 1	2.134155	0.007726	0.047807
9100	USP10	ubiquitin specific peptidase 10	-1.25337	0.008011	0.048012
6850	SYK	spleen tyrosine kinase	-2.6376	0.008158	0.048112
22928	SEPHS2	selenophosphate synthetase 2	-1.28463	0.008195	0.048138
146057	TTBK2	tau tubulin kinase 2	-1.87784	0.008232	0.048162
5780	Ptpn9	protein tyrosine phosphatase, non-receptor type 9	-1.3253	0.008278	0.048192
55589	bmp2k	BMP2 inducible kinase	1.288683	0.008296	0.048204
80025	PANK2	pantothenate kinase 2	1.453979	0.008353	0.048241
5147	PDE6D	phosphodiesterase 6D, cGMP-specific, rod, delta	-1.45298	0.00839	0.048265
2683	B4GALT1	UDP-Gal:betaGlcNAc beta 1,4- galactosyltransferase, polypeptide 1	2.401377	0.008517	0.048345
54926	ube2r2	ubiquitin-conjugating enzyme E2R 2	-1.3505	0.008526	0.048351
1849	Dusp7	dual specificity phosphatase 7	-3.18086	0.008576	0.048382
2820	Gpd2	glycerol-3-phosphate dehydrogenase 2 (mitochondrial)	1.636963	0.008589	0.04839
1788	DNMT3A	DNA (cytosine-5-)-methyltransferase 3 alpha	-1.31588	0.008628	0.048414

26191	PTPN22	protein tyrosine phosphatase, non-receptor type 22 (lymphoid)	-2.23273	0.00871	0.048464
9953	Hs3st3b1	heparan sulfate (glucosamine) 3-O-sulfotransferase 3B1	7.626608	0.008723	0.048471
65264	Ube2z	ubiquitin-conjugating enzyme E2Z	1.688868	0.008724	0.048472
2181	ACSL3	acyl-CoA synthetase long-chain family member 3	-1.37523	0.008938	0.048597
3718	JAK3	Janus kinase 3	1.859792	0.008953	0.048606
5770	ptpn1	protein tyrosine phosphatase, non-receptor type 1	1.675984	0.009007	0.048636
5771	PTPN2	protein tyrosine phosphatase, non-receptor type 2	1.869886	0.009115	0.048697
6713	sqlE	squalene epoxidase	-1.60303	0.009123	0.048701
64132	Xylt2	xylosyltransferase II	-1.52725	0.009178	0.048731
26750	RPS6KC1	ribosomal protein S6 kinase, 52kDa, polypeptide 1	1.527532	0.009302	0.048798
51251	NT5C3	5'-nucleotidase, cytosolic III	10.33578	0.009329	0.048812
31	ACACA	acetyl-Coenzyme A carboxylase alpha	-1.67031	0.009371	0.048835
64781	CERK	ceramide kinase	-1.84446	0.009492	0.048898
79858	Nek11	NIMA (never in mitosis gene a)- related kinase 11	-1.43052	0.009579	0.048942
5332	Plcb4	phospholipase C, beta 4	-2.89589	0.009661	0.048983
57097	parp11	poly (ADP-ribose) polymerase family, member 11	1.963593	0.009679	0.048992
30849	PIK3R4	phosphoinositide-3-kinase, regulatory subunit 4	-1.60315	0.00984	0.049174
8658	tnks	tankyrase, TRF1-interacting ankyrin-related ADP-ribose polymerase	-2.05439	0.009897	0.049237
51465	UBE2J1	ubiquitin-conjugating enzyme E2, J1 (UBC6 homolog, yeast)	1.266213	0.009992	0.049341
5494	PPM1A	protein phosphatase 1A (formerly 2C), magnesium-dependent, alpha isoform	-1.38216	0.010231	0.049597
1152	CKB	creatine kinase, brain	18.102	0.010332	0.049701
23387	SIK3	serine/threonine-protein kinase QSK	2.07963	0.010426	0.049797
8540	AGPS	alkylglycerone phosphate synthase	-1.95406	0.010556	0.049929
7048	Tgfbr2	transforming growth factor, beta receptor II (70/80kDa)	-1.58661	0.010738	0.050108
2241	FER	FER tyrosine kinase [Source:HGNC Symbol;Acc:HGNC:3655]	-1.51166	0.010749	0.050118
535	ATP6V0A1	ATPase, H+ transporting, lysosomal V0 subunit a1	-1.34507	0.010767	0.050136
2872	MKNK2	MAP kinase interacting serine/threonine kinase 2	-1.99963	0.010787	0.050155
124454	Ears2	glutamyl-tRNA synthetase 2, mitochondrial (putative)	-1.51881	0.010853	0.050218
8576	STK16	serine/threonine kinase 16	-1.23471	0.010856	0.050221
247	ALOX15B	arachidonate 15-lipoxygenase, type B	1.669457	0.010954	0.050342
528	ATP6V1C1	ATPase, H+ transporting, lysosomal 42kDa, V1 subunit C1	-1.36537	0.011361	0.05103
6484	ST3GAL4	ST3 beta-galactoside alpha-2,3-sialyltransferase 4	1.48017	0.011478	0.051221
5778	PTPN7	protein tyrosine phosphatase, non-receptor type 7	-1.29849	0.011706	0.051589
51611	DPH5	DPH5 homolog (S. cerevisiae)	-2.41781	0.011867	0.051844
5287	PIK3C2B	phosphoinositide-3-kinase, class 2, beta polypeptide	-1.55396	0.012067	0.052152
2582	galE	UDP-galactose-4-epimerase	-1.35184	0.012427	0.052694
152926	Ppm1k	protein phosphatase 1K (PP2C domain containing)	10.06714	0.012508	0.052812
4122	MAN2A2	mannosidase, alpha, class 2A, member 2	-1.37047	0.012552	0.052876
1890	Tymp	thymidine phosphorylase	1.79696	0.012712	0.053107
87178	Pnpt1	polyribonucleotide nucleotidyltransferase 1	5.452124	0.013163	0.053738

5321	pla2g4a	phospholipase A2, group IVA (cytosolic, calcium-dependent)	1.565368	0.013297	0.053919
55683	KIAA1310	KIAA1310	-2.33025	0.013491	0.054179
8731	rnmt	RNA (guanine-7-) methyltransferase	-1.5279	0.013565	0.054276
10068	IL18BP	interleukin 18 binding protein	-1.27637	0.013601	0.054323
5980	REV3L	REV3-like, catalytic subunit of DNA polymerase zeta (yeast)	-1.93195	0.013633	0.054365
4047	LSS	lanosterol synthase (2,3-oxidosqualene-lanosterol cyclase)	1.553256	0.013695	0.054446
993	CDC25A	cell division cycle 25 homolog A (S. pombe)	-2.48417	0.013822	0.054609
2651	GCNT2	glucosaminyl (N-acetyl) transferase 2, I-branching enzyme (I blood group)	1.984682	0.013827	0.054616
1457	Csnk2a1	casein kinase 2, alpha 1 polypeptide pseudogene; casein kinase 2, alpha 1 polypeptide	1.38179	0.013919	0.054733
9128	PRPF4	PRP4 pre-mRNA processing factor 4 homolog (yeast)	-1.42448	0.013991	0.054823
7226	TRPM2	transient receptor potential cation channel, subfamily M, member 2	-1.29721	0.014127	0.054994
5859	QARS	glutaminyl-tRNA synthetase	-1.25667	0.01416	0.055035
8790	TNNI3K	TNNI3 interacting kinase; fucose-1-phosphate guanylyltransferase	-1.51773	0.014362	0.055282
2590	GALNT2	UDP-N-acetyl-alpha-D-galactosamine:polypeptide N-acetylgalactosaminyltransferase 2 (GalNAc-T2)	1.386324	0.014649	0.055626
51086	TNNI3K	TNNI3 interacting kinase; fucose-1-phosphate guanylyltransferase	-2.05154	0.014677	0.055658
51728	POLR3K	polymerase (RNA) III (DNA directed) polypeptide K, 12.3 kDa	-1.32289	0.014793	0.055794
100	ada	adenosine deaminase	4.346509	0.014832	0.05584
57602	usp36	ubiquitin specific peptidase 36	-1.69339	0.014873	0.055888
55703	Polr3b	polymerase (RNA) III (DNA directed) polypeptide B	-1.49881	0.014967	0.055996
5292	Pim1	pim-1 oncogene	2.956011	0.015008	0.056043
8942	Kynu	kynureninase (L-kynurenine hydrolase)	1.903991	0.015012	0.056047
6733	SRPK2	SFRS protein kinase 2	-2.02216	0.015372	0.056452
8202	NCOA3	nuclear receptor coactivator 3	1.412453	0.015377	0.056458
4215	MAP3K3	mitogen-activated protein kinase kinase kinase 3	-1.49813	0.015415	0.0565
11072	Dusp14	dual specificity phosphatase 14	-1.26343	0.015518	0.056613
55033	FKBP14	FK506 binding protein 14, 22 kDa	-1.41888	0.015546	0.056643
7334	UBE2N	ubiquitin-conjugating enzyme E2N (UBC13 homolog, yeast)	1.221237	0.015598	0.0567
9583	entpd4	ectonucleoside triphosphate diphosphohydrolase 4	-1.52141	0.015776	0.056891
23305	Acsl6	acyl-CoA synthetase long-chain family member 6	2.395987	0.015854	0.056973
6790	AURKA	aurora kinase A; aurora kinase A pseudogene 1	-1.54599	0.015932	0.057056
6714	Src	v-src sarcoma (Schmidt-Ruppin A-2) viral oncogene homolog (avian)	3.263054	0.015965	0.05709
8460	TPST1	tyrosylprotein sulfotransferase 1	-1.5048	0.016073	0.057203
3707	Itpkb	inositol 1,4,5-trisphosphate 3-kinase B	-2.29458	0.016157	0.05729
10667	FARS2	phenylalanyl-tRNA synthetase 2, mitochondrial	-1.44212	0.01637	0.05751
8394	PIP5K1A	phosphatidylinositol-4-phosphate 5-kinase, type I, alpha	1.611574	0.016474	0.057617
3611	ILK	integrin-linked kinase	-1.23012	0.016648	0.057793
57486	NLN	neurolysin (metallopeptidase M3 family)	-1.41486	0.017075	0.058213
5599	mapk8	mitogen-activated protein kinase 8	1.562214	0.0171	0.058237

2983	gucy1b3	guanylate cyclase 1, soluble, beta 3	2.612677	0.017124	0.05826
23759	ppil2	peptidylprolyl isomerase (cyclophilin)-like 2	-1.35352	0.017437	0.058557
4234	mettl1	methyltransferase like 1	1.420605	0.017631	0.058738
65220	nadK	NAD kinase	1.261872	0.017681	0.058784
4117	mak	male germ cell-associated kinase	3.065857	0.017695	0.058797
8833	GMPS	guanine monphosphate synthetase	-1.41322	0.017726	0.058825
3636	INPPL1	inositol polyphosphate phosphatase-like 1	-1.35187	0.018204	0.059255
84105	pcbd2	pterin-4 alpha-carbinolamine dehydratase/dimerization cofactor of hepatocyte nuclear factor 1 alpha (TCF1) 2	-1.50775	0.018399	0.059425
790	cad	carbamoyl-phosphate synthetase 2, aspartate transcarbamylase, and dihydroorotase	-1.78901	0.018415	0.059439
23043	TNIK	TRAF2 and NCK interacting kinase	1.857638	0.018442	0.059462
18	ABAT	4-aminobutyrate aminotransferase	-1.77407	0.018497	0.05951
661	Polr3d	polymerase (RNA) III (DNA directed) polypeptide D, 44kDa	1.637942	0.018614	0.05961
4724	NDUFS4	NADH dehydrogenase (ubiquinone) Fe-S protein 4, 18kDa (NADH-coenzyme Q reductase)	1.203269	0.018836	0.059798
22929	sephs1	selenophosphate synthetase 1; similar to selenophosphate synthetase 1	-1.39607	0.018984	0.059921
84532	acss1	acyl-CoA synthetase short-chain family member 1	-2.31876	0.019061	0.059985
5832	ALDH18A1	aldehyde dehydrogenase 18 family, member A1	-1.65869	0.019124	0.060037
58497	PRUNE	prune homolog (Drosophila)	-1.22962	0.019162	0.060068
6648	Sod2	superoxide dismutase 2, mitochondrial	2.435665	0.019162	0.060068
9957	Hs3st1	heparan sulfate (glucosamine) 3-O-sulfotransferase 1	-5.66164	0.019181	0.060084
54995	OXSM	3-oxoacyl-ACP synthase, mitochondrial	-1.22026	0.019398	0.060408
8564	kmo	kynurenine 3-monooxygenase (kynurenine 3-hydroxylase)	2.401636	0.019693	0.060842
22978	NT5C2	5'-nucleotidase, cytosolic II	1.224539	0.019845	0.061065
259230	sgms1	sphingomyelin synthase 1	1.590344	0.019848	0.06107
3613	Impa2	inositol(myo)-1(or 4)-monophosphatase 2	-1.69186	0.020022	0.06132
4140	Mark3	MAP/microtubule affinity-regulating kinase 3	1.503244	0.020566	0.062092
84869	cbr4	carbonyl reductase 4	-2.94871	0.020758	0.062359
5594	MAPK1	mitogen-activated protein kinase 1	-1.26245	0.020847	0.062482
5256	PHKA2	phosphorylase kinase, alpha 2 (liver)	-1.56911	0.021261	0.063045
55904	MLL5	myeloid/lymphoid or mixed-lineage leukemia 5 (trithorax homolog, Drosophila)	-1.32216	0.021357	0.063174
953	ENTPD1	ectonucleoside triphosphate diphosphohydrolase 1	-1.73678	0.021949	0.063957
80896	NPL	N-acetylneuraminate pyruvate lyase (dihydrodipicolinate synthase)	-1.36642	0.022212	0.064297
10087	COL4A3BP	collagen, type IV, alpha 3 (Goodpasture antigen) binding protein	-1.8092	0.022266	0.064367
613	bcr	breakpoint cluster region	-1.25381	0.022293	0.064402
4258	mgst2	microsomal glutathione S-transferase 2	-1.31713	0.022528	0.0647
5286	pik3c2a	phosphoinositide-3-kinase, class 2, alpha polypeptide	-1.33913	0.023357	0.065728
5209	pfkfb3	6-phosphofructo-2-kinase/fructose-2,6-biphosphatase 3	2.616625	0.023382	0.065759
587	BCAT2	branched chain aminotransferase 2, mitochondrial	-1.33749	0.023408	0.065789
64064	OXCT2	3-oxoacid CoA transferase 2	-1.36343	0.023429	0.065815
4704	NDUFA9	NADH dehydrogenase (ubiquinone) 1 alpha subcomplex, 9, 39kDa	1.276696	0.02372	0.066165

55500	etnk1	ethanolamine kinase 1	-1.6816	0.023819	0.066282
6446	SGK1	serum/glucocorticoid regulated kinase 1	-1.57205	0.023852	0.066322
10623	POLR3C	polymerase (RNA) III (DNA directed) polypeptide C (62kD)	1.665438	0.023889	0.066366
622	BDH1	3-hydroxybutyrate dehydrogenase, type 1	-1.30987	0.02401	0.066508
5294	PIK3CG	phosphoinositide-3-kinase, catalytic, gamma polypeptide	-1.67238	0.024139	0.066659
26873	oplaH	5-oxoprolinase (ATP-hydrolysing)	-1.46179	0.024261	0.066802
4247	mgat2	mannosyl (alpha-1,6-)-glycoprotein beta-1,2-N-acetylglucosaminyltransferase	1.287292	0.024618	0.067214
2762	Gmds	GDP-mannose 4,6-dehydratase	-1.53845	0.024623	0.067219
3033	hadh	hydroxyacyl-Coenzyme A dehydrogenase	-1.36393	0.024722	0.067333
3480	IGF1R	insulin-like growth factor 1 receptor	-2.01693	0.024777	0.067395
54434	SSH1	slingshot homolog 1 (Drosophila)	-1.25296	0.024956	0.067597
58190	Ctdsp1	CTD (carboxy-terminal domain, RNA polymerase II, polypeptide A) small phosphatase 1	-1.76237	0.024983	0.067627
4548	mtr	5-methyltetrahydrofolate-homocysteine methyltransferase	-1.53185	0.025219	0.067891
84875	PARP10	poly (ADP-ribose) polymerase family, member 10	1.927591	0.025306	0.067987
54986	Ulk4	unc-51-like kinase 4 (C. elegans)	-1.88954	0.025775	0.06861
7327	UBE2G2	ubiquitin-conjugating enzyme E2G 2 (UBC7 homolog, yeast)	-1.49683	0.025857	0.068718
5442	Polrmt	polymerase (RNA) mitochondrial (DNA directed)	-1.76879	0.026139	0.069085
4217	MAP3K5	mitogen-activated protein kinase kinase kinase 5	1.563246	0.02615	0.069099
1432	Mapk14	mitogen-activated protein kinase 14	-1.39769	0.026276	0.069262
11201	poli	polymerase (DNA directed) iota	-1.55778	0.026736	0.069892
113	ADCY7	adenylate cyclase 7	-1.44613	0.027021	0.070277
158	ADSL	adenylosuccinate lyase	-1.2012	0.027719	0.071203
79813	EHMT1	euchromatic histone-lysine N-methyltransferase 1	-1.54112	0.027811	0.071324
5048	Pafah1b1	platelet-activating factor acetylhydrolase, isoform Ib, subunit 1 (45kDa)	1.348842	0.027858	0.071385
8899	prpf4b	similar to hCG1820375; PRP4 pre-mRNA processing factor 4 homolog B (yeast)	1.485916	0.027954	0.07151
3163	Hmox2	heme oxygenase (decycling) 2	-1.29953	0.028171	0.071791
11329	stk38	serine/threonine kinase 38	-1.66133	0.028668	0.072427
157285	SGK223	homolog of rat pragma of Rnd2	-3.02345	0.028912	0.072735
84693	MCEE	methylmalonyl CoA epimerase	-1.39746	0.028982	0.072822
5422	polA1	polymerase (DNA directed), alpha 1, catalytic subunit	-1.43995	0.029435	0.073386
5351	PLOD1	procollagen-lysine 1, 2-oxoglutarate 5-dioxygenase 1	-1.2086	0.029781	0.073811
6120	rpe	rcRPE; ribulose-5-phosphate-3-epimerase	-1.30809	0.029829	0.07387
3985	LIMK2	LIM domain kinase 2	4.58606	0.029932	0.073995
23031	MAST3	microtubule associated serine/threonine kinase 3	-3.41994	0.031091	0.075375
27005	USP21	ubiquitin specific peptidase 21	-1.54586	0.031269	0.075582
4836	NMT1	N-myristoyltransferase 1	-1.53829	0.031634	0.076003
23178	PASK	PAS domain containing serine/threonine kinase	-2.03636	0.031739	0.076123
80824	DUSP16	dual specificity phosphatase 16	1.930353	0.032305	0.076763
79087	Alg12	asparagine-linked glycosylation 12, alpha-1,6-mannosyltransferase homolog (S. cerevisiae)	-2.11336	0.032463	0.07694

55217	TMLHE	trimethyllysine hydroxylase, epsilon	-2.11672	0.032768	0.077279
2185	PTK2B	PTK2B protein tyrosine kinase 2 beta	1.732137	0.032899	0.077424
518	ATP5G3	ATP synthase, H+ transporting, mitochondrial F0 complex, subunit C3 (subunit 9)	-1.53326	0.033335	0.077899
9736	USP34	ubiquitin specific peptidase 34	-1.75486	0.03368	0.078272
8702	b4galt4	UDP-Gal:betaGlcNAc beta 1,4- galactosyltransferase, polypeptide 4	1.261925	0.033711	0.078305
55284	UBE2W	ubiquitin-conjugating enzyme E2W (putative)	-1.55397	0.033782	0.078381
8569	mknk1	MAP kinase interacting serine/threonine kinase 1	-1.23959	0.034079	0.078697
84340	GFM2	G elongation factor, mitochondrial 2	-1.27849	0.034378	0.079013
23395	Lars2	leucyl-tRNA synthetase 2, mitochondrial	-1.4847	0.035084	0.079745
2650	GCNT1	glucosaminyl (N-acetyl) transferase 1, core 2 (beta-1,6-N-acetylglucosaminyltransferase)	-1.8049	0.0351	0.079762
5261	phkg2	phosphorylase kinase, gamma 2 (testis)	-1.53901	0.035113	0.079775
54956	PARP16	poly (ADP-ribose) polymerase family, member 16	-1.23941	0.035229	0.079894
6303	Sat1	spermidine/spermine N1-acetyltransferase 1	1.320878	0.035497	0.080167
2585	Galk2	galactokinase 2	-1.47591	0.03609	0.080762
2591	GALNT3	UDP-N-acetyl-alpha-D-galactosamine:polypeptide N-acetylgalactosaminyltransferase 3 (GalNAc-T3)	2.230769	0.036289	0.080959
9101	usp8	ubiquitin specific peptidase 8	-1.23924	0.036409	0.081077
3643	INSR	insulin receptor	-1.57718	0.036616	0.081281
3551	IKBKB	inhibitor of kappa light polypeptide gene enhancer in B-cells, kinase beta	-1.2703	0.036968	0.081624
5091	Pc	pyruvate carboxylase	-1.30897	0.037448	0.082085
952	cd38	CD38 molecule	15.3799	0.037492	0.082127
29110	Tbk1	TANK-binding kinase 1	1.504834	0.037581	0.082212
4353	MPO	myeloperoxidase	1.387249	0.037759	0.082381
2730	GCLM	Glutamate-cysteine ligase, modifier subunit	2.376054	0.038101	0.082702
8073	ptp4a2	protein tyrosine phosphatase type IVA, member 2	-1.41321	0.038377	0.082959
126410	cyp4f22	cytochrome P450, family 4, subfamily F, polypeptide 22	1.805861	0.03847	0.083046
54625	PARP14	poly (ADP-ribose) polymerase family, member 14	3.521972	0.038508	0.083081
23228	PLCL2	phospholipase C-like 2	-1.46176	0.039218	0.083731
6391	C1orf192	chromosome 1 open reading frame 192	-1.34913	0.039999	0.08443
5589	prkcsh	protein kinase C substrate 80K-H	-1.21846	0.040041	0.084467
219333	USP12	ubiquitin specific peptidase 12	3.511667	0.040047	0.084473
51703	ACSL5	acyl-CoA synthetase long-chain family member 5	1.309798	0.040066	0.084489
55326	AGPAT5	1-acylglycerol-3-phosphate O-acyltransferase 5 (lysophosphatidic acid acyltransferase, epsilon)	-1.44594	0.040105	0.084523
132160	PPM1M	protein phosphatase 1M (PP2C domain containing)	-1.25275	0.040237	0.084639
83931	Stk40	serine/threonine kinase 40	1.278941	0.040325	0.084717
25	ABL1	c-abl oncogene 1, receptor tyrosine kinase	-1.31386	0.04041	0.084791
11221	Dusp10	dual specificity phosphatase 10	-1.6521	0.040579	0.084939
7465	wee1	WEE1 homolog (S. pombe)	-2.99546	0.040715	0.085057
58508	MLL3	myeloid/lymphoid or mixed-lineage leukemia 3	-1.4705	0.040784	0.085117
128	ADH5	alcohol dehydrogenase 5 (class III), chi polypeptide, pseudogene 4; alcohol dehydrogenase 5 (class III), chi polypeptide	-1.40619	0.041129	0.085414

262	AMD1	adenosylmethionine decarboxylase 1	1.367343	0.041176	0.085454
5164	PDK2	pyruvate dehydrogenase kinase, isozyme 2	-2.23529	0.041471	0.085706
10905	MAN1A2	mannosidase, alpha, class 1A, member 2	-1.52329	0.04198	0.086135
54961	Ssh3	slingshot homolog 3 (Drosophila)	-1.63321	0.042517	0.08658
3176	HNMT	histamine N-methyltransferase	-2.30044	0.042609	0.086656
51380	CSAD	cysteine sulfinic acid decarboxylase	-1.44705	0.042761	0.08678
8648	NCOA1	nuclear receptor coactivator 1	1.246658	0.042894	0.086889
984	Cdk11b	similar to cell division cycle 2-like 1 (PITSLRE proteins); cell division cycle 2-like 1 (PITSLRE proteins); cell division cycle 2-like 2 (PITSLRE proteins)	-1.29588	0.043237	0.087167
221	Aldh3b1	aldehyde dehydrogenase 3 family, member B1	1.21895	0.043787	0.087608
5255	PHKA1	phosphorylase kinase, alpha 1 pseudogene 1; phosphorylase kinase, alpha 1 (muscle)	-1.45131	0.044104	0.087859
178	agl	amylo-1, 6-glucosidase, 4-alpha-glucanotransferase	-1.28695	0.044421	0.088107
25778	DSTYK	dual serine/threonine and tyrosine protein kinase	2.031911	0.044696	0.088322
57396	clk4	CDC-like kinase 4	1.311973	0.044732	0.088349
64802	NMNAT1	nicotinamide nucleotide adenylyltransferase 1	-1.42073	0.044864	0.088452
54704	Pdp1	pyruvate dehyrogenase phosphatase catalytic subunit 1	-1.81725	0.044979	0.088541
3656	IRAK2	interleukin-1 receptor-associated kinase 2	3.849269	0.045149	0.088671
6675	UAP1	UDP-N-acteylglucosamine pyrophosphorylase 1	1.319292	0.045355	0.088829
6646	soat1	sterol O-acyltransferase 1	-1.26465	0.045401	0.088864
5210	Pfkfb4	6-phosphofructo-2-kinase/fructose-2,6-biphosphatase 4	-2.24328	0.045581	0.089
272	AMPD3	adenosine monophosphate deaminase (isoform E)	2.223332	0.045904	0.089244
79731	NARS2	asparaginyl-tRNA synthetase 2, mitochondrial (putative)	-1.56073	0.046124	0.089408
8408	ULK1	unc-51-like kinase 1 (C. elegans)	-1.46332	0.046278	0.089523
4820	NKTR	natural killer-tumor recognition sequence	-1.48559	0.046542	0.089719
25930	Ptpn23	protein tyrosine phosphatase, non-receptor type 23	-1.50376	0.046709	0.089841
158067	c9orf98	chromosome 9 open reading frame 98	1.715008	0.046851	0.089946
1263	plk3	polo-like kinase 3 (Drosophila)	-1.47058	0.046899	0.089981
10477	Ube2e3	ubiquitin-conjugating enzyme E2E 3 (UBC4/5 homolog, yeast)	-1.33503	0.047054	0.090094
5728	PTENP1	phosphatase and tensin homolog; phosphatase and tensin homolog pseudogene 1	-1.28449	0.047283	0.09026
2050	EPHB4	EPH receptor B4	-1.60532	0.047391	0.090338
9448	MAP4K4	mitogen-activated protein kinase kinase kinase kinase 4	1.523996	0.047778	0.090617
10000	Akt3	v-akt murine thymoma viral oncogene homolog 3 (protein kinase B, gamma)	1.62333	0.04792	0.090718
64895	PAPOLG	poly(A) polymerase gamma	-1.99907	0.048332	0.09101
5279	PIGC	phosphatidylinositol glycan anchor biosynthesis, class C	-1.82392	0.048389	0.09105
5515	PPP2CA	protein phosphatase 2 (formerly 2A), catalytic subunit, alpha isoform	1.21001	0.048486	0.091117
3055	HCK	hemopoietic cell kinase	1.778428	0.048637	0.091223
85464	SSH2	slingshot homolog 2 (Drosophila)	-1.81624	0.04936	0.091724
2047	ephb1	EPH receptor B1	-1.81499	0.049381	0.091738
10797	mthfd2	methylenetetrahydrofolate dehydrogenase (NADP+ dependent) 2, methenyltetrahydrofolate cyclohydrolase	1.554809	0.049397	0.091749

4707	NDUFB1	NADH dehydrogenase (ubiquinone) 1 beta subcomplex, 1, 7kDa	-1.34528	0.0496	0.091888
1371	CPOX	coproporphyrinogen oxidase	-1.29513	0.04964	0.091915
160851	DGKH	diacylglycerol kinase, eta	2.068368	0.049845	0.092055

Supplemental Table S2.3: A list of significantly altered gene sets identified by GSEA in the BMM dataset.

Filter	NAME	SIZE	ES	NES	NOM p-val	FDR q-val	
1	GO_ALCOHOL_CATABOLIC_PROCESS	38	-0.606	-1.842	0	0.008027	1
1	GO_DICARBOXYLIC_ACID_METABOLIC_PROCESS	71	-0.478	-1.648	0	0.046959	2
1	GO_GLYCOSAMINOGLYCAN_BINDING	106	-0.468	-1.682	0	0.036145	3
1	GO_SMALL_MOLECULE_CATABOLIC_PROCESS	211	-0.403	-1.606	0	0.063664	4
1	KEGG_GLYCOSPHINGOLIPID_BIOSYNTHESIS_LACTO_AND_NEOLACTO_SERIES	16	-0.831	-2.071	0	2.87E-04	5
1	GO_ORGANIC_HYDROXY_COMPOUND_CATABOLIC_PROCESS	43	-0.584	-1.795	0.001845	0.013283	6
1	GO_ORGANONITROGEN_COMPOUND_CATABOLIC_PROCESS	202	-0.387	-1.536	0.001866	0.100556	7
1	GO_CARBOHYDRATE_BINDING	140	-0.393	-1.517	0.001992	0.112226	8
1	GO_POSITIVE_REGULATION_OF_REACTIVE_OXYGEN_SPECIES_BIOSYNTHETIC_PROCESS	36	-0.55	-1.67	0.002004	0.039486	9
1	KEGG_GALACTOSE_METABOLISM	21	-0.689	-1.836	0.002028	0.008425	10
1	GO_REGULATION_OF_NITRIC_OXIDE_BIOSYNTHETIC_PROCESS	39	-0.563	-1.734	0.002062	0.023622	11
1	KEGG_TRYPTOPHAN_METABOLISM	23	-0.702	-1.921	0.003984	0.003121	12
1	GO_POSITIVE_REGULATION_OF_MAPK_CASCADE	284	-0.342	-1.416	0.007233	0.186908	13
1	GO_REGULATION_OF_REACTIVE_OXYGEN_SPECIES_BIOSYNTHETIC_PROCESS	49	-0.502	-1.619	0.007648	0.058081	14
1	KEGG_GLYCEROLIPID_METABOLISM	33	-0.579	-1.707	0.007843	0.029353	15
1	KEGG_HISTIDINE_METABOLISM	17	-0.641	-1.646	0.00813	0.047722	16
1	BIOCARTA_BIOPEPTIDES_PATHWAY	35	-0.531	-1.611	0.01002	0.061531	17
1	GO_LIPASE_ACTIVITY	64	-0.47	-1.586	0.014056	0.072478	18
1	GO_GLYCOSPHINGOLIPID_METABOLIC_PROCESS	51	-0.496	-1.592	0.015625	0.069857	19
1	GO_SERINE_HYDROLASE_ACTIVITY	93	-0.407	-1.48	0.019268	0.138648	20
1	GO_MEMBRANE_LIPID_CATABOLIC_PROCESS	17	-0.616	-1.597	0.020619	0.067574	21

Legend		
	1	Immune signaling and function
	2	Cellular metabolism
	3	Other biological states and processes
NAME		Name of gene set
SIZE		Number of Genes within gene set
ES		Enrichment Score for gene set (Degree to which this gene set is overrepresented at the top or bottom of the ranked lit of genes)
NES		Normalized enrichment score
NOM p-val		Nominal p-value
FDR q-val		False discovery rate (corrected for multiple testing)

129

1	KEGG_BETA_ALANINE_METABOLISM	16	-0.644	-1.597	0.021552	0.067672	22
1	GO_SPHINGOLIPID_METABOLIC_PROCESS	97	-0.391	-1.407	0.022857	0.19404	23
1	KEGG_ARGININE_AND_PROLINE_METABOLISM	34	-0.519	-1.542	0.022965	0.097655	24
1	GO_MEMBRANE_LIPID_METABOLIC_PROCESS	132	-0.364	-1.362	0.026718	0.232762	25
1	GO_CELLULAR_LIPID_CATABOLIC_PROCESS	100	-0.398	-1.436	0.028681	0.170066	26
1	BIOCARTA_CERAMIDE_PATHWAY	21	-0.565	-1.492	0.030426	0.130386	27
1	GO_CARBOHYDRATE_PHOSPHORYLATION	18	-0.599	-1.554	0.030928	0.090754	28
1	GO_ORGANOPHOSPHATE_CATABOLIC_PROCESS	80	-0.403	-1.406	0.035714	0.1943	29
1	GO_PHOSPHOLIPASE_ACTIVITY	53	-0.446	-1.439	0.037475	0.167423	30
1	GO_L_ASCORBIC_ACID_BINDING	17	-0.611	-1.568	0.037694	0.082579	31
1	GO_CELLULAR_AMINO_ACID_CATABOLIC_PROCESS	65	-0.415	-1.401	0.037924	0.198854	32
1	GO_BENZENE_CONTAINING_COMPOUND_METABOLIC_PROCESS	15	-0.647	-1.615	0.038217	0.059969	33
1	GO_TETRAHYDROFOLATE_METABOLIC_PROCESS	16	-0.619	-1.555	0.039175	0.089808	34
1	KEGG_NICOTINATE_AND_NICOTINAMIDE_METABOLISM	16	-0.59	-1.517	0.041667	0.112188	35
1	GO_RNA_PHOSPHODIESTER_BOND_HYDROLYSIS_EXONUCLEOLYTIC	26	-0.535	-1.49	0.04251	0.131591	36
1	GO_PYRIMIDINE_NUCLEOSIDE_METABOLIC_PROCESS	31	-0.513	-1.493	0.044444	0.129418	37
1	REACTOME_PYRIMIDINE_METABOLISM	17	-0.577	-1.493	0.044625	0.129332	38
1	KEGG_GLYCOLYSIS_GLUCONEOGENESIS	39	-0.486	-1.454	0.045161	0.157203	39
1	GO_PHOSPHOLIPASE_C_ACTIVITY	18	-0.602	-1.559	0.048523	0.087738	40
2	GO_CCR_CHEMOKINE_RECEPTOR_BINDING	15	-0.813	-2.012	0	8.16E-04	1
2	GO_CELLULAR_RESPONSE_TO_CYTOKINE_STIMULUS	379	-0.514	-2.213	0	2.25E-05	2
2	GO_CELLULAR_RESPONSE_TO_INTERFERON_GAMMA	64	-0.687	-2.288	0	0	3
2	GO_CELLULAR_RESPONSE_TO_VIRUS	16	-0.76	-1.875	0	0.005497	4
2	GO_CHEMOKINE_ACTIVITY	23	-0.687	-1.91	0	0.003569	5
2	GO_CHEMOKINE_RECEPTOR_BINDING	31	-0.671	-1.967	0	0.001607	6
2	GO_CYTOKINE_ACTIVITY	86	-0.572	-2.016	0	7.73E-04	7

2	GO_CYTOKINE_MEDIATED_SIGNALING_PATHWAY	277	-0.553	-2.286	0	0	8
2	GO_CYTOKINE_RECEPTOR_BINDING	145	-0.462	-1.772	0	0.016825	9
2	GO_DEFENSE_RESPONSE_TO_OTHER_ORGANISM	233	-0.529	-2.145	0	7.15E-05	10
2	GO_DEFENSE_RESPONSE_TO_VIRUS	91	-0.726	-2.581	0	0	11
2	GO_IMMUNE_EFFECTOR_PROCESS	288	-0.444	-1.831	0	0.008851	12
2	GO_INFLAMMATORY_RESPONSE	260	-0.421	-1.729	0	0.024451	13
2	GO_INNATE_IMMUNE_RESPONSE	298	-0.551	-2.316	0	0	14
2	GO_INTERFERON_GAMMA_MEDIATED_SIGNALING_PATHWAY	41	-0.717	-2.181	0	3.36E-05	15
2	GO_INTRACELLULAR_RECEPTOR_SIGNALING_PATHWAY	112	-0.439	-1.616	0	0.05963	16
2	GO_LEUKOCYTE_ACTIVATION	283	-0.349	-1.45	0	0.159365	17
2	GO_LYMPHOCYTE_CHEMOTAXIS	18	-0.723	-1.863	0	0.006418	18
2	GO_NEGATIVE_REGULATION_OF_IMMUNE_SYSTEM_PROCESS	225	-0.408	-1.654	0	0.044845	19
2	GO_NEGATIVE_REGULATION_OF_LOCOMOTION	175	-0.388	-1.52	0	0.110171	20
2	GO_NEGATIVE_REGULATION_OF_TYPE_I_INTERFERON_PRODUCTION	28	-0.675	-1.915	0	0.003356	21
2	GO_NEGATIVE_REGULATION_OF_VIRAL_GENOME_REPLICATION	30	-0.717	-2.102	0	1.60E-04	22
2	GO_NEGATIVE_REGULATION_OF_VIRAL_PROCESS	60	-0.642	-2.157	0	6.44E-05	23
2	GO_POSITIVE_REGULATION_OF_CHEMOTAXIS	78	-0.516	-1.8	0	0.01257	24
2	GO_POSITIVE_REGULATION_OF_DEFENSE_RESPONSE	241	-0.354	-1.448	0	0.160176	25
2	GO_POSITIVE_REGULATION_OF_INTERFERON_ALPHA_PRODUCTION	15	-0.831	-2.064	0	3.25E-04	26
2	GO_POSITIVE_REGULATION_OF_LEUKOCYTE_CHEMOTAXIS	54	-0.586	-1.939	0	0.002453	27
2	GO_POSITIVE_REGULATION_OF_LEUKOCYTE_MIGRATION	72	-0.538	-1.821	0	0.009989	28
2	GO_POSITIVE_REGULATION_OF_RESPONSE_TO_EXTERNAL_STIMULUS	186	-0.4	-1.596	0	0.06794	29
2	GO_REGULATION_OF_CYTOKINE_PRODUCTION	354	-0.373	-1.592	0	0.0699	30
2	GO_REGULATION_OF_DEFENSE_RESPONSE	475	-0.378	-1.642	0	0.048973	31

2	GO_REGULATION_OF_IMMUNE_EFFECTOR_PROCESS	251	-0.401	-1.657	0	0.043913	32
2	GO_REGULATION_OF_INNATE_IMMUNE_RESPONSE	243	-0.421	-1.719	0	0.026798	33
2	GO_REGULATION_OF_INTERFERON_ALPHA_PRODUCTION	18	-0.843	-2.196	0	2.20E-05	34
2	GO_REGULATION_OF_LEUKOCYTE_APOPTOTIC_PROCESS	54	-0.594	-1.937	0	0.002539	35
2	GO_REGULATION_OF_LEUKOCYTE_CHEMOTAXIS	60	-0.595	-1.969	0	0.001556	36
2	GO_REGULATION_OF_LEUKOCYTE_MIGRATION	97	-0.51	-1.837	0	0.008325	37
2	GO_REGULATION_OF_LEUKOCYTE_PROLIFERATION	122	-0.417	-1.569	0	0.08232	38
2	GO_REGULATION_OF_LYMPHOCYTE_MIGRATION	26	-0.703	-2.02	0	7.27E-04	39
2	GO_REGULATION_OF_STAT_CASCADE	79	-0.495	-1.748	0	0.020825	40
2	GO_REGULATION_OF_TYPE_I_INTERFERON_MEDIATED_SIGNALING_PATHWAY	20	-0.725	-1.916	0	0.00333	41
2	GO_REGULATION_OF_TYPE_I_INTERFERON_PRODUCTION	89	-0.515	-1.849	0	0.007535	42
2	GO_REGULATION_OF_VIRAL_ENTRY_INTO_HOST_CELL	20	-0.703	-1.86	0	0.006584	43
2	GO_REGULATION_OF_VIRAL_GENOME_REPLICATION	50	-0.62	-2.009	0	8.72E-04	44
2	GO_RESPONSE_TO_CYTOKINE	459	-0.488	-2.117	0	1.24E-04	45
2	GO_RESPONSE_TO_INTERFERON_ALPHA	17	-0.823	-2.107	0	1.36E-04	46
2	GO_RESPONSE_TO_INTERFERON_GAMMA	78	-0.664	-2.324	0	0	47
2	GO_RESPONSE_TO_TUMOR_NECROSIS_FACTOR	148	-0.439	-1.688	0	0.034537	48
2	GO_RESPONSE_TO_TYPE_I_INTERFERON	38	-0.876	-2.635	0	0	49
2	GO_RESPONSE_TO_VIRUS	148	-0.65	-2.491	0	0	50
2	GO_STAT_CASCADE	35	-0.658	-1.995	0	0.001071	51
2	HALLMARK_ALLOGRAFT_REJECTION	139	-0.522	-2.003	0	9.45E-04	52
2	HALLMARK_IL2_STAT5_SIGNALING	152	-0.45	-1.757	0	0.019207	53
2	HALLMARK_IL6_JAK_STAT3_SIGNALING	72	-0.593	-2.037	0	5.35E-04	54
2	HALLMARK_INFLAMMATORY_RESPONSE	156	-0.442	-1.721	0	0.026341	55
2	HALLMARK_INTERFERON_ALPHA_RESPONSE	74	-0.903	-3.124	0	0	56

2	HALLMARK_INTERFERON_GAMMA_RESPONSE	159	-0.826	-3.203	0	0	57
2	KEGG_CHEMOKINE_SIGNALING_PATHWAY	140	-0.425	-1.641	0	0.04959	58
2	KEGG_CYTOKINE_CYTOKINE_RECEPTOR_INTERACTION	131	-0.518	-1.954	0	0.001986	59
2	KEGG_CYTOSOLIC_DNA_SENSING_PATHWAY	36	-0.653	-1.95	0	0.002077	60
2	KEGG_JAK_STAT_SIGNALING_PATHWAY	94	-0.516	-1.85	0	0.007426	61
2	KEGG_TOLL_LIKE_RECEPTOR_SIGNALING_PATHWAY	81	-0.492	-1.733	0	0.023771	62
2	REACTOME_ANTIVIRAL_MECHANISM_BY_IFN_STIMULATED_GENES	57	-0.619	-2.027	0	6.22E-04	63
2	REACTOME_CYTOKINE_SIGNALING_IN_IMMUNE_SYSTEM	196	-0.611	-2.438	0	0	64
2	REACTOME_INTERFERON_ALPHA_BETA_SIGNALING	37	-0.867	-2.645	0	0	65
2	REACTOME_INTERFERON_GAMMA_SIGNALING	38	-0.729	-2.219	0	1.39E-05	66
2	REACTOME_INTERFERON_SIGNALING	109	-0.717	-2.602	0	0	67
2	REACTOME_NEGATIVE_REGULATORS_OF_RIG_I_MDA5_SIGNALING	22	-0.698	-1.891	0	0.004576	68
2	REACTOME_RIG_I_MDA5_MEDIATED_INDUCTION_OF_IFN_ALPHA_BETA_PATHWAYS	46	-0.588	-1.85	0	0.007426	69
2	GO_LEUKOCYTE_DIFFERENTIATION	199	-0.376	-1.478	0.001852	0.139835	70
2	GO_NEGATIVE_REGULATION_OF_CYTOKINE_PRODUCTION	129	-0.425	-1.59	0.001916	0.071031	71
2	GO_CELL_CHEMOTAXIS	106	-0.406	-1.488	0.001931	0.132835	72
2	REACTOME_INNATE_IMMUNE_SYSTEM	161	-0.405	-1.574	0.001946	0.079098	73
2	GO_REGULATION_OF_RESPONSE_TO_CYTOKINE_STIMULUS	99	-0.458	-1.645	0.001961	0.047782	74
2	GO_REGULATION_OF_CHEMOTAXIS	111	-0.462	-1.7	0.00198	0.03133	75
2	GO_LEUKOCYTE_PROLIFERATION	52	-0.531	-1.716	0.001996	0.027287	76
2	GO_POSITIVE_REGULATION_OF_INTERFERON_BETA_PRODUCTION	28	-0.634	-1.808	0.002016	0.011516	77
2	GO_NATURAL_KILLER_CELL_ACTIVATION	24	-0.653	-1.814	0.002033	0.010719	78
2	BIOCARTA_IL10_PATHWAY	16	-0.711	-1.769	0.002045	0.017192	79
2	GO_POSITIVE_REGULATION_OF_STAT_CASCADE	38	-0.571	-1.733	0.002058	0.02379	80
2	GO_MHC_PROTEIN_BINDING	17	-0.747	-1.912	0.002114	0.003434	81

2	GO_RESPONSE_TO_INTERFERON_BETA	17	-0.707	-1.825	0.002128	0.009489	82
2	GO_POSITIVE_REGULATION_OF_CYTOKINE_PRODUCTION	235	-0.359	-1.47	0.003448	0.145288	83
2	GO_RESPONSE_TO_MOLECULE_OF_BACTERIAL_ORIGIN	225	-0.355	-1.455	0.003534	0.156641	84
2	GO_NEGATIVE_REGULATION_OF_IMMUNE_EFFECTOR_PROCESS	61	-0.496	-1.677	0.003774	0.037419	85
2	GO_LYMPHOCYTE_MIGRATION	22	-0.717	-1.911	0.004016	0.003462	86
2	GO_NEGATIVE_REGULATION_OF_T_CELL_PROLIFERATION	27	-0.612	-1.772	0.00409	0.016805	87
2	GO_NEGATIVE_REGULATION_OF_LEUKOCYTE_MEDIATED_IMMUNITY	29	-0.62	-1.778	0.004149	0.015867	88
2	REACTOME_IMMUNOREGULATORY_INTERACTIONS_BETWEEN_A_LYMPHOID_AND_A_NON_LYMPHOID_CELL	28	-0.623	-1.786	0.004211	0.01465	89
2	GO_NEGATIVE_REGULATION_OF_INTERFERON_GAMMA_PRODUCTION	18	-0.682	-1.766	0.004255	0.017619	90
2	GO_NEGATIVE_REGULATION_OF_LEUKOCYTE_APOPTOTIC_PROCESS	29	-0.619	-1.763	0.004255	0.018136	91
2	GO_NEGATIVE_REGULATION_OF_INNATE_IMMUNE_RESPONSE	19	-0.669	-1.731	0.004329	0.024205	92
2	GO_IMMUNE_SYSTEM_DEVELOPMENT	390	-0.32	-1.375	0.005525	0.21944	93
2	GO_REGULATION_OF_T_CELL_APOPTOTIC_PROCESS	21	-0.622	-1.628	0.005929	0.055051	94
2	GO_CHEMOKINE_MEDIATED_SIGNALING_PATHWAY	35	-0.592	-1.774	0.006024	0.016461	95
2	GO_REGULATION_OF_LYMPHOCYTE_APOPTOTIC_PROCESS	37	-0.553	-1.657	0.006186	0.043854	96
2	KEGG_PRIMARY_IMMUNODEFICIENCY	24	-0.625	-1.716	0.006772	0.027187	97
2	GO_MYELOID_LEUKOCYTE_ACTIVATION	72	-0.443	-1.531	0.007619	0.1038	98
2	GO_POSITIVE_REGULATION_OF_TYPE_I_INTERFERON_PRODUCTION	61	-0.48	-1.605	0.007663	0.064268	99
2	GO_POSITIVE_REGULATION_OF_LEUKOCYTE_PROLIFERATION	83	-0.44	-1.556	0.007905	0.089419	100
2	GO_ANTIGEN_BINDING	28	-0.583	-1.655	0.008032	0.044545	101
2	GO_REGULATION_OF_TYROSINE_PHOSPHORYLATION_OF_STAT_PROTEIN	37	-0.546	-1.664	0.008048	0.041646	102
2	GO_REGULATION_OF_RESPONSE_TO_INTERFERON_GAMMA	17	-0.649	-1.687	0.008065	0.034773	103

2	KEGG_INTESTINAL_IMMUNE_NETWORK_FOR_IGA_PRODUCTION	25	-0.645	-1.759	0.008351	0.018745	104
2	GO_RESPONSE_TO_EXOGENOUS_DSRNA	21	-0.633	-1.684	0.008602	0.035416	105
2	KEGG_SYSTEMIC_LUPUS_ERYTHEMATOSUS	37	-0.516	-1.592	0.009785	0.069762	106
2	GO_LEUKOCYTE_CHEMOTAXIS	74	-0.43	-1.492	0.011765	0.130324	107
2	GO_REGULATION_OF_T_CELL_PROLIFERATION	81	-0.434	-1.52	0.012097	0.11046	108
2	GO_RESPONSE_TO_INTERLEUKIN_4	20	-0.656	-1.758	0.012146	0.018826	109
2	GO_NEGATIVE_REGULATION_OF_LEUKOCYTE_PROLIFERATION	38	-0.532	-1.6	0.012195	0.066222	110
2	GO_CELLULAR_RESPONSE_TO_INTERLEUKIN_4	18	-0.644	-1.651	0.01227	0.045868	111
2	GO_NEGATIVE_REGULATION_OF_CYTOKINE_BIOSYNTHETIC_PROCESS	19	-0.638	-1.642	0.01227	0.048993	112
2	GO_MONOCYTE_CHEMOTAXIS	18	-0.668	-1.694	0.012632	0.032854	113
2	GO_POSITIVE_REGULATION_OF_INFLAMMATORY_RESPONSE	66	-0.451	-1.524	0.013208	0.107306	114
2	GO_REGULATION_OF_LEUKOCYTE_MEDIATED_IMMUNITY	98	-0.411	-1.483	0.013834	0.137092	115
2	REACTOME_ANTIGEN_PROCESSING_CROSS_PRESENTATION	61	-0.467	-1.548	0.014141	0.093798	116
2	GO_CYTOPLASMIC_PATTERN_RECOGNITION_RECEPTOR_SIGNALING_PATHWAY	22	-0.598	-1.606	0.014228	0.063783	117
2	GO_POSITIVE_REGULATION_OF_LEUKOCYTE_APOPTOTIC_PROCESS	17	-0.658	-1.68	0.014463	0.036618	118
2	GO_ZYMOGEN_ACTIVATION	74	-0.451	-1.552	0.015209	0.091755	119
2	REACTOME_CHEMOKINE_RECEPTORS_BIND_CHEMOKINES	31	-0.576	-1.651	0.015842	0.045838	120
2	GO_REGULATION_OF_T_CELL_MIGRATION	15	-0.692	-1.708	0.016598	0.029133	121
2	GO_DENDRITIC_CELL_DIFFERENTIATION	21	-0.589	-1.613	0.017167	0.060817	122
2	GO_ANTIGEN_PROCESSING_AND_PRESENTATION_OF_PEPTIDE_ANTIGEN_VIA_MHC_CLASS_I	74	-0.425	-1.466	0.017375	0.148547	123
2	GO_LEUKOCYTE_MIGRATION	174	-0.348	-1.374	0.019724	0.220618	124
2	KEGG_NOD_LIKE_RECEPTOR_SIGNALING_PATHWAY	41	-0.495	-1.531	0.020367	0.103558	125
2	GO_REGULATION_OF_INTERFERON_BETA_PRODUCTION	37	-0.538	-1.623	0.021277	0.05672	126

2	GO_REGULATION_OF_PRODUCTION_OF_MOLECULAR_MEDIATOR_OF_IMMUNE_RESPONSE	60	-0.426	-1.428	0.021782	0.176893	127
2	GO_REGULATION_OF_CELL_KILLING	32	-0.543	-1.575	0.022358	0.078728	128
2	GO_LYMPHOCYTE_DIFFERENTIATION	142	-0.358	-1.367	0.02277	0.227237	129
2	GO_LYMPHOCYTE_ACTIVATION	233	-0.338	-1.359	0.023214	0.235489	130
2	GO_REGULATION_OF_INTERFERON_GAMMA_PRODUCTION	54	-0.448	-1.462	0.023529	0.151276	131
2	GO_RESPONSE_TO_PROTOZOAN	16	-0.636	-1.599	0.023861	0.067067	132
2	GO_REGULATION_OF_DEFENSE_RESPONSE_TO_VIRUS	113	-0.384	-1.407	0.025225	0.193971	133
2	REACTOME_CLASS_I_MHC_MEDIATED_ANTIGEN_PROCESSING_PRESENTATION	192	-0.342	-1.348	0.025688	0.244188	134
2	GO_MYELOID_CELL_DIFFERENTIATION	129	-0.373	-1.408	0.026769	0.193629	135
2	GO_NEGATIVE_REGULATION_OF_IMMUNE_RESPONSE	67	-0.421	-1.431	0.027613	0.174147	136
2	GO_POSITIVE_REGULATION_OF_VIRAL_GENOME_REPLICATION	25	-0.548	-1.532	0.029228	0.103297	137
2	BIOCARTA_IL2_PATHWAY	19	-0.601	-1.567	0.029644	0.082852	138
2	GO_NEGATIVE_REGULATION_OF_LYMPHOCYTE_MEDIATED_IMMUNITY	19	-0.603	-1.551	0.031513	0.092303	139
2	GO_REGULATION_OF_TYROSINE_PHOSPHORYLATION_OF_STAT3_PROTEIN	28	-0.536	-1.537	0.033126	0.100497	140
2	GO_B_CELL_PROLIFERATION	17	-0.625	-1.542	0.035197	0.09744	141
2	KEGG_RIG_I_LIKE_RECEPTOR_SIGNALING_PATHWAY	41	-0.485	-1.498	0.035565	0.125655	142
2	GO_POSITIVE_REGULATION_OF_TOLL_LIKE_RECEPTOR_SIGNALING_PATHWAY	17	-0.611	-1.608	0.035941	0.062976	143
2	GO_REGULATION_OF_TOLL_LIKE_RECEPTOR_SIGNALING_PATHWAY	36	-0.487	-1.469	0.03626	0.146389	144
2	GO_RESPONSE_TO_INTERLEUKIN_1	72	-0.401	-1.38	0.038095	0.21606	145
2	GO_REGULATION_OF_LEUKOCYTE_MEDIATED_CYTOTOXICITY	27	-0.529	-1.485	0.038544	0.135237	146
2	BIOCARTA_IL6_PATHWAY	22	-0.568	-1.51	0.04251	0.117262	147
2	GO_PATTERN_RECOGNITION_RECEPTOR_SIGNALING_PATHWAY	80	-0.396	-1.379	0.046422	0.216607	148
2	GO_HUMORAL_IMMUNE_RESPONSE	65	-0.422	-1.42	0.046967	0.183324	149
2	GO_MYELOID_LEUKOCYTE_DIFFERENTIATION	66	-0.412	-1.399	0.047337	0.200921	150

2	GO_REGULATION_OF_CYTOKINE_PRODUCTION_INVOLVED_IN_IMMUNE_RESPONSE	39	-0.463	-1.436	0.048924	0.17031	151
3	GO_CELL_CELL_SIGNALING	367	-0.347	-1.477	0	0.140528	1
3	GO_CELL_SURFACE	426	-0.327	-1.418	0	0.185459	2
3	GO_CELLULAR_RESPONSE_TO_GROWTH_HORMONE_STIMULUS	15	-0.711	-1.77	0	0.017127	3
3	GO_EXTERNAL_SIDE_OF_PLASMA_MEMBRANE	124	-0.463	-1.728	0	0.024653	4
3	GO_NAD_ADP_RIBOSYLTRANSFERASE_ACTIVITY	23	-0.741	-1.987	0	0.001233	5
3	GO_NEGATIVE_REGULATION_OF_MULTI_ORGANISM_PROCESS	97	-0.533	-1.915	0	0.003347	6
3	GO_POSITIVE_REGULATION_OF_ERK1_AND_ERK2_CASCADE	93	-0.479	-1.725	0	0.025321	7
3	GO_POSITIVE_REGULATION_OF_LYMPHOCYTE_MIGRATION	18	-0.741	-1.901	0	0.004012	8
3	GO_REGULATION_OF_ERK1_AND_ERK2_CASCADE	143	-0.42	-1.621	0	0.057411	9
3	GO_REGULATION_OF_MULTI_ORGANISM_PROCESS	309	-0.389	-1.631	0	0.05388	10
3	GO_REGULATION_OF_SYMBIOSIS_ENCOMPASSING_MUTUALISM_THROUGH_PARASITISM	152	-0.487	-1.89	0	0.004616	11
3	GO_RESPONSE_TO_BIOTIC_STIMULUS	485	-0.408	-1.771	0	0.016975	12
3	GO_SIDE_OF_MEMBRANE	247	-0.383	-1.568	0	0.082382	13
3	GO_SULFUR_COMPOUND_BINDING	146	-0.411	-1.568	0	0.08247	14
3	GO_TRANSFERASE_ACTIVITY_TRANSFERRING_GLYCOSYL_GROUPS	173	-0.413	-1.608	0	0.063202	15
3	GO_TRANSFERASE_ACTIVITY_TRANSFERRING_PENTOSYL_GROUPS	37	-0.593	-1.793	0	0.013542	16
3	GO_TRANSMEMBRANE_RECEPTOR_PROTEIN_TYROSINE_KINASE_ACTIVITY	36	-0.639	-1.891	0	0.00457	17
3	HALLMARK_KRAS_SIGNALING_UP	130	-0.44	-1.639	0	0.05033	18
3	REACTOME_TRAF6_MEDIATED_IRF7_ACTIVATION	16	-0.831	-2.101	0	1.59E-04	19
3	GO_G_PROTEIN_COUPLED_RECEPTOR_BINDING	139	-0.416	-1.6	0.001812	0.066462	20
3	GO_HEPARIN_BINDING	86	-0.517	-1.846	0.001883	0.007678	21
3	GO_GLIOGENESIS	117	-0.411	-1.521	0.001927	0.109681	22
3	REACTOME_G_ALPHA_I_SIGNALLING_EVENTS	94	-0.451	-1.624	0.001927	0.056553	23

3	GO_POSITIVE_REGULATION_OF_CALCIUM_ION_TRANSPORT	64	-0.466	-1.601	0.001946	0.065902	24
3	GO_TRANSMEMBRANE_RECEPTOR_PROTEIN_KINASE_ACTIVITY	49	-0.554	-1.77	0.001972	0.017076	25
3	GO_CALCIUM_CHANNEL_REGULATOR_ACTIVITY	25	-0.652	-1.793	0.002012	0.013469	26
3	GO_REGULATION_OF_CELL_CELL_ADHESION	226	-0.364	-1.472	0.003906	0.144601	27
3	GO_ACTIVATION_OF_CYSTEINE_TYPE_ENDOPEPTIDASE_ACTIVITY	68	-0.477	-1.619	0.003937	0.058349	28
3	GO_POSITIVE_REGULATION_OF_RESPONSE_TO_WOUNDING	98	-0.461	-1.67	0.004032	0.039444	29
3	HALLMARK_APOPTOSIS	139	-0.416	-1.578	0.00404	0.07712	30
3	GO_POSITIVE_REGULATION_OF_LOCOMOTION	281	-0.348	-1.444	0.005376	0.163865	31
3	GO_ENDOPEPTIDASE_ACTIVITY	226	-0.363	-1.468	0.005671	0.146402	32
3	GO_DOUBLE_STRANDED_RNA_BINDING	51	-0.511	-1.67	0.006036	0.039463	33
3	GO_EXONUCLEASE_ACTIVITY_ACTIVE_WITH_EITHER_RIBO_OR_DEOXYRIBONUCLEIC_ACIDS_AND_PRODUCING_5_PHOSPHOMONOESTERS	35	-0.565	-1.686	0.006036	0.035029	34
3	REACTOME_GROWTH_HORMONE_RECEPTOR_SIGNALING	18	-0.697	-1.785	0.006061	0.014728	35
3	GO_RESPONSE_TO_VITAMIN	76	-0.463	-1.597	0.006085	0.067904	36
3	REACTOME_ER_PHAGOSOME_PATHWAY	51	-0.509	-1.652	0.006198	0.045652	37
3	GO_FIBRONECTIN_BINDING	18	-0.67	-1.745	0.006438	0.021313	38
3	GO_NEGATIVE_REGULATION_OF_CELL_CELL_ADHESION	84	-0.425	-1.515	0.007843	0.113539	39
3	GO_ORGANIC_ACID_BINDING	122	-0.413	-1.546	0.009398	0.094693	40
3	GO_REGULATION_OF_HOMOTYPIC_CELL_CELL_ADHESION	182	-0.349	-1.381	0.00947	0.215539	41
3	GO_TAXIS	267	-0.33	-1.35	0.009488	0.242767	42
3	GO_PEPTIDYL_TYROSINE_MODIFICATION	122	-0.389	-1.46	0.00956	0.15343	43
3	GO_MORPHOGENESIS_OF_A_BRANCHING_STRUCTURE	104	-0.408	-1.508	0.009579	0.118869	44
3	GO_RESPONSE_TO_MECHANICAL_STIMULUS	138	-0.385	-1.456	0.01	0.156269	45
3	GO_THREONINE_TYPE_PEPTIDASE_ACTIVITY	19	-0.652	-1.664	0.010183	0.041522	46
3	GO_POSITIVE_REGULATION_OF_COAGULATION	15	-0.687	-1.687	0.010965	0.034738	47

3	GO_POSITIVE_REGULATION_OF_SEQUENCE_SPECIFIC_DNA_BINDING_TRANSCRIPTION_FACTOR_ACTIVITY	154	-0.371	-1.416	0.011299	0.186878	48
3	GO_RESPONSE_TO_BMP	53	-0.468	-1.539	0.011976	0.099439	49
3	GO_G_PROTEIN_COUPLED_RECEPTOR_SIGNALING_PATHWAY	340	-0.319	-1.345	0.012324	0.248576	50
3	GO_RESPONSE_TO_GROWTH_HORMONE	24	-0.611	-1.684	0.012605	0.035397	51
3	REACTOME_PEPTIDE_LIGAND_BINDING_RECEPTORS	70	-0.437	-1.496	0.014085	0.127231	52
3	GO_PROTEIN_TYROSINE_KINASE_ACTIVITY	114	-0.39	-1.432	0.014706	0.173519	53
3	GO_REGULATION_OF_CALCIUM_ION_TRANSPORT	127	-0.371	-1.412	0.014733	0.18997	54
3	GO_POSTSYNAPTIC_MEMBRANE	102	-0.387	-1.423	0.014815	0.180585	55
3	GO_CELLULAR_RESPONSE_TO_ALCOHOL	78	-0.429	-1.49	0.015385	0.131542	56
3	KEGG_TASTE_TRANSDUCTION	15	-0.66	-1.612	0.015521	0.061411	57
3	GO_NEGATIVE_REGULATION_OF_STRIATED_MUSCLE_CELL_DIFFERENTIATION	18	-0.638	-1.619	0.016327	0.05833	58
3	GO_FEMALE_SEX_DIFFERENTIATION	72	-0.437	-1.514	0.017928	0.114607	59
3	GO_RECEPTOR_REGULATOR_ACTIVITY	26	-0.546	-1.56	0.019027	0.0871	60
3	GO_EPIDERMIS_DEVELOPMENT	121	-0.376	-1.384	0.020147	0.214414	61
3	GO_TUBE_MORPHOGENESIS	201	-0.343	-1.378	0.020561	0.217361	62
3	GO_PROTEIN_TRIMERIZATION	25	-0.555	-1.555	0.021008	0.090123	63
3	GO_PROTEIN_MATURATION	172	-0.348	-1.374	0.022388	0.220039	64
3	GO_SYNAPTIC_MEMBRANE	141	-0.356	-1.366	0.023033	0.228839	65
3	GO_REGULATION_OF_CALCIUM_ION_IMPORT	59	-0.449	-1.452	0.023077	0.158481	66
3	GO_REGULATION_OF_RESPONSE_TO_BIOTIC_STIMULUS	141	-0.373	-1.408	0.024621	0.193682	67
3	BIOCARTA_CASPASE_PATHWAY	20	-0.643	-1.661	0.024691	0.042748	68
3	GO_POSITIVE_REGULATION_OF_CELL_CELL_ADHESION	140	-0.359	-1.36	0.026217	0.234744	69
3	GO_RESPONSE_TO_VITAMIN_D	26	-0.571	-1.612	0.026477	0.061176	70
3	GO_POSITIVE_REGULATION_OF_WOUND_HEALING	31	-0.508	-1.5	0.027723	0.124037	71
3	GO_OXIDOREDUCTASE_ACTIVITY_ACTING_ON_THE_CH_NH_GROUP_OF_DONORS	18	-0.619	-1.613	0.028986	0.060919	72

3	GO_PEPTIDYL_TYROSINE_AUTOPHOSPHORYLATION	31	-0.524	-1.514	0.029787	0.114516	73
3	GO_POSITIVE_REGULATION_OF_RELEASE_OF_SEQUESTERED_CALCIUM_ION_INTO_CYTOSOL	21	-0.574	-1.558	0.03125	0.087933	74
3	GO_ANCHORED_COMPONENT_OF_MEMBRANE	63	-0.43	-1.438	0.031434	0.168273	75
3	KEGG_CELL_ADHESION_MOLECULES_CAMS	67	-0.407	-1.389	0.03263	0.209948	76
3	GO_REGULATION_OF_CYSTEINE_TYPE_ENDOPEPTIDASE_ACTIVITY_INVOLVED_IN_APOPTOTIC_SIGNALING_PATHWAY	17	-0.611	-1.549	0.037199	0.093531	77
3	GO_PROTEIN_SERINE_THREONINE_PHOSPHATASE_ACTIVITY	46	-0.45	-1.436	0.037523	0.170187	78
3	REACTOME_TRAF6_MEDIATED_NFKB_ACTIVATION	18	-0.61	-1.538	0.038217	0.099583	79
3	GO_NEUROTRANSMITTER_RECEPTOR_ACTIVITY	23	-0.524	-1.451	0.038306	0.158575	80
3	REACTOME_EXTRACELLULAR_MATRIX_ORGANIZATION	49	-0.447	-1.437	0.039604	0.169763	81
3	GO_RESPONSE_TO_DSRNA	42	-0.479	-1.474	0.040568	0.143423	82
3	GO_PLASMA_MEMBRANE_RECEPTOR_COMPLEX	108	-0.367	-1.347	0.040665	0.2454	83
3	GO_GLIAL_CELL_MIGRATION	25	-0.56	-1.527	0.041068	0.105567	84
3	GO_POSITIVE_REGULATION_OF_PEPTIDASE_ACTIVITY	109	-0.367	-1.352	0.041746	0.241185	85
3	REACTOME_N_GLYCAN_ANTENNAE_ELONGATION_IN_THE_MEDIAL_TRANS_GOLGI	16	-0.609	-1.513	0.042035	0.115264	86
3	GO_POSITIVE_REGULATION_OF_CALCIUM_ION_IMPORT	30	-0.507	-1.485	0.042339	0.135923	87
3	GO_ALDEHYDE_DEHYDROGENASE_NAD_ACTIVITY	16	-0.621	-1.556	0.043299	0.089215	88
3	GO_NEGATIVE_REGULATION_OF_BINDING	96	-0.381	-1.378	0.043478	0.217044	89
3	GO_RESPONSE_TO_ORGANOPHOSPHORUS	94	-0.379	-1.364	0.044834	0.230599	90
3	GO_REGULATION_OF_CALCIUM_ION_TRANSPORT_INTO_CYTOSOL	52	-0.443	-1.435	0.046092	0.170155	91
3	GO_ANION_HOMEOSTASIS	30	-0.503	-1.471	0.046908	0.144539	92
3	GO_BRANCHING_MORPHOGENESIS_OF_AN_EPITHELIAL_TUBE	80	-0.394	-1.375	0.047131	0.219514	93
3	GO_LAMININ_BINDING	16	-0.627	-1.562	0.048035	0.086292	94

Supplemental Table S2.4: A list of significantly altered gene sets identified by GSEA in the MDM dataset.

Filter	NAME	SIZE	ES	NES	NOM p-val	FDR q-val	
1	KEGG_JAK_STAT_SIGNALING_PATHWAY	105	-0.587	-2.206	0	1.84E-05	1
1	GO_REGULATION_OF_INSULIN_RECEPTOR_SIGNALING_PATHWAY	27	-0.707	-2.075	0	2.16E-04	2
1	GO_REGULATION_OF_REACTIVE_OXYGEN_SPECIES_BIOSYNTHETIC_PROCESS	54	-0.597	-2.039	0	3.58E-04	3
1	GO_POSITIVE_REGULATION_OF_MAPK_CASCADE	300	-0.467	-2.018	0	4.86E-04	4
1	GO_REGULATION_OF_NITRIC_OXIDE_BIOSYNTHETIC_PROCESS	42	-0.628	-2.004	0	5.99E-04	5
1	GO_REGULATION_OF_REACTIVE_OXYGEN_SPECIES_METABOLIC_PROCESS	113	-0.514	-1.95	0	0.001255	6
1	GO_POSITIVE_REGULATION_OF_REACTIVE_OXYGEN_SPECIES_METABOLIC_PROCESS	67	-0.527	-1.857	0	0.003724	7
1	GO_POSITIVE_REGULATION_OF_REACTIVE_OXYGEN_SPECIES_BIOSYNTHETIC_PROCESS	40	-0.578	-1.85	0	0.004018	8
1	GO_REGULATION_OF_MAPK_CASCADE	437	-0.411	-1.838	0	0.004603	9
1	GO_POSITIVE_REGULATION_OF_MAP_KINASE_ACTIVITY	140	-0.451	-1.754	0	0.010498	10
1	GO_PROTEIN_POLYUBIQUITINATION	209	-0.397	-1.643	0	0.02578	11
1	GO_REGULATION_OF_MAP_KINASE_ACTIVITY	227	-0.369	-1.56	0	0.044869	12
1	GO_REGULATION_OF_GLYCOPROTEIN_METABOLIC_PROCESS	32	-0.725	-2.237	0	4.32E-06	13
1	GO_RESPONSE_TO_HYDROGEN_PEROXIDE	88	-0.563	-2.039	0	3.59E-04	14
1	GO_CELLULAR_RESPONSE_TO_LIPID	299	-0.471	-2.029	0	3.98E-04	15
1	GO_POSITIVE_REGULATION_OF_GLYCOPROTEIN_METABOLIC_PROCESS	17	-0.765	-1.983	0	8.18E-04	16
1	GO_RELEASE_OF_CYTOCHROME_C_FROM_MITOCHONDRIA	17	-0.747	-1.955	0	0.001168	17
1	GO_RESPONSE_TO_REACTIVE_OXYGEN_SPECIES	147	-0.492	-1.913	0	0.002041	18
1	GO_RESPONSE_TO_KETONE	124	-0.494	-1.911	0	0.002073	19
1	GO_RESPONSE_TO_CORTICOSTEROID	110	-0.498	-1.897	0	0.002411	20
1	BIOCARTA_CERAMIDE_PATHWAY	20	-0.685	-1.82	0	0.005559	21

Legend	
1	Immune signaling and function
2	Cellular metabolism
3	Other biological states and processes
NAME	Name of gene set
SIZE	Number of Genes within gene set
ES	Enrichment Score for gene set (Degree to which this gene set is overrepresented at the top or bottom of the ranked lit of genes)
NES	Normalized enrichment score
NOM p-val	Nominal p-value
FDR q-val	False discovery rate (corrected for multiple testing)

1	KEGG_ADIPOCYTOKINE_SIGNALING_PATHWAY	55	-0.527	-1.791	0	0.00742	22
1	HALLMARK_HYPOXIA	159	-0.439	-1.752	0	0.010636	23
1	GO_RESPONSE_TO_AMINO_ACID	77	-0.487	-1.735	0	0.012492	24
1	GO_CELLULAR_RESPONSE_TO_REACTIVE_OXYGEN_SPECIES	81	-0.474	-1.733	0	0.012733	25
1	GO_GUANYL_NUCLEOTIDE_BINDING	267	-0.401	-1.714	0	0.015091	26
1	GO_RESPONSE_TO_OXYGEN_LEVELS	226	-0.404	-1.684	0	0.019032	27
1	GO_NEGATIVE_REGULATION_OF_HYDROLASE_ACTIVITY	235	-0.394	-1.666	0	0.021841	28
1	GO_ENZYME_INHIBITOR_ACTIVITY	216	-0.377	-1.569	0	0.042438	29
1	GO_ION_HOMEOSTASIS	351	-0.33	-1.437	0	0.093456	30
1	GO_UBIQUITIN_LIKE_PROTEIN_LIGASE_BINDING	216	-0.361	-1.49	0.001672	0.068511	31
1	GO_POSITIVE_REGULATION_OF_CATABOLIC_PROCESS	319	-0.337	-1.47	0.001715	0.07719	32
1	GO_RESPONSE_TO_NUTRIENT	147	-0.417	-1.652	0.001792	0.024083	33
1	GO_REGULATION_OF_TYROSINE_PHOSPHORYLATION_OF_STAT3_PROTEIN	30	-0.644	-1.912	0.001992	0.002056	34
1	GO_RESPONSE_TO_RETINOIC_ACID	62	-0.462	-1.59	0.001992	0.037086	35
1	GO_PROTEIN_PHOSPHATASE_2A_BINDING	24	-0.686	-1.959	0.002041	0.001117	36
1	GO_POSITIVE_REGULATION_OF_CYCLIC_NUCLEOTIDE_METABOLIC_PROCESS	51	-0.513	-1.694	0.003922	0.017498	37
1	GO_RESPONSE_TO_FATTY_ACID	60	-0.456	-1.592	0.003937	0.036509	38
1	GO_REGULATION_OF_PHOSPHATIDYLINOSITOL_3_KINASE_SIGNALING	91	-0.437	-1.609	0.003984	0.032427	39
1	GO_CELLULAR_RESPONSE_TO_NUTRIENT	32	-0.568	-1.706	0.003992	0.01597	40
1	GO_REGULATION_OF_PHOSPHOLIPID_METABOLIC_PROCESS	45	-0.533	-1.74	0.004202	0.0119	41
1	GO_RESPONSE_TO_NICOTINE	25	-0.586	-1.711	0.004255	0.015415	42
1	GO_REGULATION_OF_CYCLIC_NUCLEOTIDE_METABOLIC_PROCESS	70	-0.46	-1.628	0.005703	0.028739	43
1	GO_POSITIVE_REGULATION_OF_CELLULAR_AMIDE_METABOLIC_PROCESS	84	-0.429	-1.55	0.005703	0.048073	44
1	GO_ACTIVATION_OF_MAPK_ACTIVITY	92	-0.414	-1.524	0.005941	0.056371	45
1	GO_RNA_PHOSPHODIESTER_BOND_HYDROLYSIS_EXONUCLEOLYTIC	26	-0.632	-1.835	0.006173	0.004793	46

1	GO_REGULATION_OF_CALCIUM_ION_TRANSPORT	124	-0.402	-1.556	0.007018	0.046058	47
1	GO_POSITIVE_REGULATION_OF_NUCLEOTIDE_METABOLIC_PROCESS	67	-0.467	-1.652	0.007859	0.024041	48
1	GO_REGULATION_OF_SEQUESTERING_OF_CALCIUM_ION	71	-0.448	-1.571	0.008016	0.041983	49
1	GO_MUCOPOLYSACCHARIDE_METABOLIC_PROCESS	72	-0.424	-1.501	0.008214	0.064344	50
1	GO_REGULATION_OF_LIPID_KINASE_ACTIVITY	36	-0.543	-1.682	0.008247	0.019424	51
1	GO_POSITIVE_REGULATION_OF_PHOSPHATIDYLINOSITOL_3_KINASE_SIGNALING	41	-0.511	-1.623	0.008658	0.029577	52
1	GO_REGULATION_OF_PHOSPHATIDYLINOSITOL_3_KINASE_ACTIVITY	28	-0.587	-1.718	0.010309	0.014433	53
1	GO_REGULATION_OF_NUCLEOTIDE_METABOLIC_PROCESS	110	-0.394	-1.476	0.011299	0.074384	54
1	GO_REGULATION_OF_MITOCHONDRIAL_MEMBRANE_POTENTIAL	40	-0.51	-1.61	0.01232	0.032256	55
1	GO_REGULATION_OF_CAMP_MEDIATED_SIGNALING	17	-0.641	-1.697	0.012685	0.017195	56
1	GO_REGULATION_OF_RELEASE_OF_SEQUESTERED_CALCIUM_ION_INTO_CYTOSOL	44	-0.488	-1.578	0.01378	0.039884	57
1	GO_ORGANIC_CYCLIC_COMPOUND_CATABOLIC_PROCESS	331	-0.307	-1.328	0.013937	0.163159	58
1	KEGG_MAPK_SIGNALING_PATHWAY	198	-0.328	-1.376	0.01476	0.129072	59
1	GO_SECONDARY_METABOLIC_PROCESS	24	-0.573	-1.619	0.014894	0.030564	60
1	GO_NEGATIVE_REGULATION_OF_FAT_CELL_DIFFERENTIATION	26	-0.546	-1.59	0.016529	0.036984	61
1	BIOCARTA_GSK3_PATHWAY	25	-0.561	-1.602	0.017578	0.034212	62
1	GO_LIPID_PARTICLE	38	-0.483	-1.528	0.018036	0.055139	63
1	GO_REGULATION_OF_RESPONSE_TO_OXIDATIVE_STRESS	47	-0.478	-1.546	0.018293	0.049164	64
1	GO_REGULATION_OF_FAT_CELL_DIFFERENTIATION	61	-0.451	-1.541	0.019646	0.050824	65
1	GO_REGULATION_OF_PROTEIN_CATABOLIC_PROCESS	317	-0.308	-1.339	0.019769	0.154694	66
1	GO_CELLULAR_RESPONSE_TO_KETONE	52	-0.456	-1.524	0.01992	0.056259	67
1	GO_COENZYME_BIOSYNTHETIC_PROCESS	101	-0.378	-1.438	0.020913	0.092853	68
1	GO_RESPONSE_TO_HYDROPEROXIDE	15	-0.677	-1.675	0.021413	0.020412	69

1	GO_POSITIVE_REGULATION_OF_MITOCHOND RION_ORGANIZATION	122	-0.362	-1.407	0.021544	0.110315	70
1	GO_POSITIVE_REGULATION_OF_PHOSPHOLIPI D_METABOLIC_PROCESS	30	-0.539	-1.61	0.022044	0.032382	71
1	GO_POSITIVE_REGULATION_OF_PROTEIN_CA TABOLIC_PROCESS	215	-0.324	-1.331	0.022609	0.160612	72
1	GO_PROTEIN_UBIQUITINATION	469	-0.288	-1.287	0.022989	0.198528	73
1	GO_POSITIVE_REGULATION_OF_LIPID_KINASE _ACTIVITY	22	-0.575	-1.574	0.023109	0.041002	74
1	GO_REGULATION_OF_CALCIUM_ION_TRANS MEMBRANE_TRANSPORT	67	-0.418	-1.475	0.02381	0.074861	75
1	GO_AMINOGLYCAN_METABOLIC_PROCESS	111	-0.373	-1.41	0.024074	0.108554	76
1	GO_POSITIVE_REGULATION_OF_MRNA_META BOLIC_PROCESS	37	-0.508	-1.579	0.025243	0.039799	77
1	GO_POSITIVE_REGULATION_OF_CAMP_META BOLIC_PROCESS	44	-0.468	-1.52	0.025243	0.057426	78
1	GO_CYCLIC_NUCLEOTIDE_METABOLIC_PROCE SS	31	-0.501	-1.501	0.02544	0.064303	79
1	GO_CELLULAR_RESPONSE_TO_GLUCOSE_STA RVATION	25	-0.571	-1.664	0.026432	0.022224	80
1	GO_RNA_CATABOLIC_PROCESS	194	-0.323	-1.327	0.027211	0.164254	81
1	GO_POSITIVE_REGULATION_OF_LIPID_TRANS PORT	35	-0.493	-1.543	0.028169	0.049997	82
1	GO_POSITIVE_REGULATION_OF_MONOOXYGE NASE_ACTIVITY	20	-0.585	-1.579	0.028698	0.039768	83
1	GO_NEGATIVE_REGULATION_OF_PHOSPHOR US_METABOLIC_PROCESS	372	-0.288	-1.266	0.028765	0.218233	84
1	GO_NAD_ADP_RIBOSYLTRANSFERASE_ACTIVIT Y	24	-0.563	-1.621	0.031056	0.03015	85
1	GO_REGULATION_OF_MRNA_CATABOLIC_PR OCESS	23	-0.558	-1.576	0.031373	0.040575	86
1	GO_POSITIVE_REGULATION_OF_OXIDOREDUC TASE_ACTIVITY	30	-0.504	-1.509	0.031513	0.061401	87
1	GO_REGULATION_OF_RESPONSE_TO_REACTI VE_OXYGEN_SPECIES	24	-0.538	-1.552	0.03373	0.047272	88
1	GO_PURINE_NUCLEOBASE_METABOLIC_PROC ESS	20	-0.558	-1.527	0.034091	0.055346	89
1	GO_POSITIVE_REGULATION_OF_RELEASE_OF_ SEQUESTERED_CALCIUM_ION_INTO_CYTOSOL	22	-0.552	-1.526	0.034557	0.055607	90
1	GO_NEGATIVE_REGULATION_OF_PROTEIN_C ATABOLIC_PROCESS	87	-0.384	-1.41	0.03643	0.108565	91

1	GO_POSITIVE_REGULATION_OF_LIPID_METAB OLIC_PROCESS	91	-0.389	-1.401	0.037383	0.113803	92
1	GO_REGULATION_OF_STEROID_BIOSYNTHETI C_PROCESS	28	-0.527	-1.532	0.038462	0.053955	93
1	GO_NEGATIVE_REGULATION_OF_CALCIUM_I ON_TRANSPORT	29	-0.506	-1.496	0.038855	0.066161	94
1	BIOCARTA_MITOCHONDRIA_PATHWAY	17	-0.597	-1.521	0.039301	0.057329	95
1	GO_HYALURONAN_METABOLIC_PROCESS	21	-0.537	-1.494	0.041322	0.067156	96
1	GO_REGULATION_OF_MONOOXYGENASE_AC TIVITY	47	-0.445	-1.45	0.041667	0.086515	97
1	KEGG_NICOTINATE_AND_NICOTINAMIDE_ME TABOLISM	17	-0.577	-1.522	0.042683	0.056795	98
1	GO_REGULATION_OF_CELLULAR_AMINE_MET ABOLIC_PROCESS	68	-0.41	-1.452	0.042969	0.085666	99
1	GO_POLYUBIQUITIN_BINDING	32	-0.483	-1.472	0.045098	0.076059	100
1	GO_NEGATIVE_REGULATION_OF_REACTIVE_O XYGEN_SPECIES_METABOLIC_PROCESS	30	-0.483	-1.438	0.045455	0.093063	101
1	GO_TETRAHYDROFOLATE_METABOLIC_PROCE SS	18	-0.555	-1.484	0.046512	0.07106	102
1	GO_UBIQUITIN_LIKE_PROTEIN_SPECIFIC_PRO TEASE_ACTIVITY	82	-0.371	-1.384	0.046602	0.124368	103
1	BIOCARTA_ATM_PATHWAY	20	-0.543	-1.481	0.047325	0.072358	104
1	HALLMARK_REACTIVE_OXIGEN_SPECIES_PATH WAY	44	-0.427	-1.401	0.047521	0.113651	105
1	GO_RESPONSE_TO_ATP	22	-0.564	-1.526	0.047817	0.055597	106
1	GO_REGULATION_OF_MRNA_METABOLIC_PR OCESS	81	-0.376	-1.381	0.049541	0.125461	107
2	BIOCARTA_INFLAM_PATHWAY	19	-0.852	-2.273	0	0	1
2	GO_CCR_CHEMOKINE_RECEPTOR_BINDING	19	-0.871	-2.299	0	0	2
2	GO_CELLULAR_RESPONSE_TO_BIOTIC_STIMUL US	134	-0.588	-2.309	0	0	3
2	GO_CELLULAR_RESPONSE_TO_CYTOKINE_STI MULUS	431	-0.652	-2.904	0	0	4
2	GO_CELLULAR_RESPONSE_TO_INTERFERON_G AMMA	93	-0.784	-2.93	0	0	5
2	GO_CELLULAR_RESPONSE_TO_INTERLEUKIN_ 1	63	-0.679	-2.354	0	0	6
2	GO_CHEMOKINE_ACTIVITY	28	-0.864	-2.539	0	0	7

2	GO_CHEMOKINE_MEDIATED_SIGNALING_PATHWAY	38	-0.788	-2.418	0	0	8
2	GO_CHEMOKINE_RECEPTOR_BINDING	35	-0.843	-2.649	0	0	9
2	GO_CYTOKINE_ACTIVITY	114	-0.716	-2.748	0	0	10
2	GO_CYTOKINE_MEDIATED_SIGNALING_PATHWAY	316	-0.697	-3.027	0	0	11
2	GO_CYTOKINE_RECEPTOR_BINDING	171	-0.623	-2.53	0	0	12
2	GO_DEFENSE_RESPONSE_TO_OTHER_ORGANISM	297	-0.612	-2.643	0	0	13
2	GO_DEFENSE_RESPONSE_TO_VIRUS	120	-0.753	-2.938	0	0	14
2	GO_EXTERNAL_SIDE_OF_PLASMA_MEMBRANE	137	-0.615	-2.408	0	0	15
2	GO_G_PROTEIN_COUPLED_RECEPTOR_BINDING	138	-0.591	-2.306	0	0	16
2	GO_I_KAPPAB_KINASE_NF_KAPPAB_SIGNALING	60	-0.679	-2.315	0	0	17
2	GO_IMMUNE_EFFECTOR_PROCESS	336	-0.603	-2.629	0	0	18
2	GO_INFLAMMATORY_RESPONSE	291	-0.614	-2.616	0	0	19
2	GO_INNATE_IMMUNE_RESPONSE	388	-0.626	-2.748	0	0	20
2	GO_INTERFERON_GAMMA_MEDIATED_SIGNALING_PATHWAY	62	-0.754	-2.63	0	0	21
2	GO_LYMPHOCYTE_CHEMOTAXIS	22	-0.83	-2.32	0	0	22
2	GO_LYMPHOCYTE_MIGRATION	28	-0.81	-2.412	0	0	23
2	GO_NEGATIVE_REGULATION_OF_DEFENSE_RESPONSE	105	-0.623	-2.333	0	0	24
2	GO_NEGATIVE_REGULATION_OF_EXTRINSIC_APOPTOTIC_SIGNALING_PATHWAY	76	-0.653	-2.334	0	0	25
2	GO_NEGATIVE_REGULATION_OF_MULTI_ORGANISM_PROCESS	106	-0.73	-2.814	0	0	26
2	GO_NEGATIVE_REGULATION_OF_TYPE_I_INTERFERON_PRODUCTION	31	-0.791	-2.363	0	0	27
2	GO_NEGATIVE_REGULATION_OF_VIRAL_GENOME_REPLICATION	38	-0.826	-2.588	0	0	28
2	GO_NEGATIVE_REGULATION_OF_VIRAL_PROCESS	67	-0.781	-2.725	0	0	29
2	GO_POSITIVE_REGULATION_OF_CELL_ACTIVATION	214	-0.563	-2.349	0	0	30
2	GO_POSITIVE_REGULATION_OF_CYTOKINE_BIOSYNTHETIC_PROCESS	45	-0.737	-2.427	0	0	31

2	GO_POSITIVE_REGULATION_OF_CYTOKINE_PRODUCTION	265	-0.594	-2.509	0	0	32
2	GO_POSITIVE_REGULATION_OF_DEFENSE_RESPONSE	271	-0.591	-2.52	0	0	33
2	GO_POSITIVE_REGULATION_OF_EXTRINSIC_APOPTOTIC_SIGNALING_PATHWAY	45	-0.72	-2.312	0	0	34
2	GO_POSITIVE_REGULATION_OF_I_KAPPAB_KINASE_NF_KAPPAB_SIGNALING	144	-0.628	-2.486	0	0	35
2	GO_POSITIVE_REGULATION_OF_IMMUNE_RESPONSE	404	-0.518	-2.306	0	0	36
2	GO_POSITIVE_REGULATION_OF_INFLAMMATORY_RESPONSE	71	-0.705	-2.462	0	0	37
2	GO_POSITIVE_REGULATION_OF_INNATE_IMMUNE_RESPONSE	203	-0.582	-2.406	0	0	38
2	GO_POSITIVE_REGULATION_OF_INTERFERON_GAMMA_PRODUCTION	46	-0.715	-2.301	0	0	39
2	GO_POSITIVE_REGULATION_OF_LEUKOCYTE_CHEMOTAXIS	57	-0.707	-2.385	0	0	40
2	GO_POSITIVE_REGULATION_OF_LEUKOCYTE_MIGRATION	75	-0.716	-2.549	0	0	41
2	GO_POSITIVE_REGULATION_OF_LEUKOCYTE_PROLIFERATION	98	-0.65	-2.412	0	0	42
2	GO_POSITIVE_REGULATION_OF_NF_KAPPAB_TRANSCRIPTION_FACTOR_ACTIVITY	102	-0.643	-2.418	0	0	43
2	GO_POSITIVE_REGULATION_OF_RESPONSE_TO_WOUNDING	103	-0.631	-2.39	0	0	44
2	GO_POSITIVE_REGULATION_OF_STAT_CASCADE	49	-0.679	-2.271	0	0	45
2	GO_REGULATION_OF_CHEMOTAXIS	121	-0.597	-2.31	0	0	46
2	GO_REGULATION_OF_CYTOKINE_BIOSYNTHETIC_PROCESS	71	-0.665	-2.341	0	0	47
2	GO_REGULATION_OF_CYTOKINE_PRODUCTION	398	-0.57	-2.513	0	0	48
2	GO_REGULATION_OF_EXTRINSIC_APOPTOTIC_SIGNALING_PATHWAY	122	-0.642	-2.497	0	0	49
2	GO_REGULATION_OF_EXTRINSIC_APOPTOTIC_SIGNALING_PATHWAY_IN_ABSENCE_OF_LIGAND	35	-0.765	-2.376	0	0	50
2	GO_REGULATION_OF_GRANULOCYTE_CHEMOTAXIS	28	-0.776	-2.287	0	0	51
2	GO_REGULATION_OF_I_KAPPAB_KINASE_NF_KAPPAB_SIGNALING	188	-0.621	-2.563	0	0	52

2	GO_REGULATION_OF_IMMUNE_EFFECTOR_PROCESS	294	-0.532	-2.287	0	0	53
2	GO_REGULATION_OF_INFLAMMATORY_RESPONSE	192	-0.624	-2.562	0	0	54
2	GO_REGULATION_OF_INNATE_IMMUNE_RESPONSE	280	-0.601	-2.568	0	0	55
2	GO_REGULATION_OF_INTERFERON_GAMMA_PRODUCTION	68	-0.702	-2.486	0	0	56
2	GO_REGULATION_OF_INTERLEUKIN_1_BETA_PRODUCTION	30	-0.759	-2.28	0	0	57
2	GO_REGULATION_OF_INTERLEUKIN_1_PRODUCTION	38	-0.758	-2.387	0	0	58
2	GO_REGULATION_OF_INTERLEUKIN_12_PRODUCTION	41	-0.758	-2.404	0	0	59
2	GO_REGULATION_OF_LEUKOCYTE_CHEMOTAXIS	70	-0.691	-2.43	0	0	60
2	GO_REGULATION_OF_LEUKOCYTE_MIGRATION	107	-0.658	-2.513	0	0	61
2	GO_REGULATION_OF_LEUKOCYTE_PROLIFERATION	148	-0.581	-2.317	0	0	62
2	GO_REGULATION_OF_NECROTIC_CELL_DEATH	22	-0.826	-2.301	0	0	63
2	GO_REGULATION_OF_NF_KAPPAB_IMPORT_INTO_NUCLEUS	41	-0.755	-2.397	0	0	64
2	GO_REGULATION_OF_RESPONSE_TO_CYTOKINE_STIMULUS	112	-0.623	-2.348	0	0	65
2	GO_REGULATION_OF_T_CELL_DIFFERENTIATION	74	-0.659	-2.356	0	0	66
2	GO_REGULATION_OF_T_CELL_PROLIFERATION	105	-0.595	-2.275	0	0	67
2	GO_REGULATION_OF_T_HELPER_CELL_DIFFERENTIATION	20	-0.829	-2.277	0	0	68
2	GO_REGULATION_OF_TYPE_I_INTERFERON_PRODUCTION	95	-0.641	-2.395	0	0	69
2	GO_REGULATION_OF_VIRAL_GENOME_REPLICATION	63	-0.738	-2.545	0	0	70
2	GO_RESPONSE_TO_BACTERIUM	330	-0.574	-2.523	0	0	71
2	GO_RESPONSE_TO_INTERFERON_GAMMA	109	-0.781	-2.934	0	0	72
2	GO_RESPONSE_TO_INTERLEUKIN_1	86	-0.663	-2.414	0	0	73
2	GO_RESPONSE_TO_MOLECULE_OF_BACTERIAL_ORIGIN	243	-0.589	-2.486	0	0	74

2	GO_RESPONSE_TO_TUMOR_NECROSIS_FACTOR	172	-0.651	-2.656	0	0	75
2	GO_RESPONSE_TO_TYPE_I_INTERFERON	53	-0.793	-2.605	0	0	76
2	GO_RESPONSE_TO_VIRUS	186	-0.698	-2.856	0	0	77
2	GO_TUMOR_NECROSIS_FACTOR_MEDIATED_SIGNALING_PATHWAY	93	-0.643	-2.332	0	0	78
2	HALLMARK_ALLOGRAFT_REJECTION	162	-0.637	-2.558	0	0	79
2	HALLMARK_COMPLEMENT	166	-0.617	-2.451	0	0	80
2	HALLMARK_IL2_STAT5_SIGNALING	160	-0.573	-2.285	0	0	81
2	HALLMARK_IL6_JAK_STAT3_SIGNALING	73	-0.761	-2.734	0	0	82
2	HALLMARK_INFLAMMATORY_RESPONSE	167	-0.765	-3.09	0	0	83
2	HALLMARK_INTERFERON_ALPHA_RESPONSE	87	-0.889	-3.209	0	0	84
2	HALLMARK_INTERFERON_GAMMA_RESPONSE	182	-0.864	-3.55	0	0	85
2	HALLMARK_TNFA_SIGNALING_VIA_NFKB	181	-0.729	-2.967	0	0	86
2	KEGG_CYTOKINE_CYTOKINE_RECEPTOR_INTERACTION	155	-0.697	-2.764	0	0	87
2	KEGG_CYTOSOLIC_DNA_SENSING_PATHWAY	40	-0.742	-2.379	0	0	88
2	KEGG_NOD_LIKE_RECEPTOR_SIGNALING_PATHWAY	45	-0.762	-2.495	0	0	89
2	KEGG_RIG_I_LIKE_RECEPTOR_SIGNALING_PATHWAY	49	-0.757	-2.494	0	0	90
2	KEGG_TOLL_LIKE_RECEPTOR_SIGNALING_PATHWAY	84	-0.625	-2.281	0	0	91
2	GO_REGULATION_OF_CYTOKINE_SECRETION	100	-0.599	-2.244	0	2.19E-06	92
2	GO_REGULATION_OF_ADAPTIVE_IMMUNE_RESPONSE	91	-0.61	-2.251	0	2.24E-06	93
2	GO_REGULATION_OF_LYMPHOCYTE_DIFFERENTIATION	94	-0.608	-2.252	0	2.26E-06	94
2	GO_ACTIVATION_OF_INNATE_IMMUNE_RESPONSE	173	-0.56	-2.255	0	2.28E-06	95
2	GO_POSITIVE_REGULATION_OF_INTERLEUKIN_12_PRODUCTION	26	-0.771	-2.26	0	2.29E-06	96
2	GO_MONOCYTE_CHEMOTAXIS	25	-0.796	-2.261	0	2.30E-06	97
2	GO_RESPONSE_TO_PROTOZOAN	18	-0.866	-2.264	0	2.31E-06	98
2	GO_POSITIVE_REGULATION_OF_CHEMOTAXIS	82	-0.632	-2.266	0	2.32E-06	99
2	GO_REGULATION_OF_NEUTROPHIL_CHEMOTAXIS	22	-0.799	-2.269	0	2.34E-06	100

2	GO_RESPONSE_TO_INTERFERON_BETA	17	-0.851	-2.214	0	1.65E-05	101
2	GO_REGULATION_OF_INTERFERON_BETA_PRODUCTION	38	-0.69	-2.195	0	1.81E-05	102
2	KEGG_CHEMOKINE_SIGNALING_PATHWAY	137	-0.563	-2.204	0	1.83E-05	103
2	GO_POSITIVE_REGULATION_OF_IMMUNE_EFFECTOR_PROCESS	106	-0.585	-2.205	0	1.83E-05	104
2	BIOCARTA_IL22BP_PATHWAY	15	-0.887	-2.212	0	1.85E-05	105
2	GO_REGULATION_OF_LYMPHOCYTE_APOPTOTIC_PROCESS	40	-0.688	-2.191	0	2.19E-05	106
2	GO_REGULATION_OF_CELL_ACTIVATION	333	-0.502	-2.193	0	2.19E-05	107
2	GO_REGULATION_OF_TYROSINE_PHOSPHORYLATION_OF_STAT_PROTEIN	46	-0.669	-2.193	0	2.20E-05	108
2	GO_POSITIVE_REGULATION_OF_T_CELL_PROLIFERATION	69	-0.625	-2.185	0	2.56E-05	109
2	GO_POSITIVE_REGULATION_OF_INTERLEUKIN_6_PRODUCTION	48	-0.672	-2.172	0	3.25E-05	110
2	GO_POSITIVE_REGULATION_OF_NEUTROPHIL_MIGRATION	21	-0.79	-2.163	0	3.35E-05	111
2	GO_GRANULOCYTE_MIGRATION	51	-0.633	-2.165	0	3.37E-05	112
2	GO_REGULATION_OF_VIRAL_ENTRY_INTO_HOST_CELL	22	-0.792	-2.165	0	3.38E-05	113
2	GO_REGULATION_OF_NEUTROPHIL_MIGRATION	25	-0.767	-2.166	0	3.39E-05	114
2	GO_REGULATION_OF_CD4_POSITIVE_ALPHA_BETA_T_CELL_ACTIVATION	29	-0.744	-2.166	0	3.40E-05	115
2	GO_PATTERN_RECOGNITION_RECEPTOR_SIGNALING_PATHWAY	91	-0.584	-2.16	0	3.68E-05	116
2	GO_RESPONSE_TO_INTERFERON_ALPHA	18	-0.817	-2.153	0	4.19E-05	117
2	GO_REGULATION_OF_STAT_CASCADE	82	-0.597	-2.146	0	5.23E-05	118
2	GO_INTERACTION_WITH_HOST	114	-0.562	-2.147	0	5.24E-05	119
2	BIOCARTA_IL10_PATHWAY	17	-0.828	-2.141	0	5.86E-05	120
2	GO_ZYMOGEN_ACTIVATION	85	-0.587	-2.142	0	5.87E-05	121
2	GO_REGULATION_OF_INTERLEUKIN_1_SECRETION	21	-0.787	-2.137	0	6.02E-05	122
2	GO_POSITIVE_REGULATION_OF_INTERLEUKIN_1_PRODUCTION	22	-0.782	-2.13	0	7.00E-05	123

2	GO_NEGATIVE_REGULATION_OF_EXTRINSIC_APOPTOTIC_SIGNALING_PATHWAY_VIA_DEATH_DOMAIN_RECEPTORS	27	-0.727	-2.129	0	7.47E-05	124
2	GO_POSITIVE_REGULATION_OF_INTERLEUKIN_8_PRODUCTION	31	-0.713	-2.129	0	7.48E-05	125
2	GO_POSITIVE_REGULATION_OF_INTERFERON_BETA_PRODUCTION	28	-0.708	-2.125	0	8.11E-05	126
2	GO_MYD88_INDEPENDENT_TOLL_LIKE_RECEPTOR_SIGNALING_PATHWAY	30	-0.726	-2.125	0	8.27E-05	127
2	GO_REGULATION_OF_T_CELL_MIGRATION	19	-0.769	-2.123	0	8.77E-05	128
2	GO_POSITIVE_REGULATION_OF_LYMPHOCYTE_MIGRATION	19	-0.792	-2.122	0	8.93E-05	129
2	BIOCARTA_TNFR2_PATHWAY	16	-0.794	-2.12	0	9.06E-05	130
2	BIOCARTA_HIVNEF_PATHWAY	54	-0.633	-2.121	0	9.07E-05	131
2	GO_NEGATIVE_REGULATION_OF_INFLAMMATORY_RESPONSE	67	-0.607	-2.116	0	9.84E-05	132
2	GO_CYTOPLASMIC_PATTERN_RECOGNITION_RECEPTOR_SIGNALING_PATHWAY	26	-0.734	-2.113	0	1.02E-04	133
2	GO_REGULATION_OF_LEUKOCYTE_APOPTOTIC_PROCESS	62	-0.61	-2.109	0	1.03E-04	134
2	GO_TUMOR_NECROSIS_FACTOR_RECEPTOR_SUPERFAMILY_BINDING	38	-0.661	-2.107	0	1.08E-04	135
2	GO_LEUKOCYTE_CELL_CELL_ADHESION	193	-0.521	-2.105	0	1.08E-04	136
2	GO_REGULATION_OF_ERK1_AND_ERK2_CASCADE	149	-0.537	-2.106	0	1.09E-04	137
2	GO_REGULATION_OF_TYPE_I_INTERFERON_MEDIATED_SIGNALING_PATHWAY	24	-0.763	-2.107	0	1.09E-04	138
2	GO_POSITIVE_REGULATION_OF_B_CELL_PROLIFERATION	25	-0.732	-2.105	0	1.10E-04	139
2	GO_NEGATIVE_REGULATION_OF_IMMUNE_RESPONSE	92	-0.575	-2.103	0	1.16E-04	140
2	GO_POSITIVE_REGULATION_OF_CYTOKINE_SECRETION	65	-0.613	-2.102	0	1.24E-04	141
2	GO_REGULATION_OF_LYMPHOCYTE_MIGRATION	29	-0.703	-2.101	0	1.28E-04	142
2	GO_DENDRITIC_CELL_DIFFERENTIATION	24	-0.738	-2.098	0	1.35E-04	143
2	GO_POSITIVE_REGULATION_OF_LYMPHOCYTE_DIFFERENTIATION	59	-0.609	-2.089	0	1.73E-04	144
2	GO_REGULATION_OF_CYTOKINE_PRODUCTION_INVOLVED_IN_IMMUNE_RESPONSE	40	-0.653	-2.088	0	1.76E-04	145

2	GO_NEGATIVE_REGULATION_OF_CYTOKINE_PRODUCTION	142	-0.536	-2.086	0	1.83E-04	146
2	GO_LEUKOCYTE_CHEMOTAXIS	79	-0.577	-2.085	0	1.89E-04	147
2	GO_STAT_CASCADE	39	-0.665	-2.083	0	1.91E-04	148
2	BIOCARTA_NFKB_PATHWAY	22	-0.752	-2.077	0	2.06E-04	149
2	GO_REGULATION_OF_HEMOPOIESIS	215	-0.499	-2.077	0	2.07E-04	150
2	GO_LEUKOCYTE_MEDIATED_IMMUNITY	111	-0.545	-2.076	0	2.10E-04	151
2	GO_POSITIVE_REGULATION_OF_TYPE_I_INTERFERON_PRODUCTION	62	-0.593	-2.076	0	2.11E-04	152
2	GO_REGULATION_OF_CHEMOKINE_PRODUCTION	47	-0.635	-2.072	0	2.25E-04	153
2	GO_REGULATION_OF_PRODUCTION_OF_MOLECULAR_MEDIATOR_OF_IMMUNE_RESPONSE	66	-0.596	-2.065	0	2.51E-04	154
2	GO_POSITIVE_REGULATION_OF_INTERLEUKIN_1_BETA_PRODUCTION	18	-0.79	-2.064	0	2.60E-04	155
2	GO_REGULATION_OF_ACTIVATED_T_CELL_PROLIFERATION	28	-0.716	-2.063	0	2.62E-04	156
2	GO_MYELOID_LEUKOCYTE_MIGRATION	67	-0.587	-2.059	0	2.81E-04	157
2	GO_REGULATION_OF_INTERLEUKIN_8_PRODUCTION	43	-0.637	-2.053	0	3.14E-04	158
2	GO_CELL_CHEMOTAXIS	116	-0.531	-2.05	0	3.23E-04	159
2	GO_REGULATION_OF_LEUKOCYTE_MEDIATED_IMMUNITY	110	-0.532	-2.05	0	3.23E-04	160
2	GO_ACTIVATION_OF_IMMUNE_RESPONSE	313	-0.469	-2.049	0	3.27E-04	161
2	GO_POSITIVE_REGULATION_OF_NF_KAPPAB_IMPORT_INTO_NUCLEUS	23	-0.744	-2.048	0	3.32E-04	162
2	GO_POSITIVE_REGULATION_OF_CHEMOKINE_PRODUCTION	38	-0.655	-2.047	0	3.33E-04	163
2	GO_REGULATION_OF_LEUKOCYTE_DIFFERENTIATION	166	-0.514	-2.046	0	3.35E-04	164
2	GO_POSITIVE_REGULATION_OF_CD4_POSITIVE_ALPHA_BETA_T_CELL_ACTIVATION	21	-0.756	-2.036	0	3.64E-04	165
2	GO_POSITIVE_REGULATION_OF_PRODUCTION_OF_MOLECULAR_MEDIATOR_OF_IMMUNE_RESPONSE	42	-0.633	-2.031	0	3.86E-04	166
2	GO_REGULATION_OF_B_CELL_PROLIFERATION	40	-0.632	-2.031	0	3.86E-04	167
2	GO_LIPOPOLYSACCHARIDE_MEDIATED_SIGNALING_PATHWAY	28	-0.693	-2.03	0	3.90E-04	168

2	GO_ADAPTIVE_IMMUNE_RESPONSE_BASED_ON_SOMATIC_RECOMBINATION_OF_IMMUNE_RECEPTORS_BUILT_FROM_IMMUNOGLOBULIN_SUPERFAMILY_DOMAINS	97	-0.547	-2.03	0	3.91E-04	169
2	GO_ALPHA_BETA_T_CELL_ACTIVATION	41	-0.639	-2.028	0	3.97E-04	170
2	GO_REGULATION_OF_T_HELPER_1_TYPE_IMMUNE_RESPONSE	18	-0.779	-2.029	0	3.97E-04	171
2	GO_CYTOKINE_RECEPTOR_ACTIVITY	54	-0.6	-2.025	0	4.25E-04	172
2	GO_REGULATION_OF_TUMOR_NECROSIS_FACTOR_SUPERFAMILY_CYTOKINE_PRODUCTION	78	-0.565	-2.021	0	4.61E-04	173
2	GO_REGULATION_OF_INTERFERON_ALPHA_PRODUCTION	17	-0.775	-2.02	0	4.70E-04	174
2	GO_POSITIVE_REGULATION_OF_LEUKOCYTE_APOPTOTIC_PROCESS	21	-0.738	-2.019	0	4.74E-04	175
2	KEGG_HEMATOPOIETIC_CELL_LINEAGE	57	-0.592	-2.019	0	4.78E-04	176
2	GO_REGULATION_OF_T_CELL_APOPTOTIC_PROCESS	21	-0.733	-2.018	0	4.88E-04	177
2	GO_REGULATION_OF_ALPHA_BETA_T_CELL_DIFFERENTIATION	35	-0.664	-2.017	0	4.93E-04	178
2	GO_NEGATIVE_REGULATION_OF_IMMUNE_SYSTEM_PROCESS	272	-0.478	-2.017	0	4.96E-04	179
2	GO_REGULATION_OF_T_CELL_MEDIATED_IMMUNITY	35	-0.642	-2.01	0	5.48E-04	180
2	GO_NEGATIVE_REGULATION_OF_IMMUNE_EFFECTOR_PROCESS	79	-0.563	-2.006	0	5.86E-04	181
2	KEGG_GRAFT_VERSUS_HOST_DISEASE	29	-0.674	-2.006	0	5.87E-04	182
2	GO_POSITIVE_REGULATION_OF_ADAPTIVE_IMMUNE_RESPONSE	55	-0.602	-2.005	0	5.98E-04	183
2	GO_MYELOID_DENDRITIC_CELL_DIFFERENTIATION	15	-0.773	-2.001	0	6.19E-04	184
2	GO_MYELOID_LEUKOCYTE_ACTIVATION	68	-0.581	-2.001	0	6.20E-04	185
2	KEGG_INTESTINAL_IMMUNE_NETWORK_FOR_IGA_PRODUCTION	32	-0.662	-1.996	0	6.66E-04	186
2	GO_LYMPHOCYTE_MEDIATED_IMMUNITY	83	-0.553	-1.996	0	6.71E-04	187
2	GO_REGULATION_OF_B_CELL_ACTIVATION	82	-0.551	-1.993	0	7.05E-04	188
2	GO_REGULATION_OF_EPITHELIAL_CELL_APOPTOTIC_PROCESS	35	-0.64	-1.99	0	7.40E-04	189
2	GO_POSITIVE_REGULATION_OF_PEPTIDASE_ACTIVITY	114	-0.52	-1.987	0	7.83E-04	190

2	GO_REGULATION_OF_TOLL_LIKE_RECEPTOR_SIGNALING_PATHWAY	36	-0.651	-1.98	0	8.46E-04	191
2	GO_NEGATIVE_REGULATION_OF_VIRAL_ENTRY_INTO_HOST_CELL	15	-0.79	-1.978	0	8.73E-04	192
2	GO_REGULATION_OF_ALPHA_BETA_T_CELL_ACTIVATION	52	-0.613	-1.974	0	9.26E-04	193
2	GO_REGULATION_OF_DEFENSE_RESPONSE_TO_VIRUS	136	-0.505	-1.974	0	9.27E-04	194
2	GO_REGULATION_OF_INTERLEUKIN_6_PRODUCTION	74	-0.555	-1.967	0	0.001018	195
2	KEGG_AUTOIMMUNE_THYROID_DISEASE	31	-0.645	-1.966	0	0.001031	196
2	GO_DEFENSE_RESPONSE_TO_BACTERIUM	108	-0.524	-1.965	0	0.001041	197
2	GO_NEGATIVE_REGULATION_OF_I_KAPPAB_KINASE_NF_KAPPAB_SIGNALING	40	-0.626	-1.959	0	0.001118	198
2	GO_POSITIVE_REGULATION_OF_HEMOPOIESIS	117	-0.511	-1.958	0	0.001125	199
2	GO_REGULATION_OF_LYMPHOCYTE_MEDIATED_IMMUNITY	78	-0.549	-1.955	0	0.001174	200
2	GO_ALPHA_BETA_T_CELL_DIFFERENTIATION	34	-0.627	-1.953	0	0.001204	201
2	GO_LEUKOCYTE_ACTIVATION	305	-0.453	-1.95	0	0.001246	202
2	GO_CYTOKINE_PRODUCTION	87	-0.525	-1.938	0	0.00146	203
2	GO_NIK_NF_KAPPAB_SIGNALING	75	-0.537	-1.935	0	0.001539	204
2	GO_MYELOID_DENDRITIC_CELL_ACTIVATION	19	-0.716	-1.935	0	0.001542	205
2	GO_TOLL_LIKE_RECEPTOR_SIGNALING_PATHWAY	73	-0.545	-1.933	0	0.001561	206
2	GO_NEGATIVE_REGULATION_OF_NF_KAPPAB_IMPORT_INTO_NUCLEUS	15	-0.786	-1.932	0	0.00158	207
2	GO_NEGATIVE_REGULATION_OF_RESPONSE_TO_EXTERNAL_STIMULUS	179	-0.478	-1.928	0	0.001683	208
2	KEGG_LEISHMANIA_INFECTION	58	-0.563	-1.925	0	0.001747	209
2	GO_NEGATIVE_REGULATION_OF_INNATE_IMMUNE_RESPONSE	29	-0.648	-1.92	0	0.001876	210
2	GO_REGULATION_OF_CELL_KILLING	44	-0.594	-1.916	0	0.001973	211
2	GO_PROTEASE_BINDING	84	-0.529	-1.91	0	0.002096	212
2	GO_NEGATIVE_REGULATION_OF_T_CELL_DIFFERENTIATION	19	-0.717	-1.909	0	0.002108	213
2	GO_T_CELL_HOMEOSTASIS	24	-0.66	-1.899	0	0.002347	214

2	GO_REGULATION_OF_LEUKOCYTE_MEDIATED_CYTOTOXICITY	38	-0.596	-1.896	0	0.00242	215
2	GO_POSITIVE_REGULATION_OF_ALPHA_BETA_T_CELL_ACTIVATION	38	-0.61	-1.893	0	0.002491	216
2	GO_REGULATION_OF_T_CELL_MEDIATED_CYTOTOXICITY	20	-0.683	-1.891	0	0.002573	217
2	BIOCARTA_IL7_PATHWAY	17	-0.733	-1.89	0	0.002595	218
2	GO_POSITIVE_REGULATION_OF_ACTIVATED_T_CELL_PROLIFERATION	20	-0.683	-1.888	0	0.002645	219
2	GO_POSITIVE_REGULATION_OF_B_CELL_ACTIVATION	53	-0.567	-1.887	0	0.002667	220
2	GO_CELLULAR_RESPONSE_TO_VIRUS	19	-0.702	-1.885	0	0.002726	221
2	GO_ADAPTIVE_IMMUNE_RESPONSE	182	-0.47	-1.884	0	0.002761	222
2	GO_POSITIVE_REGULATION_OF_TUMOR_NECROSIS_FACTOR_SUPERFAMILY_CYTOKINE_PRODUCTION	47	-0.58	-1.883	0	0.002783	223
2	GO_REGULATION_OF_ALPHA_BETA_T_CELL_PROLIFERATION	18	-0.714	-1.872	0	0.003165	224
2	GO_T_HELPER_1_TYPE_IMMUNE_RESPONSE	18	-0.712	-1.864	0	0.003465	225
2	GO_LEUKOCYTE_HOMEOSTASIS	41	-0.574	-1.86	0	0.003604	226
2	GO_POSITIVE_REGULATION_OF_ALPHA_BETA_T_CELL_DIFFERENTIATION	27	-0.647	-1.86	0	0.003614	227
2	GO_NEGATIVE_REGULATION_OF_NF_KAPPAB_TRANSCRIPTION_FACTOR_ACTIVITY	49	-0.553	-1.856	0	0.003784	228
2	GO_POSITIVE_REGULATION_OF_INTERLEUKIN_2_PRODUCTION	25	-0.641	-1.855	0	0.003839	229
2	GO_T_CELL_MEDIATED_IMMUNITY	23	-0.663	-1.854	0	0.003865	230
2	GO_POSITIVE_REGULATION_OF_LEUKOCYTE_DIFFERENTIATION	98	-0.494	-1.853	0	0.003912	231
2	GO_REGULATION_OF_TUMOR_NECROSIS_FACTOR_MEDIATED_SIGNALING_PATHWAY	42	-0.593	-1.852	0	0.003949	232
2	GO_REGULATION_OF_INTERLEUKIN_2_PRODUCTION	33	-0.625	-1.852	0	0.003951	233
2	GO_HUMORAL_IMMUNE_RESPONSE	89	-0.507	-1.846	0	0.004235	234
2	GO_LEUKOCYTE_PROLIFERATION	61	-0.545	-1.846	0	0.004237	235
2	GO_CD4_POSITIVE_ALPHA_BETA_T_CELL_ACTIVATION	24	-0.647	-1.842	0	0.004413	236
2	GO_RESPONSE_TO_OXIDATIVE_STRESS	270	-0.431	-1.829	0	0.005067	237

2	GO_INNATE_IMMUNE_RESPONSE_ACTIVATING_CELL_SURFACE_RECEPTOR_SIGNALING_PATHWAY	93	-0.504	-1.826	0	0.005204	238
2	KEGG_EPITHELIAL_CELL_SIGNALING_IN_HELICOBACTER_PYLORI_INFECTION	55	-0.527	-1.822	0	0.005483	239
2	GO_CELLULAR_RESPONSE_TO_OXIDATIVE_STRESS	144	-0.462	-1.821	0	0.005514	240
2	GO_LEUKOCYTE_APOPTOTIC_PROCESS	17	-0.704	-1.818	0	0.00566	241
2	GO_DEATH_RECEPTOR_BINDING	16	-0.725	-1.814	0	0.005901	242
2	GO_POSITIVE_REGULATION_OF_CYTOKINE_PRODUCTION_INVOLVED_IN_IMMUNE_RESPONSE	21	-0.664	-1.793	0	0.007316	243
2	GO_LYMPHOCYTE_ACTIVATION	256	-0.426	-1.786	0	0.007746	244
2	KEGG_NATURAL_KILLER_CELL_MEDIATED_CYTOTOXICITY	94	-0.478	-1.766	0	0.00936	245
2	GO_POSITIVE_REGULATION_OF_LEUKOCYTE_MEDIATED_IMMUNITY	59	-0.517	-1.766	0	0.009399	246
2	GO_POSITIVE_REGULATION_OF_LYMPHOCYTE_MEDIATED_IMMUNITY	49	-0.54	-1.747	0	0.011171	247
2	GO_ANTIGEN_PROCESSING_AND_PRESENTATION_OF_EXOGENOUS_PEPTIDE_ANTIGEN_VIA_MHC_CLASS_I	59	-0.51	-1.747	0	0.011208	248
2	KEGG_SYSTEMIC_LUPUS_ERYTHEMATOSUS	68	-0.493	-1.733	0	0.012666	249
2	GO_T_CELL_DIFFERENTIATION	95	-0.457	-1.706	0	0.015975	250
2	GO_SIGNAL_TRANSDUCTION_BY_PROTEIN_PHOSPHORYLATION	290	-0.401	-1.707	0	0.015977	251
2	GO_IMMUNE_RESPONSE_REGULATING_CELL_SURFACE_RECEPTOR_SIGNALING_PATHWAY	245	-0.404	-1.694	0	0.01754	252
2	GO_LYMPHOCYTE_COSTIMULATION	54	-0.501	-1.688	0	0.018505	253
2	GO_LEUKOCYTE_DIFFERENTIATION	214	-0.397	-1.649	0	0.024558	254
2	GO_IMMUNE_SYSTEM_DEVELOPMENT	412	-0.361	-1.6	0	0.034551	255
2	GO_ANTIGEN_PROCESSING_AND_PRESENTATION_OF_PEPTIDE_ANTIGEN_VIA_MHC_CLASS_I	79	-0.484	-1.755	0.001789	0.010414	256
2	GO_CELL_ACTIVATION_INVOLVED_IN_IMMUNE_RESPONSE	97	-0.454	-1.685	0.001828	0.018881	257
2	KEGG_ALLOGRAFT_REJECTION	29	-0.676	-2.003	0.001876	6.03E-04	258
2	GO_ANTIGEN_RECEPTOR_MEDIATED_SIGNALING_PATHWAY	145	-0.391	-1.546	0.001905	0.049072	259

2	GO_REGULATION_OF_MYELOID_CELL_DIFFER ENTIATION	127	-0.401	-1.58	0.001912	0.039399	260
2	GO_T_CELL_ACTIVATION_INVOLVED_IN_IMM UNE_RESPONSE	41	-0.581	-1.811	0.001923	0.006045	261
2	GO_NEGATIVE_REGULATION_OF_LEUKOCYTE _PROLIFERATION	50	-0.526	-1.739	0.001972	0.012088	262
2	GO_CELLULAR_RESPONSE_TO_HYDROGEN_PE ROXIDE	50	-0.53	-1.773	0.001984	0.00882	263
2	GO_REGULATION_OF_DEFENSE_RESPONSE_T O_VIRUS_BY_HOST	86	-0.505	-1.858	0.001988	0.003693	264
2	GO_REGULATION_OF_INTERLEUKIN_17_PROD UCTION	16	-0.685	-1.778	0.002004	0.008395	265
2	GO_TUMOR_NECROSIS_FACTOR_RECEPTOR_B INDING	24	-0.651	-1.83	0.002008	0.005007	266
2	BIOCARTA_IL1R_PATHWAY	29	-0.667	-1.96	0.002092	0.001102	267
2	GO_T_CELL_DIFFERENTIATION_INVOLVED_IN_ IMMUNE_RESPONSE	24	-0.671	-1.894	0.002146	0.002478	268
2	GO_REGULATION_OF_ANTIGEN_PROCESSING _AND_PRESENTATION	17	-0.745	-1.943	0.002151	0.001365	269
2	GO_MYELOID_CELL_DIFFERENTIATION	150	-0.384	-1.532	0.003591	0.053952	270
2	GO_FC_RECEPTOR_SIGNALING_PATHWAY	163	-0.392	-1.569	0.00363	0.042445	271
2	GO_LYMPHOCYTE_DIFFERENTIATION	148	-0.396	-1.565	0.003759	0.043417	272
2	GO_T_CELL_RECEPTOR_SIGNALING_PATHWAY	120	-0.424	-1.622	0.003774	0.029895	273
2	GO_CELLULAR_DEFENSE_RESPONSE	37	-0.534	-1.686	0.003846	0.018776	274
2	GO_B_CELL_MEDIATED_IMMUNITY	50	-0.505	-1.669	0.003906	0.021337	275
2	GO_NEGATIVE_REGULATION_OF_T_CELL_PRO LIFERATION	36	-0.562	-1.756	0.003992	0.010269	276
2	GO_POSITIVE_REGULATION_OF_ALPHA_BETA _T_CELL_PROLIFERATION	15	-0.687	-1.734	0.004	0.012579	277
2	GO_NEGATIVE_REGULATION_OF_LEUKOCYTE _MEDIATED_IMMUNITY	36	-0.561	-1.742	0.004008	0.011764	278
2	BIOCARTA_IL2RB_PATHWAY	37	-0.567	-1.763	0.00404	0.009725	279
2	GO_REGULATION_OF_MONOCYTE_CHEMOTA XIS	17	-0.682	-1.787	0.004107	0.007741	280
2	GO_REGULATION_OF_ACUTE_INFLAMMATOR Y_RESPONSE	49	-0.52	-1.7	0.004141	0.016838	281
2	GO_NEGATIVE_REGULATION_OF_STAT_CASCA DE	24	-0.624	-1.78	0.004211	0.008207	282
2	BIOCARTA_TH1TH2_PATHWAY	15	-0.705	-1.782	0.004255	0.008051	283

2	GO_NEGATIVE_REGULATION_OF_CHEMOTAXIS	35	-0.539	-1.667	0.004283	0.021637	284
2	GO_NEGATIVE_REGULATION_OF_TUMOR_NECROSIS_FACTOR_SUPERFAMILY_CYTOKINE_PRODUCTION	30	-0.554	-1.655	0.004338	0.023703	285
2	GO_POSITIVE_REGULATION_OF_T_CELL_MEDIATED_IMMUNITY	23	-0.645	-1.783	0.004357	0.007989	286
2	BIOCARTA_IL12_PATHWAY	18	-0.68	-1.804	0.004415	0.00648	287
2	GO_DEFENSE_RESPONSE_TO_GRAM_POSITIVE_BACTERIUM	44	-0.538	-1.7	0.005618	0.016772	288
2	GO_REGULATION_OF_RESPONSE_TO_INTERFERON_GAMMA	18	-0.709	-1.883	0.005814	0.002782	289
2	GO_NEGATIVE_REGULATION_OF_LYMPHOCYTE_MEDIATED_IMMUNITY	26	-0.602	-1.726	0.005848	0.013541	290
2	GO_NEGATIVE_REGULATION_OF_LEUKOCYTE_APOPTOTIC_PROCESS	33	-0.574	-1.729	0.005906	0.01323	291
2	GO_VIRUS_RECEPTOR_ACTIVITY	55	-0.476	-1.629	0.005917	0.028479	292
2	KEGG_VIRAL_MYOCARDITIS	50	-0.481	-1.575	0.006073	0.040746	293
2	KEGG_PRIMARY_IMMUNODEFICIENCY	24	-0.648	-1.841	0.006356	0.004463	294
2	GO_NEGATIVE_REGULATION_OF_DEFENSE_RESPONSE_TO_VIRUS	15	-0.726	-1.845	0.006424	0.004275	295
2	KEGG_ASTHMA	18	-0.639	-1.698	0.006479	0.016993	296
2	GO_PRODUCTION_OF_MOLECULAR_MEDIATOR_OF_IMMUNE_RESPONSE	46	-0.483	-1.58	0.00813	0.039423	297
2	GO_NEGATIVE_REGULATION_OF_LYMPHOCYTE_DIFFERENTIATION	26	-0.581	-1.705	0.00818	0.016138	298
2	GO_POSITIVE_REGULATION_OF_TYROSINE_PHOSPHORYLATION_OF_STAT3_PROTEIN	24	-0.634	-1.784	0.008197	0.00792	299
2	GO_T_CELL_PROLIFERATION	32	-0.563	-1.706	0.009785	0.016021	300
2	BIOCARTA_PDGF_PATHWAY	31	-0.555	-1.688	0.009785	0.018499	301
2	GO_POSITIVE_REGULATION_OF_IMMUNOGLOBULIN_PRODUCTION	23	-0.613	-1.733	0.009804	0.012665	302
2	GO_REGULATION_OF_INTERLEUKIN_10_PRODUCTION	29	-0.565	-1.673	0.009862	0.02076	303
2	GO_LYMPHOCYTE_ACTIVATION_INVOLVED_IN_IMMUNE_RESPONSE	70	-0.435	-1.541	0.00996	0.050828	304
2	GO_MHC_CLASS_I_PROTEIN_BINDING	16	-0.681	-1.759	0.010267	0.010003	305
2	GO_NEGATIVE_REGULATION_OF_ADAPTIVE_IMMUNE_RESPONSE	25	-0.594	-1.695	0.010616	0.017342	306

2	GO_NEGATIVE_REGULATION_OF_LEUKOCYTE_DIFFERENTIATION	56	-0.465	-1.58	0.011765	0.039398	307
2	GO_REGULATION_OF_MACROPHAGE_ACTIVATION	16	-0.693	-1.755	0.01232	0.010427	308
2	GO_CYTOKINE_SECRETION	26	-0.566	-1.612	0.012685	0.031936	309
2	GO_REGULATION_OF_TRANSFORMING_GROWTH_FACTOR_BETA_PRODUCTION	17	-0.639	-1.678	0.013043	0.019889	310
2	GO_MYELOID_LEUKOCYTE_DIFFERENTIATION	74	-0.427	-1.515	0.013462	0.059152	311
2	KEGG_ANTIGEN_PROCESSING_AND_PRESENTATION	58	-0.477	-1.597	0.014344	0.035413	312
2	GO_NEGATIVE_REGULATION_OF_CYTOKINE_PRODUCTION_INVOLVED_IN_IMMUNE_RESPONSE	17	-0.658	-1.7	0.014553	0.016824	313
2	GO_INFLAMMATORY_RESPONSE_TO_ANTIGENIC_STIMULUS	19	-0.632	-1.697	0.014614	0.01709	314
2	GO_NEGATIVE_REGULATION_OF_INTERFERON_GAMMA_PRODUCTION	25	-0.595	-1.689	0.014768	0.018238	315
2	GO_REGULATION_OF_NATURAL_KILLER_CELL_MEDIATED_IMMUNITY	25	-0.58	-1.649	0.015152	0.024534	316
2	GO_LYMPHOCYTE_HOMEOSTASIS	34	-0.539	-1.655	0.015595	0.02366	317
2	GO_REGULATION_OF_ANTIGEN_RECEPTOR_MEDIATED_SIGNALING_PATHWAY	33	-0.537	-1.636	0.016393	0.027255	318
2	GO_ACUTE_INFLAMMATORY_RESPONSE	44	-0.499	-1.613	0.016563	0.031855	319
2	GO_POSITIVE_REGULATION_OF_ACUTE_INFLAMMATORY_RESPONSE	20	-0.615	-1.686	0.016598	0.018744	320
2	GO_NATURAL_KILLER_CELL_ACTIVATION	31	-0.523	-1.563	0.016771	0.04408	321
2	BIOCARTA_IL2_PATHWAY	21	-0.589	-1.624	0.016807	0.029401	322
2	GO_ANTIGEN_PROCESSING_AND_PRESENTATION	180	-0.343	-1.388	0.017361	0.12172	323
2	GO_NEGATIVE_REGULATION_OF_LYMPHOCYTE_APOPTOTIC_PROCESS	19	-0.609	-1.636	0.018036	0.027277	324
2	KEGG_T_CELL_RECEPTOR_SIGNALING_PATHWAY	88	-0.392	-1.452	0.018315	0.085867	325
2	GO_MODULATION_BY_SYMBIONT_OF_HOST_CELLULAR_PROCESS	25	-0.57	-1.611	0.018634	0.032196	326
2	GO_POSITIVE_REGULATION_OF_RESPONSE_TO_CYTOKINE_STIMULUS	23	-0.582	-1.615	0.018828	0.031446	327
2	GO_REGULATION_OF_IMMUNOGLOBULIN_PRODUCTION	33	-0.544	-1.695	0.018908	0.017366	328

2	GO_REGULATION_OF_T_CELL_RECEPTOR_SIGNALING_PATHWAY	24	-0.589	-1.657	0.018947	0.023329	329
2	GO_PHAGOCYTOSIS	133	-0.375	-1.472	0.020599	0.076193	330
2	GO_REGULATION_OF_HUMORAL_IMMUNE_RESPONSE	25	-0.548	-1.554	0.02079	0.046786	331
2	GO_T_CELL_SELECTION	27	-0.565	-1.667	0.021053	0.021709	332
2	GO_POSITIVE_REGULATION_OF_MYELOID_CELL_DIFFERENTIATION	59	-0.433	-1.488	0.021318	0.069289	333
2	GO_NEGATIVE_REGULATION_OF_VIRAL_TRANSCRIPTION	20	-0.595	-1.618	0.021552	0.030692	334
2	GO_IMMUNOGLOBULIN_PRODUCTION	33	-0.511	-1.575	0.022495	0.040839	335
2	GO_RESPONSE_TO_INTERLEUKIN_6	21	-0.588	-1.608	0.023013	0.032824	336
2	KEGG_FC_GAMMA_R_MEDIATED_PHAGOCYTOSIS	81	-0.402	-1.428	0.023762	0.098617	337
2	GO_REGULATION_OF_MAST_CELL_ACTIVATION	30	-0.525	-1.602	0.025157	0.034154	338
2	GO_NEGATIVE_REGULATION_OF_PRODUCTION_OF_MOLECULAR_MEDIATOR_OF_IMMUNE_RESPONSE	20	-0.547	-1.486	0.028761	0.070152	339
2	BIOCARTA_IL6_PATHWAY	22	-0.555	-1.542	0.028866	0.050526	340
2	GO_POSITIVE_REGULATION_OF_INTERLEUKIN_10_PRODUCTION	19	-0.61	-1.59	0.029821	0.036982	341
2	GO_REGULATION_OF_NATURAL_KILLER_CELL_ACTIVATION	20	-0.57	-1.531	0.030501	0.054031	342
2	KEGG_AMYOTROPHIC_LATERAL_SCLEROSIS_ALS	40	-0.485	-1.527	0.030801	0.055345	343
2	GO_MYELOID_LEUKOCYTE_MEDIATED_IMMUNITY	29	-0.527	-1.545	0.031873	0.049365	344
2	GO_REGULATION_OF_MYELOID_LEUKOCYTE_DIFFERENTIATION	79	-0.398	-1.435	0.032015	0.094317	345
2	GO_RESPONSE_TO_FUNGUS	29	-0.51	-1.526	0.032609	0.055742	346
2	GO_ACUTE_PHASE_RESPONSE	25	-0.553	-1.569	0.032854	0.042422	347
2	GO_ANTIGEN_BINDING	68	-0.409	-1.434	0.035433	0.094721	348
2	GO_B_CELL_ACTIVATION	90	-0.373	-1.377	0.037244	0.128049	349
2	GO_NEGATIVE_REGULATION_OF_CYTOKINE_BIOSYNTHETIC_PROCESS	19	-0.586	-1.548	0.037422	0.04836	350
2	GO_REGULATION_OF_VIRAL_RELEASE_FROM_HOST_CELL	29	-0.509	-1.502	0.040323	0.06421	351

2	GO_FC_EPSILON_RECEPTOR_SIGNALING_PATHWAY	113	-0.35	-1.34	0.042308	0.153951	352
2	KEGG_ACUTE_MYELOID_LEUKEMIA	52	-0.441	-1.483	0.043233	0.071687	353
2	GO_MYELOID_CELL_ACTIVATION_INVOLVED_IN_IMMUNE_RESPONSE	27	-0.513	-1.506	0.045161	0.062688	354
2	GO_NEGATIVE_REGULATION_OF_TOLL_LIKE_RECEPTOR_SIGNALING_PATHWAY	18	-0.607	-1.589	0.045738	0.037342	355
2	GO_REGULATION_OF_B_CELL_APOPTOTIC_PROCESS	17	-0.603	-1.575	0.045929	0.040791	356
2	GO_CELLULAR_RESPONSE_TO_INTERLEUKIN_6	18	-0.583	-1.54	0.046122	0.05098	357
2	GO_CYTOKINE_BINDING	66	-0.405	-1.422	0.047431	0.101685	358
2	GO_POSITIVE_REGULATION_OF_AUTOPHAGY	59	-0.418	-1.412	0.04888	0.107323	359
2	GO_POSITIVE_REGULATION_OF_B_CELL_MEDIATED_IMMUNITY	20	-0.559	-1.5	0.048936	0.064608	360
3	GO_REGULATION_OF_MULTI_ORGANISM_PROCESS	343	-0.544	-2.363	0	0	1
3	GO_REGULATION_OF_RESPONSE_TO_WOUNDING	262	-0.568	-2.4	0	0	2
3	GO_REGULATION_OF_SYMBIOSIS_ENCOMPASSING_MUTUALISM_THROUGH_PARASITISM	168	-0.645	-2.603	0	0	3
3	KEGG_APOPTOSIS	75	-0.66	-2.348	0	0	4
3	GO_POSITIVE_REGULATION_OF_SEQUENCE_SPECIFIC_DNA_BINDING_TRANSCRIPTION_FACTOR_ACTIVITY	167	-0.558	-2.246	0	2.22E-06	5
3	GO_POSITIVE_REGULATION_OF_RESPONSE_TO_EXTERNAL_STIMULUS	196	-0.552	-2.267	0	2.33E-06	6
3	GO_NEGATIVE_REGULATION_OF_SIGNAL_TRANSDUCTION_IN_ABSENCE_OF_LIGAND	21	-0.847	-2.268	0	2.34E-06	7
3	GO_POSITIVE_REGULATION_OF_PEPTIDYL_TYROSINE_PHOSPHORYLATION	105	-0.583	-2.231	0	6.39E-06	8
3	GO_EXTRINSIC_APOPTOTIC_SIGNALING_PATHWAY	81	-0.618	-2.233	0	6.42E-06	9
3	GO_REGULATION_OF_CYSTEINE_TYPE_ENDOPEPTIDASE_ACTIVITY	160	-0.555	-2.223	0	1.05E-05	10
3	GO_REGULATION_OF_PEPTIDYL_TYROSINE_PHOSPHORYLATION	147	-0.562	-2.225	0	1.06E-05	11
3	GO_REGULATION_OF_CELL_CELL_ADHESION	264	-0.52	-2.227	0	1.06E-05	12
3	BIOCARTA_DEATH_PATHWAY	30	-0.748	-2.227	0	1.06E-05	13

3	GO_POSITIVE_REGULATION_OF_CELL_CELL_ADHESION	173	-0.551	-2.217	0	1.25E-05	14
3	GO_REGULATION_OF_PEPTIDASE_ACTIVITY	247	-0.512	-2.176	0	3.11E-05	15
3	GO_REGULATION_OF_HOMOTYPIC_CELL_CELL_ADHESION	216	-0.524	-2.176	0	3.11E-05	16
3	GO_REGULATION_OF_EXTRINSIC_APOPTOTIC_SIGNALING_PATHWAY_VIA_DEATH_DOMAIN_RECEPTORS	45	-0.666	-2.166	0	3.39E-05	17
3	GO_POSITIVE_REGULATION_OF_ERK1_AND_ERK2_CASCADE	100	-0.579	-2.167	0	3.41E-05	18
3	GO_RESPONSE_TO_EXOGENOUS_DSRNA	26	-0.759	-2.158	0	3.67E-05	19
3	GO_POSITIVE_REGULATION_OF_LOCOMOTION	285	-0.501	-2.152	0	4.72E-05	20
3	GO_APOPTOTIC_SIGNALING_PATHWAY	229	-0.514	-2.15	0	5.08E-05	21
3	HALLMARK_APOPTOSIS	149	-0.545	-2.147	0	5.25E-05	22
3	GO_ESTABLISHMENT_OF_ENDOTHELIAL_BARRIER	20	-0.774	-2.13	0	7.52E-05	23
3	GO_REGULATION_OF_APOPTOTIC_SIGNALING_PATHWAY	284	-0.491	-2.124	0	8.26E-05	24
3	GO_POSITIVE_REGULATION_OF_APOPTOTIC_SIGNALING_PATHWAY	146	-0.532	-2.117	0	9.52E-05	25
3	GO_RESPONSE_TO_VITAMIN_D	27	-0.722	-2.105	0	1.09E-04	26
3	GO_CELLULAR_RESPONSE_TO_HEAT	24	-0.73	-2.103	0	1.18E-04	27
3	GO_RESPONSE_TO_DSRNA	49	-0.626	-2.096	0	1.38E-04	28
3	GO_ACTIVATION_OF_CYSTEINE_TYPE_ENDOPEPTIDASE_ACTIVITY	74	-0.589	-2.094	0	1.54E-04	29
3	GO_ENDOTHELIAL_CELL_DEVELOPMENT	31	-0.705	-2.091	0	1.66E-04	30
3	GO_NECROPTOTIC_PROCESS	21	-0.761	-2.085	0	1.91E-04	31
3	GO_PROTEIN_TRIMERIZATION	29	-0.693	-2.079	0	1.97E-04	32
3	GO_NEGATIVE_REGULATION_OF_RESPONSE_TO_WOUNDING	100	-0.546	-2.069	0	2.40E-04	33
3	GO_KERATINOCYTE_DIFFERENTIATION	42	-0.635	-2.067	0	2.45E-04	34
3	GO_NECROTIC_CELL_DEATH	27	-0.71	-2.061	0	2.69E-04	35
3	GO_POSITIVE_REGULATION_OF_CYSTEINE_TYPE_ENDOPEPTIDASE_ACTIVITY_INVOLVED_IN_APOPTOTIC_SIGNALING_PATHWAY	16	-0.788	-2.057	0	2.89E-04	36
3	GO_REGULATION_OF_VASCULATURE_DEVELOPMENT	149	-0.509	-2.05	0	3.19E-04	37

3	HALLMARK_EPITHELIAL_MESENCHYMAL_TRANSITION	141	-0.521	-2.046	0	3.34E-04	38
3	GO_REGULATION_OF_ENDOTHELIAL_CELL_APOPTOTIC_PROCESS	22	-0.746	-2.036	0	3.64E-04	39
3	GO_POSITIVE_REGULATION_OF_CELL_ADHESION	263	-0.48	-2.032	0	3.83E-04	40
3	GO_NEGATIVE_REGULATION_OF_CYSTEINE_TYPE_ENDOPEPTIDASE_ACTIVITY	65	-0.572	-2.03	0	3.90E-04	41
3	GO_REGULATION_OF_PROTEIN_SECRETION	253	-0.476	-2.023	0	4.52E-04	42
3	GO_REGULATION_OF_CELL_ADHESION	438	-0.452	-2.014	0	5.17E-04	43
3	GO_POSITIVE_REGULATION_OF_TRANSCRIPTION_FACTOR_IMPORT_INTO_NUCLEUS	41	-0.636	-2.007	0	5.71E-04	44
3	GO_NEGATIVE_REGULATION_OF_CELLULAR_RESPONSE_TO_INSULIN_STIMULUS	22	-0.728	-2.007	0	5.76E-04	45
3	GO_ENDOTHELIAL_CELL_DIFFERENTIATION	46	-0.62	-2.004	0	5.99E-04	46
3	GO_REGULATION_OF_CELLULAR_RESPONSE_TO_INSULIN_STIMULUS	38	-0.634	-2	0	6.30E-04	47
3	GO_SIDE_OF_MEMBRANE	271	-0.472	-1.997	0	6.63E-04	48
3	GO_CELL_CELL_ADHESION	353	-0.455	-1.991	0	7.17E-04	49
3	GO_NEGATIVE_REGULATION_OF_CYTOKINE_SECRETION	26	-0.689	-1.989	0	7.51E-04	50
3	GO_LEUKOCYTE_MIGRATION	180	-0.49	-1.987	0	7.84E-04	51
3	GO_EXTRINSIC_APOPTOTIC_SIGNALING_PATHWAY_VIA_DEATH_DOMAIN_RECEPTORS	36	-0.645	-1.985	0	7.95E-04	52
3	GO_SINGLE_ORGANISM_CELL_ADHESION	314	-0.456	-1.979	0	8.61E-04	53
3	GO_REGULATION_OF_TRANSCRIPTION_FACTOR_IMPORT_INTO_NUCLEUS	77	-0.551	-1.97	0	9.69E-04	54
3	GO_REGULATION_OF_SEQUENCE_SPECIFIC_DNA_BINDING_TRANSCRIPTION_FACTOR_ACTIVITY	263	-0.461	-1.964	0	0.001045	55
3	GO_POSITIVE_REGULATION_OF_CARTILAGE_DEVELOPMENT	17	-0.753	-1.963	0	0.001063	56
3	GO_DEATH_RECEPTOR_ACTIVITY	17	-0.749	-1.958	0	0.001131	57
3	GO_REGULATION_OF_RESPONSE_TO_BIOTIC_STIMULUS	165	-0.484	-1.957	0	0.001142	58
3	GO_PROTEIN_HETEROOLIGOMERIZATION	68	-0.558	-1.955	0	0.001177	59
3	GO_POSITIVE_REGULATION_OF_INTRINSIC_APOPTOTIC_SIGNALING_PATHWAY	46	-0.6	-1.952	0	0.001211	60

163

3	GO_POSITIVE_REGULATION_OF_STRESS_ACTIVATED_PROTEIN_KINASE_SIGNALING_CASCADE	98	-0.52	-1.95	0	0.001256	61
3	GO_POSITIVE_REGULATION_OF_PROTEIN_SECRETION	140	-0.5	-1.948	0	0.001293	62
3	HALLMARK_KRAS_SIGNALING_UP	145	-0.494	-1.946	0	0.001322	63
3	GO_CELL_SURFACE	447	-0.434	-1.942	0	0.001388	64
3	GO_NEGATIVE_REGULATION_OF_PEPTIDASE_ACTIVITY	136	-0.491	-1.936	0	0.001521	65
3	KEGG_CELL_ADHESION_MOLECULES_CAMS	82	-0.539	-1.936	0	0.001523	66
3	KEGG_PROTEASOME	41	-0.598	-1.932	0	0.001601	67
3	GO_NEGATIVE_REGULATION_OF_APOPTOTIC_SIGNALING_PATHWAY	152	-0.483	-1.924	0	0.001769	68
3	GO_CELL_ACTIVATION	409	-0.434	-1.922	0	0.001843	69
3	GO_POSITIVE_REGULATION_OF_PROTEIN_IMPORT	77	-0.537	-1.913	0	0.002039	70
3	GO_POSITIVE_REGULATION_OF_CELL_DEATH	462	-0.425	-1.911	0	0.002071	71
3	GO_NEGATIVE_REGULATION_OF_GROWTH	160	-0.475	-1.909	0	0.002108	72
3	KEGG_TYPE_I_DIABETES_MELLITUS	34	-0.615	-1.909	0	0.002117	73
3	BIOCARTA_RELA_PATHWAY	16	-0.745	-1.908	0	0.002147	74
3	GO_MODIFICATION_BY_SYMBIONT_OF_HOST_MORPHOLOGY_OR_PHYSIOLOGY	38	-0.595	-1.9	0	0.002326	75
3	GO_RESPONSE_TO_ESTROGEN	142	-0.478	-1.888	0	0.002645	76
3	GO_NEGATIVE_REGULATION_OF_PROTEIN_SECRETION	63	-0.552	-1.887	0	0.002665	77
3	GO_RESPONSE_TO_ALCOHOL	241	-0.448	-1.887	0	0.002673	78
3	GO_REGULATION_OF_PEPTIDE_TRANSPORT	161	-0.464	-1.877	0	0.00302	79
3	GO_RESPONSE_TO_HEAT	63	-0.537	-1.876	0	0.003035	80
3	GO_MODIFICATION_OF_MORPHOLOGY_OR_PHYSIOLOGY_OF_OTHER_ORGANISM	71	-0.536	-1.875	0	0.003057	81
3	GO_GLAND_MORPHOGENESIS	60	-0.548	-1.869	0	0.003293	82
3	GO_NEGATIVE_REGULATION_OF_EPITHELIAL_CELL_APOPTOTIC_PROCESS	20	-0.695	-1.868	0	0.003297	83
3	GO_HYDROLASE_ACTIVITY_ACTING_ON_CARBON_NITROGEN_BUT_NOT_PEPTIDE_BONDS_IN_CYCLIC_AMIDINES	27	-0.639	-1.863	0	0.003469	84

3	GO_REGULATION_OF_NUCLEOCYTOPLASMIC_ TRANSPORT	177	-0.464	-1.862	0	0.00355	85
3	BIOCARTA_NTHI_PATHWAY	22	-0.665	-1.857	0	0.003762	86
3	GO_POSITIVE_REGULATION_OF_LAMELLIPODI UM_ORGANIZATION	15	-0.724	-1.856	0	0.003806	87
3	GO_NUCLEOTIDE_BINDING_DOMAIN_LEUCIN E_RICH_REPEAT_CONTAINING_RECEPTOR_SIG NALING_PATHWAY	22	-0.663	-1.855	0	0.003852	88
3	GO_REGULATION_OF_MITOCHONDRIAL_OUT ER_MEMBRANE_PERMEABILIZATION_INVOLV ED_IN_APOPTOTIC_SIGNALING_PATHWAY	37	-0.605	-1.854	0	0.003884	89
3	GO_POSITIVE_REGULATION_OF_CELL_PROLIF ERATION	489	-0.411	-1.848	0	0.004111	90
3	GO_POSITIVE_REGULATION_OF_MITOCHOND RIAL_OUTER_MEMBRANE_PERMEABILIZATIO N_INVOLVED_IN_APOPTOTIC_SIGNALING_PAT HWAY	33	-0.592	-1.847	0	0.004174	91
3	GO_POSITIVE_REGULATION_OF_NUCLEOCYTO PLASMIC_TRANSPORT	94	-0.492	-1.845	0	0.004265	92
3	GO_POSITIVE_REGULATION_OF_SECRETION	224	-0.437	-1.844	0	0.004312	93
3	GO_NEGATIVE_REGULATION_OF_ENDOTHELI AL_CELL_APOPTOTIC_PROCESS	15	-0.742	-1.843	0	0.004373	94
3	GO_REGULATION_OF_INTRACELLULAR_TRANS PORT	448	-0.412	-1.842	0	0.004416	95
3	GO_POSITIVE_REGULATION_OF_ESTABLISHM ENT_OF_PROTEIN_LOCALIZATION	359	-0.42	-1.841	0	0.004486	96
3	BIOCARTA_BIOPEPTIDES_PATHWAY	34	-0.604	-1.835	0	0.004792	97
3	GO_MOLTING_CYCLE	38	-0.58	-1.833	0	0.004875	98
3	GO_RESPONSE_TO_ESTRADIOL	93	-0.496	-1.833	0	0.004917	99
3	GO_POSITIVE_REGULATION_OF_VASCULATUR E_DEVELOPMENT	86	-0.507	-1.831	0	0.00496	100
3	GO_RESPONSE_TO_VITAMIN	82	-0.506	-1.831	0	0.004978	101
3	GO_NEGATIVE_REGULATION_OF_PROTEOLYSI S	204	-0.442	-1.827	0	0.005171	102
3	GO_CELL_CELL_SIGNALING	363	-0.413	-1.827	0	0.005177	103
3	GO_REGULATION_OF_PROTEIN_IMPORT	143	-0.463	-1.827	0	0.00518	104
3	GO_HEPARIN_BINDING	77	-0.508	-1.823	0	0.005405	105
3	GO_GROWTH_FACTOR_RECEPTOR_BINDING	79	-0.512	-1.822	0	0.005436	106

3	GO_REGULATION_OF_MEMBRANE_PERMEABILITY	57	-0.534	-1.813	0	0.005948	107
3	GO_REGULATION_OF_ENDOPLASMIC_RETICULUM_UNFOLDED_PROTEIN_RESPONSE	24	-0.639	-1.811	0	0.00603	108
3	BIOCARTA_PROTEASOME_PATHWAY	26	-0.617	-1.805	0	0.006437	109
3	GO_CELLULAR_RESPONSE_TO_MECHANICAL_STIMULUS	62	-0.52	-1.799	0	0.006855	110
3	GO_RESPONSE_TO_DRUG	304	-0.414	-1.797	0	0.006985	111
3	GO_POSITIVE_REGULATION_OF_PROTEIN_OLIGOMERIZATION	18	-0.678	-1.791	0	0.007472	112
3	GO_REGULATION_OF_SECRETION	419	-0.403	-1.79	0	0.007508	113
3	GO_RESPONSE_TO_ACID_CHEMICAL	205	-0.432	-1.785	0	0.007798	114
3	GO_POSITIVE_REGULATION_OF_INTRACELLULAR_TRANSPORT	268	-0.417	-1.78	0	0.008219	115
3	GO_NEGATIVE_REGULATION_OF_CELL_ADHESION	160	-0.444	-1.779	0	0.008305	116
3	GO_SKIN_DEVELOPMENT	104	-0.47	-1.774	0	0.008683	117
3	GO_RESPONSE_TO_STEROID_HORMONE	308	-0.408	-1.768	0	0.009263	118
3	GO_REGULATION_OF_CYTOPLASMIC_TRANSPORT	352	-0.4	-1.765	0	0.00947	119
3	GO_BLOOD_MICROPARTICLE	65	-0.506	-1.759	0	0.010068	120
3	GO_RESPONSE_TO_TOXIC_SUBSTANCE	168	-0.436	-1.756	0	0.010264	121
3	GO_GLYCOSAMINOGLYCAN_BINDING	104	-0.466	-1.755	0	0.010412	122
3	HALLMARK_UV_RESPONSE_UP	136	-0.444	-1.75	0	0.010862	123
3	GO_CELLULAR_RESPONSE_TO_EXTERNAL_STIMULUS	198	-0.429	-1.747	0	0.011155	124
3	GO_REGULATION_OF_PROTEOLYSIS	495	-0.389	-1.747	0	0.01121	125
3	GO_RESPONSE_TO_MECHANICAL_STIMULUS	142	-0.445	-1.741	0	0.011806	126
3	GO_RESPONSE_TO_OSMOTIC_STRESS	48	-0.522	-1.74	0	0.011893	127
3	GO_PROTEIN_MATURATION	182	-0.425	-1.733	0	0.012725	128
3	GO_REGULATION_OF_CELLULAR_AMINO_ACID_METABOLIC_PROCESS	55	-0.515	-1.725	0	0.01364	129
3	GO_REGULATION_OF_INTRINSIC_APOPTOTIC_SIGNALING_PATHWAY	117	-0.452	-1.723	0	0.013877	130
3	GO_INTRACELLULAR_RECEPTOR_SIGNALING_PATHWAY	114	-0.457	-1.722	0	0.013982	131

3	GO_G_PROTEIN_COUPLED_RECEPTOR_SIGNALING_PATHWAY	347	-0.395	-1.719	0	0.014328	132
3	GO_NEGATIVE_REGULATION_OF_ESTABLISHMENT_OF_PROTEIN_LOCALIZATION	145	-0.438	-1.716	0	0.014695	133
3	GO_NEGATIVE_REGULATION_OF_LOCOMOTION	184	-0.418	-1.714	0	0.015098	134
3	GO_PEPTIDASE_INHIBITOR_ACTIVITY	82	-0.469	-1.712	0	0.015273	135
3	GO_EPITHELIAL_CELL_DEVELOPMENT	115	-0.452	-1.711	0	0.015415	136
3	GO_TAXIS	286	-0.401	-1.711	0	0.01547	137
3	GO_NEGATIVE_REGULATION_OF_CELL_ACTIVATION	117	-0.445	-1.71	0	0.015546	138
3	GO_PEPTIDASE_REGULATOR_ACTIVITY	113	-0.453	-1.707	0	0.015907	139
3	GO_NEGATIVE_REGULATION_OF_CELL_PROLIFERATION	438	-0.383	-1.704	0	0.01624	140
3	GO_RESPONSE_TO_INORGANIC_SUBSTANCE	356	-0.388	-1.699	0	0.016916	141
3	GO_REGULATION_OF_MUSCLE_CONTRACTION	87	-0.463	-1.686	0	0.018764	142
3	GO_REGULATION_OF_PROTEIN_BINDING	130	-0.431	-1.685	0	0.018916	143
3	KEGG_PATHWAYS_IN_CANCER	245	-0.401	-1.675	0	0.02045	144
3	GO_POSITIVE_REGULATION_OF_KINASE_ACTIVITY	343	-0.381	-1.671	0	0.020936	145
3	GO_GROWTH_FACTOR_BINDING	82	-0.461	-1.667	0	0.021634	146
3	GO_VASCULAR_PROCESS_IN_CIRCULATORY_SYSTEM	82	-0.457	-1.661	0	0.02261	147
3	GO_NEGATIVE_REGULATION_OF_SECRETION	118	-0.432	-1.659	0	0.023006	148
3	GO_REGULATION_OF_CELLULAR_PROTEIN_LOCALIZATION	421	-0.375	-1.657	0	0.023317	149
3	GO_AGING	199	-0.406	-1.657	0	0.023408	150
3	GO_REGULATION_OF_CELL_SHAPE	100	-0.442	-1.655	0	0.023742	151
3	GO_POSITIVE_REGULATION_OF_PROTEIN_SERINE_THREONINE_KINASE_ACTIVITY	204	-0.399	-1.653	0	0.023938	152
3	GO_NEGATIVE_REGULATION_OF_INTRACELLULAR_TRANSPORT	107	-0.436	-1.653	0	0.024001	153
3	GO_DIVALENT_INORGANIC_CATION_HOMEOSTASIS	202	-0.4	-1.647	0	0.024963	154
3	GO_REGULATION_OF_INTRACELLULAR_PROTEIN_TRANSPORT	282	-0.381	-1.641	0	0.026218	155

3	GO_REGULATION_OF_PROTEIN_LOCALIZATION_TO_NUCLEUS	174	-0.407	-1.636	0	0.027271	156
3	GO_POSITIVE_REGULATION_OF_CELLULAR_PROTEIN_LOCALIZATION	267	-0.385	-1.635	0	0.027361	157
3	GO_HOMEOSTASIS_OF_NUMBER_OF_CELLS	124	-0.419	-1.626	0	0.029033	158
3	HALLMARK_APICAL_JUNCTION	138	-0.412	-1.624	0	0.029458	159
3	GO_REGULATION_OF_GROWTH	424	-0.363	-1.621	0	0.030048	160
3	GO_GTPASE_ACTIVITY	177	-0.398	-1.614	0	0.031581	161
3	GO_PROTEIN_OLIGOMERIZATION	286	-0.377	-1.614	0	0.03161	162
3	GO_NEGATIVE_REGULATION_OF_TRANSPORT	304	-0.374	-1.614	0	0.031659	163
3	GO_POSITIVE_REGULATION_OF_PROTEOLYSIS	283	-0.378	-1.613	0	0.031785	164
3	GO_POSITIVE_REGULATION_OF_CYTOPLASMIC_TRANSPORT	202	-0.385	-1.601	0	0.03434	165
3	GO_POSITIVE_REGULATION_OF_TRANSFERASE_ACTIVITY	457	-0.356	-1.597	0	0.035399	166
3	GO_NEGATIVE_REGULATION_OF_CELL_GROWTH	115	-0.409	-1.596	0	0.035628	167
3	GO_CELL_PROLIFERATION	449	-0.354	-1.58	0	0.039418	168
3	GO_POSITIVE_REGULATION_OF_INTRACELLULAR_PROTEIN_TRANSPORT	186	-0.384	-1.569	0	0.042454	169
3	GO_MEMBRANE_MICRODOMAIN	205	-0.378	-1.568	0	0.042757	170
3	GO_WOUND_HEALING	318	-0.36	-1.563	0	0.044205	171
3	GO_REGULATION_OF_PROTEIN_TARGETING	225	-0.37	-1.549	0	0.048348	172
3	GO_RESPONSE_TO_EXTRACELLULAR_STIMULUS	311	-0.359	-1.548	0	0.048375	173
3	GO_REGULATION_OF_PROTEIN_MODIFICATION_BY_SMALL_PROTEIN_CONJUGATION_OR_REMOVAL	233	-0.372	-1.546	0	0.049161	174
3	GO_NEGATIVE_REGULATION_OF_CELL_DIFFERENTIATION	354	-0.353	-1.545	0	0.049415	175
3	GO_EXTRACELLULAR_STRUCTURE_ORGANIZATION	182	-0.379	-1.54	0	0.050981	176
3	GO_NEGATIVE_REGULATION_OF_INTRACELLULAR_SIGNAL_TRANSDUCTION	329	-0.351	-1.534	0	0.053027	177
3	GO_REGULATION_OF_CELL_GROWTH	266	-0.353	-1.511	0	0.060864	178
3	GO_REGULATION_OF_SYSTEM_PROCESS	281	-0.353	-1.505	0	0.062834	179
3	GO_RESPONSE_TO_WOUNDING	370	-0.34	-1.499	0	0.065016	180

3	GO_REGULATION_OF_PROTEIN_SERINE_THRE ONINE_KINASE_ACTIVITY	345	-0.341	-1.493	0	0.067518	181
3	GO_SIGNALING_RECEPTOR_ACTIVITY	482	-0.329	-1.483	0	0.07165	182
3	GO_SECRETION	363	-0.326	-1.431	0	0.096538	183
3	GO_REGULATION_OF_BODY_FLUID_LEVELS	314	-0.334	-1.438	0.00165	0.092882	184
3	GO_CELLULAR_CHEMICAL_HOMEOSTASIS	352	-0.348	-1.529	0.001661	0.054884	185
3	GO_CELLULAR_RESPONSE_TO_ORGANIC_CYCL IC_COMPOUND	313	-0.327	-1.437	0.001672	0.09354	186
3	GO_REGULATION_OF_HOMEOSTATIC_PROCES S	306	-0.349	-1.529	0.001678	0.055004	187
3	GO_REGULATION_OF_GTPASE_ACTIVITY	441	-0.31	-1.382	0.001684	0.125186	188
3	GO_CELLULAR_HOMEOSTASIS	422	-0.326	-1.455	0.001686	0.08433	189
3	GO_SECRETION_BY_CELL	301	-0.327	-1.422	0.001701	0.101206	190
3	GO_REPRODUCTIVE_SYSTEM_DEVELOPMENT	263	-0.341	-1.461	0.001767	0.081171	191
3	GO_REGULATION_OF_BINDING	217	-0.361	-1.508	0.001776	0.061965	192
3	GO_EPIDERMIS_DEVELOPMENT	122	-0.429	-1.659	0.001779	0.022916	193
3	GO_ACTIVATION_OF_PROTEIN_KINASE_ACTIV ITY	199	-0.35	-1.436	0.001786	0.094089	194
3	GO_PROTEIN_TYROSINE_KINASE_ACTIVITY	113	-0.424	-1.626	0.001789	0.029136	195
3	GO_REGULATION_OF_STRESS_ACTIVATED_PR OTEIN_KINASE_SIGNALING_CASCADE	144	-0.392	-1.549	0.001812	0.048237	196
3	GO_POSITIVE_REGULATION_OF_CELL_PROJEC TION_ORGANIZATION	194	-0.369	-1.51	0.001842	0.061186	197
3	GO_REGULATION_OF_STEM_CELL_DIFFERENT IATION	73	-0.479	-1.707	0.001848	0.015892	198
3	GO_RESPONSE_TO_TEMPERATURE_STIMULUS	103	-0.467	-1.772	0.001855	0.008866	199
3	GO_REGULATION_OF_ENDOTHELIAL_CELL_MI GRATION	79	-0.463	-1.677	0.001855	0.020113	200
3	GO_REGULATION_OF_JNK_CASCADE	115	-0.416	-1.591	0.001862	0.03668	201
3	GO_EPIDERMAL_CELL_DIFFERENTIATION	66	-0.503	-1.733	0.001873	0.012715	202
3	GO_CYTOPLASMIC_MRNA_PROCESSING_BOD Y	55	-0.481	-1.636	0.00189	0.027129	203
3	GO_GROWTH_FACTOR_ACTIVITY	76	-0.488	-1.759	0.001898	0.010046	204
3	GO_REGULATION_OF_ION_HOMEOSTASIS	128	-0.426	-1.654	0.001908	0.023828	205
3	GO_REGULATION_OF_STRIATED_MUSCLE_CEL L_DIFFERENTIATION	50	-0.505	-1.678	0.001916	0.019985	206

3	GO_MESODERM_DEVELOPMENT	70	-0.483	-1.682	0.001923	0.019327	207
3	GO_DOUBLE_STRANDED_RNA_BINDING	56	-0.539	-1.809	0.001927	0.006187	208
3	GO_ENDOTHELIUM_DEVELOPMENT	58	-0.499	-1.698	0.001931	0.01698	209
3	GO_POSITIVE_REGULATION_OF_PROTEIN_LOCALIZATION_TO_NUCLEUS	100	-0.449	-1.669	0.001934	0.021418	210
3	GO_NEGATIVE_REGULATION_OF_CELL_CELL_ADHESION	96	-0.449	-1.658	0.001934	0.023207	211
3	GO_NEGATIVE_REGULATION_OF_HEMOPOIESIS	86	-0.428	-1.57	0.001934	0.042233	212
3	GO_REGULATION_OF_MYOTUBE_DIFFERENTIATION	31	-0.605	-1.82	0.001938	0.00556	213
3	GO_MICROVILLUS	48	-0.548	-1.764	0.001949	0.009527	214
3	GO_LUNG_ALVEOLUS_DEVELOPMENT	28	-0.571	-1.682	0.001969	0.019384	215
3	GO_SERINE_TYPE_ENDOPEPTIDASE_INHIBITOR_ACTIVITY	41	-0.55	-1.747	0.001976	0.011136	216
3	GO_NEGATIVE_REGULATION_OF_HOMOTYPIC_CELL_CELL_ADHESION	70	-0.483	-1.718	0.001992	0.01446	217
3	GO_RESPONSE_TO_GAMMA_RADIATION	44	-0.517	-1.655	0.00202	0.023714	218
3	GO_REGULATION_OF_TISSUE_REMODELING	43	-0.549	-1.748	0.002024	0.011067	219
3	GO_REGULATION_OF_PROTEIN_INSERTION_INTO_MITOCHONDRIAL_MEMBRANE_INVOLVED_IN_APOPTOTIC_SIGNALING_PATHWAY	28	-0.647	-1.916	0.002053	0.001981	220
3	GO_CELLULAR_RESPONSE_TO_GROWTH_HORMONE_STIMULUS	15	-0.7	-1.797	0.002096	0.006987	221
3	GO_CYSTEINE_TYPE_ENDOPEPTIDASE_REGULATOR_ACTIVITY_INVOLVED_IN_APOPTOTIC_PROCESS	30	-0.595	-1.782	0.002105	0.008047	222
3	GO_INTRINSIC_APOPTOTIC_SIGNALING_PATHWAY_IN_RESPONSE_TO_DNA_DAMAGE_BY_P53_CLASS_MEDIATOR	23	-0.64	-1.777	0.002105	0.00847	223
3	GO_PROSTATE_GLAND_DEVELOPMENT	29	-0.6	-1.742	0.002105	0.011766	224
3	GO_RESPONSE_TO_COPPER_ION	21	-0.624	-1.752	0.002128	0.010691	225
3	GO_NEGATIVE_REGULATION_OF_RESPONSE_TO_ENDOPLASMIC_RETICULUM_STRESS	29	-0.613	-1.811	0.002146	0.006087	226
3	GO_NEGATIVE_REGULATION_OF_RESPONSE_TO_BIOTIC_STIMULUS	21	-0.665	-1.812	0.002208	0.005989	227
3	GO_NEGATIVE_REGULATION_OF_DEVELOPMENTAL_PROCESS	477	-0.319	-1.424	0.003344	0.100674	228

3	GO_NEGATIVE_REGULATION_OF_PROTEIN_MODIFICATION_PROCESS	459	-0.3	-1.346	0.00335	0.149165	229
3	GO_RESPONSE_TO_ALKALOID	90	-0.445	-1.631	0.003597	0.028155	230
3	GO_REGULATION_OF_MUSCLE_CELL_DIFFERENTIATION	97	-0.421	-1.582	0.00363	0.038857	231
3	GO_RESPONSE_TO_TRANSITION_METAL_NANOPARTICLE	112	-0.398	-1.514	0.00363	0.059585	232
3	GO_DIGESTIVE_SYSTEM_DEVELOPMENT	86	-0.437	-1.593	0.00369	0.03638	233
3	GO_REGULATION_OF_JUN_KINASE_ACTIVITY	60	-0.45	-1.552	0.003697	0.04727	234
3	GO_REGULATION_OF_EPITHELIAL_CELL_MIGRATION	118	-0.419	-1.62	0.003711	0.030213	235
3	GO_POSITIVE_REGULATION_OF_PROTEIN_COMPLEX_ASSEMBLY	147	-0.392	-1.546	0.003731	0.049186	236
3	GO_REGULATION_OF_WOUND_HEALING	77	-0.462	-1.655	0.003781	0.023692	237
3	GO_PROTEIN_KINASE_B_SIGNALING	28	-0.6	-1.761	0.003795	0.00988	238
3	GO_INTRINSIC_APOPTOTIC_SIGNALING_PATHWAY	118	-0.417	-1.611	0.003795	0.032224	239
3	GO_NEGATIVE_REGULATION_OF_CYTOPLASMIC_TRANSPORT	90	-0.433	-1.591	0.003802	0.036801	240
3	GO_NEGATIVE_REGULATION_OF_PROTEIN_MODIFICATION_BY_SMALL_PROTEIN_CONJUGATION_OR_REMOVAL	120	-0.422	-1.615	0.003824	0.031384	241
3	GO_APOPTOTIC_MITOCHONDRIAL_CHANGES	45	-0.541	-1.762	0.003839	0.00978	242
3	GO_REGULATION_OF_CYSTEINE_TYPE_ENDOPEPTIDASE_ACTIVITY_INVOLVED_IN_APOPTOTIC_SIGNALING_PATHWAY	19	-0.765	-2.072	0.003899	2.25E-04	243
3	GO_REGULATION_OF_SMOOTH_MUSCLE_CELL_PROLIFERATION	71	-0.452	-1.599	0.003922	0.034886	244
3	GO_THREONINE_TYPE_PEPTIDASE_ACTIVITY	18	-0.664	-1.775	0.00409	0.008603	245
3	GO_CARDIAC_CELL_DEVELOPMENT	30	-0.598	-1.791	0.004141	0.007467	246
3	GO_RESPONSE_TO_PROGESTERONE	34	-0.557	-1.701	0.004175	0.016697	247
3	GO_POSITIVE_REGULATION_OF_PEPTIDYL_THREONINE_PHOSPHORYLATION	16	-0.675	-1.747	0.004264	0.011211	248
3	GO_INTRINSIC_APOPTOTIC_SIGNALING_PATHWAY_IN_RESPONSE_TO_ENDOPLASMIC_RETICULUM_STRESS	23	-0.646	-1.865	0.004338	0.003405	249
3	GO_CALCIUM_ION_BINDING	348	-0.311	-1.358	0.005008	0.14083	250
3	GO_REGULATION_OF_METAL_ION_TRANSPORT	195	-0.356	-1.464	0.005338	0.07971	251

3	GO_CELLULAR_RESPONSE_TO_EXTRACELLULAR_STIMULUS	140	-0.396	-1.547	0.005415	0.048659	252
3	GO_REGULATION_OF_RNA_STABILITY	119	-0.393	-1.512	0.005445	0.060268	253
3	GO_STRESS_ACTIVATED_PROTEIN_KINASE_SIGNALING_CASCADE	81	-0.442	-1.586	0.005474	0.038108	254
3	GO_NEGATIVE_REGULATION_OF_HOMEOSTATIC_PROCESS	97	-0.436	-1.62	0.005484	0.030194	255
3	GO_REGULATION_OF_CALCIUM_ION_TRANSPORT_INTO_CYTOSOL	54	-0.492	-1.682	0.005576	0.019345	256
3	GO_POSITIVE_REGULATION_OF_EPITHELIAL_CELL_MIGRATION	76	-0.466	-1.663	0.005714	0.022361	257
3	GO_POSITIVE_REGULATION_OF_JUN_KINASE_ACTIVITY	49	-0.493	-1.586	0.005758	0.03799	258
3	GO_MESODERM_MORPHOGENESIS	38	-0.529	-1.659	0.005769	0.023037	259
3	GO_REGULATION_OF_COAGULATION	53	-0.533	-1.788	0.006	0.00761	260
3	GO_POSITIVE_REGULATION_OF_ENDOTHELIAL_CELL_MIGRATION	49	-0.511	-1.674	0.00611	0.020551	261
3	GO_PERINUCLEAR_REGION_OF_CYTOPLASM	462	-0.3	-1.349	0.006441	0.146829	262
3	GO_EPITHELIAL_CELL_DIFFERENTIATION	280	-0.335	-1.433	0.006814	0.095422	263
3	GO_PROTEIN_HETERODIMERIZATION_ACTIVITY	286	-0.316	-1.363	0.00713	0.137328	264
3	GO_NEGATIVE_REGULATION_OF_SEQUENCE_SPECIFIC_DNA_BINDING_TRANSCRIPTION_FACTOR_ACTIVITY	98	-0.406	-1.52	0.007194	0.057548	265
3	GO_RIBONUCLEOPROTEIN_GRANULE	108	-0.42	-1.598	0.007207	0.035212	266
3	GO_NEGATIVE_REGULATION_OF_WNT_SIGNALING_PATHWAY	134	-0.363	-1.423	0.007207	0.101101	267
3	GO_REGULATION_OF_MUSCLE_SYSTEM_PROCESS	121	-0.404	-1.563	0.007366	0.04406	268
3	GO_REGULATION_OF_EPITHELIAL_CELL_PROLIFERATION	184	-0.346	-1.414	0.007394	0.106143	269
3	GO_REGULATION_OF_BLOOD_CIRCULATION	157	-0.366	-1.474	0.007477	0.07507	270
3	GO_CELLULAR_RESPONSE_TO_ACID_CHEMICAL	113	-0.424	-1.618	0.007533	0.030759	271
3	GO_NEGATIVE_REGULATION_OF_CELL_DEVELOPMENT	184	-0.354	-1.441	0.00759	0.091381	272
3	GO_NEGATIVE_REGULATION_OF_PROTEIN_BINDING	61	-0.475	-1.653	0.007752	0.023892	273
3	GO_HEAT_SHOCK_PROTEIN_BINDING	70	-0.442	-1.555	0.007874	0.046292	274

3	GO_NEGATIVE_REGULATION_OF_NUCLEOCYT OPLASMIC_TRANSPORT	59	-0.483	-1.629	0.007984	0.02862	275
3	GO_RESPONSE_TO_ISOQUINOLINE_ALKALOID	21	-0.62	-1.714	0.008	0.015088	276
3	GO_MESENCHYME_MORPHOGENESIS	24	-0.569	-1.597	0.008097	0.035327	277
3	GO_NEGATIVE_REGULATION_OF_PROTEIN_M ATURATION	26	-0.572	-1.652	0.00818	0.024075	278
3	GO_CELLULAR_RESPONSE_TO_VITAMIN	22	-0.663	-1.804	0.008264	0.006516	279
3	GO_RESPONSE_TO_PEPTIDE	280	-0.324	-1.389	0.008347	0.120975	280
3	GO_HIPPO_SIGNALING	20	-0.614	-1.694	0.008403	0.017537	281
3	GO_REGULATION_OF_PROTEIN_OLIGOMERIZ ATION	27	-0.586	-1.709	0.008421	0.015654	282
3	GO_ADENYLYLTRANSFERASE_ACTIVITY	20	-0.627	-1.699	0.008475	0.016916	283
3	GO_DEVELOPMENTAL_PROCESS_INVOLVED_I N_REPRODUCTION	365	-0.308	-1.347	0.008547	0.148952	284
3	GO_REGULATION_OF_ENDOPLASMIC_RETICU LUM_STRESS_INDUCED_INTRINSIC_APOPTOTI C_SIGNALING_PATHWAY	25	-0.607	-1.75	0.008677	0.010882	285
3	GO_NEGATIVE_REGULATION_OF_STRIATED_ MUSCLE_CELL_DIFFERENTIATION	18	-0.672	-1.737	0.008753	0.012258	286
3	GO_CYSTEINE_TYPE_ENDOPEPTIDASE_INHIBIT OR_ACTIVITY_INVOLVED_IN_APOPTOTIC_PRO CESS	15	-0.664	-1.695	0.008753	0.017384	287
3	GO_CELL_JUNCTION_ORGANIZATION	115	-0.394	-1.505	0.008945	0.062988	288
3	GO_FORMATION_OF_PRIMARY_GERM_LAYER	70	-0.452	-1.585	0.009416	0.038163	289
3	GO_REGULATION_OF_HORMONE_SECRETION	148	-0.378	-1.505	0.009615	0.062817	290
3	GO_SKIN_EPIDERMIS_DEVELOPMENT	36	-0.517	-1.611	0.009653	0.032225	291
3	GO_CELL_CYCLE_ARREST	116	-0.391	-1.496	0.009709	0.066296	292
3	GO_REGULATION_OF_ANATOMICAL_STRUCT URE_SIZE	294	-0.314	-1.355	0.009788	0.142978	293
3	GO_PHOSPHATASE_COMPLEX	36	-0.523	-1.583	0.00998	0.038763	294
3	GO_NON_MEMBRANE_SPANNING_PROTEIN_ TYROSINE_KINASE_ACTIVITY	35	-0.549	-1.689	0.010204	0.018327	295
3	GO_POSITIVE_REGULATION_OF_HOMEOSTATI C_PROCESS	144	-0.377	-1.479	0.010619	0.073014	296
3	GO_NEGATIVE_REGULATION_OF_CELL_KILLIN G	15	-0.706	-1.752	0.010776	0.010631	297
3	GO_REGULATION_OF_ORGAN_MORPHOGENE SIS	168	-0.356	-1.442	0.011009	0.091011	298

3	GO_VASODILATION	15	-0.675	-1.745	0.011013	0.011402	299
3	GO_PEPTIDYL_TYROSINE_MODIFICATION	118	-0.389	-1.513	0.011173	0.059984	300
3	GO_CYCLIC_NUCLEOTIDE_BINDING	17	-0.659	-1.737	0.011186	0.012333	301
3	KEGG_RIBOSOME	77	-0.425	-1.529	0.011472	0.054864	302
3	GO_NEGATIVE_REGULATION_OF_PHOSPHORYLATION	309	-0.305	-1.309	0.01157	0.178764	303
3	GO_RNA_POLYMERASE_II_TRANSCRIPTION_FACTOR_ACTIVITY_SEQUENCE_SPECIFIC_DNA_BINDING	351	-0.297	-1.308	0.011686	0.179638	304
3	GO_NEGATIVE_REGULATION_OF_MUSCLE_CELL_DIFFERENTIATION	36	-0.542	-1.662	0.011811	0.022389	305
3	GO_REGULATION_OF_SMOOTH_MUSCLE_CONTRACTION	31	-0.549	-1.651	0.012346	0.024182	306
3	GO_REGULATION_OF_THYMOCYTE_AGGREGATION	18	-0.638	-1.659	0.012552	0.022916	307
3	GO_ENDOCRINE_PANCREAS_DEVELOPMENT	19	-0.612	-1.653	0.012766	0.023901	308
3	GO_MICROVILLUS_ORGANIZATION	17	-0.664	-1.72	0.012793	0.014233	309
3	GO_MOVEMENT_IN_ENVIRONMENT_OF_OTHER_ORGANISM_INVOLVED_IN_SYMBIOTIC_INTERACTION	73	-0.448	-1.579	0.012868	0.03962	310
3	KEGG_TYPE_II_DIABETES_MELLITUS	32	-0.534	-1.614	0.012987	0.031599	311
3	GO_FEMALE_GAMETE_GENERATION	51	-0.484	-1.625	0.013109	0.029222	312
3	KEGG_P53_SIGNALING_PATHWAY	60	-0.436	-1.513	0.013183	0.060097	313
3	GO_REGULATION_OF_PROTEIN_COMPLEX_ASSEMBLY	269	-0.317	-1.339	0.013793	0.154672	314
3	GO_ADHERENS_JUNCTION_ORGANIZATION	42	-0.489	-1.545	0.014056	0.049491	315
3	GO_PLATELET_DERIVED_GROWTH_FACTOR_RECEPTOR_SIGNALING_PATHWAY	32	-0.554	-1.669	0.01417	0.021418	316
3	GO_MORPHOGENESIS_OF_A_BRANCHING_STRUCTURE	98	-0.38	-1.428	0.014311	0.098376	317
3	GO_RESPONSE_TO_COLD	32	-0.517	-1.55	0.014315	0.047791	318
3	GO_MAMMARY_GLAND_EPITHELIUM_DEVELOPMENT	33	-0.533	-1.612	0.014799	0.031922	319
3	GO_NEGATIVE_REGULATION_OF_BINDING	100	-0.397	-1.488	0.014842	0.069446	320
3	HALLMARK_ANDROGEN_RESPONSE	85	-0.409	-1.5	0.015209	0.064675	321
3	GO_ENDOCYTOSIS	345	-0.296	-1.298	0.015679	0.18803	322

3	GO_POSITIVE_REGULATION_OF_ORGANELLE_ASSEMBLY	35	-0.533	-1.655	0.015717	0.023682	323
3	GO_CELLULAR_RESPONSE_TO_AMINO_ACID_STIMULUS	36	-0.508	-1.538	0.015905	0.051577	324
3	GO_INTERACTION_WITH_SYMBIONT	38	-0.502	-1.587	0.015968	0.037605	325
3	GO_CELL_CELL_JUNCTION	231	-0.316	-1.331	0.016043	0.160415	326
3	GO_REGULATION_OF_VASOCONSTRICTION	32	-0.531	-1.612	0.016129	0.032024	327
3	GO_RESPONSE_TO_ZINC_ION	39	-0.5	-1.604	0.016129	0.033741	328
3	GO_POSITIVE_REGULATION_OF_VASOCONSTRICTION	18	-0.649	-1.746	0.016393	0.011252	329
3	GO_SULFUR_COMPOUND_BINDING	134	-0.365	-1.428	0.016453	0.098268	330
3	GO_POSITIVE_REGULATION_OF_CELL_DEVELOPMENT	294	-0.31	-1.325	0.016892	0.16572	331
3	GO_HETEROTYPIC_CELL_CELL_ADHESION	22	-0.574	-1.637	0.016949	0.027095	332
3	GO_PROTEIN_SECRETION	73	-0.418	-1.498	0.016981	0.065452	333
3	GO_PROTEIN_SELF_ASSOCIATION	32	-0.545	-1.653	0.017316	0.023928	334
3	GO_ER_NUCLEUS_SIGNALING_PATHWAY	30	-0.54	-1.602	0.017341	0.034162	335
3	GO_PEPTIDE_HORMONE_PROCESSING	17	-0.632	-1.646	0.017354	0.025014	336
3	GO_SEGMENTATION	49	-0.447	-1.499	0.017787	0.065099	337
3	HALLMARK_COAGULATION	94	-0.389	-1.436	0.017822	0.093795	338
3	GO_REGULATION_OF_FILOPODIUM_ASSEMBLY	28	-0.556	-1.61	0.018405	0.032407	339
3	GO_PODOSOME	20	-0.562	-1.553	0.01848	0.046864	340
3	GO_JNK_CASCADE	66	-0.444	-1.532	0.018622	0.053659	341
3	GO_RESPONSE_TO_GROWTH_FACTOR	323	-0.298	-1.292	0.018676	0.193757	342
3	BIOCARTA_CASPASE_PATHWAY	22	-0.589	-1.602	0.019048	0.034205	343
3	GO_CELLULAR_RESPONSE_TO_ALCOHOL	77	-0.402	-1.444	0.019084	0.089997	344
3	GO_VASCULATURE_DEVELOPMENT	313	-0.304	-1.306	0.019164	0.181083	345
3	GO_MAMMARY_GLAND_DUCT_MORPHOGENESIS	16	-0.616	-1.596	0.019272	0.035496	346
3	GO_CYTOSOLIC_SMALL_RIBOSOMAL_SUBUNIT	37	-0.493	-1.539	0.019313	0.051336	347
3	GO_CELL_DEATH_IN_RESPONSE_TO_OXIDATIVE_STRESS	16	-0.635	-1.622	0.019438	0.029955	348
3	GO_POSITIVE_REGULATION_OF_EPIDERMIS_DEVELOPMENT	18	-0.585	-1.561	0.019481	0.044805	349

3	GO_POSITIVE_REGULATION_OF_STEM_CELL_DIFFERENTIATION	33	-0.514	-1.528	0.019493	0.055054	350
3	HALLMARK_P53_PATHWAY	163	-0.341	-1.366	0.019538	0.135675	351
3	GO_REGULATION_OF_HORMONE_LEVELS	262	-0.315	-1.325	0.019643	0.165644	352
3	GO_REGULATION_OF_PROTEIN_TYROSINE_KINASE_ACTIVITY	46	-0.475	-1.54	0.020325	0.050983	353
3	GO_POSITIVE_REGULATION_OF_CANONICAL_WNT_SIGNALING_PATHWAY	85	-0.422	-1.535	0.020522	0.052536	354
3	GO_REGULATION_OF_VESICLE_MEDIATED_TRANSPORT	312	-0.303	-1.309	0.020548	0.178794	355
3	GO_NEGATIVE_REGULATION_OF_ANOIKIS	16	-0.646	-1.677	0.02079	0.020061	356
3	GO_POSITIVE_REGULATION_OF_PROTEIN_MODIFICATION_BY_SMALL_PROTEIN_CONJUGATION_OR_REMOVAL	165	-0.336	-1.367	0.020873	0.135071	357
3	GO_CYSTEINE_TYPE_ENDOPEPTIDASE_INHIBITOR_ACTIVITY	28	-0.533	-1.556	0.021142	0.045997	358
3	BIOCARTA_PML_PATHWAY	17	-0.615	-1.614	0.021459	0.031586	359
3	GO_NEGATIVE_REGULATION_OF_CANONICAL_WNT_SIGNALING_PATHWAY	116	-0.372	-1.435	0.021505	0.094266	360
3	GO_ACTIVATION_OF_JUN_KINASE_ACTIVITY	30	-0.525	-1.558	0.021569	0.045397	361
3	GO_NEGATIVE_REGULATION_OF_TELOMERE_MAINTENANCE	20	-0.571	-1.584	0.021978	0.038532	362
3	GO_NEGATIVE_REGULATION_OF_INTRACELLULAR_PROTEIN_TRANSPORT	74	-0.418	-1.485	0.022059	0.070758	363
3	GO_POSITIVE_REGULATION_OF_ACTIN_FILAMENT_POLYMERIZATION	45	-0.481	-1.558	0.022133	0.04568	364
3	GO_REGULATION_OF_OSTEOCLAST_DIFFERENTIATION	43	-0.47	-1.496	0.022267	0.066442	365
3	GO_POSITIVE_REGULATION_OF_TISSUE_REMODELING	21	-0.586	-1.607	0.022321	0.032967	366
3	GO_NEGATIVE_REGULATION_OF_SMOOTH_MUSCLE_CELL_PROLIFERATION	25	-0.543	-1.563	0.022573	0.044056	367
3	GO_HORMONE_RECEPTOR_BINDING	112	-0.365	-1.393	0.022599	0.11857	368
3	GO_DEVELOPMENT_OF_PRIMARY_SEXUAL_CHARACTERISTICS	122	-0.377	-1.462	0.022684	0.081108	369
3	GO_PROTEIN_ACTIVATION_CASCADE	39	-0.488	-1.528	0.022965	0.055153	370
3	GO_REGULATION_OF_MEMBRANE_PROTEIN_ECTODOMAIN_PROTEOLYSIS	16	-0.632	-1.611	0.023158	0.032252	371
3	GO_RESPONSE_TO_GONADOTROPIN	20	-0.625	-1.654	0.023404	0.023884	372

3	GO_EXONUCLEASE_ACTIVITY	58	-0.442	-1.497	0.023669	0.065916	373
3	GO_POSITIVE_REGULATION_OF_ORGANELLE_ ORGANIZATION	414	-0.287	-1.281	0.023689	0.204445	374
3	GO_TRANSCRIPTION_FROM_RNA_POLYMERA SE_II_PROMOTER	482	-0.287	-1.281	0.024077	0.203913	375
3	KEGG_PROSTATE_CANCER	79	-0.405	-1.443	0.024254	0.090173	376
3	GO_RESPONSE_TO_GROWTH_HORMONE	21	-0.615	-1.683	0.024336	0.019285	377
3	GO_SOMITOGENESIS	33	-0.501	-1.507	0.024691	0.062071	378
3	GO_OVULATION_CYCLE	70	-0.426	-1.52	0.025194	0.057556	379
3	BIOCARTA_STRESS_PATHWAY	22	-0.575	-1.594	0.025478	0.036117	380
3	GO_COLUMNAR_CUBOIDAL_EPITHELIAL_CELL _DIFFERENTIATION	63	-0.421	-1.464	0.025641	0.079972	381
3	GO_NEURAL_NUCLEUS_DEVELOPMENT	49	-0.465	-1.52	0.025794	0.057627	382
3	GO_NEGATIVE_REGULATION_OF_ADHERENS_ JUNCTION_ORGANIZATION	15	-0.641	-1.598	0.02603	0.03518	383
3	GO_CORE_PROMOTER_BINDING	113	-0.371	-1.408	0.026168	0.109991	384
3	GO_HETEROPHILIC_CELL_CELL_ADHESION_VI A_PLASMA_MEMBRANE_CELL_ADHESION_M OLECULES	23	-0.54	-1.522	0.02621	0.056946	385
3	GO_REGULATION_OF_ENDOCRINE_PROCESS	23	-0.542	-1.553	0.026423	0.046996	386
3	GO_REGENERATION	115	-0.362	-1.393	0.026465	0.118485	387
3	GO_GROWTH	246	-0.316	-1.329	0.026667	0.162137	388
3	GO_MEMBRANE_PROTEIN_PROTEOLYSIS	28	-0.513	-1.508	0.02686	0.061887	389
3	GO_SOMITE_DEVELOPMENT	39	-0.47	-1.497	0.026915	0.065837	390
3	GO_NEGATIVE_REGULATION_OF_CELL_MORP HOGENESIS_INVOLVED_IN_DIFFERENTIATION	76	-0.411	-1.494	0.026923	0.067173	391
3	GO_OUTER_MEMBRANE	142	-0.348	-1.363	0.027273	0.1379	392
3	GO_CIRCULATORY_SYSTEM_PROCESS	192	-0.33	-1.351	0.027273	0.145684	393
3	GO_TRANSLATION_ELONGATION_FACTOR_AC TIVITY	16	-0.616	-1.594	0.027368	0.036161	394
3	GO_NEGATIVE_REGULATION_OF_TRANSFERA SE_ACTIVITY	273	-0.309	-1.322	0.027372	0.1674	395
3	GO_REGULATION_OF_PEPTIDE_SECRETION	121	-0.365	-1.403	0.027473	0.11288	396
3	GO_PANCREAS_DEVELOPMENT	36	-0.498	-1.526	0.027505	0.055527	397
3	GO_TISSUE_MORPHOGENESIS	319	-0.292	-1.268	0.027539	0.215723	398

3	BIOCARTA_EGF_PATHWAY	29	-0.531	-1.575	0.027833	0.040824	399
3	GO_TRANSCRIPTIONAL_ACTIVATOR_ACTIVITY_RNA_POLYMERASE_II_TRANSCRIPTION_REGULATORY_REGION_SEQUENCE_SPECIFIC_BINDING	181	-0.321	-1.322	0.028169	0.167772	400
3	GO_RNA_POLYADENYLATION	25	-0.536	-1.527	0.029014	0.055401	401
3	GO_CARDIAC_ATRIUM_DEVELOPMENT	19	-0.569	-1.526	0.029213	0.055759	402
3	GO_SENSORY_ORGAN_DEVELOPMENT	269	-0.302	-1.284	0.029463	0.20151	403
3	GO_POSITIVE_REGULATION_OF_CALCIUM_ION_TRANSPORT	64	-0.419	-1.46	0.029586	0.081666	404
3	GO_REGULATION_OF_CATION_TRANSMEMBRANE_TRANSPORT	126	-0.353	-1.361	0.03	0.139237	405
3	GO_CYSTEINE_TYPE_PEPTIDASE_ACTIVITY	134	-0.344	-1.363	0.030075	0.137425	406
3	GO_KINASE_REGULATOR_ACTIVITY	140	-0.344	-1.357	0.030189	0.141642	407
3	GO_RESPONSE_TO_METAL_ION	246	-0.313	-1.318	0.030357	0.170743	408
3	GO_REGULATION_OF_CELL_MORPHOGENESIS	374	-0.287	-1.256	0.030405	0.227779	409
3	BIOCARTA_KERATINOCYTE_PATHWAY	41	-0.484	-1.54	0.030426	0.051057	410
3	GO_REGULATION_OF_CANONICAL_WNT_SIGNALING_PATHWAY	157	-0.348	-1.39	0.030576	0.120748	411
3	GO_FRIZZLED_BINDING	18	-0.586	-1.566	0.031683	0.043355	412
3	GO_SIGNAL_TRANSDUCTION_BY_P53_CLASS_MEDIATOR	101	-0.377	-1.418	0.031716	0.103513	413
3	GO_POSITIVE_REGULATION_OF_HORMONE_SECRETION	64	-0.419	-1.446	0.031776	0.088724	414
3	BIOCARTA_TID_PATHWAY	18	-0.634	-1.645	0.031915	0.025218	415
3	GO_NEURON_PROJECTION_REGENERATION	23	-0.579	-1.614	0.031983	0.031617	416
3	GO_REGULATION_OF_OXIDATIVE_STRESS_INDUCED_INTRINSIC_APOPTOTIC_SIGNALING_PATHWAY	23	-0.531	-1.519	0.03299	0.057988	417
3	GO_REGULATION_OF_SMOOTH_MUSCLE_CELL_MIGRATION	37	-0.478	-1.502	0.033333	0.06419	418
3	GO_EXTRACELLULAR_MATRIX	211	-0.325	-1.347	0.033989	0.148222	419
3	GO_REGULATION_OF_BMP_SIGNALING_PATHWAY	44	-0.465	-1.494	0.034115	0.067194	420
3	GO_EMBRYONIC_PLACENTA_MORPHOGENESIS	15	-0.62	-1.566	0.034274	0.043191	421
3	GO_PEPTIDYL_TYROSINE_AUTOPHOSPHORYLATION	30	-0.51	-1.539	0.034483	0.05114	422

3	GO_POSITIVE_REGULATION_OF_PROTEIN_KINASE_B_SIGNALING	54	-0.437	-1.461	0.034483	0.081212	423
3	GO_MALE_SEX_DIFFERENTIATION	90	-0.389	-1.426	0.034816	0.099716	424
3	GO_NEGATIVE_REGULATION_OF_PEPTIDYL_TYROSINE_PHOSPHORYLATION	32	-0.494	-1.497	0.035294	0.065696	425
3	GO_POSITIVE_REGULATION_OF_WNT_SIGNALING_PATHWAY	109	-0.372	-1.402	0.035336	0.112931	426
3	GO_CELLULAR_RESPONSE_TO_NITROGEN_COMPOUND	350	-0.283	-1.238	0.035889	0.24644	427
3	GO_EMBRYONIC_EYE_MORPHOGENESIS	15	-0.607	-1.561	0.036	0.044781	428
3	GO_REGULATION_OF_PROTEIN_EXPORT_FROM_NUCLEUS	30	-0.521	-1.534	0.036217	0.053082	429
3	HALLMARK_KRAS_SIGNALING_DN	85	-0.379	-1.388	0.036217	0.121575	430
3	GO_POSITIVE_REGULATION_OF_ION_TRANSPORT	134	-0.341	-1.336	0.03643	0.156903	431
3	GO_CELLULAR_RESPONSE_TO_DRUG	43	-0.469	-1.498	0.036538	0.065418	432
3	GO_POSITIVE_REGULATION_OF_OSSIFICATION	56	-0.428	-1.436	0.03668	0.094003	433
3	GO_REGULATION_OF_ENDOCYTOSIS	148	-0.334	-1.322	0.0369	0.168135	434
3	KEGG_PRION_DISEASES	27	-0.517	-1.493	0.03719	0.067279	435
3	GO_POSITIVE_REGULATION_OF_EPITHELIAL_CELL_PROLIFERATION	90	-0.38	-1.399	0.037255	0.115103	436
3	GO_POSITIVE_REGULATION_OF_EPITHELIAL_TO_MESENCHYMAL_TRANSITION	24	-0.561	-1.549	0.0375	0.048236	437
3	GO_REGULATION_OF_CELL_SUBSTRATE_ADHESION	120	-0.357	-1.357	0.038328	0.141677	438
3	GO_POSITIVE_REGULATION_OF_PROTEIN_AUTOPHOSPHORYLATION	18	-0.603	-1.587	0.03956	0.037645	439
3	GO_REGULATION_OF_NUCLEASE_ACTIVITY	20	-0.573	-1.553	0.039823	0.047111	440
3	GO_REGULATION_OF_PHOSPHOPROTEIN_PHOSPHATASE_ACTIVITY	44	-0.47	-1.508	0.040404	0.061955	441
3	GO_MAMMARY_GLAND_MORPHOGENESIS	22	-0.545	-1.503	0.040404	0.063687	442
3	GO_REGULATION_OF_PROTEIN_PHOSPHATASE_TYPE_2A_ACTIVITY	19	-0.564	-1.516	0.040984	0.059095	443
3	GO_CELL_DIFFERENTIATION_INVOLVED_IN_EMBRYONIC_PLACENTA_DEVELOPMENT	16	-0.589	-1.523	0.041237	0.056632	444
3	BIOCARTA_FAS_PATHWAY	30	-0.507	-1.517	0.041237	0.058815	445
3	GO_EMBRYONIC_DIGESTIVE_TRACT_DEVELOPMENT	19	-0.561	-1.49	0.041322	0.068545	446

3	GO_MODULATION_OF_TRANSCRIPTION_IN_OTHER_ORGANISM_INVOLVED_IN_SYMBIOTIC_INTERACTION	17	-0.591	-1.542	0.041408	0.050441	447
3	GO_VESICLE_LUMEN	58	-0.43	-1.47	0.041746	0.07716	448
3	GO_PROTEIN_KINASE_C_BINDING	38	-0.496	-1.542	0.042105	0.050542	449
3	GO_PROTEIN_K48_LINKED_UBIQUITINATION	42	-0.451	-1.44	0.042308	0.091902	450
3	GO_MEMBRANE_PROTEIN_ECTODOMAIN_PROTEOLYSIS	18	-0.565	-1.527	0.042463	0.055321	451
3	GO_ACTIN_BASED_CELL_PROJECTION	117	-0.358	-1.358	0.042593	0.141463	452
3	GO_POSITIVE_REGULATION_OF_TRANSLATIONAL_INITIATION	20	-0.538	-1.468	0.042735	0.078064	453
3	GO_ENDOCARDIAL_CUSHION_DEVELOPMENT	24	-0.526	-1.508	0.04277	0.061865	454
3	GO_REGULATION_OF_CELL_PROJECTION_ASSEMBLY	109	-0.354	-1.336	0.04291	0.156631	455
3	GO_NEGATIVE_REGULATION_OF_MYOBLAST_DIFFERENTIATION	15	-0.608	-1.528	0.042945	0.055081	456
3	GO_NEGATIVE_REGULATION_OF_CELLULAR_PROTEIN_LOCALIZATION	106	-0.368	-1.39	0.042991	0.120411	457
3	GO_GLAND_DEVELOPMENT	258	-0.299	-1.256	0.043029	0.228523	458
3	GO_REGULATION_OF_MEMBRANE_DEPOLARIZATION	30	-0.497	-1.49	0.043393	0.06852	459
3	GO_HEMOSTASIS	207	-0.311	-1.275	0.04363	0.209081	460
3	GO_CALCIUM_ION_TRANSPORT	125	-0.355	-1.375	0.044231	0.129401	461
3	GO_POSITIVE_REGULATION_OF_ORGAN_GROWTH	22	-0.528	-1.494	0.044534	0.067109	462
3	GO_POSITIVE_REGULATION_OF_CELLULAR_COMPONENT_BIOGENESIS	271	-0.301	-1.282	0.044983	0.202736	463
3	GO_MUSCLE_ADAPTATION	18	-0.578	-1.538	0.045361	0.051526	464
3	GO_PITUITARY_GLAND_DEVELOPMENT	17	-0.57	-1.516	0.046218	0.058938	465
3	GO_ESTABLISHMENT_OR_MAINTENANCE_OF_BIPOLAR_CELL_POLARITY	26	-0.511	-1.485	0.046243	0.070801	466
3	GO_TRANSCRIPTION_FACTOR_ACTIVITY_RNA_POLYMERASE_II_DISTAL_ENHANCER_SEQUENCE_SPECIFIC_BINDING	51	-0.424	-1.407	0.046243	0.110503	467
3	GO_SIGNAL_TRANSDUCTION_IN_ABSENCE_OF_LIGAND	23	-0.551	-1.55	0.046316	0.048086	468
3	GO_ANGIOGENESIS	189	-0.316	-1.3	0.046346	0.18629	469
3	GO_ENDOCRINE_PROCESS	20	-0.563	-1.517	0.046784	0.058711	470

3	KEGG_NEUROTROPHIN_SIGNALING_PATHWAY	110	-0.355	-1.359	0.046904	0.140663	471
3	GO_FEMALE_SEX_DIFFERENTIATION	67	-0.409	-1.435	0.047059	0.094241	472
3	GO_POSITIVE_REGULATION_OF_BLOOD_CIRCULATION	41	-0.455	-1.443	0.047131	0.090506	473
3	GO_REGULATION_OF_ANOIKIS	21	-0.549	-1.529	0.048319	0.054933	474
3	GO_REGULATION_OF_PROTEIN_MATURATION	54	-0.421	-1.4	0.04845	0.113937	475
3	GO_DIVALENT_INORGANIC_CATION_TRANSPORT	154	-0.336	-1.343	0.048913	0.151296	476
3	GO_POSITIVE_REGULATION_OF_PROTEIN_TYROSINE_KINASE_ACTIVITY	24	-0.525	-1.468	0.049462	0.077838	477
3	GO_POSTTRANSCRIPTIONAL_REGULATION_OF_GENE_EXPRESSION	340	-0.282	-1.239	0.049488	0.245805	478
3	GO_SIGNAL_TRANSDUCTION_IN_RESPONSE_TO_DNA_DAMAGE	83	-0.386	-1.408	0.049524	0.109547	479
3	GO_SEX_DIFFERENTIATION	149	-0.324	-1.273	0.049904	0.211077	480
3	GO_ENDOPLASMIC_RETICULUM_CALCIUM_ION_HOMEOSTASIS	17	-0.581	-1.526	0.05	0.05559	481

Chapter 3. Differential remodeling of the electron transport chain is required to support TLR3 and TLR4 signaling and cytokine production in macrophages (Ahmed *et al.*, 2019; Published in *Scientific Reports*)

3.1. Introduction

The innate immune system, including tissue macrophages, represent the first line of defence against invading microbial pathogens. Early recognition depends on a variety of pattern recognition receptors (PRRs), which detect evolutionarily conserved structures termed pathogen-associated molecular patterns (PAMPs) (1, 2). Key players in this process are the Toll-like receptors (TLR), which are capable of detecting a range of PAMPs from viruses and bacteria (1-5). Among the best characterized are TLR3 and TLR4. TLR3 recognizes double stranded RNA (dsRNA), a common PAMP associated with viral infections (6). TLR4 primarily recognizes lipopolysaccharide (LPS), the core component of the outer membrane of Gram-negative bacteria (7). Both TLR3 and TLR4 differentially and dynamically modulate nuclear factor-κB (NF-κB) and interferon regulatory factory 3 (IRF3) signaling following receptor engagement. While TLR3 activates NF-κB and IRF3 signaling via TIR-domain-containing adapter-inducing interferon-β protein (TRIF), TLR4 signals through both Myeloid differentiation primary response 88 (MyD88) and TRIF (1). Differential activation of these signaling pathways plays a critical role in fine-tuning pathogen specific antiviral and antibacterial responses (1).

Cellular metabolism has emerged as a key regulator of macrophage function. Metabolic reprogramming is required to meet the bioenergetic and biosynthetic demands of the cell and to drive effector functions (8-10). Alterations in metabolites and other bioactive metabolic products have also been shown to activate and regulate gene expression, signal transduction and epigenetic profiles (9, 11-14). Among the best characterized examples of macrophage reprogramming occurs following LPS stimulation (9, 14-18). Almost immediately after TLR4 engagement, macrophages

downregulate oxidative phosphorylation (OXPHOS) activity and dramatically increase glycolysis to support rapid ATP production (14, 15, 17-19). This repurposing of mitochondrial function also increases reactive oxygen species (ROS) production, which drives inflammatory cytokine production (9, 15, 17). ROS production is driven by the combined effects of increased mitochondrial membrane potential and the oxidation of succinate by complex II of the electron transport chain (ETC) (15) suggesting flux through the ETC may play a central role in this process. However, it is still unclear if the dynamic modulation of ETC complexes and increased ROS production contributes to signaling events following engagement of other TLRs and if differential reprogramming of these processes contributes to ligand specific immune responses.

Mitochondria are known to play an important role in innate immune responses against RNA viruses (20-23). Recognition of cytosolic viral RNA by retinoic acid-inducible gene I (RIG-I)-like receptors (RLR) and their downstream processes have been shown to require the participation of mitochondrial antiviral signaling (MAVS), a mitochondrial outer membrane adaptor protein (20, 24, 25). MAVS acts as a scaffold and recruits effector molecules to the mitochondrial outer membrane leading to the activation of NF-κB and IRF3(20). More recent studies have shown that mitochondria also contribute to antiviral signaling via MAVS independent mechanisms. Tal et al. found that mitochondrial ROS (mtROS) potentiates RLR signaling. This signaling is regulated by autophagy and clearance of dysfunctional mitochondria (26). Alternatively, Yoshizumi et al. found that RLR-mediated antiviral responses are dependent on OXPHOS activity. This dependence is regulated by the mitochondrial fusion protein optic atrophy 1 (OPA1) (23). These findings suggest that other aspects of mitochondrial function, independent of MAVS mediated scaffolding, may play a central role in facilitating antiviral responses.

While both TLR3 and RLR recognize and respond to virally derived RNAs, they signal through distinct transduction pathways to trigger antiviral immune responses (27, 28). To date, the role of the mitochondria in driving TLR3-mediated responses in macrophages is poorly understood. Previous studies have shown that engagement of TLR3 on hepatocytes and dendritic cells (DCs) causes a shift from OXPHOS towards aerobic glycolysis for energy production (29-32). In DCs, this shift is driven predominately by the *de novo* production of type I interferons (IFN) and therefore is required to rapidly meet the increased energy demands of these activated cells (30-32). Macrophages stimulated with high concentrations (10μg/mL) of the synthetic TLR3 agonist polyinosinic-polycytidylic acid (Poly(I:C) or PIC) have been shown to downregulate Complex I-associated ATP production under standard culture conditions (33). However, the functional consequences of this ETC reprogramming has yet to be elucidated.

In the current study, I used murine bone marrow-derived macrophages (BMM) to evaluate how reprogramming of mitochondrial function contributes to TLR3 and TLR4 signaling and cytokine production and how glucose availability affected these responses. I found that modulation of flux through the ETC and associated ROS production plays a critical role in cytokine production following TLR engagement. This reprogramming is ligand specific and may have differential effects on the expression of individual cytokines (e.g. accumulation of mitochondrial vs. cytosolic ROS). Further, low glucose conditions resulted in differential reprogramming of mitochondrial function following TLR3 engagement. This reprogramming upregulated complex III expression and associated mitochondrial ROS production, which amplified inflammatory and antiviral signaling and cytokine production. Collectively, these findings suggest that the ETC may act as a selective rheostat of innate immune responses that differentially regulates ligand specific responses based on nutrient availability.

3.2. Results

3.2.1. Differential production of pro-inflammatory and antiviral cytokines in PIC- and LPS-stimulated BMM.

Despite activating the same transcription factors (e.g. NF-κB and IRF3), signaling through TLR3 and TLR4 are associated with distinct inflammatory and antiviral cytokine profiles. To evaluate these differences in our model system, I stimulated BMM with PIC (10ng/ml and 10μg/ml) or LPS (100ng/ml) for 18 hours and assessed inflammatory (TNF-α, IL-1β, and IL-6) and antiviral (IFN-α, IFN-β and CXCL10) cytokine production in culture supernatants. PIC concentrations were selected to emulate responses in early (low levels of virus) and late stages of infection (high levels of virus), where Lin et al. found that only high ($\geq$ 10μg/ml) concentrations of PIC can induce robust inflammatory cytokine production (34). The LPS concentration was selected based on its ability to repurpose mitochondrial function to support ROS production (15). As previously reported (15), LPS induced a strong inflammatory response, produced intermediate levels of IFN-β and CXCL10 and no IFN-α (Figure 3.1). Alternatively, stimulation with low concentrations of PIC induced low levels of antiviral and inflammatory production. Increasing the PIC concentration (10μg/ml) significantly increased both inflammatory and antiviral cytokine production (Figure 3.1).
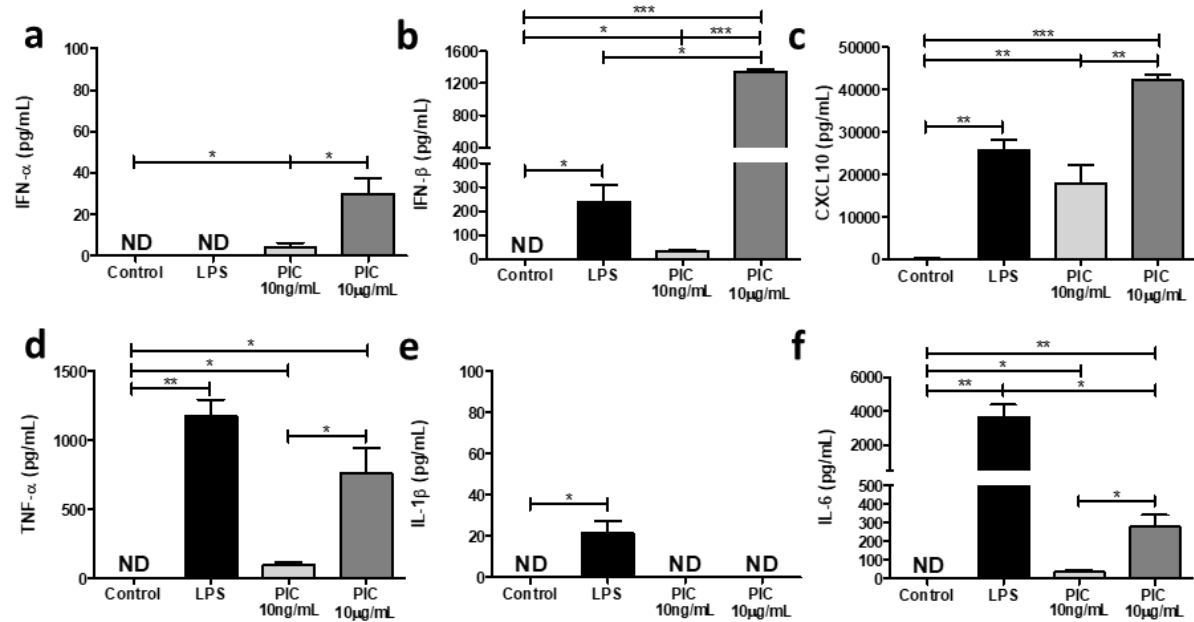
Figure 3.1: High, but not low, concentrations of Poly(I:C) are associated with pro-inflammatory cytokine production. Bone marrow-derived macrophages (BMDMs) were treated with either 100ng/mL lipopolysaccharide (LPS), 10ng/mL or 10μg/mL Poly(I:C) (PIC) for 18 hours. Supernatant was collected and assessed for antiviral (IFN-α, IFN-β, CXCL10) (a-c) and pro-inflammatory (TNF-α, IL-1β, IL-6) (d-f) cytokine expression. Data represents mean ± SEM of four individual mice (*p < 0.05, **p < 0.01, and ***p < 0.001).

3.2.2. BMM stimulated with low versus high concentrations of PIC differ in their ability to ramp up glycolytic activity under stress.

Next, I evaluated the differential effects of LPS and PIC stimulation on cellular metabolism using the Seahorse extracellular efflux analyser. As described above, BMM were stimulated with LPS (100ng/ml), low (10ng/ml) or high (10μg/ml) concentrations of PIC for 18 hours. Changes in proton efflux rate (PER) at baseline and in response to rotenone + antimycin (Rot/AA) and 2-deoxyglucose (2-DG) injections were used to evaluate changes in glycolytic parameters. As previously described (9, 35), LPS stimulation increased PER levels at baseline, increased the %PER derived from glycolysis and decreased the mitoOCR/glycoPER ratio suggesting a strong shift away from OXPHOS activity towards aerobic glycolysis (Figure 3.2). Stimulation with both concentrations of PIC also increased PER levels at baseline and increased the %PER derived from glycolysis, but this increase was significantly lower than that observed following LPS-stimulation (P<0.001). Further, the reduction in the mitoOCR/glycoPER ratio was less pronounced suggesting that PIC-stimulated cells maintain higher levels of OXPHOS activity (Figure 3.2C). Despite similar basal PER levels (Figure 3.2B), low and high concentrations of PIC differentially affected the ability of BMM to ramp up glycolysis following stress with Rot/AA. While cells stimulated with lower concentrations maintained their ability to increase glycolytic activity following exposure to Rot/AA, cells stimulated with higher concentrations were unable to do so, suggesting they may be functioning at their maximum glycolytic capacity (Figure 3.2A).
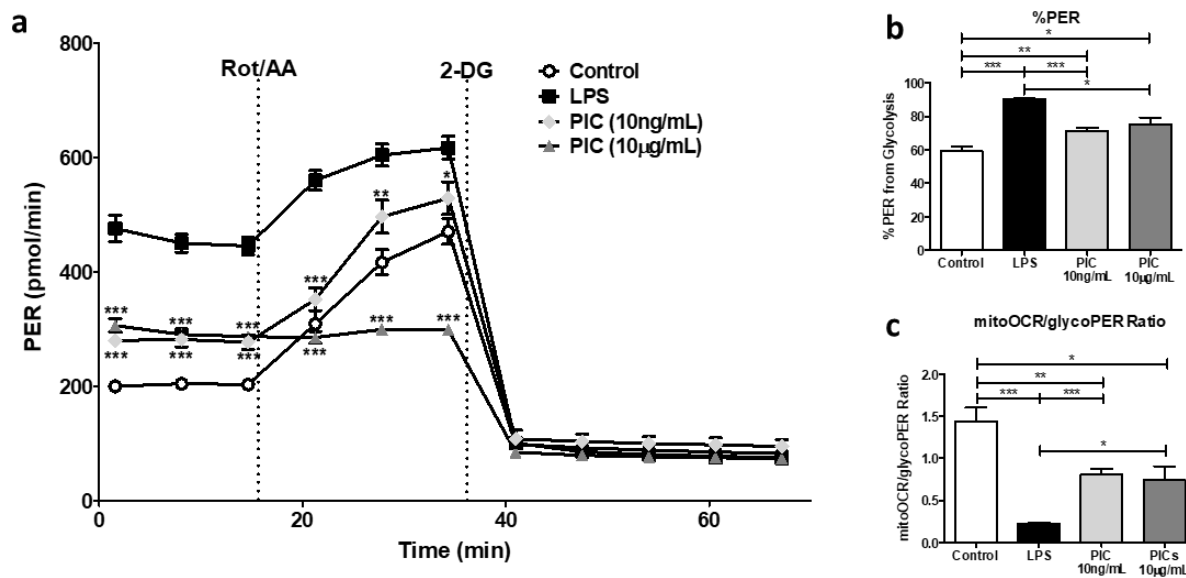
Figure 3.2: Macrophages activated using higher concentrations of Poly(I:C) are functioning near their maximum glycolytic capacity. BMDMs were seeded onto Seahorse XFp miniplates and treated with 100ng/mL LPS, 10ng/mL or 10μg/mL PIC for 18 hours. Glycolytic activity, indicated by the proton efflux rate (PER) was measured using sequential injections of rotenone plus antimycin A (Rot/AA) and 2-deoxyglucose (2-DG) (a), determining the %PER dependent on glycolysis (b) and the ratio of mitochondrial oxygen consumption rate (mitoOCR) to glycolytic PER (c). Data represents mean ± SEM of four individual mice. The levels of significance shown in Figure 2a represent pairwise comparisons against LPS-treated macrophages (*$p < 0.05$, **$p < 0.01$, and ***$p < 0.001$).

3.2.3. *Maintenance of OXPHOS activity is an important for PIC but not LPS stimulation.*

To evaluate specific changes in OXPHOS activity, I used the Cell Mito Stress Test kit from Agilent. Features of OXPHOS activity were calculated based on changes in oxygen consumption rate (OCR) in response to successive injections of oligomycin (Oligo), carbonyl cyanide 4-(trifluoromethoxy)phenylhydrazone (FCCP) and ROT/AA. Consistent with the literature (9, 19, 36), LPS stimulation dramatically reduced basal respiration, reduced mitochondrial ATP production, and reduced the ability of cells to increase oxygen consumption (e.g. spare respiratory capacity [SRC]) following FCCP treatment (Figure 3.3). High concentrations of PIC also reduced levels of basal respiration, ATP production and SRC compared to untreated cells but this impairment was less severe than that observed for LPS (basal respiration $p<0.05$, SRC $p<0.01$, ATP production $P=0.08$). Interestingly, low concentrations of PIC did not alter basal respiration or ATP production but significantly reduced SRC suggesting these cells may have a reduced capacity to deal with stress (Figure 3.3; 37). Given these differences in glycolysis and oxygen consumption the remaining experiments were performed using low concentration PIC (10ng/ml).
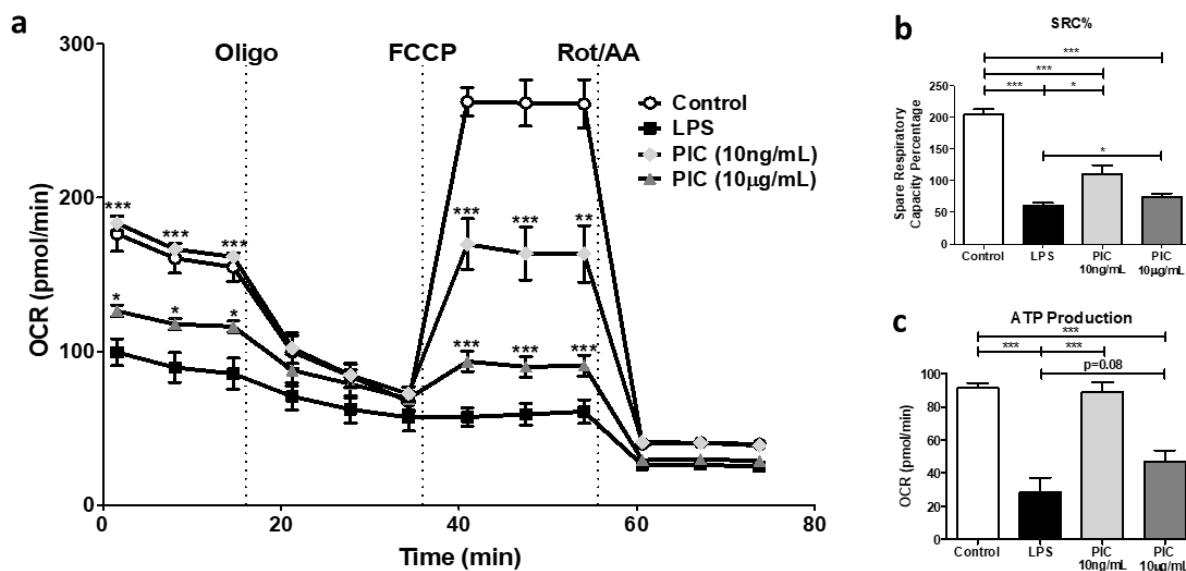
Figure 3.3: Poly(I:C) stimulation is linked to low sustained levels of oxidative phosphorylation (OXPHOS). Macrophages were plated onto Seahorse XFp miniplates and subsequently stimulated with 100ng/mL LPS, 10μg/mL or 10ng/mL PIC for 18 hours. OXPHOS function was assessed *via* successive Oligomycin (Oligo), Carbonyl cyanide-*p*-trifluoromethoxyphenylhydrazone (FCCP), and Rot/AA injections **(a)**, quantifying the spare respiratory capacity percentage (SRC%) **(b)** and ATP production **(c)**. Data represents mean ± SEM of four individual mice. The levels of significance shown in Figure 3a is based on pairwise comparisons to LPS-treated macrophages (*p < 0.05, **p < 0.01, and ***p < 0.001).

3.2.4. *Reduced glucose availability is associated with increased inflammatory and antiviral cytokine production in PIC- but not LPS-stimulated BMM*

Macrophages are highly plastic cells whose responses are modified by environmental cues including nutrient availability (38-41). A recent study in BMM showed that cells are less dependent on OXPHOS activity under condition of high glucose (>10 mM) and preferentially use aerobic glycolysis to rapidly produce ATP (23). Given the differential ability of BMM to reprogram OXPHOS activity based on glucose availability, I then evaluated how glucose levels affected TLR3 and TLR4 signaling and cytokine production. Most studies have been performed in standard culture conditions, which represent supra-physiological concentrations of glucose. For these studies, BMM were stimulated with LPS (100ng/ml) and PIC (10ng/ml) in standard (25mM) and low glucose (0.5mM) conditions. For the remainder of this paper, standard culture conditions will be referred as high glucose. Glucose levels had no effect on pro-inflammatory cytokine production in LPS-stimulated cells (Figure 3.4A-E) suggesting that even low glucose levels are sufficient to support TLR4 responses. Conversely, low glucose conditions increased pro-inflammatory (TNF-α, IL-6) and IFN-associated cytokine production (IFN-α, IFN-β, CXCL10) following PIC stimulation suggesting that glucose availability may fine tune the magnitude of the TLR3 response (Figure 3.4A-E). Interestingly, I found that high levels of glucose increase baseline OCR levels, spare respiratory capacity, and ATP production in untreated/resting cells. However, following PIC stimulation, high glucose further reduced basal OCR, spare respiratory capacity and ATP production suggesting these conditions may alter TLR3 associated mitochondrial reprogramming (Supplemental Figure S3.1).

To determine if this amplification was associated with altered signaling, I evaluated alterations in TLR3 and TLR4 adaptor protein expression and transcription factor phosphorylation following stimulation with LPS and PIC under high and low glucose conditions. While TRIF and

TRAF6 expression was not affected by glucose levels (Supplemental Figure S3.2), low glucose was associated with a dramatic increase in total and phosphorylated IRF3 in PIC-stimulated BMM. Consistent with its more downstream role (42, 43), I also found IRF7 phosphorylation was delayed but sustained at high levels in low glucose conditions (Figures 3.4F and 3.4G). Furthermore, I found that levels of phosphorylated IκBα were increased in low glucose conditions in PIC but not LPS-stimulated cells, which may explain the increased TNF-α and IL-6 production following TLR3 engagement (Figure 3.4H). Collectively, these results suggest that high glucose may limit mitochondrial reprogramming and associated antiviral and pro-inflammatory signaling and cytokine production in a TLR3 specific manner.
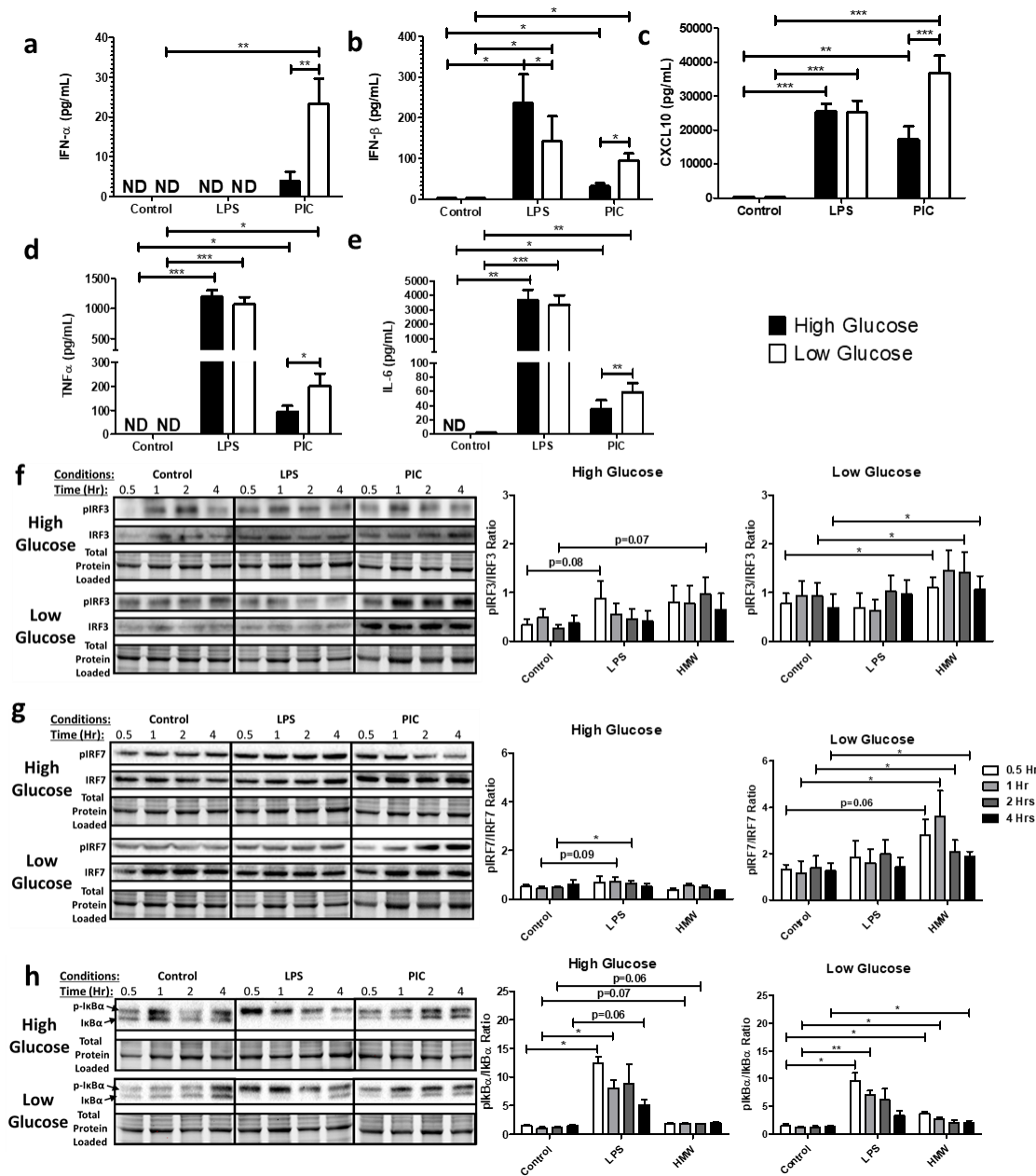
Figure 3.4: Low glucose conditions are associated with increased IRF activation and increased type I IFN production. Macrophages were stimulated with either 100ng/mL LPS or 10ng/mL PIC for 18 hours under high glucose (25mM) or low glucose (0.5mM) media conditions. Supernatant was collected for assessing antiviral (IFN-α, IFN-β, CXCL10) **(a-c)** and pro-inflammatory (TNF-α, IL-6) cytokine **(d-e)** expression. Cell lysates were harvested to quantify IRF3 **(f)**, IRF7 **(g)** and Iκbα **(h)** expression *via* immunoblotting. Data represents mean ± SEM of four individual mice (*p < 0.05, **p < 0.01, and ***p < 0.001).
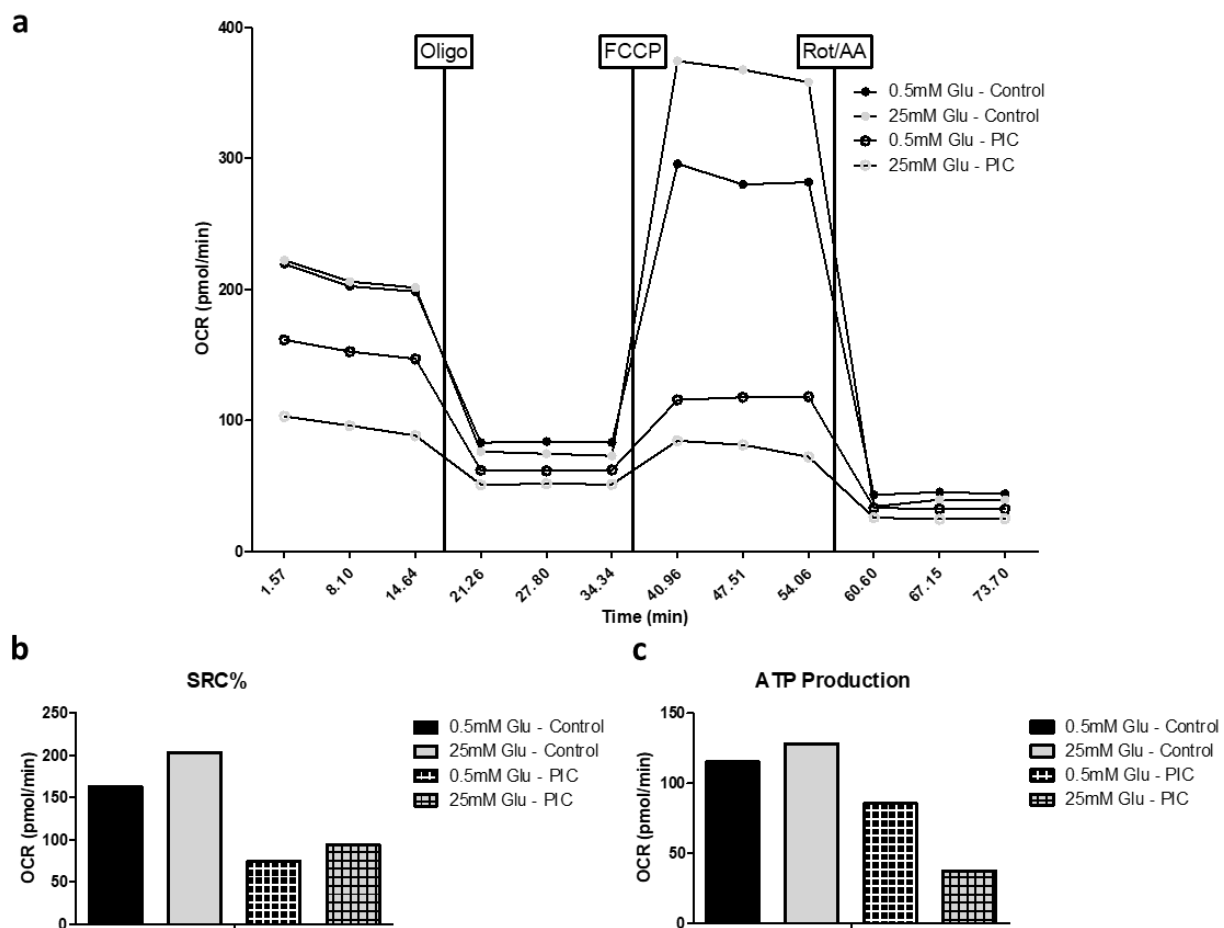
Supplemental Figure S3.1: PIC activation is associated with increased OXPHOS function under low glucose conditions. BMDMs were plated onto Seahorse XFp miniplates and treated with 10μg/mL PIC for 18 hours. OXPHOS function was assessed via successive Oligomycin (Oligo), Carbonyl cyanide-p-trifluoromethoxyphenylhydrazone (FCCP), and Rot/AA injections (a). Quantification of the spare respiratory capacity percentage (SRC%) (b) and ATP production (c). Data shown represents a test run using one representative animal.
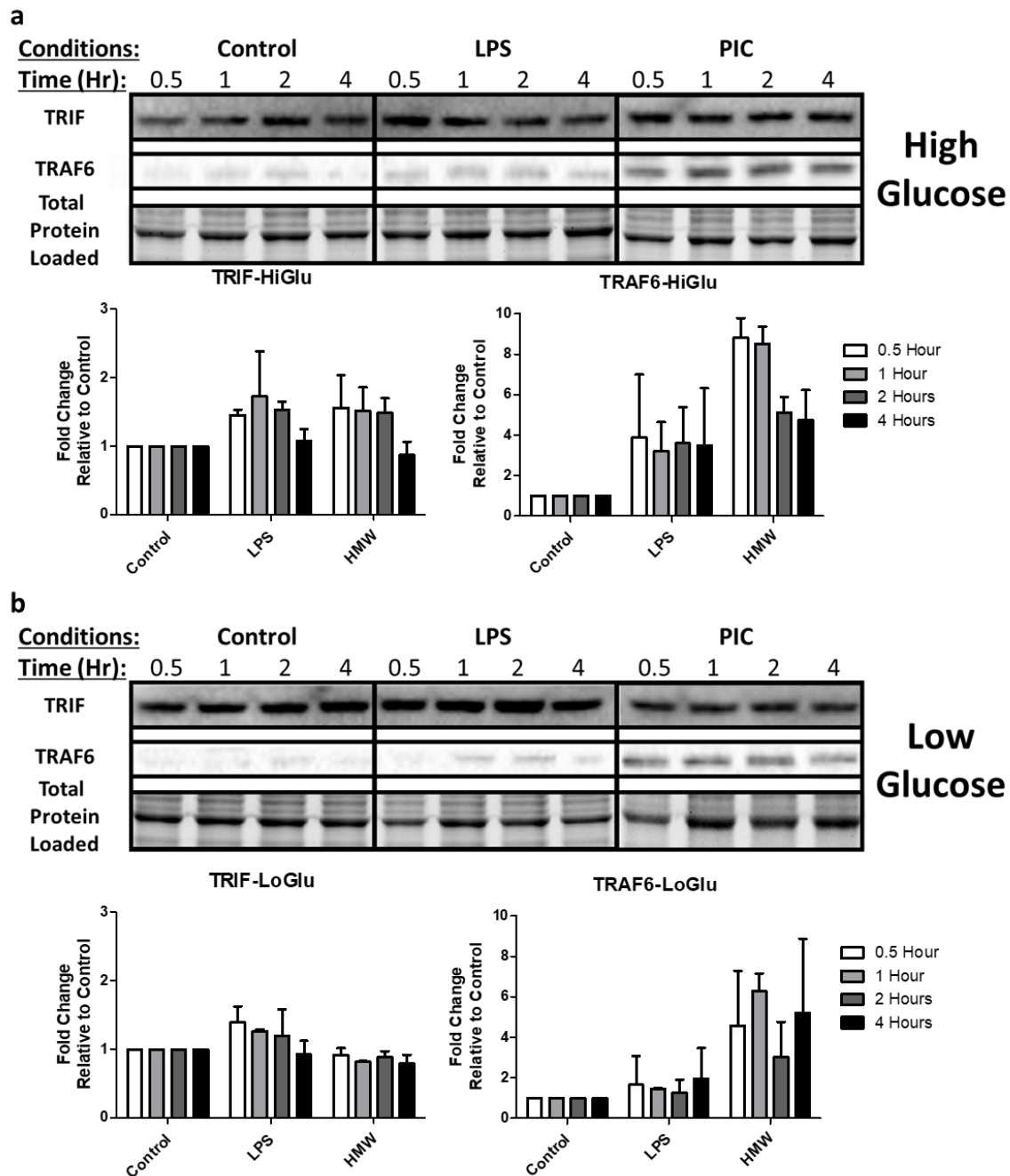
Supplemental Figure S3.2: TRIF and TRAF6 expression during PIC activation is not affected by glucose levels. Macrophages stimulated either with LPS or PIC for 18 hours under high glucose (a) or low glucose (b) media conditions were examined for differences in TLR signaling. Protein levels of TRIF and TRAF6 were measured via immunoblotting. Data shown represents blots from a representative animal while data shown represents mean ± SEM of two individual mice.

3.2.5. *Reduced glucose availability is associated with altered mitochondrial membrane potential and ETC complex expression following TLR engagement.*

To better understand how glucose levels affect TLR3 associated alterations in OXPHOS activity, I examined alterations in mitochondrial membrane potential (MMP) and ETC complex expression in high and low glucose conditions. MMP was assessed using the fluorescent dye Tetramethylrhodamine (TMRM). As previously described (15), LPS stimulation was associated with increased sequestration of TMRM by activated mitochondria (TMRM Mean Fluorescence Intensity [MFI]) in both high and low glucose conditions (Figure 3.5A). Conversely, PIC-stimulation did not significantly increase levels of TMRM sequestration in positive cells. Instead, PIC was associated with a significant increase in the number of cells expressing low levels of TMRM, which further increased under low glucose conditions (24% vs. 38%, p=0.09). To evaluate if altered ETC flux contributes to altered membrane potential, I examined ETC complex expression following LPS and PIC stimulation in high versus low glucose conditions. In high glucose conditions, alterations in expression were highly variable across animals. LPS-stimulation moderately decreased complex II (SDHB) expression whereas PIC increased complex IV (COX4) (Figure 3.5B). Alterations in ETC complex expression were more pronounced in low glucose conditions. Specifically, both LPS and PIC were associated with decreased expression of complexes I and IV. The only alteration unique to PIC in the low glucose condition was the significant increase in complex III (Figure 3.5B). In addition to its role as a proton pump, complex III is a major generator of mtROS (44) and may contribute to the amplification of inflammatory and antiviral cytokine production following TLR3 engagement under low glucose conditions.
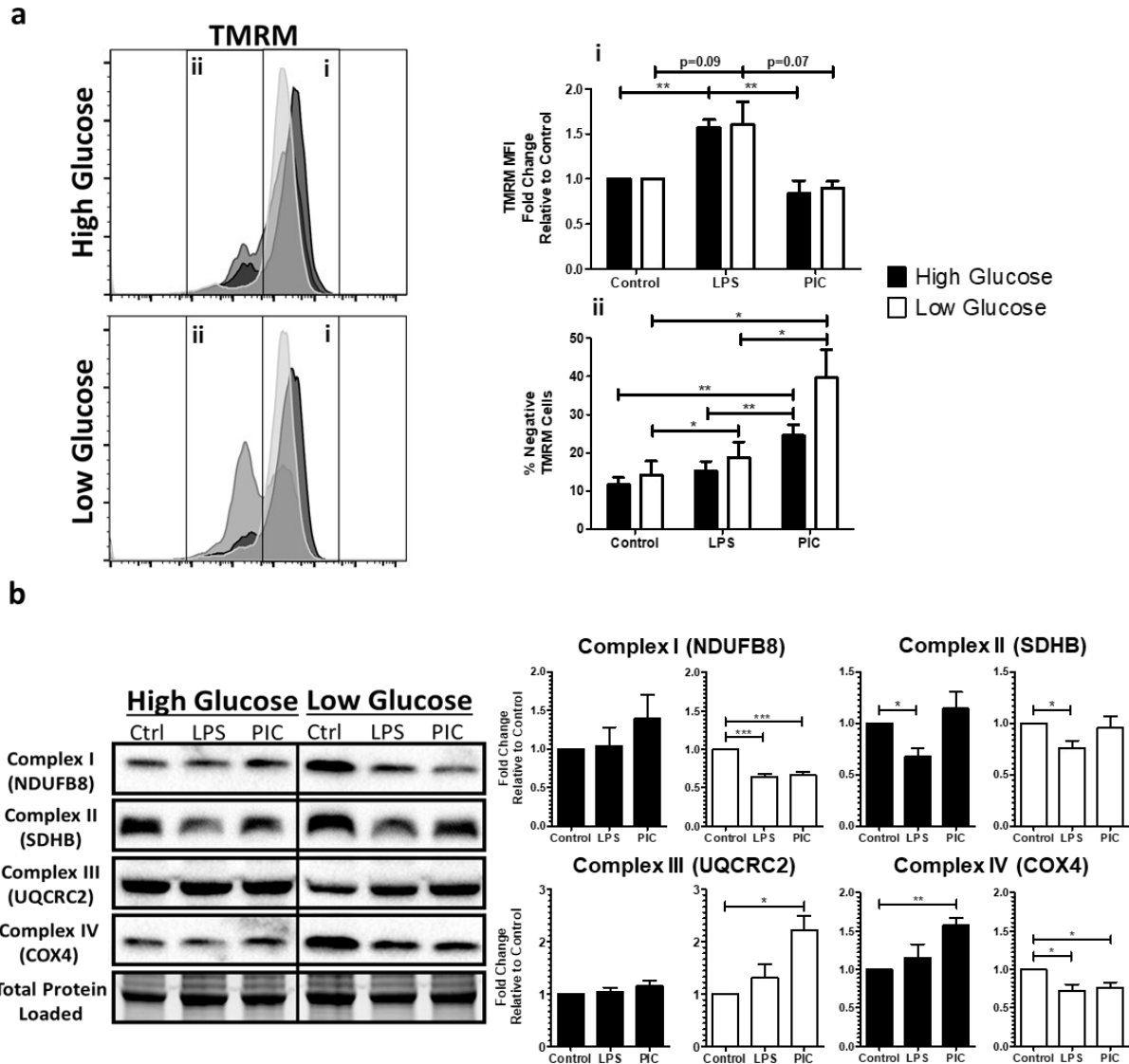
Figure 3.5: Poly(I:C) activation is linked to altered mitochondrial activity under low glucose conditions. BMDMs treated with LPS or PIC for 18 hours under high glucose or low glucose media conditions were characterized for differences in mitochondrial function. Tetramethylrhodamine (TMRM) staining was used to measure, *via* flow cytometry, mitochondrial membrane potential **(a)**. Core protein levels of Complexes I-IV of the electron transport chain was quantified *via* immunoblotting **(b)**. Data represents mean ± SEM of four individual mice (*p < 0.05, **p < 0.01, and ***p < 0.001).

3.2.6. *Flux through the ETC chain is required for inflammatory and antiviral cytokine production following TLR engagement.*

To evaluate the relative contribution of specific ETC complexes to cytokine production, BMM were stimulated with LPS (100ng/ml) and PIC (10ng/ml) under high and low glucose conditions in the presence or absence of Rotenone (Complex I inhibitor), Antimycin (Complex III inhibitor) and Cyanide (Complex IV inhibitor). Inhibition of Complex III and IV significantly reduced CXCL10 (III: ↓51%; IV: ↓72%) and TNF production (III: ↓54%; IV: ↓77%) following LPS stimulation (Figure 3.6A). Under low glucose conditions, inhibition of Complex I also limited LPS-associated cytokine production (CXCL10: ↓57%; TNF: ↓55%). Similarly, inhibition of Complexes I, III and IV significantly reduced inflammatory (TNF) and antiviral cytokine production (IFN-α, IFN-β, CXCL10) following PIC stimulation (Figure 3.6B, Supplemental Figure S3.3). The magnitude of this inhibition was further amplified under low glucose conditions, particularly for complex III (CXCL10: ↓70% vs ↓92%; TNF-α: ↓78% vs. ↓89%; IFN-β: ↓79% vs. ↓88%). These results suggest that ETC flux is required for inflammatory and antiviral cytokine production and that under low glucose conditions, alterations in complex III expression may play a central role in the amplification of these responses following TLR3 engagement.
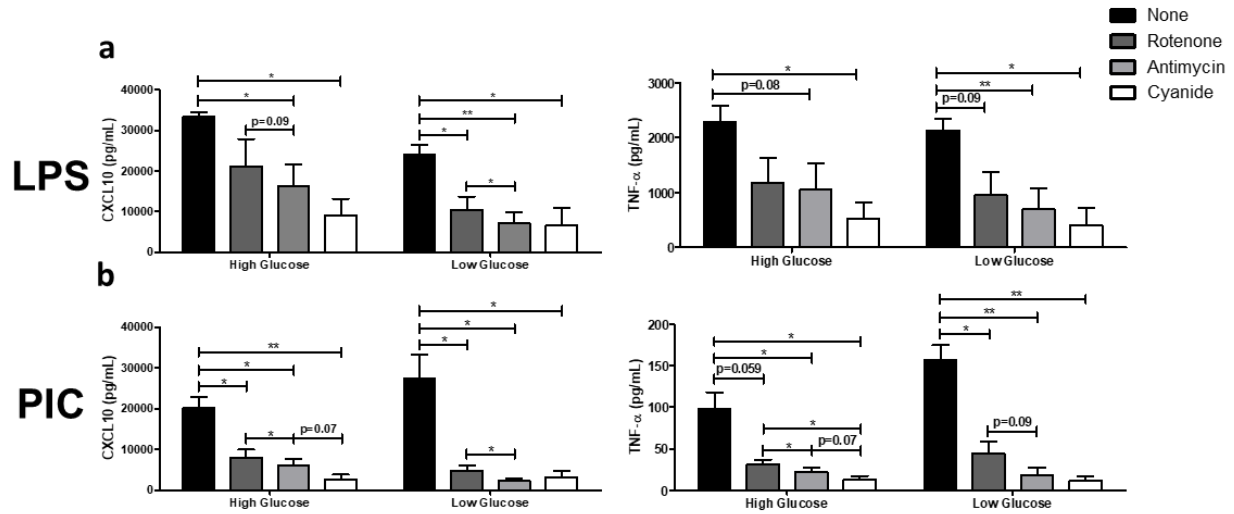
Figure 3.6: Targeting ETC activity reduces type I IFN-mediated responses during Poly(I:C) activation. LPS- **(a)** or PIC- **(b)** stimulated BMDMs were co-treated with a panel of ETC inhibitors (Rotenone, Antimycin, Cyanide) to assess the importance of mitochondrial function for antiviral responses. CXCL10 and TNF-α cytokine secretion was measured after 18 hours in high glucose or low glucose media conditions. Data represents mean ± SEM of three individual mice (*p < 0.05, **p < 0.01, and ***p < 0.001).
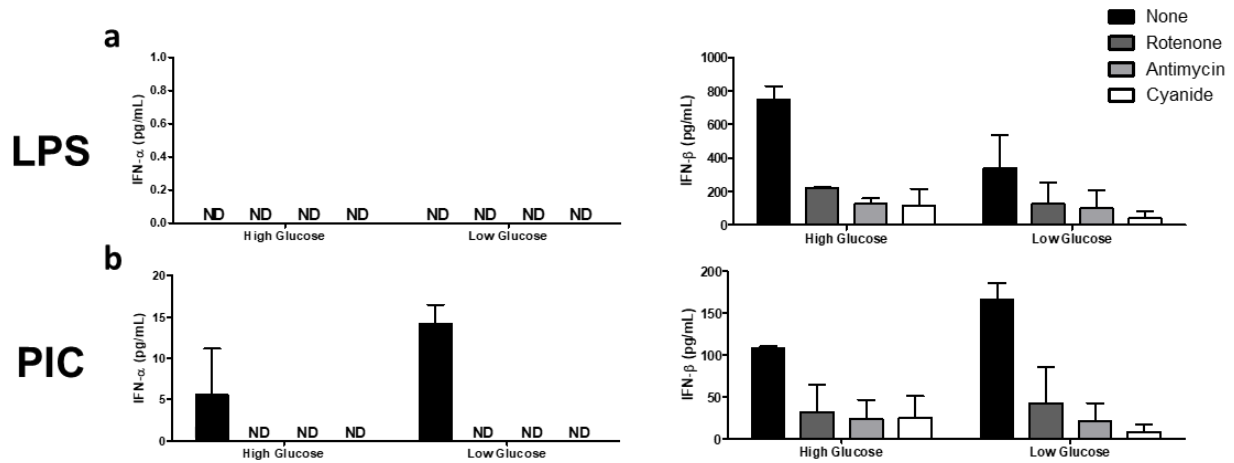
Supplemental Figure S3.3: Targeting ETC function in BMM leads to complete loss of type I IFN responses. LPS- (a) or PIC- (b) stimulated BMDMs were co-treated with a panel of ETC (Rotenone, Antimycin, Cyanide) inhibitors to assess the importance of mitochondrial function to antiviral responses. CXCL10 and TNF-α cytokine secretion was measured after 18 hours in high glucose or low glucose media conditions. Data shown represents a mean of two individual animals.

3.2.7. *Mitochondrial and cytosolic ROS accumulate in PIC stimulated BMM under low glucose conditions.*

Given the central role of complexes I and III in driving mitochondrial ROS production, I next quantified mitochondrial superoxide production using the fluorescent probe MitoSOX^{TM} Red. As previously reported (45), LPS stimulation was associated with increased mitochondrial superoxide production compared to untreated BMM. This increase was unaffected by glucose availability (Figure 3.7A). PIC stimulation was also associated with increased mitochondrial superoxide production (Figure 3.7A); however, its production was further increased under low glucose conditions. To determine if this superoxide accumulation was associated with altered antioxidant expression, cellular levels of superoxide dismutase 2 (SOD2) and mitochondrial glutathione peroxidase 4 (mtGPX4) were evaluated via western blots. In high glucose conditions, both LPS and PIC stimulated cells significantly increased SOD2 (LPS-FC=2.56±0.44; PIC-FC=1.75±0.40) and mtGPX4 expression (LPS-FC=1.40±0.07; PIC-FC=1.48±0.22) levels (Figure 3.7B). Alternatively, while LPS upregulated both antioxidant proteins under low glucose conditions (SOD2-FC=2.11±0.40; mtGPX4-FC=2.09±0.41), levels of SOD2 (FC=0.83±0.22) and mtGPX4 (FC=1.35±0.38) were not altered following PIC. This may contribute to the accumulation of superoxide in the mitochondria. To evaluate if these alterations affect the accumulation of cytosolic ROS, I used CellROX^{TM} Orange and quantified H_2O_2 levels in cell lysates. CellROX^{TM} Orange has a high affinity for hydroxyl radicals, H_2O_2 and superoxide. BMM treated with LPS exhibit increased levels of cytosolic ROS in both high and low glucose conditions (Figure 3.7C). Conversely, increased cytosolic ROS was only observed in low glucose conditions following PIC stimulation (Figure 3.7C and 3.7D). These results suggest that low glucose conditions are associated with increased mitochondrial and cytosolic ROS accumulation following PIC stimulation, which may contribute to the amplification of the cytokine response.
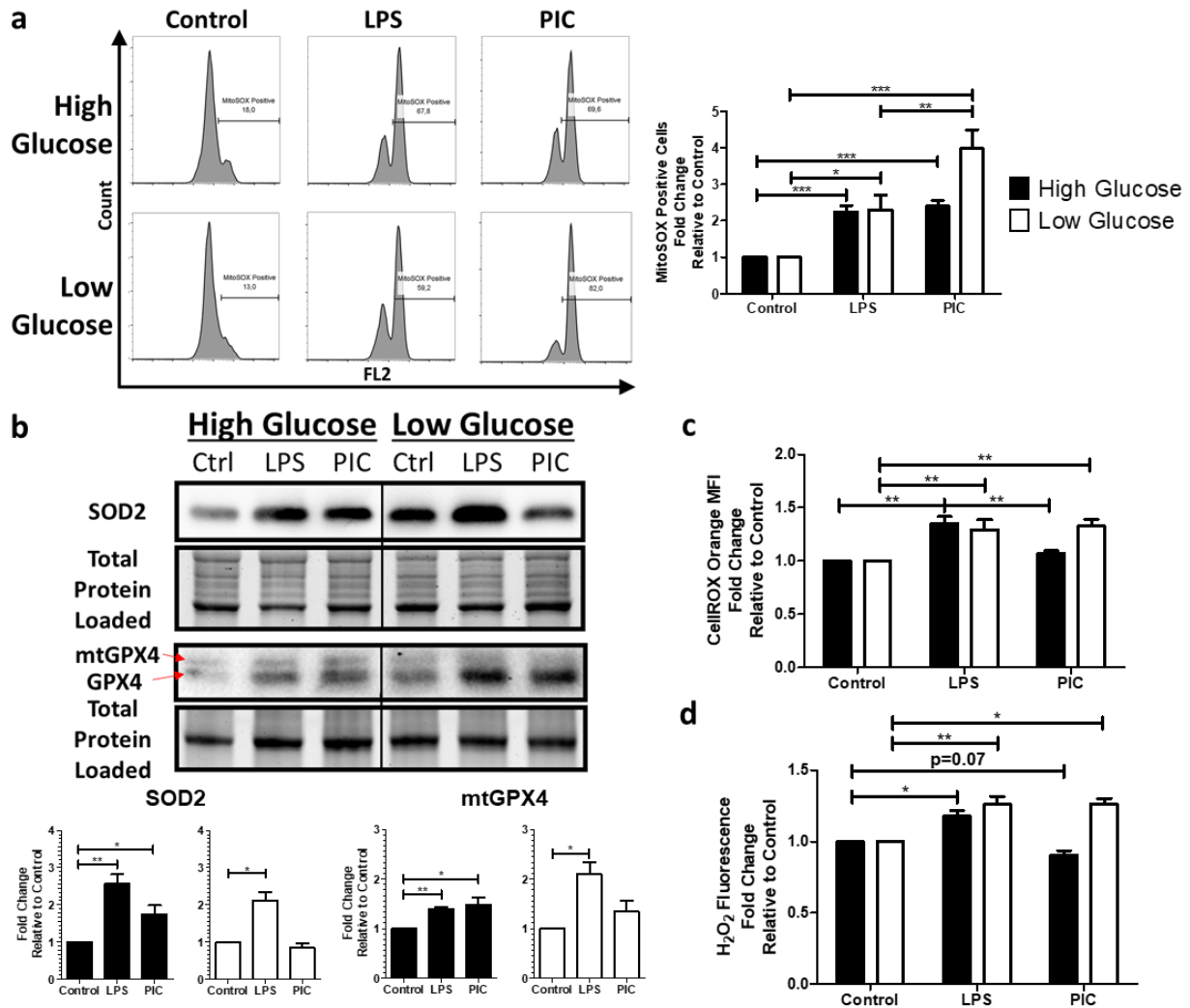
Figure 3.7: Poly(I:C) activation promotes mitochondrial ROS production and accumulation. Macrophages treated either with LPS or PIC for 18 hours under high glucose or low glucose media conditions were examined for differences in redox metabolism. Mitochondrial superoxide production was measured using MitoSOX™ Red **(a)**. Protein levels of antioxidant proteins superoxide dismutase (SOD2) and mitochondrial glutathione peroxidase 4 (mtGPX4) were measured via immunoblotting **(b)**. Cytosolic ROS production was measured using CellROX™ Orange **(c)**. Hydrogen peroxide levels were quantified using the Cell-based Hydrogen Peroxide Assay kit **(d)**. Data represents mean ± SEM of four individual mice (*p < 0.05, **p < 0.01, and ***p < 0.001).

3.2.8. *Mitochondrial and cellular ROS play a central role in TLR3 and TLR4 associated cytokine production.*

To evaluate if mtROS contributes to cytokine production following TLR3 and TLR4 engagement, cells stimulated with either LPS (100ng/ml) or PIC (10ng/ml) under high and low glucose conditions were co-treated with either antioxidants (MitoTEMPO, N-acetylcysteine) or an inhibitor of superoxide production (S3QEL). MitoTEMPO (MT) is a mitochondria-specific antioxidant that selectively scavenges mitochondrial superoxide. Alternatively, N-acetylcysteine (NAC) boosts glutathione synthesis reducing total overall cellular ROS production. S3QEL selectively inhibits superoxide production from the outer Q-binding site of the ETC complex III without altering OXPHOS. Inhibition of mitochondrial ROS had differential effects on cytokine production following LPS stimulation (Figure 3.8A; Supplemental Figure S3.4). Whereas TNF-α (MT: ↓50%; S3QEL: ↓48%) and IFN-β levels (MT: ↓60%; S3QEL: ↓61%) were decreased following MT and S3QEL production, CXCL10 levels were unaffected. CXCL10 production was only reduced following NAC treatment (CXCL10: ↓71%) suggesting cytosolic ROS may play a more important role in its production following LPS stimulation. Alternatively, inhibition of mitochondrial ROS significantly reduced TNF-α, CXCL10, IFN-α and IFN-β production in PIC-activated macrophages (Figure 3.8B; Supplemental Figure S3.4). The magnitude of S3QEL inhibition was further amplified under low glucose conditions (TNF-α: ↓54% vs. ↓66%; CXCL10: not significant vs ↓66%, IFN-β: ↓61% vs. ↓73%) suggesting complex III plays an important role in the amplification of the TLR3 responses. Similar to LPS, NAC treatment had the most pronounced effects on cytokine production in both and high low glucose conditions suggesting that both mitochondrial and cytosolic ROS contribute to TLR3 mediate cytokine production.
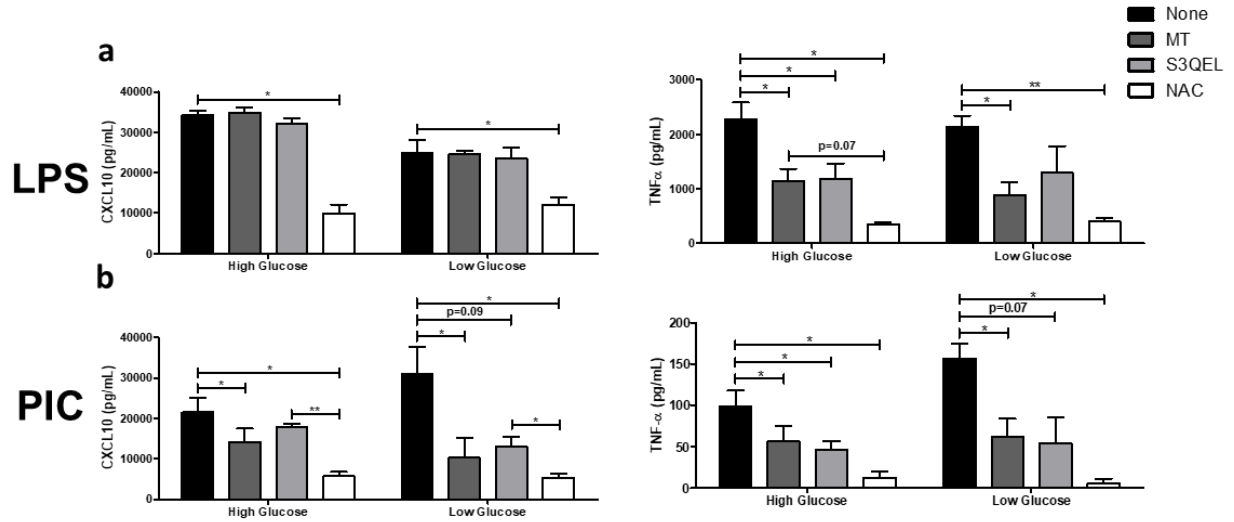
Figure 3.8: Type I IFN production can be inhibited by altering mtROS generation during Poly(I:C) activation. LPS- **(a)** or PIC- **(b)** stimulated BMDMs were co-treated with a panel of mtROS (MT, S3QEL, NAC) modulators to assess the importance of mitochondrial function for antiviral responses. CXCL10 and TNF-α cytokine secretion was measured after 18 hours in high glucose or low glucose media conditions. Data represents mean ± SEM of three individual mice (*p < 0.05, **p < 0.01, and ***p < 0.001).
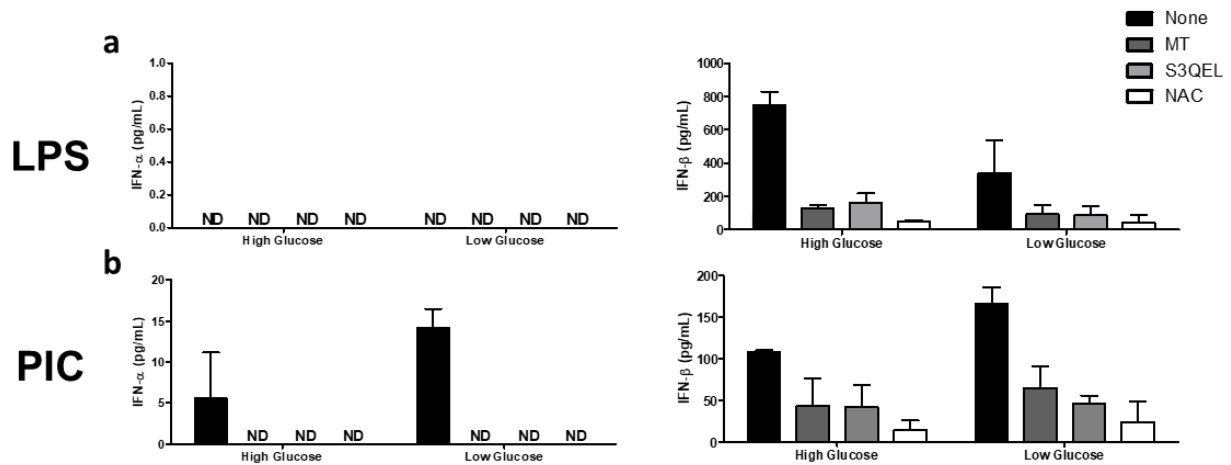
Supplemental Figure S3.4: Targeting mtROS leads to loss of type I IFN production. LPS- (a) or PIC- (b) stimulated BMDMs were co-treated with a panel of mtROS (MT, S3QEL, NAC) modulators to assess the importance of mitochondrial function to antiviral responses. CXCL10 and TNF-α cytokine secretion was measured after 18 hours in high glucose or low glucose media conditions. Data shown represents a mean of two individual animals.

3.3.   Discussion

Increasing evidence suggests that mitochondria play a critical role in driving innate immune responses against bacteria and viruses (15, 16, 20-23, 33). However, it is unclear if specific features of mitochondrial reprogramming contribute to pathogen specific immune responses or how nutrient availability may affect these processes. In the current study, I found that TLR3 and TLR4 engagement uniquely remodeled ETC complex expression, resulting in differential accumulation of mitochondrial and cytosolic ROS. This differential ROS production is required to support ligand specific inflammatory and antiviral cytokine profiles. I also found that the magnitude of TLR3 but not TLR4 responses were modulated by glucose availability. Under conditions of low glucose, TLR3 engagement was associated with increased ETC complex III expression, increased mitochondrial and cytosolic ROS, and increased inflammatory and antiviral cytokine production. This increased cytokine production was selectively reversed by targeting superoxide production from the outer Q-binding site of the ETC complex III. Collectively, these findings suggest that the ETC may act as a selective rheostat of macrophage function that regulates not only the nature (antibacterial vs. antiviral) but the magnitude of the response, which may depend on nutrient availability.

It is widely accepted that inflammatory macrophages undergo metabolic reprogramming to support cytokine production and effector functions. In LPS-stimulated cells, reprogramming is associated with a near complete inhibition of OXPHOS and an increased reliance on aerobic glycolysis to support rapid energy production (9, 15, 17, 36, 46). This switch is driven by altered flux through the tricarboxylic acid (TCA), which repurposes mitochondrial function to support superoxide production and drive intracellular anti-bacterial responses (15, 17). While it was initially assumed all "inflammatory" stimuli induce similar responses, increasing evidence

suggests this may not be the case (22, 23, 47). In the current study, I found that PIC stimulation inhibited OXPHOS activity in a dose dependent manner. However, even at its highest concentrations (10μg/ml), PIC did not completely inhibit OXPHOS and some level of cellular respiration was maintained. Consistent with these findings, Yoshizumi et al. found that RLR-mediated responses in macrophages are dependent on OXPHOS both *in vitro* and *in vivo*. In BMM, disruption of cellular respiration severely impaired RLR induced interferon and proinflammatory cytokine production (23). In mice, inhibition of OXPHOS was found to increase susceptibility to viral infection and induce significant inflammation in the lung (23). Wu et al. found that TLR9 engagement and type I IFN production in plasmacytoid dendritic cells was associated with increased OXPHOS activity. This increase was fueled by fatty acid oxidation (FAO) and was required for full cellular activation (48). *In vivo*, inhibition of FAO resulted in a diminished capacity to control lymphocytic choriomeningitis virus (48). Several IFN-stimulated genes, such as ISG15, have also been linked to the regulation of mitochondrial function during viral infection suggesting a secondary wave of mitochondrial reprogramming may occur following the TLR engagement and the induction of type I IFN responses (49). Collectively, these studies suggest that some level of OXPHOS activity may be required to mount functional antiviral immune responses but that these responses may vary by ligand and cell type.

In addition to altered cellular respiration, LPS and PIC stimulation were associated with alterations in mitochondrial membrane potential (MMP). MMP is generated by the proton pumps of the ETC (Complexes I, III and IV) to support mitochondrial ATP production (50). Various studies have reported altered MMP following macrophage activation. Mills et al. found that LPS stimulation was associated with increased MMP via reverse electron flow (RET). This RET was required to drive electrons back towards Complex I in order to support mitochondrial ROS

207

production and antimicrobial effector functions (15). Koshiba et al, have found MMP is required for MAVS-mediated antiviral signaling. Specifically, they found that inhibition of mitochondrial fusion resulted in a widespread loss of MMP. This loss in MMP correlated with the level of inhibition of RLR-induced antiviral responses (22). Unlike LPS, I found that PIC stimulation was associated with decreased MMP in a subset of cells. While it is unclear what exactly these cells represent, Tal et al. reported that when autophagy is inhibited, increased accumulation of dysfunctional mitochondria and increased mitochondrial ROS production drives excess RLR signaling (26). In this study, it is unclear if this subset of cells with decreased MMP are the main producers of ROS in our model system.

Recent studies have provided evidence that changes in the ETC, particularly in complex I and II, contribute to the regulation of antibacterial immune responses (15, 33) however, it unclear is if similar remodeling occurs during antiviral responses. Here, I found that PIC stimulated cells undergo differential remodeling of the ETC, particularly with limited glucose availability. Standard cell culture conditions represent supra-physiological levels of glucose (25mM vs. 5-7mM in fasting blood from non-diabetic individuals (51)) and may alter mitochondrial reprogramming *in vitro* (52). Under low glucose conditions, both LPS and PIC were found to downregulate complex I and IV expression. Interestingly, in the low glucose condition PIC also increased complex III expression. Importantly, this increased expression was associated with the amplification of the TLR3 cytokine production, which was reversed by the selective inhibition of ROS production by complex III. In support of our results, others have linked complex III to immune activation and function. In T cells, Sena et al. demonstrated that specific deletion of Rieske iron-sulfur protein (RISP), an essential component of Complex III, reduced mtROS production, nuclear factor of activated T cells (NFAT) activation and IL-2-mediated T cell activation and

antigen-specific expansion *in vivo* (53). Alternatively, ablation of complex III in regulatory T cells has been shown to reduce their inhibitory capacity without altering cell proliferation and survival (54). In macrophages, listeria infection has been shown to increase ROS production via complex III, which drives NF-kappa-B essential modulator (NEMO) dimerization, increasing the inhibitor of nuclear factor kappa-B kinase (IKK) activation, NF-κB signaling and cytokine production (47) Our study is among the first to identify associations between complex III mediated ROS production and TLR3 signaling and antiviral immune responses.

While ROS are generally considered toxic and damaging, increasing evidence suggests they also influence cellular signaling (55, 56). Superoxide and its more stable derivative hydrogen peroxide have been shown to regulate a variety of biological responses such as cell proliferation, differentiation, and migration (55). In the current study, I found that both mitochondrial superoxide and cytosolic ROS contribute to inflammatory and antiviral cytokine production following TLR engagement and that differential accumulation of ROS across these compartments may contribute to pathogen specific responses. Furthermore, under low glucose conditions, I found PIC but not LPS was associated with increased mitochondrial superoxide and cytosolic ROS production, which consequentially amplified cytokine production in these cells. These results suggest that the dynamic regulation of ROS production, likely through the modulation of complex III, may act as a rheostat that regulates the magnitude of antiviral immune responses. A central role for mitochondrial ROS in antiviral responses has been previously reported. Agod et al. found that mitochondrial superoxide drives increased MAVS protein expression in plasmacytoid DCs, increasing Akt and IRF3 activation and subsequent type I IFN production (57). Wang et al. showed shRNA knockout of SOD2 in cell lines increased viral replication and reduced antiviral responses (58), likely a result of decreased mitochondrial H_2O_2 production, a known redox-sensitive activator

of NF-κB and IRF signalling (47, 59-61). While I believe that mitochondrial superoxide and associated hydrogen peroxide production are the main drivers of cytokine production in our system, I cannot exclude the possibility that alternative cytosolic sources of ROS may also contribute. NADPH oxidase (NOX)-generated ROS during respiratory syncytial virus (RSV) and herpes simplex virus (HSV) infections can activate both NF-κB and IRF signalling (60, 61). Similarly, Yang et al. reported that high concentrations of PIC increase NOX2 activity and ROS production in BMMs, which was required for signal transducer and activator of transcription 1 (STAT1)-mediated signalling (62). A similar phenomenon was observed by To et al. using TLR7 ligands (63). Further studies are required to determine the specific contribution of mitochondrial vs. cytosolic derived ROS in driving these processes and the distinct roles of superoxide vs. hydrogen peroxide on signaling and effector function.

Taken together, our results suggest that dynamic remodeling of the ETC complex expression represents a mechanism by which macrophages modulate cytokine production following TLR engagement. I found that this remodeling was associated with differential accumulation of mitochondrial vs. cytosolic ROS, which may drive ligand specific cytokine profiles. I hypothesize that this differential accumulation may be driven by a dependence on complex I (LPS) versus complex III (PIC) for ROS production. Interestingly, I also found that TLR3 but not TLR4 associated mitochondrial reprogramming was dependent on glucose availability in the microenvironment. Supra-physiological levels of glucose have been shown to decrease a cell's dependence on mitochondria for energy production (52, 64). Similarly, our results suggest high glucose conditions may also alter mitochondrial reprogramming associated with TLR3 engagement. Accordingly, it is important to develop a detailed understanding of these

processes in a variety of bacterial and viral infections to identify new therapeutic approaches to help boost specific and functional effector functions.

3.4. Methods

3.4.1. Reagents

Lipopolysaccharide (LPS) and high molecular weight Poly(I:C) (PIC) were purchased from InvivoGen. MitoTEMPO (MT), N-acetylcysteine (NAC), antimycin A (AA), rotenone (ROT), potassium cyanide, 2-deoxyglucose (2-DG), oligomycin (OM) and carbonyl cyanide-p-trifluoromethoxyphenylhydrazone (FCCP) were acquired from Sigma-Aldrich while S3QEL-2 was purchased from Cedarlane. IL-1β, IL-6, IL-10, TNF-α, and CXCL10 ELISA kits were purchased from R&D Systems. The IFN-α/IFN-β 2-Plex Mouse ProcartaPlex™ Luminex Panel kit used was from Invitrogen. Tetramethylrhodamine, methyl ester (TMRM), MitoSOX Red and CellROX Orange probes were from ThermoFisher. All antibodies used in this study can be found in Table S1. Antibodies against Complex II (SDHB) was from Abcam while antibodies recognizing SOD2 was purchased from Cell Signalling Technology. Antibodies targeting IRF3, pIRF3 (Ser385), IRF7, pIRF7 (Ser477), GPX4, Iκbα, Complexes I (NDUFB8), III (UQCRC2) and IV (COX4) were purchased from ThermoFisher.

3.4.2. BMM culturing and stimulation

Total bone marrow cells were collected from the tibias and femurs of 6-13-week-old C57BL/6 mice, cryopreserved in a 90% FBS/10% DMSO solution, and frozen until use. Cells were cultured for ten days in DMEM media with 10% fetal bovine serum, 1% penicillin/streptomycin (Life Technologies), and 15% L929 fibroblast cell-conditioned medium on a 100mm Petri dish as previously described (65). On day 10, differentiated bone marrow-derived macrophages (BMM) were detached, counted, and plated into tissue-culture treated plates

at 1x106 cells/mL. BMMs were stimulated with 100ng/mL LPS, 10ng/mL or 10μg/mL PIC under high (DMEM medium supplemented with 25mM glucose) or low glucose conditions (DMEM medium supplemented with 0.5mM glucose). The relative contribution of ETC-derived ROS on BMM inflammatory and antiviral cytokine production were assessed by co-treating stimulated cells with 1μM ROT, 5μM AA, 5mM cyanide, 500μM MT, 5mM NAC or 5μM S3QEL-2.

3.4.3. *Cytokine quantification*

After the 18-hour stimulation, cytokine production was assessed in culture supernatants. IL-1β, IL-6, IL-10, TNF-α, and CXCL10 levels were assessed by ELISAs according to the manufactures instructions (R&D Systems). IFN-α and IFN-β levels were measured using IFN-α/IFN-β 2-Plex Mouse ProcartaPlex^{TM} Luminex Panel (Invitrogen).

3.4.4. *Western blot analysis*

Untreated and stimulated BMMs ($1x10^6$ cells) were lysed directly in the cell culture vessel using Pierce RIPA buffer (ThermoFisher) supplemented with HALT^{TM} Protease and Phosphatase Inhibitor (ThermoFisher). Total protein was quantified using the DC assay (Bio-Rad.) and resolved on a TGX^{TM} FastCast^{TM} Acrylamide gels (Bio-Rad). Gels were imaged directly using the Stain-Free application of a ChemiDoc XR (Bio-Rad) prior to transferring onto a PVDF membrane. Membranes were blocked overnight in 5% non-fat dry milk (w/v), washed and incubated overnight with the appropriate primary antibody. Horseradish peroxidase-conjugated secondary antibodies and Clarity^{TM} Western ECL Blotting Substrate (Bio-Rad) were used to visualize specified protein bands. Protein densitometry was analyzed according to previously described methodology (66).

3.4.5. *Assessment of mitochondrial function by flow cytometry*

BMMs were plated on 100mm Petri dishes and stimulated with 100ng/mL LPS or 10ng/mL and 10μg/mL PIC for 18 hours. Cells were then washed and stained with fluorescent probes

according to the manufacturer's instructions (30mins treatment at 37°C in select solutions). Mitochondrial membrane potential was measured using 10nM TMRM. Mitochondrial and Cellular ROS were monitored using 2.5μM MitoSOX Red in PBS and 5μM CellROX Orange in normal high glucose media, respectively. Cellular levels of fluorescence were quantified using an Attune NxT Flow Cytometer (ThermoFisher) and the results were analyzed using FlowJo Software. Results are reported as the percentage of positive cells and as mean fluorescence intensity (MFI), the latter being used to describe the level of expression on a population of positive cells.

3.4.6. *Quantification of cellular hydrogen peroxide production*

BMMs were plated onto 96-well black plates at 50,000 cells/well and stimulated with 100ng/mL LPS or 10ng/mL PIC under high or low glucose conditions for 1 hour. Cells were then washed before using the Cell-based Hydrogen Peroxide Assay Kit (Abcam) to measure H2O2 production. Cells were incubated with the AbGreen H_2O_2 indicator for 30 minutes before monitoring the relative difference in fluorescence using a fluorescence microplate reader (490nm Ex/520nm Em)

3.4.7. *Metabolic extracellular flux analysis*

BMMs were plated onto Seahorse XFp cell culture miniplates at 50,000 cells/well (Seahorse Bioscience) and stimulated with 100ng/mL LPS or 10ng/mL and 10μg/mL PIC for 18 hours. Extracellular acidification rate (ECAR) and oxygen consumption rate (OCR) were evaluated using a XFp Flux Analyzer (Seahorse Bioscience). Baseline ECAR and changes in glycolytic rate were assessed using the Seahorse XFp Glycolytic Rate Assay Kit (Agilent) according to the manufacturer's instructions. Basal respiration, ATP production-coupled respiration, maximal and reserve capacities and non-mitochondrial respiration were assessed using the Seahorse XFp Cell Mito Stress Test Kit (Agilent).

3.4.8. Statistical Analysis

Data used in this study was analyzed using GraphPad Prism software. Values shown represent the mean $\pm$ SEM of biological replicates, where the number of replicates are reported in the figure legends. Statistical significance was calculated using a paired Student's t-test (*$p < 0.05$, **$p < 0.01$, and ***$p < 0.001$).

3.5. References

1. Kawai, T., and S. Akira. 2006. TLR signaling. *Cell Death Differ.* 13: 816-825.
2. Takeda, K., and S. Akira. 2005. Toll-like receptors in innate immunity. *Int Immunol.* 17: 1-14.
3. Heil, F., H. Hemmi, H. Hochrein, F. Ampenberger, C. Kirschning, S. Akira, G. Lipford, H. Wagner, and S. Bauer. 2004. Species-Specific Recognition of Single-Stranded RNA via Toll-like Receptor 7 and 8. *Science* 303: 1526-1529.
4. Hemmi, H., O. Takeuchi, T. Kawai, T. Kaisho, S. Sato, H. Sanjo, M. Matsumoto, K. Hoshino, H. Wagner, K. Takeda, and S. Akira. 2000. A Toll-like receptor recognizes bacterial DNA. *Nature* 408: 740-745.
5. Lund, J. M., L. Alexopoulou, A. Sato, M. Karow, N. C. Adams, N. W. Gale, A. Iwasaki, and R. A. Flavell. 2004. Recognition of single-stranded RNA viruses by Toll-like receptor 7. *Proc Natl Acad Sci U S A* 101: 5598-5603.
6. Alexopoulou, L., A. C. Holt, R. Medzhitov, and R. A. Flavell. 2001. Recognition of double-stranded RNA and activation of NF-[kappa]B by Toll-like receptor 3. *Nature* 413: 732-738.
7. Chow, J. C., D. W. Young, D. T. Golenbock, W. J. Christ, and F. Gusovsky. 1999. Toll-like Receptor-4 Mediates Lipopolysaccharide-induced Signal Transduction. *J Biol Chem* 274: 10689-10692.
8. Infantino, V., V. Iacobazzi, F. Palmieri, and A. Menga. 2013. ATP-citrate lyase is essential for macrophage inflammatory response. *Biochem. Biophys. Res. Commun.* 440: 105-111.
9. Tannahill, G. M., A. M. Curtis, J. Adamik, E. M. Palsson-McDermott, A. F. McGettrick, G. Goel, C. Frezza, N. J. Bernard, B. Kelly, N. H. Foley, L. Zheng, A. Gardet, Z. Tong, S. S. Jany, S. C. Corr, M. Haneklaus, B. E. Caffrey, K. Pierce, S. Walmsley, F. C. Beasley, E. Cummins, V. Nizet, M. Whyte, C. T. Taylor, H. Lin, S. L. Masters, E. Gottlieb, V. P. Kelly, C. Clish, P. E. Auron, R. J. Xavier, and L. A. J. O/'Neill. 2013. Succinate is an inflammatory signal that induces IL-1β through HIF-1α. *Nature* 496: 238-242.
10. Errea, A., D. Cayet, P. Marchetti, C. Tang, J. Kluza, S. Offermanns, J.-C. Sirard, and M. Rumbo. 2016. Lactate Inhibits the Pro-Inflammatory Response and Metabolic Reprogramming in Murine Macrophages in a GPR81-Independent Manner. *PLoS ONE* 11: e0163694.
11. Kesarwani, P., A. K. Murali, A. A. Al-Khami, and S. Mehrotra. 2013. Redox regulation of T-cell function: from molecular mechanisms to significance in human health and disease. *Antioxid. Redox Signal.* 18: 1497-1534.
12. Wang, H., H. Flach, M. Onizawa, L. Wei, M. T. McManus, and A. Weiss. 2014. Negative regulation of Hif1a expression and TH17 differentiation by the hypoxia-regulated microRNA miR-210. *Nat. Immunol.* 15: 393-401.
13. Shirai, T., R. R. Nazarewicz, B. B. Wallis, R. E. Yanes, R. Watanabe, M. Hilhorst, L. Tian, D. G. Harrison, J. C. Giacomini, T. L. Assimes, J. J. Goronzy, and C. M. Weyand. 2016. The glycolytic enzyme PKM2 bridges metabolic and inflammatory dysfunction in coronary artery disease. *J. Exp. Med.* 213: 337-354.
14. Palsson-McDermott, E. M., A. M. Curtis, G. Goel, M. A. R. Lauterbach, F. J. Sheedy, L. E. Gleeson, M. W. M. van den Bosch, S. R. Quinn, R. Domingo-Fernandez, D. G. W. Johnston, J.-k. Jiang, W. J. Israelsen, J. Keane, C. Thomas, C. Clish, M. Vander Heiden, R. J. Xavier, and L. A. J. O'Neill. 2015. Pyruvate Kinase M2 Regulates Hif-1α Activity

and IL-1β Induction and Is a Critical Determinant of the Warburg Effect in LPS-Activated Macrophages. *Cell Metab.* 21: 65-80.

15. Mills, E. L., B. Kelly, A. Logan, A. S. H. Costa, M. Varma, C. E. Bryant, P. Tourlomousis, J. H. M. Däbritz, E. Gottlieb, I. Latorre, S. C. Corr, G. McManus, D. Ryan, H. T. Jacobs, M. Szibor, R. J. Xavier, T. Braun, C. Frezza, M. P. Murphy, and L. A. O'Neill. 2016. Succinate Dehydrogenase Supports Metabolic Repurposing of Mitochondria to Drive Inflammatory Macrophages. *Cell* 167: 457-470.e413.

16. Kelly, B., G. M. Tannahill, M. P. Murphy, and L. A. J. O'Neill. 2015. Metformin Inhibits the Production of Reactive Oxygen Species from NADH:Ubiquinone Oxidoreductase to Limit Induction of Interleukin-1β (IL-1β) and Boosts Interleukin-10 (IL-10) in Lipopolysaccharide (LPS)-activated Macrophages. *J Biol Chem* 290: 20348-20359.

17. Jha, A. K., S. C.-C. Huang, A. Sergushichev, V. Lampropoulou, Y. Ivanova, E. Loginicheva, K. Chmielewski, K. M. Stewart, J. Ashall, B. Everts, E. J. Pearce, E. M. Driggers, and M. N. Artyomov. 2015. Network Integration of Parallel Metabolic and Transcriptional Data Reveals Metabolic Modules that Regulate Macrophage Polarization. *Immunity* 42: 419-430.

18. Lampropoulou, V., A. Sergushichev, M. Bambouskova, S. Nair, E. E. Vincent, E. Loginicheva, L. Cervantes-Barragan, X. Ma, S. C.-C. Huang, T. Griss, C. J. Weinheimer, S. Khader, G. J. Randolph, E. J. Pearce, R. G. Jones, A. Diwan, M. S. Diamond, and M. N. Artyomov. 2016. Itaconate Links Inhibition of Succinate Dehydrogenase with Macrophage Metabolic Remodeling and Regulation of Inflammation. *Cell Metab.* 24: 158-166.

19. Rodríguez-Prados, J., P. G. Través, J. Cuenca, D. Rico, J. Aragonés, P. Martín-Sanz, M. Cascante, and L. Boscá. 2010. Substrate Fate in Activated Macrophages: A Comparison between Innate, Classic, and Alternative Activation. *J. Immunol.* 185: 605-614.

20. Seth, R. B., L. Sun, C.-K. Ea, and Z. J. Chen. 2005. Identification and Characterization of MAVS, a Mitochondrial Antiviral Signaling Protein that Activates NF-κB and IRF3. *Cell* 122: 669-682.

21. Castanier, C., D. Garcin, A. Vazquez, and D. Arnoult. 2010. Mitochondrial dynamics regulate the RIG-I-like receptor antiviral pathway. *EMBO Rep* 11: 133.

22. Koshiba, T. 2013. Mitochondrial-mediated antiviral immunity. *Biochim Biophys Acta* 1833: 225-232.

23. Yoshizumi, T., H. Imamura, T. Taku, T. Kuroki, A. Kawaguchi, K. Ishikawa, K. Nakada, and T. Koshiba. 2017. RLR-mediated antiviral innate immunity requires oxidative phosphorylation activity. *Sci Rep* 7: 5379.

24. Kawai, T., K. Takahashi, S. Sato, C. Coban, H. Kumar, H. Kato, K. J. Ishii, O. Takeuchi, and S. Akira. 2005. IPS-1, an adaptor triggering RIG-I- and Mda5-mediated type I interferon induction. *Nat Immunol* 6: 981-988.

25. Xu, L.-G., Y.-Y. Wang, K.-J. Han, L.-Y. Li, Z. Zhai, and H.-B. Shu. 2005. VISA Is an Adapter Protein Required for Virus-Triggered IFN-β Signaling. *Mol Cell* 19: 727-740.

26. Tal, M. C., M. Sasai, H. K. Lee, B. Yordy, G. S. Shadel, and A. Iwasaki. 2009. Absence of autophagy results in reactive oxygen species-dependent amplification of RLR signaling. *Proc Natl Acad Sci U S A* 106: 2770.

27. Kawai, T., and S. Akira. 2006. Innate immune recognition of viral infection. *Nat Immunol* 7: 131-137.

28. Meylan, E., and J. Tschopp. 2006. Toll-Like Receptors and RNA Helicases: Two Parallel Ways to Trigger Antiviral Responses. *Mol Cell* 22: 561-569.

29. Djafarzadeh, S., M. Vuda, J. Takala, M. Ochs, and S. M. Jakob. 2011. Toll-like receptor-3-induced mitochondrial dysfunction in cultured human hepatocytes. *Mitochondrion* 11: 83-88.

30. Pantel, A., A. Teixeira, E. Haddad, E. G. Wood, R. M. Steinman, and M. P. Longhi. 2014. Direct Type I IFN but Not MDA5/TLR3 Activation of Dendritic Cells Is Required for Maturation and Metabolic Shift to Glycolysis after Poly IC Stimulation. *PLoS Biol.* 12: e1001759.

31. Everts, B., E. Amiel, S. C.-C. Huang, A. M. Smith, C.-H. Chang, W. Y. Lam, V. Redmann, T. C. Freitas, J. Blagih, G. J. W. van der Windt, M. N. Artyomov, R. G. Jones, E. L. Pearce, and E. J. Pearce. 2014. TLR-driven early glycolytic reprogramming via the kinases TBK1-IKK[epsiv] supports the anabolic demands of dendritic cell activation. *Nat Immunol* 15: 323-332.

32. Hu, W., A. Jain, Y. Gao, I. M. Dozmorov, R. Mandraju, E. K. Wakeland, and C. Pasare. 2015. Differential outcome of TRIF-mediated signaling in TLR4 and TLR3 induced DC maturation. *Proc Natl Acad Sci U S A* 112: 13994.

33. Garaude, J., R. Acín-Pérez, S. Martínez-Cano, M. Enamorado, M. Ugolini, E. Nistal-Villán, S. Hervás-Stubbs, P. Pelegrín, L. E. Sander, J. A. Enríquez, and D. Sancho. 2016. Mitochondrial respiratory-chain adaptations in macrophages contribute to antibacterial host defense. *Nature immunology* 17: 1037-1045.

34. Lin, B., B. Dutta, and I. D. C. Fraser. 2017. Systematic Investigation of Multi-TLR Sensing Identifies Regulators of Sustained Gene Activation in Macrophages. *Cell Syst* 5: 25-37.e23.

35. Krawczyk, C. M., T. Holowka, J. Sun, J. Blagih, E. Amiel, R. J. DeBerardinis, J. R. Cross, E. Jung, C. B. Thompson, R. G. Jones, and E. J. Pearce. 2010. Toll-like receptor–induced changes in glycolytic metabolism regulate dendritic cell activation. *Blood* 115: 4742.

36. Van den Bossche, J., J. Baardman, Natasja A. Otto, S. van der Velden, Annette E. Neele, Susan M. van den Berg, R. Luque-Martin, H.-J. Chen, Marieke C. S. Boshuizen, M. Ahmed, Marten A. Hoeksema, Alex F. de Vos, and Menno P. J. de Winther. 2016. Mitochondrial Dysfunction Prevents Repolarization of Inflammatory Macrophages. *Cell Rep* 17: 684-696.

37. Sriskanthadevan, S., D. V. Jeyaraju, T. E. Chung, S. Prabha, W. Xu, M. Skrtic, B. Jhas, R. Hurren, M. Gronda, X. Wang, Y. Jitkova, M. A. Sukhai, F.-H. Lin, N. Maclean, R. Laister, C. A. Goard, P. J. Mullen, S. Xie, L. Z. Penn, I. M. Rogers, J. E. Dick, M. D. Minden, and A. D. Schimmer. 2015. AML cells have low spare reserve capacity in their respiratory chain that renders them susceptible to oxidative metabolic stress. *Blood*: blood-2014-2008-594408.

38. O'Neill, L. A. J., and E. J. Pearce. 2016. Immunometabolism governs dendritic cell and macrophage function. *J. Exp. Med.* 213: 15-23.

39. Wei, J., J. Raynor, T.-L. M. Nguyen, and H. Chi. 2017. Nutrient and Metabolic Sensing in T Cell Responses. *Front Immunol* 8: 247.

40. Langston, P. K., M. Shibata, and T. Horng. 2017. Metabolism Supports Macrophage Activation. *Front Immunol* 8: 61.

41. Covarrubias, A. J., H. I. Aksoylar, and T. Horng. 2015. Control of macrophage metabolism and activation by mTOR and Akt signaling. *Semin Immunol* 27: 286-296.

42. Honda, K., H. Yanai, H. Negishi, M. Asagiri, M. Sato, T. Mizutani, N. Shimada, Y. Ohba, A. Takaoka, N. Yoshida, and T. Taniguchi. 2005. IRF-7 is the master regulator of type-I interferon-dependent immune responses. *Nature* 434: 772-777.

43. Honda, K., A. Takaoka, and T. Taniguchi. 2006. Type I Inteferon Gene Induction by the Interferon Regulatory Factor Family of Transcription Factors. *Immunity* 25: 349-360.

44. Li, X., P. Fang, J. Mai, E. T. Choi, H. Wang, and X.-f. Yang. 2013. Targeting mitochondrial reactive oxygen species as novel therapy for inflammatory diseases and cancers. *J Hematol Oncol* 6: 19.

45. West, A. P., I. E. Brodsky, C. Rahner, D. K. Woo, H. Erdjument-Bromage, P. Tempst, M. C. Walsh, Y. Choi, G. S. Shadel, and S. Ghosh. 2011. TLR signalling augments macrophage bactericidal activity through mitochondrial ROS. *Nature* 472: 476-480.

46. Tan, Z., N. Xie, H. Cui, D. R. Moellering, E. Abraham, V. J. Thannickal, and G. Liu. 2015. Pyruvate Dehydrogenase Kinase 1 Participates in Macrophage Polarization via Regulating Glucose Metabolism. *J Immunol* 194: 6082.

47. Herb, M., A. Gluschko, K. Wiegmann, A. Farid, A. Wolf, O. Utermöhlen, O. Krut, M. Krönke, and M. Schramm. 2019. Mitochondrial reactive oxygen species enable proinflammatory signaling through disulfide linkage of NEMO. *Sci Signal* 12: eaar5926.

48. Wu, D., David E. Sanin, B. Everts, Q. Chen, J. Qiu, Michael D. Buck, A. Patterson, Amber M. Smith, C.-H. Chang, Z. Liu, Maxim N. Artyomov, Erika L. Pearce, M. Cella, and Edward J. Pearce. 2016. Type 1 Interferons Induce Changes in Core Metabolism that Are Critical for Immune Function. *Immunity* 44: 1325-1336.

49. Baldanta, S., M. Fernández-Escobar, R. Acín-Perez, M. Albert, E. Camafeita, I. Jorge, J. Vázquez, J. A. Enríquez, and S. Guerra. 2017. ISG15 governs mitochondrial function in macrophages following vaccinia virus infection. *PLOS Pathog* 13: e1006651.

50. Zorova, L. D., V. A. Popkov, E. Y. Plotnikov, D. N. Silachev, I. B. Pevzner, S. S. Jankauskas, V. A. Babenko, S. D. Zorov, A. V. Balakireva, M. Juhaszova, S. J. Sollott, and D. B. Zorov. 2018. Mitochondrial membrane potential. *Analytical biochemistry* 552: 50-59.

51. American Diabetes, A. 2009. Diagnosis and classification of diabetes mellitus. *Diabetes Care* 32 Suppl 1: S62-S67.

52. McKee, T. J., and S. V. Komarova. 2017. Is it time to reinvent basic cell culture medium? *Am J Physiol Cell Physiol* 312: C624-C626.

53. Sena, Laura A., S. Li, A. Jairaman, M. Prakriya, T. Ezponda, David A. Hildeman, C.-R. Wang, Paul T. Schumacker, Jonathan D. Licht, H. Perlman, Paul J. Bryce, and Navdeep S. Chandel. 2013. Mitochondria Are Required for Antigen-Specific T Cell Activation through Reactive Oxygen Species Signaling. *Immunity* 38: 225-236.

54. Weinberg, S. E., B. D. Singer, E. M. Steinert, C. A. Martinez, M. M. Mehta, I. Martínez-Reyes, P. Gao, K. A. Helmin, H. Abdala-Valencia, L. A. Sena, P. T. Schumacker, L. A. Turka, and N. S. Chandel. 2019. Mitochondrial complex III is essential for suppressive function of regulatory T cells. *Nature* 565: 495-499.

55. Holmström, K. M., and T. Finkel. 2014. Cellular mechanisms and physiological consequences of redox-dependent signalling. *Nature Reviews Molecular Cell Biology* 15: 411.

56. Nathan, C., and A. Cunningham-Bussel. 2013. Beyond oxidative stress: an immunologist's guide to reactive oxygen species. *Nature Reviews Immunology* 13: 349.

57. Agod, Z., T. Fekete, M. M. Budai, A. Varga, A. Szabo, H. Moon, I. Boldogh, T. Biro, A. Lanyi, A. Bacsi, and K. Pazmandi. 2017. Regulation of type I interferon responses by mitochondria-derived reactive oxygen species in plasmacytoid dendritic cells. *Redox Biol* 13: 633-645.

58. Wang, W., Y. Jin, N. Zeng, Q. Ruan, and F. Qian. 2017. SOD2 Facilitates the Antiviral Innate Immune Response by Scavenging Reactive Oxygen Species. *Viral Immunol* 30: 582-589.

59. Takada, Y., A. Mukhopadhyay, G. C. Kundu, G. H. Mahabeleshwar, S. Singh, and B. B. Aggarwal. 2003. Hydrogen Peroxide Activates NF-κB through Tyrosine Phosphorylation of IκBα and Serine Phosphorylation of p65: Evidence for the Involvement of IκBα Kinase and Syk Protein-Tyrosine Kinase. *J Biol Chem* 278: 24233-24241.

60. Indukuri, H., S. M. Castro, S.-M. Liao, L. A. Feeney, M. Dorsch, A. J. Coyle, R. P. Garofalo, A. R. Brasier, and A. Casola. 2006. Ikkepsilon regulates viral-induced interferon regulatory factor-3 activation via a redox-sensitive pathway. *Virology* 353: 155-165.

61. Gonzalez-Dosal, R., K. A. Horan, S. H. Rahbek, H. Ichijo, Z. J. Chen, J. J. Mieyal, R. Hartmann, and S. R. Paludan. 2011. HSV Infection Induces Production of ROS, which Potentiate Signaling from Pattern Recognition Receptors: Role for S-glutathionylation of TRAF3 and 6. *PLOS Pathog* 7: e1002250.

62. Yang, C.-S., J.-J. Kim, S. J. Lee, J. H. Hwang, C.-H. Lee, M.-S. Lee, and E.-K. Jo. 2013. TLR3-Triggered Reactive Oxygen Species Contribute to Inflammatory Responses by Activating Signal Transducer and Activator of Transcription-1. *The Journal of Immunology* 190: 6368.

63. To, E. E., R. Vlahos, R. Luong, M. L. Halls, P. C. Reading, P. T. King, C. Chan, G. R. Drummond, C. G. Sobey, B. R. S. Broughton, M. R. Starkey, R. van der Sluis, S. R. Lewin, S. Bozinovski, L. A. J. O'Neill, T. Quach, C. J. H. Porter, D. A. Brooks, J. J. O'Leary, and S. Selemidis. 2017. Endosomal NOX2 oxidase exacerbates virus pathogenicity and is a target for antiviral therapy. *Nature Communications* 8: 69.

64. Ackermann, T., and S. Tardito. 2019. Cell Culture Medium Formulation and Its Implications in Cancer Metabolism. *Trends in Cancer* 5: 329-332.

65. Weischenfeldt, J., and B. Porse. 2008. Bone Marrow-Derived Macrophages (BMM): Isolation and Applications. *CSH Protoc* 2008: pdb.prot5080.

66. Taylor, S. C., T. Berkelman, G. Yadav, and M. Hammond. 2013. A Defined Methodology for Reliable Quantification of Western Blot Data. *Mol Biotechnol* 55: 217-226.

Chapter 4. HIF-1α regulation of pro-inflammatory cytokine production following TLR3 engagement is dependent on viral nucleic acid length and glucose availability (Ahmed *et al.* under revision, submitted to *Journal of Immunology*)

4.1. Introduction

Macrophages serve as sentinels of the innate immune response, surveying tissues and quickly removing pathogens and apoptotic debris to re-establish and maintain homeostasis (1-3). Emerging evidence suggests cellular metabolism is an important regulator of macrophage function, however the mechanisms underlying these processes are not fully understood. Macrophages require a dynamic metabolism to satisfy their bioenergetic and biosynthetic demands, it but also to modulate their gene expression, signal transduction and epigenetic profiles (4-11). As the metabolic hub of the cell, mitochondria play a central role in these processes (5, 6, 10, 11). They serve as a scaffold for innate immune signaling, producing bioactive molecules and metabolites that amplify inflammatory and antiviral signaling through pattern recognition receptors (PRR) (6, 11-15). For example, reactive oxygen species (ROS) produced by mitochondria act as rheostats to modulate the magnitude of inflammatory and antiviral signaling in macrophages based on their surrounding nutrient environment (11, 16-18).

Hypoxia-inducible factor-1α (HIF-1α) is a transcription factor that has been shown to regulate mitochondrial function, oxygen consumption and substrate choices to support energy metabolism (19-23). Originally discovered as part of the cellular hypoxic response, it is now recognized that HIF-1α is induced by a wide range of cellular stressors, including bacterial and viral infection (24-26). It modulates cellular migration, phagocytosis and increases intracellular killing of bacteria (23, 25, 27, 28). It has also been shown to upregulate inflammatory cytokines (IL-1β, TNF-α, IL-6) and glycolytic enzyme (GLUT1, PKM2, PDK1) gene expression (19, 20, 25, 27, 29, 30) to support macrophage activation during bacterial infections (19, 20, 25, 27). In viral

infections, HIF-1α expression promote pathogenesis. For example, the interplay between HIF-1α and the HIV accessory protein Vpr induces viral gene expression and dysregulates multiple host pathways to support infection (31, 32). HIF-1α also drives the release of extracellular vesicles, which increase inflammation and contribute to HIV-associated immune dysfunction (33). In Hepatitis C, viral proteins activate HIF-1α by normoxic stabilization (34, 35). This stabilization is required to increase the expression of glycolytic enzymes, which promotes survival of infected cells via nonoxidative glucose utilization (34). Consistent with these findings, HIF-1α has also been shown to promote survival of infected cells in Hepatitis B, Kaposi's sarcoma-associated herpesvirus and Epstein-Barr infections (36-38). While certain viruses modulate HIF-1α for their own benefit, it is unclear if this transcription factor is also required to initiate or support aspects of an antiviral immune response.

A variety of PRRs, including Retinoic acid-inducible gene-I (RIG-I)-like receptors (RLR) and Toll-like receptors (TLR; TLR3/7/9), sense and recognize viral nucleic acids to initiate antiviral immune responses (13, 14, 39-43). This recognition results in the phosphorylation and homo- or heterodimerization of the interferon regulatory factor (IRF) transcription factors IRF3 and IRF7, which drive type I interferon (IFN) production (44). It also activates NF-κB through TRIF, TRAF3 or TRAF6, all of which stimulates inflammatory cytokine production (45). Polyinosinic:polycytidylic acid or Poly(I:C) is a double-stranded homopolymer commonly used to model antiviral immune responses to viral double stranded RNA (dsRNA). In the cytosol, Poly(I:C) interacts with either RIG-I or melanoma differentiation–associated gene 5 (MDA5), depending on the length of the dsRNA. RIG-I preferentially interacts with shorter dsRNA (<1 kb), whereas MDA5 interacts with longer strands (>2 kb) (43, 46). In the endosome, Poly(I:C) interacts with TLR3 irrespective of length (41). However, Mian et al. (47) found that long strands of

Poly(I:C) (10 μg/mL) (2-8 kb) induced strong inflammatory responses in fibroblasts, whereas shorter lengths (0.5-1.5 kb) were more potent in activating macrophage-like cell lines (RAW264.7) and human PBMCs. Furthermore, the magnitude of antiviral and inflammatory responses in human monocyte-derived dendritic cells was found to depend on the form (ssRNA versus dsRNA) and length of the RNA as well as the level of 5' phosphorylation (48). While further investigation is required, these differences are likely related to differential engagement of TLR3. Stable TLR3 dimerization requires a minimum of 40-50 bp, and dsRNA binding affinity can be altered depending on strand length (49-51).

Here, I show that the magnitude of the inflammatory response following TLR3 engagement on mouse bone marrow-derived macrophages (BMM) differs based on the length of Poly(I:C) (HMW; 1.5-8 kb vs. LMW; 0.2-1 kb) and is linked to differential accumulation of HIF-1α, which is strengthened under conditions of stress, including glucose deprivation. I also show that HIF-1α is differentially regulated by ROS (mitochondrial and cytosolic) and pyruvate kinase M2 (PKM2), depending on the length of Poly(I:C) used. Collectively, these results suggest HIF-1α may be used to fine-tune TLR3-specific inflammatory responses under conditions of stress.

4.2. Materials and Methods

4.2.1. Reagents

High glucose Dulbecco's Modified Eagle Media (DMEM) (with 4 mM L-glutamine and 1 mM sodium pyruvate), DMEM without glucose/glutamine/pyruvate/phenol red, fetal bovine serum (FBS), penicillin/streptomycin (PenStrep), glucose, sodium pyruvate and L-glutamine were purchased from Life Technologies. Lipopolysaccharide (LPS), high molecular weight Poly(I:C) (HMW) and low molecular weight Poly(I:C) (LMW) were obtained from InvivoGen. Acriflavine (ACR), N-acetylcysteine (NAC), antimycin A (AA), rotenone (ROT), 2-deoxyglucose (2-DG), oligomycin (OM) and carbonyl cyanide-p-trifluoromethoxyphenylhydrazone (FCCP) were acquired from Sigma-Aldrich, while DASA-58 was from Cayman Chemical. Tetramethylrhodamine, methyl ester (TMRM), MitoSOX™ Red and CellROX™ Orange probes were purchased from ThermoFisher. IL-6, IL-10, and TNF-α ELISA kits were attained from R&D Systems. Antibodies against HIF-1α (D2U3T) and PKM2 (D78A4) were obtained from Cell Signalling Technology. Polyclonal antibodies targeting IκBα were from ThermoFisher, whereas the GAPDH (6C5) antibody was purchased from Advanced ImmunoChemical Inc.

4.2.2. Isolation, differentiation, and treatment of bone marrow-derived macrophages (BMM)

All animal procedures were approved by the Carleton University Animal Care Committee and were conducted in accordance with the guidelines provided by the Canadian Council for Animal Care. Bone marrow progenitor cells were isolated from the tibias and femurs of 6-13-week-old C57BL/6 mice and cryopreserved until use. Progenitors were cultured on a 100 mm Petri dish for 10 days in high glucose DMEM media with 10% FBS, 1% PenStrep, and 15% L929 fibroblast cell-conditioned medium (11, 52). L929 conditioned media was prepared as previously described (52). Once differentiated, BMM were collected, counted, and plated onto tissue-culture treated plates at a density of $1x10^6$ cells/mL and allowed to rest overnight. BMMs were then

stimulated with 10 ng/mL high molecular weight (HMW; 1.5-8 kb) or 10 ng/mL low molecular weight Poly(I:C) (LMW; 0.2-1 kb) (Sigma-Aldrich) in complete DMEM media with either high (25 mM) or low glucose (0.5 mM). Low glucose media was prepared using the no glucose/glutamine/pyruvate/phenol red DMEM media that was subsequently supplemented with 0.5 mM glucose and matching concentrations of glutamine (4 mM) and sodium pyruvate (1 mM). Cells were stimulated for a range of 0.5 to 18 hours depending on the endpoint analysis. To better understand if oxygen levels can further alter HIF-1α accumulation, treatments were done under normoxic (atmospheric O_2 levels) and hypoxic (1%) conditions using a hypoxic incubator. To evaluate the role of HIF-1α, PKM2 and ROS in inflammatory signaling and cytokine production, BMM cells were stimulated with HMW- or LMW-Poly(I:C) in the presence or absence of inhibitor (1 μM ACR, 20 μM DASA-58, or 5 mM NAC respectively).

4.2.3. *Quantification of Cytokine Production in Culture Supernatants*

Cell culture supernatants were collected from BMM after 18 hours of stimulation with HMW or LMW Poly(I:C) and spun at 1,800 RPM for 10 minutes to remove cellular debris. TNF-α, IL-6 and IL-10 levels were evaluated using ELISAs according to the manufacturer's instructions (R&D Systems).

4.2.4. *Evaluation of protein expression in total BMM lysates*

Following the stimulation of BMM with HMW or LMW Poly(I:C) in high or low glucose media, cells were lysed using Pierce RIPA buffer supplemented with HALT™ Protease and Phosphatase Inhibitor (ThermoFisher). Total protein content in each sample was quantified using the DC assay (Bio-Rad). For each protein tested, 30 μg of total protein was loaded onto 12% TGX™ FastCast™ Acrylamide gels (Bio-Rad) and imaged using the ChemiDoc XR's Stain-Free program (Bio-Rad). Resolved proteins were transferred onto PVDF membranes using the Trans-

Blot® Turbo™ Transfer System and blocked overnight in 5% non-fat powdered milk (w/v) prior to overnight incubation with the appropriate primary antibody in TBS with 5% BSA (w/v) and 0.1% Tween-20. Horseradish peroxidase-conjugated secondary antibodies and Clarity™ Western ECL Blotting Substrate (Bio-Rad) were used to visualize protein bands of interest. Protein band densitometry was analyzed using methods previously described (53). In short, the chemiluminescence intensity of target bands was normalized to the amount of total protein loaded in its respective lane, as determined by the Stain-Free application on the ChemiDoc™ XR imager (Bio-Rad). The levels of target protein expression were further normalized relative to its respective control samples and presented as a fold change value. For IκBα, following normalization described above, the protein expression data was presented as the ratio between phosphorylated IκBα levels divided by total IκBα levels.

4.2.5. Evaluation of Mitochondrial Membrane Potential, Mitochondrial ROS and Total Cytosolic ROS using Flow Cytometry

Untreated and stimulated BMMs were detached and stained with fluorescent probes according to the manufacturer's instructions. Differences in mitochondrial membrane potential (MMP) were evaluated using 10 nM TMRM (ThermoFisher), which is a lipophilic cationic dye that accumulates in the mitochondrial matrix in proportion to the magnitude of MMP across the inner mitochondrial membrane. Mitochondrial and cellular ROS levels were monitored using 2.5 μM MitoSOX™ Red (ThermoFisher) in PBS and 5 μM CellROX™ Orange (ThermoFisher). MitoSOX™ Red is a fluorogenic probe that specifically localizes to active mitochondria via MMP detection and selectively reacts with superoxide in the mitochondrial matrix to create a highly florescent red product. CellROX™ Orange is a cell-permeable fluorogenic dye that localizes to the cytoplasm and strongly fluoresces upon oxidation by various ROS. Single cell analysis was measured using an Attune NxT Flow Cytometer (ThermoFisher). A minimum of 10,000 events

were captured per sample. Data was analyzed using FlowJo Software (version 10.0.7). After gating upon the macrophage population based on size (via FSC and SSC), events were characterized based on their fluorescent profiles of the respective probes. For experiments where the TMRM and MitoSOX^{TM} Red stains were used, sub-populations were categorized as either "positive" cells (high fluorescence) or "negative" cells (low fluorescence) for their respective stain. TMRM data was presented as the percentage of "TMRM negative" cells. MitoSOX^{TM} Red data was presented as the percentage of "MitoSOX Red positive" cells. For experiments where the CellROX^{TM} Orange probe was used, samples were characterized based on changes in the median fluorescence intensity (MFI) of the total population. The MFI value of each sample was normalized to its respective control sample and presented as a fold change value.

4.2.6. *Characterization of Energy Metabolism of BMM*

Harvested BMMs were plated onto Seahorse XFp cell culture miniplates (Agilent) at a density of 50,000 cells/well before stimulation. Cells were then stimulated with either 10 ng/mL HMW or LMW Poly(I:C) for 18 hours. Measurement of extracellular acidification rate (ECAR) and oxygen consumption rate (OCR) were done using a XFp Flux Analyzer (Agilent). Changes in glycolytic rate were assessed using the Seahorse XFp Glycolytic Rate Assay Kit (Agilent) according to the manufacturer's instructions. BMMs treated under high or low glucose conditions were exposed to sequential rotenone plus antimycin A (ROT/AA) and 2-deoxyglucose (2-DG) injections, and ECAR measurements were recorded. ECAR measurements were converted to proton efflux rate (PER) using the Wave Desktop software (Seahorse Bioscience) to better represent extracellular acidification. PER measurements were used to determine differences in basal glycolytic rate, %PER dependent on glycolysis and the ratio of mitochondrial oxygen consumption rate (mitoOCR) to glycolytic PER (glycoPER) across different samples.

Mitochondrial function was evaluated using the Seahorse XFp Cell Mito Stress Test Kit (Agilent). OCR measurements were recorded after HMW- and LMW-activated BMM were exposed to successive injections of OM, FCCP, and ROT/AA. Changes in OCR were used to measure the spare respiratory capacity percentage (SRC%) and ATP production of activated BMM.

Glucose consumption of BMM treated with HMW or LMW was done using a Contour® Next glucometer (54). After 18 hours of HMW or LMW treatment, cell culture supernatants were collected and spun down (as described above) to remove cellular debris. Afterwards, 5☐L of supernatant was loaded onto a test strip attached to a glucometer, and the amount of glucose remaining in sample after treatment was recorded. Prior to treatment, glucose levels in both high and low glucose media were recorded, and the percent glucose consumption was calculated for each sample by dividing the amount of glucose that remained after 18hrs by the amount of glucose present before treatment. As a positive control, BMM were also treated with 100 ng/mL LPS, a TLR ligand known to cause BMM to heavily depend on glucose as a primary energy source to mount a proper effector response (19, 21, 55, 56).

4.2.7. *Statistical Analyses*

Data used in this study was analyzed using GraphPad Prism software. Values shown represent the means ± SEM of biological replicates, where the number of replicates is reported in the figure legends. Statistical significance was calculated using a paired Student's t-test (*$p < 0.05$, **$p < 0.01$, and ***$p < 0.001$).

4.3.   Results:

4.3.1.   *HIF-1α is induced following TLR3 engagement and is regulated by glucose availability*

Emerging evidence suggests HIF-1α is regulated by certain viruses to promote viral replication and survival of infected cells (31, 32, 34, 35); however, it is unclear if its accumulation is required to support antiviral immune responses. To evaluate if HIF-1α is modulated during early antiviral immune responses, HIF-α protein expression was quantified via western blot after BMM were stimulated with HMW or LMW Poly(I:C) (10 ng/mL each) for 18 hours. Under standard cell culture conditions (high glucose; 25 mM), HMW but not LMW Poly(I:C) stimulation was associated with HIF-1α accumulation, compared to unstimulated control cells (FC=1.72, p=0.042) (Figure 4.1). However, in glucose deprived conditions (0.5 mM), both HMW and LMW Poly(I:C) stimulation increased HIF-1α (HMW FC=2.91, p=0.039; LMW FC=2.24, p=0.004). Given its established role in regulating gene expression under hypoxic conditions (57), I investigated if HIF-1α expression levels were further modified by oxygen levels. To do this, BMMs were stimulated with HMW and LMW Poly(I:C) in high or low glucose and under hypoxic conditions (1% O_2). In high glucose conditions, hypoxia increased HIF-1α levels in control cells and further increased accumulation of HIF-1α following stimulation with HMW and LMW Poly(I:C) (Supplemental Figure S4.1). In contrast, under conditions of glucose and oxygen deprivation, HMW and LMW Poly(I:C) stimulation were not associated with any further increase in HIF-1α compared to control cells. Collectively, these data suggest that, while HIF-1α may be important in antiviral responses in HMW-stimulated cells, it only contributes to LMW Poly(I:C) responses under conditions of stress. Furthermore, they suggest that macrophages may have a maximal capacity to respond to stress.
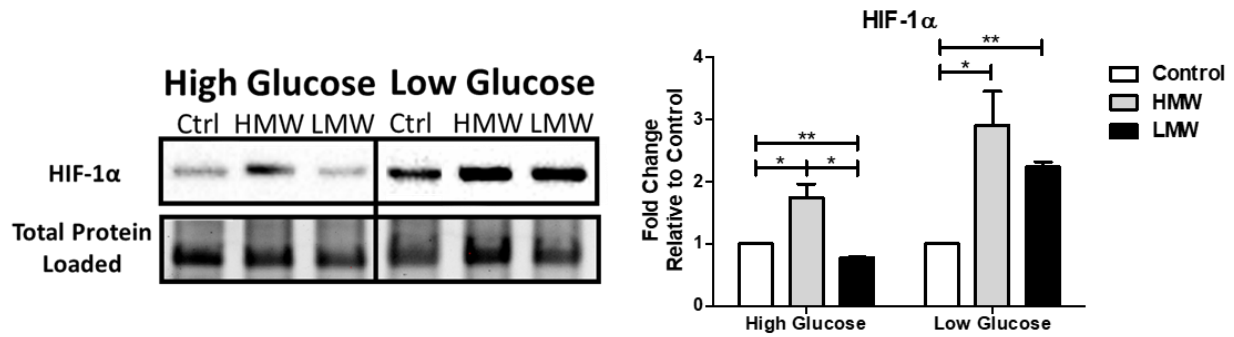
Figure 4.1: HIF-1α differentially accumulates in BMM following stimulation with HMW *vs.* LMW Poly(I:C) in low and high glucose. BMM were stimulated with either 10 ng/mL HMW- or 10 ng/mL LMW Poly(I:C) for 18 hours under high glucose (25 mM) or low glucose (0.5 mM) conditions. Total cell lysates were used to quantify HIF-1α expression *via* immunoblotting. Band intensity was normalized to the total protein levels in each of their respective lanes using the Bio-Rad Stain-Free Application. Afterwards, the expression of HIF-1α in each glucose condition was normalized to its respective control sample and presented as a fold change value. Data represents means ± SEM of four individual mice (*p < 0.05, **p < 0.01, and ***p < 0.001).
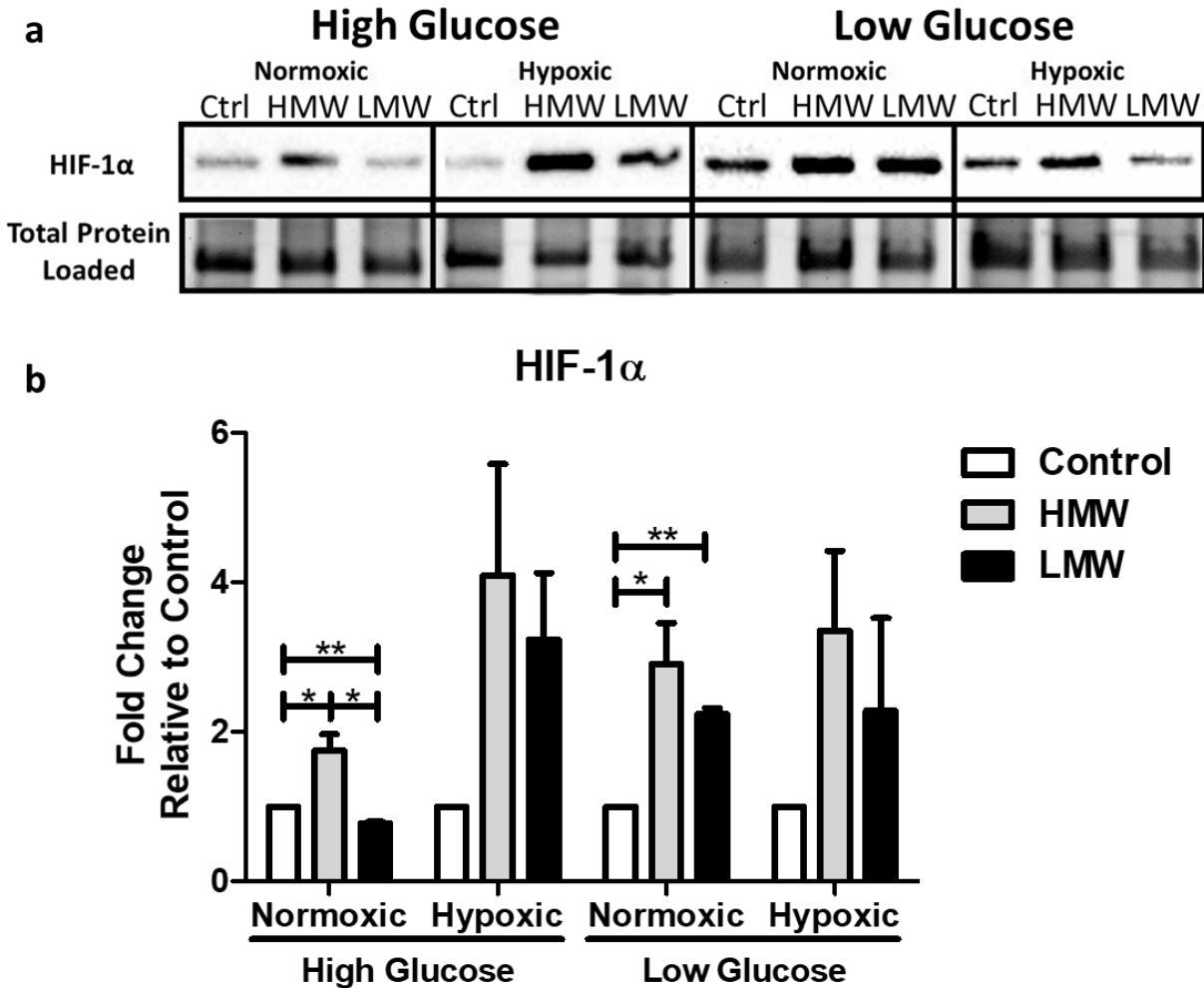
Supplemental Figure S4.1: HIF-1α expression is activated under glucose and/or oxygen deprivation conditions. BMM were stimulated with either HMW or LMW Poly(I:C) for 18 hours under high glucose or low glucose conditions. Total cell lysates were used to quantify HIF-1α expression via immunoblotting. Band intensity was normalized to the total protein levels in each of their respective lanes using the Bio-Rad Stain-Free Application. Afterwards, the expression of HIF-1α in each glucose condition was normalized to their respective control sample and presented as a fold change value. Data represents mean ± SEM of four individual mice (*p < 0.05, **p < 0.01, and ***p < 0.001).

4.3.2. *Stimulation of BMM with LMW Poly(I:C) does not alter glycolytic activity*

Given the role of HIF-1α in regulating glycolytic gene expression, I then investigated if TLR3 engagement was associated with differential modulation of glycolysis. I have previously shown that stimulation with HMW Poly(I:C) is associated with increased glycolytic activity, but this increase is significantly lower than that observed following LPS stimulation (11). To determine if similar changes are observed with LMW Poly(I:C), BMM were stimulated with HMW and LMW Poly(I:C) in high and low glucose media. Changes in glycolytic rate were evaluated using Agilent's Glycolytic Rate Assay and are reported as changes in proton efflux rate (PER) at baseline and in response to treatments of rotenone and antimycin A (ROT/AA) and 2-deoxyglucose (2-DG). As previously reported (11), HMW stimulation in high and low glucose conditions increased PER levels following stimulation, increased %PER derived from glycolysis and decreased the mitoOCR/glycoPER ratio (Figure 4.2A-C). However, LMW stimulation was not associated with any significant changes in glycolytic function despite the marked upregulation of HIF-1α in low glucose conditions (Figure 4.2A-C). To verify these results, I examined if HMW and LMW Poly(I:C) stimulations were associated with altered glucose uptake from the culture supernatant. In high glucose media, HMW but not LMW Poly(I:C) stimulation increased glucose consumption. As seen in the glycolytic rate assay, this increase was less pronounced than that observed following LPS stimulation (Figure 4.2D). In low glucose media, however, neither HMW nor LMW Poly(I:C) stimulation were associated with significant glucose uptake, suggesting these cells may adapt to the environment and use alternative energy sources under stressed conditions. In contrast, LPS stimulated cells further increased its glucose uptake to compensate for the reduced glucose in the environment (Figure 4.2D). These results suggest that cells stimulated with HMW and LMW Poly(I:C) may have differential dependencies on glycolysis to support their activation

status. Moreover, it appears that HIF-1α accumulation following glucose deprivation has a limited effect on glycolytic activity.

4.3.3. *Preventing HIF-1 dimerization blocks pro-inflammatory cytokine production via inhibition of NF-κB activation*

To determine if the differential accumulation of HIF-1α is associated with altered cytokine production, BMM were stimulated with HMW and LMW Poly(I:C) for 18 hours under high and low glucose conditions. Cytokine production in the culture supernatant was evaluated. Under high glucose conditions, HMW stimulated cells produced significantly higher levels of TNF-α (HMW: 93.1 pg/mL, p=0.013 vs. LMW: 25.0 pg/mL, p=0.048), IL-6 (HMW: 35.3 pg/mL, p=0.034 vs. LMW: 13.9 pg/mL, p=0.076) and IL-10 (HMW: 128.4 pg/mL, p=0.024 vs. LMW: 47.9 pg/mL, p=0.592) (Figure 4.3A-C). IL-1β was not detected in any condition following TLR3 engagement (data not shown). Consistent with this increase in TNF-α and IL-6, levels of p-IκBα in HMW stimulated cells remained elevated at 2- and 4-hours post-stimulation relative to controls (Figure 4.3D). Interestingly, LMW stimulation transiently increased p-IκBα levels at 0.5 hours before returning to control levels 2- and 4-hours after stimulation (Figure 4.3D). Low glucose conditions were associated with a significant increase in cytokine production in both HMW and LMW stimulated cells (TNF-α [HMW: FC=2.16, p=0.045 vs. LMW: FC=1.61, p=0.012], IL-6 [HMW: FC=1.68, p=0.003 vs. LMW: FC=2.51, p=0.017] and IL-10 [HMW: FC=1.33, p=0.014 vs. LMW: FC=1.91, p=0.008]) (Figure 4.3A-C). Additionally, both stimuli maintained and demonstrated sustained levels of p-IκBα for up to 4 hours post-stimulation (Figure 3d).

To determine if HIF-1α plays a direct role in regulating inflammatory cytokine production, cells were then stimulated for 18 hours with HMW or LMW under high or low glucose conditions in the presence or absence of ACR, which directly binds to HIF-1α and block HIF complex dimerization and limits its transcriptional activity without preventing its accumulation (58;

Supplemental Figure S4.2). Under high glucose conditions, preventing dimerization slightly reduced TNF-α (HMW: ↓31.6%, p=0.417 vs. LMW: ↓37.8%, p=0.08) and IL-6 production (HMW: ↓49.6%, p=0.049 vs. LMW: ↓100%, p=0.021) but did not reduce IL-10 levels (Figure 4.4A-D; Supplemental Figure S4.3A-B). Under low glucose conditions, ACR was associated with a more dramatic decrease in pro-inflammatory cytokine production following HMW Poly(I:C) stimulation (TNF-α: 57.1%, p=0.024, IL-6: 57.6%, p=0.043) and an almost complete inhibition of production following LMW Poly(I:C) (TNF-α: 93.7%, p<0.001, IL-6: 100%, p=0.004) (Figure 4.4A-D). Consistent with these findings, ACR had a more pronounced effect on reducing p-IκBα levels and the p-IκBα/IκBα ratio in low glucose conditions (Figure 4.4E). These results suggest that HIF-1α, through the modulation of NF-κB, contributes to inflammatory cytokine production following TLR3 engagement. They also suggest that HIF-1α's role in regulating inflammatory cytokine production, but not glycolysis, may become more important under conditions of stress.
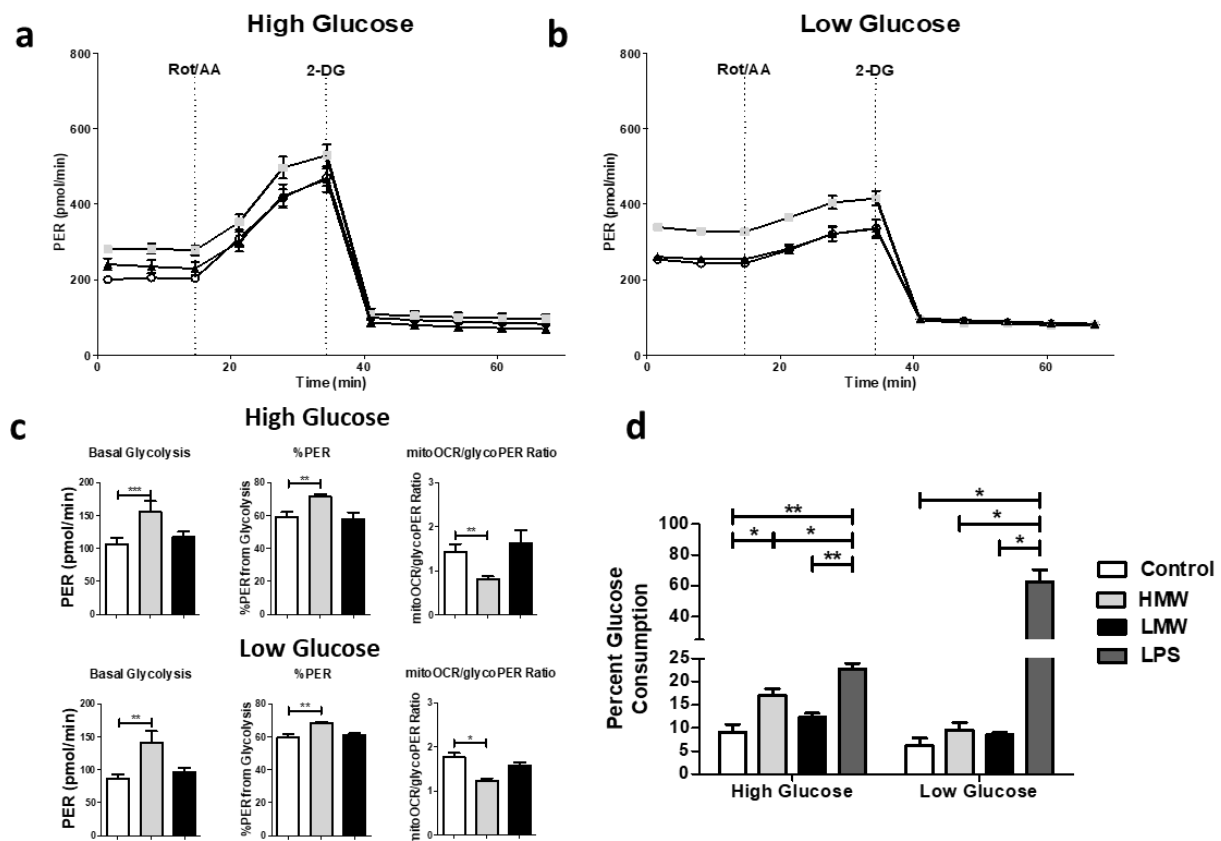
Figure 4.2: HMW Poly(I:C) stimulation is associated with increased glycolytic demands compared to LMW. Macrophages were stimulated with 10 ng/mL HMW Poly(I:C) or 10 ng/mL LMW Poly(I:C) for 18 hours. Glycolytic activity, as measured by Proton efflux rate (PER), was determined using a Seahorse efflux analyzer. Cells treated under high or low glucose conditions were exposed to sequential rotenone plus antimycin A (Rot/AA) and 2-deoxyglucose (2-DG) injections (**a, b**) in order to determine basal glycolytic rate, %PER dependent on glycolysis and the ratio of mitochondrial oxygen consumption rate (mitoOCR) to glycolytic PER (**c**). Glucose consumption by BMM after stimulation with HMW and LMW Poly(I:C) and LPS was determined using a glucometer (**d**). Data represents means ± SEM of four individual mice (*p < 0.05, **p < 0.01, and ***p < 0.001).
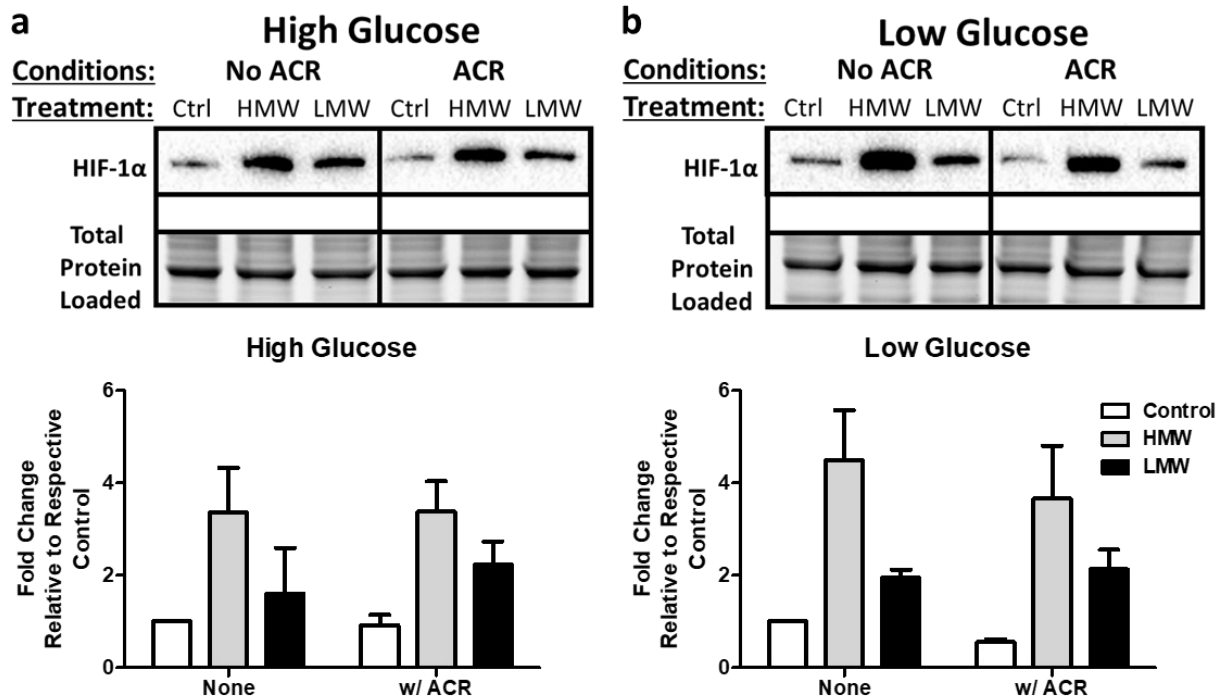
Supplemental Figure S4.2: Acriflavine treatment does not affect HIF-1α accumulation during HMW or LMW activation. HMW- or LMW-Poly(I:C) stimulated macrophages were co-treated with acriflavine (ACR) under high glucose (a) or low glucose (b) conditions for 18 hours. Total cell lysates were used to quantify HIF-1α expression via immunoblotting. Band intensity was normalized to the total protein levels in each of their respective lanes using the Bio-Rad Stain-Free Application. HIF-1α levels in each glucose condition was normalized to their respective control sample and presented as a fold change value. Data represents mean ± SEM of two individual mice.

235
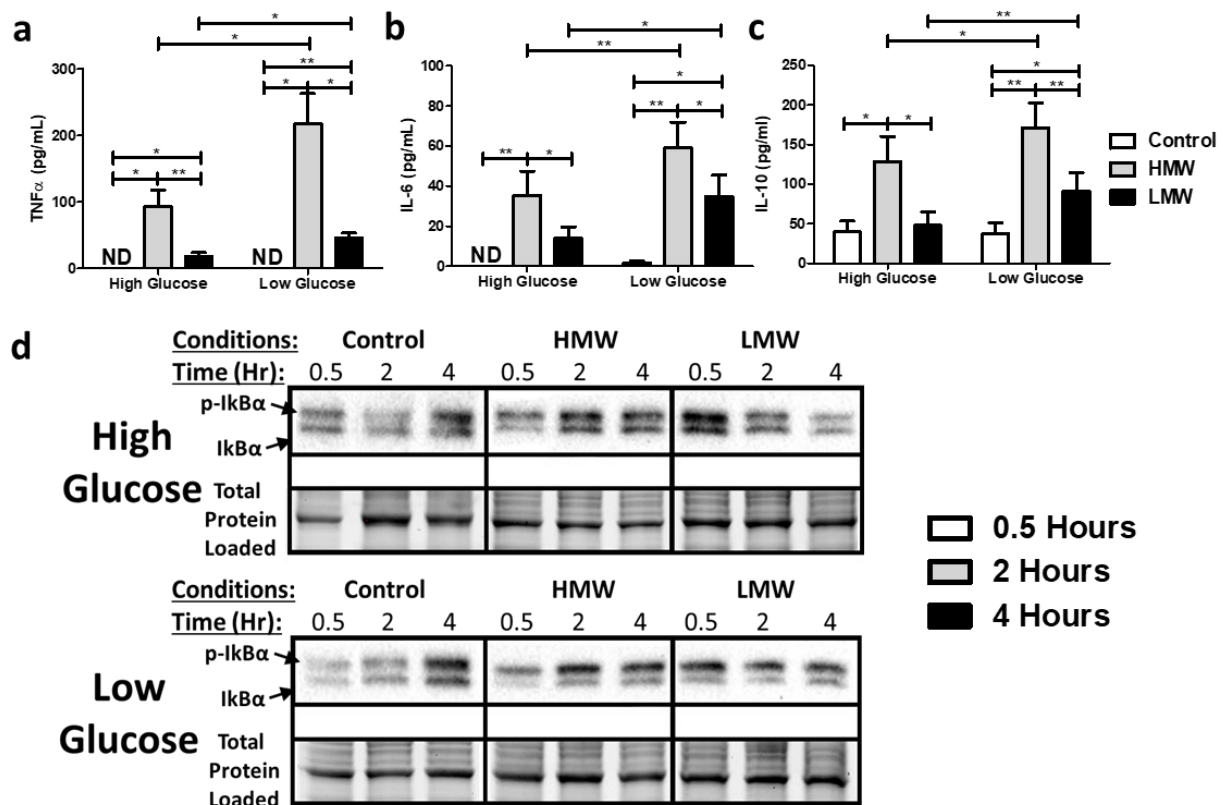
Figure 4.3: Low glucose conditions increased NF-κB activation and pro-inflammatory cytokine production. BMM were treated with 10 ng/mL HMW or 10 ng/mL LMW Poly(I:C) for 18 hours under high or low glucose media conditions. Pro-inflammatory cytokine production (TNF-α (**a**), IL-6 (**b**) and IL-10 (**c**)) was evaluated in culture supernatant. Total cell lysates were harvested to measure total and phosphorylated IκBα expression using immunoblotting at 0.5-, 2- and 4-hours post-stimulation (**d**). Band intensity was normalized to the total protein levels in each of their respective lanes using the Bio-Rad Stain-Free Application. Afterwards, the expression of IκBα in each glucose condition was normalized to its respective control sample collected at the same time point and presented as a fold change value. Data represents means ± SEM of four individual mice (*p < 0.05, **p < 0.01, and ***p < 0.001).
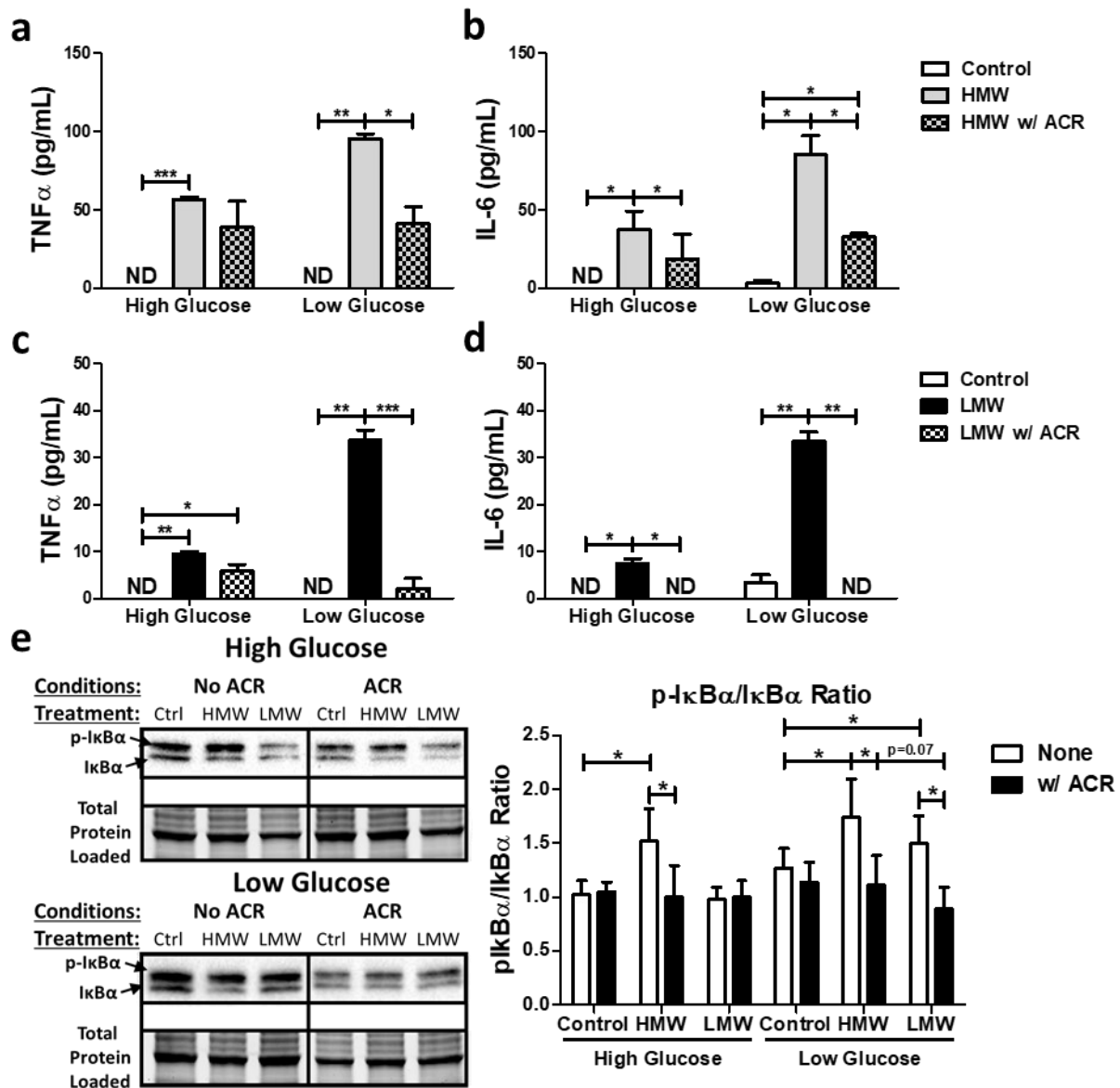
Figure 4.4: Targeting HIF-1 dimerization blunts pro-inflammatory but not anti-inflammatory cytokine expression. HMW or LMW Poly(I:C) stimulated macrophages were co-treated with acriflavine (ACR) under high glucose or low glucose conditions for 18 hours. Production of TNF-α (**a, c**) and IL-6 (**b, d**) in culture supernatant after HMW (**a-b**) or LMW activation (**c-d**) was measured using ELISA. Total protein and phosphorylation levels of IκBα from total cell lysates were quantified using immunoblotting after 18 hours (**e**). Band intensity was normalized to the total protein levels in each of their respective lanes using the Bio-Rad Stain-Free Application. Afterwards, the expression of IκBα in each glucose condition was normalized to its respective control sample and presented as a fold change value. Data represents means ± SEM of three individual mice (*p < 0.05, **p < 0.01, and ***p < 0.001).

237
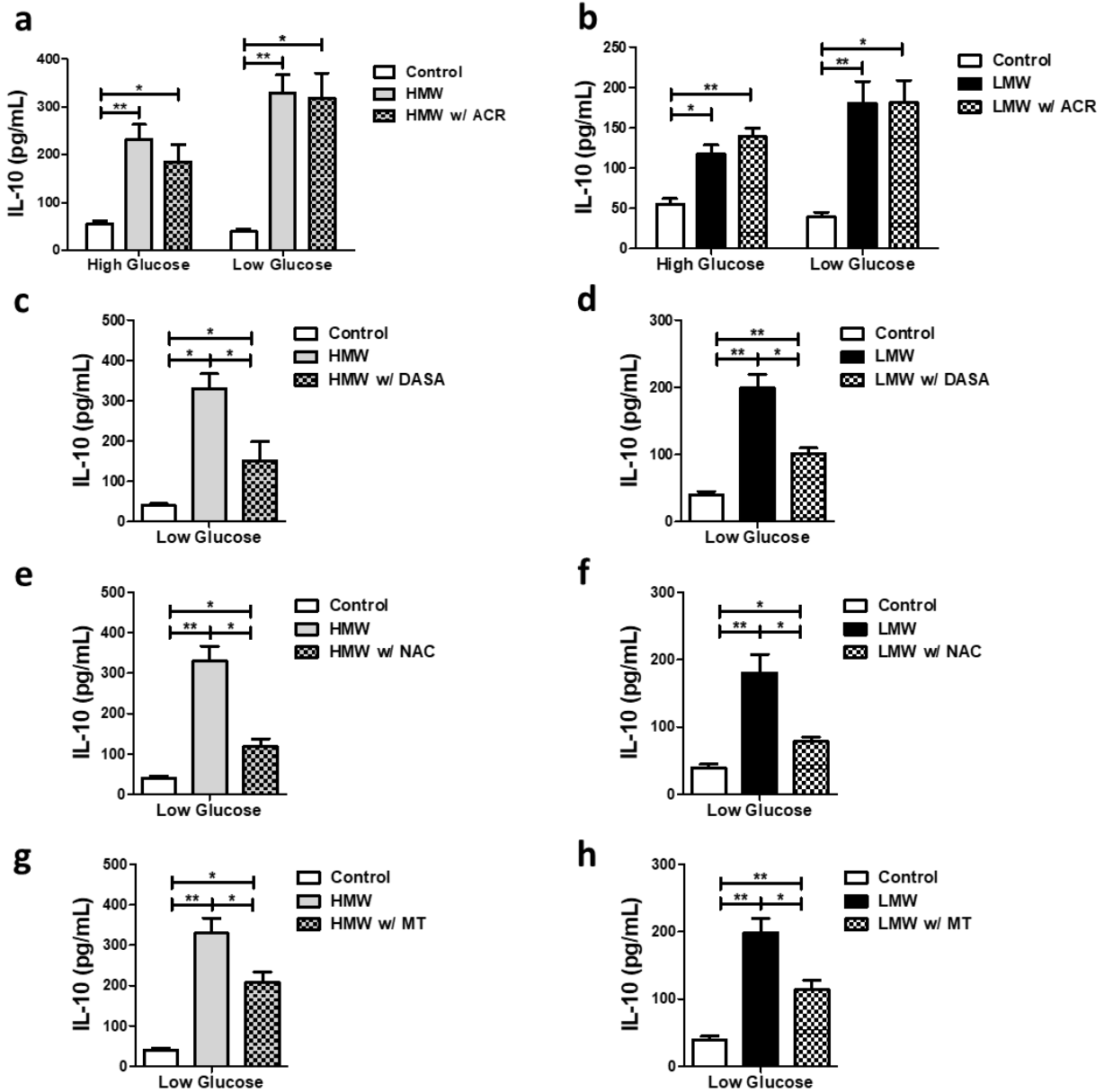
Supplemental Figure S4.3: HIF-1α does not directly regulate IL-10 expression. HMW- or LMW-Poly(I:C) stimulated macrophages were co-treated with either acriflavine (ACR) (a, b), DASA-58 (c, d), N-acetylcysteine (NAC) (e, f) or MitoTEMPO (MT) (g, h) under high glucose (a, c, e, g) or low glucose (b, d, f, h) conditions for 18 hours. IL-10 expression levels in culture supernatant were measured via ELISA. Data represents mean ± SEM of three individual mice (*p < 0.05, **p < 0.01, and ***p < 0.001).

4.3.4. PKM2 dimerization is important for HIF-1α- and NF-κB-driven inflammatory responses following TLR3 engagement

The stability and accumulation of HIF-1α is highly regulated at various levels by inhibitory proteins and metabolites (20, 59, 60), redox status (30, 61, 62) and transcriptional co-activators (19, 21). In particular, pyruvate kinase M2 (PKM2) has been shown to co-activate HIF-1α under inflammatory conditions (19, 21, 62). To evaluate if PKM2 is required for the co-activation of HIF-1α following TLR3 engagement, BMM were stimulated with HMW and LMW Poly(I:C) under low glucose conditions in the presence or absence of DASA-58, which is a PKM2 "activator" that locks the protein in an active glycolytic tetrameric state, preventing its interactions with HIF-1α. These experiments were conducted in low glucose conditions as this condition potently encourages HIF-1α accumulation. As seen with LPS (19), co-treatment with DASA-58 significantly reduced inflammatory cytokine production in cells stimulated with HMW and LMW Poly(I:C) (Figure 4.5A-D). However, as observed for ACR, the effects of DASA-58 on TNF-α (HMW: ↓54%, p=0.026 vs. LMW: ↓93%, p=0.017) and IL-6 (HMW: ↓80%, p=0.032 vs. LMW: ↓100%, p=0.004) production were more pronounced in LMW compared to HMW Poly(I:C) stimulated cells. Consistent with these findings, maintaining PKM2 in its tetrameric state significantly reduced the levels of phosphorylated IκBα and the phosphorylated IκBα to IκBα ratio (HMW: ↓37.4%, p=0.048 vs. LMW: ↓50.1%, p=0.038) (Figure 4.5F). Interestingly, unlike ACR, DASA-58 also reduced IL-10 production (Supplemental Figure S4.3C-D). This is likely related to the ability of PKM2 to modulate STAT3 (21, 63). Collectively, these data suggest that the effects of PKM2 on the co-activation (and potentially accumulation [Figure 4.5E]) of HIF-1α, and not its own role in glycolysis, contribute to the regulation of inflammatory cytokine production during antiviral immune responses. Further, while PKM2 and HIF-1α may be the central regulators of

inflammatory cytokine production following LMW Poly(I:C) stimulation, other factors may contribute to the regulation following HMW.

4.3.5. *Cytosolic and mitochondrial ROS differentially regulate HMW and LMW inflammatory cytokine production*

Previous studies have shown that ROS, whether generated in the cytosol or by mitochondria, are key modulators of HIF-1α stability during stress responses (21, 30, 61, 64). As such, I examined if both types of ROS might play a role in regulating HIF-1α accumulation following 18-hour HMW and LMW Poly(I:C) stimulation under low glucose conditions. MitoSOX™ Red was used to measure mitochondrial superoxide production and CellROX™ Orange was used to measure cytosolic ROS (Figures 4.6A and 4.7A). Both HMW and LMW Poly(I:C) stimulations were associated with increased mitochondrial superoxide accumulation (HMW FC=4.02, p<0.001; LMW FC=2.97, p=0.007) (Figure 4.6A). To evaluate if this increase in mitochondrial superoxide contributes to the stabilization of HIF-1α, I used MitoTEMPO to scavenge superoxide from active mitochondria. This co-treatment significantly reduced HIF-1α levels in both HMW and LMW stimulated cells (HMW: ↓49%, p=0.014 vs. LMW: ↓56%, p=0.013) (Figure 4.6B). Consistent with these findings, levels of IκBα phosphorylation (HMW: ↓35%, p=0.042 vs. LMW: ↓30%, p=0.019) (Figure 4.6G) and cytokine production were decreased following MT co-treatment (TNF-α [HMW: ↓33%, p=0.023 vs. LMW: ↓45%, p=0.049] and IL-6 [HMW: ↓75%, p=0.048 vs. LMW: ↓45%, p=0.045]) (Figure 4.6C-F). These findings suggest that mitochondrial ROS play a role in stabilizing HIF-1α following TLR3 engagement.

Next, I wanted to see if cytosolic ROS also contribute to the accumulation of HIF-1α following TLR3 engagement. Only HMW-treated cells were associated with a detectable increase in cytosolic ROS (HMW FC=1.33, p=0.003; LMW FC=1.09, p=0.096) (Figure 4.7A). Consistent with these findings, the antioxidant *N*-acetylcysteine (NAC) which targets total cellular ROS

production, only reduced HIF-1α accumulation in HMW stimulated cells (Figure 4.7B). Interestingly, NAC resulted in a near complete loss in TNF-α (HMW: ↓93%, p=0.006 vs. LMW: ↓100%, p=0.004) and IL-6 secretion (HMW: ↓81%, p=0.022 vs. LMW: ↓100%, p=0.004) (Figure 4.7C-F) following both HMW and LMW stimulation. NAC was also associated with significant loss in both forms of IκBα as well as the p-IκBα/IκBα ratio (HMW: ↓29%, p=0.040 vs. LMW: ↓19%, p=0.049) (Figure 4.7G). In addition to the scavenging of cellular ROS, NAC has been shown to increase the levels of cysteine, which is used as a substrate to generate glutathione (GSH), the principal antioxidant produced by the cell (65). GSH can also mediate post-translational modifications to signaling proteins such as IKK-β, which may reduce NF-κB activity (66). Collectively, these data suggest cytosolic ROS may only contribute to HIF-1α accumulation (and potentially associated cytokine production) following HMW-mediated engagement of TLR3.
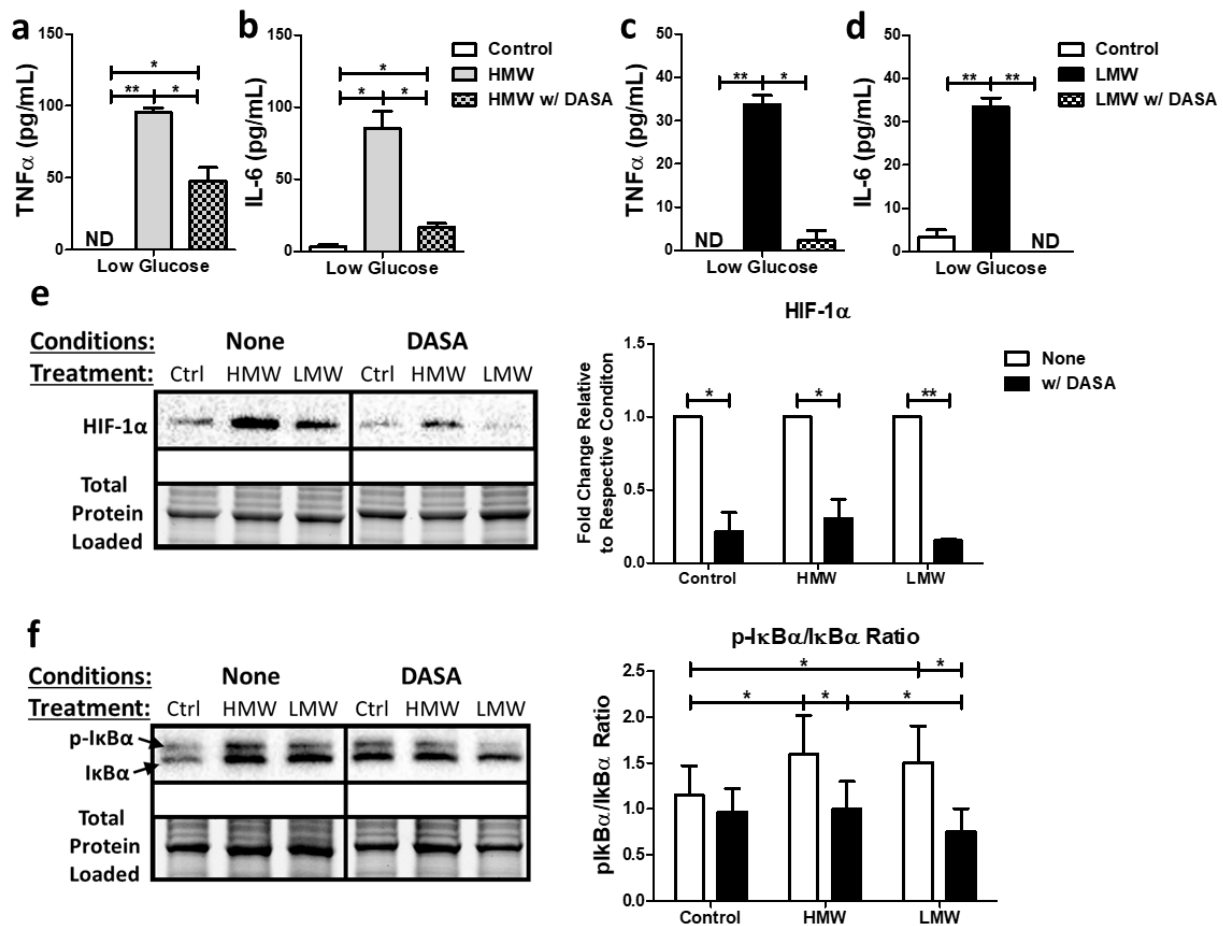
Figure 4.5: Maintenance of PKM2 in tetramer form reduces inflammatory cytokine production under low glucose conditions by reducing HIF-1α accumulation and NF-κB activation. Inflammatory cytokine production was measured in culture supernatant from cells stimulated with HMW or LMW Poly(I:C) for 18 hours in the presence of DASA-58. These experiments were performed under low glucose conditions. Secretion (**a-d**) of TNF-α (**a, c**) and IL-6 (**b, d**) under low glucose conditions after HMW (**a-b**) or LMW activation (**c-d**) were quantified *via* ELISA. Expression of HIF-1α (**e**) and IκBα (**f**) under low glucose conditions were assessed using immunoblotting. Band intensity was normalized to the total protein levels in each of their respective lanes using the Bio-Rad Stain-Free Application. Afterwards, the expression of IκBα in each glucose condition was normalized to its respective control sample and presented as a fold change value. Data represents means ± SEM of three individual mice (*p < 0.05, **p < 0.01, and ***p < 0.001).
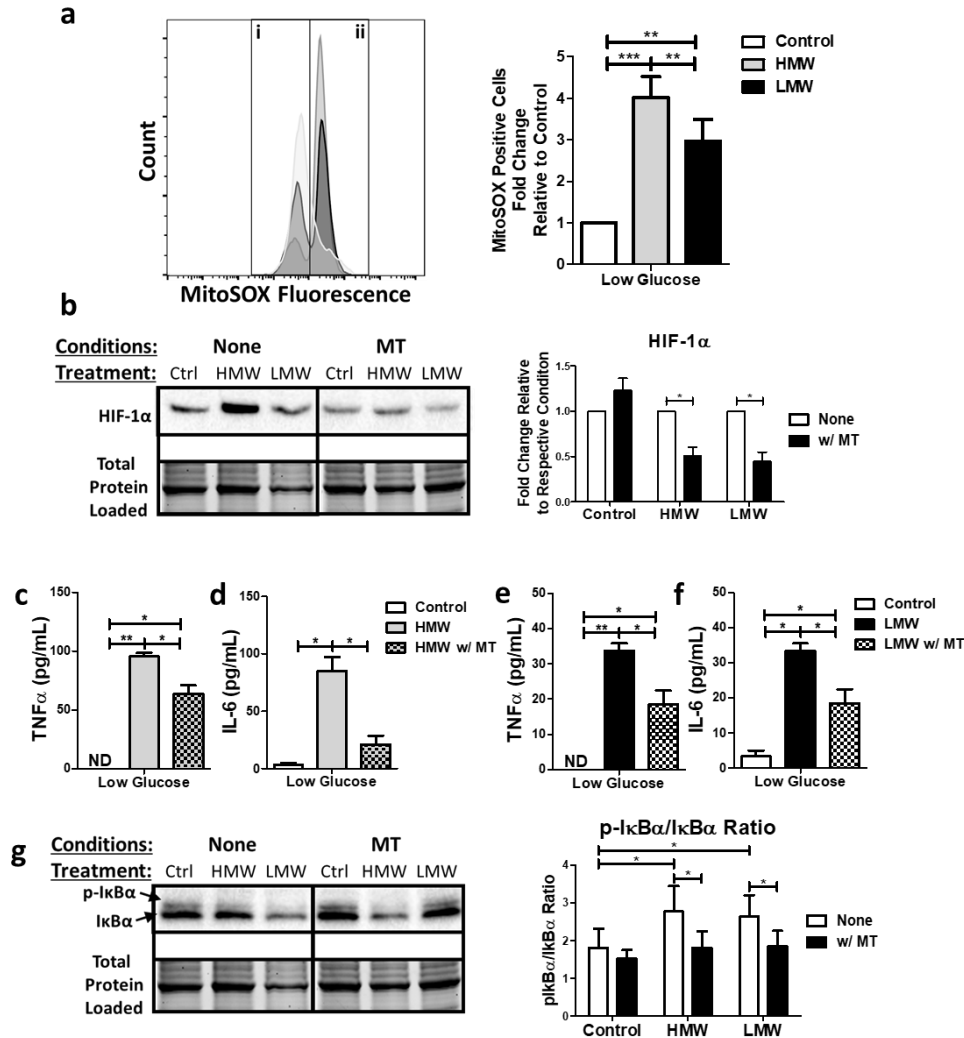
Figure 4.6: HMW- and LMW-mediated inflammatory cytokine production is blunted by mitochondrial ROS scavenging. HMW- and LMW-stimulated macrophages were examined for their differences in mitochondrial ROS production after 18 hours. Mitochondrial superoxide production was quantified using MitoSOX^{TM} Red staining. Cells stained with MitoSOX^{TM} Red were categorized into either a "negative" cell population (*i*) or a "positive" population (*ii*), where fold change difference in the percentage of positive cells relative to the control sample was shown in the bar graph to the right of the histogram (**a**). Next, BMM were treated with HMW or LMW in the presence or absence of MitoTEMPO (MT) for 18 hours. Expression of HIF-1α (**b**) and IκBα (**g**) under low glucose conditions was assessed using immunoblotting. Band intensity was normalized to the total protein levels in each of their respective lanes using the Bio-Rad Stain-Free Application. Afterwards, the expression of IκBα in each glucose condition was normalized to its respective control sample and presented as a fold change value. The effects of mitochondrial superoxide loss on inflammatory responses were assessed my measuring cytokine production (TNF-α (**c, e**) & IL-6 (**d, f**)) using ELISA. Data represents means ± SEM of three individual mice (*p < 0.05, **p < 0.01, and ***p < 0.001).
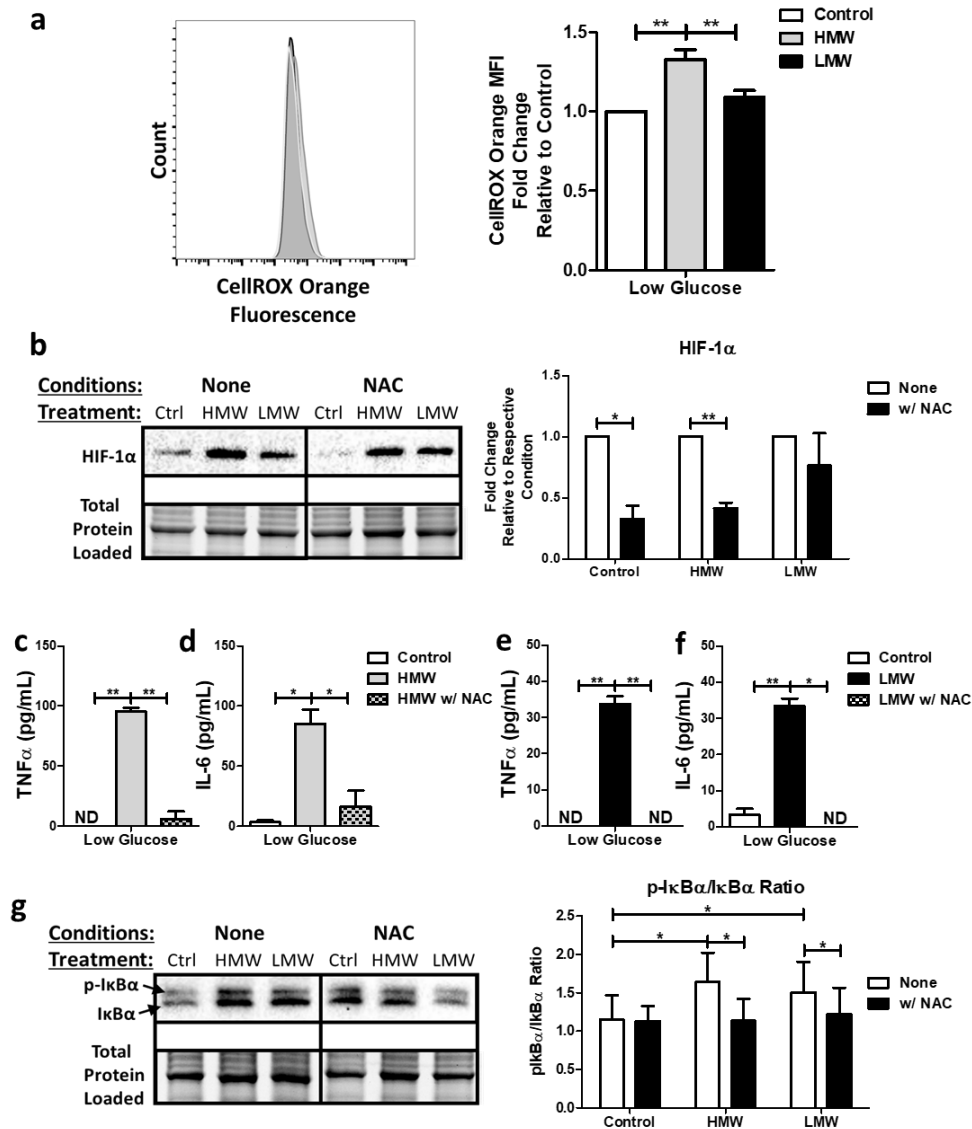
Figure 4.7: NAC differentially alters HIF-1α accumulation and completely inhibits inflammatory responses following HMW and LMW. HMW- and LMW-stimulated macrophages were examined for their differences in ROS production after 18 hours. Cytosolic ROS production was measured using CellROX™ Orange staining (**a**). For CellROX™ Orange staining, cells were analyzed based on changes in MFI. Next, to evaluate the effects of total cellular ROS on inflammatory responses, BMM were stimulated with HMW and LMW Poly(I:C) in the presence or absence of N-acetylcysteine (NAC). Expression of HIF-1α (**b**) and IκBα (**g**) under low glucose conditions was assessed using immunoblotting. Band intensity was normalized to the total protein levels in each of their respective lanes using the Bio-Rad Stain-Free Application. Afterwards, the expression of IκBα in each glucose condition was normalized to its respective control sample and presented as a fold change value. Cytokine production (TNF-α (**c, e**) & IL-6 (**d, f**)) was measured using ELISA. Data represents mean ± SEM of three individual mice (*$p < 0.05$, **$p < 0.01$, and ***$p < 0.001$).

244

4.4. Discussion:

The role of HIF-1α in regulating cellular metabolism and inflammation during antibacterial immune responses has been widely investigated (19, 20, 25, 27, 29, 30). However, its potential role in supporting antiviral immune responses is not fully understood. Here, I show that TLR3 activation and inflammatory cytokine production are differentially modulated by short and long dsRNA and that this process is dependent on HIF-1α accumulation, which is modified by glucose availability. Engagement of TLR3 by long dsRNAs (e.g., HMW Poly(I:C)) increased glycolytic activity and pro-inflammatory cytokine production in both high and low glucose conditions. This cytokine production is regulated by HIF-1α accumulation and is stabilized by PKM2, mitochondrial ROS, and cytosolic ROS. Conversely, engagement of TLR3 by short dsRNAs (e.g., LMW Poly(I:C)) did not alter glycolysis but rather induce a subdued inflammatory response in high glucose conditions. In contrast, stress (low glucose) conditions, increased HIF-1α expression and enhanced inflammatory cytokine production. In these activated cells, HIF-1α was stabilized by PKM2 and mitochondrial ROS, but not cytosolic ROS. Collectively, these data suggest that HIF-lα seems to fine tune the level of inflammatory cytokine production in antiviral immune responses and may act to drive differential responses to diverse activating ligands as well as nutrient availability in tissue microenvironments. These findings also suggest that HIF-1α and the proteins/molecules that stabilize its accumulation may represent potential targets to reduce pro-inflammatory cytokine production in antiviral immune responses.

While HIF-1α was originally identified under hypoxic conditions, studies have shown that nonhypoxic stimuli can also activate this transcription factor in a cell specific manner (24). In LPS-stimulated cells, over one hundred HIF-1α-related target genes are upregulated, including those associated with glucose metabolism (e.g. *PFKL, GAPDH, LDHA, PDK1*), inflammation (e.g.

IL1B, iNOS) and redox homeostasis (e.g. *GPX3, HMOX1, SOD2*) (19, 67, 68). HIF-1α plays a central role in inducing the Warburg effect in these inflammatory cells (21, 24, 25, 62, 69). This inflammatory phenotype can be reversed by genetic deletion of HIF-1α or by inhibiting glycolysis (e.g., 2-DG) (60, 70, 71). Furthermore, HIF-1α overexpression in macrophages induce a hyperinflammatory state with heightened IL-1β, IL-6 and TNF-α expression (62). Taken together, these studies suggest HIF-1α-induced glycolysis is required to support inflammatory cytokine production. Here, I found that HMW but not LMW Poly(I:C) was associated with increased glycolysis in standard culture conditions (high glucose). In stark contrast to LPS stimulated cells, neither HMW nor LMW Poly(I:C) stimulation increased glucose uptake under low glucose conditions. Interestingly, while HMW was associated with a more pronounced inflammatory response, potentially linked to increased glycolysis, inflammatory cytokine production in LMW stimulated cells depended more on HIF-1α accumulation (Figure 4). Collectively, our results suggest HIF-1α may regulate antiviral inflammatory responses, at least in part, using mechanisms independent of glycolysis.

HIF-1α/NF-κB crosstalk has been shown to play a critical role in mounting effective immune responses (26, 72, 73). Traditionally, NF-κB is thought to regulate HIF-1α function. Bonello et al. (74) found an NF-κB binding element in the HIF-1α promoter and showed that hydrogen peroxide (H$_2$O$_2$), and the activation of NOX4-containing NADPH oxidase, increased NF-κB-mediated HIF-1α expression. In bacterial infections, IKK-β has been shown to regulate HIF-1α accumulation (26, 73) Further, Hepatitis C infection has been shown to boost HIF-1α expression in a NF-κB- and MAPK-dependent manner (35). In this study, I found that HIF-1α may also regulate NF-κB activity. Consistent with these findings, HIF-1α has been shown to drive the expression of NF-κB-regulated inflammatory mediators in LPS-stimulated macrophages (25, 75),

and knocking out HIF-1α has been shown to protect against LPS-induced mortality (75). HIF-1α-mediated activation of NF-κB and IL-1β is also required for neutrophil survival and function (76). While further studies are required to better understand the specific mechanisms by which HIF-1α regulates NF-κB, our studies suggest there may be bidirectional communication between HIF-1α and NF-κB, creating a feed-forward loop to activate inflammatory cells.

Several studies show that short and long cytosolic dsRNA differentially interact with RIG-I and MDA5, respectively (43, 46). I have shown that extracellular short (LMW: 200-1000 bp) vs. long (HMW: 1500-8000 bp) Poly(I:C) differentially engage TLR3, inducing distinct inflammatory and metabolic responses. Leonard et al. (51) found that dsRNA binds to TLR3 dimers in a saturable, specific, and reversible manner. To induce these dimers, dsRNA strands must be long enough (40-50 bp) to weakly interact with three separate contact sites on each monomer (49, 50). Binding affinity increases with strand length, with longer dsRNAs binding to multiple TLR3 dimers to induce differential signaling (51). Emerging evidence suggests that TLR3 responsiveness may differ between cell types (47, 48, 77). While MEF responsiveness is greater with longer dsRNA strands, RAW264.7 cells are more responsive to shorter dsRNA strands (47). Similarly, Jiang et al. (48) found human monocyte-derived dendritic cells produce more robust antiviral and pro-inflammatory responses to short synthetic and influenza A specific-dsRNA strands. It is unclear what drives these cell-specific responses, but dsRNA has been shown to interact with other cellular receptors, including CCR5 (78). The idea of functional sensing is not specific to TLR3. Engagement of TLR4 with increasing concentrations of LPS selectively activates intracellular adaptor molecules. For example, picogram concentrations activate TRAM/TRIF signaling, whereas nanogram concentrations are required to also activate MyD88

signaling and induce robust inflammatory responses (79-81). This highlights the remarkable ability of TLRs to sense stimuli and respond based on ligand type, length, and concentration.

HIF-1α expression and function are regulated at multiple levels: post-translationally, metabolically, and at the level of complex formation. Under normoxic conditions, prolyl hydroxylases (PHDs) and the Factor Inhibiting HIF-I (FIH-I) hydroxylate proline and asparagine residues respectively along HIF-1α, leading to the destabilization and degradation of HIF-1α (82-86). These hydroxylation reactions are impeded in the absence of oxygen, resulting in HIF-1α stabilization and accumulation (84). In this study, I found that HIF-1α was stabilized by several factors including PKM2, which exists in tetramer and dimer forms in the cytosol. In its tetramer form, PKM2 serves as the final enzyme of glycolysis. As a dimer, it translocates into the nucleus and co-activates HIF-1α (19, 87, 88), which promotes an inflammatory state by increasing the expression of lactose dehydrogenase (LDH) and pyruvate dehydrogenase (PDH) kinase (PDK). This inactivates the conversion of pyruvate to acetyl-CoA by PDH and forces pyruvate towards LDH to produce lactate (88-91). This, consequentially, increases the expression of IL-1β, IL-6 and TNF-α (20, 21, 75, 92). The PKM2 dimer also functions as a protein tyrosine kinase. It phosphorylates STAT3 in the nucleus leading to IL-6 and IL-1β expression (21, 63). Small molecule activators, which lock PKM2 into its glycolytically active tetramer form, decrease glycolytic-associated inflammation (19, 21). This secondary "moonlighting" function of PKM2 is not limited to inflammatory macrophages, as it is also important for proper Th1 and Th17 differentiation. Silencing, inhibiting, or locking PKM2 resulted in reduced T cell activation, proliferation, and associated cytokine production (93, 94). Here, I found that locking PKM2 into its tetramer using DASA-58 resulted in decreased accumulation of HIF-1α, NF-κB activation, and inflammatory cytokine production in low glucose conditions. Interestingly, locking PKM2 into its

tetramer form produced a more pronounced effect on LMW responses, suggesting other factors may also contribute to HIF-1α stabilization following stimulation with HMW Poly(I:C).

Exogenous or endogenous H_2O_2 and siRNA-mediated inhibition of mitochondrial superoxide dismutase 2 (SOD2) have also been shown to stabilize HIF-1α protein levels under normoxic conditions, suggesting ROS may help stabilize HIF-1α levels (95-98). Both superoxide and H_2O_2 have also been shown to directly inhibit PHD activity by oxidizing the iron cofactor of these enzymes (99, 100). Furthermore, H_2O_2 can induce disulfide bond-mediated PHD2 dimerization, which inactivates the protein and results in HIF-1α stabilization (101). Mitochondrial ROS have also been shown to stabilize HIF-1α by possibly oxidizing the iron cofactor of PHDs (102). Additionally, targeting superoxide production from Complex III of the ETC without the loss of OXPHOS has been shown to reduce HIF-1α accumulation (103). Here, I found that mitochondrial and cytosolic ROS differentially contribute to HIF-1α stabilization following HMW vs. LMW Poly(I:C) stimulations. In HMW-stimulated macrophages, both cellular and mitochondrial ROS contributed to HIF-1α accumulation, NF-κB activation and the secretion of inflammatory cytokines. However, in LMW-activated macrophages only mitochondrial ROS were found to be critical in driving a pro-inflammatory state. Interestingly, Li et al. (104) found that a small amount of HIF-1α localizes to the outer mitochondrial membrane under hypoxic conditions or after H_2O_2 treatment. In addition, the authors developed a mitochondrial-targeted form of HIF-1α. This ectopic form of HIF-1α attenuates apoptosis, reduces mtDNA release, and increases MMP (104). Cells with depleted mtDNA have diminished respiration, TCA cycle activity, and MMP leading to reduced HIF-1α levels (105). Genetic reconstitution of MMP restored ROS levels in these cells, which was critical for HIF-1α accumulation (105). This highlights the importance of ROS and mitochondrial function to HIF-1α transcriptional activity.

Interestingly, I found that co-treatment with NAC resulted in a near complete reduction of inflammatory cytokine production in both HMW and LMW stimulated cells, irrespective of cytosolic ROS accumulation. NAC functions by replenishing the cysteine supply in the cells, which is used to produce GSH (106). While GSH is an important ROS scavenger, it has also been shown to post-translationally modify proteins (glutathionylation) associated with TLR3 signaling (17, 66, 107, 108). Reynaert et al. (107) found that glutathionylation reduces IKK-β activity, resulting in the loss of IκBα phosphorylation and reduced NF-κB activity. The direct glutathionylation of IκBα has also been shown to prevent its phosphorylation, and therefore preventing NF-κB activation (66). Furthermore, the DNA-binding site of the p50 subunit of NF-κB can be S-glutathionylated, leading to reduced pro-inflammatory cytokine expression (108).

In summary, I show that HIF-1α plays an important role in regulating the magnitude of inflammatory responses in mouse BMM following TLR3 engagement. HIF-1α amplifies these inflammatory responses following strong engagement of TLR3 and under stress conditions, such as glucose deprivation. This may play a role in a macrophage's ability to survey tissues for pathogens and shape its response based on the pathogen and the tissue microenvironment (109). I also show that this amplifying effect is largely mediated by increasing IκBα phosphorylation and NF-κB activity. Based on these findings, it is tempting to speculate that targeting HIF-1α or its stabilizing factors may represent a potential therapeutic strategy to reduce high levels of damaging inflammation during acute and chronic viral infections.

4.5. References

1. Ross, J. A., and M. J. Auger. 2002. Biology of the Macrophage. In *The Macrophage*, 2nd ed. B. Burke, and C. E. Lewis, eds. Oxford University Press, New York, New York. 1-57.
2. Pearce, Erika L., and Edward J. Pearce. 2013. Metabolic pathways in immune cell activation and quiescence. *Immunity* 38: 633-643.
3. Mosser, D. M., and J. P. Edwards. 2008. Exploring the full spectrum of macrophage activation. *Nat Rev Immunol* 8: 958-969.
4. Djafarzadeh, S., M. Vuda, J. Takala, M. Ochs, and S. M. Jakob. 2011. Toll-like receptor-3-induced mitochondrial dysfunction in cultured human hepatocytes. *Mitochondrion* 11: 83-88.
5. Koshiba, T. 2013. Mitochondrial-mediated antiviral immunity. *Biochim Biophys Acta* 1833: 225-232.
6. Yoshizumi, T., H. Imamura, T. Taku, T. Kuroki, A. Kawaguchi, K. Ishikawa, K. Nakada, and T. Koshiba. 2017. RLR-mediated antiviral innate immunity requires oxidative phosphorylation activity. *Sci Rep* 7: 5379.
7. Pantel, A., A. Teixeira, E. Haddad, E. G. Wood, R. M. Steinman, and M. P. Longhi. 2014. Direct type I IFN but not MDA5/TLR3 activation of dendritic cells is required for maturation and metabolic shift to glycolysis after Poly IC stimulation. *PLoS Biol.* 12: e1001759.
8. Everts, B., E. Amiel, S. C.-C. Huang, A. M. Smith, C.-H. Chang, W. Y. Lam, V. Redmann, T. C. Freitas, J. Blagih, G. J. W. van der Windt, M. N. Artyomov, R. G. Jones, E. L. Pearce, and E. J. Pearce. 2014. TLR-driven early glycolytic reprogramming via the kinases TBK1-IKKε supports the anabolic demands of dendritic cell activation. *Nat Immunol* 15: 323-332.
9. Garaude, J., R. Acín-Pérez, S. Martínez-Cano, M. Enamorado, M. Ugolini, E. Nistal-Villán, S. Hervás-Stubbs, P. Pelegrín, L. E. Sander, J. A. Enríquez, and D. Sancho. 2016. Mitochondrial respiratory-chain adaptations in macrophages contribute to antibacterial host defense. *Nat Immunol* 17: 1037-1045.
10. Wu, D., David E. Sanin, B. Everts, Q. Chen, J. Qiu, Michael D. Buck, A. Patterson, Amber M. Smith, C.-H. Chang, Z. Liu, Maxim N. Artyomov, Erika L. Pearce, M. Cella, and Edward J. Pearce. 2016. Type 1 Interferons induce changes in core metabolism that are critical for immune function. *Immunity* 44: 1325-1336.
11. Ahmed, D., D. Roy, A. Jaworski, A. Edwards, A. Abizaid, A. Kumar, A. Golshani, and E. Cassol. 2019. Differential remodeling of the electron transport chain is required to support TLR3 and TLR4 signaling and cytokine production in macrophages. *Sci Rep* 9: 18801.
12. Seth, R. B., L. Sun, C.-K. Ea, and Z. J. Chen. 2005. Identification and characterization of MAVS, a mitochondrial antiviral signaling protein that a ctivates NF-κB and IRF3. *Cell* 122: 669-682.
13. Kawai, T., K. Takahashi, S. Sato, C. Coban, H. Kumar, H. Kato, K. J. Ishii, O. Takeuchi, and S. Akira. 2005. IPS-1, an adaptor triggering RIG-I- and MDA5-mediated type I interferon induction. *Nat Immunol* 6: 981-988.
14. Xu, L.-G., Y.-Y. Wang, K.-J. Han, L.-Y. Li, Z. Zhai, and H.-B. Shu. 2005. VISA is an adapter protein required for virus-triggered IFN-β Ssgnaling. *Mol Cell* 19: 727-740.
15. Tal, M. C., M. Sasai, H. K. Lee, B. Yordy, G. S. Shadel, and A. Iwasaki. 2009. Absence of autophagy results in reactive oxygen species-dependent amplification of RLR signaling. *Proc Natl Acad Sci U S A* 106: 2770.

16. Indukuri, H., S. M. Castro, S.-M. Liao, L. A. Feeney, M. Dorsch, A. J. Coyle, R. P. Garofalo, A. R. Brasier, and A. Casola. 2006. Ikkε regulates viral-induced interferon regulatory factor-3 activation via a redox-sensitive pathway. *Virology* 353: 155-165.

17. Gonzalez-Dosal, R., K. A. Horan, S. H. Rahbek, H. Ichijo, Z. J. Chen, J. J. Mieyal, R. Hartmann, and S. R. Paludan. 2011. HSV infection induces production of ROS, which potentiate signaling from pattern recognition receptors: Role for S-glutathionylation of TRAF3 and 6. *PLOS Pathog* 7: e1002250.

18. Yang, C.-S., J.-J. Kim, S. J. Lee, J. H. Hwang, C.-H. Lee, M.-S. Lee, and E.-K. Jo. 2013. TLR3-triggered reactive oxygen species contribute to inflammatory responses by activating Signal transducer and activator of transcription-1. *J Immunol* 190: 6368.

19. Palsson-McDermott, E. M., A. M. Curtis, G. Goel, M. A. R. Lauterbach, F. J. Sheedy, L. E. Gleeson, M. W. M. van den Bosch, S. R. Quinn, R. Domingo-Fernandez, D. G. W. Johnston, J.-k. Jiang, W. J. Israelsen, J. Keane, C. Thomas, C. Clish, M. Vander Heiden, R. J. Xavier, and L. A. J. O'Neill. 2015. Pyruvate kinase M2 regulates Hif-1α activity and IL-1β induction and is a critical determinant of the warburg effect in LPS-activated macrophages. *Cell Metab.* 21: 65-80.

20. Tannahill, G. M., A. M. Curtis, J. Adamik, E. M. Palsson-McDermott, A. F. McGettrick, G. Goel, C. Frezza, N. J. Bernard, B. Kelly, N. H. Foley, L. Zheng, A. Gardet, Z. Tong, S. S. Jany, S. C. Corr, M. Haneklaus, B. E. Caffrey, K. Pierce, S. Walmsley, F. C. Beasley, E. Cummins, V. Nizet, M. Whyte, C. T. Taylor, H. Lin, S. L. Masters, E. Gottlieb, V. P. Kelly, C. Clish, P. E. Auron, R. J. Xavier, and L. A. J. O'Neill. 2013. Succinate is an inflammatory signal that induces IL-1β through HIF-1α. *Nature* 496: 238-242.

21. Shirai, T., R. R. Nazarewicz, B. B. Wallis, R. E. Yanes, R. Watanabe, M. Hilhorst, L. Tian, D. G. Harrison, J. C. Giacomini, T. L. Assimes, J. J. Goronzy, and C. M. Weyand. 2016. The glycolytic enzyme PKM2 bridges metabolic and inflammatory dysfunction in coronary artery disease. *J. Exp. Med.* 213: 337-354.

22. Karshovska, E., Y. Wei, P. Subramanian, R. Mohibullah, C. Geißler, I. Baatsch, A. Popal, J. Corbalán Campos, N. Exner, and A. Schober. 2020. HIF-1α (Hypoxia-inducible factor-1α) promotes macrophage necroptosis by regulating miR-210 an d miR-383. *Arterioscler Thromb Vasc Biol* 40: 583-596.

23. Palazon, A., A. W. Goldrath, V. Nizet, and R. S. Johnson. 2014. HIF transcription factors, inflammation, and immunity. *Immunity* 41: 518-528.

24. Blouin, C. C., E. L. Pagé, G. M. Soucy, and D. E. Richard. 2004. Hypoxic gene activation by lipopolysaccharide in macrophages: Implication of Hypoxia-inducible factor 1α. *Blood* 103: 1124-1130.

25. Peyssonnaux, C., V. Datta, T. Cramer, A. Doedens, E. A. Theodorakis, R. L. Gallo, N. Hurtado-Ziola, V. Nizet, and R. S. Johnson. 2005. HIF-1α expression regulates the bactericidal capacity of phagocytes. *J. Clin. Invest.* 115: 1806-1815.

26. Rius, J., M. Guma, C. Schachtrup, K. Akassoglou, A. S. Zinkernagel, V. Nizet, R. S. Johnson, G. G. Haddad, and M. Karin. 2008. NF-κB links innate immunity to the hypoxic response through transcriptional regulation of HIF-1α. *Nature* 453: 807-811.

27. Cramer, T., Y. Yamanishi, B. E. Clausen, I. Förster, R. Pawlinski, N. Mackman, V. H. Haase, R. Jaenisch, M. Corr, V. Nizet, G. S. Firestein, H.-P. Gerber, N. Ferrara, and R. S. Johnson. 2003. HIF-1α is essential for myeloid cell-mediated inflammation. *Cell* 112: 645-657.

28.   Anand, R., S. Gribar, J. Li, J. W. Kohler, M. F. Branca, T. D. Dubowski, C. Sodhi, and D. Hackam. 2007. Hypoxia causes an increase in phagocytosis by macrophages in a Hif-1α-dependent manner. *J Leukoc Biol* 82.

29.   Frede, S., C. Stockmann, P. Freitag, and J. Fandrey. 2006. Bacterial lipopolysaccharide induces HIF-1 activation in human monocytes via p44/42 MAPK and NF-kappaB. *Biochem J* 396: 517-527.

30.   Mills, E. L., B. Kelly, A. Logan, A. S. H. Costa, M. Varma, C. E. Bryant, P. Tourlomousis, J. H. M. Däbritz, E. Gottlieb, I. Latorre, S. C. Corr, G. McManus, D. Ryan, H. T. Jacobs, M. Szibor, R. J. Xavier, T. Braun, C. Frezza, M. P. Murphy, and L. A. O'Neill. 2016. Succinate dehydrogenase supports metabolic repurposing of mitochondria to drive inflammatory macrophages. *Cell* 167: 457-470.e413.

31.   Deshmane, S. L., R. Mukerjee, S. Fan, L. Del Valle, C. Michiels, T. Sweet, I. Rom, K. Khalili, J. Rappaport, S. Amini, and B. E. Sawaya. 2009. Activation of the oxidative stress pathway by HIV-1 Vpr leads to induction of hypoxia-inducible factor 1alpha expression. *J Biol Chem* 284.

32.   Deshmane, S. L., S. Amini, S. Sen, K. Khalili, and B. E. Sawaya. 2011. Regulation of the HIV-1 promoter by HIF-1α and Vpr proteins. *Virol J* 8: 477.

33.   Duette, G., P. Pereyra Gerber, J. Rubione, P. S. Perez, A. L. Landay, S. M. Crowe, Z. Liao, K. W. Witwer, M. P. Holgado, J. Salido, J. Geffner, O. Sued, C. S. Palmer, and M. Ostrowski. 2018. Induction of HIF-1α by HIV-1 infection in CD4(+) T cells promotes viral replication and drives extracellular vesicle-mediated inflammation. *mBio* 9: e00757-00718.

34.   Ripoli, M., A. D'Aprile, G. Quarato, M. Sarasin-Filipowicz, J. Gouttenoire, R. Scrima, O. Cela, D. Boffoli, M. H. Heim, D. Moradpour, N. Capitanio, and C. Piccoli. 2010. Hepatitis C virus-linked mitochondrial dysfunction promotes Hypoxia-inducible factor 1α-mediated glycolytic adaptation. *J Virol* 84: 647-660.

35.   Nasimuzzaman, M., G. Waris, D. Mikolon, D. G. Stupack, and A. Siddiqui. 2007. Hepatitis C virus stabilizes Hypoxia-inducible factor 1α and stimulates the synthesis of Vascular endothelial growth factor. *J Virol* 81: 10249.

36.   Yoo, Y.-G., S. H. Oh, E. S. Park, H. Cho, N. Lee, H. Park, D. K. Kim, D.-Y. Yu, J. K. Seong, and M.-O. Lee. 2003. Hepatitis B virus X protein enhances transcriptional activity of Hypoxia-inducible factor-1α through activation of Mitogen-activated protein kinase pathway. *J Biol Chem* 278: 39076-39084.

37.   Cai, Q.-L., J. S. Knight, S. C. Verma, P. Zald, and E. S. Robertson. 2006. EC5S ubiquitin complex is recruited by KSHV latent antigen LANA for degradation of the VHL and p53 tumor suppressors. *PLOS Pathog* 2: e116.

38.   Kondo, S., S. Y. Seo, T. Yoshizaki, N. Wakisaka, M. Furukawa, I. Joab, K. L. Jang, and J. S. Pagano. 2006. EBV latent membrane protein 1 up-regulates Hypoxia-inducible factor 1α through Siah1-mediated down-regulation of Prolyl hydroxylases 1 and 3 in nasopharyngeal epithelial cells. *Cancer Res* 66: 9870.

39.   Heil, F., H. Hemmi, H. Hochrein, F. Ampenberger, C. Kirschning, S. Akira, G. Lipford, H. Wagner, and S. Bauer. 2004. Species-specific recognition of single-stranded RNA via Toll-like receptor 7 and 8. *Science* 303: 1526-1529.

40.   Lund, J., A. Sato, S. Akira, R. Medzhitov, and A. Iwasaki. 2003. Toll-like receptor 9–mediated recognition of herpes simplex virus-2 by plasmacytoid dendritic cells. *J Exp Med* 198: 513-520.

41.	Alexopoulou, L., A. C. Holt, R. Medzhitov, and R. A. Flavell. 2001. Recognition of double-stranded RNA and activation of NF-[kappa]B by Toll-like receptor 3. *Nature* 413: 732-738.

42.	Yoneyama, M., M. Kikuchi, T. Natsukawa, N. Shinobu, T. Imaizumi, M. Miyagishi, K. Taira, S. Akira, and T. Fujita. 2004. The RNA helicase RIG-I has an essential function in double-stranded RNA-induced innate antiviral responses. *Nat Immunol* 5: 730-737.

43.	Kato, H., O. Takeuchi, S. Sato, M. Yoneyama, M. Yamamoto, K. Matsui, S. Uematsu, A. Jung, T. Kawai, K. J. Ishii, O. Yamaguchi, K. Otsu, T. Tsujimura, C.-S. Koh, C. Reis e Sousa, Y. Matsuura, T. Fujita, and S. Akira. 2006. Differential roles of MDA5 and RIG-I helicases in the recognition of RNA viruses. *Nature* 441: 101-105.

44.	Takeuchi, O., and S. Akira. 2009. Innate immunity to virus infection. *Immunol Rev* 227: 75-86.

45.	Kawai, T., and S. Akira. 2007. Signaling to NF-κB by Toll-like receptors. *Trends Mol Med* 13: 460-469.

46.	Kato, H., O. Takeuchi, E. Mikamo-Satoh, R. Hirai, T. Kawai, K. Matsushita, A. Hiiragi, T. S. Dermody, T. Fujita, and S. Akira. 2008. Length-dependent recognition of double-stranded ribonucleic acids by Retinoic acid-inducible gene-I and Melanoma differentiation-associated gene 5. *J Exp Med* 205: 1601-1610.

47.	Mian, M. F., A. N. Ahmed, M. Rad, A. Babaian, D. Bowdish, and A. A. Ashkar. 2013. Length of dsRNA (poly I:C) drives distinct innate immune responses, depending on the cell type. *J Leukoc Biol* 94: 1025-1036.

48.	Jiang, M., P. Österlund, L. P. Sarin, M. M. Poranen, D. H. Bamford, D. Guo, and I. Julkunen. 2011. Innate immune responses in human Monocyte-derived dendritic cells are highly dependent on the size and the 5′ phosphorylation of RNA molecules. *J Immunol* 187: 1713.

49.	Wang, Y., L. Liu, D. R. Davies, and D. M. Segal. 2010. Dimerization of Toll-like receptor 3 (TLR3) is required for ligand binding. *J Biol Chem* 285: 36836-36841.

50.	Liu, L., I. Botos, Y. Wang, J. N. Leonard, J. Shiloach, D. M. Segal, and D. R. Davies. 2008. Structural basis of Toll-like receptor 3 signaling with double-stranded RNA. *Science* 320: 379-381.

51.	Leonard, J. N., R. Ghirlando, J. Askins, J. K. Bell, D. H. Margulies, D. R. Davies, and D. M. Segal. 2008. The TLR3 signaling complex forms by cooperative receptor dimerization. *Proc Natl Acad Sci U S A* 105: 258-263.

52.	Weischenfeldt, J., and B. Porse. 2008. Bone marrow-derived macrophages (BMM): Isolation and applications. *CSH Protoc* 2008: pdb.prot5080.

53.	Taylor, S. C., T. Berkelman, G. Yadav, and M. Hammond. 2013. A defined methodology for reliable quantification of Western blot data. *Mol Biotechnol* 55: 217-226.

54.	Achari, A. E., and S. K. Jain. 2016. L-Cysteine supplementation increases adiponectin synthesis and secretion, and GLUT4 and glucose utilization by upregulating disulfide bond A-like protein expression mediated by MCP-1 inhibition in 3T3-L1 adipocytes exposed to high glucose. *Mol Cell Biochem* 414: 105-113.

55.	Rodríguez-Prados, J., P. G. Través, J. Cuenca, D. Rico, J. Aragonés, P. Martín-Sanz, M. Cascante, and L. Boscá. 2010. Substrate fate in activated macrophages: A comparison between innate, classic, and alternative activation. *J Immunol* 185: 605-614.

56.	Freemerman, A. J., A. R. Johnson, G. N. Sacks, J. J. Milner, E. L. Kirk, M. A. Troester, A. N. Macintyre, P. Goraksha-Hicks, J. C. Rathmell, and L. Makowski. 2014. Metabolic

reprogramming of macrophages: Glucose transporter 1 (GLUT1)-mediated glucose metabolism drives a proinflammatory phenotype. *J Biol Chem* 289: 7884-7896.

57.   Semenza, G. L. 1998. Hypoxia-inducible factor 1 and the molecular physiology of oxygen homeostasis. *J Lab Clin Med* 131: 207-214.

58.   Lee, K., H. Zhang, D. Z. Qian, S. Rey, J. O. Liu, and G. L. Semenza. 2009. Acriflavine inhibits HIF-1 dimerization, tumor growth, and vascularization. *Proc Natl Acad Sci U S A* 106: 17910-17915.

59.   Swain, L., M. Wottawa, A. Hillemann, A. Beneke, H. Odagiri, K. Terada, M. Endo, Y. Oike, K. Farhat, and D. M. Katschinski. 2014. Prolyl-4-hydroxylase domain 3 (PHD3) is a critical terminator for cell survival of macrophages under stress conditions. *J Leukoc Biol* 96: 365-375.

60.   Semba, H., N. Takeda, T. Isagawa, Y. Sugiura, K. Honda, M. Wake, H. Miyazawa, Y. Yamaguchi, M. Miura, D. M. R. Jenkins, H. Choi, J.-w. Kim, M. Asagiri, A. S. Cowburn, H. Abe, K. Soma, K. Koyama, M. Katoh, K. Sayama, N. Goda, R. S. Johnson, I. Manabe, R. Nagai, and I. Komuro. 2016. HIF-1α-PDK1 axis-induced active glycolysis plays an essential role in macrophage migratory capacity. *Nat Commun* 7: 11635.

61.   Shatrov, V. A., V. V. Sumbayev, J. Zhou, and B. Brüne. 2003. Oxidized low-density lipoprotein (oxLDL) triggers hypoxia-inducible factor-1α (HIF-1α) accumulation via redox-dependent mechanisms. *Blood* 101: 4847-4849.

62.   Wang, T., H. Liu, G. Lian, S.-Y. Zhang, X. Wang, and C. Jiang. 2017. HIF1α-induced glycolysis metabolism is essential to the activation of inflammatory macrophages. *Mediators Inflamm* 2017: 10.

63.   Gao, X., H. Wang, Jenny J. Yang, X. Liu, and Z.-R. Liu. 2012. Pyruvate kinase M2 regulates gene transcription by acting as a protein kinase. *Mol Cell* 45: 598-609.

64.   Wang, D., D. Malo, and S. Hekimi. 2010. Elevated mitochondrial reactive oxygen species generation affects the immune response via hypoxia-inducible factor-1α in long-lived Mclk1+/- mouse mutants. *J Immunol* 184: 582.

65.   De Rosa, S. C., M. D. Zaretsky, J. G. Dubs, M. Roederer, M. Anderson, A. Green, D. Mitra, N. Watanabe, H. Nakamura, I. Tjioe, S. C. Deresinski, W. A. Moore, S. W. Ela, D. Parks, and L. A. Herzenberg. 2000. N-acetylcysteine replenishes glutathione in HIV infection. *Eur J Clin Invest* 30: 915-929.

66.   Kil, I. S., S. Y. Kim, and J.-W. Park. 2008. Glutathionylation regulates IκB. *Biochem Biophys Res Commun* 373: 169-173.

67.   Wenger, R. H., D. P. Stiehl, and G. Camenisch. 2005. Integration of oxygen signaling at the consensus HRE. *Sci STKE* 2005: re12.

68.   Dengler, V. L., M. Galbraith, and J. M. Espinosa. 2014. Transcriptional regulation by hypoxia inducible factors. *Crit Rev Biochem Mol Biol* 49: 1-15.

69.   Everts, B., and E. J. Pearce. 2014. Metabolic control of dendritic cell activation and function: recent advances and clinical implications. *Front Immunol* 5: 203.

70.   Li, C., Y. Wang, Y. Li, Q. Yu, X. Jin, X. Wang, A. Jia, Y. Hu, L. Han, J. Wang, H. Yang, D. Yan, Y. Bi, and G. Liu. 2018. HIF1α-dependent glycolysis promotes macrophage functional activities in protecting against bacterial and fungal infection. *Sci Rep* 8: 3603.

71.   Liu, L., Y. Lu, J. Martinez, Y. Bi, G. Lian, T. Wang, S. Milasta, J. Wang, M. Yang, G. Liu, D. R. Green, and R. Wang. 2016. Proinflammatory signal suppresses proliferation and shifts macrophage metabolism from Myc-dependent to HIF1α-dependent. *Proc Natl Acad Sci U S A* 113: 1564.

72.	D'Ignazio, L., D. Bandarra, and S. Rocha. 2016. NF-κB and HIF crosstalk in immune responses. *FEBS J* 283: 413-424.

73.	Fitzpatrick, S. F., M. M. Tambuwala, U. Bruning, B. Schaible, C. C. Scholz, A. Byrne, A. O'Connor, W. M. Gallagher, C. R. Lenihan, J. F. Garvey, K. Howell, P. G. Fallon, E. P. Cummins, and C. T. Taylor. 2011. An intact canonical NF-κB pathway is required for inflammatory gene expression in response to hypoxia. In *J Immunol*, United States. 1091-1096.

74.	Bonello, S., C. Zähringer, S. BelAiba Rachida, T. Djordjevic, J. Hess, C. Michiels, T. Kietzmann, and A. Görlach. 2007. Reactive oxygen species activate the HIF-1α promoter via a functional NFκB site. *Arterioscler Thromb Vasc Biol* 27: 755-761.

75.	Peyssonnaux, C., P. Cejudo-Martin, A. Doedens, A. S. Zinkernagel, R. S. Johnson, and V. Nizet. 2007. Cutting edge: Essential role of Hypoxia inducible factor-1α in development of Lipopolysaccharide-induced sepsis. *J Immunol* 178: 7516-7519.

76.	Walmsley, S. R., C. Print, N. Farahi, C. Peyssonnaux, R. S. Johnson, T. Cramer, A. Sobolewski, A. M. Condliffe, A. S. Cowburn, N. Johnson, and E. R. Chilvers. 2005. Hypoxia-induced neutrophil survival is mediated by HIF-1alpha-dependent NF-kappaB activity. *J Exp Med* 201: 105-115.

77.	Zhou, Y., M. Guo, X. Wang, J. Li, Y. Wang, L. Ye, M. Dai, L. Zhou, Y. Persidsky, and W. Ho. 2013. TLR3 activation efficiency by high or low molecular mass poly I:C. *Innate Immun* 19: 184-192.

78.	Shaheen, Z. R., B. S. Christmann, J. D. Stafford, J. M. Moran, R. M. L. Buller, and J. A. Corbett. 2019. CCR5 is a required signaling receptor for macrophage expression of inflammatory genes in response to viral double-stranded RNA. *Am J Physiol Regul Integr Comp Physiol* 316: R525-R534.

79.	Maitra, U., L. Gan, S. Chang, and L. Li. 2011. Low-dose Endotoxin induces inflammation by selectively removing nuclear receptors and activating CCAAT/enhancer-binding protein δ. *J Immunol* 186: 4467-4473.

80.	Maitra, U., H. Deng, T. Glaros, B. Baker, D. G. S. Capelluto, Z. Li, and L. Li. 2012. Molecular mechanisms responsible for the selective and low-grade induction of proinflammatory mediators in Murine macrophages by Lipopolysaccharide. *J Immunol* 189: 1014-1023.

81.	Yuan, R., S. Geng, and L. Li. 2016. Molecular mechanisms that underlie the dynamic adaptation of innate monocyte memory to varying stimulant strength of TLR ligands. *Front Immunol* 7: 497.

82.	Ohh, M., C. W. Park, M. Ivan, M. A. Hoffman, T.-Y. Kim, L. E. Huang, N. Pavletich, V. Chau, and W. G. Kaelin. 2000. Ubiquitination of hypoxia-inducible factor requires direct binding to the β-domain of the von Hippel–Lindau protein. *Nat Cell Biol* 2: 423-427.

83.	Maxwell, P. H., M. S. Wiesener, G.-W. Chang, S. C. Clifford, E. C. Vaux, M. E. Cockman, C. C. Wykoff, C. W. Pugh, E. R. Maher, and P. J. Ratcliffe. 1999. The tumour suppressor protein VHL targets hypoxia-inducible factors for oxygen-dependent proteolysis. *Nature* 399: 271-275.

84.	Brahimi-Horn, C., N. Mazure, and J. Pouysségur. 2005. Signalling via the hypoxia-inducible factor-1α requires multiple posttranslational modifications. *Cell Signal* 17: 1-9.

85.	Mahon, P. C., K. Hirota, and G. L. Semenza. 2001. FIH-1: A novel protein that interacts with HIF-1α and VHL to mediate repression of HIF-1 transcriptional activity. *Genes Dev* 15: 2675-2686.

86. Lando, D., D. J. Peet, J. J. Gorman, D. A. Whelan, M. L. Whitelaw, and R. K. Bruick. 2002. FIH-1 is an asparaginyl hydroxylase enzyme that regulates the transcriptional activity of Hypoxia-inducible factor. *Genes Dev* 16: 1466-1471.

87. Luo, W., H. Hu, R. Chang, J. Zhong, M. Knabel, R. O'Meally, R. N. Cole, A. Pandey, and G. L. Semenza. 2011. Pyruvate kinase M2 Is a PHD3-stimulated coactivator for Hypoxia-inducible factor 1. *Cell* 145: 732-744.

88. Luo, W., and G. L. Semenza. 2011. Pyruvate kinase M2 regulates glucose metabolism by functioning as a coactivator for Hypoxia-inducible factor 1 in cancer cells. *Oncotarget* 2: 551-556.

89. Imtiyaz, H. Z., and M. C. Simon. 2010. Hypoxia-inducible factors as essential regulators of inflammation. *Curr. Top. Microbiol. Immunol.* 345: 105-120.

90. Jantsch, J., D. Chakravortty, N. Turza, A. T. Prechtel, B. Buchholz, R. G. Gerlach, M. Volke, J. Gläsner, C. Warnecke, M. S. Wiesener, K.-U. Eckardt, A. Steinkasserer, M. Hensel, and C. Willam. 2008. Hypoxia and Hypoxia-inducible factor-1α modulate Lipopolysaccharide-induced dendritic cell activation and function. *J Immunol* 180: 4697-4705.

91. Papandreou, I., R. A. Cairns, L. Fontana, A. L. Lim, and N. C. Denko. 2006. HIF-1 mediates adaptation to hypoxia by actively downregulating mitochondrial oxygen consumption. *Cell Metab* 3: 187-197.

92. Das Gupta, K., M. R. Shakespear, J. E. B. Curson, A. M. V. Murthy, A. Iyer, M. P. Hodson, D. Ramnath, V. A. Tillu, J. B. von Pein, R. C. Reid, K. Tunny, D. M. Hohenhaus, S. V. Moradi, G. M. Kelly, T. Kobayashi, J. H. Gunter, A. J. Stevenson, W. Xu, L. Luo, A. Jones, W. A. Johnston, A. Blumenthal, K. Alexandrov, B. M. Collins, J. L. Stow, D. P. Fairlie, and M. J. Sweet. 2020. Class IIa Histone deacetylases drive Toll-like receptor-inducible glycolysis and macrophage inflammatory responses via Pyruvate kinase M2. *Cell Rep* 30: 2712-2728.e2718.

93. Kono, M., K. Maeda, I. Stocton-Gavanescu, W. Pan, M. Umeda, E. Katsuyama, C. Burbano, S. Y. K. Orite, M. Vukelic, M. G. Tsokos, N. Yoshida, and G. C. Tsokos. 2019. Pyruvate kinase M2 is requisite for Th1 and Th17 differentiation. *JCI Insight* 4: e127395.

94. Angiari, S., M. C. Runtsch, C. E. Sutton, E. M. Palsson-McDermott, B. Kelly, N. Rana, H. Kane, G. Papadopoulou, E. L. Pearce, K. H. G. Mills, and L. A. J. O'Neill. 2020. Pharmacological activation of Pyruvate kinase M2 inhibits CD4(+) T cell pathogenicity and suppresses autoimmunity. *Cell Metab* 31: 391-405.e398.

95. Guzy, R. D., B. Hoyos, E. Robin, H. Chen, L. Liu, K. D. Mansfield, M. C. Simon, U. Hammerling, and P. T. Schumacker. 2005. Mitochondrial complex III is required for hypoxia-induced ROS production and cellular oxygen sensing. *Cell Metab* 1: 401-408.

96. Brunelle, J. K., E. L. Bell, N. M. Quesada, K. Vercauteren, V. Tiranti, M. Zeviani, R. C. Scarpulla, and N. S. Chandel. 2005. Oxygen sensing requires mitochondrial ROS but not oxidative phosphorylation. *Cell Metab* 1: 409-414.

97. Chandel, N. S., D. S. McClintock, C. E. Feliciano, T. M. Wood, J. A. Melendez, A. M. Rodriguez, and P. T. Schumacker. 2000. Reactive oxygen species generated at mitochondrial Complex III stabilize Hypoxia-inducible factor-1α during hypoxia: A mechanism of O_2 sensing. *J Biol Chem* 275: 25130-25138.

98. Kaewpila, S., S. Venkataraman, G. R. Buettner, and L. W. Oberley. 2008. Manganese Superoxide dismutase modulates Hypoxia-inducible factor-1α induction via superoxide. *Cancer Res* 68: 2781.

99.   Chua, Y. L., E. Dufour, E. P. Dassa, P. Rustin, H. T. Jacobs, C. T. Taylor, and T. Hagen. 2010. Stabilization of Hypoxia-inducible factor-1α protein in hypoxia occurs independently of mitochondrial reactive oxygen species production. *J Biol Chem* 285: 31277-31284.

100.   Brüne, B., and J. Zhou. 2007. Hypoxia-inducible factor-1α under the control of Nitric oxide. *Methods Enzymol* 435: 463-478.

101.   Lee, G., H.-S. Won, Y.-M. Lee, J.-W. Choi, T.-I. Oh, J.-H. Jang, D.-K. Choi, B.-O. Lim, Y. J. Kim, J.-W. Park, P. Puigserver, and J.-H. Lim. 2016. Oxidative dimerization of PHD2 is responsible for its inactivation and contributes to metabolic reprogramming via HIF-1α activation. *Sci Rep* 6: 18928.

102.   Bell, E. L., T. A. Klimova, J. Eisenbart, C. T. Moraes, M. P. Murphy, G. R. S. Budinger, and N. S. Chandel. 2007. The Qo site of the mitochondrial complex III is required for the transduction of hypoxic signaling via reactive oxygen species production. *J Cell Biol* 177: 1029-1036.

103.   Orr, A. L., L. Vargas, C. N. Turk, J. E. Baaten, J. T. Matzen, V. J. Dardov, S. J. Attle, J. Li, D. C. Quackenbush, R. L. S. Goncalves, I. V. Perevoshchikova, H. M. Petrassi, S. L. Meeusen, E. K. Ainscow, and M. D. Brand. 2015. Suppressors of superoxide production from mitochondrial complex III. *Nat Chem Biol* 11: 834-836.

104.   Li, H.-S., Y.-N. Zhou, L. Li, S.-F. Li, D. Long, X.-L. Chen, J.-B. Zhang, L. Feng, and Y.-P. Li. 2019. HIF-1α protects against oxidative stress by directly targeting mitochondria. *Redox Biol* 25: 101109.

105.   Martínez-Reyes, I., Lauren P. Diebold, H. Kong, M. Schieber, H. Huang, Christopher T. Hensley, Manan M. Mehta, T. Wang, Janine H. Santos, R. Woychik, E. Dufour, Johannes N. Spelbrink, Samuel E. Weinberg, Y. Zhao, Ralph J. DeBerardinis, and Navdeep S. Chandel. 2016. TCA cycle and mitochondrial membrane potential are necessary for diverse biological functions. *Mol Cell* 61: 199-209.

106.   Haddad, J. J., and H. L. Harb. 2005. L-gamma-Glutamyl-L-cysteinyl-glycine (glutathione; GSH) and GSH-related enzymes in the regulation of pro- and anti-inflammatory cytokines: a signaling transcriptional scenario for redox(y) immunologic sensor(s)? *Mol Immunol* 42: 987-1014.

107.   Reynaert, N. L., A. van der Vliet, A. S. Guala, T. McGovern, M. Hristova, C. Pantano, N. H. Heintz, J. Heim, Y.-S. Ho, D. E. Matthews, E. F. M. Wouters, and Y. M. W. Janssen-Heininger. 2006. Dynamic redox control of NF-κB through glutaredoxin-regulated S-glutathionylation of inhibitory κB kinase β. *Proc Natl Acad Sci U S A* 103: 13086.

108.   Pineda-Molina, E., P. Klatt, J. Vázquez, A. Marina, M. García de Lacoba, D. Pérez-Sala, and S. Lamas. 2001. Glutathionylation of the p50 subunit of NF-κB: A mechanism for redox-induced inhibition of DNA binding. *Biochemistry* 40: 14134-14142.

109.   Takenaka, S., S. McCormick, E. Safroneeva, Z. Xing, and J. Gauldie. 2009. Influence of the Tissue Microenvironment on Toll-Like Receptor Expression by CD11c^{+} Antigen-Presenting Cells Isolated from Mucosal Tissues. *Clin Vaccine Immunol* 16: 1615.

Chapter 5. dsRNA strand length dictates the manner of mitochondrial reprogramming and ROS-activated antiviral response during TLR3 engagement (Ahmed *et al.* in preparation, to be submitted to *Frontiers Immunology*)

5.1. Introduction

Macrophages are highly dynamic cells that are very responsive to their local microenvironment (1-3). They develop region-specific transcriptional identities, which drive tissue specific immune responses (4-8). During viral infections, macrophages play an important role in initiating antiviral responses to inhibit viral dissemination and activate the adaptive immune response. To do this, they surveil the microenvironment using pattern-recognition receptors (PRRs) such as Toll-like receptors (TLR3/7/8/9) and Retinoic acid-inducible gene-I (RIG-I)-like receptors (RLRs) (9-12). Recognition of viral ligands (e.g, viral nucleic acids) and engagement of their respective PRR activates downstream signaling pathways that upregulates type I interferon (IFN) production, which promotes antiviral programming in infected and uninfected bystander cells (13-16). Emerging evidence suggests these responses are modulated by nutrient availability and the metabolic status of the cell but the mechanisms underlying these processes remain incompletely understood (17-22).

It is increasingly recognized that mitochondria many represent a rheostat of the cell, regulating macrophage activation and function (19, 22-27). First, they support cellular bioenergetics and biosynthetic demands by metabolizing glucose (18, 28-31), glutamine (32, 33), branched-chain amino acids (34-36), and fatty acids (37, 38). The intermediate metabolites and bioactive molecules derived from these pathways (e.g., TCA metabolites, reactive oxygen species (ROS)) also regulate cellular signaling, transcription and epigenetics and have been shown to control cell fate decision and in regulate immune responses (19, 21, 24, 39-43). In antiviral immune responses, the mitochondria has been shown to act as a scaffold to support cytosolic RLR

activation through the aggregation of the mitochondrial antiviral signaling (MAVS) protein (26, 44-47). Oxidative phosphorylation (OXPHOS) (22, 48) and mitochondrial fusion/fission dynamics (49, 50) have also been shown to modulate RLR-mediated antiviral responses, but it is unclear if other PRR engage similar mitochondrial processes.

TLR3 is an endosomal PRR, which is activated by viral dsRNA resulting in the phosphorylation and homo- or heterodimerization of the interferon regulatory factor (IRF) transcription factors IRF3 and IRF7 and the production type I IFN (51). This PRR has been shown to recognize a wide range of dsRNA lengths (min: 40-50bp; max: >8kb) in order to mount responses against a variety of viruses, which can possess segmented genomes of various lengths (52-56). Recent studies suggest that short and long dsRNA differentially engage TLR3 to induce cell and pathogen specific immune responses (57, 58). Consistent with these findings, I recently reported that engagement of TLR3 by high molecular weight (HMW; 1.5-8 kb) vs. low molecular weight (LMW; 0.2-1 kb) Poly(I:C) differentially activates NF-kB transcription and inflammatory cytokine production in a HIF-1α dependent manner (59). However, it is unclear if differential engagement of TLR3 also modulates type I IFN responses.

I have recently shown that TLR3-mediated responses require both OXPHOS activity and Complex III-derived mtROS to support antiviral signaling in macrophages (21). However, it is unknown if TLR3 engagement with short vs. long dsRNA dictates the manner of mitochondrial reprogramming that occurs. In this study, I investigated the differential effects of short and long dsRNA (i.e., HMW vs. LMW Poly(I:C)) on type I IFN responses and mitochondrial function in murine bone marrow derived macrophages (BMM). I found that responses to both HMW and LMW Poly(I:C) requires sustained OXPHOS to drive mtROS-mediated antiviral responses. Further, I found the reliance of TLR3 on mitochondrial OXPHOS activity and mtROS production

is amplified in conditions of low glucose suggesting nutrient availability plays a critical in defining local immune responses. Importantly, this study also showed that engagement of TLR3 by HMW and LMW Poly(I:C) is associated with differential production of mtROS by Complex I and Complex III of the electron transport chain (ETC). This differential production of mtROS regulated the magnitude of the type I IFN responses and suggests the ETC may act as a rheostat to regulate pathogen specific immune responses.

5.2. Materials and Methods

5.2.1. *Reagents*

High glucose Dulbecco's Modified Eagle Media (DMEM) (with 4 mM L-glutamine and 1 mM sodium pyruvate), DMEM without glucose/glutamine/pyruvate/phenol red, fetal bovine serum (FBS), penicillin/streptomycin (PenStrep), glucose, sodium pyruvate and L-glutamine were purchased from Life Technologies. High molecular weight Poly(I:C) (HMW) and low molecular weight Poly(I:C) (LMW) were obtained from InvivoGen. N-acetylcysteine (NAC), antimycin A (AA), rotenone (ROT), oligomycin (OM), carbonyl cyanide-p-trifluoromethoxyphenylhydrazone (FCCP), and SQ1EL-1 were acquired from Sigma-Aldrich, while S3QEL-2 was from Cedarlane. Tetramethylrhodamine, methyl ester (TMRM) and MitoSOX^{TM} Red probes were purchased from ThermoFisher. CXCL10 ELISA kit were attained from R&D Systems. The IFN-α/IFN-β 2-Plex Mouse ProcartaPlex^{TM} Luminex Panel kit used was from Invitrogen. The Cell-based Hydrogen Peroxide Assay Kit and antibodies detecting Complex II (SDHB) was from Abcam while antibodies recognizing SOD2 was purchased from Cell Signaling Technology. Antibodies against IRF3, pIRF3 (Ser385), IRF7, pIRF7 (Ser477), GPX4, Iκbα, Complexes I (NDUFB8), III (UQCRC2) and IV (COX4) were from ThermoFisher.

5.2.2. Animals

All animal procedures were approved by the Carleton University Animal Care Committee and were conducted in accordance with the guidelines provided by the Canadian Council for Animal Care. C57BL/6 mice colonies are maintained at the Carleton University Vivarium. The bone marrow cells from the tibias and femurs of 6-13-week-old mice were isolated and cryopreserved in a 90% FBS/10% dimethylsulfoxide (DMSO) mixture until use.

5.2.3. Culture and Treatment of Mouse Bone Marrow-derived Macrophages (BMMs)

As previously described (21, 60), mouse bone marrow progenitors were differentiated for 10 days in high glucose DMEM media supplemented with 10% FBS, 1% PenStrep and 15% L929 fibroblast cell-conditioned medium on a 100mm Petri dish. L929-conditional media was prepared as previously described (21). On day 10, the differentiated BMMs were harvested, counted, and seeded onto tissue culture-treated plates at a concentration of 1×10^6 cells/mL and allowed to rest overnight.

BMMs were stimulated with 10 ng/mL high molecular weight (HMW) or low molecular weight Poly(I:C) (LMW) in complete DMEM media with either high (25mM) or low glucose (0.5mM). Low glucose media was prepared by supplementing DMEM media without glucose/glutamine/pyruvate/phenol red with 0.5mM glucose and matching concentrations of glutamine (4mM) and sodium pyruvate (1mM) present in high glucose DMEM media. Cells were stimulated for 0.5 to 18 hours depending on the endpoint assay. To evaluate the role of Complex I and III activity and ROS production on antiviral signaling, BMMs were co-treated with 500μM MT, 5mM NAC, 5μM S1QEL or 5μM S3QEL-2.

5.2.4. Measurement of Cytokine Secretion

Cell culture supernatants were collected from activated BMM after 18 hours of stimulation and then centrifuged to remove cellular debris. CXCL10 levels were assessed by ELISAs according to the manufacturer's instructions. IFN-α and IFN-β levels were measured using IFN-α/IFN-β 2-Plex Mouse ProcartaPlex[TM] Luminex Panel.

5.2.5. Western Blot Analysis

Following stimulations, BMMs were lysed with Pierce RIPA buffer supplemented with HALT[TM] Protease and Phosphatase Inhibitor (ThermoFisher). Total protein levels in each sample were measured using the DC assay (Bio-Rad). A total of 30ug of protein from each sample was loaded onto 12% TGX[TM] FastCast[TM] Acrylamide gels (Bio-Rad) and imaged using the ChemiDoc[TM] XR's Stain-Free program (Bio-Rad). Resolved proteins were transferred onto PVDF membranes using the Trans-Blot® Turbo[TM] Transfer System and blocked overnight in 5% non-fat dry milk (w/v) prior to overnight incubation with the appropriate primary antibody in 5% BSA (w/v) in TBS with 0.1% Tween-20. Horseradish peroxidase-conjugated secondary antibodies and Clarity[TM] Western ECL Blotting Substrate (Bio-Rad) were used to visualize protein bands of interest. The protein band chemiluminescence intensity of target proteins were normalized to the amount of total protein loaded in its respective lane, as determined by the Stain-Free application on the ChemiDoc[TM] XR imager (Bio-Rad). For IκBα, IRF3 and IRF7, following normalization described above, the protein expression data was presented as the ratio between phosphorylated protein levels divided by total protein levels.

5.2.6. Assessment of Mitochondrial Function using Flow Cytometry

BMMs were plated onto 60mm Petri dishes (at a concentration of $1x10^6$ cells/mL) and allowed to rest overnight before treatment with either 100ng/mL LPS, 10ng/mL HMW Poly(I:C)

or 10ng/mL LMW Poly(I:C) for 18 hours. Cells were then collected, washed, and stained with fluorescent probes according to manufacturer's instructions. Mitochondrial abundance was measured using 150nM MitoTracker Green (ThermoFisher) in serum free DMEM media. Differences in mitochondrial membrane potential (MMP) was evaluated using 10nM TMRM (ThermoFisher) in complete media. Mitochondrial and Cellular ROS levels were monitored using 2.5μM MitoSOX^{TM} Red (ThermoFisher) in PBS and 5μM CellROX^{TM} Orange (ThermoFisher) in complete media. Cellular levels of fluorescence were quantified using an Attune NxT Flow Cytometer (ThermoFisher) and the results were analyzed using FlowJo Software. Results are reported as the percentage of positive cells and as mean fluorescence intensity (MFI), the latter being used to describe the level of expression on positive cells.

5.2.7. *Measurement of Cellular H$_2$O$_2$Production by fluorescence spectrometry*

BMMs were plated onto 96-well black plates at 50,000 cells/well and stimulated with 100ng/mL LPS, 10ng/mL HMW Poly(I:C) or 10ng/mL LMW Poly(I:C) for 1 hour. Cells were then washed before using the Cell-based Hydrogen Peroxide Assay Kit (Abcam) to measure H2O2 production. Cells were incubated with the AbGreen H$_2$O$_2$ indicator for 30 minutes before monitoring the relative difference in fluorescence using a fluorescence microplate reader (490nm Ex/520nm Em).

5.2.8. *Characterization of Energy Metabolism of BMMs*

Harvested BMMs were plated onto Seahorse XFp cell culture miniplates (Seahorse Bioscience) at a density of 50,000 cells/well before stimulation. Cells were then stimulated with either 10ng/mL HMW Poly(I:C) or 10ng/mL LMW Poly(I:C) for 18 hours. Measurement of extracellular acidification rate (ECAR) and oxygen consumption rate (OCR) were evaluated using a XFp Flux Analyzer (Seahorse Bioscience). Alterations in mitochondrial function was assessed

using the Seahorse XFp Cell Mito Stress Test Kit (Agilent). BMM were exposed to successive injections of Oligomycin (OM), Carbonyl cyanide-p-trifluoromethoxyphenylhydrazone (FCCP), and Rot/AA and OCR levels were used to evaluate changes in spare respiratory capacity percentage (SRC%) and ATP production across stimulations and culture conditions.

5.2.9. *Statistical Analyses*

Data used in this study was analyzed using GraphPad Prism software. Values shown represent the mean ± SEM of biological replicates, where the number of replicates is reported in the figure legends. Statistical significance was calculated using a paired Student's t-test (*$p < 0.05$, **$p < 0.01$, and ***$p < 0.001$).

5.3. Results

5.3.1. *TLR3 associated type I IFN responses are amplified under low glucose conditions*

It is increasingly recognized that the composition of cell culture media can alter intracellular metabolic responses *in vitro* (61). For example, high glucose has been shown to alter metabolic responses following RLR engagement by reducing cellular dependence on OXPHOS and increasing reliance on glycolysis (22). Given this finding, I first wanted to evaluate if HMW vs. LMW Poly(I:C) induce differential activation of type I IFN responses and if these responses were affected by glucose availability (high [25mM] vs. low [0.5mM]). Irrespective of the glucose concentration, I found that HMW stimulation induced higher levels of IFN-α, IFN-β and CXCL10 production compared to LMW Poly(I:C) (Figure 5.1A-C). I also found that low glucose resulted in an amplification of type I IFN responses in both HMW- (IFNα FC: 5.935, p=0.008; IFN-β FC: 2.972, p=0.006; CXCL10 FC: 2.195, p=0.005) and LMW-stimulated cells (IFNα FC: 2.081, p=0.036; IFN-β FC: 3.349, p=0.003; CXCL10 FC: 4.866, p=0.025). Consistent with these findings, low glucose was also associated with a dramatic upregulation in both total and

phosphorylated IRF3 (pIRF3) expression (Figure 5.1D) and a sustained increased in pIRF7 following TLR3 engagement (Figure 5.1E), which may explain the increase in type I IFN production under these conditions.

5.3.2. Low glucose conditions are associated with increased cellular respiration to compensate for increased proton leak

Given the central role of the mitochondria is regulating TLR3 responses (21), I wanted to see if HMW and LMW Poly(I:C) stimulations differentially reprogram OXPHOS activity. I also wanted to see if these processes were altered by glucose availability. To do this, I used Agilent's Cell Mito Stress Test kit and the Seahorse XF Analyzer. Unlike LPS (21), HMW and LMW Poly(I:C) stimulation did not alter levels of basal respiration or ATP production compared to unstimulated controls (Figure 5.2A-D). However, both stimuli were associated with a significant decrease in the spare respiratory capacity, with HMW having a more pronounced effect compared to LMW Poly(I:C). Interestingly, glucose availability did not alter the effects of HMW vs. LMW Poly(I:C) on %SRC. However, it did result in an increase in cellular respiration and proton leak in both control and stimulated BMMs (Figure 5.2A, B, E). Given that changes in proton leak can directly alter mitochondrial membrane potential (MMP) across the inner mitochondrial membrane (68), I evaluated MMP in stimulated cells using the fluorescent dye Tetramethylrhodamine (TMRM). I found that TLR3 engagement was associated with a significant increase in the proportion of cells with low TMRM sequestration but not in overall decrease in the frequency of mitochondria (Figure 5.2F and Supplemental Figure S5.1). Consistent with observed increase in proton leak, I also found the portion of TMRM negative cells further increased in low glucose conditions. Collectively, these results suggest that limited glucose availability may cause BMM to increase their respiratory activity and compensate with proton leak to limit mitochondrial ROS accumulation.
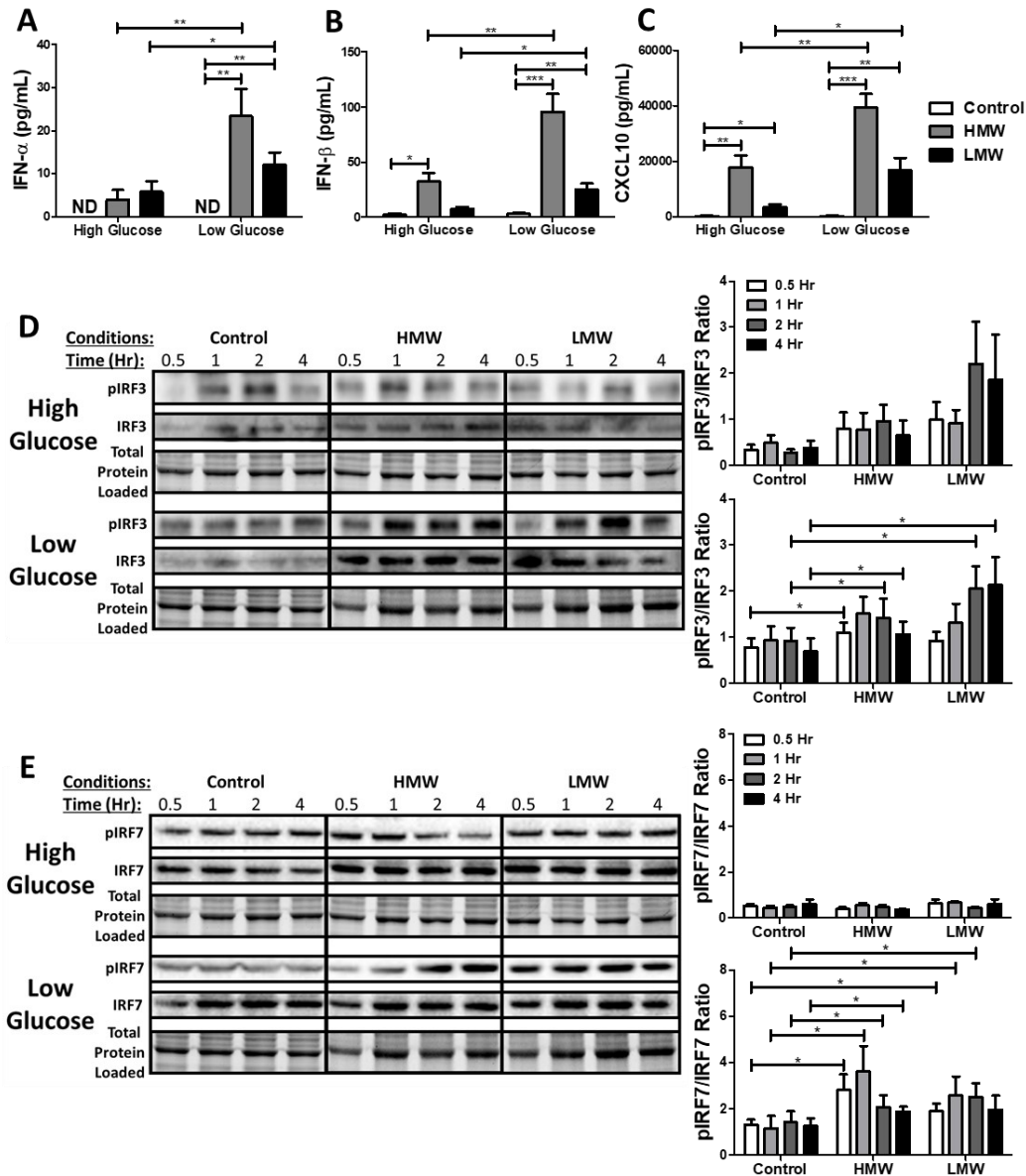
Figure 5.1: Low glucose conditions are associated with amplified antiviral signalling and subsequent cytokine production. BMMs were treated with 10ng/mL HMW or 10ng/mL LMW Poly(I:C) for 18 hours under high or low glucose media conditions. Cytokine expression (IFN-α (**A**), IFN-β (**B**) and CXCL10 (**C**)) was evaluated in culture supernatant. Total cell lysates were harvested to measure total and phosphorylated IRF3 (**D**) and IRF7 (**E**) expression using immunoblotting at 0.5, 1, 2 & 4 hours after treatment. Band intensity was normalized to the total protein levels in each of their respective lanes using the Bio-Rad Stain-Free Application. Afterwards, the expression of IRF3 and IRF7 in each glucose condition was normalized respective to the intensity of their phosphorylated forms (pIRF3 and pIRF7) to their respective control sample collected at the same time point and presented as a fold change value. Data represents mean ± SEM of four individual mice (*p < 0.05, **p < 0.01, and ***p < 0.001).
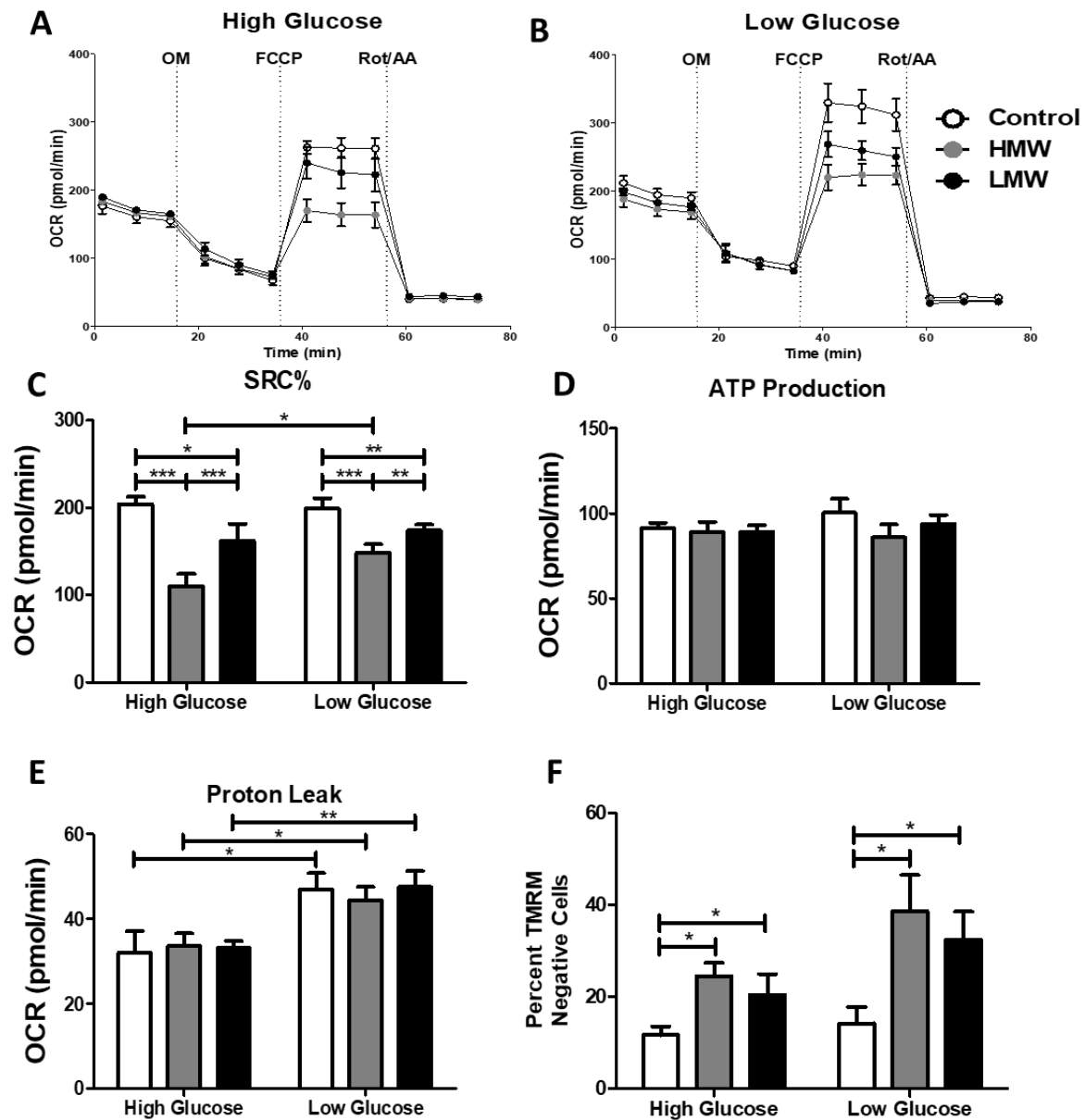
Figure 5.2: Increased proton leak drives boost in respiration under low glucose conditions. BMMs were plated onto Seahorse XFp miniplates and subsequently stimulated with HMW or LMW for 18 hours under high (**A**) and low (**B**) glucose conditions prior to assessing OXPHOS activity *via* consecutive Oligomycin (Oligo), Carbonyl cyanide-p-trifluoromethoxyphenylhydrazone (FCCP), and Rot/AA injection. This allowed for the quantification of OXPHOS features such as spare respiratory capacity percentage (SRC%; **C**), ATP production (**D**) and proton leak (**E**). Tetramethylrhodamine (TMRM) staining was used to measure changes in mitochondrial membrane potential (**F**) and reported as the percentage of TMRM negative cells. Data represents mean ± SEM of four individual mice. (*p < 0.05, **p < 0.01, and ***p < 0.001).
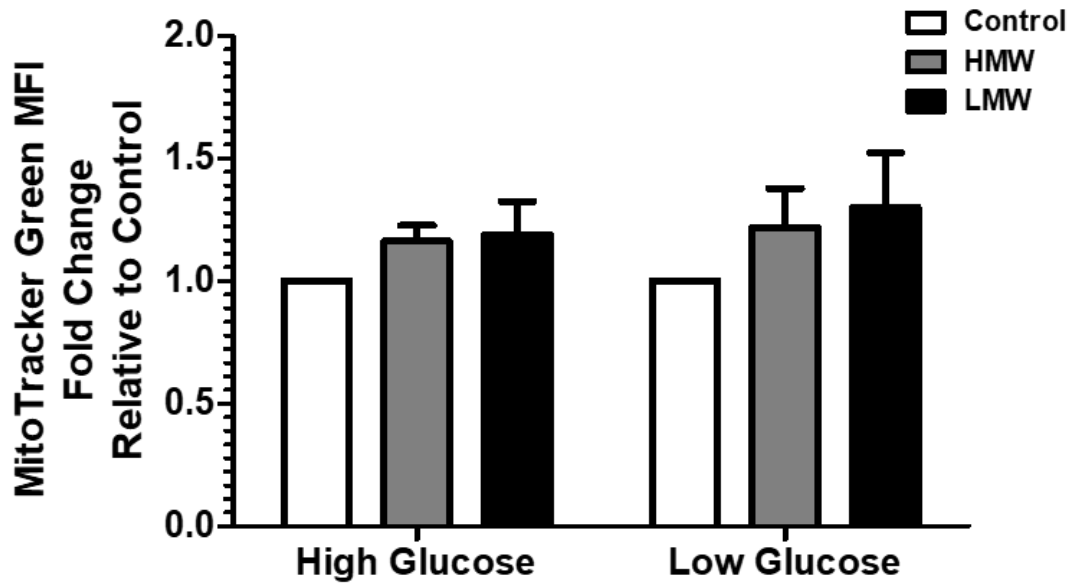
Supplemental Figure S5.1: TLR3 engagement does not alter mitochondrial mass. BMMs treated with HMW or LMW for 18 hours in high or low glucose media were evaluated for changes in mitochondrial abundance. MitoTracker Green staining was used to measure mitochondrial abundance. Data represents mean $\pm$ SEM of four individual mice (*$p < 0.05$, **$p < 0.01$, and ***$p < 0.001$).

5.3.3. The amplification of type I IFN responses in low glucose conditions is driven by increased mitochondrial ROS accumulation

I have previously shown that HMW Poly(I:C) is associated with increased mitochondrial and cytosolic ROS accumulation, which regulates cytokine production (21). Here, I wanted to investigate if differential accumulation of mitochondrial ROS (mtROS) contributes to the observed differences in type I IFN cytokine production following HMW vs. LMW Poly(I:C) stimulation. For these studies, mitochondrial superoxide production was measured using the fluorescent probe MitoSOX^{TM} Red. As expected, TLR3 engagement increased mitochondrial superoxide production in stimulated cells compared to unstimulated controls (Figure 5.3A). However, mtROS accumulation was more pronounced in cells stimulated with HMW compared to LMW Poly(I:C) (HMW FC: 2.396, LMW FC: 1.370, p<0.001) and was further increased under low glucose conditions (HMW: 2.396 vs. 4.020, LMW: 1.370 vs 2.974). Interestingly, I also found that low glucose conditions were associated with increased hydrogen peroxide levels, which was absent in high glucose suggesting a more global change in cellular redox status (Figure 5.3B). To determine if this accumulation was associated with altered mitochondrial antioxidant responses, I measured changes in SOD2 and mtGPX4 levels using western blot. Unlike the increased levels of antioxidants observed in high glucose conditions, Poly(I:C) stimulations in low glucose did not altered antioxidant expression (Figure 5.3C and D). This lack of induction may further potentiate ROS accumulation in these cells.

Next, to determine if mtROS accumulation contributes to antiviral signaling and cytokine production, BMM were stimulated with HMW or LMW Poly(I:C) in the presence or absence of antioxidants (MitoTEMPO [MT], N-acetylcysteine [NAC]). MT scavenges superoxide from active mitochondria whereas NAC targets total cellular ROS production. Both MT and NAC treatments resulted in a near complete loss of type I IFN (IFN-α, IFN-β) production following

TLR3 engagement across conditions (Figure 5.4). This ROS scavenging also dramatically reduced CXCL10 levels (Figure 5.4). The complete loss in CXCL10 production in NAC but not MT treated cells (HMW HG: ↓92%, LG: ↓94%; LMW HG: ↓83%, LG: ↓96%) suggests non-mitochondrially derived ROS may also potentiate this signaling.

5.3.4. *Complex I expression is differentially modulated by HMW vs. LMW Poly(I:C)*

To better understand what may be driving the increased accumulation of mtROS, I evaluated changes in ETC protein expression using western blot. Again, I found that glucose availability dramatically affected the ability of the mitochondria function. In high glucose conditions, alterations in ETC expression were highly variable across animals. The only difference that was significant was an increase in Complex IV (COX4) (Figure 5.5). However, under low glucose conditions, both HMW and LMW Poly(I:C) were associated with decreased Complex I (NDUFB8) (HMW FC: 0.669, LMW FC: 0.540) and Complex IV expression (HMW FC: 0.783, LMW FC: 0.711) as well as an increase Complex III (UQCRC2) expression (HMW FC: 2.219, LMW FC: 2.293) (Figure 5.5). Importantly, the downregulation of Complex I was more pronounced in LMW compared to HMW Poly(I:C) (p=0.038) (Figure 5.5).
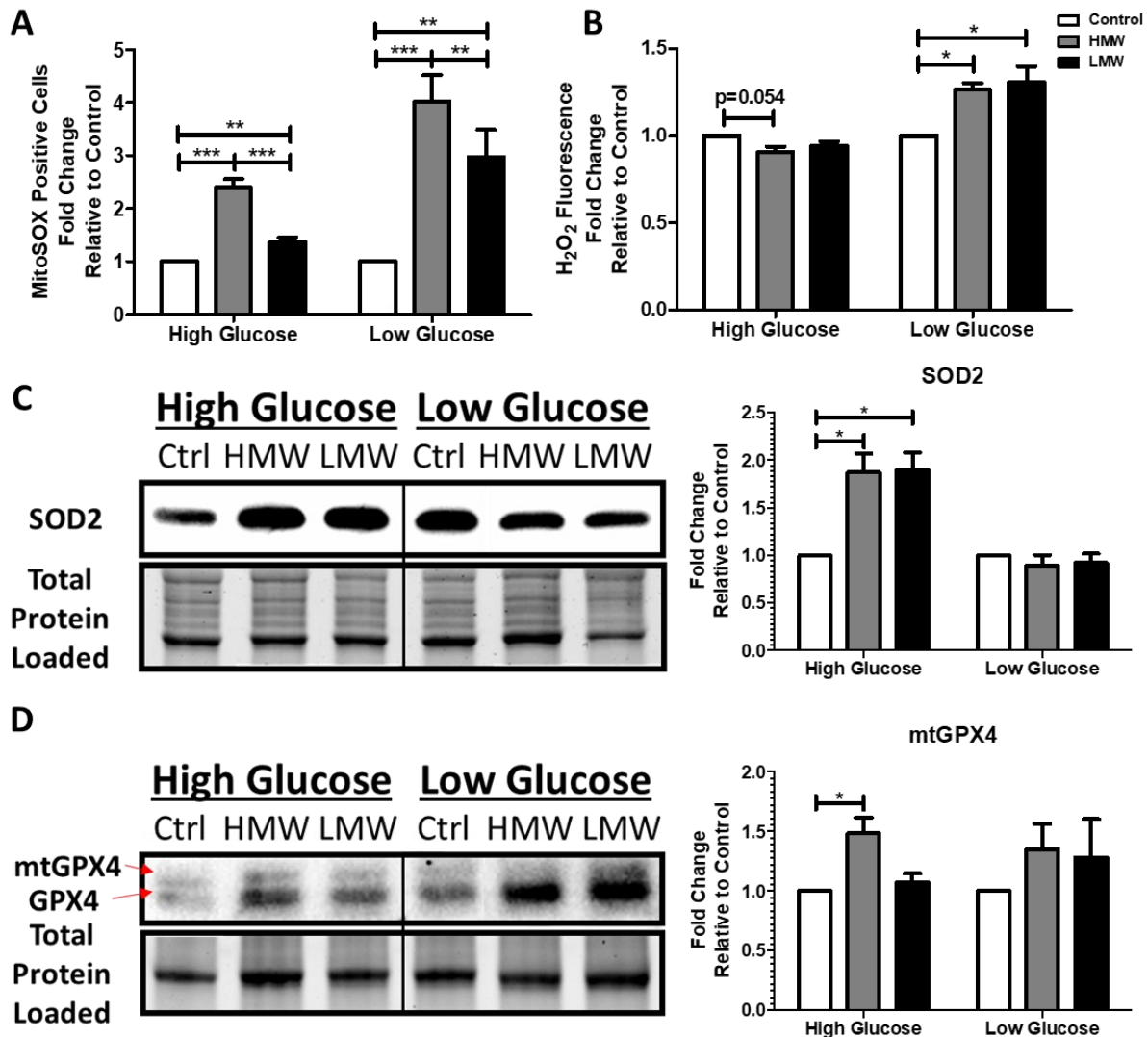
Figure 5.3: HMW and LMW activation is linked to elevated mitochondrial ROS and loss of mitochondrial antioxidant response under low glucose conditions. HMW- and LMW-stimulated BMMs were probed for changes in redox metabolism under high or low glucose conditions. Mitochondrial superoxide levels were measured using MitoSOX™ Red (**A**). Hydrogen peroxide levels were quantified using the Cell-based Hydrogen Peroxide Assay kit (**B**). Expression levels of antioxidant proteins superoxide dismutase 2 (SOD2) (**C**) and mitochondrial glutathione peroxidase 4 (mtGPX4) (**D**) were quantified using immunoblotting. Data represents mean ± SEM of four individual mice (*p < 0.05, **p < 0.01, and ***p < 0.001).
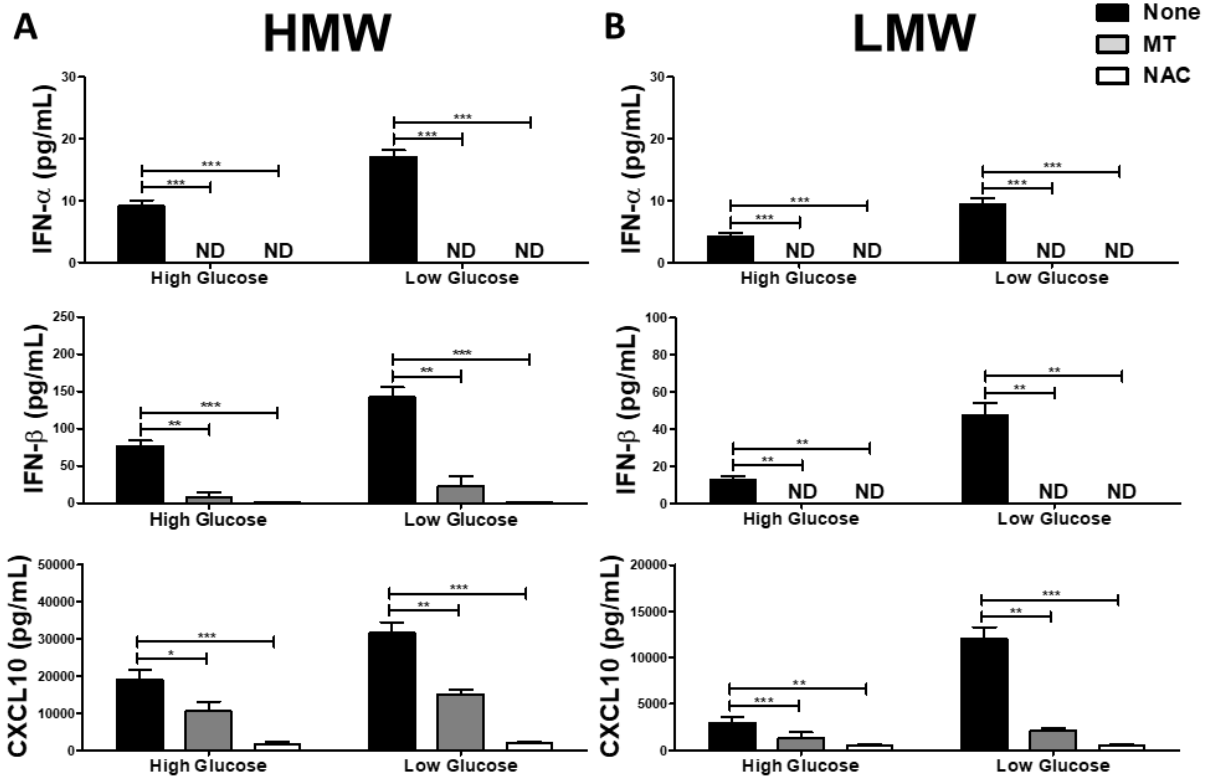
Figure 5.4: Scavenging ROS blunts Poly(I:C)-mediated type I IFN production. HMW- (**A**) or LMW-activated BMMs (**B**) were co-treated with two different ROS scavengers (MT, NAC) under high or low glucose conditions to better understand the importance of ROS to drive antiviral responses. IFN-α, IFN-β and CXCL10 cytokine production were quantified after 18 hours *via* ELISA. Data represents mean ± SEM of four individual mice (*p < 0.05, **p < 0.01, and ***p < 0.001).
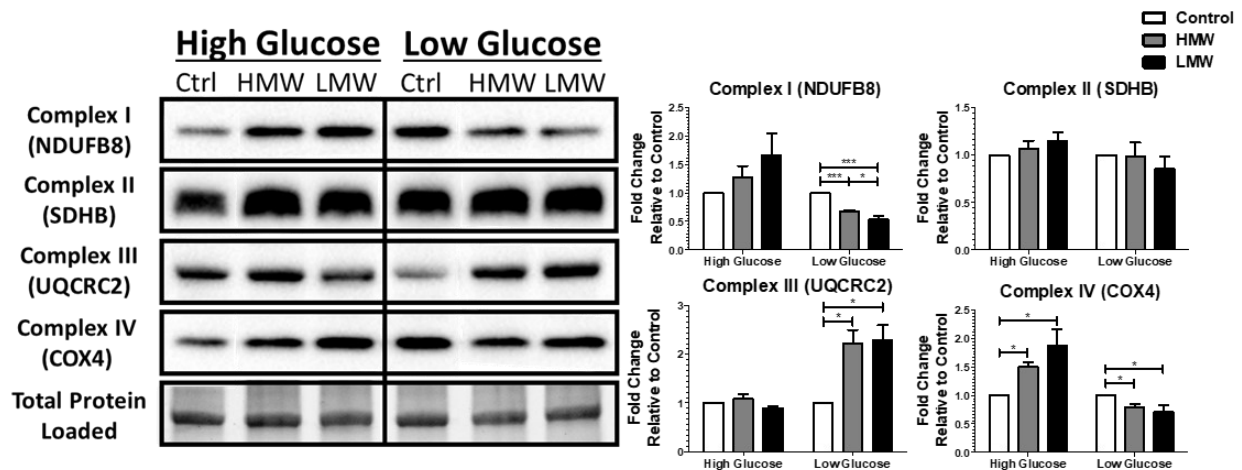
Figure 5.5: dsRNA length-dependent TLR3 engagement determines the degree of Complex I expression under low glucose conditions. Macrophages treated with HMW or LMW for 18 hours in high or low glucose media were evaluated for differences in mitochondrial function. Protein levels of Complexes I-IV of the ETC was quantified *via* immunoblotting. Band intensity was normalized to the total protein levels in each of their respective lanes using the Bio-Rad Stain-Free Application. Data represents mean ± SEM of four individual mice (*$p < 0.05$, **$p < 0.01$, and ***$p < 0.001$).

5.3.5. *Mitochondrial ROS from Complexes I and III differentially drive type I IFN responses following stimulation with HMW or LMW Poly(I:C)*

Mitochondrial superoxide production is a by-product of cellular respiration that occurs because of electron leakage across the ETC (62-64). Given complexes I and III are the major producers of mtROS, I wondered if their altered expression following HMW and LMW stimulation contributed to increased mtROS production and type I IFN responses in low glucose conditions. For these experiments BMM were stimulated with HMW or LMW Poly (I:C) in the presence or absence of S1QEL or S3QEL. These inhibitors prevent superoxide production from Complex I (S1QEL) or Complex III (S3QEL) without impairing OXPHOS activity. Under these low glucose conditions S1QEL and S3QEL were found to have differing effects on HMW vs. LMW Poly(I:C) responses. Whereas ROS production by complexes I and III was required to drive type I IFN and CXCL10 production in LMW Poly (I:C) stimulated cells (Figure 5.6B), complex I ROS production was not required for IFN-β production following HMW Poly (I:C) (Figure 5.6A). In fact, it appears that high levels of mtROS derived from complex I may inhibit the production IFN-β under these conditions (↑21%, p=0.038). Consistent with these findings, S1QEL and S3QEL were found to dramatically reduced the levels of pIRF3/7 following LMW. However, treatment with S1QEL did not affect pIRF3 levels in HMW treated cells (Figures 5.6C and D). Interestingly, Honda et al. (13) have shown that pIRF3 plays a central role in driving early type I IFN responses including IFN-β production. Alternatively, IRF7 phosphorylation is required to support later phases of these responses, which include IFN-α, CXCL10 and further IFN-β production.
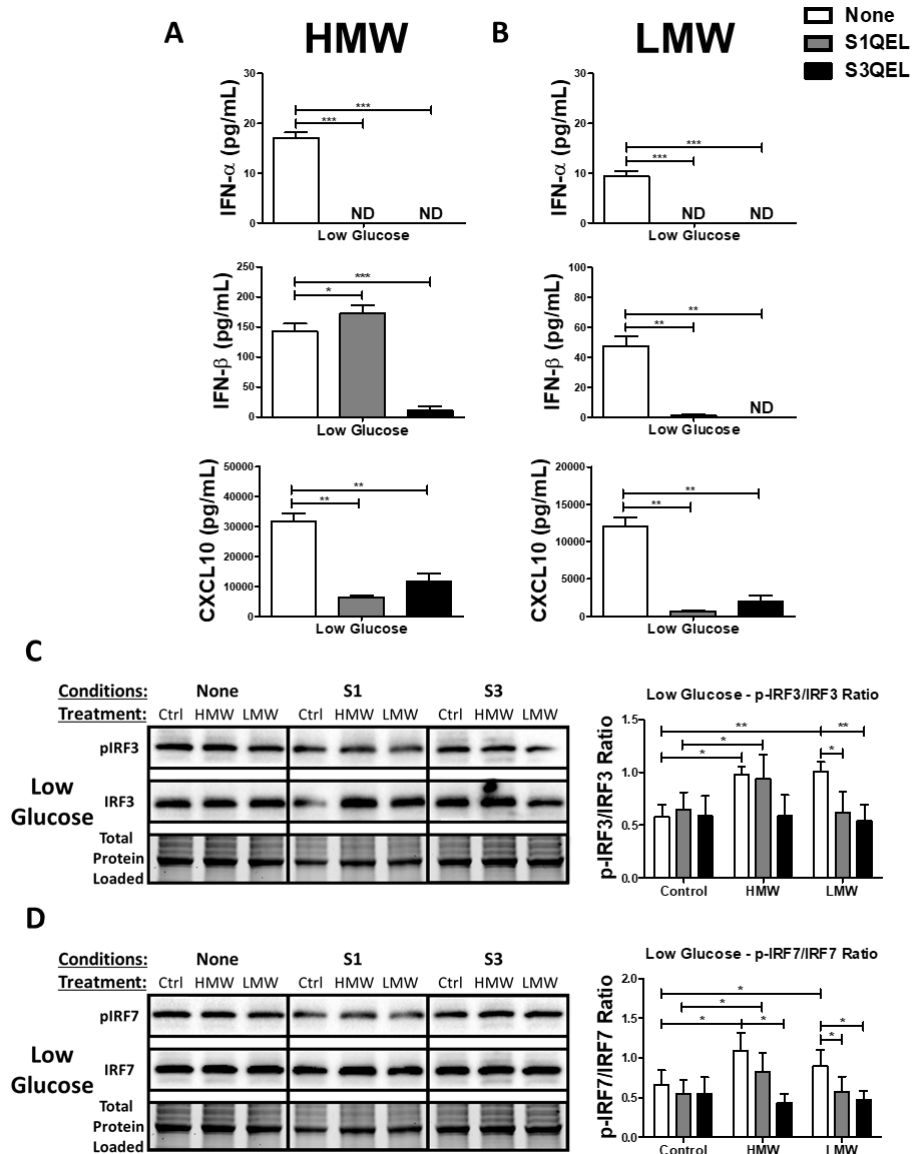
Figure 5.6: Preventing the production of Complex I generated mtROS can unlock HMW-mediated IFN production *via* increased IRF3/7 activation. BMMs treated with either HMW (**A**) or LMW (**B**) were co-treated with specific suppressor of electron leak from Complex I (S1QEL) or Complex III (S3QEL) under high or low glucose conditions to better understand the importance of mtROS to proper antiviral response. IFN-α, IFN-β and CXCL10 cytokine production were quantified after 18 hours. Total cell lysates were harvested to measure total and phosphorylated IRF3 (**C**) and IRF7 (**D**) after S1QEL and S3QEL co-treatment using immunoblotting. Band intensity was normalized to the total protein levels in each of their respective lanes using the Bio-Rad Stain-Free Application. Afterwards, the expression of IRF3 and IRF7 in each glucose condition was normalized respective to the intensity of their phosphorylated forms (pIRF3 and pIRF7) to their respective control sample collected at the same time point and presented as a fold change value. Data represents mean ± SEM of four individual mice (*p < 0.05, **p < 0.01, and ***p < 0.001).

5.4. Discussion

dsRNA viruses are a diverse family of microorganisms capable of infecting everything from bacteria to animals (53, 55, 56). The genomes of these viruses are highly diverse and can be either monopartite or segmented in structure (up to 12 dsRNA fragments of varying sizes) (53, 54, 56). For example, the genome of the Megabirnaviridae family consist of two segments between 7.0-9.0 kb in length, the Partitiviridae family have between 2-3 segments of 1.4-2.3 kb in length and the Reoviridae family possess 10-12 genomic segments between 0.7-5.0 kb in length (55). To effectively respond to these viruses, macrophages must recognize both long and short dsRNA. While cytosolic PRR differentially recognize short vs. long nucleic acids (e.g., RIG-I (<1 kb) and MDA5 (>2 kb)) (65, 66), endosomal TLR3 must recognize all forms and lengths of dsRNA >40-50 bp (51, 52). In the current study, I found that TLR3 engagement by long vs. short dsRNA differentially reprograms mitochondrial function to support early antiviral responses and that these processes are tightly regulated by glucose availability. I show that strong type I IFN responses, as seen following stimulation with HMW Poly(I:C) and in low glucose conditions, require significant accumulation of mtROS to drive IRF3 and IRF7 phosphorylation and cytokine production. Further, this accumulation is regulated by the modulation complex I (↓) and III (↑) of the ETC. I also show there may be a maximal capacity of mtROS to drive type I IFN responses. When these levels exceed a certain threshold, for example following HMW stimulation in low glucose conditions, mtROS derived from Complex I may suppress type I IFN responses.

Previous work has identified an intimate link between mitochondrial function and antiviral responses. Central to this relationship is the requirement of sustained OXPHOS activity and MMP across the inner mitochondrial membrane (19, 22-27). Yoshimuzi et al. (22) demonstrated the importance of OXPHOS activity to RLR-mediated responses of macrophages. Targeting

OXPHOS led to increased viral susceptibility and the induction of robust inflammatory responses in the lung (22). Furthermore, complete dissipation of MMP was shown to blunt RLR-mediated antiviral signaling due to reduced MAVS aggregation (50). This dependency on OXPHOS is directly associated with the inhibitory effects of glucose metabolism (48). The rate-limiting glycolytic protein hexokinase 2 (HK2) directly interacts with MAVS along the outer mitochondrial membrane natively, which is lost during RIG-I activation leading to reduced glycolytic activity and lactate production (48). Further, lactate is a natural suppressor of MAVS signaling and can limiting the magnitude of an antiviral immune response (48). Unlike LPS (18, 19, 25, 32), I found that irrespective of the length of dsRNA, some level of cellular respiration is required to support TLR3-mediated response. Further, while I did not specifically evaluate the inhibitory effects of glycolysis on these processes, I found that low glucose conditions supported higher levels of cellular respiration, proton leak and mtROS production, IRF3/7 signaling and type I IFN production. Interestingly, Wu et al. have shown that increased OXPHOS activity in TLR9-activated plasmacytoid dendritic cells is linked to an autocrine type I IFN-mediated boost in fatty acid oxidation (FAO) (67). Future studies are required to see if FAO plays a role in these TLR3 responses.

One key factor that influences MMP and ultimately OXPHOS function is passive or active proton leak, which facilitates the transport of protons back into the matrix independent of OXPHOS (68). I have found that the amplification of TLR3-mediated antiviral responses under low glucose conditions was associated with increased mitochondrial respiration due to elevated proton leak. This elevation in proton leak is also likely responsible for the increase in the proportion of BMM with low MMP. This contrasts with RIG-I signaling, where overexpression of uncoupling protein 2 (UCP2) in MEFs resulted in increased active proton leak, inactivating

MAVS-mediated signaling (50). There has been some debate as to the effect of proton leak on mtROS production. Koshiba et al. (50) show that the over expression of UCP2 caused attenuated mtROS generation which is critical to driving its antiviral response (42). In our study, I show that the increase in proton leak during both HMW and LMW stimulation under low glucose conditions resulted in augmented mtROS production, which was also vital to facilitating increased IRF3/7 phosphorylation. Despite these differences, both RIG-I- and TLR3-mediated antiviral signaling is driven in part by mtROS (21, 42, 69).

Our previous work was among the first to link complex III-mediated mtROS to increased antiviral signaling in HMW-activated macrophages (21). In this study, I show that complex III-associated ROS production is also required to induce early (IFN-β) and later (IFN-α and CXCL10) type I IFN responses following stimulation with HMW and LMW Poly(I:C). I also show that mtROS from Complex I contributes to TLR3 signaling. However, unlike complex III, I found that complex I is downregulated by HMW and LMW Poly(I:C) stimulation in low glucose conditions. I speculate this downregulation, which is more pronounced in LMW- vs. HMW-stimulated cells, may represent a protective mechanism to limit the accumulation of mtROS and the detrimental effects of these oxidizing species. Consistent with these findings, HMW-stimulated cells in low glucose support the highest levels of mtROS. Further, I found that inhibition of complex I ROS production increased IFN-β production. This may be related to the dependence of early antiviral immune responses on OXPHOS activity and their ability of these cells to form supercomplexes. ETC supercomplex formation reduces the travel path of electrons between individual complexes and limit the chance of electron leakage and subsequent mitochondrial superoxide production (70, 71). During antibacterial responses, macrophages undergo ETC supercomplex disassembly to mount a robust inflammatory response, mediated by mtROS production and subsequent NLRP3

inflammasome activation (24, 72). Yet, studies that have investigated the role of ETC supercomplexes during viral infections is limited. Champagne et al. (73) show that during Influenza infection, methylation-controlled J protein (MCJ) KO CD8+ T cells have improved immunity due to increased ETC supercomplex assembly. The resulting increase in OXPHOS activity and MMP led to increased IFN-γ and IL-2 secretion (73). Bladanta et al. (74) conducted studies using vaccinia-infected BMM and found that knocking out the mitochondrial-associated interferon-stimulating gene (ISG) ISG15 caused a reduction of free Complex I and more supercomplex formation. But while the loss of ISG15 resulted in reduced mtROS, ISG15$^{-/-}$ BMM were more susceptible to vaccinia infection (74). Further studies are required to better understand how the dynamics of ETC supercomplexes affect the antiviral capabilities of macrophages.

In summary, I have shown that ETC complex architecture during TLR3 engagement is influenced by the dsRNA strand length. TLR3 engagement requires OXPHOS to mount mtROS-driven antiviral responses regardless of strand length and this dependency is exaggerated under low glucose conditions. Yet, Complex I-derived mtROS dampen type I IFNs production during HMW responses while LMW activation requires mtROS from complexes I and III for a proper response. Interestingly, blocking superoxide production from complex I without hampering electron flow significantly improved HMW-derived type I IFN production. This demonstrates the functional plasticity of macrophages and their capability to sufficiently shape its response to various viruses and in different tissue microenvironments. These findings not only highlight the role of the ETC as a modulator that is capable of fine-tuning antiviral response based on the microenvironment but provides a potential new approach for enhancing antiviral therapies in patients with acute viral infections.

5.5.   References

1. Ross, J. A., and M. J. Auger. 2002. Biology of the macrophage. In *The macrophage*, 2nd ed. B. Burke, and C. E. Lewis, eds. Oxford University Press, New York, New York. 1-57.
2. Varol, C., A. Mildner, and S. Jung. 2015. Macrophages: Development and Tissue Specialization. *Annual Review of Immunology* 33: 643-675.
3. Mosser, D. M., and J. P. Edwards. 2008. Exploring the full spectrum of macrophage activation. *Nat Rev Immunol* 8: 958-969.
4. Gordon, S., and P. R. Taylor. 2005. Monocyte and macrophage heterogeneity. *Nat Rev Immunol* 5: 953-964.
5. Yu, X., A. Buttgereit, I. Lelios, S. G. Utz, D. Cansever, B. Becher, and M. Greter. 2017. The cytokine TGF-β promotes the development and homeostasis of alveolar macrophages. *Immunity* 47: 903-912 e904.
6. Naito, M., G. Hasegawa, Y. Ebe, and T. Yamamoto. 2004. Differentiation and function of Kupffer cells. *Medical Electron Microscopy* 37: 16-28.
7. Biswas, S. K., and E. Lopez-Collazo. 2009. Endotoxin tolerance: new mechanisms, molecules and clinical significance. *Trends in Immunology* 30: 475-487.
8. Smythies, L. E., R. Shen, D. Bimczok, L. Novak, R. H. Clements, D. E. Eckhoff, P. Bouchard, M. D. George, W. K. Hu, S. Dandekar, and P. D. Smith. 2010. Inflammation Anergy in Human Intestinal Macrophages Is Due to Smad-induced IκBα Expression and NF-κB Inactivation. *Journal of Biological Chemistry* 285: 19593-19604.
9. Murphy, K. M. 2011. *Janeway's Immunobiology*. Taylor & Francis Group.
10. Bianchi, M. E. 2007. DAMPs, PAMPs and alarmins: all we need to know about danger. *J. Leukoc. Biol.* 81: 1-5.
11. Fitzgerald, K. A., and J. C. Kagan. 2020. Toll-like receptors and the control of immunity. *Cell* 180: 1044-1066.
12. Reikine, S., J. B. Nguyen, and Y. Modis. 2014. Pattern recognition and signaling mechanisms of RIG-I and MDA5. *Front Immunol* 5: 342-342.
13. Honda, K., A. Takaoka, and T. Taniguchi. 2006. Type I Inteferon Gene Induction by the Interferon Regulatory Factor Family of Transcription Factors. *Immunity* 25: 349-360.
14. Ivashkiv, L. B., and L. T. Donlin. 2014. Regulation of type I interferon responses. *Nat. Rev. Immunol.* 14: 36-49.
15. Kawai, T., and S. Akira. 2006. Innate immune recognition of viral infection. *Nat Immunol* 7: 131-137.
16. Schneider, W. M., M. D. Chevillotte, and C. M. Rice. 2014. Interferon-Stimulated Genes: A Complex Web of Host Defenses. *Annu. Rev. Immunol.* 32: 513-545.
17. Zhu, L., T. Yang, L. Li, L. Sun, Y. Hou, X. Hu, L. Zhang, H. Tian, Q. Zhao, J. Peng, H. Zhang, R. Wang, Z. Yang, L. Zhang, and Y. Zhao. 2014. TSC1 controls macrophage polarization to prevent inflammatory disease. *Nat Commun* 5.
18. Rodríguez-Prados, J., P. G. Través, J. Cuenca, D. Rico, J. Aragonés, P. Martín-Sanz, M. Cascante, and L. Boscá. 2010. Substrate fate in activated macrophages: A comparison between innate, classic, and alternative activation. *J Immunol* 185: 605-614.
19. Mills, E. L., B. Kelly, A. Logan, A. S. H. Costa, M. Varma, C. E. Bryant, P. Tourlomousis, J. H. M. Däbritz, E. Gottlieb, I. Latorre, S. C. Corr, G. McManus, D. Ryan, H. T. Jacobs, M. Szibor, R. J. Xavier, T. Braun, C. Frezza, M. P. Murphy, and L. A. O'Neill. 2016. Succinate dehydrogenase supports metabolic repurposing of mitochondria to drive inflammatory macrophages. *Cell* 167: 457-470.e413.

20. Van den Bossche, J., J. Baardman, Natasja A. Otto, S. van der Velden, Annette E. Neele, Susan M. van den Berg, R. Luque-Martin, H.-J. Chen, Marieke C. S. Boshuizen, M. Ahmed, Marten A. Hoeksema, Alex F. de Vos, and Menno P. J. de Winther. 2016. Mitochondrial Dysfunction Prevents Repolarization of Inflammatory Macrophages. *Cell Rep* 17: 684-696.

21. Ahmed, D., D. Roy, A. Jaworski, A. Edwards, A. Abizaid, A. Kumar, A. Golshani, and E. Cassol. 2019. Differential remodeling of the electron transport chain is required to support TLR3 and TLR4 signaling and cytokine production in macrophages. *Sci Rep* 9: 18801.

22. Yoshizumi, T., H. Imamura, T. Taku, T. Kuroki, A. Kawaguchi, K. Ishikawa, K. Nakada, and T. Koshiba. 2017. RLR-mediated antiviral innate immunity requires oxidative phosphorylation activity. *Sci Rep* 7: 5379.

23. Koshiba, T. 2013. Mitochondrial-mediated antiviral immunity. *Biochim Biophys Acta* 1833: 225-232.

24. Garaude, J., R. Acín-Pérez, S. Martínez-Cano, M. Enamorado, M. Ugolini, E. Nistal-Villán, S. Hervás-Stubbs, P. Pelegrín, L. E. Sander, J. A. Enríquez, and D. Sancho. 2016. Mitochondrial respiratory-chain adaptations in macrophages contribute to antibacterial host defense. *Nat Immunol* 17: 1037-1045.

25. Kelly, B., G. M. Tannahill, M. P. Murphy, and L. A. J. O'Neill. 2015. Metformin Inhibits the Production of Reactive Oxygen Species from NADH:Ubiquinone Oxidoreductase to Limit Induction of Interleukin-1β (IL-1β) and Boosts Interleukin-10 (IL-10) in Lipopolysaccharide (LPS)-activated Macrophages. *J Biol Chem* 290: 20348-20359.

26. Seth, R. B., L. Sun, C.-K. Ea, and Z. J. Chen. 2005. Identification and characterization of MAVS, a mitochondrial antiviral signaling protein that a ctivates NF-κB and IRF3. *Cell* 122: 669-682.

27. Castanier, C., D. Garcin, A. Vazquez, and D. Arnoult. 2010. Mitochondrial dynamics regulate the RIG-I-like receptor antiviral pathway. *EMBO Rep* 11: 133.

28. Jiang, H., H. Shi, M. Sun, Y. Wang, Q. Meng, P. Guo, Y. Cao, J. Chen, X. Gao, E. Li, and J. Liu. 2016. PFKFB3-Driven Macrophage Glycolytic Metabolism Is a Crucial Component of Innate Antiviral Defense. *J. Immunol.* 197: 2880-2890.

29. Semba, H., N. Takeda, T. Isagawa, Y. Sugiura, K. Honda, M. Wake, H. Miyazawa, Y. Yamaguchi, M. Miura, D. M. R. Jenkins, H. Choi, J.-w. Kim, M. Asagiri, A. S. Cowburn, H. Abe, K. Soma, K. Koyama, M. Katoh, K. Sayama, N. Goda, R. S. Johnson, I. Manabe, R. Nagai, and I. Komuro. 2016. HIF-1α-PDK1 axis-induced active glycolysis plays an essential role in macrophage migratory capacity. *Nat Commun* 7: 11635.

30. Wang, T., H. Liu, G. Lian, S.-Y. Zhang, X. Wang, and C. Jiang. 2017. HIF1α-induced glycolysis metabolism is essential to the activation of inflammatory macrophages. *Mediators Inflamm* 2017: 10.

31. Aki, T., T. Funakoshi, K. Noritake, K. Unuma, and K. Uemura. 2020. Extracellular glucose is crucially involved in the fate decision of LPS-stimulated RAW264.7 murine macrophage cells. *Scientific Reports* 10: 10581.

32. Jha, A. K., S. C.-C. Huang, A. Sergushichev, V. Lampropoulou, Y. Ivanova, E. Loginicheva, K. Chmielewski, K. M. Stewart, J. Ashall, B. Everts, E. J. Pearce, E. M. Driggers, and M. N. Artyomov. 2015. Network Integration of Parallel Metabolic and Transcriptional Data Reveals Metabolic Modules that Regulate Macrophage Polarization. *Immunity* 42: 419-430.

33. Liu, M., R. S. O'Connor, S. Trefely, K. Graham, N. W. Snyder, and G. L. Beatty. 2019. Metabolic rewiring of macrophages by CpG potentiates clearance of cancer cells and overcomes tumor-expressed CD47−mediated 'don't-eat-me' signal. *Nature Immunology* 20: 265-275.

34. Ko, J. H., A. Olona, A. E. Papathanassiu, N. Buang, K. S. Park, A. S. H. Costa, C. Mauro, C. Frezza, and J. Behmoaras. 2020. BCAT1 affects mitochondrial metabolism independently of leucine transamination in activated human macrophages. *J Cell Sci* 2020: jcs.247957.

35. Papathanassiu, A. E., J.-H. Ko, M. Imprialou, M. Bagnati, P. K. Srivastava, H. A. Vu, D. Cucchi, S. P. McAdoo, E. A. Ananieva, C. Mauro, and J. Behmoaras. 2017. BCAT1 controls metabolic reprogramming in activated human macrophages and is associated with inflammatory diseases. *Nat Commun* 8: 16040.

36. Yoon, B. R., Y.-J. Oh, S. W. Kang, E. B. Lee, and W.-W. Lee. 2018. Role of SLC7A5 in metabolic reprogramming of Human monocyte/macrophage immune responses. *Front Immunol* 9: 53.

37. Huang, S. C.-C., B. Everts, Y. Ivanova, D. O'Sullivan, M. Nascimento, A. M. Smith, W. Beatty, L. Love-Gregory, W. Y. Lam, C. M. O'Neill, C. Yan, H. Du, N. A. Abumrad, J. F. Urban Jr, M. N. Artyomov, E. L. Pearce, and E. J. Pearce. 2014. Cell-intrinsic lysosomal lipolysis is essential for alternative activation of macrophages. *Nat Immunol* 15: 846-855.

38. Malandrino, M. I., R. Fucho, M. Weber, M. Calderon-Dominguez, J. F. Mir, L. Valcarcel, X. Escoté, M. Gómez-Serrano, B. Peral, L. Salvadó, S. Fernández-Veledo, N. Casals, M. Vázquez-Carrera, F. Villarroya, J. J. Vendrell, D. Serra, and L. Herrero. 2015. Enhanced fatty acid oxidation in adipocytes and macrophages reduces lipid-induced triglyceride accumulation and inflammation. *Am J Physiol Endocrinol Metab* 308: E756-769.

39. Tannahill, G. M., A. M. Curtis, J. Adamik, E. M. Palsson-McDermott, A. F. McGettrick, G. Goel, C. Frezza, N. J. Bernard, B. Kelly, N. H. Foley, L. Zheng, A. Gardet, Z. Tong, S. S. Jany, S. C. Corr, M. Haneklaus, B. E. Caffrey, K. Pierce, S. Walmsley, F. C. Beasley, E. Cummins, V. Nizet, M. Whyte, C. T. Taylor, H. Lin, S. L. Masters, E. Gottlieb, V. P. Kelly, C. Clish, P. E. Auron, R. J. Xavier, and L. A. J. O'Neill. 2013. Succinate is an inflammatory signal that induces IL-1β through HIF-1α. *Nature* 496: 238-242.

40. Palsson-McDermott, E. M., A. M. Curtis, G. Goel, M. A. R. Lauterbach, F. J. Sheedy, L. E. Gleeson, M. W. M. van den Bosch, S. R. Quinn, R. Domingo-Fernandez, D. G. W. Johnston, J.-k. Jiang, W. J. Israelsen, J. Keane, C. Thomas, C. Clish, M. Vander Heiden, R. J. Xavier, and L. A. J. O'Neill. 2015. Pyruvate kinase M2 regulates Hif-1α activity and IL-1β induction and is a critical determinant of the warburg effect in LPS-activated macrophages. *Cell Metab.* 21: 65-80.

41. West, A. P., I. E. Brodsky, C. Rahner, D. K. Woo, H. Erdjument-Bromage, P. Tempst, M. C. Walsh, Y. Choi, G. S. Shadel, and S. Ghosh. 2011. TLR signalling augments macrophage bactericidal activity through mitochondrial ROS. *Nature* 472: 476-480.

42. Tal, M. C., M. Sasai, H. K. Lee, B. Yordy, G. S. Shadel, and A. Iwasaki. 2009. Absence of autophagy results in reactive oxygen species-dependent amplification of RLR signaling. *Proc Natl Acad Sci U S A* 106: 2770.

43. Herb, M., A. Gluschko, K. Wiegmann, A. Farid, A. Wolf, O. Utermöhlen, O. Krut, M. Krönke, and M. Schramm. 2019. Mitochondrial reactive oxygen species enable proinflammatory signaling through disulfide linkage of NEMO. *Sci Signal* 12: eaar5926.

44. Yoneyama, M., M. Kikuchi, T. Natsukawa, N. Shinobu, T. Imaizumi, M. Miyagishi, K. Taira, S. Akira, and T. Fujita. 2004. The RNA helicase RIG-I has an essential function in double-stranded RNA-induced innate antiviral responses. *Nat Immunol* 5: 730-737.

45. Yoneyama, M., M. Kikuchi, K. Matsumoto, T. Imaizumi, M. Miyagishi, K. Taira, E. Foy, Y.-M. Loo, M. Gale, and S. Akira. 2005. Shared and unique functions of the DExD/H-box helicases RIG-I, MDA5, and LGP2 in antiviral innate immunity. *J Immunol* 175: 2851-2858.

46. Kawai, T., K. Takahashi, S. Sato, C. Coban, H. Kumar, H. Kato, K. J. Ishii, O. Takeuchi, and S. Akira. 2005. IPS-1, an adaptor triggering RIG-I- and MDA5-mediated type I interferon induction. *Nat Immunol* 6: 981-988.

47. Hou, F., L. Sun, H. Zheng, B. Skaug, Q.-X. Jiang, and Z. J. Chen. 2011. MAVS forms functional prion-like aggregates to activate and propagate antiviral innate immune response. *Cell* 146: 448-461.

48. Zhang, W., G. Wang, Z. G. Xu, H. Tu, F. Hu, J. Dai, Y. Chang, Y. Chen, Y. Lu, H. Zeng, Z. Cai, F. Han, C. Xu, G. Jin, L. Sun, B. S. Pan, S. W. Lai, C. C. Hsu, J. Xu, Z. Z. Chen, H. Y. Li, P. Seth, J. Hu, X. Zhang, H. Li, and H. K. Lin. 2019. Lactate is a natural suppressor of RLR signaling by targeting MAVS. *Cell* 178: 176-189.e115.

49. Yu, C.-Y., J.-J. Liang, J.-K. Li, Y.-L. Lee, B.-L. Chang, C.-I. Su, W.-J. Huang, M. M. C. Lai, and Y.-L. Lin. 2015. Dengue virus impairs mitochondrial fusion by cleaving mitofusins. *PLoS pathog* 11: e1005350.

50. Koshiba, T., K. Yasukawa, Y. Yanagi, and S.-i. Kawabata. 2011. Mitochondrial membrane potential is required for MAVS-mediated antiviral signaling. *Sci Signal* 4: ra7.

51. Alexopoulou, L., A. C. Holt, R. Medzhitov, and R. A. Flavell. 2001. Recognition of double-stranded RNA and activation of NF-[kappa]B by Toll-like receptor 3. *Nature* 413: 732-738.

52. Liu, L., I. Botos, Y. Wang, J. N. Leonard, J. Shiloach, D. M. Segal, and D. R. Davies. 2008. Structural basis of Toll-like receptor 3 signaling with double-stranded RNA. *Science* 320: 379-381.

53. Wickner, R. 1993. Double-stranded RNA virus replication and packaging. *J Biol Chem* 268: 3797-3800.

54. Roldão, A., A. C. Silva, M. C. M. Mellado, P. M. Alves, and M. J. T. Carrondo. 2011. 1.47 - Viruses and Virus-Like Particles in Biotechnology: Fundamentals and Applications. In *Comprehensive Biotechnology (Second Edition)*. M. Moo-Young, ed. Academic Press, Burlington. 625-649.

55. Jia, H., K. Dong, L. Zhou, G. Wang, N. Hong, D. Jiang, and W. Xu. 2017. A dsRNA virus with filamentous viral particles. *Nature Commun* 8: 168.

56. King, A. M. Q., E. Lefkowitz, M. J. Adams, and E. B. Carstens. 2011. *Virus taxonomy: ninth report of the International Committee on Taxonomy of Viruses*. Elsevier.

57. Mian, M. F., A. N. Ahmed, M. Rad, A. Babaian, D. Bowdish, and A. A. Ashkar. 2013. Length of dsRNA (poly I:C) drives distinct innate immune responses, depending on the cell type. *J Leukoc Biol* 94: 1025-1036.

58. Jiang, M., P. Österlund, L. P. Sarin, M. M. Poranen, D. H. Bamford, D. Guo, and I. Julkunen. 2011. Innate immune responses in human Monocyte-derived dendritic cells are highly dependent on the size and the 5′ phosphorylation of RNA molecules. *J Immunol* 187: 1713.

59. Ahmed, D., A. Humphrey, D. Roy, M.-E. Sheridan, A. Jaworski, A. Edwards, J. Donner, A. Abizaid, W. Willmore, A. Kumar, A. Golshani, and E. Cassol. 2020. HIF-1α regulation of pro-inflammatory cytokine production following TLR3 engagement is dependent on viral nucleic acid length and glucose availability [Manuscript submitted for publication]. *J Immunol*: 1-20.

60. Weischenfeldt, J., and B. Porse. 2008. Bone marrow-derived macrophages (BMM): Isolation and applications. *CSH Protoc* 2008: pdb.prot5080.

61. Lagziel, S., E. Gottlieb, and T. Shlomi. 2020. Mind your media. *Nat Metab*.

62. Voet, D., J. G. Voet, and C. W. Pratt. 2016. *Fundamentals of biochemistry: life at the molecular level*. John Wiley & Sons.

63. Berg, J. M., J. L. Tymoczko, and L. Stryer. 2008. *Biochemistry*. Macmillan.

64. Spinelli, J. B., and M. C. Haigis. 2018. The multifaceted contributions of mitochondria to cellular metabolism. *Nat Cell Biol* 20: 745-754.

65. Kato, H., O. Takeuchi, S. Sato, M. Yoneyama, M. Yamamoto, K. Matsui, S. Uematsu, A. Jung, T. Kawai, K. J. Ishii, O. Yamaguchi, K. Otsu, T. Tsujimura, C.-S. Koh, C. Reis e Sousa, Y. Matsuura, T. Fujita, and S. Akira. 2006. Differential roles of MDA5 and RIG-I helicases in the recognition of RNA viruses. *Nature* 441: 101-105.

66. Kato, H., O. Takeuchi, E. Mikamo-Satoh, R. Hirai, T. Kawai, K. Matsushita, A. Hiiragi, T. S. Dermody, T. Fujita, and S. Akira. 2008. Length-dependent recognition of double-stranded ribonucleic acids by Retinoic acid-inducible gene-I and Melanoma differentiation-associated gene 5. *J Exp Med* 205: 1601-1610.

67. Wu, D., David E. Sanin, B. Everts, Q. Chen, J. Qiu, Michael D. Buck, A. Patterson, Amber M. Smith, C.-H. Chang, Z. Liu, Maxim N. Artyomov, Erika L. Pearce, M. Cella, and Edward J. Pearce. 2016. Type 1 Interferons induce changes in core metabolism that are critical for immune function. *Immunity* 44: 1325-1336.

68. Jastroch, M., A. S. Divakaruni, S. Mookerjee, J. R. Treberg, and M. D. Brand. 2010. Mitochondrial proton and electron leaks. *Essays Biochem* 47: 53-67.

69. Agod, Z., T. Fekete, M. M. Budai, A. Varga, A. Szabo, H. Moon, I. Boldogh, T. Biro, A. Lanyi, A. Bacsi, and K. Pazmandi. 2017. Regulation of type I IFN responses by mitochondria-derived ROS in plasmacytoid dendritic cells. *Redox Biol* 13: 633-645.

70. Acín-Pérez, R., P. Fernández-Silva, M. L. Peleato, A. Pérez-Martos, and J. A. Enriquez. 2008. Respiratory active mitochondrial supercomplexes. *Mol Cell* 32: 529-539.

71. Garlid, K. D., M. Jabůrek, P. Ježek, and M. Vařecha. 2000. How do uncoupling proteins uncouple? *Biochim Biophys Acta* 1459: 383-389.

72. Su, Y., T. P. Miettinen, L. Mu, E. Mirek, S. R. Manalis, T. G. Anthony, H. Sesaki, and J. Chen. 2020. Disassembly of ETC Complexes Drives Macrophage Inflammatory Responses by Reprogramming Cellular Metabolism and Translation [Manuscirpt submitted for publication]. *Cell Rep* Available at SSRN: https://ssrn.com/abstract=3611881: 1-54.

73. Champagne, Devin P., Ketki M. Hatle, Karen A. Fortner, A. D'Alessandro, Tina M. Thornton, R. Yang, D. Torralba, J. Tomás-Cortázar, Yong W. Jun, Kyo H. Ahn, Kirk C. Hansen, L. Haynes, J. Anguita, and M. Rincon. 2016. Fine-tuning of CD8+ T cell mitochondrial metabolism by the respiratory chain repressor MCJ dictates protection to Influenza virus. *Immunity* 44: 1299-1311.

74. Baldanta, S., M. Fernández-Escobar, R. Acín-Perez, M. Albert, E. Camafeita, I. Jorge, J. Vázquez, J. A. Enríquez, and S. Guerra. 2017. ISG15 governs mitochondrial function in macrophages following vaccinia virus infection. *PLOS Pathog* 13: e1006651.

Chapter 6.   CONCLUSIONS AND PRESPECTIVES

A host's response to a viral infection is a complex and multifaceted set of processes that attempts to overcome the virus' ability to exploit host cellular machinery and circumvent the immunological countermeasures designed to prevent such a takeover (1). On the front lines against infection, macrophages are responsible for sensing and immediately respond to invading viruses in almost every tissue in the body (2, 3). To initiate antiviral immune responses, macrophages possess a series of PRRs that can detect conserved viral PAMPs such as genomic DNA and RNA (2-5). They also play an important role in attracting and activating other immune cells to help in the fight against viral invasion (2, 6, 7). If the immune system is successful, they also assist in re-establishing tissue homeostasis in the host at the end of the infection (6-9). As a result, this versatility of functions demonstrates the macrophage's role as a bridge between the innate and adaptive immune systems.

Recent evidence suggests cellular metabolism is a central regulator of macrophage effector functions. Macrophages undergo profound metabolic changes to not only meet the biosynthetic and bioenergetic needs of the cell but to regulate various cellular processes including transcription factor activity, cytokine production and cell differentiation (10-12). To date, the majority of work conducted in the field of immunometabolism concerning macrophages centers on the dichotomy of metabolic profiles between pro-inflammatory M1 macrophages (i.e. LPS/TLR4 engagement) and anti-inflammatory M2 macrophages (i.e. IL-4/IL-10 activation) (13, 14). The prevailing theory over the last half decade has been that the metabolic reprogramming associated with LPS activation was consistently observed across the other inflammatory states. However, more recent work has slowly started to erode this notion and has generated a hypothesis that PRR engagement induces a diverse spectrum of metabolic and activation states. To better elucidate the metabolic

mechanisms that drive and support TLR-mediated responses further studies are required. Interestingly, as more data is generated, it is becoming increasingly clear that the mitochondria is at the center at regulating the dynamic nature of macrophage function and activation.

In this thesis, I endeavored to development a better understanding of the mechanics surrounding the metabolic regulation of macrophages during antiviral responses. In particular, I was interested in understanding how cellular metabolism contributes to the regulation of TLR-mediated antiviral responses. I hypothesized that mitochondrial function was a central regulator of these responses in macrophages and that dynamic modulation of mitochondrial function could serve to drive ligand specific immune responses. To perform these studies, I employed a combination of immunological techniques and systems biology approaches to systematically evaluate the metabolic pathways associated with antiviral responses in macrophages. Using these profiles, I then functionally evaluated the roles of select metabolic pathways and networks on antiviral immune responses using a primary macrophage model system. These studies evaluated associations between bioenergetic profiles and immune function.

In Chapter 2, I conducted one of the first studies to systematically evaluate how type I IFNs modulate cellular metabolism in macrophages using transcriptional profiling. Using publicly available microarray datasets available through the Gene Expression Omnibus (GEO) database at the NCBI, I developed metabolic gene signatures associated with early IFN-α responses in mouse BMMs and human MDMs. I found that in both model systems, short-term treatments with IFN-α were associated with an extensive metabolic reprogramming, with >500 metabolic genes linked to bioenergetic pathways, cellular redox balance, branched chain amino acid catabolism, cell membrane composition, FA synthesis and FAO. By conducting this untargeted comparative study,

my work provided novel insights into the metabolic processes required to support and facilitate type I IFN responses in mouse and human macrophages.

With this understanding, I then focused my *in vitro* functional studies on two well-characterized inducers of type I IFN responses (LPS, Poly(I:C)). The purpose of these studies was to evaluate differences in metabolic reprogramming between TLR3- and TLR4-mediated responses in mouse BMMs. In Chapter 3, I show that differences in mitochondrial reprogramming between TLR3 and TLR4 engagement is directly linked to changes in the expression of ETC complexes. These changes resulted in differential production of mitochondrial vs. cytosolic ROS, which drove their ligand specific inflammatory and antiviral programs. Interestingly, TLR3-assocaited responses were found to be associated with increased mtROS production by Complex III and that this accumulation of mtROS played a central role in driving cytokine production in these cells. This work is among the first to suggest that targeting complex III mtROS production may provide a novel means of modulating macrophage antiviral responses. Another key insight from this study was the role of glucose availability in manipulating these TLR3-mediated responses. I showed that in low glucose conditions, TLR3, but not TLR4 responses had amplified pro-inflammatory and antiviral cytokine production. This was linked to increased Complex III expression and subsequent elevated mitochondrial and cytosolic ROS.

These studies also showcased the preferred energy sources for TLR3 vs. TLR4 responses. While LPS activation primarily relies on glycolysis for energy, maintaining some OXPHOS activity is a requisite feature of Poly(I:C) activation. Standard culture conditions contain supraphysiological levels of most nutrients in order to maintain cells *ex vivo* (15-17). For example, glucose levels in standard DMEM media (25mM) are more than five times found in the fasting blood of non-diabetic individuals and more than twice as high as found in hyperglycemic patients

(15, 18). Moreover, levels of glucose found in the tissues are a small percentage compared to the levels found in blood under homeostasis, which drops further during infection as a result of increased consumption (19, 20). My findings are consistent with another study that demonstrated that macrophages were less dependent on OXPHOS activity in high glucose media, skewing antiviral immune responses (21). Collectively, these results suggest that assessing immune function under more oxidative conditions by reducing the concentrations of glucose in the media may provide a better representation of effector function *in vivo*.

The latter two studies in this thesis were performed to evaluate how metabolic reprogramming contributes to differential engagement TLR3 and activation of antiviral immune responses using short and long dsRNA. I also conducted these experiments under high and low glucose conditions to evaluate how these responses differed under standard *in vitro* conditions and conditions more conducive to *in vivo* comparisons. In Chapter 4, I found that HIF-1α could modulate the inflammatory response of TLR3-activated macrophages and that this modulation differed based on the length of the Poly(I:C) ligand and the nutrient environment, where low glucose conditions resulted in a more robust inflammatory response. Given the fact that dsRNA viruses possess segmented genomes with variable lengths, macrophages must retain plasticity to proper respond to all ligands. Differential engagement of TLR3 and distinct metabolic profiles may play a central role is driving ligand specific immune functions. Further, this study highlights the possibility of differentially targeting HIF-1α function depending on the specific viral infection to diminish potentially damaging inflammation during antiviral responses.

In Chapter 5, I further examined the relationship between Poly(I:C) ligand length, differential mitochondrial reprogramming, and the regulation of type I IFN responses. Under low glucose conditions, I found this dependency was further exaggerated leading to an amplification

in mtROS production. The increase in mtROS resulted in increased IRF-3 and -7 signalling and increased type I IFN production. Interestingly, I also found that the length of Poly(I:C) strand directly influences the manner of ETC restructuring required to support antiviral responses. While mtROS accumulation drives IRF3/7 activation and subsequent antiviral responses during TLR3 engagement, Complex I-derived mtROS diminish type I IFNs production during HMW responses and blocking superoxide production from Complex I without hindering electron flow through the complex, improves HMW-mediated type I IFN production. This suggests that a dependence on OXPHOS activity during the early phase of the antiviral response is more important to LMW-mediated response, which requires mtROS from complexes I and III for a proper response. This highlights the role of the ETC as a key modulator of antiviral responses and potentially positions the complexes of the ETC as new targets to improve antiviral therapies by targeting components that are harmful to macrophage antiviral function during acute viral infections.

Further investigation from this chapter suggests a role for ETC supercomplexes in facilitating macrophage antiviral responses. Recent studies have investigated ETC supercomplexes in the context of macrophage antibacterial responses and linked its disassembly to an increase in mtROS production which enables its robust inflammatory responses and NLRP3 inflammasome activation (22, 23). Su et al. (23) also examined if ETC supercomplex disassembly was conserved across TLR stimuli. Using a high concentration of Poly(I:C) (10μg/mL), which in Chapter 3 was found to caused severe OXPHOS impairment and boosted pro-inflammatory cytokine production, TLR3-activated macrophages underwent a similar disassembly to LPS-activated macrophages including a loss of Complex I-associated ETC supercomplex structures. It is possible that the effects of Complex I-derived mtROS observed in HMW-stimulated BMM is due to increased free Complex I in mitochondria and subsequent mtROS production from that site. Thus, developing

mechanisms to maintain Complex I-associated ETC supercomplex structures may be one possibility to augment macrophage antiviral responses. But more work is required to elucidate whether this possibility is a reality.

Taken together, this thesis brings together a plethora of investigative techniques to probe the importance of cellular metabolism in driving the antiviral response in macrophages. The research completed in this thesis provides the foundational work required to better understand the complicated relationship between metabolic networks and effector function. A systematic understanding of these processes non-diseased models can be translated to provide critical insights into the dysregulation of these networks in diseased states such as live acute and chronic viral infections. In addition, I identified potential metabolic targets that can modulate the magnitude of inflammatory and antiviral responses and thus represent new prospective targets for the improvement of antiviral therapies.
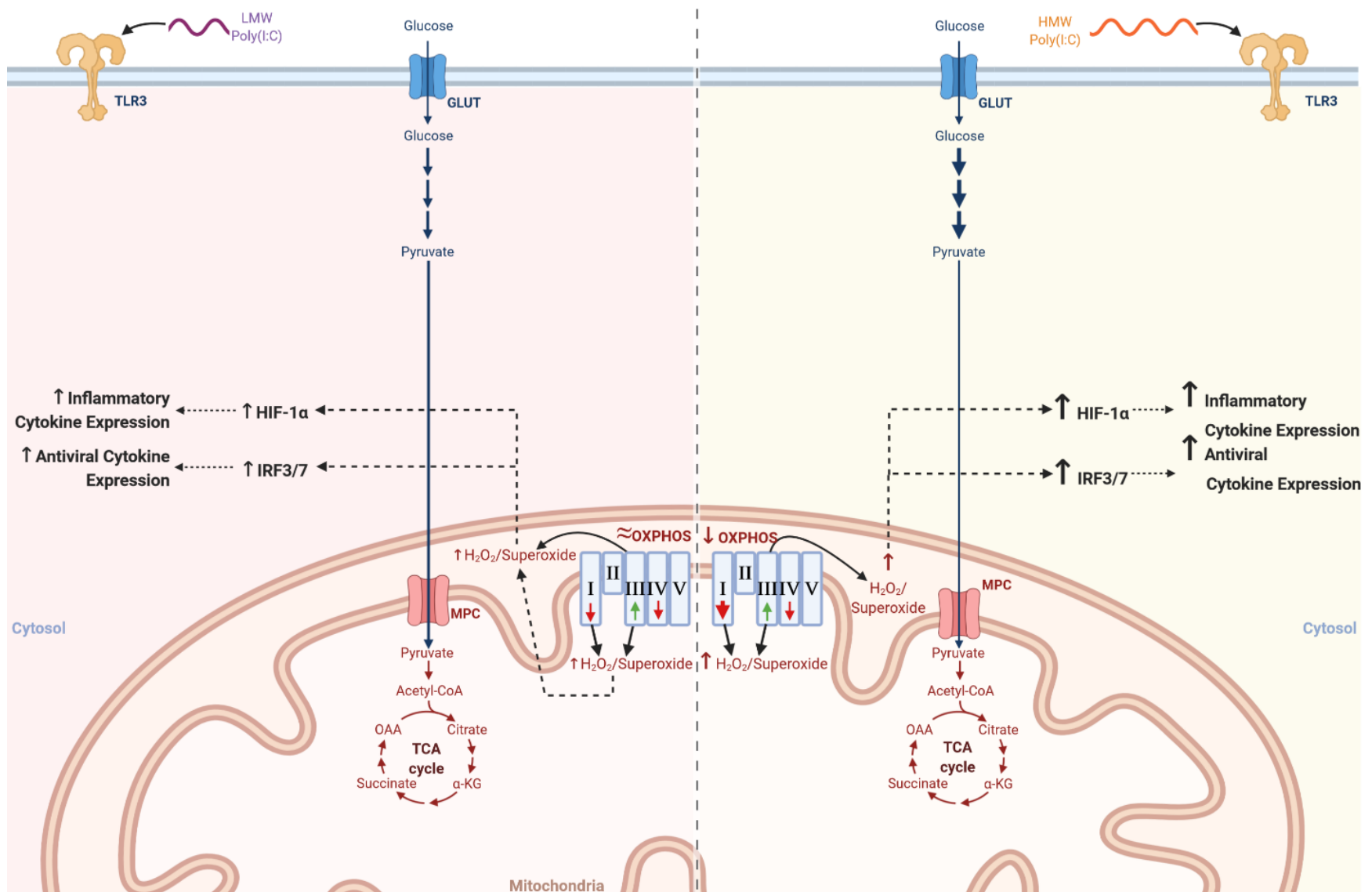
Figure 6.1: A summary of the findings pertaining to the role of cellular metabolism in TLR3-mediated responses.

6.1. References

1. Fritsch, S. D., and T. Weichhart. 2016. Effects of Interferons and Viruses on Metabolism. *Front. Immunol.* 7: 630.
2. Murphy, K. M. 2011. *Janeway's Immunobiology*. Taylor & Francis Group.
3. Bianchi, M. E. 2007. DAMPs, PAMPs and alarmins: all we need to know about danger. *J. Leukoc. Biol.* 81: 1-5.
4. Fitzgerald, K. A., and J. C. Kagan. 2020. Toll-like receptors and the control of immunity. *Cell* 180: 1044-1066.
5. Reikine, S., J. B. Nguyen, and Y. Modis. 2014. Pattern recognition and signaling mechanisms of RIG-I and MDA5. *Front Immunol* 5: 342-342.
6. Ross, J. A., and M. J. Auger. 2002. The biology of the macrophage. In *The macrophage*, 2nd ed. B. Burke, and C. E. Lewis, eds. Oxford University Press, New York, New York. 1-57.
7. Mosser, D. M., and J. P. Edwards. 2008. Exploring the full spectrum of macrophage activation. *Nat Rev Immunol* 8: 958-969.
8. Fadok, V. A., D. L. Bratton, A. Konowal, P. W. Freed, J. Y. Westcott, and P. M. Henson. 1998. Macrophages that have ingested apoptotic cells in vitro inhibit proinflammatory cytokine production through autocrine/paracrine mechanisms involving TGF-beta, PGE2, and PAF. *Journal of Clinical Investigation* 101: 890-898.
9. Fadok, V. A., P. P. McDonald, D. L. Bratton, and P. M. Henson. 1998. Regulation of macrophage cytokine production by phagocytosis of apoptotic and post-apoptotic cells. *Biochem Soc Trans* 26: 653-656.
10. Kesarwani, P., A. K. Murali, A. A. Al-Khami, and S. Mehrotra. 2013. Redox regulation of T-cell function: from molecular mechanisms to significance in human health and disease. *Antioxid. Redox Signal.* 18: 1497-1534.
11. Tannahill, G. M., A. M. Curtis, J. Adamik, E. M. Palsson-McDermott, A. F. McGettrick, G. Goel, C. Frezza, N. J. Bernard, B. Kelly, N. H. Foley, L. Zheng, A. Gardet, Z. Tong, S. S. Jany, S. C. Corr, M. Haneklaus, B. E. Caffrey, K. Pierce, S. Walmsley, F. C. Beasley, E. Cummins, V. Nizet, M. Whyte, C. T. Taylor, H. Lin, S. L. Masters, E. Gottlieb, V. P. Kelly, C. Clish, P. E. Auron, R. J. Xavier, and L. A. J. O'Neill. 2013. Succinate is an inflammatory signal that induces IL-1β through HIF-1α. *Nature* 496: 238-242.
12. Wang, H., H. Flach, M. Onizawa, L. Wei, M. T. McManus, and A. Weiss. 2014. Negative regulation of Hif1a expression and TH17 differentiation by the hypoxia-regulated microRNA miR-210. *Nat. Immunol.* 15: 393-401.
13. Zhu, L., Q. Zhao, T. Yang, W. Ding, and Y. Zhao. 2015. Cellular metabolism and macrophage functional polarization. *Int Rev Immunol* 34: 82-100.
14. Wynn, T. A., A. Chawla, and J. W. Pollard. 2013. Origins and Hallmarks of Macrophages: Development, Homeostasis, and Disease. *Nature* 496: 445-455.
15. McKee, T. J., and S. V. Komarova. 2017. Is it time to reinvent basic cell culture medium? *Am J Physiol Cell Physiol* 312: C624-C626.
16. Ackermann, T., and S. Tardito. 2019. Cell Culture Medium Formulation and Its Implications in Cancer Metabolism. *Trends in Cancer* 5: 329-332.
17. Kedia-Mehta, N., and D. K. Finlay. 2019. Competition for nutrients and its role in controlling immune responses. *Nat Commun* 10: 2123.
18. American Diabetes, A. 2009. Diagnosis and classification of diabetes mellitus. *Diabetes Care* 32 Suppl 1: S62-S67.

19.	Gey, K. F. 1956. The concentration of glucose in rat tissues. *Biochem J* 64: 145-150.

20.	Varanasi, S. K., D. Donohoe, U. Jaggi, and B. T. Rouse. 2017. Manipulating Glucose Metabolism during Different Stages of Viral Pathogenesis Can Have either Detrimental or Beneficial Effects. *J Immunol*.

21.	Yoshizumi, T., H. Imamura, T. Taku, T. Kuroki, A. Kawaguchi, K. Ishikawa, K. Nakada, and T. Koshiba. 2017. RLR-mediated antiviral innate immunity requires oxidative phosphorylation activity. *Sci Rep* 7: 5379.

22.	Garaude, J., R. Acín-Pérez, S. Martínez-Cano, M. Enamorado, M. Ugolini, E. Nistal-Villán, S. Hervás-Stubbs, P. Pelegrín, L. E. Sander, J. A. Enríquez, and D. Sancho. 2016. Mitochondrial respiratory-chain adaptations in macrophages contribute to antibacterial host defense. *Nat Immunol* 17: 1037-1045.

23.	Su, Y., T. P. Miettinen, L. Mu, E. Mirek, S. R. Manalis, T. G. Anthony, H. Sesaki, and J. Chen. 2020. Disassembly of ETC Complexes Drives Macrophage Inflammatory Responses by Reprogramming Cellular Metabolism and Translation [Manuscirpt submitted for publication]. *Cell Rep* Available at SSRN: https://ssrn.com/abstract=3611881: 1-54.